Structural Basis for Specific Inhibition of the Deubiquitinase UCHL1

Dissertation

For the achievement of the academic degree of the

Doctor of Natural Sciences

(Dr. rer. nat.)

Submitted to

The Faculty of Chemistry and Chemical Biology

TU Dortmund University

by

Christian Grethe, M.Sc.

Menden 2023

The work presented in this thesis was performed during the period from December 2018 to Mai 2023 under the supervision of Dr. Malte Gersch at the Chemical Genomics Centre, the Max Planck Institute for Molecular Physiology Dortmund, and the Faculty of Chemistry and Chemical Biology at the TU Dortmund University.

Dekan:	Prof. Dr. Stefan Kast
1st Examiner:	Dr. Malte Gersch
2nd Examiner:	Prof. Dr. Dr. h.c. Herbert Waldmann
Supervisor:	Dr. Malte Gersch

"Success is not final; failure is not fatal: it is the courage to continue that counts."

WINSTON CHURCHILL

University of Miami, 1946

Disclaimer

The first part of this thesis (project 1) was carried out in collaboration with MSc. Mirko Schmidt, a PhD student in the Gersch lab. Although he has contributed equally to the work and success of this project, this thesis focuses mainly on experiments and results performed and analysed by myself. Results of important experiments carried out by Mr Schmidt are attributed and briefly discussed where necessary for the logical development of this work. Mr Schmidt synthesised the probes MS023 and MS037 that were used in the initial profiling assay. He also performed most of the cell-based experiments shown in this thesis, including Ubiquitin-probe assays, western blots, cellular target ID and target validation experiments, and proteomic profiling of the probes. My own work focused on the chemical synthesis of inhibitors and probes, their *in vitro* characterisation, and protein crystallisation experiments. Cell viability measurements were performed by Dr. Rachel O' Dea and cellular characterisation experiments were performed by MSc. Kai Gallant and MSc. Mirko Schmidt.

Parts of this dissertation (project 1) have been published in *Grethe and Schmidt et al., 2022*[1] and as part of the bachelor and master theses of Gian Marvin Kipka 2019[2] and 2022[3], respectively, or will be published as part of Mr Schmidt's dissertation[4].

Acknowledgments

I am profoundly grateful to have had the opportunity to work on this thesis under the guidance of my supervisor, Dr. Malte Gersch. Your steady support, invaluable insights, and dedication to the advancement of knowledge have been instrumental in shaping both the direction and the quality of this research. Your mentorship has not only enriched my academic experience, but has also impelled me to pursue excellence in all facets of my work.

I am deeply grateful to Prof. Herbert Waldmann, who not only took on the role of my second examiner, but also played a foundational role in establishing the Chemical Genomics Centre. His resolute dedication to advancing scientific research and fostering the development of emerging researchers like myself is truly commendable. Prof. Waldmann's visionary leadership and unwavering commitment have not only enabled pioneering research, but also provided me with the opportunity to contribute to this dynamic and thriving scientific community.

I would also like to express my sincere gratitude to Mirko Schmidt for his significant contributions made to this research. Your expertise, thoughtful discussions, and collaborative spirit have played a crucial role in the development and execution of the ideas presented in this thesis. Your generosity in sharing your knowledge and time has been immeasurable, and I am truly fortunate to have had the privilege of working alongside you.

To Gian M. Kipka, I am indebted for your extraordinary dedication and contributions to this work. Beginning as my Bachelor’s student and continuing as my Master‘s student, your commitment to excellence and your diligent efforts have left an indispensable mark on this research. Your insights, hard work, and enthusiasm have greatly enriched the depth of this thesis.

I would like to extend my gratitude to Sven Brandherm from the Rauh Lab at TU Dortmund University. Your contributions, especially to one particular synthesis, have been invaluable to my journey. Countless scientific discussions have not only expanded my understanding, but opened up new perspectives for my research.

I extend my heartfelt gratitude to my research group, the Gersch Lab, for their essential contributions to this journey. Your never-ending support, invaluable insights, and continuous engaging discussions have been instrumental in shaping the conduct of this research. Beyond the academic realm, the camaraderie and shared moments, including our private get-togethers, have provided a sense of solidarity that has sustained me through challenging times. The synergy and team spirit within our group has not only helped to withstand stressful situations, but has also played a significant role in the achievements of this thesis.

I am also grateful to the entire team at the CGC and MPI Dortmund for fostering an environment of intellectual curiosity and creativity. The camaraderie and support from fellow researchers have undoubtedly enhanced the quality of this work.

I would like to thank all the individuals, institutions, and resources that have contributed to the realisation of this research. Your collective efforts have made this thesis into what it is today.

My heartfelt appreciation also goes to my fiancée, Lisa Hölzel. Your willingness to listen and offer comfort and understanding has eased the weight of burdens and doubts. Your friendship, care, and support have been an immeasurable source of strength. Despite 5 years of repeated moments of stress and missed opportunities to spend quality time together, you remained by my side and your belief in me never wavered. Your love and constant encouragement, even during the most difficult times, provided the emotional strength I needed to endure and overcome challenges, and influenced my personal growth and development beyond the academic realm. I wholeheartedly acknowledge that I would not have reached this point without your genuine love and guidance.

To both Mirko Schmidt and Sven Brandherm, I am immensely thankful for your friendship and personal support. Our shared moments of laughter and relaxation, whether through "cornern" at Möllerbrücke/Westpark or during lively Mario Kart sessions in the "Saloon", have provided a much-needed contrast to the intensity of my scientific pursuits. Our friendship, which began in the early days of our studies, has developed into a bond that extends far beyond scientific endeavours. Your company has been a constant source of encouragement and comfort, giving me strength not only in my research but also in facing life's challenges.

Furthermore, I would like to express my appreciation to my family and friends for their encouragement and belief in my abilities. Countless get-togethers, including meals, visits to restaurants/beer gardens, brewing and drinking of cold beverages, card game evenings, shared moments of laughter and your constant emotional support have provided the motivation to overcome challenges and to persevere.

Finally, I would like to raise a frothy mug of appreciation to Hansa Pils, a trusty companion that has expertly helped to cool down both my experiments and my nerves after a hard day's work. In moments of stress and after numerous failed experiments, your crisp embrace has provided a unique kind of comfort. As I navigated through the intricate pathways of research, you stood by like a faithful lab assistant, providing a refreshing interlude amidst the data storms. Your bubbly personality and refreshing qualities have truly contributed to the successful brewing of this thesis. Cheers to Hansa Pils for being the unofficial stress reliever of this scientific odyssey!

Table of Contents

Disclaimer III
Acknowledgments IV
Abstract VIII
Zusammenfassung X
1 Introduction 1
1.1 The Ubiquitin system 1
1.2 Ubiquitin chain topology determines target fate and function 3
1.3 Deubiquitinases influence the entire complexity of the Ubiquitin system 5
1.3.1 Mechanisms of DUB specificity 7
1.3.2 Regulation of DUB abundance and activity 8
1.4 DUBs – rays of hope for new drugs and tools 9
1.4.1 Important roles in tumour progression 10
1.4.2 Important roles in neurodegenerative diseases 10
1.5 UCHL1 – still an unsolved mystery 13
1.5.1 The structure of UCHL1 13
1.5.2 Functional roles 15
1.5.3 UCHL1-deficient mouse models 15
1.5.4 Disease association 16
1.6 Activity-based probes – tools to investigate DUB function 17
1.6.1 Small molecule ABPs 19
1.7 Advancing the validation of UCHL1 as a promising drug target 20
2 Motivation and Aim 23
3 Structural basis for specific inhibition of the deubiquitinase UCHL1 (Project 1) 26
3.1 Design and synthesis of a focused activity-based probe library targeting DUBs 26
3.1.1 Targeting UCHL3 and USP2 27
3.1.2 Targeting USP20 and USP33 29
3.1.3 Targeting USP30 – synthesis of probe CG050 31
3.1.4 Targeting UCHL1 32
3.1.5 Targeting USP7/USP8 38
3.1.6 Targeting USP9x/USP24 39
3.2 A Ubiquitin-VS competition workflow identifies DUB-binding probes 39
3.3 A set of chemogenomic probes for UCHL1 40
3.4 GK13S potently inhibits recombinant and cellular UCHL1 43
3.5 Inhibition of UCHL1 by GK13S does not impair cell growth 45

3.6 Glioblastoma cells treated with GK13S but not GK16S phenocopy a UCHL1 mutant mouse 47
3.7 A compound-induced hybrid conformation underlies GK13S-mediated inhibition of UCHL1 50
3.8 Structural basis for specific inhibition of UCHL1 54
4 Conclusion (Project 1) 58
5 Structural basis for enhanced piperazine-specific inhibition of UCHL1 (Project 2) 62
5.1 Design of GK13S analgoues to enhance UCHL1 selectivity 62
5.2 Synthesis of 3-carboxy-*N*-cyanopyrrolidine-based GK13S analogues 66
5.3 GK13S analogue CG390 shows improved UCHL1 over PARK7 selectivity *in vitro* 70
5.4 *N*-Cyanopiperidine CG305 shows stereoselective labelling of UCHL1, but not of PARK7 72
5.5 Synthesis of piperidine-, morpholine- and piperazine-warhead analogues of GK13S 75
5.6 *N*-Cyanopiperazines CG306 and CG341 show greatly improved selectivity towards UCHL1 *in vitro* 77
5.7 CG341 and CG306 successfully prevent binding to USP30 – a common target of 3-carboxy-*N*-cyanopyrrolidines 81
5.8 *N*-Cyanopiperazines CG306 and CG341 potently inhibit UCHL1 in cells 84
5.9 Structural basis for enhanced piperazine-specific inhibition of UCHL1 88
6 A dual-functional-warhead approach to address novel DUBs (Project 3) 92
7 Summary and Conclusion (Project 2 & 3) 95
8 Outlook 99
8 Appendix 101
9 Methods 115
9.1 Biological Methods 115
9.2 Chemical Synthesis 119
9.2.1 Structural basis for specific inhibition of UCHL1 (Project 1) 120
9.2.2 Structural basis for piperazine-specific inhibition of UCHL1 (Project 2) 133
9.2.3 A Dual-Functional-Warhead Approach to Address novel DUBs (Project 3) 163
9.2.4 CG306 Binding Element Improvement 180
References 189
Abbreviations 197
Eidesstaatliche Versicherung (Affidavit) 199

Abstract

Highly enriched in neurons, the DUB UCHL1 accounts for up to 2% of the total soluble protein in the human brain. Loss of UCHL1 is associated with neurodegenerative diseases, and its dysregulation contributes to the promotion of cancer metastasis and invasive behaviour. Despite its multiple associations with diseases and disease-related pathways, the precise functions of UCHL1 remain poorly understood. A comprehensive understanding of the role of UCHL1 in these pathways is currently hampered by an insufficiently defined set of UCHL1 substrate proteins and a lack of suitable pharmacological tools to specifically inhibit UCHL1 activity. Efforts to improve the specificity and efficacy of DUB inhibitors face significant challenges due to limited structural information about inhibitor:DUB complexes.

This dissertation reports on the design, synthesis and target validation of an activity-based probe library derived from putative covalent DUB inhibitors. This led to the discovery of a chemogenomic pair of 3-carboxy-cyanopyrrolidine-based compounds GK13S and GK16S that enable the selective investigation of UCHL1 activity in a cellular setting. Detailed biochemical characterisation of the lead probe GK13S revealed nanomolar and stereoselective binding to UCHL1. The crystal structure of UCHL1 in complex with GK13S bound to the catalytic cysteine revealed that the enzyme is trapped in a hybrid conformation between apo- and ubiquitin-bound states, explaining its exquisite UCHL1 specificity relative to other members of the UCH family. Consistent with neural tissue from UCHL1 mutant mice, inhibition of UCHL1 in glioblastoma but not epithelial cells resulted in a probe-dependent decrease in mono-Ubiquitin levels. *In vitro* analyses of GK13S and GK16S in combination with activity-based protein profiling revealed PARK7 as a major off-target protein of 3-carboxy-cyanopyrrolidines. A crystal structure of PARK7 in co-complex with the minimal probe GK16S revealed differences in the binding site compared to UCHL1. Based on these findings, repeated cycles of chemical synthesis as well as cellular and biochemical analyses led to the discovery of piperazine-based compounds that did not target PARK7. CG341 and CG306 were found to be non-toxic, nanomolar potent and selective inhibitors of UCHL1, overcoming the limitations of previously reported UCHL1-targeting probes. In addition, this dissertation introduces a novel “dual-functional warhead“ strategy that offers an initial framework for efficiently creating extensive and varied libraries of activity-based probes. These libraries have the potential to facilitate the discovery of novel and precise probes targeting specific DUB enzymes.

In conclusion, this dissertation advances the knowledge of DUB biology and inhibitor development, offering selective tools to study UCHL1 in cellular contexts. The work delves into the structural underpinnings of UCHL1 inhibition, validates the selectivity of the developed probes, and proposes their utility in investigating intricate disease-related pathways. This

approach holds promise for advancing drug development efforts and devising diagnostic tools, thereby contributing to a comprehensive understanding of DUB function in the context of various diseases.

Zusammenfassung

Hoch angereichert in Neuronen macht die Deubiquitinase (DUB) UCHL1 bis zu 2% des gesamten löslichen Proteins im menschlichen Gehirn aus. Der Verlust von UCHL1 ist mit neurodegenerativen Krankheiten assoziiert, und seine Fehlregulierung trägt zur Förderung von Krebsmetastasen und invasivem Verhalten bei. Trotz der vielfachen Verbindungen zu Krankheiten und krankheitsrelevanten Signalwegen sind die genauen Funktionen von UCHL1 noch immer schlecht verstanden. Ein umfassendes Verständnis der Rolle von UCHL1 in diesen Signalwegen wird derzeit durch unzureichend definierte Substratproteine von UCHL1 und einen Mangel an geeigneten pharmakologischen Werkzeugen zur gezielten Hemmung der UCHL1-Aktivität behindert. Bemühungen, die Spezifität und Wirksamkeit von DUB-Inhibitoren zu verbessern, stehen vor erheblichen Herausforderungen aufgrund begrenzter struktureller Informationen über Inhibitor:DUB-Komplexe.

Diese Dissertation berichtet über das Design, die Synthese und die Validierung einer auf vermeintlich kovalenten DUB-Inhibitoren basierenden Aktivitäts-basierten Sonden Bibliothek. Dies führte zur Entdeckung eines chemogenomischen Paares von 3-Carboxy-Cyanopyrrolidin-basierten Verbindungen GK13S und GK16S, die die selektive Untersuchung der UCHL1 Aktivität in einem zellulären Umfeld ermöglichen. Eine detaillierte biochemische Charakterisierung der Leitsonde GK13S zeigte nanomolare und stereoselektive Bindung an UCHL1. Die Kristallstruktur von UCHL1 im Komplex mit GK13S, das kovalent an das katalytische Cystein gebunden ist, zeigte, dass das Enzym in einer hybriden Konformation zwischen apo- und Ubiquitin-gebundenem Zustand gefangen ist, was seine exquisite UCHL1-Spezifität im Vergleich zu anderen Mitgliedern der UCH-Familie erklärt. Konsistent mit Gewebe aus dem Gehirn von UCHL1-Mutantenmäusen führte die Hemmung von UCHL1 in Glioblastomen, aber nicht in Epithelzellen, zu einer Sonden-abhängigen Abnahme der Mono-Ubiquitin Level. *In vitro* Analysen von GK13S und GK16S in Kombination mit aktivitätsbasiertem Proteinprofiling enthüllten PARK7 als das vorwiegende *off-target*-Zielprotein von 3-Carboxy-Cyanopyrrolidinen. Eine Kristallstruktur von PARK7 im Komplex mit der Minimalsonde GK16S zeigte Unterschiede in der Umgebung der Bindungsstelle im Vergleich zu UCHL1. Basierend auf diesen Ergebnissen führten wiederholte Zyklen von chemischer Synthese sowie zelluläre und biochemische Analysen zur Entdeckung von Piperazin-basierenden Verbindungen, die PARK7 nicht binden. CG341 und CG306 erwiesen sich als ungiftige, nanomolar-potente und selektive Inhibitoren von UCHL1 und überwanden die Einschränkungen zuvor berichteter Kleinmolekül-Sonden zur Untersuchung von UCHL1. Darüber hinaus führt diese Dissertation eine neuartige „Doopelfunktionale warhead“-Strategie ein, die einen initialen Rahmen für die effiziente Herstellung umfangreicher und vielfältiger Bibliotheken von aktivitätsbasierten Sonden bietet. Diese Bibliotheken haben das Potenzial,

die Entdeckung neuartiger und präziser Sonden zur gezielten Hemmung spezifischer DUB-Enzyme zu erleichtern.

Zusammenfassend trägt diese Dissertation zur Weiterentwicklung des Wissens über DUB-Biologie und Inhibitor-Entwicklung bei, indem sie selektive Werkzeuge zur Untersuchung von UCHL1 in zellulären Kontexten bietet. Die Arbeit geht auf die strukturellen Grundlagen der Inhibition von UCHL1 ein, validiert die Selektivität der entwickelten Sonden und legt ihre Nützlichkeit bei der Untersuchung komplexer, krankheitsrelevanter Signalwege dar. Zukünftig bietet diese Arbeit einen Ansatz für Fortschritte bei der Entwicklung von Medikamenten und diagnostischen Werkzeugen und hilft somit zu einem umfassenden Verständnis der DUB-Funktion im Kontext verschiedener Krankheiten beizutragen.

1 Introduction

1.1 The Ubiquitin system

The discovery of ubiquitination as a post translational modification (PTM) between the late 1970s and early 1980s set the foundation for a new era in almost all fields of scientific research. Over the years, it became increasingly clear that ubiquitination is a regulatory mechanism, playing an essential role in the majority of cellular processes in eukaryotes.[5] Ubiquitination describes the covalent attachment of the highly conserved, small protein Ubiquitin (Ub) to target proteins by the help of E1, E2 and E3 enzymes, a process that is reversible by deubiquitinases (DUBs) (**Figure 1A-C**).

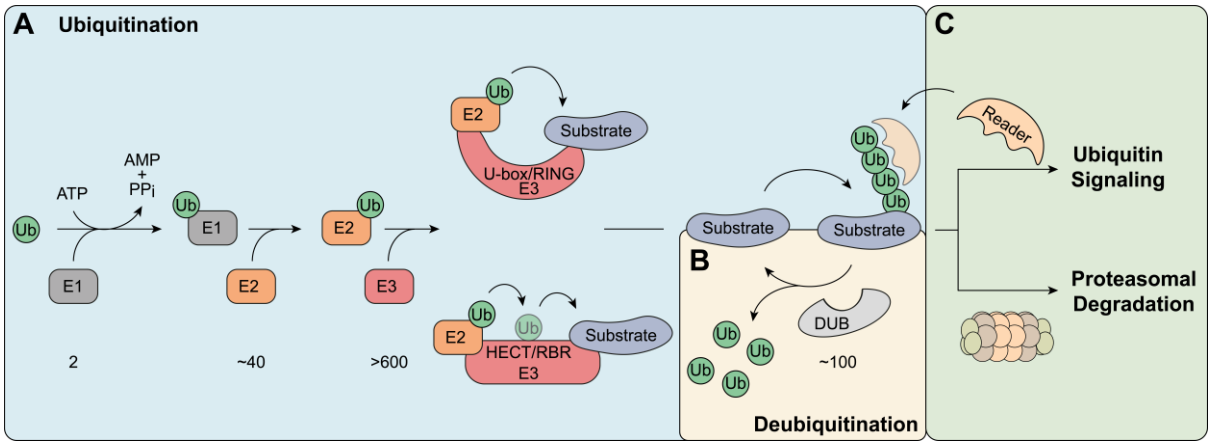

Figure 1. The Ubiquitin system. A. Schematic representation of the ubiquitination cascade consisting of E1 activating enzymes, E2 conjugating enzymes and E3 ligases, facilitating the transfer of Ubiquitin (Ub) onto a substrate. **B.** Deubiquitinases are able to reverse ubiquitination. **C.** Depending on the ubiquitination pattern and linkage type, ubiquitinated proteins can either be bound by enzymes containing reader domains, thereby affecting cellular processes, or directed to proteasomal degradation. Numbers below enzymes reflect the quantity of known representatives of each class. Figure adapted from Schmidt et al.[6]

In a two-step reaction, the C-terminus of Ubiquitin is transferred to the catalytic Cys of an E1 activating enzyme in an ATP-dependent manner, forming a thioester bond (**Figure 1A**). Subsequently, an E2 conjugating enzyme transmits Ubiquitin to its own catalytic Cys in a transthioesterfication reaction. Further, an E3 ligase, which is able to bind both, E2 enzyme and target substrate, catalyses the transfer of Ubiquitin to the protein in a direct or indirect manner.[5] In general there are at least four different types of E3 ligases: The HECT (Homologous to E6AP C-terminus), RING (Really Interesting New Gene)-finger, U-box and RBR (RING-between-RING) E3 ligases.[7] The HECT and RBR E3 ligases form a Ubiquitin-thioester intermediate with the E3 active site Cys during Ubiquitin transfer to a substrate, whereas the RING and U-box E3 ligases directly transfer Ubiquitin from the conjugating E2 enzyme to the substrate (**Figure 1A**).[5,7] With over 600 enzymes, members of the E3 protein

family facilitate E2 and target protein selectivity, thus providing specificity of the Ubiquitin transfer in the last step of the enzymatic E1-E3 cascade.[7]

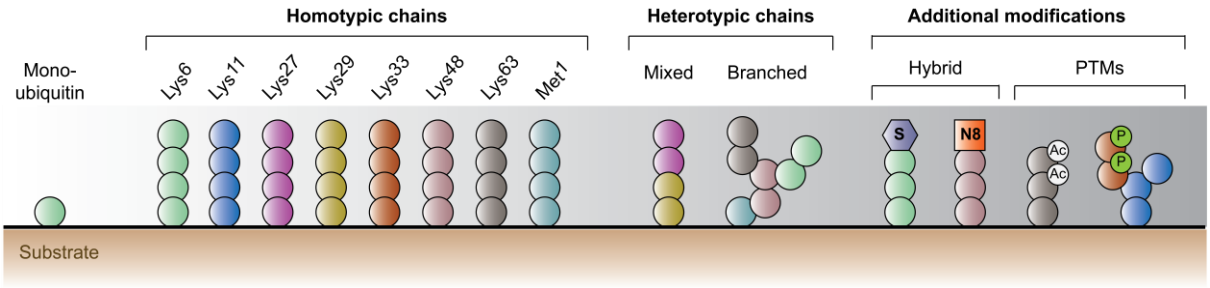

Figure 2. The structural complexity of Ubiquitin chain linkage types. A substrate can be (multiple) mono ubiquitinated or poly-ubiquitinated, where 3 different types of the latter are differentiated. In homotypic chains, Ubiquitin is connected continuously via the same Lys side chain to the preceding Ubiquitin. Heterotypic chains contain more than one linkage type in mixed (different linkage types in one chain) or branched (connection of more than one Ubiquitin molecule to a single Ubiquitin) arrangement. Additional modifications of Ubiquitin by Ubiquitin-like (Ubl) modifier (hybrid chains) such as Sumo (S) or Nedd8 (N8) or attachment of PTMs including phosphorylation (P) or acetylation (Ac) result in higher levels of Ubiquitin signalling complexity. Figure adapted from Mevissen et al.[8]

The C-terminal Gly76 of Ubiquitin is attached to a free ε-amino group of a lysine side chain of the target protein, resulting in the formation of an isopeptide bond. Ubiquitin itself in turn bears seven internal Lys residues (Lys6, Lys11, Lys27, Lys29, Lys33, Lys48, Lys63) and one N-terminal Met residue (Met1), which can be utilised for further modification.[9] Addition of more Ubiquitin monomers via the same N-terminal Met (linear chain), or the same Lys residue (homotypic chain) results in poly-Ubiquitin chains with distinct topology and function (**Figure 2**). Further, Ubiquitin monomers can be linked together via varying Lys residues, resulting in heterotypic chains. A chain bearing multiple sites of connection on one Ubiquitin is called branched Ubiquitin chain, whereas a Ubiquitin chain comprising several linkage types is referred to as mixed Ubiquitin chain. Structurally, Ubiquitin bears a globular β-grasp fold. This structural feature is conserved in the protein family of Ubiquitin-like (Ubl) modifiers, with distinct sequence, but complementary signalling functions to Ubiquitin.[10,11,12,13] Ubl modifiers, such as SUMO, NEDD8 and ISG15 are similarly ligated to proteins by their respective enzyme machineries.[14] An additional layer of complexity can be added by further modifying Ubiquitin chains with Ubl modifiers and other PTMs such as phosphorylation (which can possibly occur on every Ser, Thr and Tyr residue of Ubiquitin[15]) or acetylation (to date verified on Lys residues[16]), resulting in a huge number of possible chain topologies.[8] Single mono-ubiquitination, multiple mono-ubiquitination or Ubiquitin chains of different linkage types, topologies and lengths determine the fate and function of substrate proteins in different ways, e.g. by affecting proteasomal degradation, cellular localisation, catalytic activity or protein interactions (**Figure 1C**).[17,18] Each linkage type displays a unique three dimensional structure,

allowing interaction with effector proteins via specific Ubiquitin binding domains (UBDs) and thereby regulating numerous cellular processes.[19]

1.2 Ubiquitin chain topology determines target fate and function

Protein degradation in cells is regulated by two major pathways: autophagy and the Ubiquitin proteasome system (UPS), both fundamentally involved in protein homeostasis.[20] The UPS, first described in late 1970s by Hershko[21] and Ciechanover[22] and in 2004 rewarded with the Nobel prize, relates to the degradation of damaged, misfolded or short-lived proteins via the proteasome, thus regulating the degradation of over 80% of all proteins in cells.[20] In this process, predominantly Lys48-linked poly-Ubiquitin chains are assembled via the enzymatic E1-E3 cascade onto a protein (**Figure 1A**), targeting it for degradation by the 26S proteasome.[23] Although ubiquitination was originally referred to as the signal for proteolysis, many linkage types have been associated with distinct cellular functions (**Figure 3**).[9] The most abundant types of ubiquitination are mono-ubiquitination as well as Lys48- and Lys63-linked poly-ubiquitination. While the more compact Lys48-linked poly-Ubiquitin chains mostly target proteins for degradation, Lys63-linked chains feature a more flexible and extended topology allowing them to be bound by distinct effector proteins, thus playing roles in cell signalling, intracellular trafficking, DNA damage response and many more cellular processes.[9,23,24,25] Mono-ubiquitination was shown to facilitate protein recognition, complex formation or allosteric regulation of target proteins via nonproteolytic mechanisms.[8] Proteomic profiling upon inhibition of the proteasome revealed that Lys6-, Lys11-, Lys27- and Lys33-linked chains may also play a role in proteasomal degradation.[26] Further, Lys6-linked poly-Ubiquitin chains regulate DNA damage response, whereas Lys11-linked chains facilitate cell cycle regulation and membrane trafficking.[27,28] Activation of the innate immune response, protein secretion, DNA damage repair and mitochondrial damage response is controlled by Lys27-linked chains. In Parkinson's Disease (PD), the TNF-receptor associated factor 6 (TRAF6) enhances the aggregation of mutant PARK7 (Parkinsonism Associated Deglycase) and α-synuclein through Lys29-, but also Lys6- and Lys27-linked poly-Ubiquitin chains.[29] Apart from association with the TNF signalling pathway and neuronal diseases, Lys29-linked chains have been associated with the regulation of the MAP kinase (MAPK) pathway and proteasomal degradation.[30] Lys33-linked ubiquitination, the least studied homotypic linkage type, is engaged in protein sorting mechanisms such as transport of membrane proteins.[29] Linear (Met1-linked) Ubiquitin chains are assembled by the linear Ubiquitin chain assembly complex (LUBAC), a multi-protein complex consisting of HOIL-1, HOIP and SHARPIN. HOIP possesses a catalytic centre in its RING2 domain and is responsible for assembling linear ubiquitin chains, whereas HOIL-1L and SHARPIN have been recognised as accessory

proteins in this process.[31] Linear chains mediate NFκB[32] and Wnt signalling as well as angiogenesis, craniofacial and neural development[33].

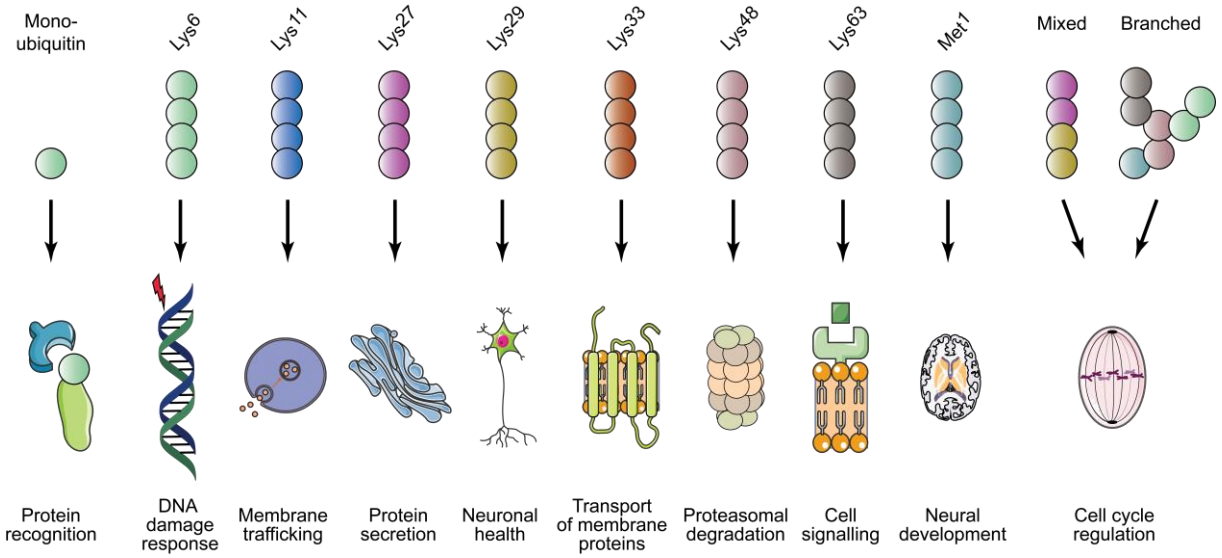

Figure 3. Ubiquitin linkage topology determines substrate fate and function. Shown is one of often many examples of signals induced by different Ubiquitin chain linkage topologies. Figure adapted from Meyer and Rape[34].

Apart from homotypic chains, the function of heterotypic Ubiquitin chains remains poorly understood. The group of Michael Rape intensively studied, among others, the function of Lys11/Lys48- and Lys11/Lys63-branched chains in context of the anaphase promoting complex (APC/C). They identified these branched-chains as key players in quality control through facilitating the degradation of cell cycle regulators (**Figure 3**).[35,36,37] Through additional modification of Ubiquitin with Ubl modifiers, hybrid Ubiquitin/Ubl chains are formed (**Figure 2**) that either regulate the original function of the Ubiquitin chain or encode for a completely new one.[38] Studies revealed that Ubiquitin can also be modified with Ubls such as SUMO, NEDD8 and ISG15.[37] SUMOylated Ubiquitin chains were shown to influence genomic stability and DNA damage response, while NEDDylated Ubiquitin chains regulate proteotoxic stress response, possibly playing a role in pathogenesis and progression of neurodegenerative diseases.[38,39,40,41] On the contrary, little is known about the function of ISG15-Ubiquitin chains, serendipitously detected in a proteomic study in 2005.[42] Since ISG15 has not been reported to generate polymeric chains and no ISG15-interacting motifs are known so far, it is supposed to potentially function as a chain termination moiety to rescue ubiquitinated proteins from degradation.[38] However, research on mixed Ubiquitin chains is still in its infancy and need to be further elucidated in future studies.

1.3 Deubiquitinases influence the entire complexity of the Ubiquitin system

Dysregulation of the UPS has been divulged in a multitude of neurodegenerative disorders, viral diseases and most hallmarks of cancer, highlighting the importance of this pathway in the regulation of multiple cellular processes.[7,43] Deubiquitinases (DUBs) constitute an important regulatory component of the UPS by catalysing the removal of Ubiquitin, thus being directly involved in Ubiquitin associated signalling processes. To counterbalance ubiquitination, DUBs not only remove Ubiquitin from substrates, but also alter Ubiquitin chain topology.[44] Modulation and processing of Ubiquitin chains can be accomplished through UBDs, allowing specific interaction with either Ubiquitin or Ubiquitin chains.[45]

Nature has brought forth a comprehensive range of deubiquitinating enzymes with ~100 of them discovered so far.[46] Most DUBs are isopeptidases, catalysing the hydrolysis of the isopeptide-bond between the C-terminal Gly76 of Ubiquitin and the attached Lys side chain. One important function of DUBs lies in maintaining the free Ubiquitin pool in cells, primarily at the proteasome. The proteasome is a key protease complex for degradation of proteins, consisting of a barrel-shaped 20S catalytic core particle and one or two 19S regulatory particles (RPs), serving as proteasome activator(s). Three known DUBs are associated with the 19S RP and are responsible for recycling Ubiquitin from chains. Two DUBs, USP14 and UCHL5 (/UCH37) are located at the tip of the 19S RP. They belong to the family of Cys proteases and cleave the distal Ubiquitin of a chain. The third DUB, RPN11, is part of the metalloprotease family of DUBs and is found at the base of the 19S RP, cleaving the proximal linkage between Ubiquitin chain and target protein.[47]

DUBs are divided into two main classes according to their active site characteristics: metalloproteases and Cysteine proteases. The catalytic mechanism of metalloproteases is zinc ion dependent.[9] Two zinc ions are coordinated within their active site by His, Asp and Ser side chains. The function of the zinc ion is the activation of a water molecule to form a hydroxide ion, which is able to attack the carbonyl group of the isopeptide linkage.[48] The ε-amino group of the Lys side chain is subsequently eliminated and replaced by the previously generated hydroxide ion. An adjacent Glu residue serves as proton acceptor and donor during catalysis.[48] The Cys protease DUBs contain a catalytic triad or diad, featuring a similar mechanism to the protease papain: A reactive Cys residue, activated via deprotonation of an adjacent His, performs a nucleophilic attack on the isopeptide bond of a ubiquitinated Lys side chain (**Figure 4**). This leads to the formation of a tetrahedral intermediate with a negatively charged oxygen, stabilised by the oxyanion hole. Elimination of the Lys-amine leads to substrate release, while Ubiquitin stays bound to the Cys via a thioester bond. In a second step, a water molecule performs a nucleophilic attack on the thioester bond, followed by elimination and subsequent release of Ubiquitin, regenerating the active site Cys.[49] In many

Cys proteases the catalytic His residue needs to be aligned and polarised by a third residue, usually Asp or Asn (**Figure 4**).[48]

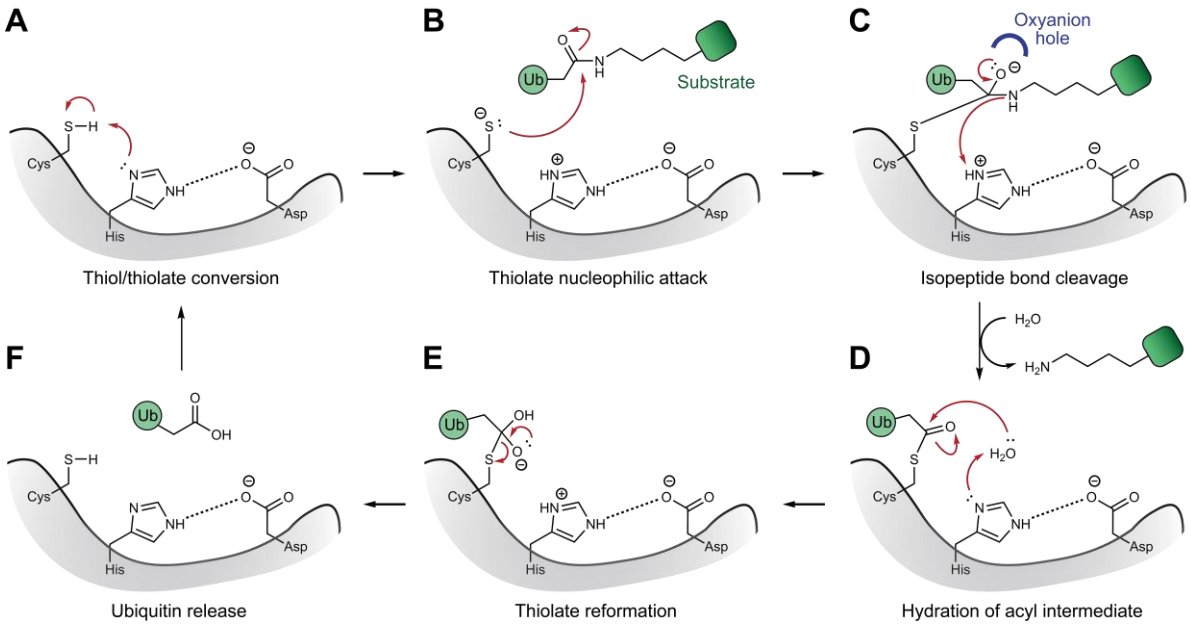

Figure 4. Catalytic cleavage mechanism of DUB Cys proteases. Exemplified by the three most common members of the catalytic triad Cys, His and Asp. **A.** His, which is depolarised by Asp, deprotonates the catalytic Cys, thereby converting it into a reactive thiolate. **B.** The Cys thiolate performs a nucleophilic attack on the isopeptide bond between Ubiquitin and substrate-Lys, forming a tetrameric intermediate, stabilised by the oxyanion hole (as shown in **C**). **C.** The isopeptide bond is cleaved via proton transfer from His to the Lys-amine group, releasing the substrate. **D.** Hydration of the Cys acyl intermediate by utilizing a water molecule. **E.** Hydrolysis and cleavage of water leads to **F.** Ubiquitin release from the active site. Figure adapted from Kwasna et al.[50]

The Cys proteases are further categorised into 6 superfamilies, of which 60 USPs (Ubiquitin-specific proteases), 17 OTUs (ovarian tumour proteases), 4 MJDs/Josephins (Machado-Joseph disease domain DUBs), 4 UCHs (Ubiquitin C-terminal hydrolases), 4 MINDYs (motif interacting with Ubiquitin-containing novel DUB family) and one member of the ZUFSP (Zinc finger with UFM1 Specific Peptidase domain) family were discovered so far (**Figure 5**).[18,51] The metalloprotease DUBs contain one superfamily of JAMM/MPN+ domain containing proteins (JAMMs) with 12 identified representatives.[18,51]

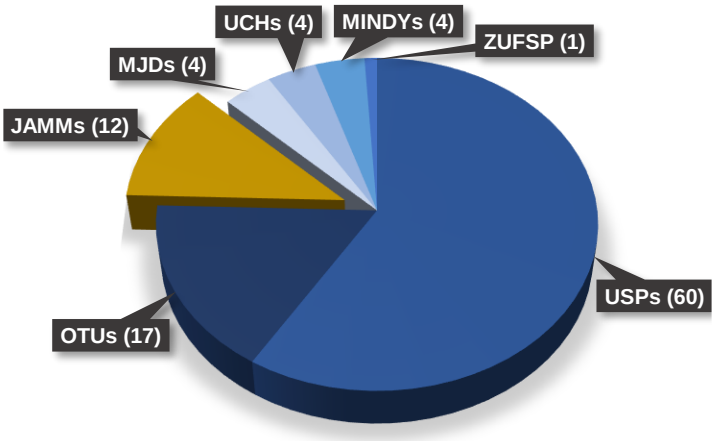

Figure 5. Human DUBs across their different enzyme subfamilies. More than 100 DUBs are known, divided into two main classes by their catalytic mechanism: the metalloproteases (yellow) and cysteine proteases (blue, mono-chromatic). OUTs: ovarian tumour proteases; USPs: Ubiquitin-specific proteases; ZUFSP: Zinc finger-containing Ubiquitin peptidase 1; MINDYs: motif interacting with Ubiquitin-containing novel DUB family; UCHs: Ubiquitin C-terminal hydrolases; MJDs: Machado-Joseph disease domain DUBs; JAMMs: JAMM/MPN+ domain containing proteins.

1.3.1 Mechanisms of DUB specificity

Given the great complexity of Ubiquitin chain linkage types, also referred to as the "Ubiquitin code", it is not surprising that DUBs show different preferences by recognizing mono-Ubiquitin, different Ubiquitin chain linkages or even the position within a Ubiquitin chain (**Figure 6A,B**).[48,52] All DUBs have at least one Ubiquitin binding site, the S1 site, positioning the Ubiquitin C-terminus and scissile bond in the active site to ensure catalysis.[8] Depending on the Ubiquitin binding sites, different chain cleavage modes are possible (**Figure 6C**): Some DUBs can cleave the distal Ubiquitin from a chain such as UCHL5, whereas others are able to only partially trim and thereby edit chains (endo-specific cleavage).[48,53] Then again there are DUBs lacking the S1' Ubiquitin binding site, but instead having a S1' substrate binding site that mediates the cleavage between substrate and proximal Ubiquitin (base-specific cleavage) (**Figure 6C**).[5,48] In the event of an exo-specific DUB binding to a di-ubiquitinated substrate, the S1 site is bound by the distal Ubiquitin, while the proximal, protein-bound Ubiquitin occupies the S1' site.[8] Some DUBs feature additional Ubiquitin binding sites such as S2, S2', S3 or S3' sites to facilitate the binding of longer Ubiquitin chains, contributing to linkage specificity.[5,8]

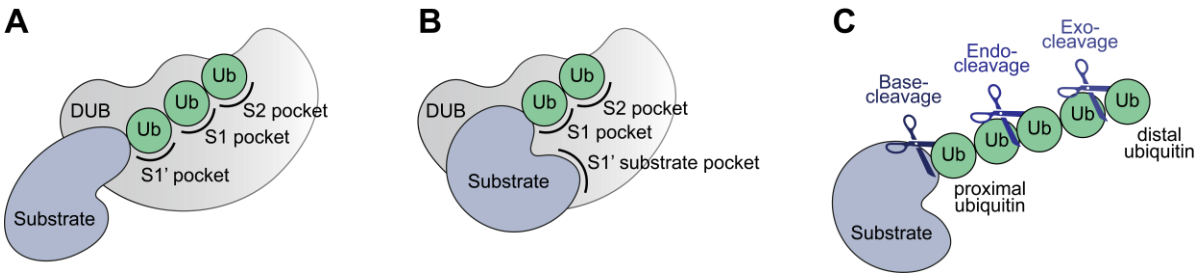

Figure 6. DUB specificity and cleavage modes. A, **B.** DUBs can exert specificity for certain Ubiquitin linkage types (**A**), or substrates (**B**), determined by their Ubiquitin binding sites (e.g. S1', S1, S2). **C.** DUBs can cleave the distal Ubiquitin from a chain (exo-cleavage), cleave in between Ubiquitin chains (endo-cleavage), or cleave Ubiquitin chains between substrate and proximal Ubiquitin (base-cleavage).[5,54]

1.3.2 Regulation of DUB abundance and activity

The simplest mechanism for modulating a protein's activity or abundance is by regulating its intracellular localisation or concentration. The same principle holds true for DUBs, whose activity is not solely based on linkage- or substrate specificity, but can further underly (even cell type specific) transcriptional and translational control or degradation.[44] Various DUBs are regulated by transcription factors, enabling high protein levels in the presence of certain events. The protein levels of USP37, for instance, greatly depend on the current cell-cycle state and are controlled by E2F transcription factors, allowing the upregulation of USP37 levels during the G1/S transition.[55] While some DUBs are targeted for proteasomal degradation by poly-ubiquitination, others such as USP14 are able to auto-deubiquitinate, thus opposing their own degradation.[44,56]

Other DUBs, like most proteins of the USP family, do not show any Ubiquitin linkage specificity. Their activity and specificity are regulated via protein-protein-interaction (PPI) domains on their surface or even in their catalytic domains, allowing them to selectively bind to target proteins.[57,58] These interacting partners can play key roles in the biological function or activity of the DUB. In the case of all three proteasome-associated DUBs (USP14, UCHL5 and Rpn11) for example, significant activity can only be achieved by incorporation in the 19S RP.[59,60] UCHL5 is part of the chromatin-remodelling INO80 complex, auto-inhibiting its catalytical function. At the proteasome, UCHL5 activity is modulated by DUB adaptor (DEUBAD) domains, present in both the proteins INO80G and Rpn13. The DEUBAD domain of Rpn13 facilitates structural rearrangements in UCHL5, resulting in inhibition of INO80 and thus activation of UCHL5. In contrast, the DEUBAD domain of INO80G inhibits UCHL5 by exploiting similar structural elements, but promotes a radically different conformation and blocks Ubiquitin binding.[61] Similarly, the catalytic activities of USP1, USP12 and USP46 are regulated by UAF1 (USP1-associated factor 1) and WD repeat-containing proteins, indicating the versatile possibilities of DUB regulation by interacting partners.[62,63,64] Besides their interconnection with partner proteins, DUBs are often found in complexes with proteins of the Ubiquitin system, where they, inter alia, stabilise E3 ligases by counteracting auto-ubiquitination, or function as a negative regulator by reversing the E3 enzymes function.[44,65]

Physiological processes often happen in certain locations inside the cell. Subcellular localisation of DUBs is realised through particular localisation signals, allowing them for instance to interact with cellular compartments. This is crucial in the case of USP30 that shows a highly restricted intracellular localisation to the outer mitochondrial membrane and is thereby able to regulate mitochondrial morphology.[44,66] Additional localisation factors can mediate nucleolar (in the case of USP36), endosomal (AMSH and USP8) or transmembrane (USP19) localisation.[67,68,69]

Regulation of DUBs can further be achieved by a wide variety of PTMs such as phosphorylation, ubiquitination or modification with Ubl modifiers. Especially phosphorylation plays an important role in directing DUB activity. Depending on the DUB and its activation state, phosphorylation can upregulate (USP1, USP10, USP14, USP37, USP9X, OTUD5), inhibit (CYLD) or modulate (A20) the catalytic activity of DUBs, but can also affect their subcellular localisation (USP4, OTUB1) or interaction with other proteins.[8,15,44,55,70,71]

The possible presence of multiple such interaction- and localisation domains, PTMs and Ubiquitin binding sites in one DUB gives rise to almost infinite capabilities to impact DUB function, activity and regulation.

1.4 DUBs – rays of hope for new drugs and tools

Since DUBs themselves, as antagonists of the Ubiquitin system, maintain the balance of almost all cellular processes (**Figure 7**), the aberrant regulation of DUBs generally leads to the occurrence and progression of a series of diseases, including neurodegenerative disorders, such as Parkinson's (PD) and Alzheimer's Disease (AD) or multiple types of cancer.

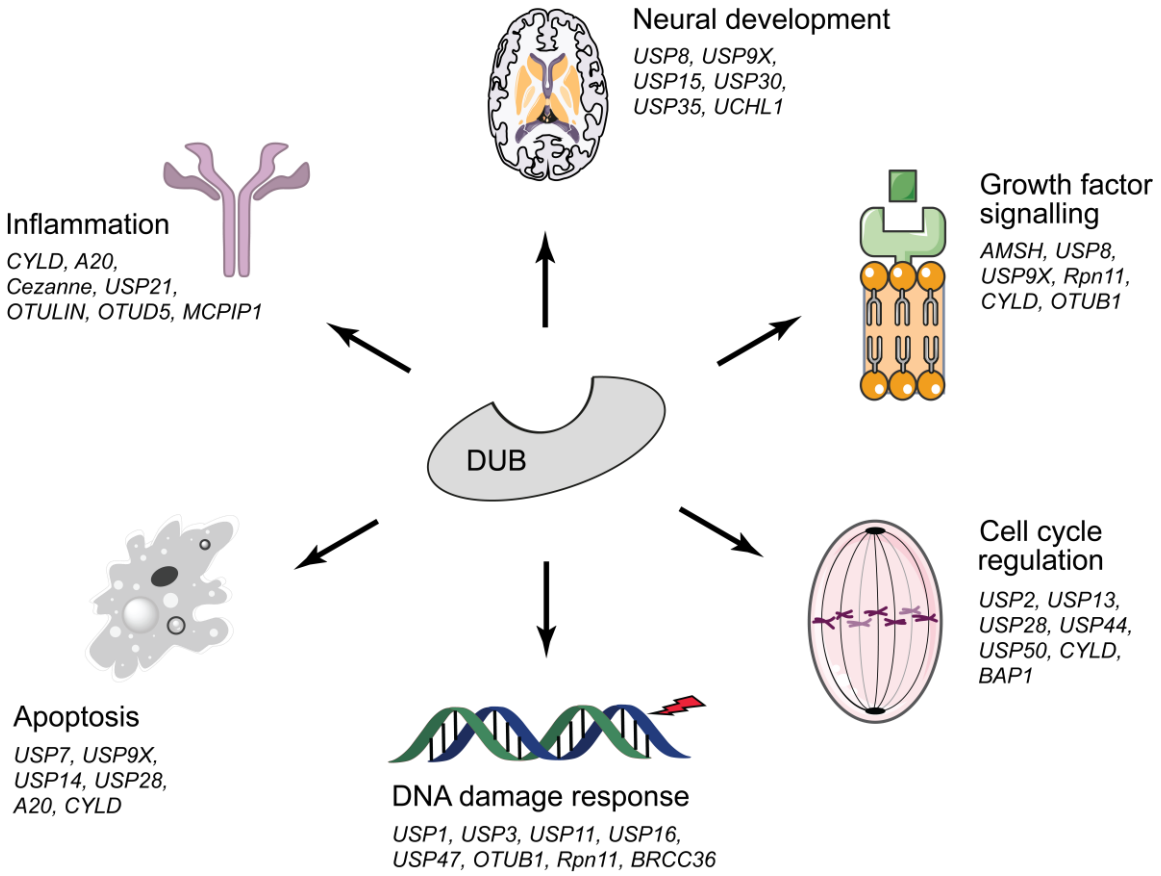

Figure 7. Human DUBs regulate multiple cellular pathways. Selection of DUBs, playing key roles in disease relevant pathways. Figure adapted from Heideker and Wertz[9].

DUBs regulate many disease relevant pathways such as apoptosis, DNA damage response, growth factor signalling, cell cycle regulation and inflammation (**Figure 7**).[32,57,72,73] Moreover,

DUBs were identified to control the activity and function of important oncogenes including the E3 ligase MDM2 (via USP7), transcription factor MYC (via USP28) and apoptosis regulator MCL1 (via USP9x), as well as tumour suppressors including PTEN (via USP7, ATXN and JOSD1) and p53 (via USP7, USP10 and OTUB1).[9,74,75,76,77,78,79,80]

1.4.1 Important roles in tumour progression

The tumour suppressor protein p53 is a regulatory protein which is involved in cellular stress regulation, such as DNA damage response, hypoxia, cell cycle arrest and cell death.[81] Since loss of function mutations in the p53 gene are present in over 50% of human cancers, it became one of the most intensive studied proteins in history, particularly in the drug development field.[81] In healthy cells, the E3 Ubiquitin ligase MDM2 (mouse double minute 2 homolog) functions as a negative regulator of p53 by poly-ubiquitinating and thereby targeting it for proteasomal degradation. A proper equilibrium in MDM2 levels is maintained by the DUB USP7, deubiquitinating and thereby activating MDM2, leading to p53 ubiquitination via MDM2 and reduction of p53 levels.[18] Over the past years, increasing roles of USP7 in the direct regulation of numerous cancer-associated pathways became apparent. USP7 was shown to promote cell growth and proliferation in breast cancer cells by interacting with estrogen receptor α (ERα).[82] Further, crucial roles for USP7 in prostate, cervical and colorectal cancer are described in the literature.[83,84,85,86] Since USP7 inhibition is directly related to cancer regression, extensive research was carried out over the years for the purpose of developing specific USP7 inhibitors. In the years 2007 – 2010, the pharma companies *Hybrigenics* and *Progenra* used screening campaigns to develop USP7 inhibitors such as HBX41108 and P22077, respectively. HBX41108 was shown to be a reversible inhibitor of USP7 with an IC_{50} of 0.42 µM, but later studies revealed multiple off-target proteins, including several DUBs[87]. Further, P22077 was found to inhibit both USP7 and USP47 with IC_{50} values of 8.0 µM and 8.7 µM, respectively. Despite the weak inhibitory potency against USP7, P22077 was tested *in vivo* in a mouse model for human multiple myeloma, leading to tumour growth inhibition and prolonged survival.[88,89] Later studies revealed the compound being additionally active against USP9x, USP10 and USP20 at 1 µM concentration.[87] A multitude of improved USP7 inhibitors were discovered bearing different structural and functional features, but none of them were able to enter clinical trials so far.

1.4.2 Important roles in neurodegenerative diseases

Mitochondria are crucial cell organelles with the function of coordinating numerous metabolic processes.[90] Quality control of mitochondria is therefore a key mechanism, tightly regulated by the proteins PINK1 and Parkin. Parkin is an E3 ligase, ubiquitinating mitochondrial outer membrane proteins to trigger degradation of defect mitochondria, a process called mitophagy.

Malfunction of Parkin leads to impaired mitochondrial degradation and has been directly linked to diseases such as type 2 diabetes, AD and PD. As DUBs are able to counteract ubiquitination, some have been reported to function as “breaks” of mitophagy, counteracting Parkin (**Figure 8**).

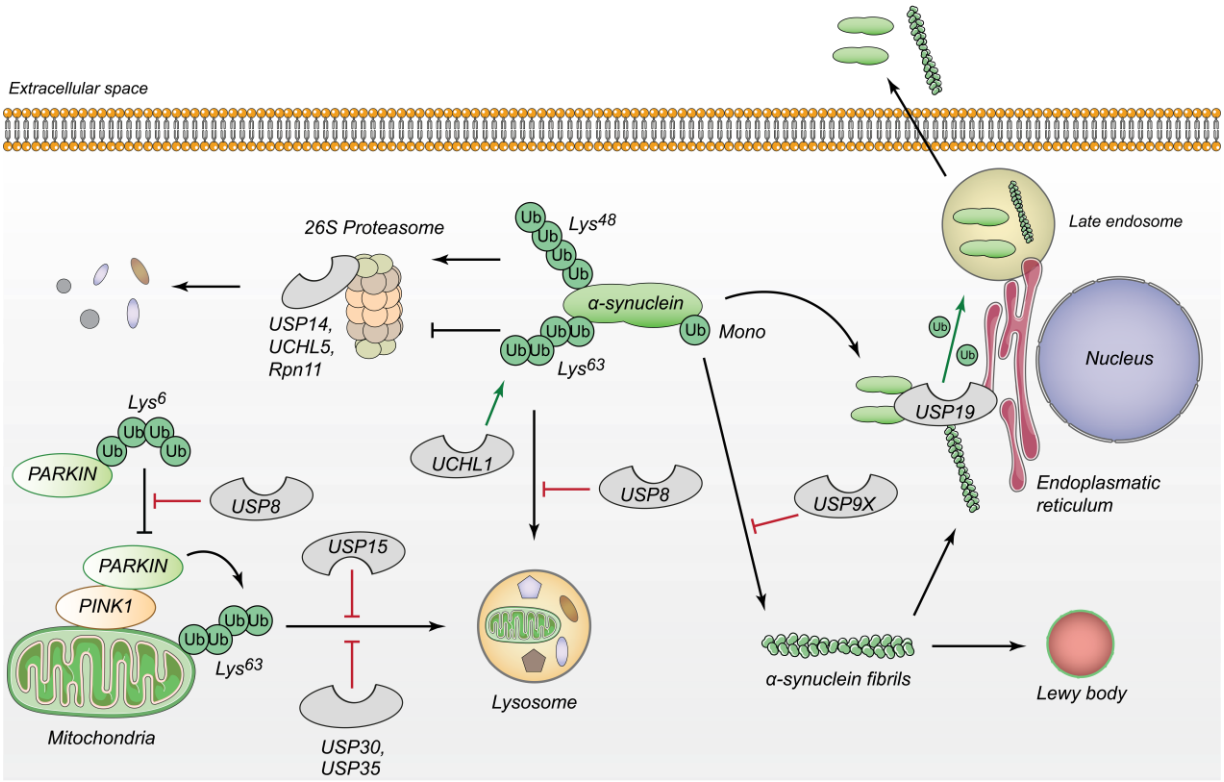

Figure 8. Roles of DUBs in PD. α-Synuclein forms fibrils through nucleated polymerization. These fibrils can accumulate and create intracellular structures called Lewy bodies. The stability of α-synuclein is controlled by DUBs UCHL1 and USP8. Another enzyme, USP9X, helps prevent the formation of fibrils by decreasing mono-ubiquitination of α-synuclein. Misfolded α-synuclein is recruited to the endoplasmic reticulum by USP19 for deubiquitination. Thereafter, the deubiquitinated α-synuclein is moved to late endosomes for secretion. The toxic fibrils of α-synuclein can harm mitochondria, which is a key aspect of Parkinson's disease (PD). The removal of damaged mitochondria through mitophagy is crucial for maintaining the health of mitochondria and is regulated by enzymes USP8, USP15, USP30, and USP35. Figure adapted from Durcan et al.[91]

Ataxin-3 (ATXN3), member and eponym of the Machado–Joseph disease DUB family, was found to regulate Parkin auto-ubiquitination. ATXN3 stabilises the complex of Parkin and its corresponding E2 Ubiquitin-conjugating enzyme and thereby impedes efficient Ubiquitin transfer to Parkin. [92,93] Further, various studies showed that knock down of the mitochondria associated DUBs USP15, USP30 and USP35 rescued Parkin-driven mitophagy defects.[91] USP8 deubiquitinates and thereby acts as an activator of Parkin, which is usually auto-inhibited by Lys6 linked poly-Ubiquitin (**Figure 8**).[94] Notably, USP8 knockdown also protects from α-synuclein–induced locomotor deficits and cell loss in dopaminergic neurons in a *Drosophila* model of PD.[93,95] In a study of Stockum et al., genetic inhibition of USP8 by RNA interference (RNAi) and knock down, as well as inhibition by the small molecule DUB-IN-2

(Cpd22e[96], IC_{50} = 0.28 µM, **Figure 9**) improved mitochondrial function and lifespan, indicating therapeutic potential of USP8 inhibition.[97] USP30 reverses ubiquitination of Parkin substrates on mitochondria (**Figure 8**) and knock down of USP30 was shown to enhance ubiquitination of multiple Parkin substrates and promote mitophagic flux, thereby rescuing defects in impaired mitochondrial morphology.[98,99] Thus, inhibition of USP30 represents an interesting therapeutic target to antagonize pathologies associated with mitochondrial dysfunction.[99]

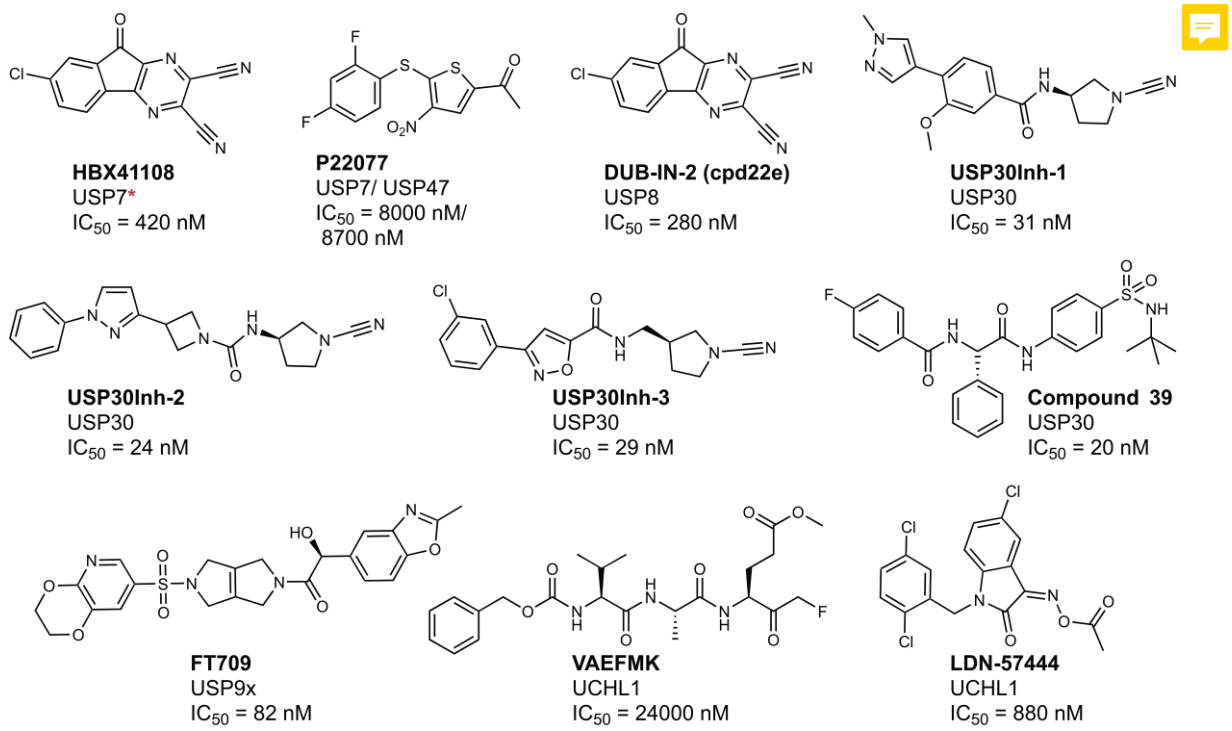

Figure 9. A selection of early discovered DUB inhibitors with their respective target and inhibitory potency. *USP7 is one of many targets.

Many independent research groups and pharmaceutical companies such as *Mission Therapeutics* intensively investigated and developed small molecule inhibitors targeting USP30. In principle, two classes of inhibitors were shown to be suitable for USP30 inhibition: non-covalent inhibitors with a benzosulphonamide scaffold and covalent, cyanopyrrolidine based inhibitors (**Figure 9**).[100] Rusilowicz-Jones et al.[101] characterised USP30 inhibitors with a benzosulphonamide scaffold, that were already reported in earlier studies.[101,102] Compound 39 (**Figure 9**) was demonstrated to potently (IC_{50} = 20 nM) and selectively inhibit USP30. Upon treatment with compound 39 for 24 h, an upregulation in mitophagy was observed in neuronal SHSY5Y cells.[101] The group of Tsefou et al.[103] synthesised USP30 inhibitors (USP30Inh-1, USP30Inh-2, and USP30Inh-3) with a reactive cyanopyrrolidine moiety (**Figure 9**), based on inhibitors reported by Mission Therapeutics.[104] In a screening against more than 40 DUBs, these inhibitors showed good selectivity at 1 µM concentration, but decreased selectivity and off-target inhibition at 10 µM.[100,103] Notably, in April 2022

Mission Therapeutics launched clinical studies of a cyanopyrrolidine-based inhibitor (MTX652) for the treatment of chronic kidney disease (CKD) as a cause of mitochondrial dysfunction.[105]

Several studies indicate that the DUB USP9X is also involved in the genesis of PD and other neurodegenerative disorders. USP9X is able to deubiquitinate α-Synuclein and thereby influence autophagic degradation. Patients suffering from PD were shown to exhibit reduced levels of USP9X, which is believed to be the cause for accumulation and aggregation of α-Synuclein, subsequently leading to neuronal malfunction.[93,106] Recently, Clague et al. from *Forma Therapeutics* developed a small-molecule inhibitor of USP9X (FT709, **Figure 9**) with an IC_{50} of 82 nM *in vitro*. FT709 showed specificity both across a panel of 20 tested DUBs, and in mass spectrometry (MS)-based chemoproteomic studies, indicating its therapeutic potential.[107]

1.5 UCHL1 – still an unsolved mystery

UCHL1 (also called PGP9.5 or PARK5) is with its 25 kDa the smallest of the four members belonging to the UCH protein family, but one of the most studied DUBs in the field. Not long after its discovery more than 20 years ago[108], UCHL1 attracted attention as a specific marker of neuronal cells to visualise different populations and subtypes of nerves. Later, UCHL1 even found application in the use as an FDA-approved specific plasma biomarker for Traumatic Brain Injury (TBI).[109,110] Already early studies suggested that UCHL1 is highly expressed in the central and peripheral nervous system, where it makes up to 5% of soluble proteins in the brain.[111] In contrast to its closest homologue UCHL3, that is universally expressed in all tissues, UCHL1 is expressed exclusively in neurons and testis/ovary.[112]

1.5.1 The structure of UCHL1

UCHL1 is a globular protein with a complex structure featuring a knotted backbone comprising a peptidase C12 catalytic domain with short N- and C-terminal extensions.[113] The protein's 3D structure consists of two lobes of α-helices surrounding a tightly-packed hydrophobic core of β-strands.[111,113] This unique knotted structure is considered the most complicated eukaryotic protein structure known to date.[114] The knotted backbone is thought to have evolved as a protective mechanism for UCH class DUBs, preventing unintended proteasomal unfolding and degradation.[115]

UCHL1 undergoes three populated states during unfolding, transitioning from folded to fully denatured. In the intermediate stage, the α-helices unfold while the central hydrophobic core of β-strands remains intact.[116] Removing of relatively few amino acids from the N- or C-terminus destabilises the structure, leading to unfolding and protein aggregation.[114,117] Eliminating eleven amino acids from the N-terminus reduces affinity for Ubiquitin and causes

insoluble aggregate formation.[118] Similarly, removing four amino acids from the C-terminus abolishes binding to Ubiquitin-substrates, resulting in neuronal death.[117] UCHL1 unfolding leads to toxic gain-of-function, exposing hidden hydrophobic regions and causing abnormal interactions with other proteins and cellular membranes.[111,119,120,121]

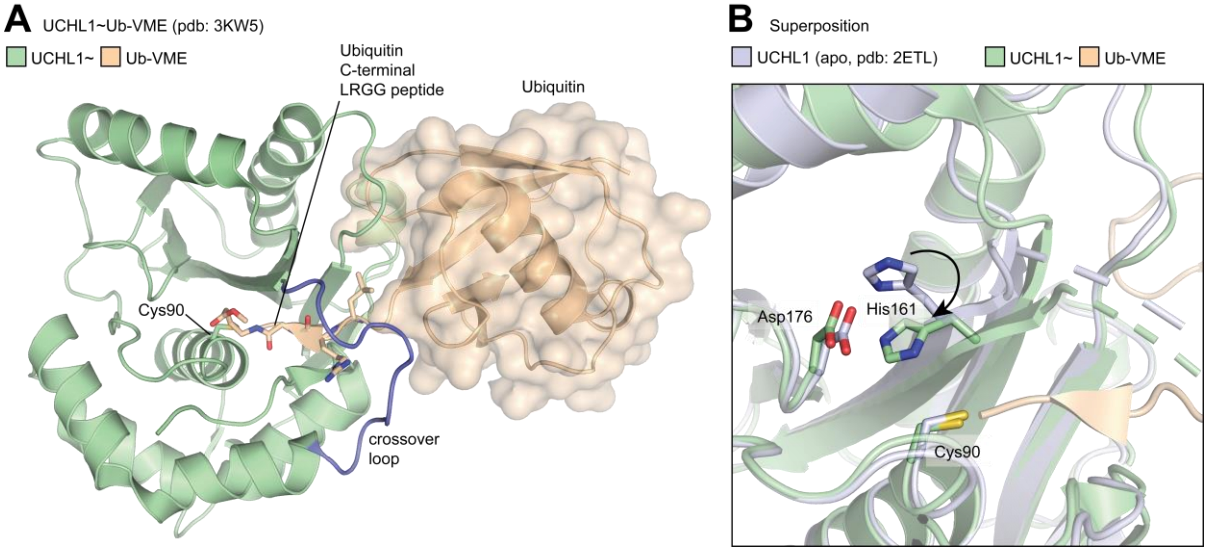

Figure 10. A. Structure of UCHL1 (green) in complex with Ub-VME (gold) (pdb: 3KW5). The short crossover loop (blue) limits the access of substrates to the active site of UCHL1. **B.** Superposition of **A** with apo UCHL1 (pdb: 2ETL) and zoom into the binding pocket. Catalytic triad residues Cys90, His161, and Asp176 are highlighted. His161 is undergoing a conformational change upon Ubiquitin binding as indicated by the black arrow.

Many DUBs are initially in an inactive state and require protein-protein interactions to become active, a protection mechanism against abnormal hydrolytic activity.[122] In the unbound state, the geometry of the UCHL1 catalytic triad (Asp176, His161, and Cys90) is distorted, rendering the enzyme non-functional, with the His161 and Cys90 residues 8.2 Å apart.[113] Crystallographic data with the UCHL1-bound probe Ubiquitin vinyl methyl ester (Ub-VME) revealed that Ubiquitin binding induces a conformational change, bringing the catalytic triad residues closer together and enhancing its enzymatic activity.[111,123]

All UCH class DUBs share a common feature of having a flexible crossover loop that limits access to their active site.[111] UCHL1 has the shortest loop among the UCH family members, making it accessible only to very short disordered peptides conjugated to Ubiquitin.[113] This limits its substrate range since folded proteins cannot access the catalytic centre.[113,123] UCHL1 can efficiently hydrolyse ubiquitin-AMC but not slightly larger Ubiquitin-sepharose conjugates.[108,124] In contrast, UCHL3 with an extended loop can bind larger Ubiquitin-conjugates and peptide sequences up to 80 amino acids.[111] It has been hypothesised that the short active site loop of UCHL1 could adopt an extended, accessible conformation upon binding the correct substrate, but experimental evidence is still lacking.[113]

1.5.2 Functional roles

One of the functions of UCHL1 is related to maintaining Ubiquitin homeostasis. It can cleave short disordered peptides from the C-terminus of Ubiquitin, increasing monomeric Ubiquitin levels, and helping to maintain a pool of available Ubiquitin in the cytosol.[125] Exogenously expressed UCHL1 binds to and increases free Ubiquitin in mouse embryonic fibroblasts (MEFs), as does the hydrolase-deficient C90S mutant, but not the non-Ubiquitin binding (D30K) mutant of UCHL1.[112] These discoveries suggest that UCHL1's ability to bind Ubiquitin and extend its half-life, rather than its hydrolytic function, is responsible for the increase in free Ubiquitin levels.[111,126]

UCHL1 has been suggested to deubiquitinate certain exogenously expressed proteins in cell lines.[127,128] However, due to spatial constraints limiting access to folded proteins at its catalytic site, it is unclear how UCHL1 can have general deubiquitinating activity. Recent *in vitro* experiments with UCH deubiquitinases and ubiquitinated substrates show that UCHL1 is far less efficient than its homolog UCHL3.[129] Current data implies that the deubiquitinase activity of UCHL1 does not target fully folded ubiquitinated substrates directly. Instead, it efficiently cleaves mono-Ubiquitin from small disordered peptides linked to the C-terminus of a Ubiquitin molecule.[108]

UCHL1 participates in larger protein complexes, and co-immunoprecipitation studies identified interaction partners such as amyloid precursor protein (APP) and tubulin.[130,131] A high-throughput mass spectrometry screen of the human deubiquitinase interactome revealed the interaction of UCHL1 with two keratin proteins and an uncharacterised coiled-coil domain-containing protein (CCDC14).[65] However, up to date there are still relatively few functionally verified interaction partners of UCHL1.[111] Further proteomic analysis of UCHL1 in neurons is expected to uncover novel interactors, providing a better understanding of UCHL1's tissue-specific functions.[111]

1.5.3 UCHL1-deficient mouse models

There are currently two naturally occurring UCHL1 mutant mouse lines and one UCHL1 knockout mouse described in the literature[132,133,134]: The gad mouse, the nm3419 mouse, and the UCHL1 knockout mouse. The phenotypes observed in all three lines are remarkably consistent, showing ataxic phenotypes, including sensory and motor disturbances, leading to paralysis and death at different ages.[111] The gad mouse has an in-frame deletion in the UCHL1 gene, resulting in the loss of UCHL1 protein, leading to axonal degeneration and inclusion bodies in nerve terminals.[132,135] The nm3419 mouse has a premature stop codon in UCHL1, leading to reduced Ubiquitin levels and ER stress in corticospinal motor neurons.[133,136] The UCHL1 knockout mouse shows a similar ataxic phenotype with impaired

synaptic transmission at neuromuscular junctions, loss of synaptic vesicles, accumulation of tubulovesicular structures at the presynaptic nerve terminals and denervation of muscles[134]. These models collectively demonstrate that while UCHL1 is not necessary for neuronal development, it is crucial for maintaining axonal integrity and that the dysregulation of UCHL1 is playing an important role in the development of severe neurological disorders.[137]

1.5.4 Disease association

Cells have developed various mechanisms to handle misfolded proteins, involving Ubiquitin-mediated degradation pathways.[111,138] However, when these mechanisms fail, as seen in neurons under prolonged stress, they can contribute to disease pathogenesis.[111,139]

Oxidative modifications in UCHL1 are a common feature in neurodegenerative diseases, making the protein prone to unfolding and leading to toxic gain-of-function.[111] The fatty-acid metabolite 15d-PGJ2, derived from COX2, was shown to modify UCHL1 at Cys152, leading to destabilisation and aggregation, which could be linked to neurological diseases.[140] Proteomic studies revealed that UCHL1 undergoes oxidative modification in AD and PD, resulting in decreased solubility proportional to tau-immunoreactive tangles.[141,142] The shift from soluble to insoluble UCHL1 with reduced hydrolytic activity is likely due to oxidation of Cys and Met residues disrupting its native structure, promoting aggregation and potentially contributing to disease pathogenesis.[143]

Parkinson's disease (PD) involves the loss of dopaminergic neurons and the formation of Lewy Bodies with ubiquitinated aggregates and protein oxidative modification.[144] A UCHL1 I93M mutation has been linked to PD susceptibility, leading to abnormal dopaminergic neuron morphology and degeneration, possibly through a dominant toxic gain-of-function mechanism.[111] On the other hand, a S18Y mutation in UCHL1 has conflicting reports, with some suggesting a neuroprotective effect against PD, possibly mediated by altered protein-protein interactions.[111] Further, a Glu7Ala mutation in UCHL1 was shown to be the cause for early onset neurodegeneration in three siblings by affecting Ubiquitin binding and hydrolysis, leading to an ataxic phenotype.[137]

Apart from its association with neurological diseases, UCHL1 was identified as an oncogene in various cancer types including non-small cell lung cancer[145], breast cancer[146,147] and multiple myeloma[148]. Overexpression of UCHL1 in germinal centre B-cells was shown to substantially impact gene expression and thereby influence cell cycle progression, cell death and proliferation as well as DNA replication.[149] In transgenic mice, its overexpression leads to lymphomas and lung tumours.[150] On the contrary, inhibiting UCHL1 activity in certain cancer cell lines by either knock down or overexpression of a catalytically inactive mutant results in a significant decrease in metastatic behaviour as well as elevation of cell invasion,

transformation and self-renewal properties. This promotes UCHL1 as a key regulator of tumour cell invasion.[146,151,152,153] In a separate study using DUB activity profiling, Liu et al.[147] identified UCHL1 as an exceptionally active DUB in TNBC (Triple-Negative Breast Cancer). The study proposed that UCHL1 plays a role in promoting TGF-β-induced metastasis in TNBC by deubiquitinating and stabilizing TGFβR1 and SMAD2. Using genetic approaches, the authors revealed that UCHL1 interacts with TGFβR1 and SMAD2/3 via its N-terminal region, effectively rescuing these proteins from ubiquitination and proteasomal degradation. In doing so, UCHL1 emerges as a key regulator of TGF-β signalling. Other studies show that UCHL1 is playing a role in multiple other pathways as well by regulating key proteins including the Protein Kinase B (PKB, or AKT)[145,150], mTOR[154], Wnt[153] and the Von Hippel-Lindau (pVHL) tumour suppressor. A plethora of additional functions have been reported, involving control of metabolism, protein aggregation and autophagy.[111]

Despite its manifold associations with diseases and disease relevant pathways, the target spectrum and the exact functions of UCHL1 remain poorly understood. A comprehensive understanding of how UCHL1 is involved in these pathways is presently hindered by an insufficiently defined set of UCHL1 substrate proteins and a lack of appropriate pharmacological tools to specifically inhibit UCHL1 activity.[155] In addition, efforts to improve the efficacy and precision of DUB inhibitors are often hampered by a lack of structural insight into specific inhibitor:DUB complexes, a challenge also faced in the context of UCHL1.[156,157]

1.6 Activity-based probes – tools to investigate DUB function

Cancer biologists face a considerable hurdle in connecting genotype to phenotype, primarily due to the frequent disparity between protein expression and protein activity. Post-translational activation or inhibition often contributes to this discrepancy, making it challenging to measure protein activity using conventional proteomic methods.[155] To address this issue, activity-based probes (ABPs) have emerged as valuable chemical tools.[158] ABPs enable the quantification of a particular enzyme's activity or a class of enzymes in a physiologically relevant setting, independently of protein expression levels.[159] Moreover, ABPs facilitate the monitoring of specific target engagement by inhibitors or drugs, aid in identifying on and off-target effects, and support live cell or in vivo imaging of enzyme activity or inhibition.[155,160,161] In general, ABPs encompass 1) a central specificity element for selective binding to the protein of interest, 2) a reactive group (warhead) for covalent target protein modification and 3) a part to facilitate detection (e.g. a fluorescent dye) or isolation (e.g. biotin).[17] In the context of studying DUB biology, the first generation of ABPs comprise a single Ubiquitin moiety as natural substrate and specificity element, ensuring DUB specific binding.[17] An additional warhead is fused to the Ubiquitin C-terminus. As most DUBs are Cys proteases, functional

groups with variable reactivity and reaction profiles are used to covalently target the catalytic Cys such as alkylbromides (Ubiquitin-Br_2, reaction via nucleophilic substitution), propargylamides (Ubiquitin-PA, direct (1,2) addition) or vinylsulphones (Ubiquitin-VS, conjugate (1,4) addition).[5,162] As reporter group, often Hemagglutinin (HA) is applied for the visualisation of the targeted protein via fluorescent readout by an HA antibody.[17] Alternatively, a bioorthogonal group, such as an azide or an alkyne handle is used to facilitate the subsequent attachment of reporter tags via click-chemistry. This way, the probe stays as natural as possible upon target binding and the tag does not interfere with reactivity, selectivity or physiochemical properties of the probe.[5]

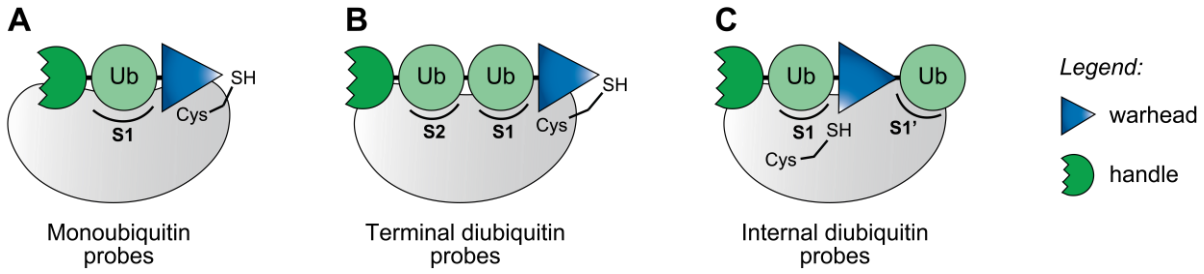

Figure 11. Ubiquitin-based ABPs to investigate the specificities and functions of DUBs targeting different Ub-binding sites. A. Mono-Ubiquitin probes targeting the S1 pocket. **B.** Terminal di-Ubiquitin probes targeting the S1 & S2 pocket. **C.** Internal di-Ubiquitin probes targeting the S1 & S1' pocket. Figure adapted from Gui et al.[5]

Mono-Ubiquitin-based probes are useful tools to selectively target DUBs in a cellular lysate, but show little selectivity within the protein family of DUBs. To further get insides on the selective recognition/cleavage of Ubiquitin linkage types by individual DUBs, a multitude of probes, based on di- or even tri-Ubiquitin as recognition element have been invented.[162] For all linkage types, terminal (the reactive group is located at the proximal end) and/or internal di-Ubiquitin ABPs (the reactive group is located between two Ubiquitin moieties) have been reported, enabling detailed mechanistic studies of binding specificity and binding mechanisms of a DUB or report on its substrate spectrum (**Figure 11**).[17,53,163,164,165] Recently, a DUB ABP containing a methyl disulphide reactive group has been reported[166], allowing the release of the DUB under mild conditions by preserving its catalytic activity, thus making it possible to study the targeted DUB in isolation.

Many regulatory mechanisms in a cell take place on the posttranslational level. The disadvantage of Ubiquitin-based ABPs, however, is that the large size of the Ubiquitin recognition element prevents cell permeability[158], thus allowing utilization only in cell lysates. Cell lysis on the other hand causes dilution of cytoplasmic and nuclear proteins and disrupts cellular organisation and localisation.[167] This can lead to altered ubiquitination patterns and dissociation of PPIs, potentially important for DUB activity, resulting in a limited use of these probes to study DUB biology.[5,162] Different attempts were made to address cell penetration of

DUB ABPs, including pore-forming toxins[168], electroporation[169] and cell-penetrating peptide (CPP) ABPs[167], but found little application in the literature, owed, among others, to laborious manufacturing processes and missing or altered DUB interfamily specificity. In contrast, changing the specificity element from a general, all DUBs targeting Ubiquitin moiety to a selective and cell permeable small molecule inhibitor is readily accessible and found broader application.

1.6.1 Small molecule ABPs

One of the key advantages of small molecule ABPs is their chemical adaptability, which offers the potential to optimise these probes to exhibit high specificity for specific DUBs, minimising cross-reactivity with other non-target proteins.[170] This enhanced selectivity ensures more accurate and reliable results, allowing precise investigation of individual DUBs and their role in cellular processes. Another important advantage of small molecule ABPs is their ability to efficiently access the active sites of DUBs. In contrast, larger ubiquitin-based ABPs may encounter steric hindrance issues when attempting access certain DUB active sites[171]. Small molecule ABPs circumvent this limitation, ensuring effective labelling and detection of DUBs. In addition, small molecule ABPs often exhibit enhanced cellular permeability, allowing them to access their target in living cells,[158,172] providing a more physiological context for studying DUB activities in their native cellular environment.

The first small-molecule based ABP with the aim to target DUBs was published by Ward et al. in 2016[173] and was based on a chloroacetyl pyrrole scaffold (compound 1[a], **Figure 12A**).[162] Originally identified in a high-throughput screening by *Mission Therapeutics*, the compound was intended to inhibit USP4 and USP11. By modifying the compound with an alkyne handle (compound 2[a], **Figure 12A**), Ward et al. were able to perform activity-based protein profiling (ABPP, **Figure 12B**) studies. They identified in total 12 DUBs and many non-DUB proteins targeted by their probe in intact U2OS cells. In 2018 VLX1570 (**Figure 12A**), a small molecule USP14 inhibitor for the use in refractory multiple myeloma, has been put on full clinical hold due to adverse side effects.[174] Later, in 2020, Ward et al.[175] prepared an alkyne-based VLX1570 analogue (compound 1[b], **Figure 12A**) and were able to show in a proteomic approach that the compound targets a wide range of proteins in addition to various DUBs. Further, the authors found out that this compound class induces nonspecific protein aggregation, thus providing an explanation for its toxicity.[175] This shows that the evaluation of an inhibitor's target spectrum in a cellular environment, apart from commonly used *in vitro* assays, is of utmost importance in the process of drug development.

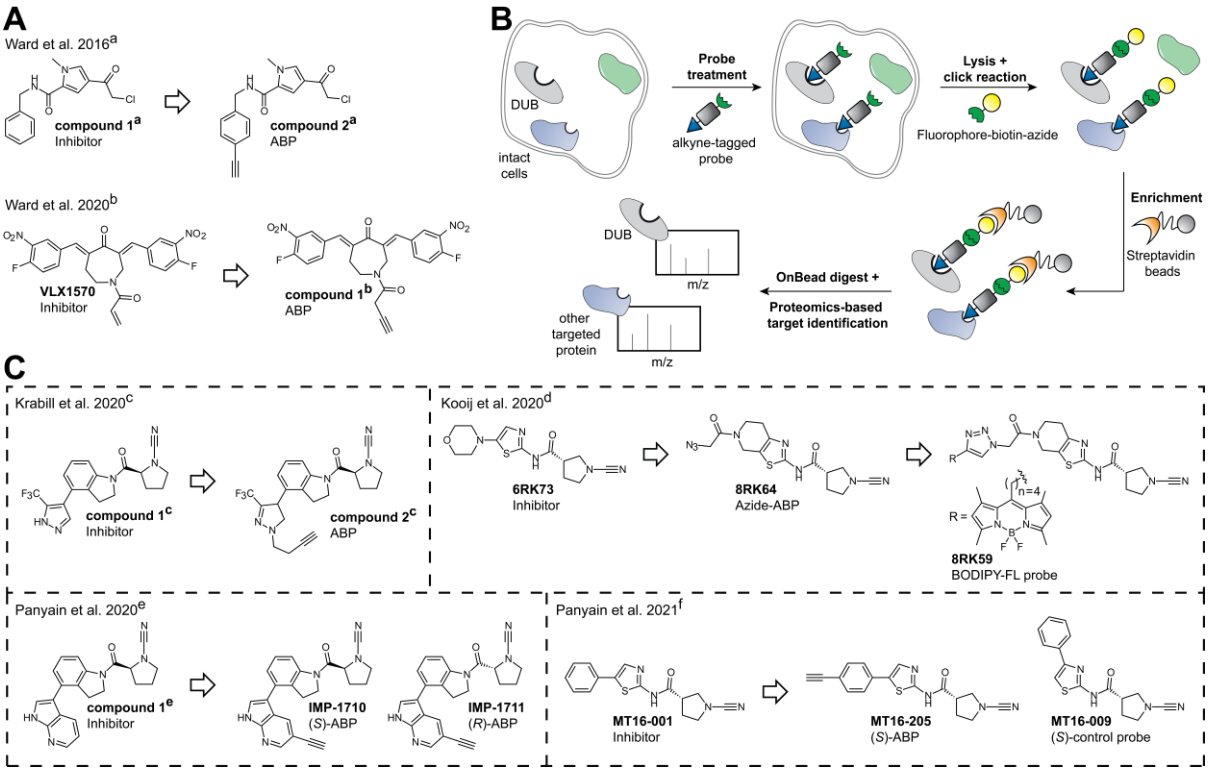

Figure 12. Small molecule ABPs are valuable tools to study DUBs in their native cellular environment. A. Chemical structure of small molecule DUB ABPs and their respective parent inhibitors. a: Ward et al. 2016[173], **b**: Ward et al. 2020[175]. **B. Schematic workflow of cellular activity-based protein profiling (ABPP) for target identification.** In the depicted example intact cells are treated with an alkyne-tagged probe and subsequently lysed. An azide-functionalised fluorophore-biotin reporter is introduced via click chemistry. Streptavidin beads are used to enrich the probe-bound proteins, which can be further analysed by either in-gel fluorescence or subjected to proteomics-based mass spectrometry experiments. Figure adapted from Grethe and Schmidt et al.[1] **C. Chemical structure of recently published small molecule UCHL1 ABPs and their respective parent inhibitors. c:** Krabill et al. 2020[152], **d:** Kooij et al. 2020[176], **e:** Panyain et al. 2020[177], **f:** Panyain et al. 2021[178].

1.7 Advancing the validation of UCHL1 as a promising drug target

As mentioned above, there is substantial evidence for the involvement of UCHL1 in neurodegenerative disorders and several types of cancer. However, the lack of selective and potent small molecule inhibitors or ABPs has hindered the exploration of the translational potential of these findings. The widely used UCHL1 inhibitor, LDN-57444[179] (**Figure 9**), fails to label UCHL1 in cells and studies suggest that its reported biochemical activity may be assay dependent, raising doubts about its efficacy in previous experiments.[89,177]

In recent years, several covalent small-molecule UCHL1 inhibitors containing a cyanopyrrolidine moiety have been reported in the patent literature.[89,180,181,182] Biochemical activity has been evaluated for over 400 small molecules using a fluorescence polarisation (FP) assay, identifying several highly potent UCHL1 inhibitors with IC_{50} values of ≤ 0.1 µM. However, critical data on their selectivity over other DUBs or protein classes were not

provided. Recently, peer-reviewed papers have been published based on these compounds, reporting covalent UCHL1 inhibitors and ABPs with varying quality (**Figure 12C**).[152,176,177,178] In 2020, Krabill et al.[152] conducted a study on a previously reported cyanopyrrolidine-based covalent inhibitor (compound 1^c, **Figure 12C**) targeting UCHL1[182]. The authors confirmed that compound 1^c covalently binds to the catalytic Cys90 of UCHL1, with slow reversibility due to hydrolysis over time.[152] To assess its selectivity, the authors used the broad-spectrum DUB ABP HA-Ub-VME in a gel shift assay and observed that compound 1^c not only inhibited UCHL1 but also targeted at least one other DUB in HEK293 cell lysate. However, the identity of this off-target DUB was not determined. Compound 1^c was also shown to exhibit growth inhibition against B-cell and lung cancer cell lines (KMS11 and SW1271), that had high endogenous UCHL1 expression levels and were sensitive to UCHL1 knockdown. Furthermore, the inhibitor also induced moderate growth inhibition in a myeloma cell line (KMS12) with low UCHL1 expression levels that did not rely on UCHL1 for proliferation, indicating significant off-target effects. In addition, an ABPP approach using an alkyne-tagged version of compound 1^c (compound 2^c, **Figure 12C**) revealed a wide range of off-targets. However, no quantification of engagement of these off-targets relative to UCHL1 was reported, resulting in an undefined selectivity profile for these compounds.

Lately, fluorescent small molecule ABPs have been developed by the Geurink and Ovaa labs[176] that effectively label UCHL1 both in vitro and in several cell lines, as well as *in vivo* in zebrafish embryos. These ABPs are based on the cyanopyrrolidine inhibitor 6RK73 (**Figure 12C**), originally reported by Mission Therapeutics[181], coupled to various fluorescent reporters, with the most extensively studied being BODIPY-FL probe 8RK59 (**Figure 12C**). The fluorescent analogues showed similar biochemical activities to the parent compound, efficiently labelling and inhibiting recombinant UCHL1, both *in vitro* and in HEK293T cell lysates. The authors confirmed that 8RK59 specifically binds to the active site Cys90 of UCHL1, as validated by its interaction with a catalytically inactive C90A mutant expressed in HEK293T cells. However, 8RK59 showed another significant off-target signal at 60 kDa in cells during in-gel fluorescence analysis, with a labelling efficiency comparable to that of UCHL1. To further investigate these off-targets, the authors performed proteomic profiling experiments using azide-tagged (8RK64, **Figure 12C**) or biotinylated ABP analogues of 6RK73. These experiments identified several off-target proteins from different classes, including PARK7, which showed higher labelling than UCHL1. This suggests limited cellular selectivity of 6RK73 as a UCHL1 inhibitor. Despite uncertain evidence for specific UCHL1 labelling in cells, the authors used microscopy to investigate whether 8RK59 could visualise and track UCHL1 activity *in vivo* in zebrafish embryos.[176] Fluorescence imaging showed that

8RK59 was predominantly localised in the eye, face, and brain, leading to the hypothesis that this distribution may be due to a higher density of neurons expressing UCHL1.

In a separate study, Panyain et al.[177], in collaboration with Mission Therapeutics, reported the development of UCHL1 inhibitors with low nanomolar potency. One of these compounds, the cyanopyrrolidine-based compound 1^{e} (**Figure 12C**), was further refined into an alkyne-tagged ABP (IMP-1710, **Figure 12C**). Both parent inhibitor 1^{e} and IMP-1710 showed strong binding to UCHL1, with IC_{50} values of 90 and 38 nM, respectively, in a fluorescence polarisation (FP) assay using Ub-Lys-TAMRA. Notably, the (*R*)-enantiomer of IMP-1710 (IMP-1711, **Figure 12C**), which exhibited over 1000-fold less potency than the (*S*)-enantiomer, served as an effective control compound and demonstrated specific and stereoselective interaction with UCHL1. IMP-1710 and compound 1^{e} effectively engaged UCHL1 in a breast cancer cell line (Cal51) stably expressing FLAG-tagged UCHL1, with EC_{50} values of 110 and 820 nM, respectively. These compounds displayed high selectivity for UCHL1 when tested against a panel of 20 recombinant DUBs and in HEK293 cells. However, ABPP of probe IMP-1710 at a concentration of 200 nM revealed several other covalently bound targets, with fibroblast growth factor receptor 2 (FGFR2) being the second most enriched protein.

In 2021, Panyain et al.[178] identified the previously reported compounds MT16-001 and MT16-205 (**Figure 12C**; previously reported in Jones et al.[181] as example 1 and example 205, respectively) as UCHL1 inhibitors with similar IC_{50} values of 550 and 160 nM, respectively. MT16-009 (**Figure 12C**), a less-potent analogue, was used as a negative control due to its similar physicochemical properties to MT16-001. Both MT16-001 and MT16-205 effectively inhibited UCHL1, but not UCHL3 *in vitro*, demonstrating selectivity for UCHL1 over the closely related UCH family member. Further screening against a panel of 19 DUBs revealed that MT16-001 and MT16-205 inhibited UCHL1 and the structurally unrelated DUB, USP30, with similar potency. However, both MT16-001 and MT16-205 showed pronounced cytotoxicity, which is inconsistent with the viability of many UCHL1 knockout cell lines.[183] Cellular target engagement experiments using HA-Ub-VME in human breast cancer cells (Cal51) expressing UCHL1 confirmed that both compounds engaged UCHL1 in intact cells. However, several other covalently bound targets were identified that could not be detected with the used set of control probes.[178]

Despite intensive research efforts, neither clear phenotype upon UCHL1 inhibition, nor a substrate of UCHL1 could be assigned in the above examples. This highlights the need for improved, selective and non-toxic ABPs, as well as appropriate control probes to unveil the function and target spectrum of UCHL1 in future studies.

2 Motivation and Aim

The development of specific tools to study DUBs in a cellular context has been hampered by an incomplete understanding of DUB biology and a general lack of thoroughly characterised inhibitors.[18] Efforts to improve the efficacy and specificity of DUB inhibitors are often hampered by a lack of structural information from specific inhibitor:DUB complexes.[156,157] The establishment of small molecule probes for UCHL1 and DUBs in general may lead to tool compounds for investigating their target proteins in complex cellular environments, or may even act as tools to help eliminate promiscuous drug candidates at an early stage of inhibitor development.[162]

Different types of nitriles, such as aliphatic nitriles, aryl nitriles, and cyanamides of various scaffolds, have been found to be effective covalent inhibitors for several enzymes. Similarly, several nitrile-based inhibitors for deubiquitinases of the USP and UCH families have been reported, but are often poorly characterised in terms of potency and specificity.[104,181,182,184,185,186,187]

Project 1 of this work aimed to characterise a selected panel of putative covalent, structurally diverse nitrile-based DUB inhibitors (**Figure 13**, top panel). Following the design and synthesis of the corresponding alkyne-tagged ABP analogues, the cellular target engagement of the probes was to be elucidated. The most selective and covalent probe should then be biophysically characterised using experiments such as fluorescence-based target cleavage, kinetic measurements, thermal stability assays (TSA) and isothermal titration calorimetry (ITC). In combination with further cellular characterisation and crystallographic studies in co-complex with its protein target, insights into potency, selectivity, stability as well as kinetic binding properties and mode of binding should be elucidated.

The second project of the thesis aimed to structurally improve the probe by chemical synthesis along with cellular and biochemical analysis to improve selectivity (**Figure 13**, bottom panel). Key properties of the improved ABP were to be compared with the probe established in part 1 of the thesis. In addition, a crystal structure of the new probe in complex with its protein target should provide further information on the binding mode and target association and may explain the different binding properties between the two probes. Ultimately, both projects should aim to acquire an activity-based probe suitable for investigating the function and substrate spectrum of target DUBs in a cellular environment (**Figure 13**, overlapping).

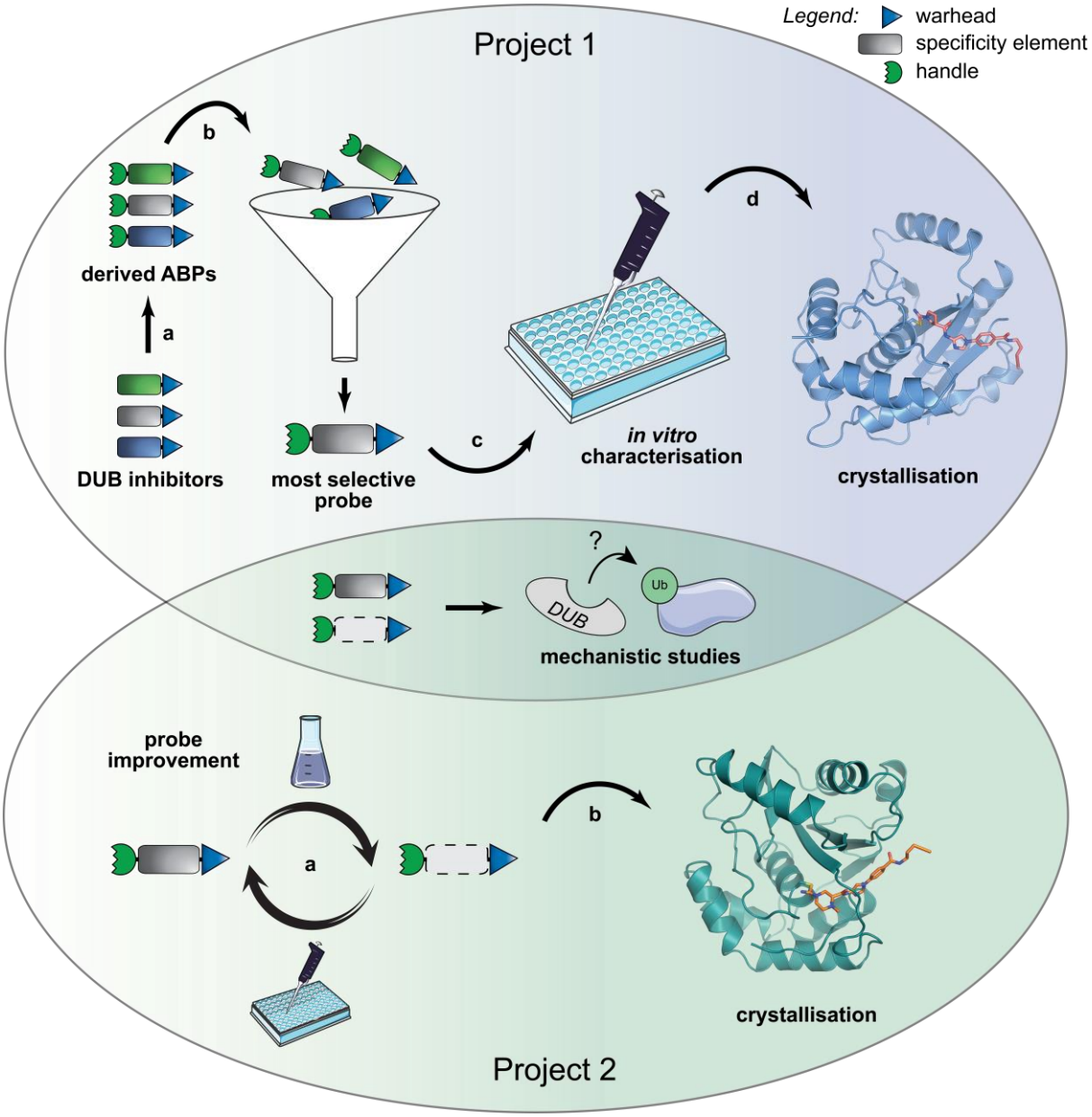

Figure 13. Overview of projects 1 and 2. Project 1 (top panel). **a.** A panel of DUB inhibitors should be synthetically converted into their corresponding activity-based probe (ABP) analogues. **b.** Cellular characterisation of the probes should provide first insights into covalent binding properties and target engagement. **c.** The most selective covalently binding probe should be further evaluated in various *in vitro* assays. **d.** Crystal structure analysis in co-complex with its target protein should shed light on the structural binding properties of the ABP. **Project 2** (bottom panel). **a.** Cycles of chemical synthesis and biochemical evaluation of the most selective probe derived in project 1 should aim for an activity-based probe with improved selectivity profile and binding properties. **b.** A crystal structure in co-complex with the probe target protein could help explain differences between selectivity and potency between new and old probe. The overall aim of both projects is to establish suitable ABPs for mechanistic studies of DUBs in a cellular context (overlapping).

Techniques for the generation of small molecule regulators of protein activity have proven to be effective tools for the development of new drug-like molecules.[188] Methods such as phage display, DNA-encoded libraries and multi-component reactions are well known tools for the

rapid generation of small molecule libraries.[188] In view of the scarce number of small molecule DUB ABPs in the literature, such a library would be of great benefit. However, to generate small molecule-based ABP libraries, a suitable attachment position for the incorporation of an alkyne-handle must be considered. This not only requires a free position in a small molecule, but also often means tedious synthetic work, as methods may need to be adapted for each library molecule.

In the third project of this dissertation, a novel "dual-functional warhead" approach to generate an activity-based probe library featuring distinct binding elements, with the aim to target (novel) DUBs should be developed (**Figure 14**). The main focus of this approach was the design and synthesis of cyclic, *N*-cyano-nitrile containing, putative DUB targeting warheads. These warheads should be designed to have an additional alkyne handle for biorthogonal functionalisation and a suitable chemical group for easy attachment to various binding elements. To initially validate whether DUB binding of dual-functional warhead-bearing molecules is still given, a known DUB-binding scaffold should be fused to the newly developed warheads and target binding assessed in a cellular context. Finally, a library of ABPs with warheads of different ring sizes should be fused to a variety of readily accessible binding elements and probe binding assessed by cellular and biochemical target engagement.

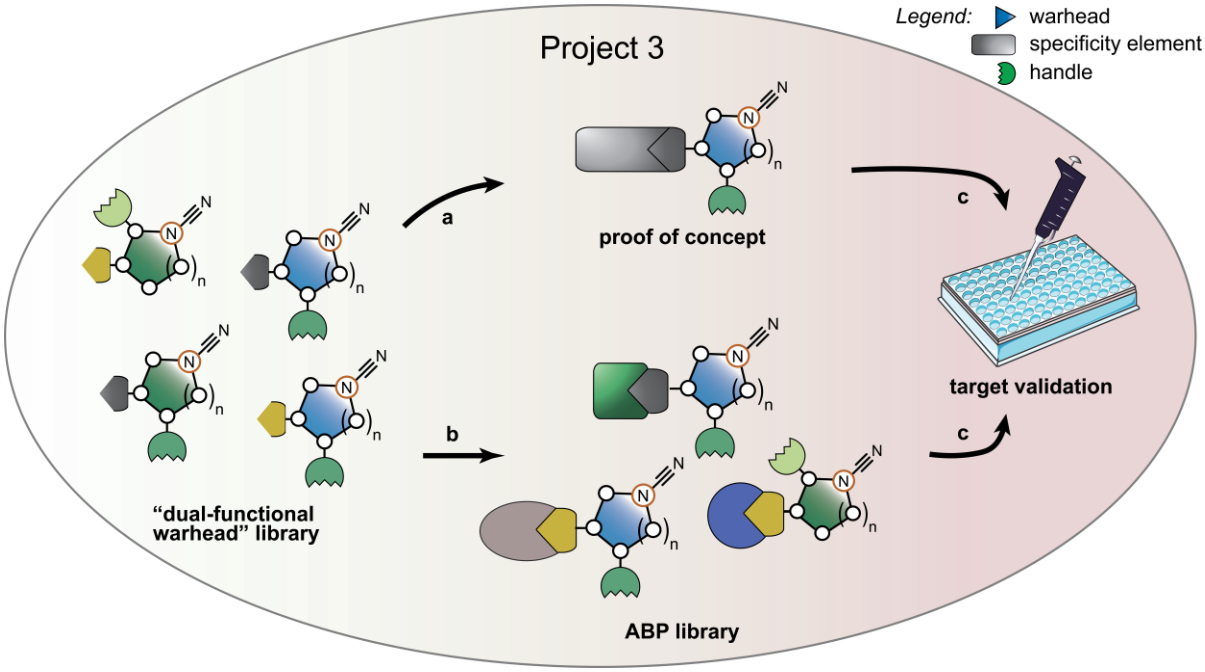

Figure 14. Overview of project 3. A library of dual-functional warheads should be synthetically addressed. These molecules should contain a reactive cyclic *N*-cyano-nitrile moiety in various ring sizes. Further, alkyne-handle and different reactive groups should be incorporated at varying ring positions for efficient and diverse library generation. **a** A dual-functional warhead is fused to a known DUB-binding moiety to evaluate target association. **b** An ABP library is generated by connecting dual-functional warheads to readily accessible and diverse binding elements. **c** Target validation of novel dual-functional warhead-bearing molecules in cells.

3 Structural basis for specific inhibition of the deubiquitinase UCHL1 (Project 1)

Altering DUB function by genetic depletion often results in a combination of direct and indirect effects that are challenging to separate for specific substrate determination. This is mainly due to the prolonged time frame of genetic depletion experiments, as well as many DUBs being involved in multiple pathways, influencing other DUBs or E3 ligases and regulating transcriptional activity. These factors have not only hindered a deeper understanding of the roles DUBs play in the Ubiquitin system, but have also impeded efforts to create DUB inhibitors for therapeutic applications.[18,46]

Tools such as small molecule based ABPs, with their ability to enter cells and alter their target proteins function significantly faster, display a considerable alternative to genetic depletion methods.

3.1 Design and synthesis of a focused activity-based probe library targeting DUBs

While there are over 100 DUBs discovered so far, only a limited number of inhibitors has been reported in the literature, many with unknown specificity. For many DUBs, such as UCHL1, the absence of suitable, well characterised tool compounds hindered research on their biological function. The work in the first part of this thesis comprised the design and chemical synthesis of alkyne-tagged activity-based probes based on patent-known inhibitors (**Figure 15A**), with the further aim to profile their cellular target engagement, thus to inform on the suitability as tool compounds to study the cellular function and substrate spectrum of DUBs.

Inhibitors were selected based on diverse chemical scaffolds, an assigned DUB target and the presence of a nitrile group to form covalent thioimidate adducts (**Figure 15B**) with the active site cysteine of DUBs and thus report on their covalent cellular targets in an unbiased manner.

Further information, such as patent-derived structure-activity relationships, partially allowed for identification of suitable positions for the attachment of an alkyne handle for later bioorthogonal modification with reporter tags.

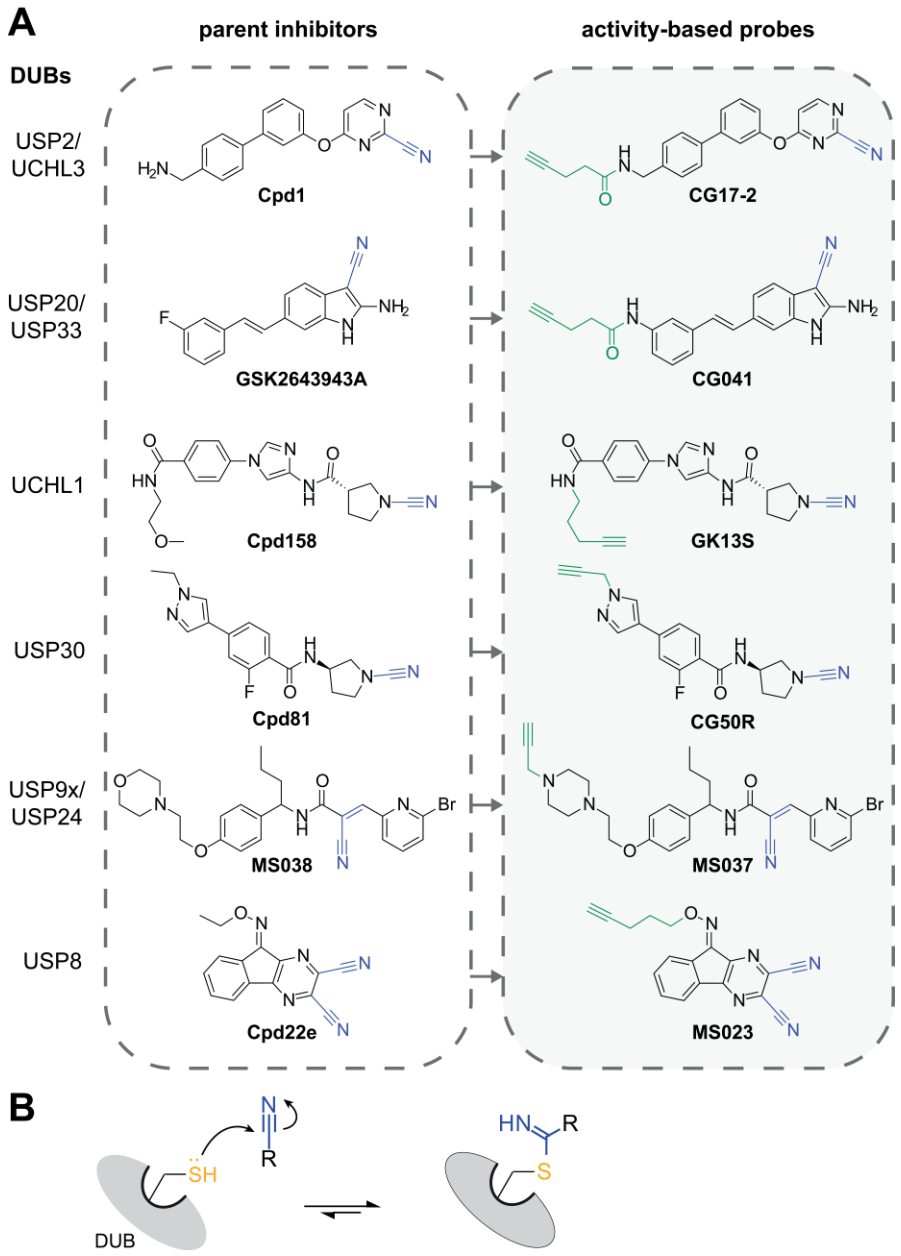

Figure 15. Design and synthesis of an activity-based probe library derived from nitrile-based DUB inhibitors.
A. Synthesised activity-based probes (right panel) derived from known inhibitors (left panel), containing a potential nitrile-based warhead (blue) for covalent protein modification and an alkyne handle (green) for bioorthogonal functionalisation.
B. Mechanism of thioimidate formation between DUB active site cysteine and small molecule nitrile.

3.1.1 Targeting UCHL3 and USP2

Aryl nitriles have been described in various publications as covalent inhibitors, targeting the active site cysteine.[189] In 2010, *Novartis* reported a small set of 2-cyanopyrimidines as inhibitors of UCHL3 and USP2 for the treatment of proliferative diseases such as cancer.[184] This set of compounds demonstrated a drug-like scaffold, since similar 2-cyanopyrimidines, such as Dutacatib, are already established cathepsin K inhibitors. With the aim to develop an ABP that is capable of reporting target protein binding, an inhibitor with a suitable position for alkyne linker attachment had to be found. In this respect the benzylamine group of Cpd1 (**Figure 15A**) showed two major advantages: 1) the amine facilitates easily accessible amide coupling reactions to introduce an alkyne and 2) interference with covalent modification of the active site Cys can be prevented by placing warhead and alkyne at large distance. First, the

parent inhibitor Cpd1 was synthesised based on the procedure described in the patent[184] (**Scheme 1a-e**).

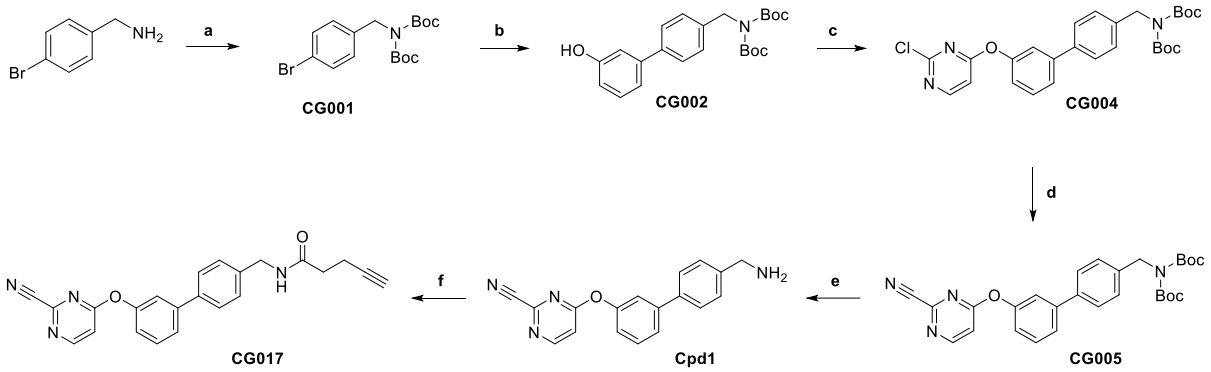

Scheme 1. Synthesis of CG017 based on patent US7700605B2[184]. a. Boc_2O, DIPEA, DMAP, THF, rt, 16 h, 99%. **b.** (3-hydroxyphenyl)boronic acid, super stable Pd(0), K_2CO_3, DMF:H_2O = 5:1, 90 °C, 6 h, 44%. **c.** 2,4-dichloropyrimidine, K_2CO_3, DMF, rt, 20 h, 98% **d.** $Zn(CN)_2$, $Pd[(PPh)_3]_4$, DMF, µW, 130 °C, 20 min, 71%. **e.** 20% TFA in DCM, rt, 4 h. **f.** Pent-4-ynoic acid, EDC-HCl, DIPEA, DCM, rt, 2 h, 10% over 2 steps. The synthesis procedures for steps **a-e** were based on appropriate methods described in the patent[184], with minor refinements, including insights from the research of Gian M. Kipka[2].

Starting from 4-bromobenzylamine, Boc-protection was implemented to prevent side reactions of the free amine in the following reaction steps (**a**). In a Suzuki-Miyaura cross-coupling reaction, (3-Hydroxyphenyl)boronic acid was fused to the C4-position of intermediate CG001, forming a biphenyl moiety that acts as specificity element for target protein binding (**b**). The reaction was catalysed by a super stable palladium (0) complex containing an electron-deficient trifluoromethylated phosphine ligand, which exhibited thermo- and air-stability. The palladium(0) binds CG001 in an oxidative addition, forming an organo-palladium(II) intermediate. The halide is replaced by a phenolate anion, generated by K_2CO_3. During transmetallation, the aromatic ring of the (3-hydroxyphenyl)boronic acid is transferred to the palladium, resulting in an organo-palladium(II) species with both aryl residues bound. Reductive elimination finally regenerates the Pd(0) catalyst and releases intermediate CG002. The highly electron-deficient pyrimidine ring of 2,4-dichloropyrimidine allowed for a nucleophilic aromatic substitution (S_NAr) reaction with CG002 (**c**) and subsequent palladium-catalysed cyanation (**d**) generating aryl nitrile CG005. Although the C4-position of 2,4-dichloropyrimidine tends to be more reactive, the exclusive formation of a single regioisomer is challenging.[190] After purification, NMR spectroscopy was used to confirm the presence of only the desired regioisomer. The nearly quantitative yield (98%) further indicates regioselectivity of the ether synthesis (**c**). Boc-deprotection and purification by preparative HPLC yielded the parent inhibitor Cpd1. Finally, the ABP CG017 was synthesised via an amide coupling reaction of Cpd1 with pent-4-ynoic acid, serving as alkyne handle. In order to ensure highest purity for biological testing of final compounds, only fractions containing pure

product were combined, explaining some low yields of final reaction steps throughout this thesis.

3.1.2 Targeting USP20 and USP33

The pharma company *AstraZeneca* filed a patent in 2001 describing indole derivatives with vascular damaging activity. One of the presented indole derivatives, GSK2643943A, reappeared in a screening campaign by *GlaxoSmithKline* as a hit against USP20 with an IC_{50} of 160 nM.[89] No DUB selectivity data were shown, but the compound was found to penetrate the cell membrane by modulating USP33 levels.[89] Ubiquitin-specific peptidase 20 (USP20) is a vital member of the Ubiquitin-specific proteolytic enzyme family and plays a key role in regulating the stability of proteins via multiple signalling pathways. Recent research has highlighted the important role of USP20 in the tumourigenesis of various types of cancer, including breast cancer, colon cancer, lung cancer, gastric cancer, and adult T cell leukemia.[191]

Following *AstraZeneca's* patent US7030123B2[185], the inhibitor GSK2643943A was synthesised (**Scheme 2**).

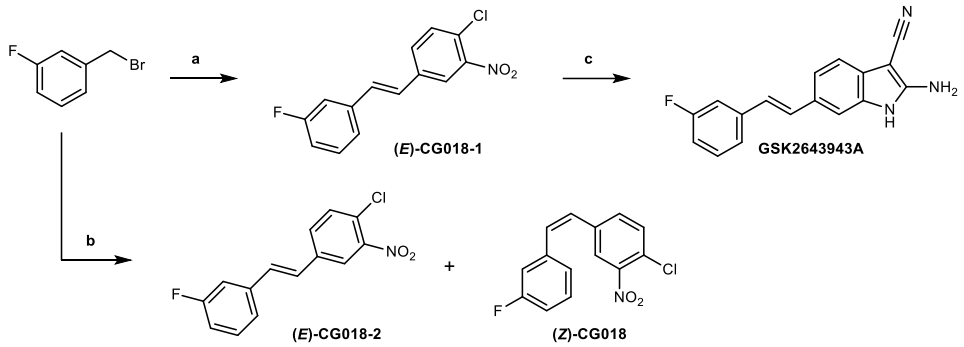

Scheme 2. Synthesis of GSK2643943A based on patent US7030123B2[185]. a. 1) $POEt_3$, 120 °C, 1 h, 2) 4-chloro-3-nitrobenzaldehyde, NaH, DMF, 0 °C, on, 13%. **b.** 1) PPh_3, DMF, reflux, 1 h, 2) 4-chloro-3-nitrobenzaldehyde, NaH, DMF, 0 °C, 18 h, 32% for (*E*)-CG018-2, 38% for (*Z*)-CG018. **c.** 1) malononitrile, K_2CO_3, DMF, 50 °C, on, 2) $Na_2S_2O_3$, DMF, 110 °C, 15 min, 46%. The synthesis procedures for steps **a-c** were based on appropriate methods described in the patent[185].

Starting from 1-(bromomethyl)-3-fluorobenzene, an Arbuzov reaction with $POEt_3$ yielded diethyl (3-fluorobenzyl)phosphonate (**a**, step 1), which was subsequently used in a Horner-Wadsworth-Emmons (HWE) reaction with 4-chloro-3-nitrobenzaldehyde to produce (*E*)-CG018-1 (**a**, step 2). In an HWE reaction a ketone or an aldehyde (here 4-chloro-3-nitrobenzaldehyde) reacts with a phosphonate (diethyl (3-fluorobenzyl)phosphonate) in a two-step mechanism to form an alkene ((*E*)-CG018-A).[192] The reaction mechanism involves the deprotonation of the phosphonate, nucleophilic addition of the carbanion onto the aldehyde/ketone and final elimination of the alkene, predominantly in (*E*)-configuration.[192] To evaluate the configuration of the product, a second, (*E*)/(*Z*)-unselective Wittig reaction was

performed (**b**). In the Wittig reaction, a phosphorus ylide reacts with an aldehyde or ketone (here 4-chloro-3-nitrobenzaldehyde) to form an alkene.[193] The ylide (here (3-fluorobenzyl)triphenylphosphonium bromide) is generated from a phosphonium salt (PPh_3) by deprotonation with a strong base (NaH).[193] Thin layer chromatography (TLC) after step **b** showed the presence of two product species, presumably (*E*)- and (*Z*)-CG018. Subsequent silica column chromatography successfully separated both. The configuration was determined by comparing $J_{H\text{-}H}$ coupling constants of the alkene protons of both NMR spectra. One NMR spectrum showed two prominent proton peaks with typical $J_{H\text{-}H}$ coupling constants for (*Z*)-alkenes of $J_{H\text{-}H}$ = 12 Hz, thereby assigned to (*Z*)-CG018, whereas the other NMR displayed two prominent proton peaks with typical $J_{H\text{-}H}$ coupling constants for (*E*)-alkenes of $J_{H\text{-}H}$ = 16 Hz, thereby assigned to (*E*)-CG018. Comparison with the product from step **a** confirmed the formation of the (*E*)-isomer, since both NMR spectra showed related peak patterns and coupling constants. Following a publication of Volovenko 2001[194], describing a method for the synthesis of 2-amino-6-nitroindoles, (*E*)-CG018 was converted into GSK2643943A by the use of malononitrile, base K_2CO_3 and aprotic solvent DMF (**b**). In this reaction, the base deprotonates the malononitrile, activating it for nucleophilic aromatic substitution of the halogen atom. Intramolecular rearrangement and ring-closing then leads to the formation of parent inhibitor GSK2643943A.

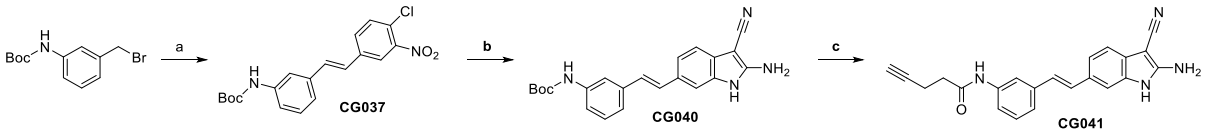

Scheme 3. Synthesis of CG041 based on patent US7030123B2[185]. **a.** 1) $POEt_3$, 130 °C, 1 h, 2) 4-chloro-3-nitrobenzaldehyde, NaH, DMF, 0 °C, on, 27%. **b.** 1) malononitrile, K_2CO_3, DMF, 50 °C, on, 2) $Na_2S_2O_3$, DMF, 110 °C, 15 min, 39%. **c.** 1) 20% TFA in DCM, rt, 2 h, 2) pent-4-ynoic acid, EDC-HCl, DIPEA, DCM, rt, 4 h, 10%. The synthesis procedures for steps **a-b** were based on appropriate methods described in the patent[185].

To further validate DUB selectivity in a cellular context, the ABP CG041 was designed, based on compound GSK2643943A. As the fluorine group in GSK2643943A provides a possible position for derivatisation, an alkyne handle should be incorporated there. For facile alkyne conjugation, *tert*-butyl (3-(bromomethyl)phenyl)carbamate was selected as starting material (**Scheme 3**) since it is compatible with amide coupling reactions after Boc-deprotection during the final step of the synthesis. Starting with *tert*-butyl (3-(bromomethyl)phenyl)carbamate, an Arbuzov reaction employing POEt3 led to the formation of *tert*-butyl (3-((diethoxyphosphoryl)-methyl)phenyl)carbamate, which was subsequently reacted with 4-chloro-3-nitrobenzaldehyde in an HWE reaction, yielding CG037 in (*E*)-configuration (**a**). NMR spectroscopy confirmed the formation of the (*E*)-isomer ($J_{H\text{-}H}$(alkene) = 16 Hz). In a similar ring-closing reaction as described for the synthesis of GSK2643943A, CG037 was reacted to

CG040 (**b**). Boc-deprotection of the aniline further allowed for alkyne handle introduction via amide coupling with pent-4-ynoic acid (**c**).

3.1.3 Targeting USP30

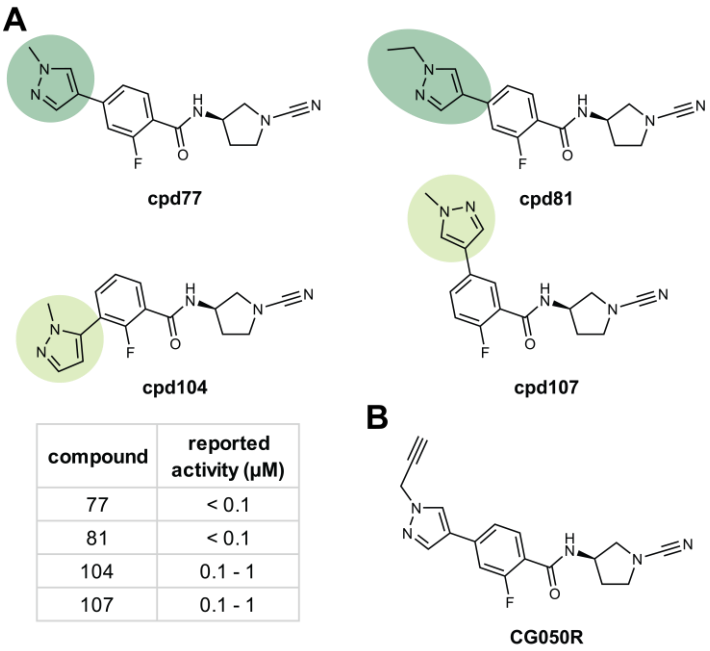

compound	reported activity (µM)
77	< 0.1
81	< 0.1
104	0.1 - 1
107	0.1 - 1

Figure 16. Patent-derived[104] structure-activity relationships of inhibitors gave a first overview about possible sites for alkyne-handle incorporation for the design of probe CG050R. A. A 2-fluorobenzamide-based scaffold, bearing a 1-methyl-1*H*-pyrazole in 4-position of the benzyl ring (cpd77) demonstrated good inhibitory potency and the possibility to synthetically incorporate an alkyne-handle through a nucleophilic substitution at the pyrazole group. The likewise good USP30 inhibition by cpd81 pointed out, that bulkier groups in 4-position are tolerated as well, thereby validating it as a suitable starting point for the development of an activity-based probe. **B.** Structure of the activity-based probe GK050R, derived from inhibitor cpd81.

The DUB USP30 has been reported as an actionable target considered for the treatment of conditions associated with mitochondrial defects.[101] USP30 depletion enhances mitophagic clearance of mitochondria and also enhances parkin-induced cell death.[104,195] In 2016 Mission Therapeutics described in a patent[104] small molecule inhibitors of USP30, nearly all bearing a reactive cyanopyrrolidine moiety. The patent[104] provided sufficient information about structure-activity-relationships (**Figure 16A**), allowing to evaluate an appropriate position for modification with an alkyne, which lead to the design of probe CG050R (**Figure 16B**). Compounds cpd77, cpd104 and cpd107 all showed a 1-methyl-1*H*-pyrazole in C4-, C3- and C2-position of the benzyl ring (**Figure 16A**). Whereas cpd77 was found to have nanomolar potency against its target protein USP30, cpd104 and cpd107 demonstrated weaker binding. Compound cpd81, bearing an ethyl group at the pyrazole, exhibited equally potent inhibition to cpd77. This suggests that larger groups might also be tolerated in C4-position, making cpd77 a suitable starting point for developing an activity-based probe. The pyrazole group in cpd77 further allows modification with an alkyne via a nucleophilic substitution reaction (**Scheme 4**).

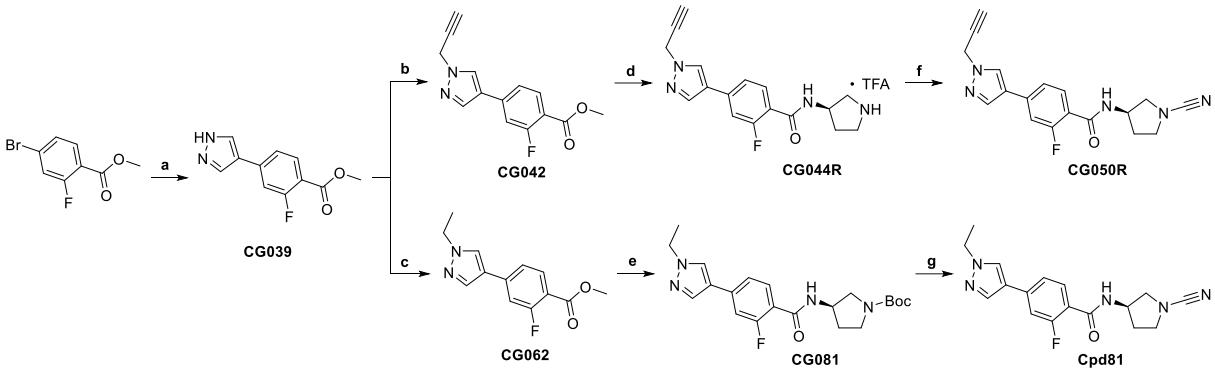

Scheme 4. Synthesis of inhibitor Cpd81 and probe CG050R based on patent WO2016156816A1[104]. a. (1-(*tert*-butoxycarbonyl)-1*H*-pyrazol-4-yl)boronic acid, $Pd(PPh_3)_4$, Na_2CO_3, Dioxane:H_2O = 5:1, 90 °C, on, 78%. **b.** propargyl bromide, K_2CO_3, acetone, rt, on, 57%. **c.** iodoethane, K_2CO_3, DMF, rt, on, 25%. **d.** 1) LiOH, THF, rt, on, 2) *tert*-butyl (*R*)-3-aminopyrrolidine-1-carboxylate, HATU, DIPEA, DMF, rt, on, 3) 10% TFA in DCM, rt, 4 h, 12%. **e.** 1) LiOH, MeOH, rt, on, 2) *tert*-butyl (*R*)-3-aminopyrrolidine-1-carboxylate, HATU, DIPEA, DMF, rt, on, 65%. **f.** BrCN, K_2CO_3, THF, rt, 2 h, 12%. **g.** 1) 20% TFA in DCM, rt, 4 h, 2) BrCN, K_2CO_3, DCM, rt, 2 h, 75%. Steps **a**, **c**, **e**, and **g** were synthesised according to the patent[104], while the procedures for steps **b**, **d**, and **f** were based on appropriate methods described in the same patent.

Synthesis of inhibitor Cpd81 and probe CG050 both started with a Suzuki coupling reaction between methyl 4-bromo-2-fluorobenzoate and (1-(*tert*-butoxycarbonyl)-1*H*-pyrazol-4-yl)boronic acid under palladium catalysis, yielding intermediate CG039 (**a**). A following nucleophilic substitution reaction between the pyrazole of CG039 and propargyl bromide (**b**) resulted in the formation of CG042. Introduction of the alkyne at this early stage of the synthesis route was necessary to prevent possible side reactions of the nucleophilic pyrazole N-atom. After basic ester hydrolysis, amide coupling with *tert*-butyl (*R*)-3-aminopyrrolidine-1-carboxylate and subsequent acidic Boc-deprotection CG044R was formed. To generate the final probe CG050R, an electrophilic cyanation of the pyrrolidine nitrogen-atom was performed using cyanogen bromide (BrCN) as source for an electrophilic nitrile group and K_2CO_3 as base. The pyrrolidine's secondary nitrogen, acting as a nucleophile, attacks the electrophilic carbon of BrCN, leading to the release of bromide and the formation of the final probe CG050R. The inhibitor Cpd81 was synthesised in a similar reaction sequence as described for CG050R (**c**, **e**, **g**), using iodoethane instead of propargylbromide in step **c**.

3.1.4 Targeting UCHL1

3.1.4.1 Synthesis of probes GK12S/R and GK13S/R

The DUB UCHL1 has been reported to play central roles as an oncogene in the progression of many cancers.[111] While small molecules that target UCHL1 would be useful tools for studying its function, specific inhibitors are scarce. In 2016 *Mission Therapeutics* filed a patent describing N-cyanopyrrolidines as UCHL1 inhibitors.[181] Offering detailed structure-activity-

relationships (**Figure 17A**), the patent allowed to determine a suitable position for alkyne-handle introduction, leading to the design of probe GK13S (**Figure 17B**).

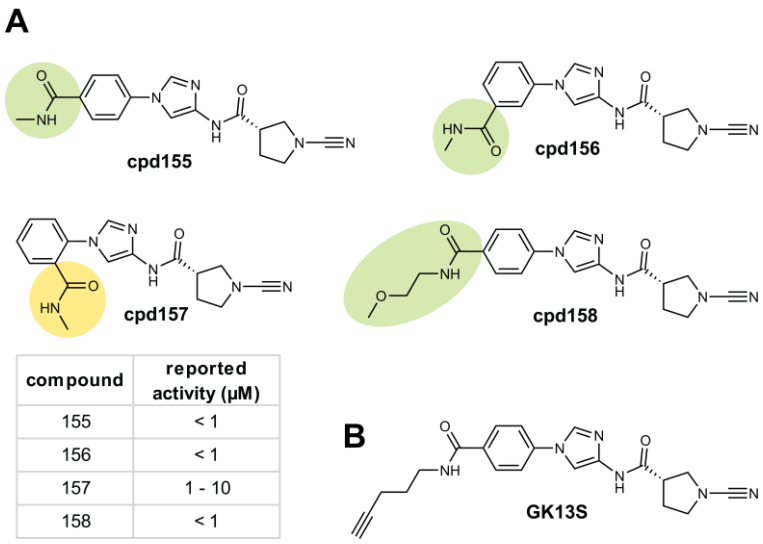

compound	reported activity (µM)
155	< 1
156	< 1
157	1 - 10
158	< 1

Figure 17. Patent-derived[181] structure-activity relationships of inhibitors gave a first overview about possible sites for alkyne-handle incorporation for the design of probe GK13S. A. A 1-phenyl-1*H*-imidazole-based scaffold, bearing a *N*-methyl acetamide in 4- (cpd155) or 3- (cpd156) position demonstrated good inhibitory potency and the possibility to synthetically incorporate an alkyne-handle via amide coupling. The likewise good UCHL1 inhibition of *N*-(2-methoxyethyl)benzamide compound cpd158 pointed out, that bulkier groups in 4-position are tolerated as well, thereby validating it as a suitable starting point for the development of an activity-based probe. **B.** Structure of the activity-based probe GK13S, derived from inhibitor cpd158.

Compounds cpd155 and cpd156 (**Figure 17A**), bearing a *N*-methyl acetamide group in C4- and C3-position of the benzyl ring respectively, were reported to potently inhibit UCHL1. Compound cpd158, bearing a *N*-(2-methoxyethyl)benzamide, presented likewise potent inhibition, indicating that bulkier groups are tolerated in C4-position as well and thus validating cpd158 as a suitable starting point for the development of an activity-based probe. Further, the benzamide group in cpd158 allows for the synthetic addition of a 4-pentyn-1-amine as an alkyne-handle via an amide coupling reaction (**Scheme 5**).

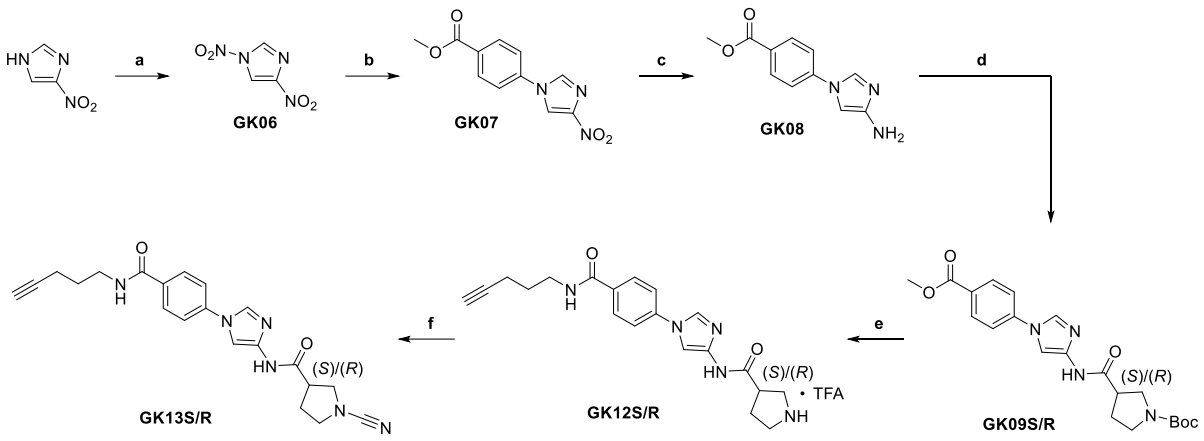

Scheme 5. Synthesis of GK13S/R based on patent WO2016046530A1[181]. a. HNO_3, Ac_2O, AcOH, rt, 5 h, 91%. **b.** methyl 4-aminobenzoate, MeOH:H_2O = 1:1, rt, 2 d, 68%. **c.** Pd/C, H_2, EtOH, H_2O, rt, 2 h, 96%. **d.** (*S*)/(*R*)-1-Boc-pyrrolidine-3-carboxylic acid, HATU, DIPEA, DCM, rt, 4 h, (*S*): 76%, (*R*): 75%. **e.** 1) LiOH, MeOH, rt, 30 h, 2) pent-4-yn-1-amine HCl, HATU, DIPEA, DCM, rt, 1 h, 3) 20% TFA in DCM, rt, 1 h, (*S*): 33%, (*R*): 10%. **f.** BrCN, K_2CO_3/DIPEA, DCM/DMF, 0 °C -> rt, 2 h, (*S*): 86%, (*R*): 44%. The procedures for steps **a**-**f** were based on corresponding methods described in the patent[181], with minor refinements, including insights from the research of Gian M. Kipka[2].

The 6-step synthesis route of probe GK13S was first established by G. M. Kipka during his bachelor thesis, based on the synthesis of cpd158 as described in the patent[181]. In the first reaction, 4-nitro imidazole was converted to 1,4-dinitro-imidazole in an electrophilic aromatic substitution (**a**). Concentrated nitric acid and acetic anhydride in acetic acid were used to prepare the electrophilic species acetyl nitrate *in situ* (**Scheme 6A**). In this process, a nucleophilic attack of nitric acid on the carbonyl carbon atom of acetic anhydride with cleavage of acetate and subsequent proton transfer, lead to the formation of acetyl nitrate. In the subsequent electrophilic aromatic substitution, the electrophilic acetyl nitrate forms a bond with the π electrons of the N1-nitrogen atom under cleavage of the acetate group. This results in loss of aromaticity and formation of a σ complex. In the second reaction step, deprotonation of the nitrogen occurs, leading to re-aromatization of the heterocycle (**Scheme 6B**).

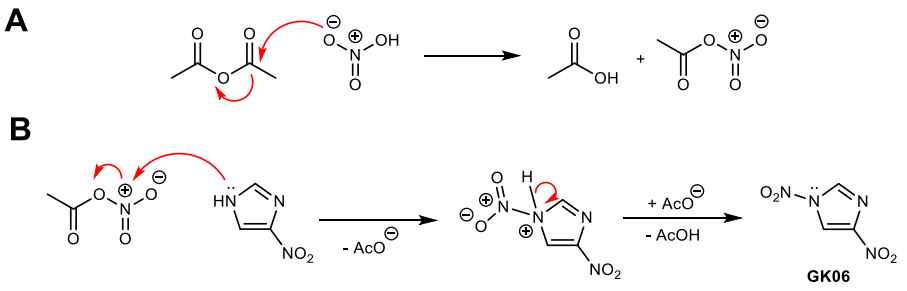

Scheme 6. A. Formation of the electrophilic species acetyl nitrate. **B.** Electrophilic aromatic substitution at the N1-nitrogen atom of imidazole. Scheme adapted from reference [2].

GK06 was further reacted with methyl 4-aminobenzoate in an *ANRORC* (addition of nucleophile, ring opening, ring closure) reaction to form GK07 (**Scheme 5b**). In this reaction a nucleophilic addition of the aniline (methyl 4-aminobenzoate) occurs at the C5-carbon atom

of GK06, since this is the most electrophilic position of the heterocycle due to the strong electron-withdrawing effect of the nitro group at the C4-carbon atom (**Scheme 7a**).

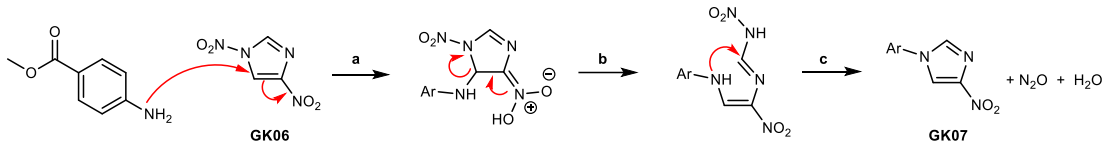

Scheme 7. GK06 and 4-aminobenzoate react in an *ANRORC* reaction to form GK07. a. Nucleophilic addition of the aniline at the C5-carbon atom of **GK06**. **b.** Ring-opening via electron transfer results in an open intermediate **c.** Nucleophilic attack of the nitrogen leads to cyclization and elimination of N_2O and water. Scheme adapted from reference [2].

Subsequently, a ring-opening reaction results in an “open” intermediate (**Scheme 7b**). In the last step, the nucleophilic attack of the nitrogen leads to cyclization and elimination of nitramide (H_2NNO_2), which subsequently decomposes to dinitrogen monoxide and water (**Scheme 7c**). In the next reaction step, the nitro group was reduced to an amine by use of palladium on activated charcoal under hydrogen atmosphere (**Scheme 5c**). In an amide coupling, the chiral *N*-Boc-protected (*S*)/(*R*)-1-Boc-pyrrolidine-3-carboxylic acid was attached to the free amine of GK08 (**Scheme 5d**). The synthesis of both enantiomers enabled to evaluate the impact of stero-configuration on protein binding in later biochemical assays. To avoid side reactions of commonly used carbodiimide coupling reagents, potentially affecting the chirality, HATU was used as the coupling reagent. In the next reaction, basic ester hydrolysis of GK09R and GK09R to cleave the methyl ester and subsequent amide coupling with pent-4-yn-1-amine HCl yielded GK12R and GK12S, respectively (**Scheme 5e**). In the final reaction (**Scheme 5f**), a cyanide group was introduced at the pyrrolidine *N*-atom via BrCN, yielding the final probes GK13R and GK13S. Chiral HPLC evaluated that both probes were enantiopure (ee >99%) and approved that no side reactions, affecting the stereochemistry occurred throughout the synthesis.

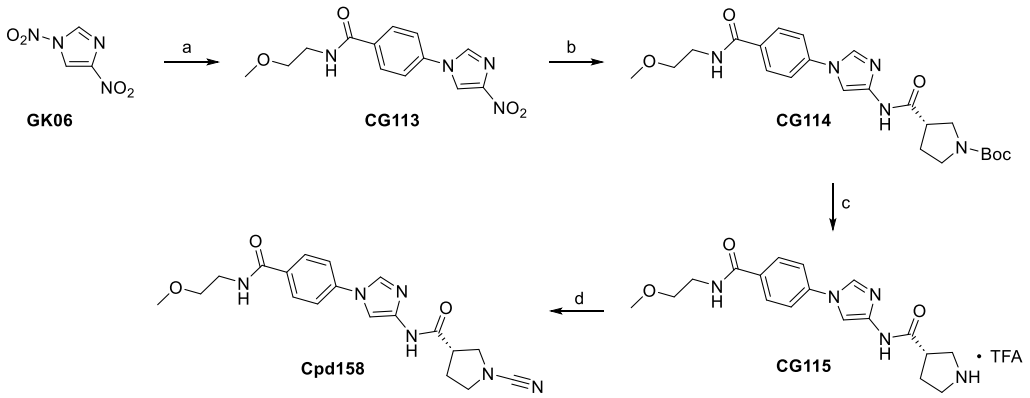

Scheme 8. Synthesis of inhibitor Cpd158 based on patent WO2016046530A1[181]. a. 4-amino-N-(2-methoxyethyl)benzamide, MeOH:H_2O = 1:1, rt, 2 d, 84%. **b.** 1) Pd/C, H_2, EtOH, H_2O, rt, 2 h, 2) (*S*)-1-Boc-pyrrolidine-3-carboxylic acid, HATU, DIPEA, DMF, rt, 2 h, 52%. **c.** 20% TFA in DCM, rt, 2 h, 76%. **d.** BrCN, DIPEA, DCM, DMF, 0 °C -> rt, 2 h, 56%. All reaction steps were synthesised according to the patent[181].

An ANRORC reaction of GK06 with 4-amino-*N*-(2-methoxyethyl)benzamide yielded precursor CG113. Based on CG113, the inhibitor Cpd158 was synthesised in a similar reaction sequence as described for GK13S/R (**Scheme 8**).

3.1.4.2 Synthesis of probes CG166 and CG173

In addition to the above described phenyl-imidazole based probes, *Mission Therapeutics* published another patent[182] in 2018, describing small molecule inhibitors of UCHL1. Among others, multiple *N*-cyanopyrrolidines with an indoline scaffold were shown. One major difference to the UCHL1 probes described above was the connectivity of their specificity element to the warhead. Whereas the *N*-cyanopyrrolidine warhead of the phenyl-imidazole probes presented a connection via the C3-position of the pyrrolidine ring, the same warhead was connected to an indole scaffold in the patent from 2017[182] in C2-position.

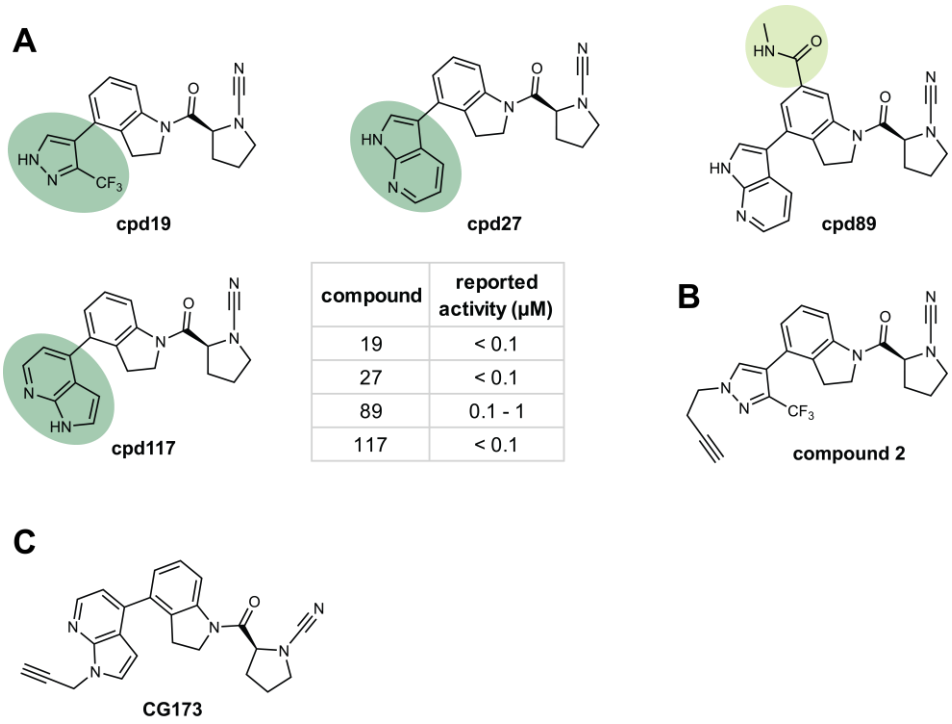

Figure 18. Patent-derived[182] structure-activity relationships of inhibitors gave an overview about possible sites for alkyne-handle incorporation. A. A selection of *N*-cyanopyrrolidine-based inhibitors with indoline-based specificity element show potent UCHL1 inhibition (cpd19, 27 and 117), whereas *N*-methyl acetamide substitution at the indoline (cpd89) decreases potency. **B.** Structure of compound 2 published in Krabill et al.[152], based on inhibitor cpd19 (compare **Figure 12C**). **C.** Structure of the activity-based probe CG173 derived from inhibitor cpd117.

In 2020, Krabill et al.[152] published a paper on the covalent, cyanopyrrolidine-based ABP compound 2 (**Figure 12C**, **Figure 18**). Compound 2 was derived from cpd19 (**Figure 18A**), originating in the *Mission Therapeutics* patent[182]. In a Ubiquitin-Rhodamine (Ub-Rho) assay, compound 2 was shown to retain UCHL1 activity (IC_{50} value of 6.4 µM) albeit with a 10-fold reduction in potency compared to its parent inhibitor cpd19 (IC_{50} value of 0.67 µM). In a gel-based labelling assay, the group further evaluated probe binding in KMS11 and SW1271 cell

lines and observed labelling of UCHL1 among other covalently modified proteins. An additional ABPP in KMS11 cells confirmed the presence of several off-target proteins. However, the study did not quantify probe engagement of these off-targets relative to UCHL1, and their definite identities were not determined, resulting in an undefined selectivity profile for this probe.

With the aim to further evaluate and compare protein binding of this compound class in our own biological assays, an indoline-based activity-based probe was designed (**Figure 18C**). However, the patent did not provide any information about potency differences upon substitution of free amines that are present in a variety of the inhibitors. A multitude of potent compounds from the patent were exposing two adjacent nitrogen-atoms with one of them being able to act as an electron donor and the other as an electron acceptor. Alkyne introduction at the pyrrolopyridine N1-atom might lead to a potential reduction of activity through either loss of a proton donor H-Atom, or reduced nucleophilicity of the nitrogen to form hydrogen bonds. A comparison of compound 2 (**Figure 18B**) to the 10-times higher, reported activity of cpd19[152] suggests that withdrawal of a proton-donor by introducing an alkyne handle might lead to reduction of potency, but in an acceptable extent, since low micromolar inhibition is still given. Loss of potency might also arise from interference of the alkyne handle with backbone amino acids in the adjacent environment of the UCHL1 binding pocket. Since acetamide substitution at the indoline (cpd89) in C6-position decreases potency, the alkyne handle was planned to be incorporated at the nucleophilic N1-atom of the pyrrolopyridine ring of cpd117 in a substitution reaction, leading to the design of probe CG173 (**Figure 18C**).

The synthesis of inhibitor and probe (**Scheme 9**) both started with an amide coupling of 4-bromoindoline and *N*-Boc-*L*-proline to afford CG119 (**a**). Cross-coupling with bis(pinacolato)diboron in a Miyaura borylation reaction under palladium catalysis further provided CG124 (**b**). The selection of an appropriate base is a determining factor for the success of borylation reactions, as strong activation of the product can facilitate the competing Suzuki reaction. The utilization of potassium acetate (KOAc) was derived from a screening of varying reaction conditions performed by the Miyaura group.[196] After oxidative addition of the aryl bromide (CG119) to the palladium catalyst, an (acetato)palladium(II) complex is formed under removal of the halide. The newly formed Pd-O bond, consisting of a hard Lewis base and a soft Lewis acid, impacts the reaction rate of the following transmetalation step, since it is more reactive than a Pd-Br bond.[196] Transmetalation with bis(pinacolato)diboron and reductive elimination under regeneration of the catalyst finally led to the formation of pinacolester CG124. CG124 was further reacted in a Suzuki coupling with 4-bromo-1*H*-pyrrolo[2,3-*b*]pyridine providing intermediate CG127 (**c**) as a joint starting point for the synthesis of inhibitor and probe. Acidic Boc-deprotection of CG127 and subsequent cyanation

with BrCN led to the formation of inhibitor Cpd117 (**e**). Nucleophilic substitution of the pyrrolopyridine N1-atom of CG127 and subsequent Boc-deprotection provided CG166 (**d**), which was further reacted to the final probe CG173 in a cyanation reaction with BrCN (**f**).

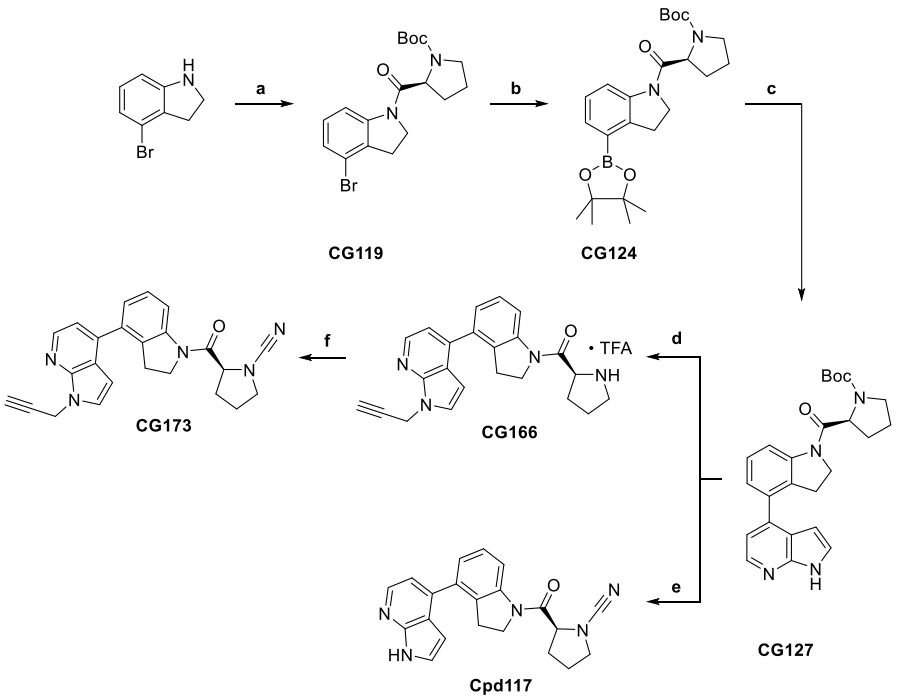

Scheme 9. Synthesis of probe CG173 and inhibitor Cpd117 based on patent US20180194724A1[182]. a. *N*-Boc-*L*-proline, HATU, DIPEA, THF, rt, on, 90%. **b.** Bis(pinacolato)diboron, KOAc, $PdCl_2$(dppf), 1,4-dioxane, 89%. **c.** 4-bromo-1H-pyrrolo[2,3-b]pyr-dine, XPhos Pd G2, K_3PO_4, 1,4-dioxane:water = 5:1, 60 °C, on, 70%. **d.** 1) propargyl bromide, K_2CO_3, DMF, rt, on, 2) 20% TFA in DCM, rt, 2 h, 36%. **e.** 1) 20% TFA in DCM, rt, 2 h, 2) BrCN, DIPEA, DCM, DMF, rt, 2 h, 68%. **f.** BrCN, K_2CO_3, DCM, rt, 3 h, 60%. Steps **a-e** were synthesised according to the patent[182].

3.1.5 Targeting USP7/USP8

The DUB USP7 has been the subject of extensive research due to its involvement in regulating key substrates linked to cancer progression, such as MDM2, N-MYC, and PTEN, making USP7 a promising candidate for drug development.[197] In 2009, *Hybrigenics* screened 65 000 compounds using a Ub-AMC assay and found HBX41108 (**Figure 9**) to be a USP7 inhibitor with an IC_{50} of 0.42 µM, but later studies from Ritorto et al.[87] revealed multiple off-target proteins, including several DUBs. In a study of Stockum et al., inhibition of USP8 by a very similar molecule DUB-IN-2 (Cpd22e[96], IC_{50} = 0.28 µM, **Figure 9**) improved mitochondrial function and lifespan, indicating therapeutic potential of USP8 inhibition.[97] Based on cpd22e, MSc. M. Schmidt designed and synthesised the probe MS038 (**Figure 15**) in an accompanying project; details will be part of his dissertation.

3.1.6 Targeting USP9x/USP24

MSc. M. Schmidt further developed probe MS037, based on compounds published in 2015 by the Donato group, demonstrating USP9x and USP24 inhibition. The highly conserved DUB USP9x has been reported to have several crucial functions, especially in maintaining cell survival, development and polarity as well as in protein trafficking.[198] Furthermore, it is assumed that USP9x plays a role in the development of Parkinson's disease such as, among others, USP8 and USP24. In addition, USP24 promotes drug resistance during cancer therapy. This highlights the need for inhibitors targeting these DUBs along with activity-based probes to evaluate the specificity of target protein binding in disease relevant models. Synthetic considerations, mechanistic details and further information will be part of Mr Schmidt's dissertation and are therefore not discussed here.

3.2 A Ubiquitin-VS competition workflow identifies DUB-binding probes

In order to evaluate cellular target engagement of the previously synthesised small molecule probes in a complex proteome, a Ubiquitin vinyl sulfone (Ub-VS) competition experiment was performed (**Figure 19**). HEK293 cell lysate was either pretreated with Ub-VS, followed by probe treatment (**Figure 19A**, left panel), or directly treated with the compounds (**Figure 19A**, right panel). Probe-bound proteins were then modified with a fluorophore via copper-catalysed click chemistry (**Figure 19B**) and the samples were analysed by SDS-PAGE (**Figure 19C**). Ub-VS acts as a potent and irreversible DUB-selective inhibitor through covalent modification of the active site cysteine. In samples pretreated with Ub-VS, the probes can only bind to potential non-DUB proteins in the cell lysate. Comparison with non-pretreated samples indicated whether the probe-modified proteins are DUBs.

Two of the tested probes, the 2- and 3-cyanopyrrolidines GK13S and CG173, showed a Ub-VS competitive band of approximal 30 kDa (**Figure 19C**). Both probes were derived from inhibitors targeting UCHL1 with a molecular weight of 25 kDa, indicating that these probes bind to their proposed DUB target. Other bands appearing in both, Ub-VS pretreated and non-pretreated samples implied additional non-DUB targets for these compounds. Despite the presence of a large number of active DUBs in HEK293 cells[199], no other Ub-VS-competitive bands were observed. The related binding pattern of non-DUB proteins for probes GK13S and CG50R, including a pronounced one with lower molecular weight, potentially arises from unspecific interactions of their similar phenyl-pyrazole/phenyl-imidazole specificity element or 3-cyanopyrrolidine warhead. The probe MS023 displayed a multitude of prominent bands, but none of them were Ub-VS competitive, indicating covalent binding of non-DUB proteins. Further, MS037 did not show DUB binding in this assay and CG017 and CG041 did not show any covalent-irreversibly bound proteins at all (**Figure 19C**).

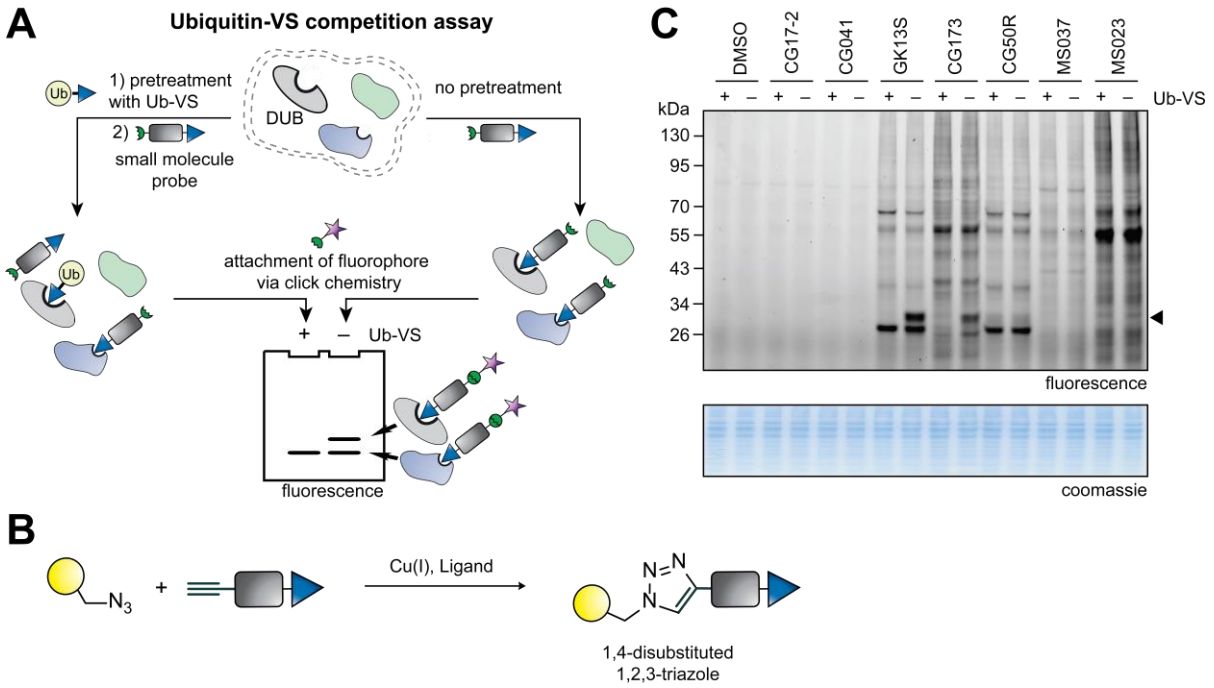

Figure 19. A Ubiquitin-VS competition assay identifies target engagement of an activity-based probe library in HEK293 cell lysate. A. Ub-VS competition workflow. Cell lysates were either incubated directly with compounds (right panel) or pretreated with Ub-VS followed by small molecule probe treatment (left panel). Attachment of a fluorophore to the probes via click chemistry and comparison of both workflows by fluorescent readout indicates whether the probe-modified proteins are DUBs. **B.** Copper(I)-catalysed azide-alkyne cycloaddition (CuAAC) between terminal alkyne of the probe and azide-functionalised fluorophore (yellow) under formation of a 1,4-disubstituted 1,2,3-triazole. **C.** Activity-based protein profiling in HEK293 cell lysate with indicated compounds (1 µM, 1 h). Proteomes were pretreated with a Ub-VS probe where shown. The black arrow indicates a Ub-VS competitive protein target in GK13S- and CG173-treated samples. The assay was performed by MSc. M. Schmidt.

3.3 A set of chemogenomic probes for UCHL1

The probe GK13S showed the most prominent Ub-VS competitive signal in cell lysate. Apart from one prominent off-target protein binding, only a few faint bands on the gel indicated good selectivity at a concentration of 1 µM. To further verify, if off-target protein binding arose from unselective binding of the probe's specificity element or too high reactivity of the warhead, a systematic set of chemogenomic probes comprising probes of both stereoisomers (GK13S and GK13R, **Scheme 5**), inactive controls lacking the warhead (GK12S and GK12R, **Scheme 5**) as well as minimal probes lacking the central aromatic specificity element (GK16S and GK16R, **Scheme 10**) were synthesised (**Figure 20**).

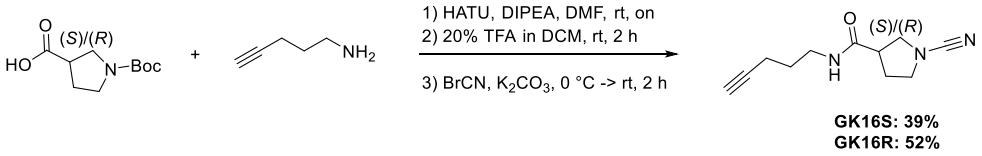

Scheme 10. Synthesis of minimal probes GK16S and GK16R.

Synthesis of inactive controls GK12S and GK12R followed the same route as shown in **Scheme 5 a-e** as precursors of probes GK13S and GK13R. The minimal probes were prepared in a 3-step synthesis starting from (S)/(R)-1-Boc-pyrrolidine-3-carboxylic acid (**Scheme 10**). After an amide coupling reaction with the alkyne pent-4-yn-1-amine and subsequent acidic Boc-deprotection, electrophilic cyanation yielded the minimal probes GK16S and GK16R.

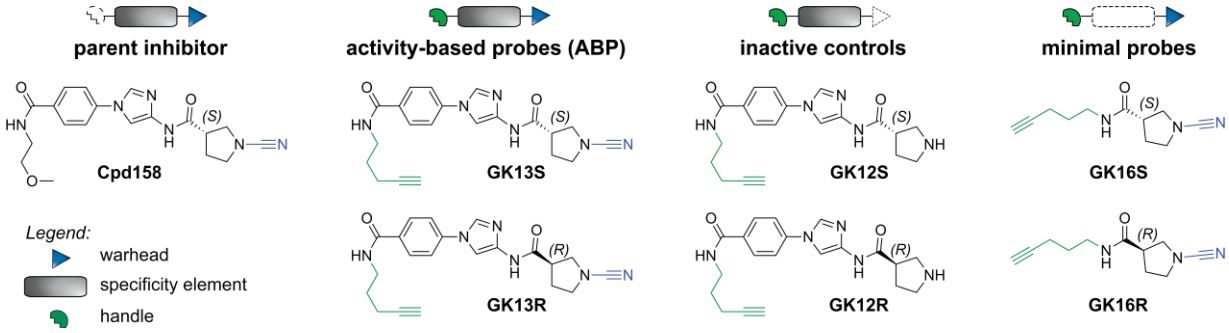

Figure 20. A set of chemogenomic, 1,3-linked cyanopyrrolidine probes for UCHL1. Schematic representations and chemical structures of synthesised probes and controls comprising warhead (blue), specificity element (grey) and alkyne handle (green).

The specificity of the probes in cells was evaluated by treating intact HEK293 cells and visualising covalently bound proteins after 24 h via activity-based profiling (**Figure 21A**). At a high concentration of 10 µM, all probes exhibited binding to a lower molecular weight protein. However, at concentrations of 0.1 and 1 µM, only the GK13S probe displayed a strong signal for a band of approximately 30 kDa. To further validated that this protein corresponds to the Ubiquitin-probe competitive band observed in the cell lysate, a reverse Ubiquitin-probe competition experiment was performed (**Figure 21B**). Intact cells were treated with the compounds and the resulting lysates incubated with the HA-Ub-VS probe. The presence of active DUBs was then visualised via anti-HA Western blotting (**Figure 21B**). The molecular weight and significant signal decrease in the HA-Ub-VS competition experiment were in agreement with UCHL1, the DUB target of the parent inhibitor.

An activity-based protein profiling workflow was employed to identify probe-bound proteins, which involved the enrichment of bound proteins through streptavidin and protein analysis by quantitative mass spectrometry (**Figure 11B**). The most enriched protein from cells treated with 5 µM of GK13S could be identified as UCHL1, showing a 3000-fold enrichment (**appendix, Figure 63A**), which is consistent with the strong signal observed in the gel-based labelling assays (**Figure 19C**, **Figure 21A**). Further, GK13S also resulted in the strong enrichment of PARK7 (also referred to as DJ-1) and the PARK7-homolog C21orf33 (also known as GATD3, a mitochondrial glutamine amidotransferase), as well as several aldehyde dehydrogenases. At a lower concentration of 1 µM, GK13S showed a similar enrichment pattern (**appendix, Figure 63B**). Notably, the (*R*)-Isomer GK13R, and the minimal probe

GK16S showed strong enrichment for both PARK7 and C21orf33, while UCHL1 was only weakly enriched (**appendix, Figure 63C**).

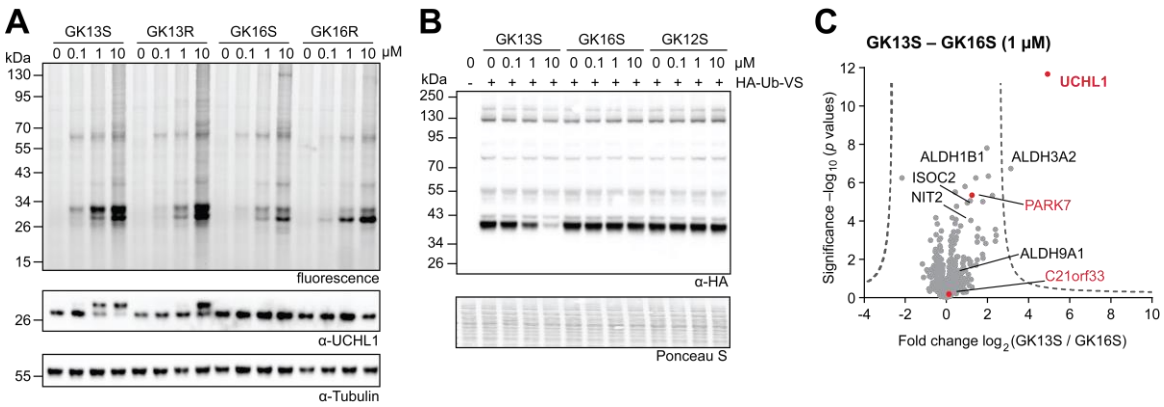

Figure 21. Cellular characterisation of 1,3-linked cyanopyrrolidines. A. Cellular activity-based protein profiling with intact HEK293 cells and indicated compounds (24 h incubation). The fluorescence image visualises probe-bound endogenous proteins. **B.** Cellular HA-Ub-VS competition experiment. HEK293 cells were treated with indicated compounds for 24 h. Lysates were then incubated with a HA-Ub-VS probe, followed by western blotting visualising Ub-VS-reactive DUBs. **C.** Proteomics-based target identification of GK13S in comparison to GK16S. The volcano plot shows the relative label-free abundance ratio (fold change) of proteins between GK13S and the minimal probe GK16S. Cells were treated for 24 h at indicated concentrations. UCHL1, PARK7, and PARK7-homolog C21orf33 are marked in red. Assays were performed and evaluated by MSc. M. Schmidt.

When a probe, specific to a single protein is not available, the comparison of two chemogenomic probes may provide specific insights into a non-overlapping protein target. The comparison of GK13S to GK16S-enriched proteins (**Figure 21C**) indicated that GK13S binds to all targets of GK16S, as well as UCHL1. This pattern was also observed for the enantiomer GK13R, but showed a lower enrichment of UCHL1 compared to GK13S. These results collectively suggest that GK13S and GK16S are a suitable set of chemogenomic probes for small molecule-mediated investigation of the cellular functions of UCHL1.

The targets of the probes were further validated through genetic perturbation using siRNA-mediated depletion, leading to the unambiguous identification of the upper band labelled by GK13S as UCHL1 and the lower band labelled by both GK13S and GK16R as PARK7 (**appendix, Figure 64A**). Additionally, the experiment confirmed that the faint band observed in GK16S-treated samples above PARK7 (**Figure 21A**) is not UCHL1. Instead, it is consistent with the molecular weight of C21orf33. Overexpression of catalytically inactive mutants further confirmed the active site cysteine of UCHL1 as the site of labelling by GK13S and the catalytic cysteine of PARK7 as the site of labelling by all probes tested (**appendix, Figure 64B,C**).

3.4 GK13S potently inhibits recombinant and cellular UCHL1

To obtain a more comprehensive understanding of the specificity of GK13S for UCHL1, an analysis of its binding affinity and inhibitory activity utilizing recombinant protein was performed (**Figure 22**).

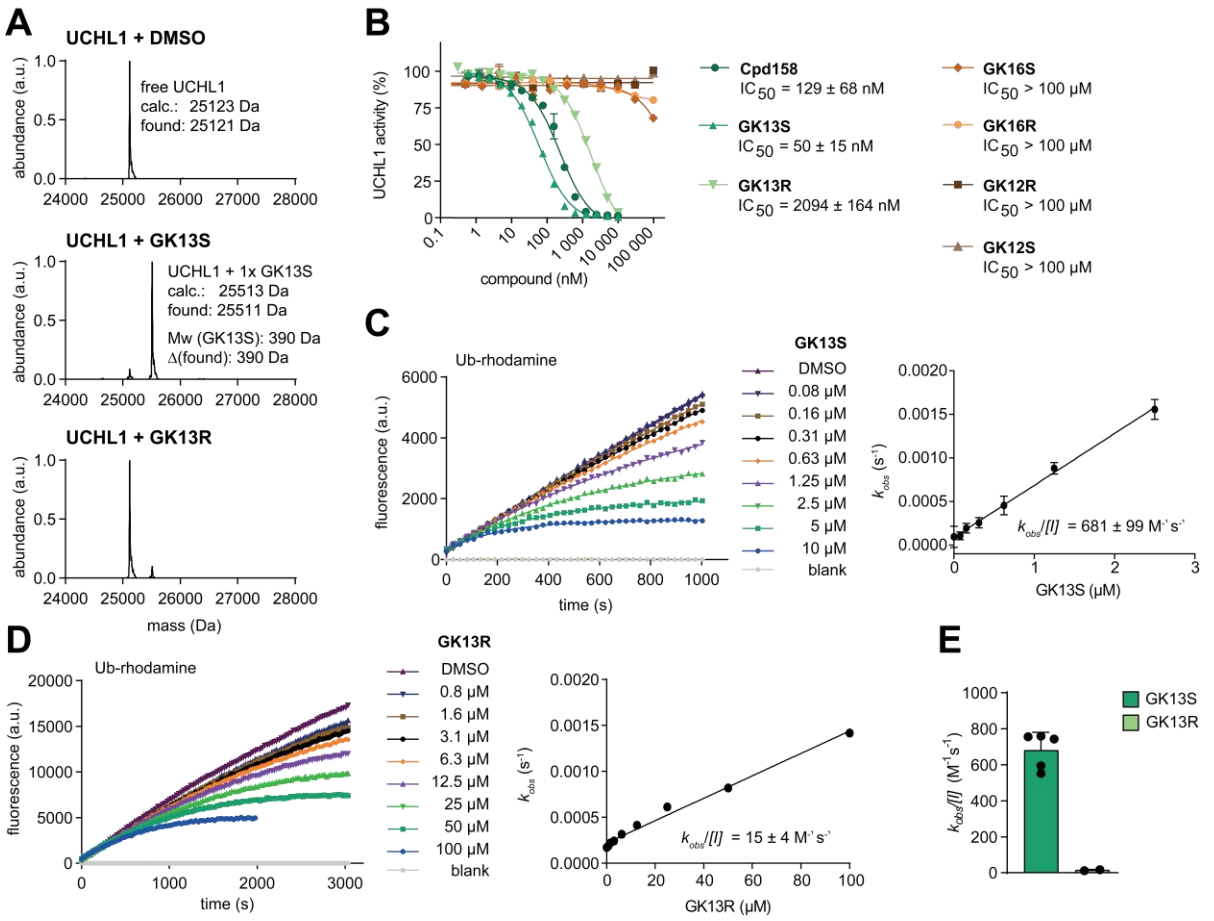

Figure 22. GK13S potently inhibits UCHL1 *in vitro*. A. Intact protein mass spectrometry revealed covalent binding of GK13S and GK13R to recombinant UCHL1. UCHL1 (0.8 µM) was treated with compound (1 µM) or DMSO for 2 h. **B.** Inhibitory potencies of indicated compounds, preincubated with UCHL1 for 1 h, determined from a Ubiquitin-Rhodamine cleavage assay. Data points are shown as mean ± standard deviation (SD) from two independent experiments. IC_{50} values were determined from 5 (Cpd158), 3 (GK13S), or 2 (GK13R) independent experiments. **C.** $k_{obs}/[I]$ kinetic assay of GK13S binding to UCHL1 at indicated concentrations. Data points are shown as means calculated from N = 3 wells (N = 6 wells for DMSO and blank (Ubiquitin-Rhodamine without enzyme)). Rate constants k_{obs} were determined from the plot on the left, and then plotted against inhibitor concentrations as shown on the right for a representative experiment. The $k_{obs}/[I]$ value was determined as the slope and is given as means ± SD calculated from five independent experiments. **D.** $k_{obs}/[I]$ kinetic assay of GK13R binding to UCHL1 at indicated concentrations. $k_{obs}/[I]$ values were calculated from 2 independent experiments. **E.** Comparison of $k_{obs}/[I]$ values of GK13S and GK13R from assays shown in **C**-**D**.

Intact mass spectrometry at a probe concentration of 1 µM revealed that GK13S, but not its enantiomer GK13R, bound UCHL1 in a 1:1 ratio (**Figure 22A**). IC_{50} measurements at an incubation time of 1 h revealed that the probe and the parent inhibitor have comparable potencies of 50 and 129 nM, respectively, whereas the enantiomer GK13R inhibited UCHL1

~40-times worse (**Figure 22B**). The control probes lacking the warhead and the minimal probes exhibited no significant inhibition (IC_{50} greater than 100 µM), emphasizing the importance of both the warhead and the aromatic specificity element in GK13S for inhibiting UCHL1. These data are in agreement with the cell-based labelling experiments (**Figure 21A,B**) and LC-MS binding experiments at a higher compound concentration of 10 µM (**appendix, Figure 65**). Protein inhibition by covalent compounds is strongly dependent on the incubation time. To compare binding of the probes in a secondary assay, the covalent mode of inhibition was further characterised in a fluorescence-based Ubiquitin-rhodamine (Ub-Rho) cleavage assay. Time-dependent target association of the inhibitors to UCHL1 was measured at various concentrations to determine concentration dependent observed rates of inactivation (k_{obs}) (**Figure 22C-D**). By plotting k_{obs} values against inhibitor concentration [I], the apparent second-order rate constant $k_{obs}/[I]$ was determined, reflecting the combined kinetic and binding parameters involved in the sequence of events leading to UCHL1 inhibition, including the rate of UCHL1~inhibitor formation.[200] In line with the relatively weak electrophilicity of the cyanamide and comparable to other warheads,[201] GK13S exhibited a $k_{obs}/[I]$ value of 681 M^{-1} s^{-1} (**Figure 22C**). The potency of the (*R*)-isomer was ~40-fold lower, validating the results of the IC_{50} measurements (**Figure 22D-E**).

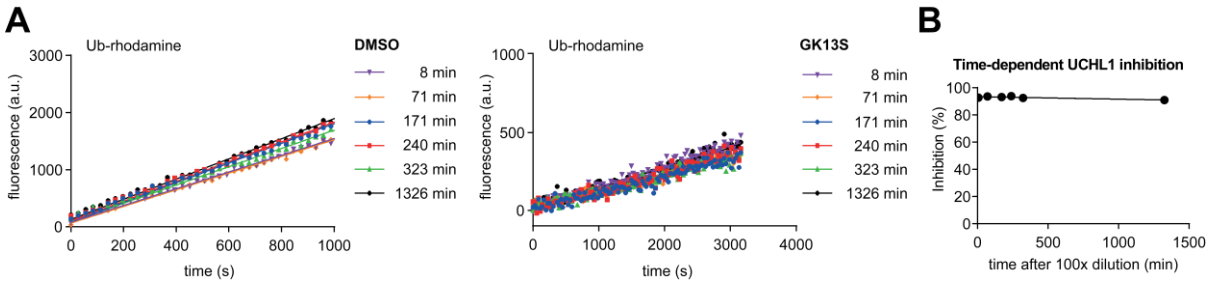

Figure 23. A Jump dilution experiment determines covalent-irreversible binding mode of GK13S. A. Jump-dilution assay. UCHL1 (12 nM) was treated with DMSO (1.25 µM) or an excess of GK13S (1.25 µM) for 2 h. Parts of this solution were diluted 100-fold at indicated time points, then diluted 1:2 with Ub-Rho (100 nM) and UCHL1 activity was measured in a Ub-Rho cleavage assay. **B.** Time-dependent UCHL1 inhibition based on slopes of individual time points from jump-dilution assay (as shown in **A**).

The binding mode was further characterised in a jump-dilution assay (**Figure 23**). GK13S was incubated with UCHL1 at a concentration of 1.25 µM for 2 h to ensure full protein labelling, followed by 100x dilution at different time points. In the case of GK13S being a reversible inhibitor, dilution to a concentration of 12.5 nM (after 100x dilution) would correlate with UCHL1 activity increasement over time (12.5 nM GK13S relates to ~75% UCHL1 activity in a Ub-Rho assay (**Figure 22B**)). Over a time period of more than 22 h nearly no reduction in inhibition could be observed (**Figure 23B**), characterising GK13S as a covalent irreversible inhibitor. To validate this result, GK13S was incubated with 5 M urea in a dialysis tube

overnight. In a subsequent LC-MS analysis no unbound UCHL1 could be observed, confirming a covalent irreversible binding mode (**appendix, Figure 66**).

Consistent with the validated potency of the probes, GK13S and parent inhibitor Cpd118 both increased UCHL1 stability upon binding by 6 °C in a thermal shift assay, whereas the inactive control probes GK12R/S and the minimal probes GK16R/S did not show any stabilisation at concentrations up to 5 µM (**Figure 24A**). GK13R demonstrated only weak stabilisation of 1 °C at the highest concentration.

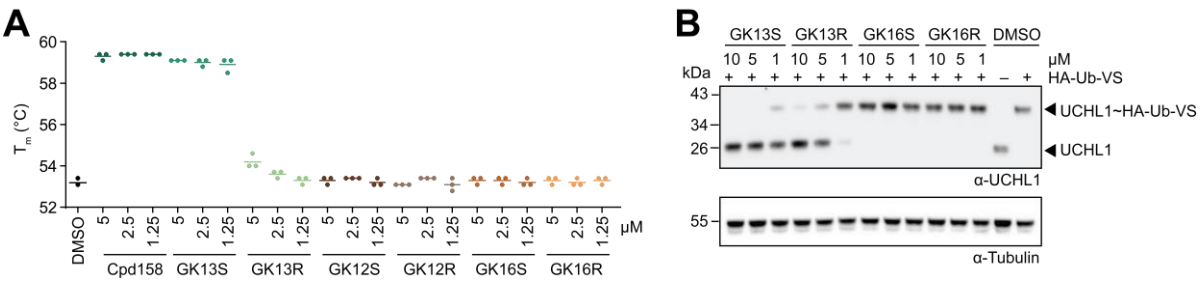

Figure 24. GK13S stabilises and potently inhibits recombinant and cellular UCHL1. A. Thermal shift assay showing the melting temperature (Tm) of UCHL1 (1 µM) pre-treated for 1 h with compounds at indicated concentrations. **B.** Inhibition of cellular UCHL1. Western blot analysis of endogenous UCHL1 labelled with HA-Ub-VS after treatment of HEK293 cells with either the indicated compounds or DMSO for 24 h. The cellular assay (**B**) was performed and evaluated by MSc. M. Schmidt.

To assess the degree of inhibition of cellular UCHL1, a Ub-VS competition experiment in HEK293 cells was performed (**Figure 24B**). Treatment with 5-10 µM GK13S for 24 h lead to complete inhibition of UCHL1. Even at a lower concentration of 1 µM near complete inhibition could be observed. The enantiomer GK13R showed near complete labelling of UCHL1 at 5 µM concentration, whereas at 1 µM nearly no labelling of UCHL1 could be observed. Given that covalent inhibitors act in a time-dependent manner, it is reasonable that the pronounced specificity window of GK13S compared to GK13R observed in the *in vitro* assay, where the incubation time was 1 h (50 nM vs. > 2 µM), may be diminished when a cellular inhibition assay is performed with a 24 h incubation period (near complete inhibition of UCHL1 at 1 µM vs. 5 µM). The minimal probes did not show any UCHL1 binding at concentrations up to 10 µM, further highlighting the use of the minimal probe GK16S, but not of the enantiomer GK13R, as a chemogenomic control for GK13S to investigate the specific inhibition of UCHL1.

3.5 Inhibition of UCHL1 by GK13S does not impair cell growth

Since the results of the binding assay (**Figure 19C**) demonstrated binding of both the 3-carboxypyrrolidine GK13S and the 2-carboxypyrrolidine CG173 probes to UCHL1, both compounds were compared *in vitro* (**Figure 25A-E**). Considering the weak UCHL1 binding (**Figure 19C**), it was surprising that CG173 showed very similar binding kinetics (k_{obs}/[I]

= 597 M^{-1} s^{-1}) and inhibitory potency (IC_{50} = 43 nM) compared to GK13S (**Figure 25A,D**). The parent inhibitor Cpd117 inhibited UCHL1 even ~ 5-times more potent (IC_{50} = 8 nM).

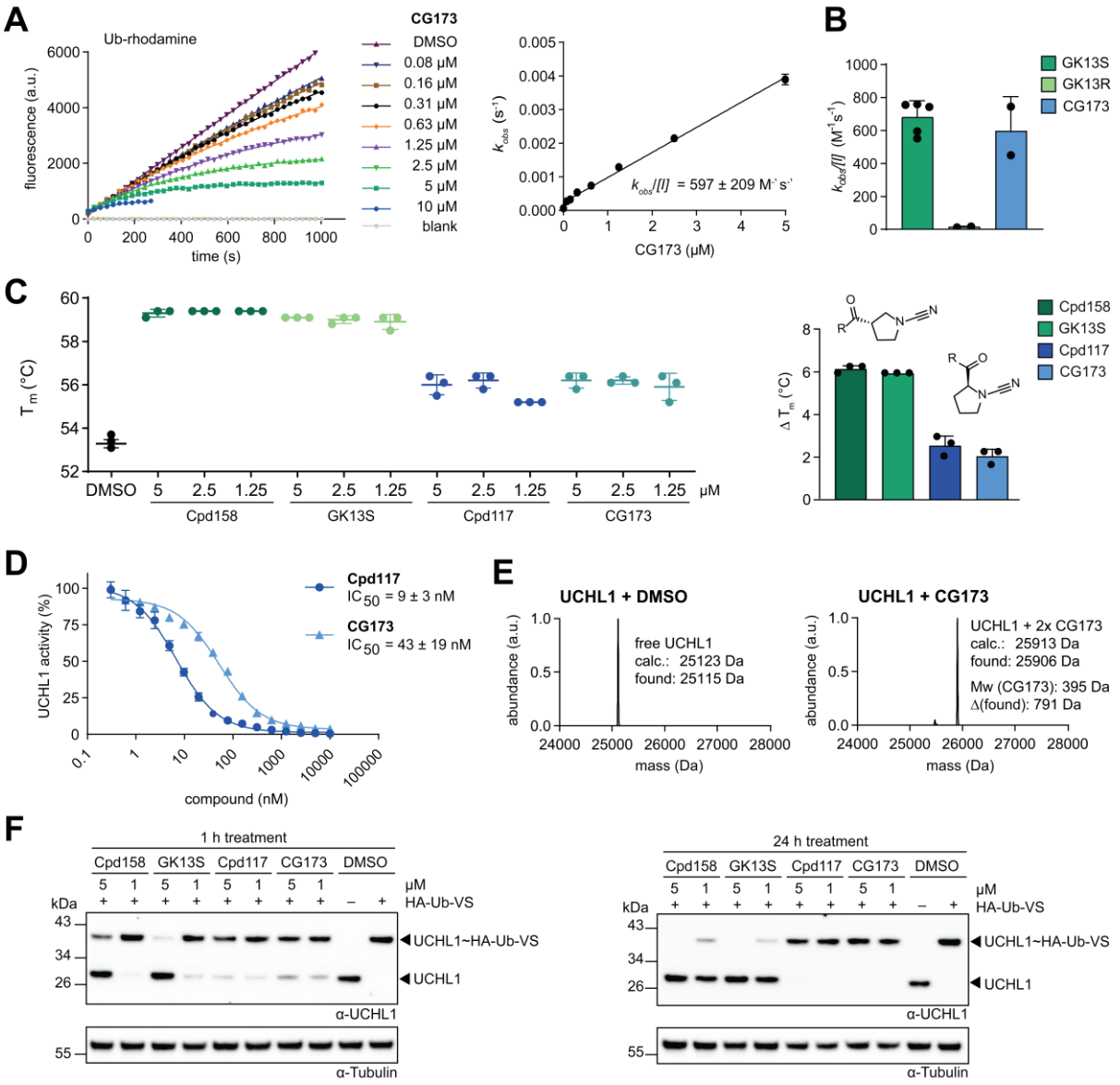

Figure 25. *In vitro* comparison of 2- and 3-carboxy-N-cyanopyrrolidine UCHL1 inhibitors. **A.** $k_{obs}/[I]$ kinetic assay of CG173 binding to UCHL1 at indicated concentrations. $k_{obs}/[I]$ values were calculated from 2 independent experiments. **B.** Comparison of $k_{obs}/[I]$ values of indicated compounds. Related experiments are shown in **Figure 22C-D**. **C.** Thermal shift assay showing the melting temperature (T_m) of UCHL1 (1 µM) pre-treated for 1 h with compounds at indicated concentrations (left panel) and comparison of changes in UCHL1 protein melting temperatures (ΔT_m) after binding to 3- and 2-carboxy-N-cyanopyrrolidine-based compounds (right panel). Values are given as mean ± SD from 3 technical replicates. **D.** Inhibitory potencies of indicated compounds were determined from Ub-Rho cleavage assays (compare **Figure 22B**). IC_{50} values were determined from 2 independent experiments and are given as mean ± standard deviation. **E.** Intact protein mass spectrometry data of compound CG173 covalently binding recombinant UCHL1 twice. UCHL1 (3 µM) was treated with compound (10 µM) or DMSO for 16 h. **F.** Comparison of inhibitory potency of cellular UCHL1 for 2- and 3-carboxy-N-cyanopyrrolidine-based compounds. Same workflow as in **Figure 24B**. Cellular assays (**F**) were performed and evaluated by MSc. M. Schmidt.

However, CG173 and Cpd117 both led to reduced protein stabilisation (**Figure 25C**), indicating less tight binding. In regards to the higher potency compared to GK13S, this suggests a potentially more reactivity driven binding mechanism. LC-MS analysis revealed that CG173 bound UCHL1 covalently in a 2:1 stoichiometry, under the same conditions where GK13S bound only once (**Figure 25E**), further supporting this hypothesis.

In contrast to the potent *in vitro* binding, Cpd117 and CG173 both showed a very low degree of cellular UCHL1 inhibition after 1 h, and no inhibition at all after 24 h incubation, whereas GK13S and parent inhibitor Cpd158 demonstrated a time- and concentration-dependent inhibition (**Figure 25F**).

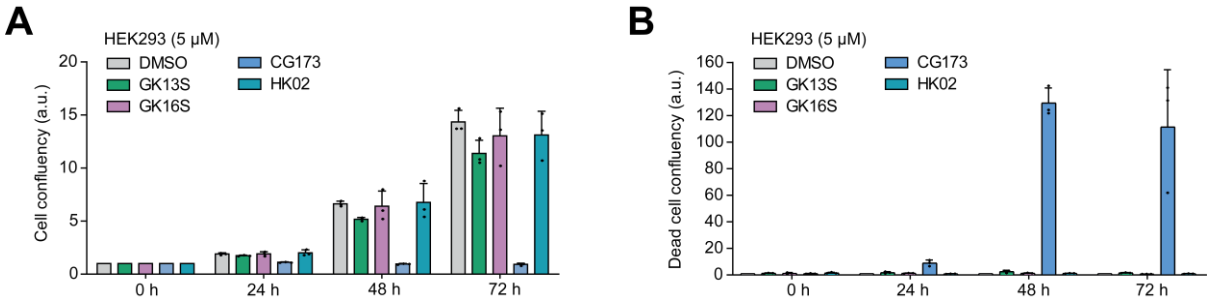

Figure 26. 2-, but not 3-carboxy-N-cyanopyrrolidines induce apoptosis in HEK293 cells. A. Quantification of HEK293 cell confluency observed at 24, 48 and 72 h post treatment with 5 µM of the indicated compounds. Confluency is normalised to that at 0 h. Data are shown as means of N = 3 independent experiments. Error bars represent standard deviation. **B.** Quantification of HEK293 propidium iodide (PI) positive cells observed at 24, 48 and 72 h post treatment with 5 µM of the indicated compounds. Confluency is normalised to DMSO at each time point. PI positive cell confluency is adjusted to overall cell confluency. Data are shown as means of N = 3 independent experiments. Error bars represent standard deviation. HK02S was used as a minimal probe for CG173; See **appendix, Figure 67** for complete chemical structure. The assay was performed, and data as well as graphs kindly provided by Dr. Rachel O'Dea.

Notably, cell treatment with CG173 and Cpd117 showed strong induction of apoptosis and growth arrest of HEK293 cells at a concentration of 5 µM and an incubation time of up to 72 h. Neither GK16S nor GK13S showed any growth arrest or apoptosis under the same conditions (**Figure 26**). These results are in agreement with previous reports of the viability of multiple cell lines upon knockout of UCHL1[183] and suggest that the toxicity associated with CG173 is not related to UCHL1. Hence, the collective data indicate that GK13S, but not CG173 is suitable for characterising the function of UCHL1 in cells.

3.6 Glioblastoma cells treated with GK13S but not GK16S phenocopy a UCHL1 mutant mouse

In mice, mutations of UCHL1 are associated with gracile axonal dystrophy (gad)[132] and reduced levels of free mono-Ubiquitin in neurons.[112,202] Accordingly, inhibition of UCHL1 in COS-7 monkey kidney cells has previously been shown to increase free Ubiquitin levels in

cells.[203] With the aim to validate GK13S and GK16S as a probe pair for the investigation of UCHL1 in a human neuro-cellular system, their use in the human glioblastoma cell line U-87 MG was investigated (**Figure 27**). Comparable to the results observed in HEK293 cells, GK13S and GK16S were non-toxic in concentrations up to 5 µM for up to 72 h in U-87 MG cells (**appendix, Figure 67A-D**) and demonstrated a pattern of bound proteins that was highly similar to that observed in HEK 293 cells (**Figure 27A**).

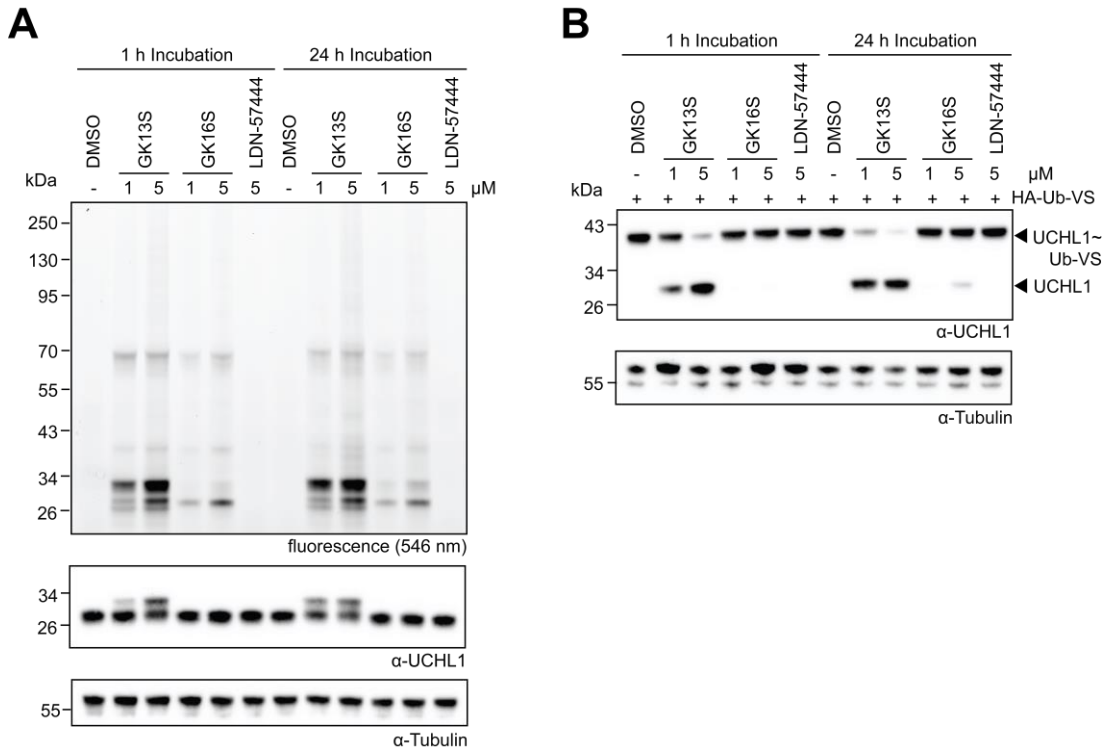

Figure 27. Probe pair binding in U87 MG cells show a similar pattern to that observed in HEK293 cells. A. Cellular activity-based protein profiling of intact U-87 MG cells treated with indicated compounds or DMSO for 1 or 24 h. **B.** Inhibition of cellular UCHL1. Western blot analysis of endogenous UCHL1 labelled with HA-Ub-VS after treatment of U-87 MG cells with either the indicated compounds or DMSO for 1 or 24 h. Assays were performed and evaluated by MSc. M. Schmidt.

The widely used UCHL1 inhibitor LDN-5744443 (**Figure 9**) was included to evaluate its recently questioned effectiveness.[176,177] GK13S, but not GK16S nor LDN-57444, led to complete inhibition of UCHL1 in U-87 MG cells (**Figure 27B**). This further confirms the suspicion of ineffective UCHL1 inhibition by LDN-5744443 and establishes the use of GK13S and GK16S as chemogenomic probes in U-87 MG cells. In line with the increase of free Ubiquitin levels in COS-7 cells, UCHL1 inhibition by GK13S, but not GK16S, led to reduced Ubiquitin levels in U-87 MG cells. (**Figure 28A-B**). This reduction was unchanged in the presence of siRNA-mediated depletion of PARK7 (**appendix, Figure 67E-F**) or UCHL3 (**Figure 28A**), supporting the non-redundant function of these two homologous DUBs.[111] These data collectively show that inhibition of UCHL1 by GK13S in the glioblastoma cell line U-87 MG, on a molecular level, phenocopies a pathogenic UCHL1 mutation in mice.[112] They

further validate the use of the chemogenomic pair of probes to investigate the function of UCHL1 in a cellular context (**Figure 28C**).

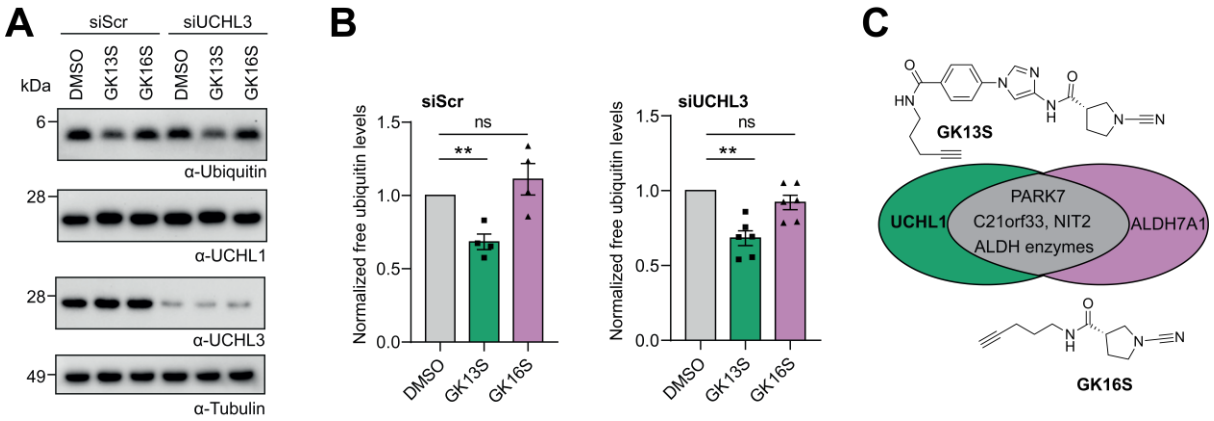

Figure 28. GK13S, but not GK16S, reduces mono-Ubiquitin in U-87 MG cells, phenocopying the effect of a UCHL1 mutant mouse. A. Western blots showing mono-Ubiquitin levels in U-87 MG cells treated with GK13S or GK16S. An additional knockdown of UCHL3 does not aggravate the effect. **B.** Quantification of mono- Ubiquitin intensities upon treatment of U-87 MG cells with DMSO, GK13S, or GK16S (as shown in a). Values correspond to the mean of four or six independent experiments for control or UCHL3 knockdown, respectively. Error values represent the standard error of the mean (s.e.m.). Statistical significance was analysed using individual one-sample, two-tailed t-tests compared to the mean of "1" as set for the DMSO-treated samples. **p < 0.01 (exact p = 0.0095 for DMSO/GK13S comparison in siScr background and p = 0.0014 for the DMSO/GK13S comparison in the siUCHL3 background); ns, not significant. **C.** Schematic representation of overlapping and individual cellular targets of GK13S and GK16S, supporting their application as chemogenomic probes for the investigation of UCHL1. Assays were performed and evaluated by MSc. M. Schmidt and MSc. K. Gallant.

3.7 A compound-induced hybrid conformation underlies GK13S-mediated inhibition of UCHL1

The next aim was to structurally characterise the binding of GK13S to UCHL1 in order to understand the basis for its specificity. Several attempts to crystallise full length UCHL1 in co-complex with GK13S or crystal soaking of GK13S into UCHL1 apo crystals failed. Since N- and C-terminal truncation of UCHL1 both lead to destabilisation[117,118], methylation of lysine residues was applied as a rescue strategy[204] (**Figure 29**). This increases surface hydrophobicity in order to drive the formation of a crystal form which is compatible with compound binding. Near complete di-methylation of all 16 Lys residues plus the N-terminus could be achieved as judged by LC-MS analysis (**Figure 29**).

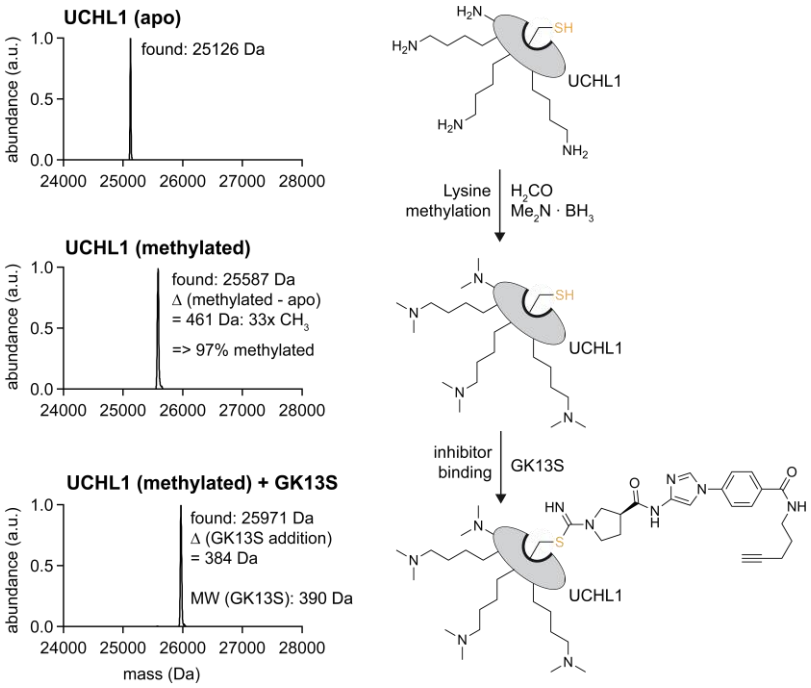

Figure 29. Lysine methylation of UCHL1 enabled co-crystallisation of GK13S and UCHL1. Lysine methylation of the crystallised human UCHL1 construct (residues 1-223 with N-terminal GS-linker). Left panel: Intact protein mass spectrometry data of apo UCHL1, methylated UCHL1 and GK13S-bound methylated UCHL1. Right panel: Corresponding schematic representations of the methylation workflow and compound binding.

After complex formation between GK13S and UCHL1, several coarse and fine screenings resulted in suitable conditions for successful co-crystallisation of GK13S~UCHL1. After anisotropic scaling, the crystal structure was solved to 2.24 Å resolution (**Figure 30**). The asymmetric unit contained ten copies of the complex, with well-defined density for the ligand in eight copies and partially defined ligand density in two copies (**appendix, Figure 68**). Superposition of all copies indicated identical positioning of the ligand (**Figure 30B-C**).

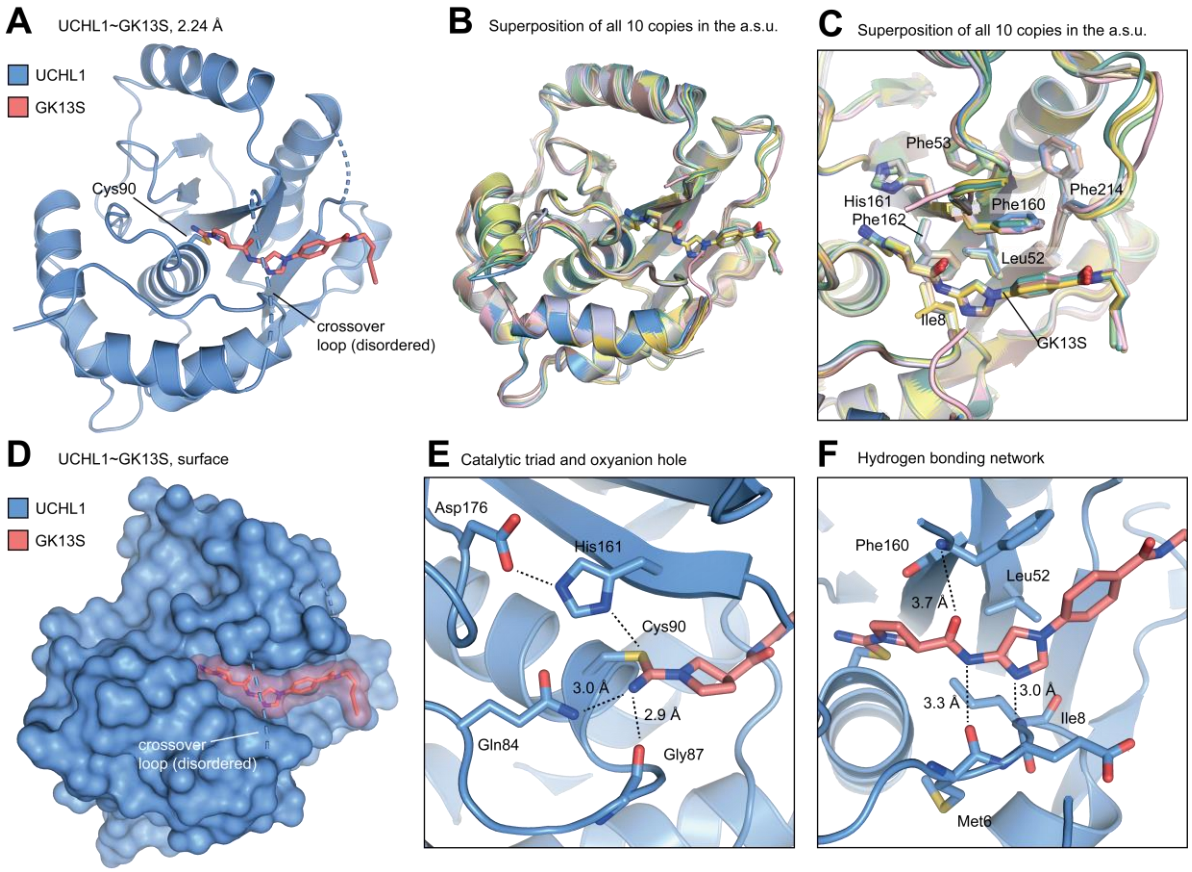

Figure 30. Structural analysis of specific binding of GK13S to UCHL1. A. Structure of UCHL1 (blue) in complex with GK13S (red). The covalently bound active site cysteine 90 and the disordered crossover loop are indicated. **B, C.** Superposition of all 10 copies within the asymmetric unit of the UCHL1~GK13S structure showing the entire protein (**B**) or the compound binding site (**C**). Labelled residues and the compound are shown as sticks, demonstrating that the same binding mode is observed in all copies. **D.** Surface representation of **A**. **E.** Close-up view on **A**, highlighting the oxyanion hole (Gln84 and Gly87) bound by the isothiourea nitrogen and the aligned catalytic triad residues Cys90, His161, and Asp176. Hydrogen bonds are shown as dotted lines, and their length is given. **F.** Close-up view on **A**, highlighting residues of UCHL1 interacting with GK13S.

GK13S binds covalently to the catalytic cysteine Cys90 through an isothiourea bond (**Figure 30**) and occupies a shallow cleft that guides the Ubiquitin C-terminal LRGG peptide to the active site (**Figure 31**). The stability of the isothiourea bond is maintained by the oxyanion hole formed by Gln84 and Gly87 and by hydrogen bonding with the residues of the catalytic triad (**Figure 30E-F**). The central amide and imidazole ring of GK13S form hydrogen bonds with Phe160, Met6, and Ile8 on both sides of the cleft, which also coordinate the backbone of the Ubiquitin C-terminal peptide (**Figure 31B-D**). The hydrogen bonding acceptors and donors of GK13S are geometrically similar to those of Ubiquitin, and the phenyl ring of GK13S mimics the hydrophobic side chain of Leu73 in Ubiquitin that is recognised by Phe160.

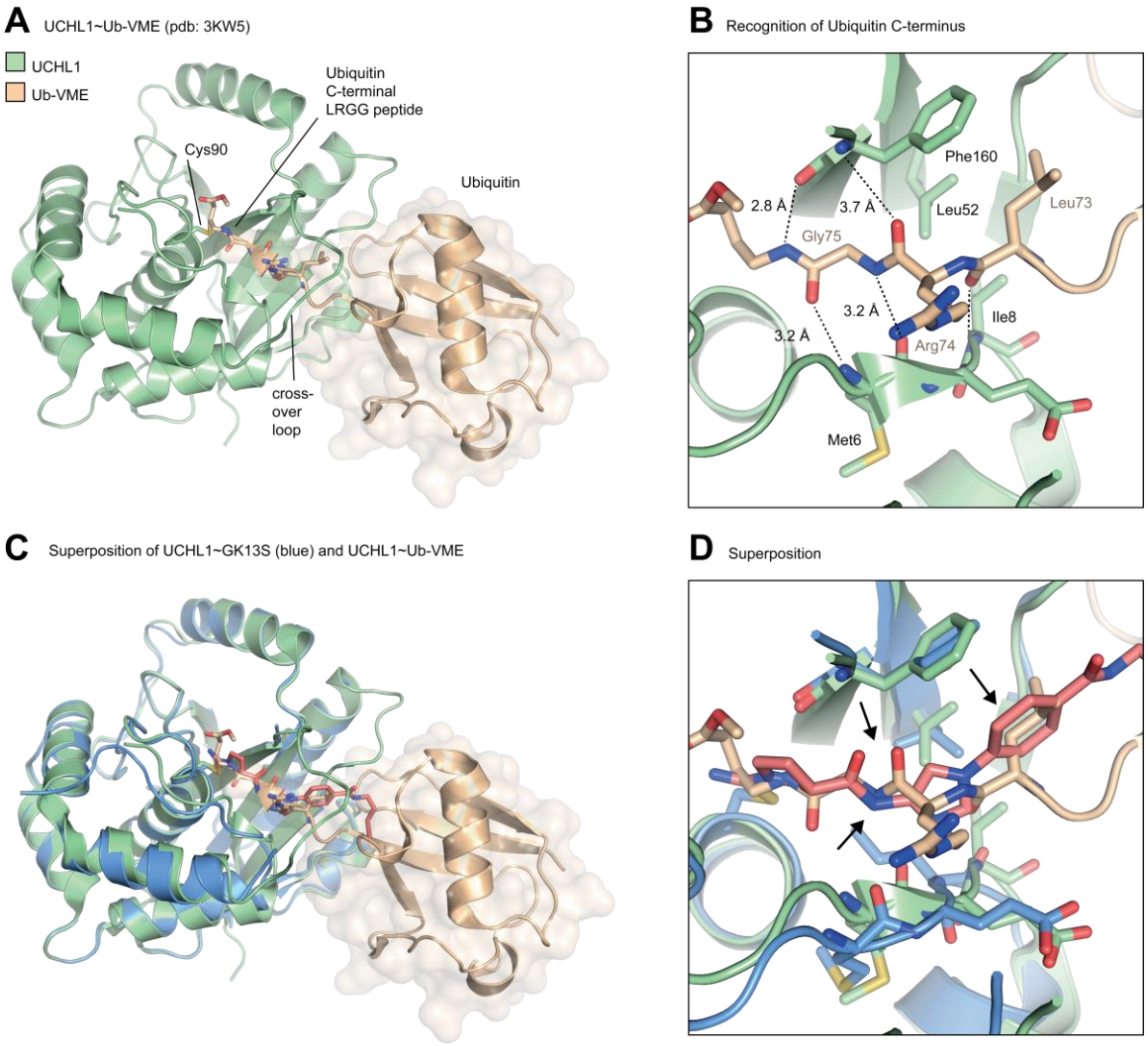

Figure 31. GK13S mimics the C-terminal peptide of Ubiquitin. A, B. Structure of UCHL1 (green) in complex with Ub-VME (gold) (pdb: 3KW5) showing the entire protein (**A**) or the compound binding site, highlighting key interactions of the Ubiquitin C-terminus with the binding cleft of UCHL1 (**B**). The Ubiquitin C-terminal residues 73–76 are also shown as sticks. VME vinyl methyl ester. **C, D.** Superposition of **A** and UCHL1~GK13S, highlighting that the compound binds into the cleft, which is guiding the Ubiquitin C-terminus to the active site (**A**) and close-up view on the binding cleft of UCHL1 (**B**). Ubiquitin residues mimicked by GK13S are indicated with black arrows (a hydrogen bond acceptor, a hydrogen bond donor and the hydrophobic Leu73 side chain).

The literature of crystal structures with an inhibitor bound to UCHL1 is limited to a co-complex with the peptide-based inhibitor VAEFMK[205] (**Figure 9**), which was soaked into apo UCHL1 crystals. It is important to note that the binding site of GK13S to UCHL1 is distinct, since VAEFMK interacts with hydrophobic residues in neighbouring copies in the crystal lattice, but not in the Ubiquitin binding cleft near the modified cysteine (**Figure 33**).

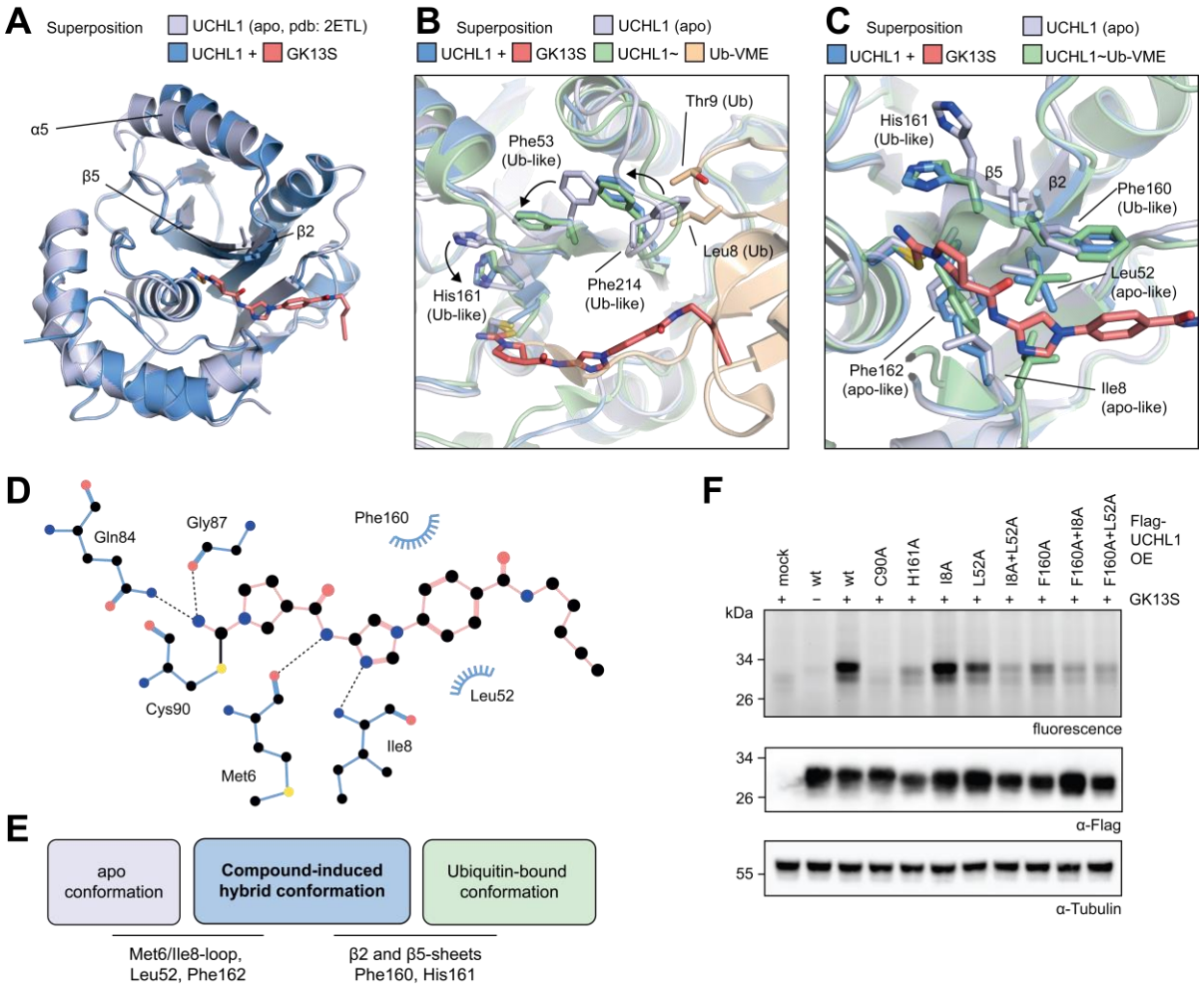

Figure 32. A compound-induced hybrid conformation underlies GK13S-mediated inhibition of UCHL1. A. Superposition of UCHL1~GK13S with UCHL1 apo (pdb: 2ETL). Secondary structure elements changed by GK13S binding are labelled. **B, C.** Superposition of UCHL1~GK13S with UCHL1 apo (pdb: 2ETL) and UCHL1~Ub-VME (pdb: 3KW5). **B.** An allosteric relay composed of Phe214, Phe53 and catalytic His161 was described previously[123] to activate the catalytic triad of UCHL1 through engaging the Leu8 loop of Ubiquitin binding when bound to the S1 site. GK13S triggers the same conformational change. Indicated residues are shown as sticks. **C.** GK13S induces a hybrid UCHL1 conformation of apo and Ubiquitin-bound states; Residues in the UCHL1~GK13S structure are labelled as either apo-like or Ub-like, depending on whether they resemble the orientation observed in the apo or the Ub-VME-bound structures, respectively. **D.** 2D representation of the ligand binding pocket observed in the UCHL1~GK13S structure. **E.** Schematic overview of structural changes underlying the GK13S-induced hybrid conformation. **F.** Validation of the binding site in cells. Indicated Flag-UCHL1 constructs with mutations in the GK13S binding site were overexpressed in HEK293 cells. Cells were treated with compound where indicated, and GK13S-bound proteins were visualised by in-gel fluorescence. The cellular assay (**F**) was performed and evaluated by MSc. M. Schmidt.

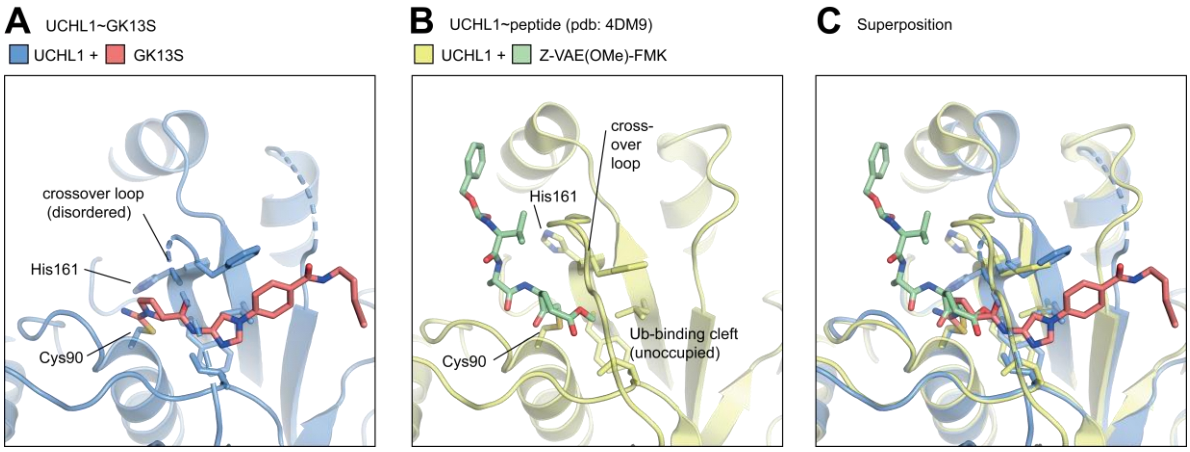

Figure 33. The binding site of GK13S to UCHL1 is distinct from that of the peptide VAEFMK. A. Close-up view of the GK13S binding site in UCHL1. The covalently targeted active-site cysteine 90 and catalytic histidine 161 are shown as sticks. **B.** Close-up view of UCHL1 bound to VAEFMK, obtained from the soaking of apo crystals (pdb: 4DM9). The peptide and the catalytic Cys90 and His161 are shown as sticks. Crossover loop and unoccupied Ubiquitin binding cleft are indicated. **C.** Superposition of **A** and **B**. Both compounds bind in opposite orientations. GK13S establishes contacts with residues of the same UCHL1 copy to which it is covalently bound. The phenyl ring in the CbZ group of the peptide inhibitor is coordinated through a crystal contact to a neighbouring copy.

3.8 Structural basis for specific inhibition of UCHL1

The co-complex structure of GK13S~UCHL1 revealed that GK13S mimics the C-terminal peptide of Ubiquitin, which is commonly recognised by DUBs, through hydrogen bonding and hydrophobic interactions. The question arose how GK13S could lead to such a high specificity in the whole proteome (**Figure 21**) and especially towards its UCH family members. The UCH family comprises UCHL3 as the closest homologue to UCHL1 as well as UCHL5 and BAP1, featuring additional C-terminal extensions to the catalytic domain with regulatory functions (**Figure 34A**). All four proteins show relatively high sequence similarity, particularly with regards to their active site (**Figure 35F** & **appendix, Figure 69**).

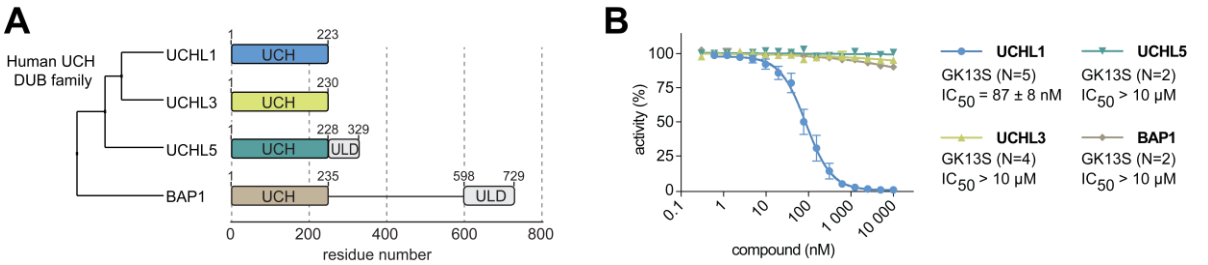

Figure 34. GK13S is UCHL1 specific within the UCH DUB family. A. Average distance alignment and schematic representation of domain architecture of human UCH family deubiquitinases. Boundaries of bacterially expressed UCH catalytic domain constructs are given. ULD, UCH37-like domain. **B.** Ub-Rho cleavage assay of indicated recombinant UCH DUBs, preincubated with GK13S dilutions for 1 h. Data points are shown as mean ± standard error from N = 2–5 independent experiments, as indicated in the figure.

In vitro LC-MS analysis (**appendix, Figure 70**) as well as a Ub-Rho assay featuring all UCH family members revealed that GK13S potently inhibits UCHL1 (**Figure 34B**). On the contrary,

no inhibition of UCHL3, UCHL5 and BAP1 at concentrations up to 1 µM could be observed. Only at concentrations near 10 µM, GK13S showed slight inhibition (~ 10%) of UCHL3 and BAP1 in the Ub-Rho assay, whereas no covalent binding could be observed during LC-MS analysis (**appendix, Figure 70**).

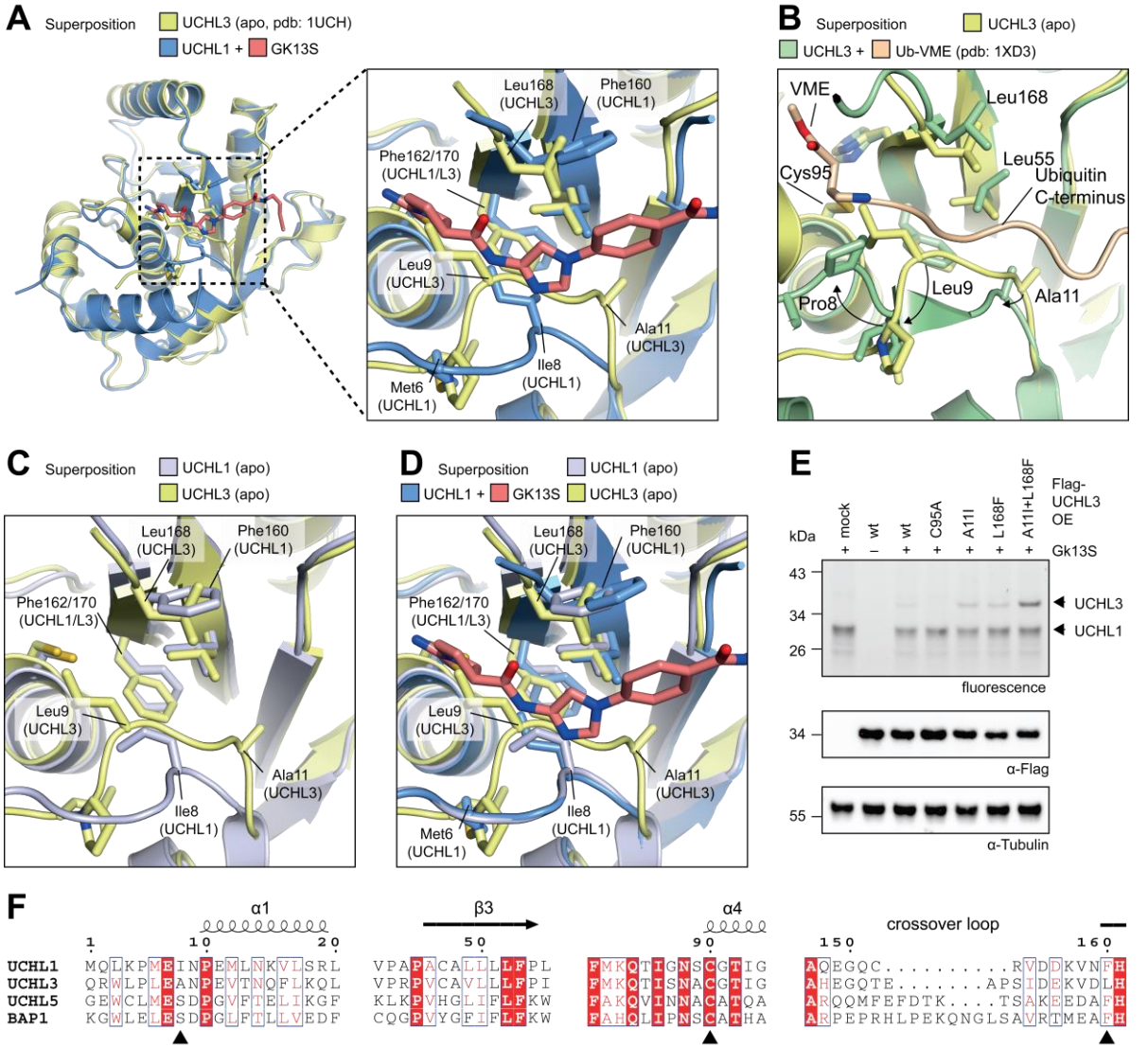

Figure 35. Structural basis for specific inhibition of UCHL1. A. Superposition of UCHL1~GK13S with apo UCHL1 (pdb: 2ETL) and apo UCHL3 (pdb: 1UCH) and close-up view of the binding pocket. Labelled residues are shown as sticks. **B.** Superposition of the equivalent to the compound binding pocket in apo UCHL3 and UCHL3~Ub-VME (pdb: 1XD3). The Ubiquitin C-terminus is shown in cartoon representation. Residues undergoing a conformational change upon Ubiquitin binding are indicated with arrows. **C, D.** Superposition and close-up view on the binding pocket of apo UCHL1 (pdb: 2ETL) and apo UCHL3 (pdb: 1UCH) (**C**) and UCHL1~GK13S (**D**). Labelled residues are shown as sticks. **E.** Indicated Flag-UCHL3 constructs with mutations introducing a GK13S binding site were overexpressed in HEK293 cells. Cells were treated with compound where indicated, and GK13S-bound proteins were visualised by in-gel fluorescence. **F.** Sequence alignment of human Ubiquitin C-terminal Hydrolase (UCH) family members. Secondary structure assignments are based on the UCHL1~GK13S structure. Black arrows indicate residues mutated in **E**.

Superposition of the GK13S~UCHL1 and apo UCHL3 structure showed that UCHL3 adopts a different conformation in its N-terminal residues (**Figure 35A**) and undergoes a distinct conformational transition upon Ubiquitin binding (**Figure 35B**). Leu9 in apo UCHL3 (corresponding to Met6 in UCHL1) is shifted into the cleft where GK13S would bind, thus sterically hinders its binding. On the contrary, binding of Ubiquitin by UCHL3 is possible, since the Ubiquitin C-terminus is able to induce a conformational change, shifting down Leu9 and thereby activating UCHL3 for Ubiquitin binding (**Figure 35B**). Further, the large hydrophobic Ile8 in UCHL1 is able to form a hydrophobic pocket for the pyrrolidine ring of GK13S, whereas the corresponding residue Ala11 in UCHL3 lacks hydrophobicity, further reducing optimal binding conditions (**Figure 35C-D**). In UCHL3, Leu168 forms a different environment for the phenyl ring of GK13S than the more hydrophobic Phe160 in UCHL1, which is potentially further stabilising ligand binding via π-π-stacking. These results suggest that the specificity of GK13S to UCHL1 relies on the aromatic Phe160 side chain and a specific apo conformation triggered by Ile8. To test this hypothesis, UCHL3 was overexpressed in HEK293 cells with point mutations in these residues, exchanged to the corresponding residues in UCHL1 and screened for potential GK13S binding (**Figure 35E**). Whereas both wt UCHL3 and catalytically inactive UCHL3 (C95A mutant) did not show any GK13S binding, as expected, the introduction of a point mutation in Ala11 to the corresponding residue Ile8 in UCHL1 (A11I) displayed weak binding of GK13S. Similar inhibition could be achieved by mutating Leu168 in UCHL3 to the aromatic Phe160 (L168F). A double mutation of both A11I and L168F led to potent binding of GK13S (**Figure 35E**). To confirm these results, binding of GK13S to wt UCHL3 and all three mutants was evaluated in a Ub-Rho cleavage assay (**Figure 36A**). Accordingly, GK13S did not show any binding to wt UCHL3 (IC_{50} > 100 µM), whereas both single mutations resulted in near identical IC_{50} values of ~ 30 µM. The double mutant was able to be inhibited by GK13S with a 3-times lower IC_{50} of 11 µM, consistent with the binding observed in the gel-based assay (**Figure 35E**).

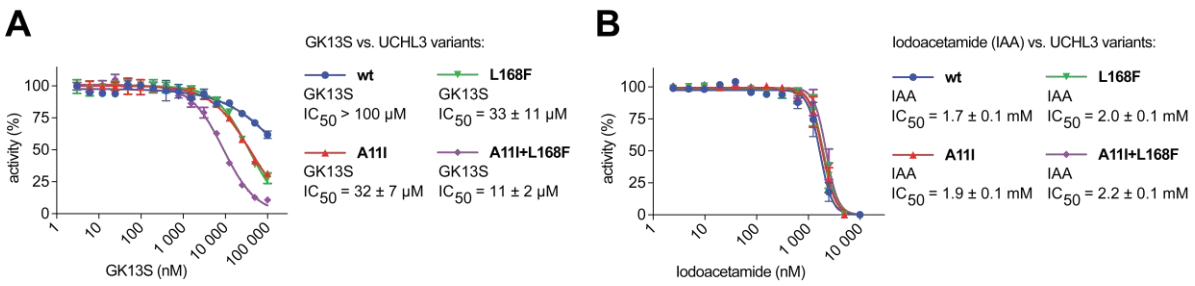

Figure 36. Functional mutation of the UCHL3 active site enables binding of GK13S. A. Inhibitory potencies of GK13S against indicated UCHL3 catalytic domains determined from Ub-Rho cleavage assays. IC_{50} values were determined from 3 independent experiments. Data are shown from a representative experiment as mean ± SD. **B.** Inhibitory potencies of iodoacetamide (IAA) against indicated UCHL3 catalytic domains determined from Ubiquitin-Rhodamine cleavage assays. IC_{50} values were determined from 3 independent experiments. Values are plotted as mean ± standard error from 3 independent experiments.

Although the double mutant still displayed a lower potency than wt UCHL1, these results suggest that the UCHL1-specific “inhibition-competent” conformation can at least partially be triggered by these mutations in UCHL3. In contrast, the non-specific alkylating agent iodoacetamide inhibited all UCHL3 variants with similar potency, indicating that the binding of GK13S to UCH enzymes is not primarily driven by the chemical reactivity of the catalytic cysteine (**Figure 36B**).

UCHL5 activity is allosterically regulated through conformational changes upon interaction with the proteasome and regulatory complexes. In the proteasome-unbound state, UCHL5 is part of the auto-inhibiting INO80 complex. Activation can only be achieved by adaptors, such as INO80G, leading to structural rearrangements in UCHL5, resulting in inhibition of INO80 and thus activation of UCHL5. Furthermore, the apo state of both the full-length and catalytic domain structures of UCHL5, as well as its complex with INO80G, exhibits an occupied cleft that is not suitable for GK13S binding (**Figure 37**). Additionally, substitution of Ile8 with a smaller and polar serine (Ser13 in UCHL5 or Ser10 in BAP1) likely interferes with the hydrophobic coordination of the pyrrolidine as the space is occupied by a phenylalanine (**Figure 37**). These differences likely explain why GK13S does not bind to UCHL5 or BAP1.

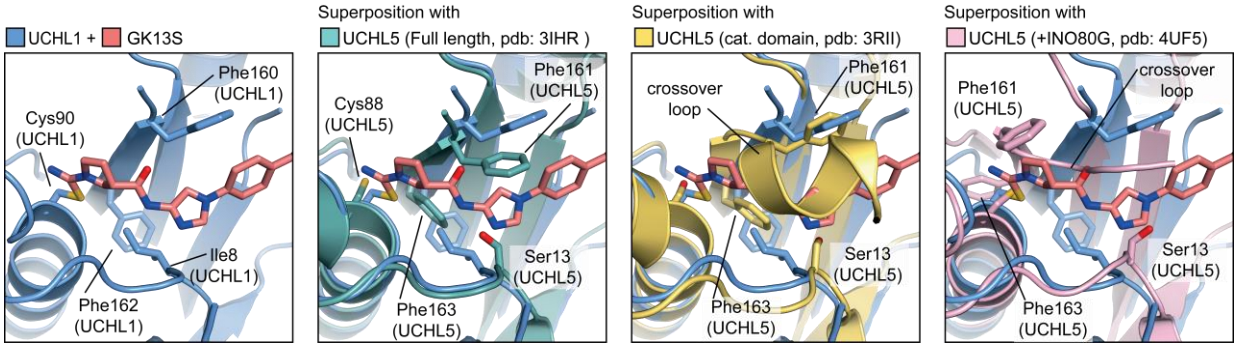

Figure 37. Structural features of UCHL5 and associated domains block binding of GK13S. Close-up view of the binding pocket of UCHL1~GK13S (left panel) and superposition with full-length UCHL5 (pdb: 3IHR), the catalytic domain of UCHL5 (pdb: 3RII) and UCHL5 in co-complex with an inhibitory fragment of INO80G (pdb: 4UF5) (from left to right).

Taken together, the crystal structure of UCHL1 in co-complex with the probe GK13S revealed detailed information about a novel UCHL1-specific conformation with subtle differences on both sides of the catalytic cleft in the binding pocket. In combination with the illustrated conformational adaptivity of UCHL1, this accounts for the in-class specificity of GK13S towards the UCH family of proteins. The study further demonstrated that UCHL1 inhibition by GK13S is not driven by increased reactivity or abundance of UCHL1, but is based on specific interactions in the active site.

4 Conclusion (Project 1)

DUBs are enzymes that play a crucial role in the regulation of protein function by removing Ubiquitin from proteins. Aberrant regulation of DUB activity has been implicated in a variety of diseases, making them attractive targets for the development of drugs. Among the various families of DUBs, the UCH family, including UCHL1, is particularly well-studied and is known to be involved in several diseases, including neurodegeneration, cancer, and autoimmune disorders. Despite its manifold associations with diseases and disease relevant pathways, the lack of selective and potent small molecule inhibitors or ABPs has hindered a comprehensive understanding of how UCHL1 is involved in in these pathways.[155]

In the first part of this dissertation, a selected panel of putative covalent, structurally diverse nitrile-based DUB activity-based probes was designed and synthesised, based on patent-derived inhibitors (**Figure 15A**). Cellular activity-based protein profiling in combination with a Ub-VS competition assay (**Figure 19**) revealed prominent DUB-binding of the probe GK13S, derived from an inhibitor targeting UCHL1.

A set of probes based on GK13S was established, featuring the corresponding (*R*)-isomer, inactive controls (lacking the warhead) GK12R and GK12S as well as minimal probes (featuring only warhead and alkyne handle) GK16R and GK16S (**Figure 20**). The set of probes was used for detailed *in vitro* and cellular studies, revealing that GK13S, but not the control probes, potently inhibits recombinant and cellular UCHL1 (**Figure 22** - **Figure 25**). This concludes that UCHL1 binding is only possible when both, the specificity element and warhead are present and further underlines the preference of UCHL1 towards inhibitors featuring a 3-carboxy-*N*-cyanopyrrolidine warhead in (*S*)-configuration.

A proteomics-based target identification approach revealed that UCHL1 is the highest enriched protein by the probe GK13S in HEK293 cells (**Figure 21C** & **appendix, Figure 63**). A number of non-DUB proteins could be identified with PARK7 being the second highest enriched protein, followed by the PARK7 family member C21orf33 as well as the aldehyde dehydrogenases ISOC1 and NIT2. The comparison of GK13S to GK16S-enriched proteins (**Figure 21C**) indicated that GK16S binds to all targets of GK13S, but showing significantly less enrichment of UCHL1. The large difference in the potencies of GK13S and GK16S both *in vitro* and in cells allowed for formation of a chemogenomic pair of probes for the specific investigation of cellular UCHL1.

The comparison of the reaction mechanisms of endogenous PARK7 and C21orf33 substrates to their irreversible reactions with GK16S (**Figure 38**) revealed that 3-carboxy-*N*-cyanopyrrolidines and glutamine both have a similar size and connection between their

electrophilic centre and carbonyl group. The findings suggest that these off-target proteins primarily respond in a reactivity-driven manner due to the electrophilic nature of the cyanamide warhead. Further studies examining cyanamides with different geometries will be necessary to clarify their target range, substrate recognition, and cellular distribution of these and other targets.

A comparison of the established set of 3-carboxy-*N*-cyanopyrrolidine probes with the 2-carboxy-*N*-cyanopyrrolidine CG173 revealed that CG173, but not GK13S or GK16S induced cell death in HEK293 and U-87 MG cells at concentrations of up to 5 µM and an incubation time of up to 72 h (**Figure 26** & **appendix, Figure 67**). As many cell lines were shown to be viable following UCHL1 knockout[183], these data indicate non-UCHL1-related toxicity of CG173 and related compounds. The *in vitro* binding of CG173 to UCHL1 shows modification of both the catalytic Cys90 and hyperreactive Cys152 (**Figure 25E**), implying a high compound reactivity, which is is consistent with the strong binding to UCHL1 observed in the Ub-Rho assay (**Figure 25D**). On the contrary, CG173 shows less stabilisation of recombinant UCHL1 compared to GK13S (**Figure 25C**) and only weak inhibition of cellular UCHL1 that decreases over time with longer incubation (**Figure 25F**). Whether this behaviour and toxicity are common features of the 2-carboxy-*N*-cyanopyrrolidine scaffold, requires further investigation using larger compound libraries.

Genetic studies have established a connection between UCHL1 and neurodegeneration.[137] Reduced levels of mono-Ubiquitin have been observed in the brain tissue of a UCHL1 mutant mouse[112,132], which had been previously investigated in a monkey cell line[203] where mutant UCHL1 was overexpressed. The probe pair GK13S+GK16S was successfully applied in the human glioblastoma cell line U-87 MG showing that GK13S, but not GK16S phenocopies a UCHL1 mutant mouse by upregulation of free Ubiquitin levels upon inhibtion of UCHL1 (**Figure 28**). This validates the chemogenomic probe pair for studying cellular UCHL1 and establishes U-87 MG cells as a model system for UCHL1-dependent phenotypes. Since GK13S binds to the catalytic cysteine of UCHL1, blocking engagement with Ubiquitin, it not only inhibits its catalytic function, but potentially also other non-catalytic functions. Therefore it cannot be determined whether the observed reduced levels of Ubiquitin are due to inhibition of the hydrolase activity of UCHL1, decreasing the processing of its substrates, or due to reduced binding of free Ubiquitin. A potential function of the large amounts of cellular UCHL1 might be the regulation of free Ubiquitin levels, thereby acting as kind of molecular rheostat to determine global Ubiquitination activities. Further investigations are required to understand these mechanisms and the link to neurodegeneration.

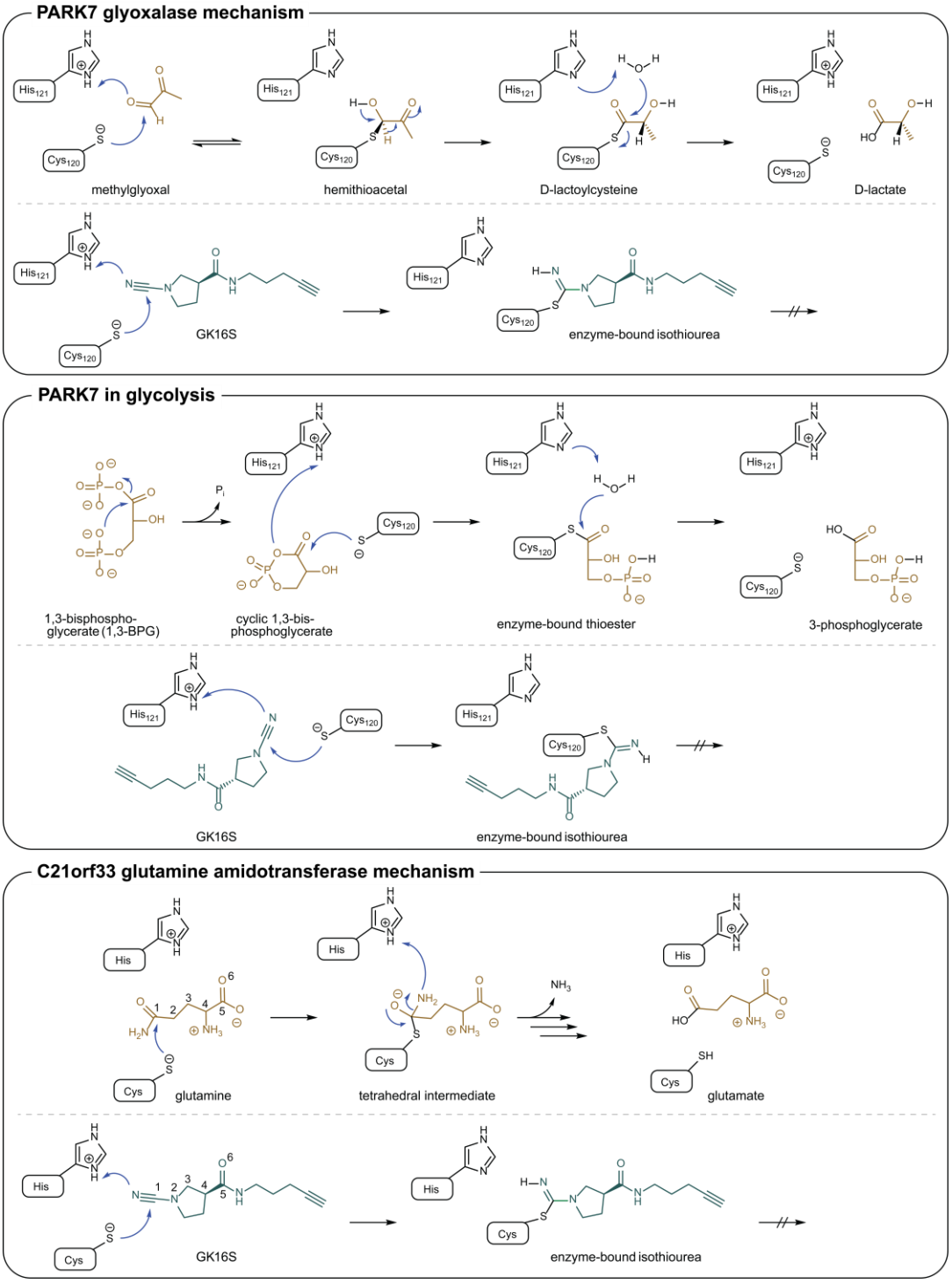

Figure 38. Potential chemical basis for cross-reactivity of cyanamide-containing probes with PARK7 and C21orf33/GATD3. PARK7 glyoxylase mechanism[206] Methylglyoxal is attacked by the active site cysteine forming a reversible hemithioacetal. Proton transfer and subsequent hydrolysis lead to release of D-lactate and free catalytic cysteine. **PARK7 in glycolysis.**[207] PARK7 prevents phosphoglycerate modifications on proteins from reactive cyclic-1,3-phosphoglycerate by forming a reversible enzyme-bound thioester, followed by hydrolysis to yield 3-phosphoglycerate. Minimal probe GK16S is proposed to be attacked by the active site cysteine of PARK7 in a similar manner, forming an irreversible isothiourea. **C21orf33 glutamine amidotransferase mechanism.**[208] Deamidation of glutamine proceeds via a tetrahedral intermediate and release of ammonia. GK16S displays a similar size and chemical characteristics as the glutamine substrate (indicated by the numbers) and thereby is proposed to be recognised by C21orf33 in a similar manner.

X-ray crystallography was used to solve the 2.24 Å crystal structure of UCHL1 in co-complex with GK13S (**Figure 30**). The structure was compared with those of apo UCHL1 (**Figure 32**) and other members of the UCH family, including UCHL3 (**Figure 35**) and UCHL5 (**Figure 37**), to identify the differences that contribute to the specificity of GK13S towards UCHL1. The apo conformation of UCHL1 presents an unaligned catalytic triad and a partially occupied binding cleft. However, when the globular part of Ubiquitin engages, it triggers a conformational change that aligns the triad and opens the cleft, making it capable of directing the Ubiquitin C-terminal LRGG peptide to the catalytic cysteine. GK13S mimics the C-terminal peptide through key hydrogen bonding and hydrophobic interactions (**Figure 31**) and specifically inhibits UCHL1 by locking the enzyme in a hybrid conformation of apo and Ubiquitin-bound states (**Figure 32**).The specific inhibition of UCHL1 by GK13S is the result of a combination of (I) the conformational plasticity of UCHL1, which allows it to form a complex with GK13S, (II) the apo UCHL1 structure that creates a unique binding site for GK13S, by positioning its pyrrolidine in a pocket unique to the apo conformation of UCHL1 (**Figure 32A-C**) and (III) the subtle differences in the binding pocket on both sides of the catalytic cleft within the UCH family of DUBs (**Figure 35D-F** & **Figure 37**).

5 Structural basis for enhanced piperazine-specific inhibition of UCHL1 (Project 2)

The highly potent and well-characterised probe GK13S, together with its chemogenomic probe pair GK16S, has been shown in part 1 of this thesis to allow the specific study of cellular UCHL1, and thus offers a promising pharmacological tool to advance knowledge of how UCHL1 is involved in disease-relevant pathways. However, both probes share a common off-target with almost all other *N*-cyanopyrrolidine-based and UCHL1-targeting probes known in the literature: PARK7. Given that both UCHL1 and PARK7 are implicated in neurodegenerative diseases, the proper function of (some) UCHL1-related pathways may depend on the activity of PARK7. In this case, binding of GK13S to PARK7 would not preclude misinterpretation of probe-based UCHL1 inhibition results.

5.1 Design of GK13S analgoues to enhance UCHL1 selectivity

Covalent inhibitor engagement is first driven by molecular recognition between specificity element and target protein, followed by covalent bond formation between the electrophilic warhead and a nearby nucleophilic residue.[209] Since GK13S and GK16S both bind PARK7 and share the common structural feature of a 3-carboxy-*N*-cyanopyrrolidine, the next aim was to modify this warhead in order to prevent PARK7 binding, while still preserving UCHL1 activity. While information regarding the binding environment of GK13S in UCHL1 were available from the established co-crystal structure (**Figure 39A**), detailed information of 3-carboxy-*N*-cyanopyrrolidines binding to PARK7 were not available at that time[210]. In order to compare the binding of 3-carboxy-*N*-cyanopyrrolidines to both UCHL1 and PARK7 and to structurally design new inhibitors, co-crystallisation of PARK7 with the chemogenomic probe GK16S was established. Various co-crystallisation efforts led to a crystallisation condition from which the structure of PARK7 in complex with GK16S was solved to a resolution of 1.53 Å resolution (**Figure 39B**).

GK16S is bound covalently to the catalytic cysteine Cys106 of PARK7 and occupies a well defined, narrow binding pocket, formed in particular by residues Glu18, Arg48, Asn76, His126, Leu128 and Pro158 (**Figure 39B**). In comparison, UCHL1 displays a rather broad active site, especially located around the warhead of GK13S, defined by residues such as Pro5, Met6, Gln84, Gly87, Asn88 and Asn159 (**Figure 39A** & **Figure 30E-F**). Size and binding-angle of a compound might be rather limited by the small crossover loop of UCHL1, which results in a tube-like binding cleft (**Figure 30A,D** & **Figure 31A**). Considering both co-crystal structures, substitutions at the pyrrolidine warhead of GK13S might be able to occupy available space in UCHL1 (**Figure 39A**), that might not be accessible in the well-defined active site of PARK7

(**Figure 39B**). The pyrrolidine C5-atom of GK13S for instance, might be able to occupy a cleft formed by UCHL1 residues Gln84, Gly87 and Arg178, whereas PARK7 binding seems to be hindered by surrounding residues His126 and Leu128. This could lead to an improved UCHL1 over PARK7 selectivity by promoting UCHL1- and at the same time reducing PARK7-binding.

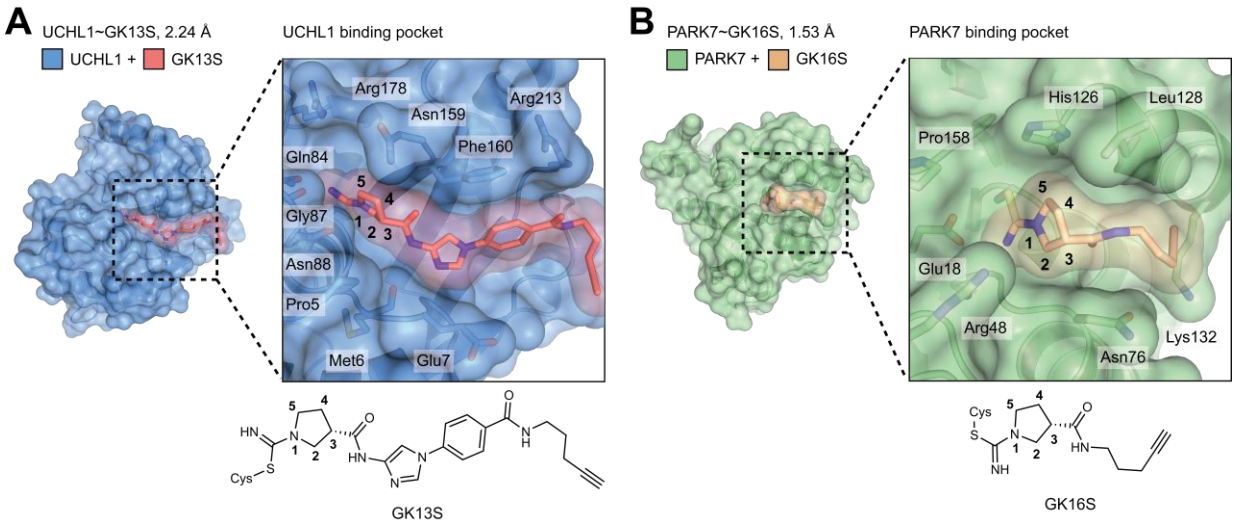

Figure 39. A,B. Structural comparison of warhead-to-protein binding between UCHL1~GK13S (A) and PARK7~GK16S (B). A. Structure of UCHL1 (blue) in complex with GK13S (red) and zoom into the binding cleft occupied by GK13S (right panel) with important structural residues indicated. **B.** Structure of PARK7 (green) in complex with GK16S (gold) and zoom into the binding cleft occupied by GK16S (right panel) with important structural residues indicated.

A patent by Kemp et al.[181] reveals additional information about potential pyrrolidine ring extensions at truncated analogues of GK13S (**Figure 40**). A methyl group in (*S*)-configuration at the pyrrolidine C2-position of cpd74 retains potent binding to UCHL1. Inhibitors with methyl- and ethyl-substituents at the pyrrolidine C4-position (cpd85 and cpd87) also show UCHL1 binding, although with reduced affinity. These results indicate the potential of GK13S derivatisation at the pyrrolidine C2- and C4-position while at least partially retaining UCHL1 activity.

compound	reported activity (µM)
cpd41	< 1
cpd74	< 1
cpd85	1 - 10
cpd87	1 - 10

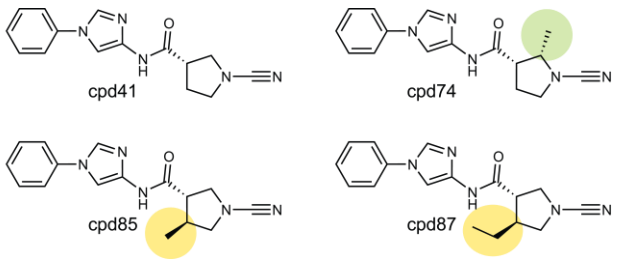

Figure 40. Structure-activity relationship of selected, patent-derived[181] and UCHL1 binding compounds featuring a 3-carboxy-*N*-cyanopyrrolidine warhead. The GK13S-analogue Cpd41 (partially) retains UCHL1 potency upon derivatisation at the pyrrolidine C2- (cpd74) and C4-atom (cpd85 and cpd87).

Based on this information, GK13S-analogues CG287, CG288, CG385-*anti*, CG385-*syn* and CG390, with modifications at different pyrrolidine C-atoms were designed (**Figure 41**) to test their influence on UCHL1 affinity and selectivity *in silico*.

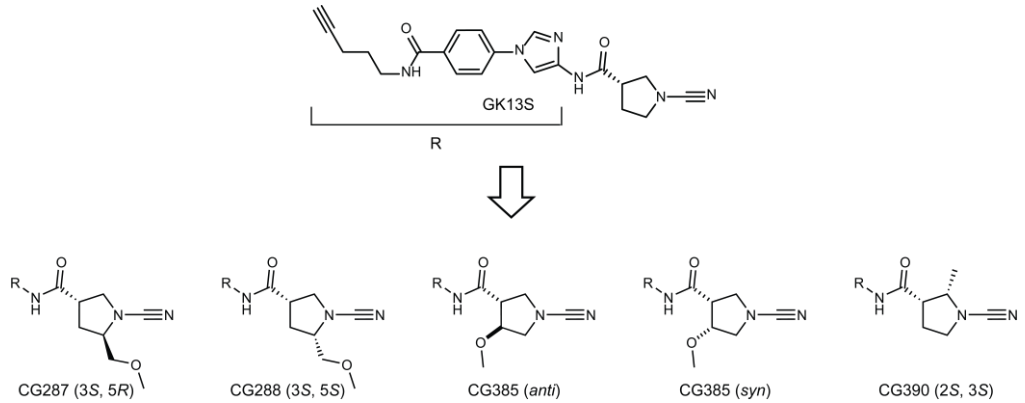

Figure 41. Chemical structures of GK13S-derived probes with modifications on different pyrrolidine C-atoms to evaluate positive and negative influences on UCHL1 and PARK7 binding respectively. R = specificity element and alkyne handle.

The lack of a suitable enantiopure educt to introduce a methoxy group at the C3-position led to the racemic design of CG385-s*yn* and CG385-*anti*. Although the (*R*)-isomer of GK13S (GK13R) only showed very weak targeting of UCHL1 (**Figure 22**), the binding analysis of CG385, containing 50% of the active (*S*)-conformation, will still be able to inform about the selectivity difference between UCHL1 and PARK7.

To verify, if the designed probes are potentially able to bind UCHL1, the software *LigandScout* was used to perform a structure-based docking into the binding cleft of UCHL1, based on the covalently bound GK13S in UCHL1~GK13S. The binding cleft residues were kept static during docking, allowing an alignment of all docking-poses to visualise and analyse the influence of different ring extensions (**Figure 42A**). All probes were able to be fitted into the binding cleft of UCHL1 and showed similar positioning of both specificity element and warhead in comparison to GK13S (**Figure 42A-D**), while occupying additional space. The docking pose of CG287 (**Figure 42B**) shows that the (*R*)-configurated methyl-methoxy group in C5-position of CG287 could be able to engage an unoccupied cleft below Asn88, whereas the (*S*)-configurated methyl-methoxy group of CG288 might be able to occupy a cleft formed by UCHL1 residues Gln84, Gly87 and Arg178 (**Figure 42C**). The methyl-group in C2-position of CG390 (**Figure 42F**) was calculated to fit perfectly into a small cavity below Asn159, whereas docking of CG385-*anti* positioned its methoxy-group in C4-position pointing out of the binding pocket of UCHL1 (**Figure 42E**). While the warheads of most probes showed very similar positioning compared to GK13S (**Figure 42A**), docking of CG385-*syn* was only possible by shifting the warhead to the lower part of the binding pocket, potentially hindering UCHL1 binding (**Figure 42D**).

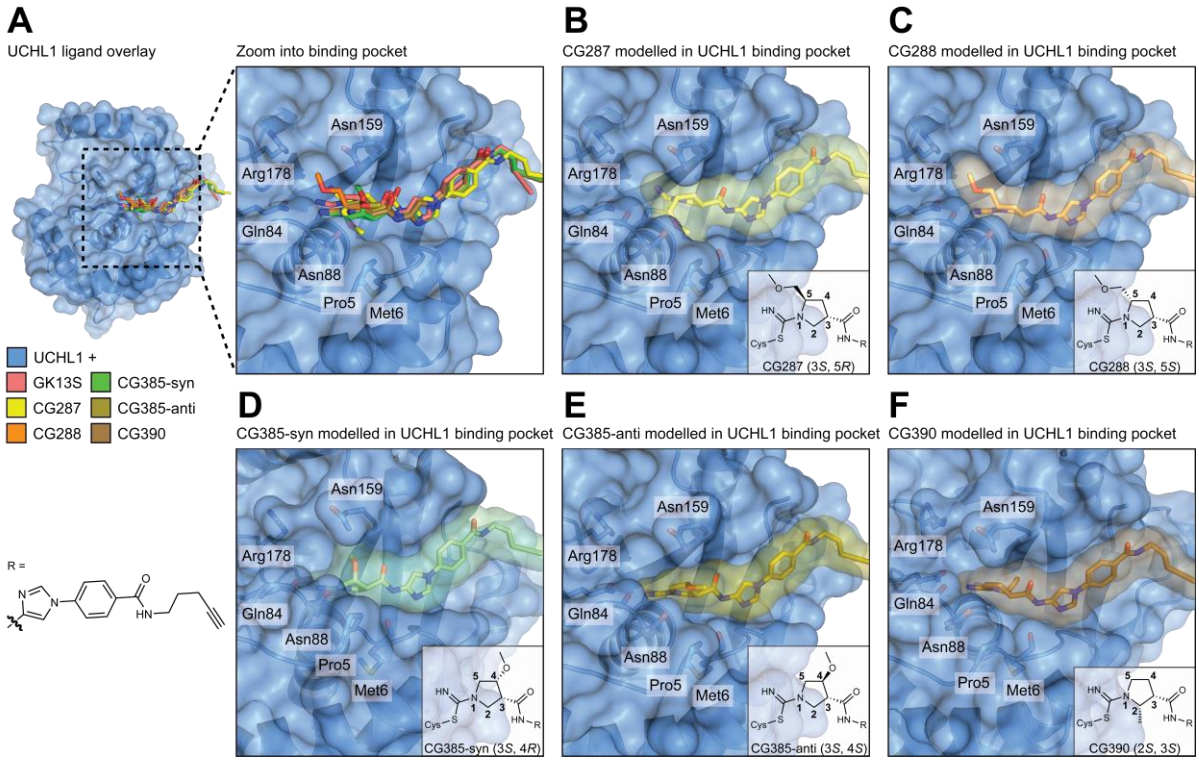

Figure 42. Modelling of *N*-cyanopyrrolidine analogues of GK13S in the binding cleft occupied by GK13S. A. Superposition of modelled probes CG287 (yellow), CG288 (orange), CG385 (*syn*) (green), CG385 (*anti*) (olive) and CG390 (brown) with GK13S (white) in complex with UCHL1 (blue). **B-F.** Individual structures of probes CG287 (**B**), CG288 (**C**), CG385 (*syn*) (**D**), CG385 (*anti*) (**E**) and CG390 (**F**) with ligand surface, fitted into the binding cleft of UCHL1. Probes were generated with the structure-based interface of *LigandScout*, based on GK13S in the co-crystal structure of UCHL1~GK13S, followed by energy minimization (MMFF94 force field). The superposition was carried out by aligning the resulting UCHL1~ligand structures with UCHL1~GK13S. The energy minimization was performed without changing the protein environment.

With the exception of CG385-*syn*, all of the designed probes were then synthesised. Synthesis followed a similar reaction sequence as described for GK13S (**Figure 43A**), requiring 1) the shared intermediate GK07 and 2) acid-functionalised building blocks with different ring substitutions (**Figure 43B**).

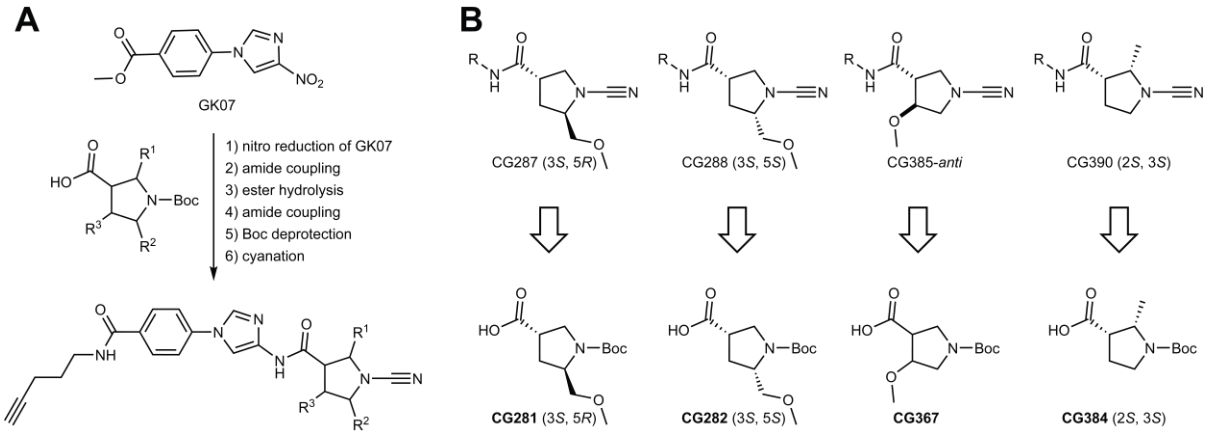

Figure 43. Synthesis of 3-carboxy-*N*-cyanopyrrolidine-based GK13S analogues. A. Schematic representation of the reaction sequence for the synthesis of GK13S analogues, comprising 1) nitro-reduction of GK07 to the corresponding amine, 2) amide coupling with acid-functionalised building blocks, 3) ester hydrolysis of the methyl benzoate-group to the corresponding benzoic acid, 4) subsequent amide coupling with pent-4-yn-1-amine, 5) acidic Boc-deprotection and final 6) cyanation using BrCN. **B.** Acid-functionalised building blocks as starting points for the synthesis of 3-carboxy-*N*-cyanopyrrolidine-based GK13S analogues.

5.2 Synthesis of 3-carboxy-*N*-cyanopyrrolidine-based GK13S analogues

The synthesis of building blocks CG281 and CG282 followed a similar reaction sequence starting at either 1-(*tert*-butyl) 2-methyl (2*R*,4*R*)-4-hydroxypyrrolidine-1,2-dicarboxylate for the synthesis of CG281 or its (2*S*,4*R*)-analogue for CG282 (**Scheme 11**). Via tosylate activation and subsequent nucleophilic substitution with sodium cyanide (**a**), the hydroxy group was converted to a cyanide with inversion of the stereo configuration, as judged by distinct chemical shifts in the NMR spectra compared to the corresponding (2*R*,4*S*)- and (2*S*,4*S*)-diastereomer (methods, CG243 and CG245, respectively). Selective ester to alcohol reduction in presence of the cyanide group was performed with lithium borohydrate (**b**). Methylation of the resulting hydroxy group by methyl iodide resulted in the formation of CG273 and CG274 (**c**). In a Pinner reaction, the nitrile was converted under acid catalysis into an imino ester salt (Pinner salt), immediately reacting in a nucleophilic addition with excess of methanol to the corresponding methyl ester (**d**). Basic ester hydrolysis with 2M lithium hydroxide gave the acid building blocks CG281 and CG282 (**e**). Comparison of ^{1}H NMR spectra after peak assignment revealed that after ester reduction of CG244 (**b**) nearly 40% of the *cis*-oriented CG247 (2*S*,4*S*) epimerised to its *trans* (2*S*,4*R*)-enantiomer. A hydride ion, formed by $LiBH_4$, is able to react not only as a nucleophile, as intended in the ester reduction, but also as a base, probably being able to deprotonate the cyanide αH-atom of CG244. Since the corresponding carbanion can be re-protonated from both sides, this would lead to a loss of stereo information. This hypothesis was further confirmed by NMR evaluation of CG274, where 50% of the wrong *trans*-oriented product (2*S*, 4*R*) could be detected, probably due to the use of the strong base NaH. Likewise, the presence of nearly 50% of the wrong *cis*-oriented product (2*R*,4*R*) could

be detected for its diastereomer CG274. Surprisingly, the ^{1}H NMR spectrum of CG276 (3*S*,5*S*) shows 70% epimerisation to the wrong *trans*-product (3*R*,5*S*), whereas the spectrum of its diastereomer CG275 (3*S*,5*R*) only shows 25% of the wrong *cis*-product (3*R*,5*R*), suggesting a *trans*-preference probably due to sterically hindrance of the *cis*-configuration.

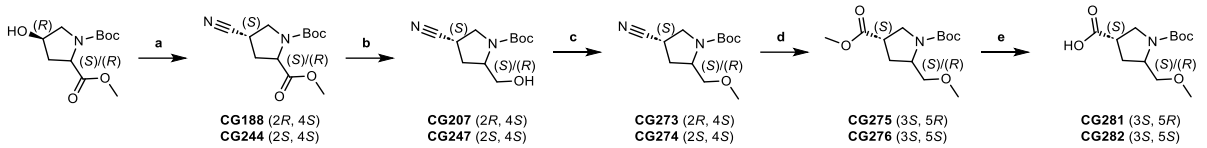

Scheme 11. Synthesis of acid-functionalised building blocks CG281 and CG282. a. 1) TsCl, Et_3N, DCM, 0°C -> rt, on. 2) NaCN, DMSO, 60°C, on. CG188: 55%; CG244: 70%. **b.** 2M $LiBH_4$ in THF, 0°C, 4.5 h. **c.** MeI, NaH, THF, rt, 3.5 h. CG273: 47% over two steps; CG274: 48% over two steps. **d.** 1) 4M HCl in 1,4-dioxane, MeOH, rt, on. 2) Boc_2O, sat. aq. $NaHCO_3$, EA, rt, 12 h. CG275: 86%; CG276: 59%. **e.** 2M LiOH, 1,4-dioxane, 50°C, 3 h. CG281: quant.; CG282: quant. As no literature was found for the coherent and stereoselective synthesis of CG281/CG282, the synthetic procedures for steps **a**[211], **b**[212], **c**[213], and **d**[214] were adapted from individual references describing the same (**a**) or similar (**b**-**d**) structures.

Both acid building blocks CG281 and CG282 were reacted in an amide coupling reaction with GK07, after previous palladium catalysed nitro-group reduction, resulting in the formation of CG283 and CG284, respectively (**Scheme 12a**).

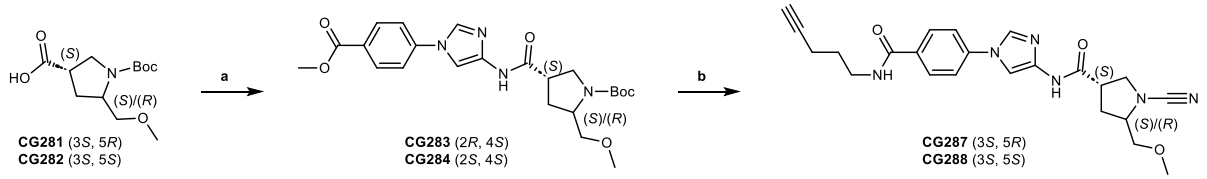

Scheme 12. Synthesis of final probes CG287 and CG288. a. 1) GK07, H_2, Pd/C, EtOH, rt, 4 h. 2) HATU, DIPEA, DMF, rt, on. CG283: 85%, CG284: 53%. **b.** 1) 2M LiOH, 1,4-dioxane, 50°C, 6 h. 2) pent-4-yn-1-amine HCl, HATU, DIPEA, DMF, rt, 2 h. 3) 20% TFA in DCM, rt, 1 h. 4) BrCN, K_2CO_3, DCM, 0°C -> rt, 2 h. CG287: 2%, CG288: 1%. Although the compounds CG287 and CG288 are novel, the synthetic procedures shown are based on appropriate methods from the patent WO2016046530A1[181].

Ester hydrolysis of the methyl benzoate-group to the corresponding benzoic acid, amide coupling with pent-4-yn-1-amine, acidic Boc-deprotection and final BrCN reaction led to the desired probes CG287 and CG288 (**b**), featuring a methoxy-methyl group in C2-position of the pyrrolidine ring. Even after thorough selection of pure fractions after preparative HPLC purification of both CG284 and CG288 (**Scheme 12**), isolation of pure CG288 (3*S*,5*S*) could not be achieved, as 25% of the epimerised (3*R*,5*S*)-product was detected in the ^{1}H NMR spectrum. Due to its poor purity of 75%, CG288 was excluded from further biological testing. For CG287 a high purity of >95% (<5% (3*R*,5*R*)-product), as judged by NMR analysis, could be achieved, yielding sufficient amounts for further biological characterisation.

Although the synthesis of racemic pyrrolidines such as CG367 (**Figure 43B**) by [3+2] cycloaddition is known from the literature[215,216], the acid building block CG367 (**Scheme**

13) was synthesised using a reaction sequence that later allowed functionalisation of the hydroxy group of CG216 (cf. CG238, Chapter 6). Selective reduction of the keto group of 1-(*tert*-butyl) 3-ethyl 4-oxopyrrolidine-1,3-dicarboxylate with sodium borohydride (**a**), basic ester hydrolysis (**b**) and subsequent methylation of the hydroxy group (**c**) led to the formation of CG367. LC-MS analysis of pure CG180 revealed the formation of both chemically different diastereomers *syn*- and *anti*-CG180, by showing two peaks with identical product mass. However, no separation during the purification step was possible.

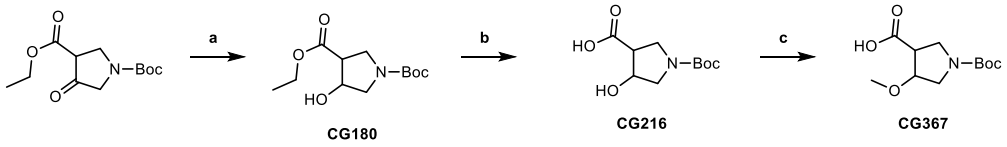

Scheme 13. Synthesis of acid-functionalised building block CG216. a. $NaBH_4$, MeOH, 0°C, 6 h, pH 3-4, 86%. **b.** 2M LiOH, 1,4-dioxane, 60°C, 4 h, quant. **c.** MeI, NaH, THF, 0°C -> rt, on. As no literature was found for the coherent synthesis of CG367, the synthetic procedures for steps **a**[217], **b**[218] and **c**[213] were adapted from individual references describing the same (**a**) or similar (**b**, **c**) structures.

In an identical sequence of reactions as described for CG283 and CG284, CG367 was converted into CG373 (**Scheme 14a**). Both *syn*- and *anti*-diastereomers were successfully separated by preparative HPLC, the latter being subsequently reacted to the final probe CG385-*anti*, hereinafter referred to as CG385.

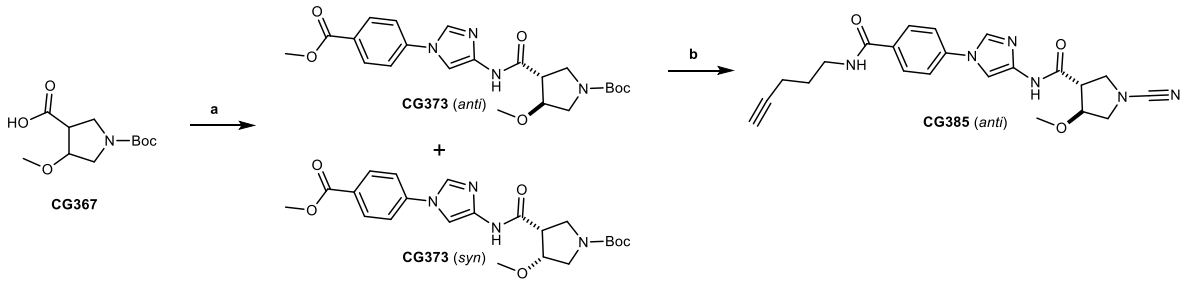

Scheme 14. Synthesis of final probe CG385 (*anti*). a. 1) GK07, H_2, Pd/C, EtOH, rt, 5 h. 2) HATU, DIPEA, DMF, rt, on. CG373 (*anti*): 7%, CG373 (*syn*): 8%. **b.** 1) 2M LiOH, 1,4-dioxane, rt, on. 2) pent-4-yn-1-amine HCl, HATU, DIPEA, DMF, rt, on. 3) 20% TFA in DCM, rt, 2 h. 4) BrCN, K_2CO_3, DCM, rt, 2 h, 32%. Although the compounds CG373 and CG385 are novel, the synthetic procedures shown are based on appropriate methods from the patent WO2016046530A1[181].

Even after thorough selection of pure fractions after preparative HPLC, as judged by LC-MS, an impurity of 4% could be observed in the ^{1}H NMR spectrum of CG385, characterised as the elimination product 1-cyano-*N*-(1-(4-(pent-4-yn-1-ylcarbamoyl)phenyl)-1*H*-imidazol-4-yl)-2,5-dihydro-1*H*-pyrrole-3-carboxamide (CG385 impurity, **Scheme 15**) as judged by 1D- and 2D-NMR analysis. Characteristic chemical shifts in the ^{1}H NMR spectrum of CG385 such as the alkene proton H^1 [δ = 6.91 ppm (s, 1H)] (**Scheme 15**) as well as the chemically equivalent pyrrolidine protons H^2 [δ = 4.48 ppm (s, 4 H) could be assigned to the impurity. With an overall purity of 96%, CG385 was suitable for further biological characterisation.

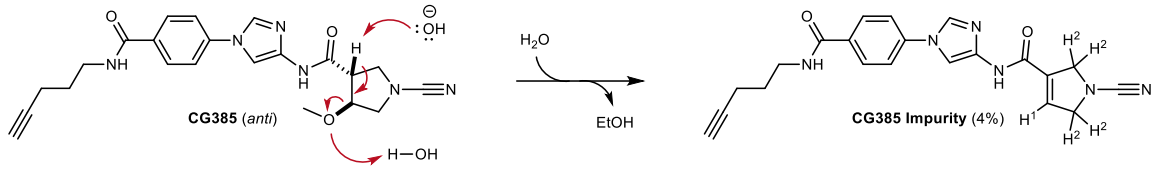

Scheme 15. Proposed elimination mechanism of CG385. Protons of the impurity with characteristic chemical shifts in the ^{1}H NMR spectrum are assigned.

The preparation of chiral pyrrolidine CG384 (**Scheme 16**) started with a nucleophilic substitution of methyl 3-oxobutanoate and 1,2-dibromoethane (**a**), followed by a condensation reaction with the chiral auxiliary (*S*)-1-phenylethan-1-amine (**b**), yielding the 4,5-dihydro-1*H*-pyrrole CG366. The chiral auxiliary allowed for subsequent stereoselective pyrrole reduction to the corresponding pyrrolidine CG372 (**c**), followed by palladium catalysed cleavage of the auxiliary and Boc-protection of the resulting free amine (**d**). Basic ester hydrolysis using 2M lithium hydroxide yielded acid building block CG384 (**e**).

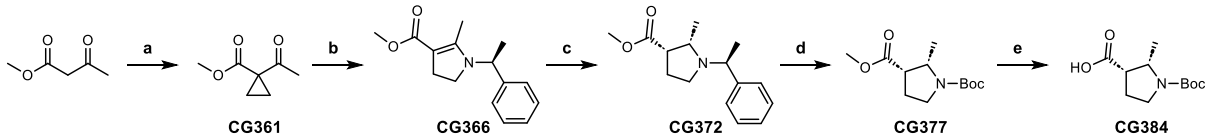

Scheme 16. Synthesis of acid-functionalised building block CG384 based on patent WO2016046530A1[181]. a. 1,2-dibromoethane, K_2CO_3, acetone, 70°C, on, 30%. **b.** (*S*)-1-phenylethan-1-amine, toluene, 130°C, on, 61%. **c.** $NaBH(OAc)_3$, AcOH, ACN, 0°C, 5 h, recrystallisation, 63%. **d.** 1) Pd/C, H_2, EtOH, rt, on. 2) THF, sat. aq. $NaHCO_3$, Boc_2O, rt, 4 h, 84%. **e**. 2M LiOH, 1,4-dioxane, 50°C, 3 h. All reaction steps were synthesised according to the patent[181].

The final probe CG390 was synthesised based on CG384 (**Scheme 17**), following the general procedure as described in **Figure 43A**.

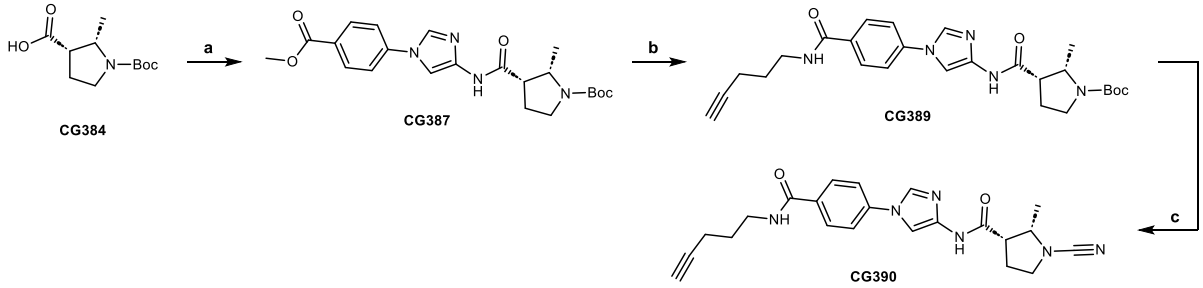

Scheme 17. Synthesis of final probe CG390. a. 1) GK07, H_2, Pd/C, THF, rt, on. 2) HATU, DIPEA, THF, rt, on, 50%. **b.** 1) 2M LiOH, 1,4-dioxane, 50°C, 4 h. 2) pent-4-yn-1-amine HCl, HATU, DIPEA, DMF, rt, on, 31%. **c.** 1) 20% TFA in DCM, rt, 3 h. 2) BrCN, K_2CO_3, DMF, rt, 3 h, 55%. Although the compounds CG389 and CG390 are novel, the synthetic procedures shown are based on appropriate methods from the patent WO2016046530A1[181].

The ^{1}H NMR spectra of intermediates CG387 and CG389 revealed the presence of 11% and 16% of an impurity, respectively, characterised by NMR analysis as the respective (2*S*, 3*R*)-diastereomer. This could either indicate that the reduction of CG366 was not entirely stereo selective and all respective peaks in the ^{1}H NMR spectrum of CG372 where overlapping (since

no impurity could be detected), or base-induced and reversible abstraction of the acidic αH-atom adjacent to the ester group in CG377 resulted in epimerisation (**e**). Purification by preparative HPLC after the final step (**c**) finally resulted in successful separation of the impurity, yielding pure CG390, which was used for further biological characterisation.

5.3 GK13S analogue CG390 shows improved UCHL1 over PARK7 selectivity *in vitro*

In order to evaluate UCHL1 binding and selectivity of the aforementioned probes, their *in vitro* binding affinity to UCHL1 and PARK7 was measured by means of Intact protein mass spectrometry (**Figure 44**). UCHL1 and PARK7 (3 µM) were either treated with DMSO (10 µM) or directly with the compounds (10 µM) for 1 h. Probe binding (in %) was evaluated as the difference of the area under the curve between probe treated and DMSO treated samples and visualised as blue (UCHL1 binding) or green (PARK7 binding) boxes (**Figure 44A**). In contrast to the modelled binding pose for CG287 (**Figure 42B**) that predicted the methyl-methoxy group to bind a cleft, unoccupied by the parent probe GK13S, CG287 did neither show covalent modification of UCHL1 nor PARK7 (**Figure 44B**). Due to the promising docking pose of CG288 (**Figure 42B**), protein binding of the probe was evaluated, despite being only 75% pure (**appendix, Figure 72A**). In line with the results for CG287 (**Figure 44B**), its diastereomer CG288 did not show any UCHL1 engagement, excluding both as suitable UCHL1-selective probes.

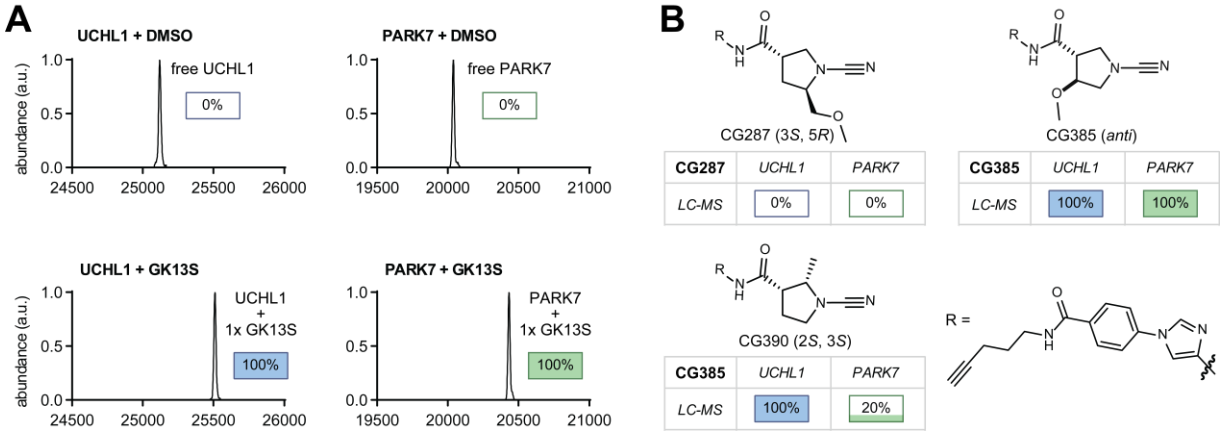

Figure 44. GK13S analogue CG390 improves PARK7 selectivity *in vitro*. A. Intact protein mass spectrometry data of GK13S binding to recombinant UCHL1 (left panel) or PARK7 (right panel). UCHL1 (3 µM) or PARK7 (3 µM) were treated with GK13S (10 µM) or DMSO for 1 h. Observed masses were assigned to given species with listed expected masses. Differences in area-under-the-curve (AUC) values between GK13S and DMSO were calculated and illustrated in blue (UCHL1 binding) and green (PARK7 binding) boxes, where 100% relates to full protein labelling. **B.** Chemical structures and covalent UCHL1 and PARK7 modification of indicated compounds, as measured by LC-MS. For **i**ntact protein mass spectrometry UCHL1 (3 µM) or PARK7 (3 µM) were treated with compound (10 µM) or DMSO for 1 h. Differences in AUC values between compound and DMSO treated samples were calculated and illustrated as in **A**. For related LC-MS spectra see **appendix, Figure 72A**.

Flexible ligands often have multiple binding modes or bound conformations that differ by rotation of a portion of the molecule around internal rotatable bonds.[219] Introduction of a methyl-methoxy group increases rotational flexibility of CG287 and CG288. Despite calculation of the best binding pose in consideration of the protein environment (by MMFF94 force field) (**Figure 42**), both probes might actually adopt a different conformation that interferes with UCHL1 binding. In addition, the methyl-methoxy group might hinder the probes to trigger an allosteric relay in UCHL1 (apo), which would lock the protein in a compound-induced hybrid conformation, a process crucial for binding of GK13S (**Figure 32**). CG385 on the other hand, demonstrating a methoxy group with reduced rotational flexibility (compared to a methyl-methoxy group), did show complete covalent modification of UCHL1, but also of PARK7. This supports the docking pose (**Figure 42E**), where the methoxy group points towards the solvent exposed environment of the binding cleft, probably not affecting the probes selectivity. In line with its predicted docking pose (**Figure 42F**), CG390 was able to retain full UCHL1 modification and even showed increased UCHL1 over PARK7 selectivity, as intact protein binding to PARK7 at 10 µM compound concentration could be reduced to 20%, compared to 100% for GK13S.

IC_{50} measurements at an incubation time of 1 h (**Figure 45**) revealed that probes CG385 and CG390 have comparable potencies of 183 and 135 nM, respectively, slightly (~2-times) less potent compared to the parent probe GK13S (IC_{50} = 66 nM), whereas probes CG287 and CG288 exhibited no significant UCHL1 inhibition (IC_{50} greater than 10 µM). These data are in agreement with the previous LC-MS binding experiment (**Figure 44**).

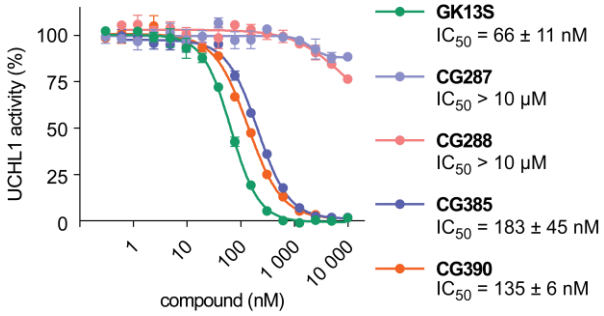

Figure 45. A Ub-Rhodamine assay validates probe binding to UCHL1. Inhibitory potencies of indicated compounds, preincubated with UCHL1 for 1 h, determined from a Ub-Rho cleavage assay. IC_{50} values were determined from N = 5 (GK13S) or 2 (CG287, CG288, CG385, CG390) independent experiments. Data are shown from a representative experiment as mean ± standard deviation.

To further assess specificity in a cellular environment, HEK293 cell lysate was treated with the probes for 4 h and covalently bound proteins were either visualised through activity-based protein profiling (**Figure 46A**), or their degree of cellular UCHL1 inhibition was assessed in a Ub-VS competition assay (**Figure 46B**).

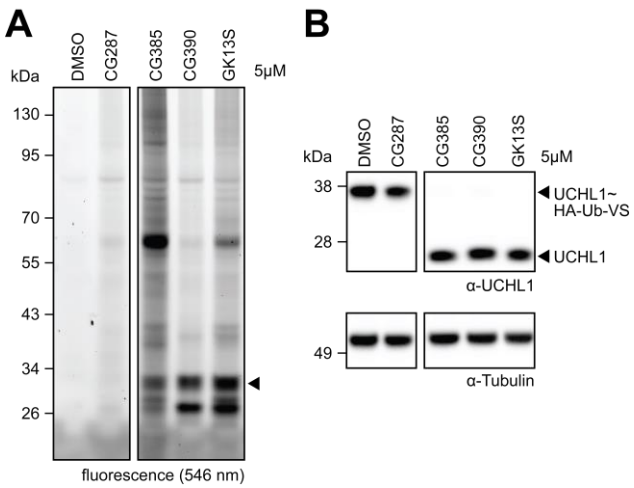

Figure 46. Cellular characterisation of improved 3-carboxy-*N*-cyanopyrrolidine probes. A. Cellular activity-based protein profiling with HEK293 cell lysate and indicated compounds or DMSO at 5 µM concentration (4 h incubation). The fluorescence image visualises probe-bound endogenous proteins. The black arrow indicates a protein band at the height of UCHL1. Data shown are from the same experiment and gel. **B.** Inhibition of cellular UCHL1. Western blot analysis of endogenous UCHL1 labelled with HA-Ub-VS after treatment of HEK293 cell lysate with either the indicated compounds or DMSO at 5 µM concentration for 4 h. Data shown are from the same experiment and gel. Assays were performed and evaluated by MSc. M. Schmidt.

Complete inhibition of UCHL1 was observed after treating the cell lysate with 5 µM of the probes CG385, CG390 and GK13S, respectively, whereas CG287 did not inhibit UCHL1 under these conditions (**Figure 46B**). These data are in agreement with the LC-MS labelling experiment of UCHL1 (**Figure 44**) as well as their *in vitro* potency (**Figure 45**). Activity-based protein profiling of covalently bound proteins (**Figure 46A**) after treatment with 5 µM GK13S demonstrated a similar binding pattern as observed for the labelling experiment in intact HEK293 cells at 10 µM probe concentration and 24 h incubation time (**Figure 21**). In line with previous *in vitro* experiments, hardly any covalent-irreversible binding of proteins could be observed for CG287 in a cellular setting. The probe CG385 seemed to modify multiple cellular proteins, including a pronounced one with a molecular weight of approximately 60 kDa that was also detectable in the GK13S treated sample, but with much lower intensity. In comparison to the GK13S treated sample, only a faint band at the height of UCHL1 could be observed, classifying the probe CG385 inferior to GK13S in terms of UCHL1 specificity in a cellular environment. For CG390, a pattern similar to that of GK13S could be observed with overall reduced band intensity, possibly arising from lower cellular potency. In line with the selectivity profile of GK13S, a prominent protein band at the height of PARK7 could be identified for probe CG390 as well, with comparable intensity to the band at the height of UCHL1. Overall, this led to the conclusion that an improvement of cellular UCHL1 over PARK7 selectivity could not be achieved by the aforementioned probes.

5.4 *N*-Cyanopiperidine CG305 shows stereoselective labelling of UCHL1, but not of PARK7

The catalytic mechanisms of PARK7 (**Figure 38**) suggest that substrate binding is primarily reactivity-driven. Since GK13S and GK16S are binding similar off-targets (**appendix, Figure 63**) it is thus to reason that the reactivity of the electrophilic 3-carboxy-*N*-cyanopyrrolidine

warhead might be too high. Since all attempts to improve UCHL1 selectivity by modification of the 3-carboxy-*N*-cyanopyrrolidine warhead failed, a new approach featuring 3-carboxy-*N*-cyanopiperidine analogues of GK13S was established (**Figure 47**). The change in warhead size from a 5-membered pyrrolidine to a 6-membered piperidine, and the associated change and increase in structural conformations[220], was hypothised to affect the binding cleft occupancy and catalytic cysteine reactivity of the cyanamide warhead in a way that could positively influence UCHL1 selectivity. Following this hypothesis, the *N*-cyanopiperidine probe CG305 was synthesised along with its (*R*)-enantiomer CG322 (**Figure 47A**). UCHL1 and PARK7 selectivity was first evaluated by LC-MS analysis (**Figure 47B**). Treatment of 3 µM protein with 10 µM CG305 resulted in near complete (83%) modification of recombinant UCHL1, while no labelling of PARK7 could be observed. Under the same conditions, CG305 showed no binding to either of the enzymes, indicating a preference of UCHL1 for the (*S*)-configured stereoisomer. This stereo preference is consistent with the previously described results for GK13S. IC_{50} measurements at a fixed incubation time of 1 h revealed a potency of 1496 nM for the probe CG305, whereas the enantiomer did not show any appreciable degree of inhibition (**Figure 47C**), confirming the results of the LC-MS labelling experiment.

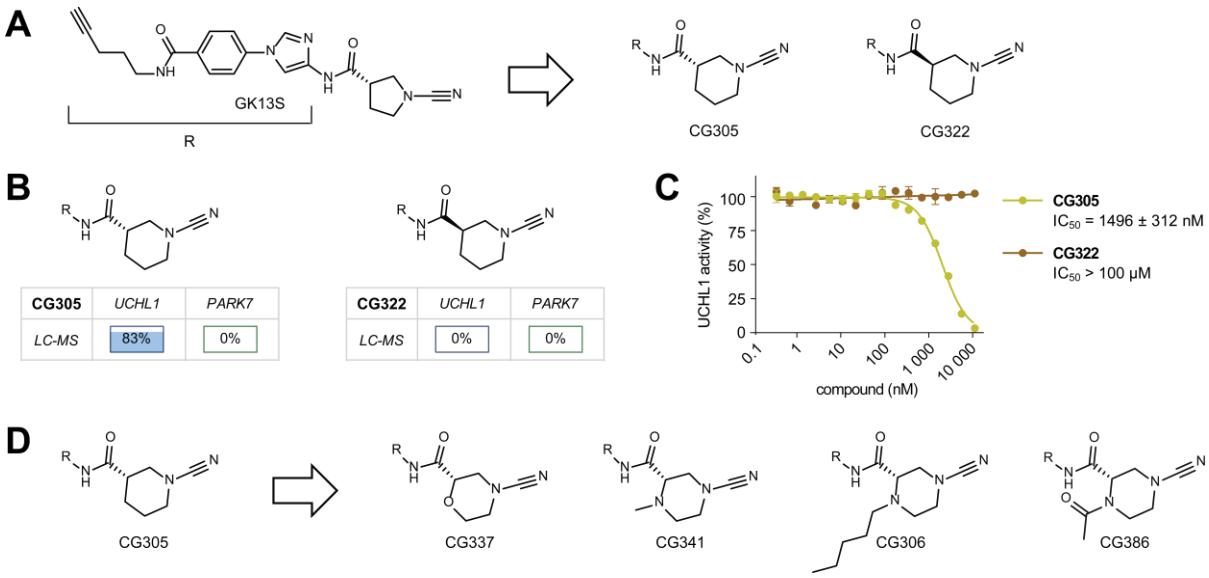

Figure 47. Piperidine-analogue CG305 shows stereoselective labelling of UCHL1, but not PARK7. A. Schematic representation of *N*-cyanopiperidine probe CG305 and its (*R*)-enantiomer CG322, based on an identical structural scaffold as GK13S (defined as "-R"). **B.** Covalent modification of UCHL1 and PARK7 by CG305 and its enantiomer CG322, as measured by LC-MS. For **i**ntact protein mass spectrometry UCHL1 (3 µM) or PARK7 (3 µM) were treated with compound (10 µM) or DMSO for 1 h. Differences in AUC values between compound and DMSO samples were calculated and illustrated as described for **Figure 44**. Respective LC-MS spectra are shown in **appendix, Figure 72B**. **C.** Inhibitory potencies of CG305 and CG322, preincubated with UCHL1 for 1 h, determined from a Ub-Rho cleavage assay. Data points are shown as mean ± standard deviation. IC_{50} values were determined from 5 (CG305) or 3 (CG322) independent experiments. **D.** Schematic representation of CG305 analogues with different 6-membered ring warheads.

CG305 demonstrated a promising UCHL1 over PARK7 selectivity profile *in vitro*, accompanied by a ~20-fold reduction in potency compared to GK13S (**Figure 47B-C**). These results support the hypothesis of enhanced UCHL1 selectivity through warhead ring expansion and classify CG305 as a suitable starting point for additional modifications to further improve UCHL1 potency.

Morpholines and piperazines are frequently encountered structural motifs in the field of pharmaceutical research. These motifs have the potential to enhance various pharmacokinetic (PK) properties of molecules, including their water solubility and metabolic stability, while not being essential for direct receptor binding.[221,222,223,224,225] Morpholines are utilised as functional groups to improve the potency of drug candidates through molecular interaction with target proteins.[221,222] For instance, the ether oxygen atom in morpholine serves as a crucial binding motif in inhibitors. Additionally, morpholine groups can be employed to modulate the physicochemical properties of molecules as the weak basicity of morpholine (e.g., *N*-methyl morpholine, pK_a = 7.4) closely resembles the pH of blood and often leads to improvements in solubility without compromising permeability to the same extent as stronger bases.[221] Piperazine-based compounds have gained considerable interest due to their favourable physicochemical properties and the orthogonal applicable, ready derivatisation of the nitrogen atoms with substituents.[223,224] Derivatization at the piperazine can be tailored to either retain or diminish the basicity of the compound.[223,224].

Based on the piperidine warhead in CG305, four probes featuring a morpholine (CG337) or piperazine moiety (CG341, CG306 and CG386) were designed (**Figure 47D**). To evaluate the influence of different warheads on molecular properties of the probes, the number of H-bond donors, -acceptors and rotational bonds as well as their hydrophobicity (miLogP) was calculated using the *Molinspiration Cheminformatics* online platform (**Table 1**). Additional H-bond acceptors at different positions (“O” in CG337, “N” and “O” in CG386) were rationalised to establish stronger protein-ligand interactions. The N-alkylated piperazine moiety (“N^+-H” in CG341/ CG306) will likely be protonated under physiological conditions (electron donating (+I) effect of alkyl), serving as a prospective H-bond donor (**Table 1**), whereas N-acetylation (electron-withdrawing group, -M-effect) in CG386 rather suppresses the basicity. Hydrophobicity, in the form of the logarithmic octanol-water partition coefficient (log P), is widely used as a measurement for solubility and cell permeability of a drug (**equation 1**).[226]

$$\log P = \frac{c_{octanol}}{c_{water}} \quad (1)$$

A higher hydrophobicity is linked to reduced water solubility, whereas low hydrophobicity can impede cell permeability. Since *N*-methyl-piperazine CG341 was predicted to show a substantially lower LogP value (miLogP = -3.01) compared to the cell permeable probe GK13S

(miLogP = -0.77) (**Table 1**), CG306 (miLogP = -1.07) was designed as *N*-pentyl-piperazine to increase hydrophobicity and overcome potential permeability issues.

Table 1. Different warhead composition influences molecular properties of probes. Molecular properties were calculated using the *Molinspiration Cheminformatics* online platform. n(N, O): Number of N- and O-atoms. n(N-H, O-H): Number of H-bound N-and O-atoms. n(rot. bond): Number of rotational bonds. miLogP: molinspiration LogP; Method for logP prediction developed at *Molinspiration* (miLogP2.2 - November 2005), based on a training set with more than twelve thousand, mostly drug-like molecules.

compound	GK13S	CG305	CG337	CG386	CG341	CG306
n(N, O)	8	8	9	10	9	9
n(N-H, O-H)	2	2	2	2	3	3
n(rot. bond)	7	7	7	7	7	11
miLogP	0.77	1.04	0.10	-0.49	-3.01	-1.07

5.5 Synthesis of piperidine-, morpholine- and piperazine-warhead analogues of GK13S

The synthesis of piperidine-, morpholine- and piperazine-warhead analogues of GK13S followed two similar reaction sequences, resting upon the shared intermediate GK07 as well as different acid-functionalised building blocks (**Figure 48**). Whereas enantiopure acid-intermediates were commercially available for piperidine- and morpholine-probes, synthesis of the piperazine acid-intermediates was based on precursor 1-Boc-3-methyl (*S*)-piperazine-1,3-dicarboxylate (**Figure 48A**). Reductive amination of the free piperazine N-atom with either formaldehyde (**a**) or valeraldehyde (**b**) resulted in the N-alkylated intermediates CG295 and CG296, respectively, whereas amidation with acetyl chloride yielded amide CG364 (**c**). In a final hydrolysis reaction, the ester intermediates were converted into their respective acids (**d**) using 2M lithium hydroxide.

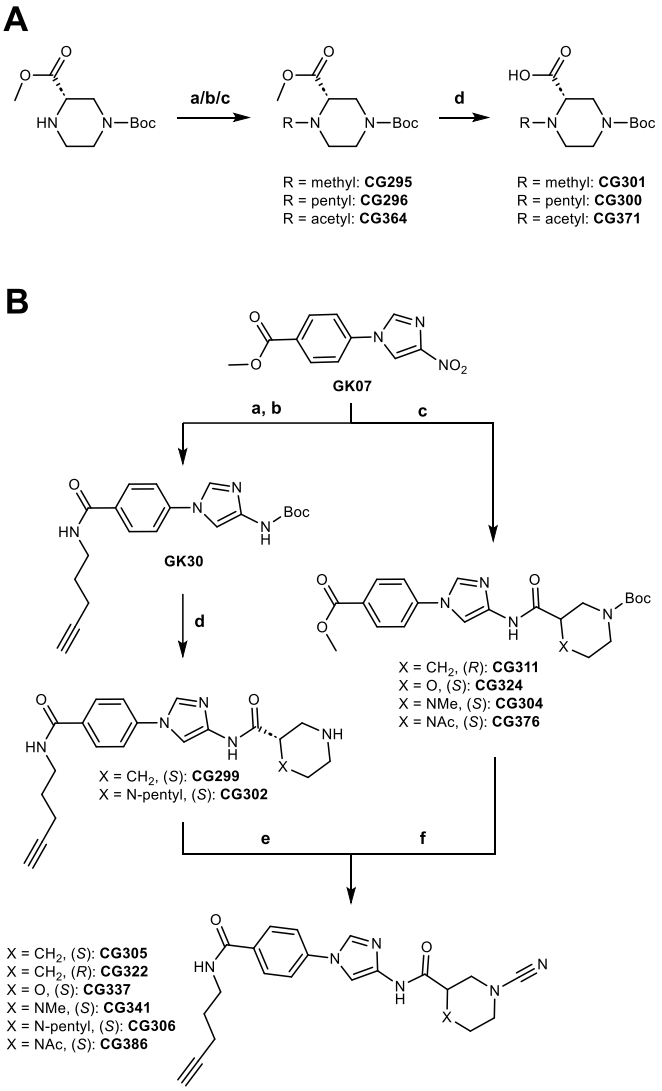

Figure 48. Synthesis of piperidine-, morpholine- and piperazine-warhead analogues of GK13S. A. Synthesis of piperazine precursors. a. Formaldehyde, $NaBH(OAc)_3$, AcOH, ACN:MeOH (1:1), rt, on, 66%. **b.** Valeraldehyde, $NaBH(OAc)_3$, AcOH, DCM, rt, on, 95% **c.** Acetyl chloride, Et_3N, DCM, 0 °C -> rt, on, 52%. **d.** 2M LiOH, 1,4-dioxane, 50 °C, 4 h. CG301 (quant.), CG300 (94%), CG371 (quant.). The synthetic procedures for steps **a**[227], **b**[228], and **c**[229] were adapted from references describing the same (**a**, **c**) or similar (**b**) structures. **B. Synthesis of probes.** Compounds were synthesised using two similar procedures (left and right panel). **a.** 1) GK07, Pd/C, H_2, EtOH, rt, 5 h. 2) Boc_2O, DIPEA, EtOH, MeOH, rt, 20 h, 20%. **b.** 1) LiOH, MeOH, 50°C, 5 h. 2) pent-4-yn-1-amine, HATU, DIPEA, DCM, rt, 1 d, 80%. **c.** 1) GK07, Pd/C, H_2, EtOH, rt, 5 h. 2) 1-Boc-*D*-nipecotic acid/ (*S*)-4-Boc-morpholine-2-carboxylic acid/ CG301/ CG371, HATU, DIPEA, DMF, rt, on. CG311: quant., CG324: 51%, CG304: 68%, CG376: 70%. **d.** 1) GK30, 20% TFA/DCM, rt, 4 h. 2) 1-Boc-*L*-nipecotic acid/ CG300, HATU, DIPEA, THF, rt, on. 3) 20% TFA/DCM, rt, 3 h. CG299: 31%, CG302: 18%. **e.** CG299/ CG302, BrCN, K_2CO_3, DMF, rt, 1-2 h. CG305: 77%, CG306: 53%. **f.** 1) CG311/ CG324/ CG304/ CG376, 2M LiOH, 1,4-dioxane, 50°C, 4-6 h. 2) pent-4-yn-1-amine HCl, HATU, DIPEA, DMF, rt, on. 3) 20% TFA/DCM, rt, 2-3 h. 4) BrCN, K_2CO_3, DMF, rt, 2-3 h. CG322: 54%, CG337: 50%, CG341: 52%, CG386: 79%. Although the compounds described are novel, the synthetic procedures of steps c, e, and f are based on appropriate methods from the patent[181].

Synthesis of the corresponding probes followed two similar reaction sequences (**Figure 48B**). For CG305 and CG341, the nitro-group of GK07 was reduced using hydrogen and palladium on activated charcoal, followed by Boc-protection of the resulting heteroaromatic amine (**a**). In the next reaction, basic ester hydrolysis of the methyl ester and subsequent amide coupling with pent-4-yn-1-amine HCl yielded GK30 (**b**). Deprotection of the Boc-group and subsequent amide coupling to 1-Boc-*L*-nipecotic acid or acid intermediate CG300 yielded free amines CG299 and CG302, respectively (**d**). Electrophilic cyanation of the piperidine/ piperazine N-atom using cyanogen bromide (BrCN) provided final probes CG305 and CG322 (**e**). GK30 was thought to function well as a common intermediate for the synthesis of all probes by shortening the overall reaction sequence. However, in line with previously reported results,

suggesting an instability of GK07 after nitro-group reduction[2], a rapid decomposition of GK30 after Boc-deprotection could be observed during the synthesis of CG299 and CG302, eventually resulting in poor yields (31% and 18%, respectively). These results support the hypothesis of molecular instability of the resulting amino-imidazole (GK08) and further indicate that TFA may even accelerate decomposition by functioning as an acidic catalyst. To circumvent the need for high amounts of GK30, successive probes were synthesised using the previously described sequence of reactions (**Figure 43A**). Following palladium catalysed nitro-group reduction of GK06, amide coupling reactions, using either commercially available acids such as 1-Boc-*R*-nipecotic acid and (*S*)-4-Boc-morpholine-2-carboxylic acid, or piperazine-intermediates CG301 and CG371 (**Figure 48B**), yielded intermediates CG311, CG324, CG304 and CG376, respectively (**c**). Ester hydrolysis of the methyl benzoate-group to the corresponding benzoic acid, amide coupling with pent-4-yn-1-amine, acidic Boc-deprotection and final BrCN reaction resulted in the desired probes CG322, CG337, CG341 and CG386, respectively (**f**).

5.6 *N*-Cyanopiperazines CG306 and CG341 show greatly improved selectivity towards UCHL1 *in vitro*

As a first step to characterise the specificity of the new probes for UCHL1 and PARK7, binding to recombinant protein was analysed by LC-MS (**Figure 49**).

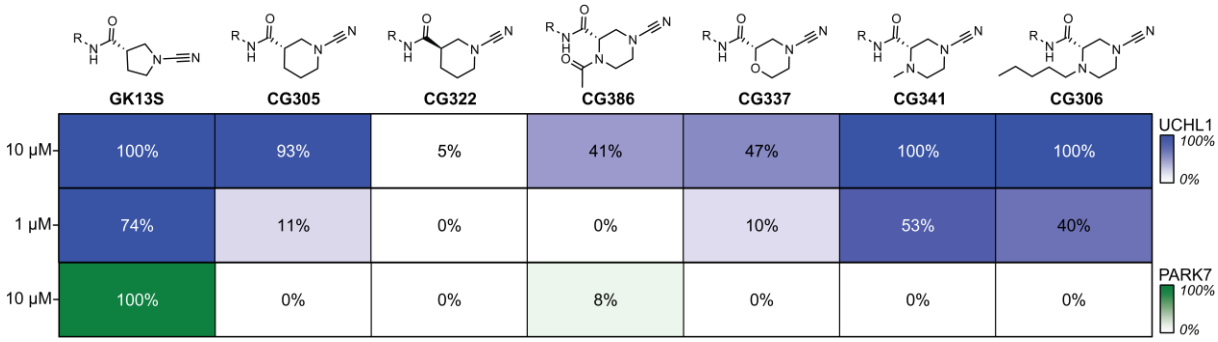

Figure 49. Covalent modification of recombinant UCHL1 and PARK7, as measured by LC-MS, reveals improved UCHL1 selectivity profile of N-alkylated piperazines *in vitro*. 10 µM: UCHL1 (3 µM) or PARK7 (3 µM) were treated with indicated compounds (10 µM) or DMSO for 1 h. 1 µM: UCHL1 (0.8 µM) was treated with indicated compounds (1 µM) or DMSO for 1 h. Differences in AUC values between compound and DMSO samples were calculated and illustrated as a heat map with covalent probe-protein modification in %. Values were determined from 2-5 independent experiments. Respective LC-MS spectra are shown in **appendix, Figure 73** & **Figure 74A**.

At a probe concentration of 10 µM, the *N*-alkyl-piperazine probes CG341 and CG306 showed complete covalent modification of UCHL1 (3 µM), whereas the morpholine- and *N*-acetyl-piperazine probes CG337 and CG386 presented only 47% and 41% UCHL1 binding, respectively. Probe incubation with PARK7 under the same conditions showed 8% labelling of CG386, whereas no covalent PARK7 modification was observed for the other optimised

probes. To gain further insights into the potency differences between the probes, a reduced amount of UCHL1 (0.8 µM) was incubated with a small excess of probe (1 µM). As intended, all probes showed a lower percentage of UCHL1 labelling compared to the 10 µM probe treatment. However, as none of the probes showed complete labelling of UCHL1 under these conditions, a better comparability of their respective binding affinities is given. After reducing the concentration to 1 µM, probe treatment with CG341 and CG306 for 1 h resulted in decent UCHL1 labelling of 53% and 40% respectively. GK13S, previously shown to inhibit recombinant UCHL1 with nanomolar potency, showed 74% labelling under the same conditions, indicating a high potency for probes CG341 and CG306 as well. The piperidine CG305 and the morpholine CG337 showed a lower binding affinity, labelling UCHL1 to an extent of only 11% and 10%, respectively, while CG386 showed no binding at all. A complementary labelling experiment under the same conditions but with a longer incubation time (14 h) revealed that the probes GK13S, CG337, CG341 and CG306 were able to fully modify UCHL1 (**appendix, Figure 74B**). The results also suggest slow binding kinetics for CG337 (10% labelling after 1 h vs. 100% labelling after 14 h), whereas the piperidine-based probe CG305 may react significantly slower and/or in a covalent-reversible manner, as only 66% labelling of UCHL1 was observed after 14 h treatment.

Based on the LC-MS labelling results, the probes CG337, CG341 and CG306 were selected for further *in vitro* characterisation (**Figure 50**). A set of corresponding minimal probes, lacking the central aromatic specificity element, was synthesised and binding to recombinant UCHL1 evaluated. IC_{50} measurements at a fixed incubation time of 1 h revealed that the piperazine-probes CG341 and CG306 have comparable potencies of 191 and 254 nM, respectively, only slightly (~ threefold) less potent than the parent probe GK13S (66 nM) (**Figure 50A-B**). The morpholine-probe CG337 inhibited UCHL1 approximately 7-fold less than GK13S. In line with the results for GK13S and its corresponding minimal probe GK16S, none of the synthesised minimal probes showed any appreciable degree of UCHL1 labelling or inhibition (IC_{50} > 100 µM), confirming the need for both the warhead and the aromatic specificity element for the optimised probes as well (**Figure 50A-B**).

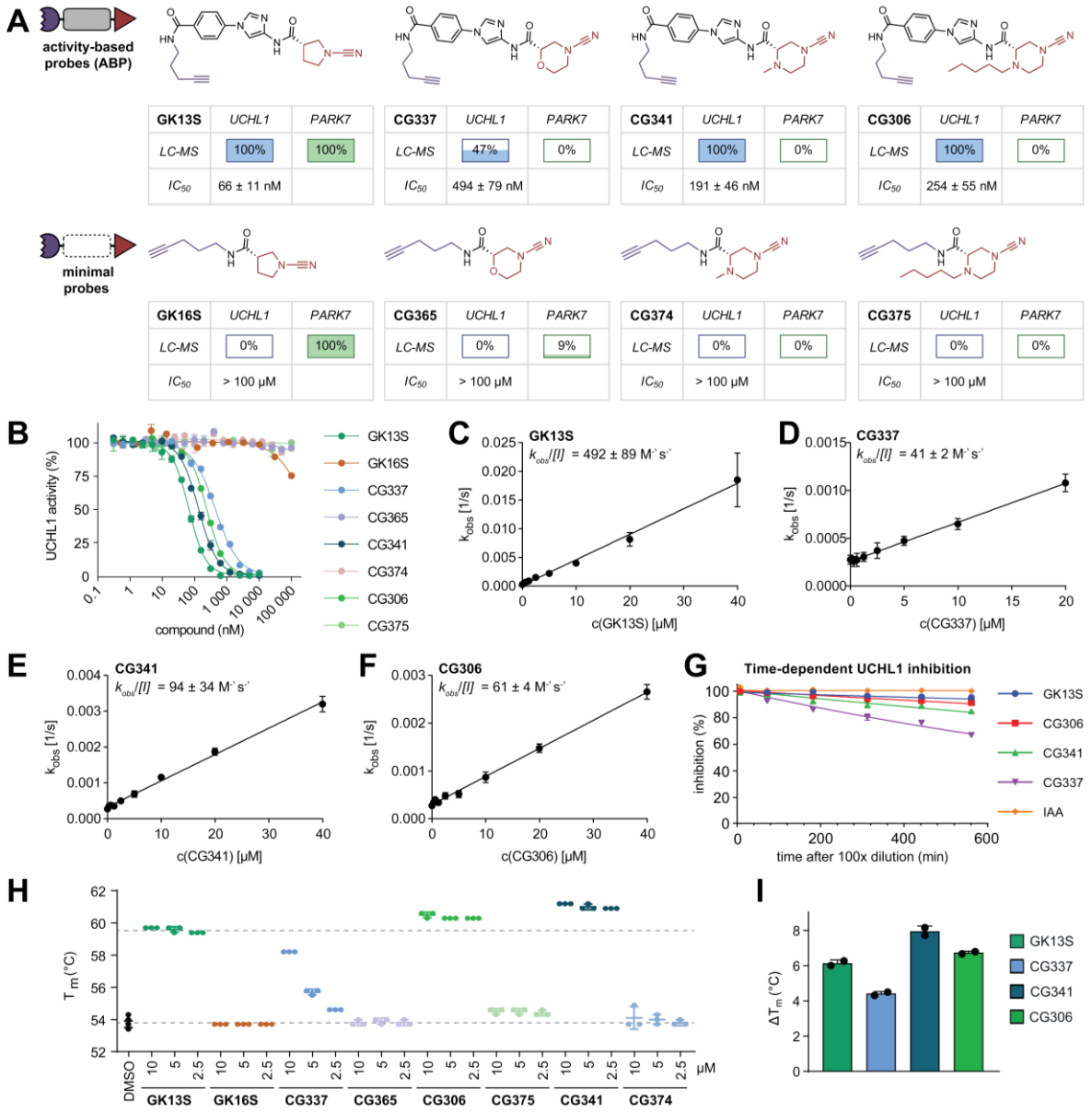

Figure 50. Alkylated *N*-cyanopiperazines CG306 and CG341 show clear selectivity to UCHL1 over PARK7, while retaining UCHL1 potency. A. Schematic representation, chemical structures and tabular *in vitro* results of indicated probes and controls comprising warhead (red), specificity element (grey) and alkyne handle (magenta). For **i**ntact protein mass spectrometry UCHL1 (3 µM) or PARK7 (3 µM) were treated with compound (10 µM) or DMSO for 1 h. Differences in AUC values between compound and DMSO samples were calculated and illustrated as described above. Respective LC-MS spectra are shown in **appendix, Figure 73** & **Figure 75A**. IC_{50} values were derived from **B**. **B.** Inhibitory potencies of indicated compounds, preincubated with UCHL1 for 1 h, determined from a Ub-Rho cleavage assay. Data points are shown as mean ± SD. IC_{50} values were determined from 5 (GK13S), 4 (CG341), 3 (CG306 and GK16S) or 2 (CG337, CG365, CG374 and CG375) independent experiments. **C-F.** $k_{obs}/[I]$ kinetic assay of GK13S (**C**), CG337 (**D**), CG341 (**E**) and CG306 (**F**) binding to UCHL1. Rate constants k_{obs} were determined from the respective Ub-Rho plot (**appendix, Figure 76**) and plotted against inhibitor concentrations as shown for a representative experiment, respectively. The $k_{obs}/[I]$ values were determined as the slope and are given as mean ± SD calculated from three independent experiments. **G.** Time-dependent UCHL1 inhibition based on slopes of individual time points from jump-dilution assay shown in **appendix, Figure 77**. **H.** Thermal shift assay showing the melting temperature (T_m) of UCHL1 (1 µM) pre-treated for 1 h with compounds at indicated concentrations. **I.** Comparison of changes in UCHL1 protein melting temperatures (ΔT_m) after binding to pyrrolidine-, morpholine- and piperazine-based compounds. Values are given as mean ± SD from 3 biological replicates.

At a probe concentration of 10 µM and an incubation time of 1 h, GK16S labelled recombinant PARK7 completely, as determined by intact protein mass spectrometry. This supports the previously established hypothesis that the 3-carboxy-*N*-cyanopyrrolidine warhead binds PARK7 in a reactivity driven manner. Interestingly, the morpholine-based minimal probe CG365 labels PARK7 to an extent of 9%, whereas the two N-alkylated piperazine minimal probes CG374 and CG375 showed no labelling. As PARK7 has a well-defined active site (**Figure 39**), the additional space occupied by the methyl/pentyl groups as well as the different structural conformations and protonation states (unprotonated morpholine O-atom vs. protonated piperazine *N*-alkyl-atom), may be of help to impede PARK7 binding and thereby improve the specificity towards UCHL1.

To compare the time-dependent target association of the probes to UCHL1, the covalent mode of inhibition was further characterised in a fluorescence-based Ub-Rho cleavage assay (**appendix, Figure 76**). The observed concentration dependent inactivation rates (k_{obs}) were plotted against the inhibitor concentration [I] to determine the rate constant k_{obs}/[I] (**Figure 50C-F**). GK13S exhibited the highest $k_{obs}/[I]$ value of 492 M^{-1} s^{-1}, followed by CG341 (94 M^{-1} s^{-1}), CG306 (61 M^{-1} s^{-1}) and CG337 (41 M^{-1} s^{-1}). Although the specificity window of GK13S vs. CG341 is slightly increased compared to the IC_{50} measurements (fivefold vs. threefold), there is a clear trend in potency, consistent with the LC-MS labelling and IC_{50} results (**Figure 50A,B**). In line with the LC-MS labelling experiments at 1 µM and different time points (**Figure 81**, **appendix, Figure 74B**), CG337 showed the slowest binding. The observed differences in potency between the improved probes also correlate well with their IC_{50} values. Overall, the slower binding kinetics of the improved probes compared to the parent probe GK13S indicate the successful reduction of reactivity to avoid unselective and reactivity-driven off-target binding. It is tempting to speculate that an increased ring size correlates with a weaker electrophilicity of the cyanamide warhead. This would result in a more specificity-driven binding mode, which would be consistent with the increased specificity of the improved probes towards UCHL1. Future experiments that calculate or measure the reactivity difference (e.g. binding to a free thiol) will provide more detailed information in the future.

The binding mode was further characterised in a jump-dilution assay (**Figure 50G**, **appendix, Figure 77**). Over a time period of 10 h, no significant reduction in UCHL1 inhibition was observed for GK13S and CG306, compared to the positive probe IAA, characterising both as covalent-irreversible inhibitors. Under the same conditions, CG341 showed a slight decrease to 85% inhibition after 100-fold dilution (final concentration: 5 nM) for 10 h, suggesting an exceptionally slow dissociation and therefore a covalent-reversible binding mechanism. Surprisingly, inhibition of UCHL1 was reduced to ~65% after 10 h treatment with CG337. Although this still represents a slow reversibility, it also indicates that a different reactivity of

the cyanamide warhead can be achieved by sterically and electronically altering its nature, which is in line with the observed results of the $k_{obs}/[I]$ kinetic assay. A slight decrease in inhibition could also be due to a change in sample properties over time, as the incubation was performed at room temperature. This would result in different compositions between the samples measured. Additional assays, such as surface plasmon resonance (SPR), will be required to further clarify a potential reversibility of the compounds.

Consistent with a rather specificity-driven binding mode, the binding of both piperazine-based probes CG341 and CG306 led to an increase in UCHL1 stability of 7 °C, slightly higher than that of GK13S (ΔT_m = 6 °C). In comparison, the probe CG337 led to a weaker stabilisation (ΔT_m = 4 °C), which is in line with its lower IC_{50} and incomplete protein labelling under comparable conditions (**Figure 49**). Almost none of the minimal probes tested, except CG375, showed any protein stabilisation, supporting the specific recognition of their respective parent probe by UCHL1. Surprisingly, the CG306-derived minimal probe CG375 resulted in a modest 1 °C stabilisation of UCHL1, although it did not show any inhibition or covalent protein modification under comparable conditions (**Figure 50A,B**). A possible explanation could be that the long alkyl-moiety of CG375 is able to interact with hydrophobic sites in UCHL1, thereby stabilising them.

5.7 CG341 and CG306 successfully prevent binding to USP30 – a common target of 3-carboxy-*N*-cyanopyrrolidines

In recent years, the interest in developing small molecule inhibitors targeting USP30 greatly increased, in particular by pharmaceutical companies. Between 2016 – 2018 at least seven patents were filed merely by *Mission Therapeutics* (WO2016156816A1[104], WO2017009650A1[182], WO2017163078A1[230], WO2018060689A1[231], WO2018060691A1[232], WO2018060742A1[233], and WO2018065768A1[229]), showing various *N*-cyano-based, covalent USP30 inhibitors (**Figure 51A**). A large number of inhibitors contain 3-aminopyrrolidine as a warhead, which is linked to a specificity element in mostly (*R*)-configuration. Interestingly, a variety of molecules that feature pyrrolidine warheads with direct linkage to a heterocycle (Cpd 8), linkage via an intermediate carbon bridge (Cpd 6), (*S*)-2-aminopyrrolidines (Cpd 127) or multiple substitutions at the pyrrolidine ring in different stereo-orientations (Cpds 1, 28, 70, 174) are reported to inhibit USP30 with submicromolar potency. Even piperidine-, morpholine- and piperazine-based inhibitors were reported for USP30 in both (*R*)- and (*S*)-configuration (Cpds 55+56, 20+33 and 58+57, respectively). Whereas the majority of morpholine-based inhibitors shows only poor USP30 inhibition (**Figure 51A**), (*R*)-morpholine-based inhibitor Cpd 20 was reported to inhibit USP30 with an IC_{50} between 0.1 – 1 µM. Recently, the lab of Edward W. Tate developed the 3-carboxy-*N*-cyanopyrrolidine

MT16-001[178] in an attempt to develop an activity-based probe for UCHL1. Surprisingly, they discovered a dual-reactivity of MT16-001 against UCHL1 and USP30 at 1 µM compound concentration (**Figure 51B**). In conclusions this indicates that USP30 seems to have a high affinity for *N*-cyanopyrrolidine-based inhibitors, but tolerates various linkage types and structural properties of the warhead.

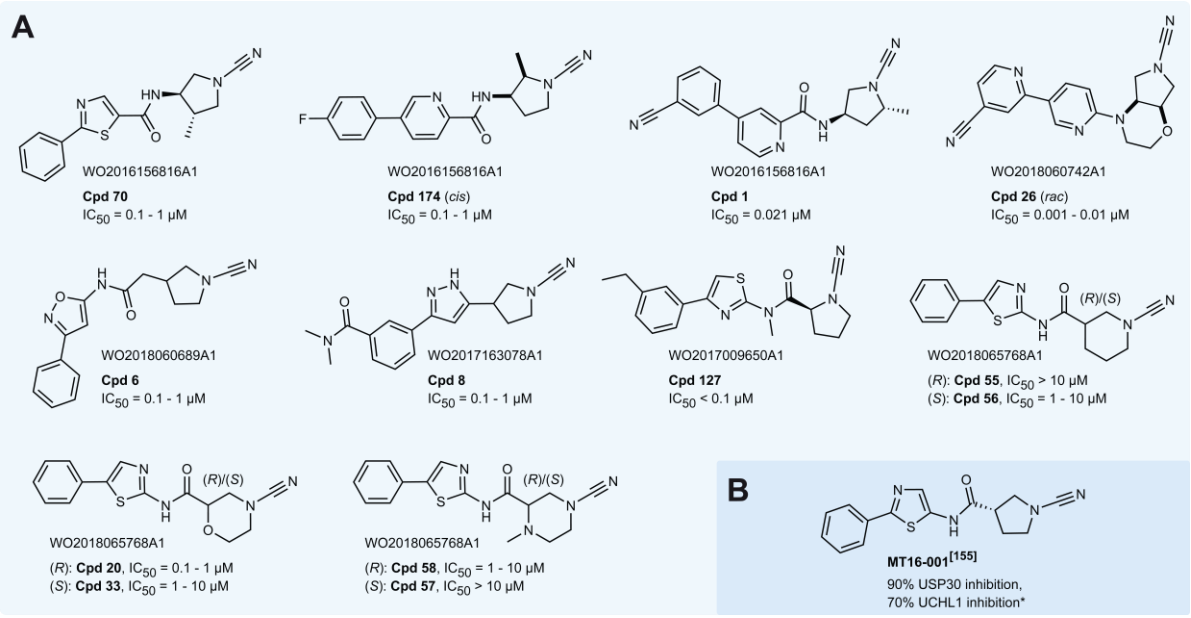

Figure 51. *N*-Cyano-based covalent USP30 inhibitors. A. A selection of USP30 inhibitors with *N*-cyano-based warheads from indicated *Mission Therapeutics* patents. **B.** Compound MT18-001 was found to have dual reactivity towards UCHL1 and USP30. * At 1 µM compound concentration, screened against 19 DUBs using fluorescence polarisation (FP) and fluorescence intensity (FI) assays[178].

Due to the structural similarity of MT16-001 to GK13S, and because both morpholine- and piperazine-based inhibitors have been reported to inhibit USP30[229], the covalent binding of the previously optimised probes and their controls (**Figure 50A**) was assessed by intact protein mass spectrometry (**Figure 52**). Consistent with the presumed high tolerance of the USP30 active site to 3-carboxy-*N*-cyanopyrrolidines, both GK13S and the minimal probe GK16S covalently modified USP30 to an extent of 50% and 68%, respectively, after 1 h treatment at a concentration of 10 µM. For GK13S this translates into a half-maximal USP30 inhibition at ~5 µM, which is in line with an IC_{50} of 2.14 µM as measured in a Ub-Rho cleavage assay (**appendix, Figure 78**). Under the same conditions no binding to USP30 could be observed for the morpholine- and piperazine-based probes (**Figure 52**). This is in agreement with the reported inactivity of (*S*)-cyanomorpholine Cpd33 and (*S*)-cyanopiperazine Cpd57 (**Figure 51**) (IC_{50} > 10 µM).

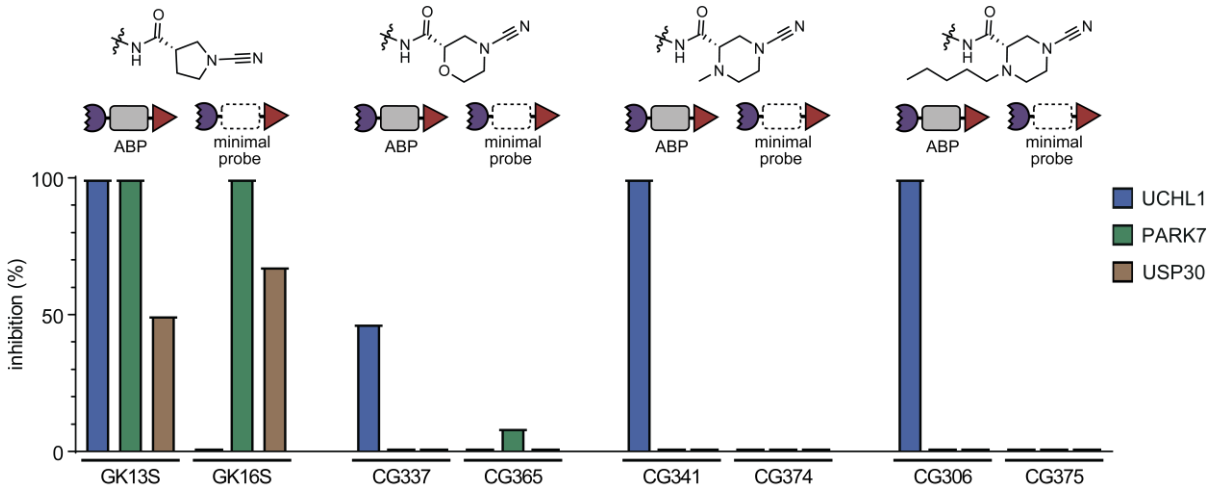

Figure 52. Intact protein mass spectrometry reveals enhanced selectivity profile of alkylated *N*-cyanopiperazines by preventing USP30 binding. LC-MS labelling experiments of indicated compounds (10 µM) to 3 µM of UCHL1 (blue), PARK7 (green) or USP30 (blue). were treated with indicated compounds (10 µM) or DMSO for 1 h. 1 µM: UCHL1 (0.8 µM) was treated with indicated compounds (1 µM) or DMSO for 1 h. Differences in AUC values between compound and DMSO samples were calculated and illustrated as a heat map with covalent probe-protein modification in %. Values were determined from 2-5 independent experiments. Respective LC-MS spectra are shown in appendix **Figure 75B**.

In a Ub-Rho assay with reduced incubation time (20 min), GK13S inhibited USP30 near equipotent compared to 1 h incubation time (IC_{50} = 2.27 µM vs. 2.14 µM), while potency towards UCHL1 was reduced ~threefold (IC_{50} = 226 nM vs. 66 nM), indicating a potentially more reactivity-driven inhibition of USP30 (**Figure 53**). Under the same conditions (20 min incubation), CG341 (IC_{50} = 1.48 µM) and CG306 (IC_{50} = 1.74 µM) show a ~sevenfold potency reduction towards UCHL1, while no inhibition of USP30 could be observed, even at high concentrations up to 10 µM, confirming the results of the LC-MS labelling experiment (**Figure 52**). The overall potency-reduction at shorter incubation times is in line with the time-dependent reaction of covalent inhibitors. Further, the comparably higher potency difference between GK13S and CG341/CG306 is in agreement with the results of the $k_{obs}/[I]$ kinetic assay (**Figure 50C-F**).

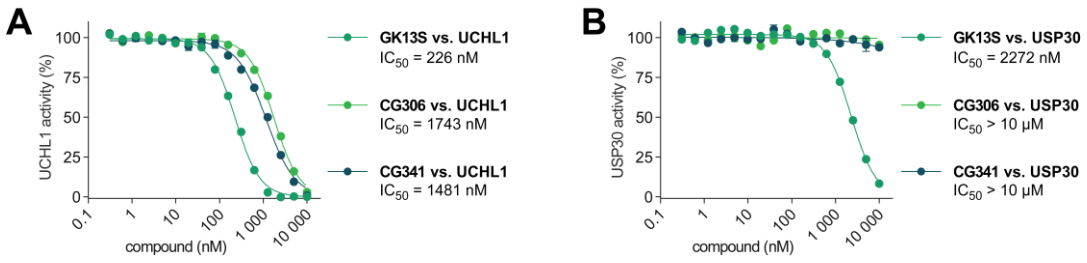

Figure 53. Ub-Rho cleavage assay with shorter incubation time clarifies potency differences of probe-selectivity between UCHL1 and USP30. A, B. Inhibitory potencies of indicated compounds, preincubated with UCHL1 (**A**) or USP30 (**B**) for 20 min, determined from a Ubiquitin-Rhodamine cleavage assay. Data points are shown for one biological experiment.

Overall, these findings indicate an improved selectivity profile of the morpholine- and piperazine-based probes towards UCHL1 with regard to PARK7 and USP30 off-target binding. Considering all previous labelling experiments and potency measurements, (*S*)-*N*-cyanopiperazines CG341 and CG306 clearly stand out as probes with an excellent selectivity profile towards UCHL1, by preventing PARK7 and USP30 binding, while retaining nanomolar UCHL1 potency.

5.8 *N*-Cyanopiperazines CG306 and CG341 potently inhibit UCHL1 in cells

In order to evaluate the ability of the probes to inhibit UCHL1 in the background of a complex protein mixture, a Ub-VS mediated target engagement assay was employed (**Figure 54A,B**). Following treatment of HEK293 cell lysate for 4 h with 1 µM (**Figure 54A**) of the probes, inhibition of UCHL1 was near complete for GK13S, which is in line with the previous target engagement assay (**Figure 24B**). However, CG341 and CG306 inhibited UCHL1 to the extent of only ~40% and ~10%, respectively (**Figure 54A**), as quantified by the ratio of band intensities between free UCHL1 (lower band) and the total amount of UCHL1 (free UCHL1 and HA-Ub-VS-bound UCHL1). Increasing the probe concentration to 5 µM (**Figure 54B**) resulted in complete UCHL1 inhibition for GK13S and CG341 and ~80% inhibition for CG306. These results are in accordance with the lower $k_{obs}/[I]$-values of the piperazine probes compared to GK13S (~fivefold/ ~8-fold lower for CG341 and CG306, respectively) (**Figure 50C-F**). Under the same conditions, none of the tested minimal probes did show any inhibition of UCHL1, which is in agreement with the LC-MS labelling experiment (**Figure 50A**) and the Ub-Rho cleavage assay (**Figure 50B**).

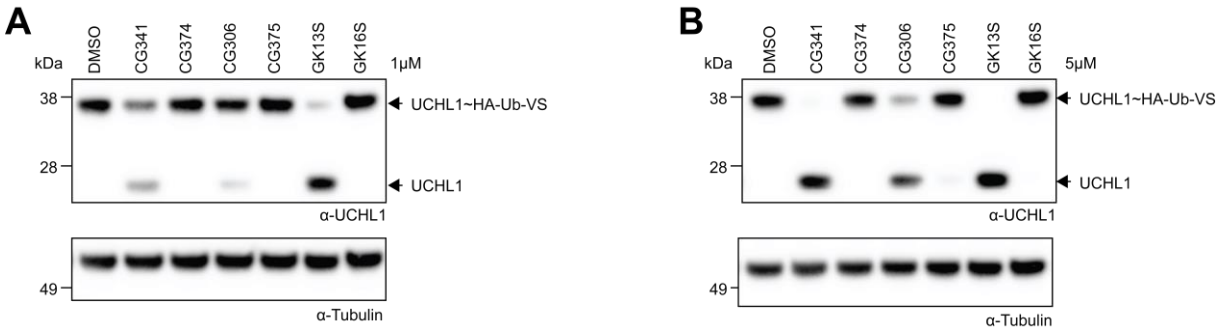

Figure 54. *N*-Cyanopiperazines CG306 and CG341 potently inhibit UCHL1 in HEK293 cell lysate. A, B. Comparison of inhibitory potency on cellular UCHL1 for *N*-cyanopiperazine-based compounds and their minimal probes. Western blot analysis of endogenous UCHL1 labelled with HA-Ub-VS after treatment of HEK293 cell lysate with indicated compounds or DMSO at either 1µM (**A**) or 5µM (**B**) concentration for 24 h. Experiments were performed by MSc. M. Schmidt.

Since CG341 and CG306 were shown to assess UCHL1 in a cellular context to a similar extent as GK13S, their specificity was investigated in intact U-87 MG cells, a human cellular system already established for the use of the probe pair of GK13S and GK16S. In an ABPP

experiment in intact U-87 MG cells at 1 µM (**Figure 55A**) and 5 µM (**Figure 55B**) probe concentration and 48 h treatment, CG306 showed strong binding of a protein band at the height of UCHL1, whereas the related minimal probe CG375 showed no protein labelling under these conditions. At a probe concentration of 1 µM, CG341 showed a less prominent protein band at the height of UCHL1 compared to the CG306 treated sample (**Figure 55A**). Although increasing the probe concentration of CG341 to 5 µM resulted in a higher overall signal of band intensity, as judged by the overall background reduction (**Figure 55B**), the band intensity of the protein at the height of UCHL1 at 1 µM probe treatment appeared to be slightly reduced compared to two other bands at the height of ~70 kDa (**Figure 55A,B**). Furthermore, the related minimal probe CG374 showed a weak signal for the potential UCHL1 protein band at both concentrations (**Figure 55A,B**). Importantly, none of the probes tested showed an additional protein band at the height of PARK7.

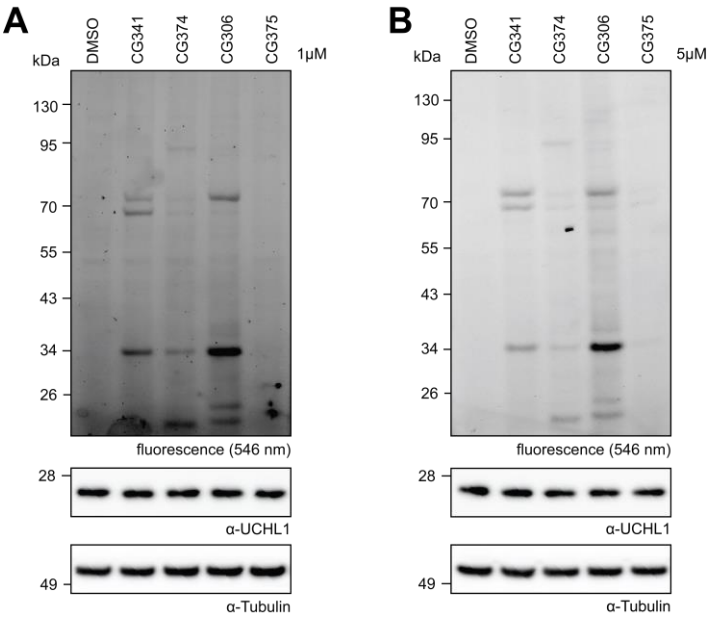

Figure 55. *N*-Cyanopiperazines CG341 and CG306 show improved selectivity towards UCHL1 in cells. A, B. Cellular activity-based protein profiling of intact U-87 MG cells treated with indicated compounds or DMSO at a concentration of 1µM (**A**) or 5µM (**B**) for 48 h.

To investigate whether the effect of phenocopying a UCHL1 mutant mouse, as shown for GK13S (**Figure 28A,B**), could be replicated with the piperazine probe pairs, quantification of free mono-Ubiquitin levels was performed by western blot analysis (**appendix, Figure 79**). As the band intensity for the DMSO control appeared to be reduced compared to the control probes (**appendix, Figure 79A,B**), and the experiment was only repeated once at the current time of writing, CG375 was used as a control for quantification of band intensities (**appendix, Figure 79C**), as it showed no protein labelling at probe concentrations up to 5 µM (**Figure 55B**). Ubiquitin levels in U-87 MG cells were reduced by 28% after incubation with 5 µM GK13S, consistent with the previous experiment (**Figure 28B**), where a reduction of 32% was observed. Under the same conditions, piperazines CG341 and CG306 induced a reduction of free Ubiquitin levels by ~17% and ~20%, respectively (**appendix, Figure 79C**). This is in line with their overall reduced potency compared to GK13S (**Figure 54A,B**) and the observed

difference in labelling intensity between CG341 and CG306 as seen on the gel (**Figure 55A,B**). Pursuant to the observed faint labelling of UCHL1 by minimal probe CG374 (**Figure 55B**), western blot analysis indicated a slight reduction of Ubiquitin levels by ~5% at 5 µM probe concentration (**appendix, Figure 79B**). Reduction of the probe concentration to 1 µM led to similar results with a slightly decreased effect on Ubiquitin level reduction (**appendix, Figure 79A**). Since this experiment was only be performed once at the current time of writing, these results have to be validated by additional repetitions.

Collectively, these data imply that piperazine probes CG306 and CG341 both show an increased UCHL1 selectivity in cells compared to parent probe GK13S. Neither CG306, nor CG341 displayed prominent off-target protein labelling in intact U-87 MG cells (**Figure 55A,B**), compared to a prominent PARK7 protein band in GK13S-treated samples (**Figure 19C**, **Figure 21A**, **Figure 27A**). Cellular analysis further indicates a better target engagement for CG341 compared to CG306 in HEK293 cell lysate (**Figure 54A,B**), whereas CG306 shows a stronger UCHL1 band intensity in intact U-87 MG cells (**Figure 55**), indicating an improved membrane permeability, further confirmed by an increased ability to reduce free Ubiquitin levels (**appendix, Figure 79A-C**). Since no protein labelling could be observed for the CG306 related minimal probe CG375 (**Figure 54A,B**), reactivity-driven off-target labelling seemed to be successfully evaded by this type of warhead. Along with its excellent selectivity profile at concentrations up to 5 µM in U-87 MG cells (**Figure 55**), these data qualify CG306 to further investigate the function of UCHL1 in a cellular context, even without the necessity for an additional control probe.

Despite superior *in vitro* properties of CG341, CG306 shows a stronger UCHL1 band intensity after treatment of intact U-87 MG cells (**Figure 55**) and an increased ability to reduce free Ubiquitin levels (**appendix, Figure 79A-C**). This indicates an improved membrane permeability of CG306 over CG341, which is in line with its higher calculated miLogP value (-1.07 vs. -3.01) (**Table 1**). The membrane permeability of small molecules is influenced by various physicochemical properties such as molecular weight, the quantity of hydrogen bond donors and acceptors and their polar surface area[234,235,236]. Previous studies have indicated that the number of hydrogen bond donors exposed to solvent in a lipophilic environment is a crucial determinant of membrane permeability[234,236]. Small molecules with a higher number of exposed amide NH-groups typically exhibit reduced lipophilicity and passive membrane permeability due to high desolvation penalties[234]. It has been shown that amide-to-ester substitution as well as N-methylation of amide groups that are exposed in a lipophilic environment improves membrane permeability.[234,237] Moreover, substitution of a hydrogen- by a fluorine-atom was shown to positively influence potency and cell permeability of small molecules.[238,239]

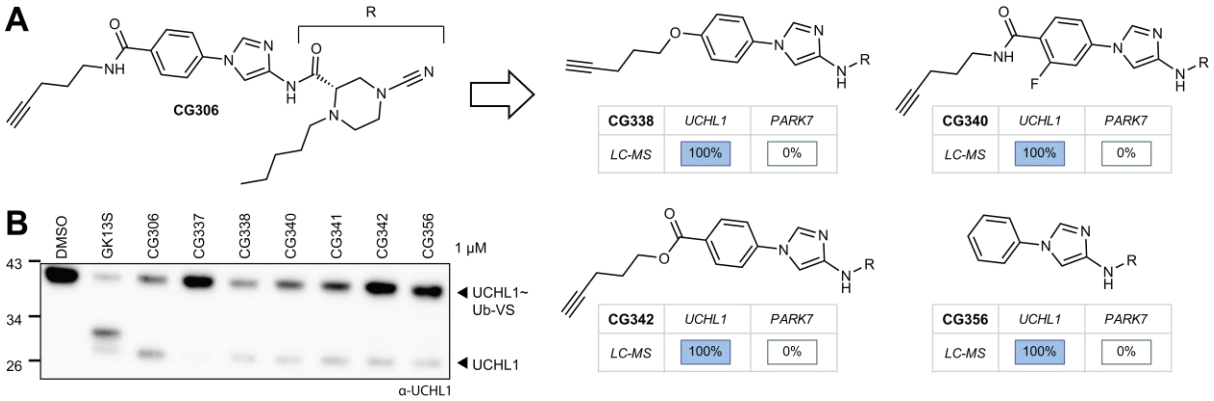

Figure 56. Different substitutions at the specificity element of CG306 fail to improve membrane permeability. A. Schematic representation and covalent, LC-MS derived UCHL1 and PARK7 modification of CG306-derived probes with shared warhead (-R), but different specificity element. For intact protein mass spectrometry UCHL1 (3 µM) or PARK7 (3 µM) were treated with compound (10 µM) or DMSO for 1 h. Differences in AUC values between compound and DMSO samples were calculated and illustrated as described for **Figure 44**. Respective LC-MS spectra are shown in **appendix, Figure 80B**. **B.** Inhibition of cellular UCHL1. Western blot analysis of endogenous UCHL1 labelled with HA-Ub-VS after treatment of intact HEK293 cells with either the indicated compounds or DMSO at 1 µM concentration for 24 h.

In an attempt to further improve membrane permeability of CG306, four analogues were synthesised during this thesis, bearing the same warhead as CG306, but different specificity elements (**Figure 56A**). Unfortunately, whether amide-to-ester (CG342), nor amide-to-ether (CG338) substitution led to an increased cellular labelling of UCHL1 (**Figure 56B**). Further, introduction of a fluorine in ortho position to the amide bond (CG340) which was thought to form F···H-N hydrogen bonds that potentially prevent repulsive interactions with the hydrophobic compartment of the cell membrane, failed to increase membrane permeability (**Figure 56B**). Even omission of the alkyne handle (CG356) led to reduced labelling of cellular UCHL1 compared to CG306, indicating that the benzylamide scaffold in combination with the alkyne handle is positively affecting membrane permeability. Future fluorine substitutions at the imidazole ring or N-methylation of the central amide might be able to improve membrane permeability of CG306.

5.9 Structural basis for enhanced piperazine-specific inhibition of UCHL1

In order to structurally characterise the binding of the piperazine warhead (CG341, CG306) and to identify different binding properties towards the pyrrolidine warhead (GK13S), crystallisation of a probe with a piperazine warhead in co-complex with UCHL1 should be established. Following lysine methylation, UCHL1 was covalently modified with CG341, as binding of the probe showed a higher degree of protein stabilisation (**Figure 50H-I**). Several fine screenings, based on the previously established condition for the meUCHL1~GK13S structure, resulted in the formation of crystals from which the structure of UCHL1 in complex with CG341 was solved to 2.20 Å resolution (**Figure 57A-C**).

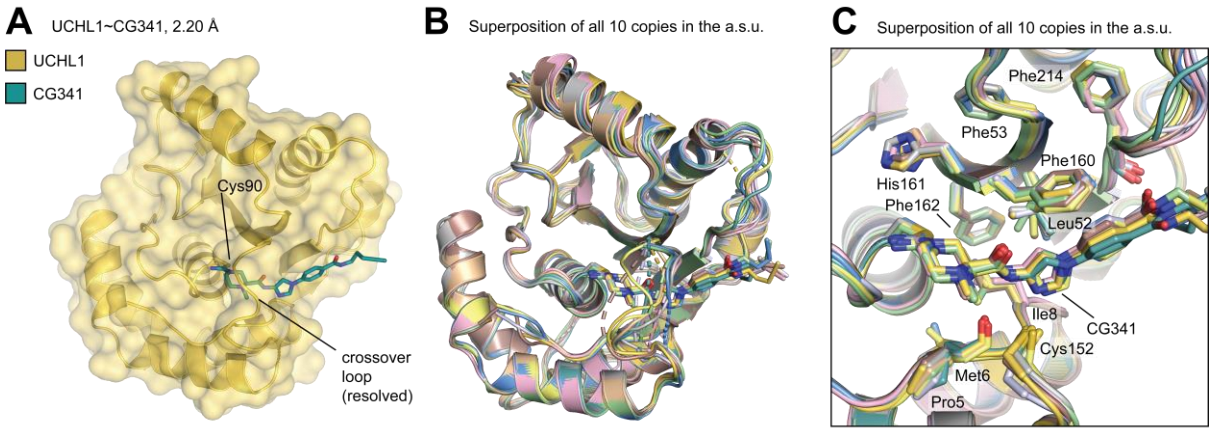

Figure 57. Structural analysis of specific binding of CG341 to UCHL1. A. Structure and surface of UCHL1 (yellow) in complex with CG341 (cyan). The covalently bound active site Cys90 and the resolved crossover loop are indicated. **B, C.** Superposition of all 10 copies within the asymmetric unit of the UCHL1~CG341 structure showing the entire protein (**B**) or the compound binding site (**C**). Labelled residues and the compound are shown as sticks, demonstrating that the same binding mode is observed in all copies.

Compared to meUCHL1~GK13S, no anisotropy scaling was necessary to solve the structure of meUCHL1~CG341. Although both structures show 10 copies in their asymmetric unit, they differ in their spatial arrangement (**appendix, Figure 81A-B**) and space group (P1 for meUCHL1~CG341 compared to $P2_12_12_1$ for the GK13S-bound structure). The ligand density of CG341 is remarkably well defined (in 5 copies fully defined, in 5 copies defined up to the alkyne handle) (**appendix, Figure 81C**) and the crossover loop is completely resolved (chains A, C, and G) or almost completely resolved (missing crossover loop residues: chains B and D: 2, chains E, H, and I: 3, chain J: 4 and chain F: 5). Superposition of all 10 copies revealed near identical positioning of the ligand in the active site (**Figure 57B-C**). CG341 is covalently bound to the catalytic cysteine Cys90 via an isothiourea with its cyanamide warhead, stabilised by the oxyanion hole (Gln84 and Gly87) and the residues of the catalytic triad are in hydrogen bonding distance (**Figure 58A-B**).

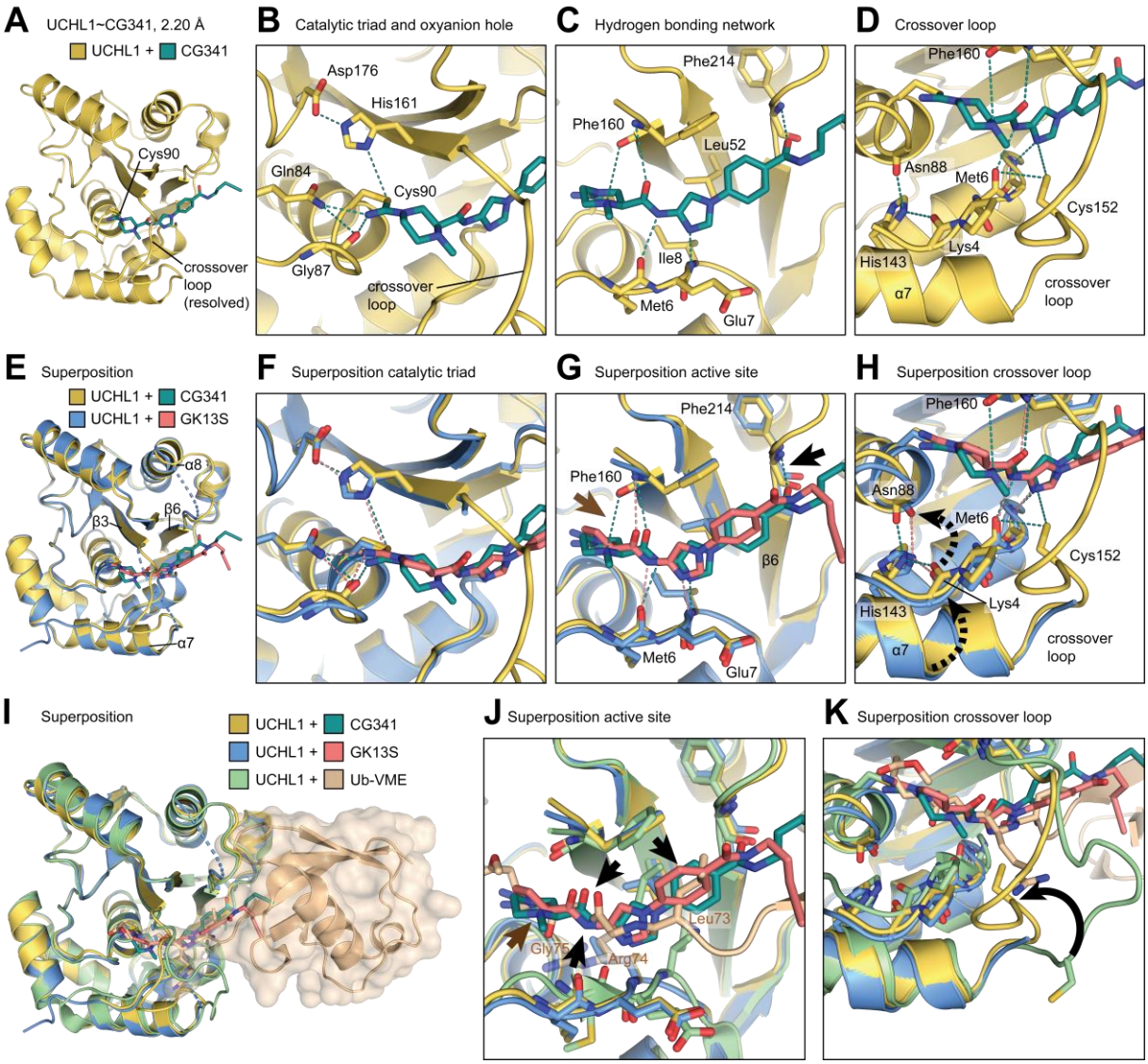

Figure 58. Piperazine-mediated hydrogen bonding promotes stabilisation of crossover loop. A-D. Structure of UCHL1 (yellow) in complex with CG341 (cyan) showing the entire protein (**A**), the catalytic triad and oxyanion hole (**B**), the compound binding site (**C**), or the crossover loop (**D**). CG341 (cyan) and key interacting residues are shown as sticks. Hydrogen bonds are shown as dotted lines for CG341 (cyan). **E-H.** Superposition of **A** with the structure of UCHL1 (blue) in complex with GK13S (red) (pdb: 7ZM0) showing the same protein sections as in **A-D**. Hydrogen bonds are shown as dotted lines in cyan for CG341 and red for GK13S. Differences in hydrogen binding are indicated with black arrows in **G**. Residues of UCHL1~CG341 adopting a different conformation compared to the GK13S-bound structure are indicated with dotted arrows in **H**. **I-K.** Superposition of **E** with UCHL1 (green) in complex with Ub-VME (gold) (pdb: 3KW5) showing the same protein sections as in **E**, **G** and **H**. Ubiquitin residues mimicked by both CG341 and GK13S are indicated with black arrows (a hydrogen bond acceptor, a hydrogen bond donor and the hydrophobic Leu73 side chain). An additional hydrogen bond mimicked by CG341 only is indicated with a brown arrow. Residues undergoing a conformational change upon Ubiquitin binding are indicated with black arrows in **K**.

The protonated *N*-methyl-piperazine, the central amide and the imidazole ring of CG341 extend to either side of the active site, forming hydrogen bonds with the backbone of Met6, Ile8 and Phe160, which also coordinate the C-terminal peptide of Ubiquitin (**Figure 58C**, **Figure 31B**). In chains C, D, E and I the decentral amide of CG341 and the backbone of

Phe214 are in hydrogen bond distance (**Figure 57C, Figure 58C**). Closer examination of the crossover loop revealed that Cys152 is in hydrogen bond distance to the backbone of Met6 and the imidazole ring of CG341 (**Figure 58D**), potentially stabilising the crossover loop. Superposition with the GK13S-bound structure (**Figure 58E-H**) showed overall high similarity (**Figure 58E**) and near identical positioning of the central amide and hydrogen bonding to the catalytic triad and oxyanion hole (**Figure 58F**). However, closer inspection of the compound binding site and the crossover loop revealed characteristic differences (**Figure 58G-H**). The hydrogen bond between the carbonyl adjacent to the phenyl ring in CG341 and the backbone of Phe214 (**Figure 58G**) potentially stabilises the C-terminal loop connecting α-helix 8 and β-sheet 6 of UCHL1 (**Figure 58E**), which is fully resolved in 9 chains and partly resolved in chain D (residues 209-211 missing) (**Figure 57B**). In comparison, the same loop is only resolved in 5 chains (B, D, E, H, I) for the GK13S-bound structure (**Figure 30B**). The most striking difference, however, is the additional hydrogen bond between the protonated *N*-methyl-piperazine of CG341 and the backbone oxygen atom of Phe160 (**Figure 58G**, brown arrow). Superposition of the two compound-bound UCHL1 structures with the Ubiquitin-bound structure (**Figure 58I-K**) revealed that the protonated nitrogen atom of the piperazine is in close proximity to the amide N-atom of Gly76 of the Ubiquitin C-terminus, both stabilising the crossover loop via a hydrogen bond to Phe160, whereas this stabilisation is absent in the meUCHL1~GK13S structure (**Figure 58G**). In addition, the benzyl ring of CG341 is slightly tilted towards the binding cleft compared to GK13S, resulting in a positioning that more closely resembles the hydrophobic side chain of Leu73 of the Ubiquitin C-terminus (**Figure 58J**). Furthermore, binding of CG341 to the active site Cys90 in UCHL1 induces rotation of the adjacent Asn88 and the, via a hydrogen bond connected, His143 (**Figure 58H**). This results in an upshift of the active site backbone (**Figure 58H**, top arrow) as well as the α7 helix (**Figure 58H**, bottom arrow). Compared to the Ubiquitin-bound structure, where the crossover loop points in the opposite direction of the active site, stabilisation via hydrogen bonding of Cys152 in the meUCHL1~CG341 structure leads to a different positioning of the crossover loop, closer to the active site (**Figure 58K**); a rearrangement that is hindered in the Ubiquitin-bound structure by the large C-terminal Ubiquitin residue Arg74. Since the crossover loop was not resolved in any copy of the GK13S-bound structure, the conformational change and stabilisation upon additional hydrogen bonding of the piperazine moiety in the CG341-bound structure is likely to account for the significant difference in the resolution of the crossover loop between the two structures and provides a possible explanation for the different space groups and spatial arrangements of their asymmetric unit (**appendix, Figure 81A,B**).

Although CG341 and GK13S bind the active site of UCHL1 in a very similar manner (**Figure 58G**), closer examination of the warhead binding environment revealed that CG341, but not

GK13S, occupies a small cleft in UCHL1 formed by the surrounding residues Pro5, Met6 and Cys152 (**Figure 59**). The piperazine warhead of CG341 directs the *N*-methyl substituent into the aforementioned pocket (**Figure 59B**) that is unoccupied in the GK13S-bound structure (**Figure 59C**), demonstrating a better recognition of CG341 by UCHL1 and further contributing to its specificity.

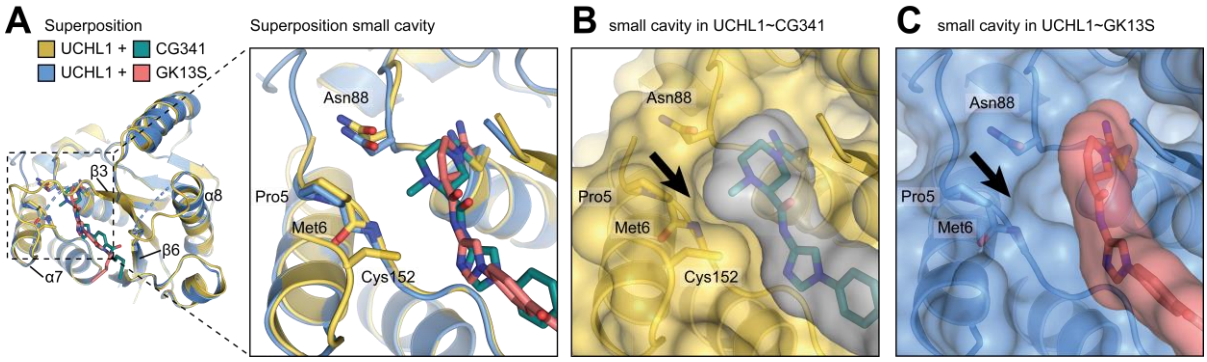

Figure 59. The *N*-methyl piperazine moiety of CG341 occupies a small cavity near the active site of UCHL1. A. Superposition of UCHL1~CG341 with UCHL1~GK13S and close-up view of a small cleft near the active site, formed by the indicated residues. **B-C.** Structures of UCHL1~CG341 (**B**) and UCHL1~GK13S (**C**) in surface representation, showing the same protein section as in **A**. The black arrow indicates a small cavity near the active site of UCHL1 formed by Pro5, Met6 and Cys152.

Taken together, CG341 induces a similar hybrid conformation as GK13S, but is able to undergo additional hydrogen bonding (**Figure 58G**). This triggers a slight conformational change (**Figure 58H**) leading to stabilisation of the crossover loop. The stabilisation of the protein by additional hydrogen bonding is consistent with the higher melting temperature of UCHL1 upon CG341 binding, compared to GK13S binding (**Figure 50H**). Although the piperazine warhead of CG341 was shown to bind considerably slower than the pyrrolidine warhead of GK13S (**Figure 50C-F**), the enhanced ability of CG341 to mimic the Ubiquitin C-terminal tail, together with the additional occupancy of a small cavity near the active site of UCHL1 (**Figure 59**), demonstrates that CG341 is more tightly recognised by UCHL1 than GK13S. This further supports the hypothesis of a more specificity-driven binding mechanism of the piperazine- compared to the pyrrolidine warhead, providing an explanation for the enhanced UCHL1 specificity of CG341 towards off-target proteins such as PARK7 and USP30, compared to GK13S (**Figure 52**).

6 A dual-functional-warhead approach to address novel DUBs (Project 3)

Structural information about specific inhibitors with cellular potency is only available for a limited number of DUBs[156,240], including USP14[241], USP7[240,242], and the coronavirus protease PLpro[243]. It is noteworthy that in these cases, despite the entirely different DUB fold, the C-terminal tail of Ubiquitin is recognised via a tube-like structural scaffold, similar to the crossover loop of UCHL1, featuring the property of being solvent-accessible at both ends (**Figure 60**).

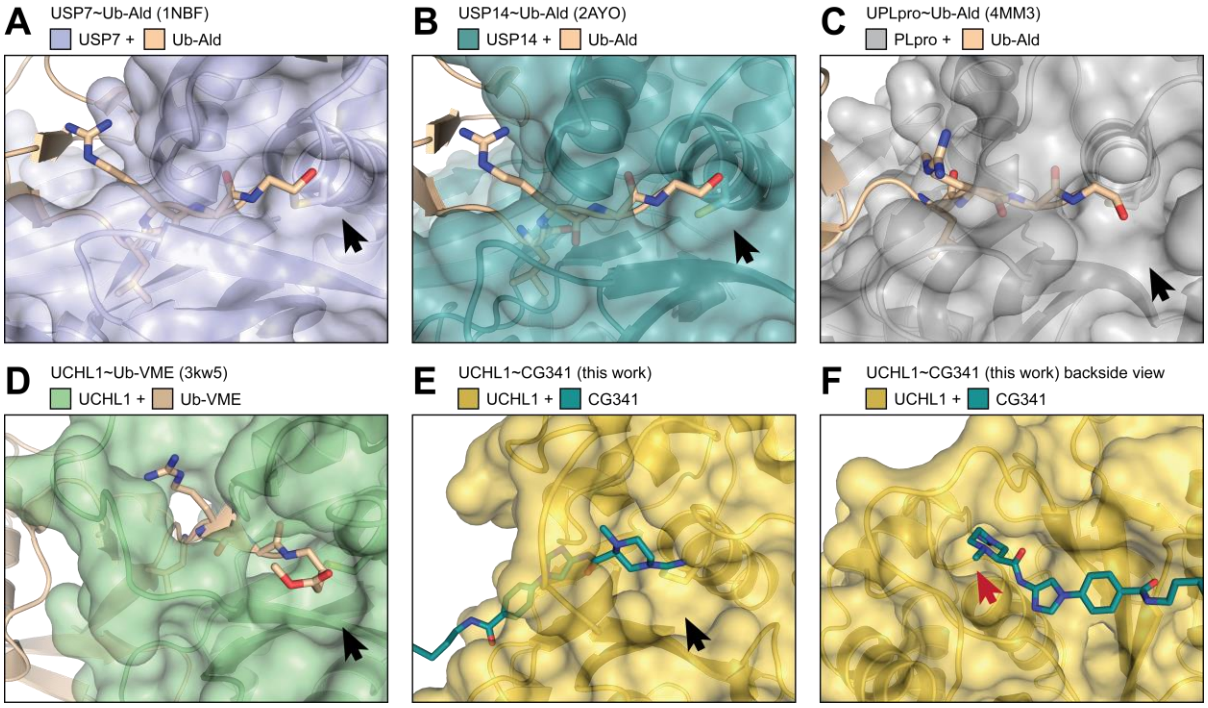

Figure 60. The general recognition of the Ubiquitin C-terminus by DUBs is based on a shared, structural scaffold, that is solvent accessible at both ends. A-D. Selection of structurally characterised DUB inhibitors of USP7 (**A**), USP14 (**B**), SARS PLpro (**C**) and UCHL1 (**A**). Shown is a close-up view of their binding pockets from Ubiquitin-bound co-crystal structures. **E.** Close-up view of the UCHL1~CG341 binding pocket. Same orientation as in **A**-**D**. The black arrows indicate solvent-exposed areas offering potential space for additional alkyne-handle modifications. **F.** Backside view of **E**. The red arrow indicates the putative position of the alkyne-handle in probes CG225 and CG227.

This characteristic makes it likely for ABPs, that bind to the active site and additionally present an alkyne-handle that is connected to the warhead, to still be accessible for click-chemistry (**Figure 60**, black arrows). Based on this hypothesis, cyclic, *N*-cyano-nitrile containing, putative DUB-targeting warhead-precursors of different ring size were designed and synthesised, bearing an additional alkyne handle for biorthogonal functionalisation and a carboxylic acid group for readily connection to various specificity elements (**Figure 61A**).

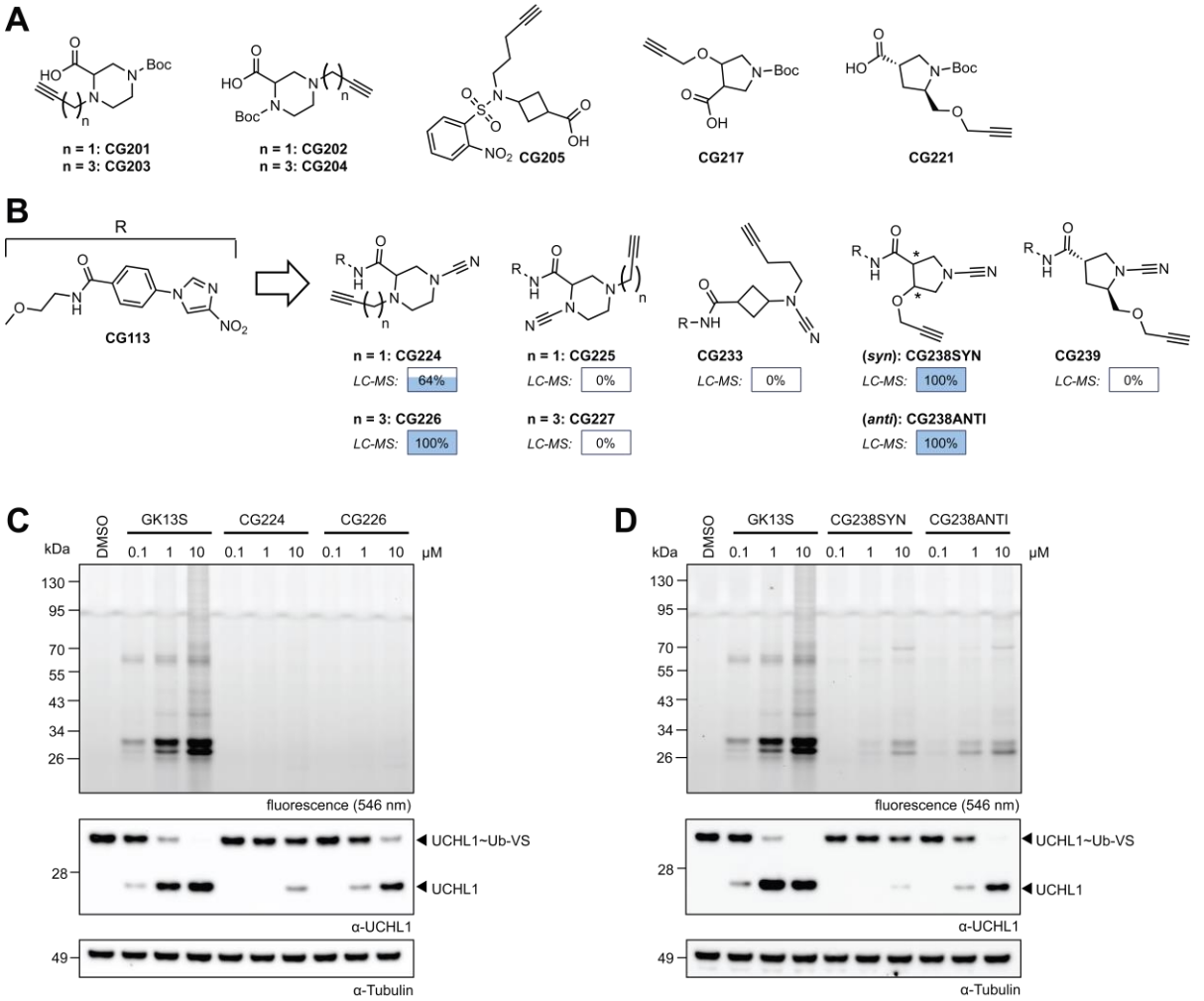

Figure 61. Cellular activity-based protein profiling of a selection of probes with warhead-attached alkyne handle indicated general feasibility of the dual-functional-warhead approach. A. A selection of dual functional warheads was designed and synthesised based on commercially available 4-6 membered ring scaffolds. **B.** Dual-functional-warheads from **A** were fused to Cpd118-precursor CG113 to generate the illustrated activity-based probes. Then binding of these probes (10 µM) to recombinant UCHL1 (3 µM) was evaluated by intact protein mass spectrometry. For related LC-MS spectra see **appendix, Figure 82**. **C, D.** Cellular activity-based protein profiling of intact HEK293 cells treated with indicated compounds or DMSO for 24 h (upper panel) as well as associated western blot analysis of cellular UCHL1 labelled with HA-Ub-VS (lower panel). Assays in **C-D** were performed by MSc. M. Schmidt.

To initially validate, if DUB-binding of dual-functional warhead-bearing molecules is still given, the UCHL1-specific binding element of GK13S parent inhibitor CG118 was fused to the new developed warheads and UCHL1 binding assessed *in vitro* (**Figure 61B**). At a probe concentration of 10 µM, 2-carboxy-*N*-cyano-piperazines CG225 and CG227 and cyclobutene-based probe CG233 did not show any covalent modification of UCHL1. Future studies have to reveal whether this could be explained by the general disability of these types of warheads to label UCHL1. Likewise, 3-carboxy-*N*-cyanopyrrolidine CG239 did not bind to UCHL1 under these conditions, but CG238-SYN and CG238-ANTI were able to label UCHL1 in full extent. This is in line with the results of the labelling experiments (**Figure 44**) of their analogue probes

CG287 and CG385, respectively. While the rather short alkyne-handle of 3-carboxy-*N*-cyanopiperazine CG224 might clash with the active site of UCHL1 (**Figure 60F,** red arrow) and hence counteract binding (~60% UCHL1 modification, **Figure 61B**), CG306-analogue CG226 demonstrated full UCHL1 modification, which is in agreement with previous CG306 labelling experiments (**Figure 49**, **Figure 50A**) and available, solvent accessible space as judged from the meUCHL1~CG341 co-crystal structure (**Figure 60F,** red arrow).

7 Summary and Conclusion (Project 2 & 3)

A crystal structure of PARK7 in co-complex with the minimal probe GK16S revealed differences in the binding site compared to that of UCHL1 (**Figure 39**). Whereas UCHL1 features a broader binding site environment surrounding the pyrrolidine warhead of GK13S, the binding cleft of PARK7 is rather enclosing the same structural element in the GK16S-bound structure. Following the reported activity of truncated GK13S analogues towards UCHL1 (**Figure 40**), the design of probes based on a GK13S binding element, but with modifications at the pyrrolidine ring was established (**Figure 41**). Computational docking of the designed probes into the GK13S binding environment of UCHL1 revealed that binding of almost all probes is theoretically possible, while maintaining a similar binding position of the warhead as in the GK13S-bound structure (**Figure 42**). Five analogues of GK13S with substitutions at different positions of the pyrrolidine ring and in varying stereochemical configurations were planned to be synthesised (**Figure 43**, **Scheme 11**-**Scheme 17**). During the synthesis of the acid precursors for probes CG287 and CG288, epimerisation, based on deprotonation of an acidic Cα-atom led to the formation of the less sterically hindered *anti*-intermediate (CG281) in large access. As a consequence, only the pure *anti*-oriented probe CG287 could be synthesised (**Scheme 12**). Similar difficulties were encountered in the synthesis of *syn*- and *anti*-CG385 (**Scheme 14**). Although *syn*- and *anti*-CG373 could be successfully separated by preparative HPLC, subsequent basic ester hydrolysis resulted in deprotonation of a Cα-atom at C4-position of the pyrrolidine ring. This resulted in 1) epimerisation that led to the formation of only *anti*-CG385, which appears to be the thermodynamically favoured product, and 2) elimination of MeOH with formation of a double bond between the C2- and C3-atoms of the pyrrolidine ring (**Scheme 15**).

After effective synthesis of the probes CG287, *anti*-CG385 and CG390 with pyrrolidine ring-modifications at the C2-, C3- and C5-positions, respectively, *in vitro* characterisation revealed potent, nanomolar inhibition of recombinant UCHL1 by probes CG385 and CG390, whereas CG287 showed no UCHL1 binding (**Figure 45**). The high rotational freedom of the methyl-methoxy group at the warhead of CG287 could either lead to a different orientation in the binding site of UCHL1 as predicted (**Figure 42B**) and thereby impede binding, or prevent the probe from locking UCHL1 in a compound-induced hybrid conformation, a process critical for binding of GK13S (**Figure 32**). To rule out false negative binding of CG287 due to incorrect stereochemistry of the educts or errors during synthesis, chiral HPLC could in future provide information on the actual stereo configuration of CG287. However, even the (*R*)-isomer of GK13S (GK13R) inhibited recombinant UCHL1 with an IC_{50} of 2 µM (vs. 66 nM for GK13S),

whereas no significant degree of inhibition could be observed for CG287, disqualifying the probe for further studies regardless of its stereo configuration.

While both GK13S and CG385 showed equipotent binding to PARK7 and UCHL1 *in vitro* at a concentration of 10 µM (**Figure 44**), an improved UCHL1 over PARK7 selectivity was observed for CG390. Cellular characterisation in HEK293 cell lysate revealed reduced off-target labelling for CG390 compared to the other probes tested. However, a prominent protein band at the height of PARK7 indicated that CG390 does not retain UCHL1 selectivity in a cellular environment. Further cellular target validation by siRNA-mediated knockdown of UCHL1 and PARK7 is required to verify the identity of the protein bands.

By changing the warhead to a piperidine scaffold in CG305, PARK7 labelling was effectively prevented even at a probe concentration of 10 µM (**Figure 47A-C**). To antagonise the associated ~20-fold reduction in UCHL1 potency compared to GK13S (IC_{50} of 1496 nM vs. 66 nM), morpholine and piperazine warhead analogues of CG305 with different physicochemical properties were designed and synthesised (**Figure 47D, Table 1, Figure 48**). In-depth *in vitro* characterisation revealed that the 3-carboxy-*N*-cyanopiperazines CG306 and CG341 exhibit high UCHL1 over PARK7 selectivity (**Figure 49**, **Figure 62**), while retaining UCHL1 potency with IC_{50} values of 254 nM and 191 nM, respectively (**Figure 50A-B**). While GK13S shows additional *in vitro* labelling of the DUB USP30, a common (off-)target of *N*-cyanopyrrolidine-based inhibitors, both *N*-cyanopiperazines were able to prevent USP30 labelling (**Figure 52**). An ongoing DUB-wide *in vitro* screen will provide further details on the selectivity profile of cyanopiperazines versus cyanopyrrolidines.

The rate constant $k_{obs}/[I]$, which describes the covalent mode of inhibition, was found to be lower for CG341 and CG306 compared to GK13S ($k_{obs}/[I]$ = 94 M^{-1} s^{-1} and 61 M^{-1} s^{-1} vs. 492 M^{-1} s^{-1}), indicating a more selectivity-driven binding mechanism (**Figure 50C-G**) that could lead to the observed improvement in selectivity towards off-target protein labelling. Further improvement in UCHL1 potency and/or acceleration of binding to UCHL1 could be achieved by further modification of the piperazine warhead. Homopiperazine, for instance, adopts a pseudo-chair conformation with flexible N-N distance depending on the presence and nature of a bridged ring system[223]. Since chemical constitution of the warhead seemed to greatly influence UCHL1 potency and selectivity of the probe, the conformational flexibility of the homopiperazine scaffold may offer new perspectives and opportunities to further improve binding properties.

Neither CG306 and CG341, nor their related minimal probes CG374 and CG375, showed labelling of a protein band at the height of PARK7 in intact U-87 MG cells (**Figure 55**). Furthermore, none of these probes showed covalent binding to recombinant PARK7 (**Figure**

50A), ruling out a fully reversible binding mode, highlighting their value for the specific investigation of cellular UCHL1 (**Figure 62**). Both CG341 and CG306, but not their minimal probes, were able to phenocopy the effect of reduced mono-Ubiquitin levels upon mutant UCHL1 overexpression, as shown for GK13S (**Figure 28A,B**), but with slightly reduced efficiency. This not only validates the use of U-87 MG cells as a suitable model system for UCHL1-dependent phenotypes, but also highlights the success of optimising the selectivity of GK13S in terms of reduced off-target labelling of piperazine-based probes towards UCHL1.

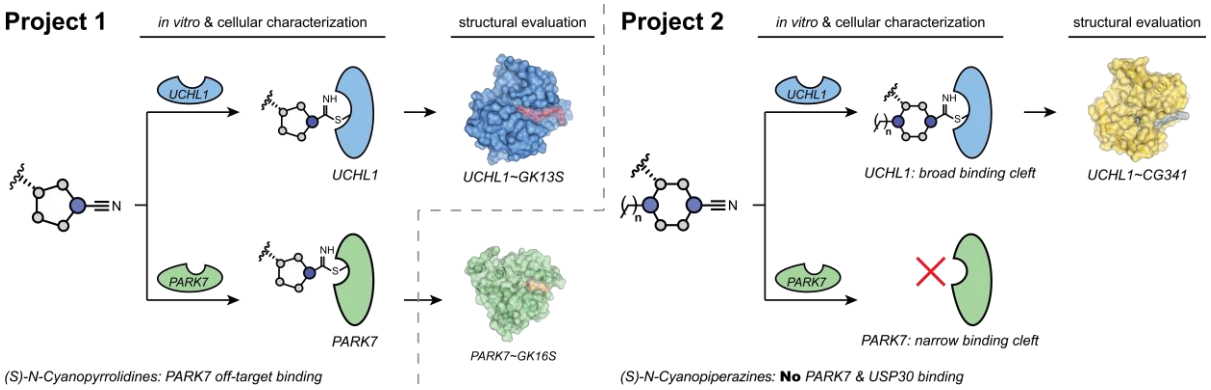

Figure 62. Schematic summary of project 1 and 2. In-depth *in vitro* and co-crystal structure analysis of the chemogenomic probe pair GK13S and GK16S in combination with ABPP revealed PARK7 as the major off-target protein of 3-carboxy-*N*-cyanopyrrolidines. A Change of the warhead to a 3-carboxy-*N*-cyanopiperazine moiety could be shown to effectively avoid PARK7 and also USP30 off-target labelling *in vitro* and in cells.

The crystal structure of UCHL1 in co-complex with CG341 (**Figure 57**) shows a high overall similarity to the GK13S-bound structure (**Figure 58E**), and both GK13S and CG341 induce a homologous hybrid conformation in UCHL1 (**Figure 58E-K**) and bind to the active site of UCHL1 in a closely related manner (**Figure 58F,G**). However, detailed comparison of the two structures revealed that the different size, shape and composition of the piperazine warhead of CG341 facilitates additional interactions with the UCHL1 binding site (**Figure 58G,H**), accounting for the observed improvement in selectivity of piperazine-based probes towards UCHL1 (**Figure 62**). Binding of CG341 induces a slight conformational change compared to the GK13S-bound structure (**Figure 58H**), and the protonated *N*-methyl piperazine moiety allows for additional hydrogen bonding (**Figure 58G,H**) as well as hydrophobic interactions with a small cavity near the active site (**Figure 59**). Notably, the involvement of crossover loop residues Phe160 and Cys152 in these interactions contributes significantly to the stabilisation of the crossover loop of UCHL1, a feature lacking in the GK13S-bound structure (**Figure 30A**). Although catalysis of UCH enzymes does not rely on the physical integrity of the crossover loop, it provides connectivity for critical active site residues.[244] In the absence of substrate, the crossover loop is flexible and often not visible in crystal structures, as seen in the structure of GK13S in co-complex with UCHL1 (**Figure 30A, D**, **Figure 58E**). The functional significance

of this loop and its dynamic behaviour during catalysis remains unclear, but it has been suggested that the loop contributes to the precise positioning of the active site of the enzyme to accommodate the substrate.[244] The structural integrity of the crossover loop provides the basis for future studies in order to understand its functions in catalysis. It contributes a structural basis for the design of novel inhibitors with improved crossover loop stabilisation features to further enhance UCHL1 selectivity. In addition, the crossover loop residue Cys152 may serve as an additional site for covalent modification by probes with “dual”-warheads, an approach that has been shown to significantly increase target protein selectivity of inhibitors targeting fibroblast growth factor receptors (FGRs) and potentially overcome drug-induced resistant mutations.[245]

Comparison of available Ubiquitin-bound DUB crystal structures revealed a common structural tube-like scaffold that guides the Ubiquitin C-terminal peptide to the catalytic cysteine (**Figure 60**). Based on the property of the scaffold to be solvent accessible at both ends, novel dual-functional warheads were synthesised to readily generate libraries of diverse, DUB-targeting probes. Proof of concept was achieved by demonstrating that the known UCHL1-binding scaffold of CG118, fused to a 3-carboxy-*N*-cyanopyrrolidine warhead with an alkyne handle on the pyrrolidine ring, is still able to access cellular UCHL1 association. It is tempting to speculate that the tubular structural scaffold of other DUBs (**Figure 60**) may also allow targeting of probes with dual-functional warheads, and that the additional alkyne moiety may help to prevent binding to non-DUB proteins, as seen with CG238-ANTI. Thereupon, a library of ABPs with warheads of different ring sizes and shapes, fused to a variety of readily accessible specificity elements will have to be synthesised in the future. Cellular and biochemical target engagement of these probes will hopefully confirm the advantage of this approach and identify novel DUB targets.

In conclusion, the results of this thesis shed light on the molecular mechanism underlying the specificity of the pyrrolidine-based small molecule probe GK13S and the piperazine-based probes CG341 and CG306 towards UCHL1. The findings of the study have important implications for the development of more specific and effective tools to target and investigate UCHL1 and other DUBs in disease relevant pathways. The study highlights the importance of a conformational adaptability in the specificity of inhibitors targeting UCHL1 and provides a basis for future studies aimed at developing new drugs targeting UCHL1 and other members of the UCH family of DUBs. It also proposes a dual-functional warhead approach that can serve as a starting point for the easy generation of large and diverse ABP libraries to identify new and specific DUB-targeting probes, thereby helping to investigate the importance of these DUBs in disease-relevant pathways or enabling the development of novel drugs.

8 Outlook

Worryingly, numerous papers have relied on LDN-57444 as a compound, despite its inherent limitations. These studies have been widely cited and have formed the basis for follow-up studies. For example, LDN-57444 has been used in cancer-related research to identify UCHL1 as a prognostic marker in neuroblastoma cell differentiation, and attempts have been made to improve its aqueous solubility for the treatment of invasive carcinomas.[246] However, recent data suggest that LDN-57444 lacks the necessary potency and selectivity to serve as a reliable UCHL1 probe, casting doubt on the robustness of these studies.[1,177] To complicate matters further, LDN-57444 contains an N-oxime chemical moiety, which is known to be unstable at mildly acidic or physiological pH, making interpretation of experiments with this compound difficult.[247] In the field of successful drug discovery, the use of high quality chemical probes plays a critical role in the validation of biological targets. Unfortunately, the use of poor quality probes such as LDN-57444 can easily lead to misleading results in these investigations. A truly high quality probe must possess experimentally proven attributes, including high potency, selectivity, cellular efficacy, and permeability, to serve as a reliable tool for testing biochemical hypotheses and validating novel therapeutic targets.[248,249] The probe pair GK13S & GK16S as well as the probes CG341 and CG306 stand out as high quality chemical probes, with GK13S & GK16S currently commercially available. They are valuable for the study of UCHL1 not only in cancer-related pathways, but also in any disease or mechanistic investigation involving UCHL1. Their versatility extends to other cancer contexts where UCHL1 plays a role in regulating EGFR expression, such as EGFR+ colorectal cancer[250], drug-resistant breast cancer[251] as well as thyroid and glioma carcinomas[252]. In addition, they can find relevance in cancers that respond to UCHL1 inhibition, such as non-small-cell lung cancer (NSCLC), where UCHL1 has recently been shown to regulate the expression of programmed cell death ligand 1 (PD-L1) within the AKT/P65 signalling pathway.[253] Beyond cancer, the probes may serve as powerful tools to explore UCHL1-mediated TGF-β signalling in non-cancerous contexts, such as cardiac remodelling.[254] They will be useful tools for understanding the intricate involvement of UCHL1 in maintaining protein quality control and preventing protein aggregation, thereby helping to uncover important insights into the mechanisms underlying neurodegenerative diseases such as Alzheimer's, Parkinson's, and Huntington's disease.[255] By helping to identify how UCHL1 dysfunction or dysregulation contributes to the accumulation of toxic protein aggregates and neuronal damage, the probes may advance the development of targeted therapies aimed at restoring proper protein degradation pathways and ameliorating disease progression, particularly with regard to their non-toxic properties.

In future investigations, it will be essential to gain a comprehensive understanding of the regulatory mechanisms that control UCHL1 expression and activity, as current knowledge remains limited. Demonstrating the impact of modulating UCHL1 on disease-related pathways using the herein described probes could provide stronger evidence of its relevance to disease progression and pave the way for the development of more effective and targeted treatments. Due to their non-toxic properties, the probes could be optimised to design therapeutic compounds that modulate UCHL1 activity in a controlled and safe manner, potentially leading to innovative treatments for neurodegenerative diseases and cancer. Non-toxic UCHL1-targeting probes could also have diagnostic applications. They could be used to monitor UCHL1 activity levels in patient samples or living organisms, providing insights into disease progression and response to treatment. This could contribute to early diagnosis and personalised medicine approaches. In essence, the herein described, specific and non-toxic UCHL1-targeting small molecule-based probes could revolutionise our understanding of the role of UCHL1 in diseases, allowing precise control of its activity and shedding light on its contribution to cancer and neurodegenerative diseases. This knowledge could pave the way for the development of novel treatments and diagnostic tools for these challenging diseases.

8 Appendix

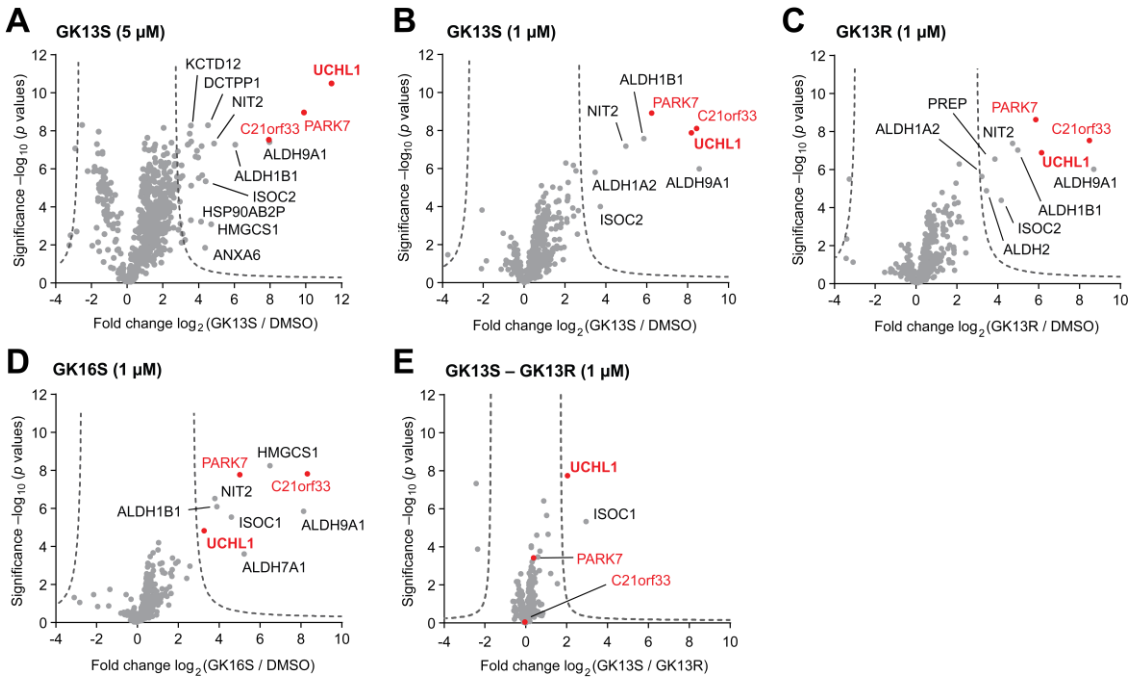

Figure 63. Identification of cellular targets. Proteomics-based target identification of indicated probes. Volcano plots show the relative label-free abundance ratio (fold change) of proteins between indicated samples. Compare **Figure 21C**. Cells were treated for 24 h at indicated concentrations. UCHL1, PARK7 and the PARK7-homologue C21orf33 are marked in red. Assays were performed and evaluated by MSc. M. Schmidt.

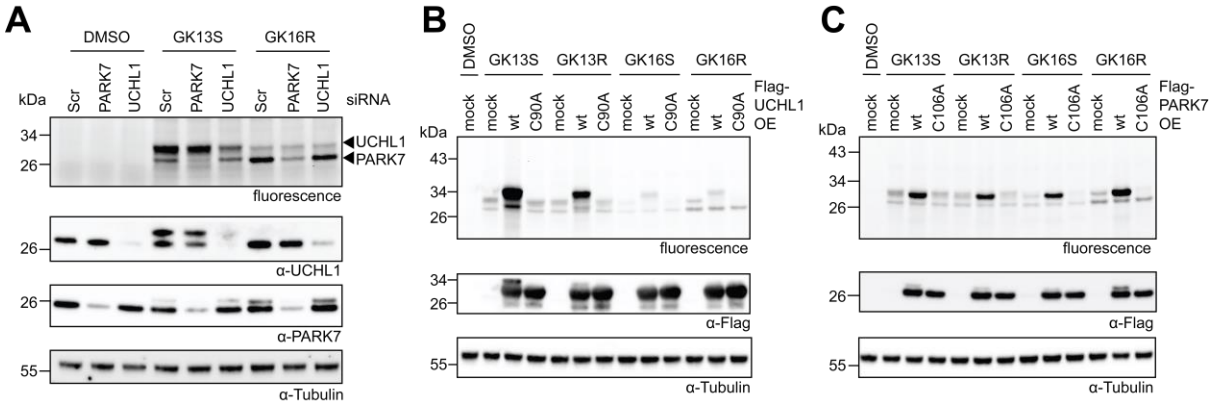

Figure 64. Cellular target validation of the probe pair GK13S and GK16S. A. Target validation through siRNA-mediated knockdown of UCHL1 and PARK7 in HEK293 cells after treatment with indicated compounds (1 µM, 1 h). Fluorescence gel band identities of UCHL1 and PARK7 derived from western blots are shown as black arrows. **B, C.** Determination of sites of covalent modification through overexpression (OE) of Flag-UCHL1 (wt and C90A active site mutant, **B**) and Flag-PARK7 (wt and C106A active site mutant, **c**) in HEK293 cells after treatment with indicated compounds (1 µM, 1 h). wt, wildtype. Assays were performed and evaluated by MSc. M. Schmidt.

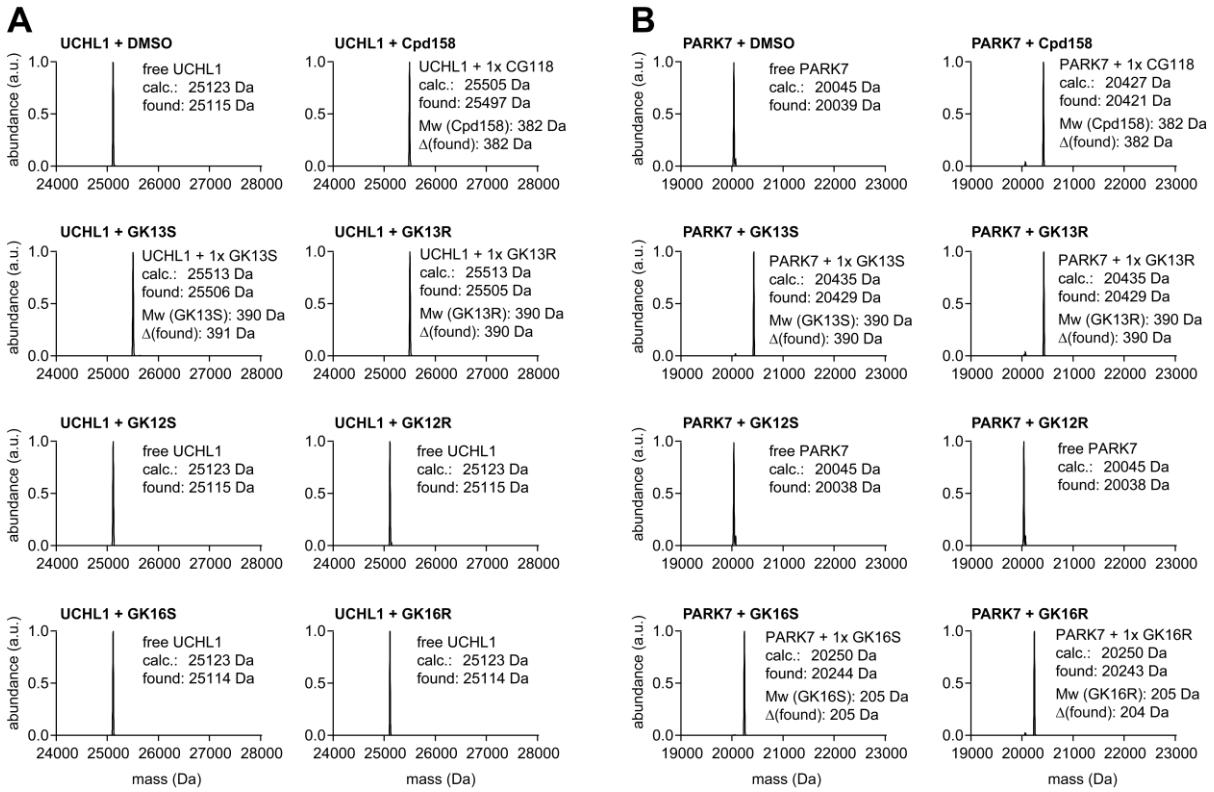

Figure 65. In vitro characterisation of probe binding. A, B. Intact protein mass spectrometry data of indicated compounds binding to recombinant UCHL1 (**A**) or PARK7 (**B**). UCHL1 (3 µM) or PARK7 (3 µM) were treated with compounds (10 µM) or DMSO for 16 h. Observed masses were assigned to given species with listed expected masses.

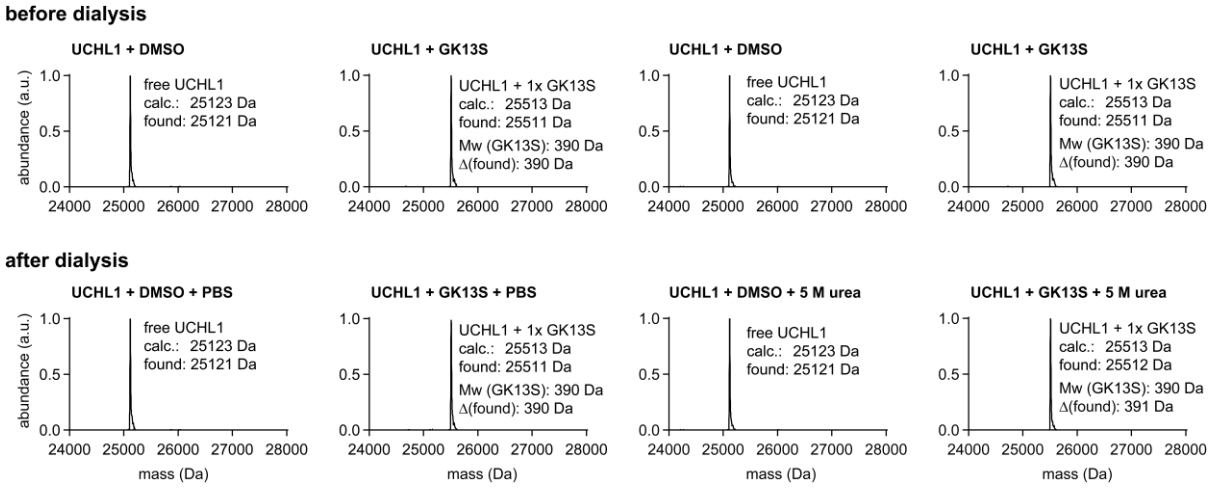

Figure 66. Dialysis dilution assay. UCHL1 was treated with DMSO or an excess of GK13S (upper panel), then diluted 5-fold with PBS or 5 M urea as indicated, dialysed overnight into PBS and its protein mass was determined (lower panel).

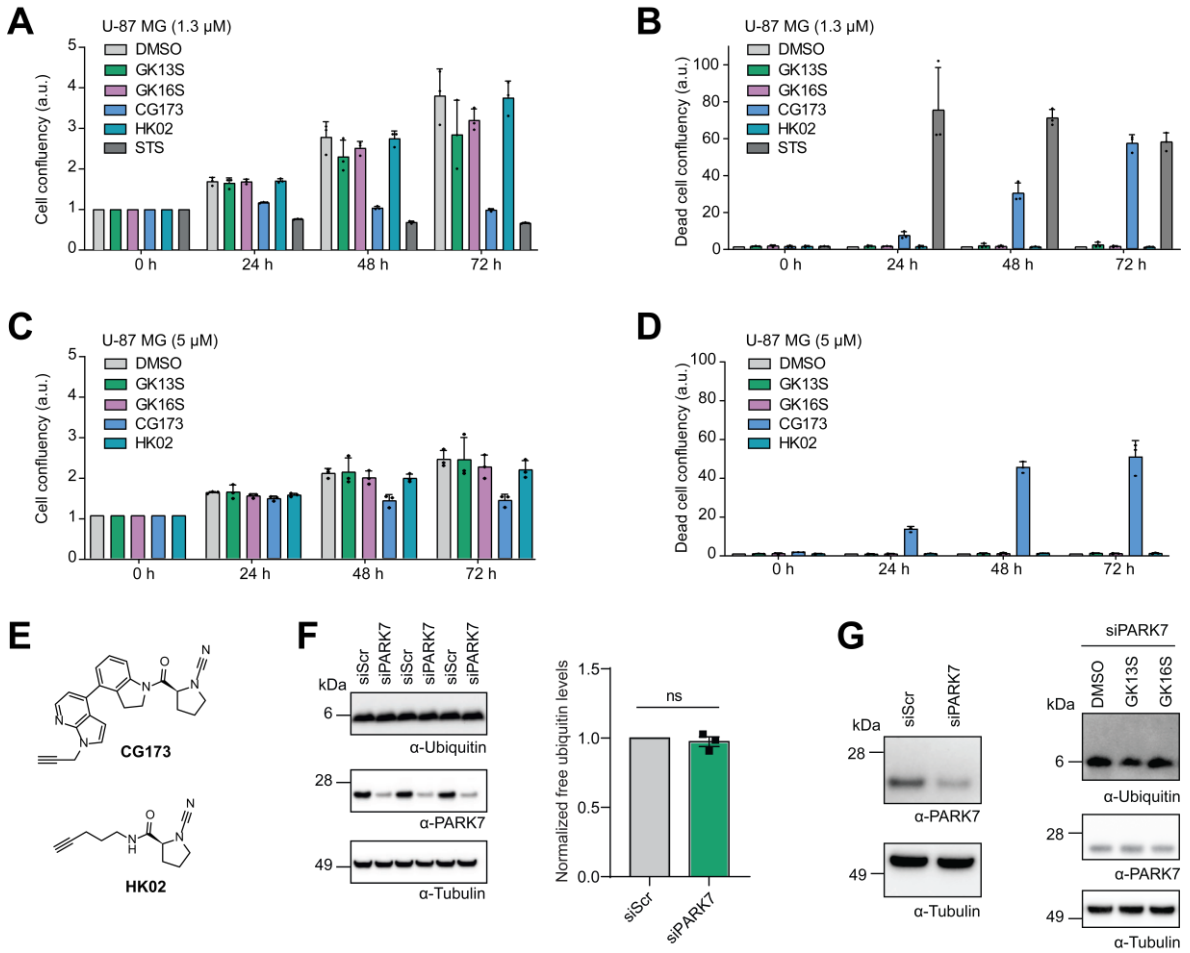

Figure 67. 2-, but not 3-carboxy-*N*-cyanopyrrolidines induce apoptosis in U-87 MG cells. **A.** Quantification of U-87 MG confluency observed at 24, 48 and 72 h post treatment with 1.3 µM of the indicated compounds. Confluency is normalised to that observed at 0 h. Data are shown as means of N = 3 independent experiments. Error bars represent standard deviation. **B.** Quantification of U-87 MG PI positive cells observed at 24, 48 and 72 h post treatment with 1.3 µM of the indicated compounds. Confluency is normalised to that observed for DMSO at each time point. PI positive cell confluency is adjusted to overall cell confluency. Data are shown as means of N = 3 independent experiments. Error bars represent standard deviation. **C.** Quantification of U-87 MG confluency observed at 24, 48 and 72 h post treatment with 5 µM of the indicated compounds as in **A**. Data are shown as means of N = 3 independent experiments. Error bars represent standard deviation. **D.** Quantification of U-87 MG PI positive cells observed at 24, 48 and 72 h post treatment with 5 µM of the indicated compounds as in **B**. Data are shown as means of N = 3 independent experiments. Error bars represent standard deviation. **E.** Structural comparison of probe CG173 and corresponding minimal probe HK02S. **F.** Western blots showing that depletion of PARK7 in U-87 MG does not change mono-Ubiquitin levels. Quantitation as in **Figure 28A**. N = 3, values are plotted as mean ± standard error of the mean. Statistical significance was analysed using a one sample, two-tailed t-test compared to the mean of '1' as set for the siScr samples. ns, not significant. **G.** Western blots showing effective depletion of PARK7 in U-87 MG cells (left panel). Samples were treated with DMSO for 48 h to exactly mimic the conditions used for experiments shown in **Figure 28A**. Western blots showing mono-Ubiquitin levels in PARK7-depleted U-87 MG cells treated with GK13S or GK16S (right panel). Compare **Figure 28A**. The assay was performed, and data as well as graphs kindly provided by Dr. Rachel O'Dea and MSc. Kai Gallant.

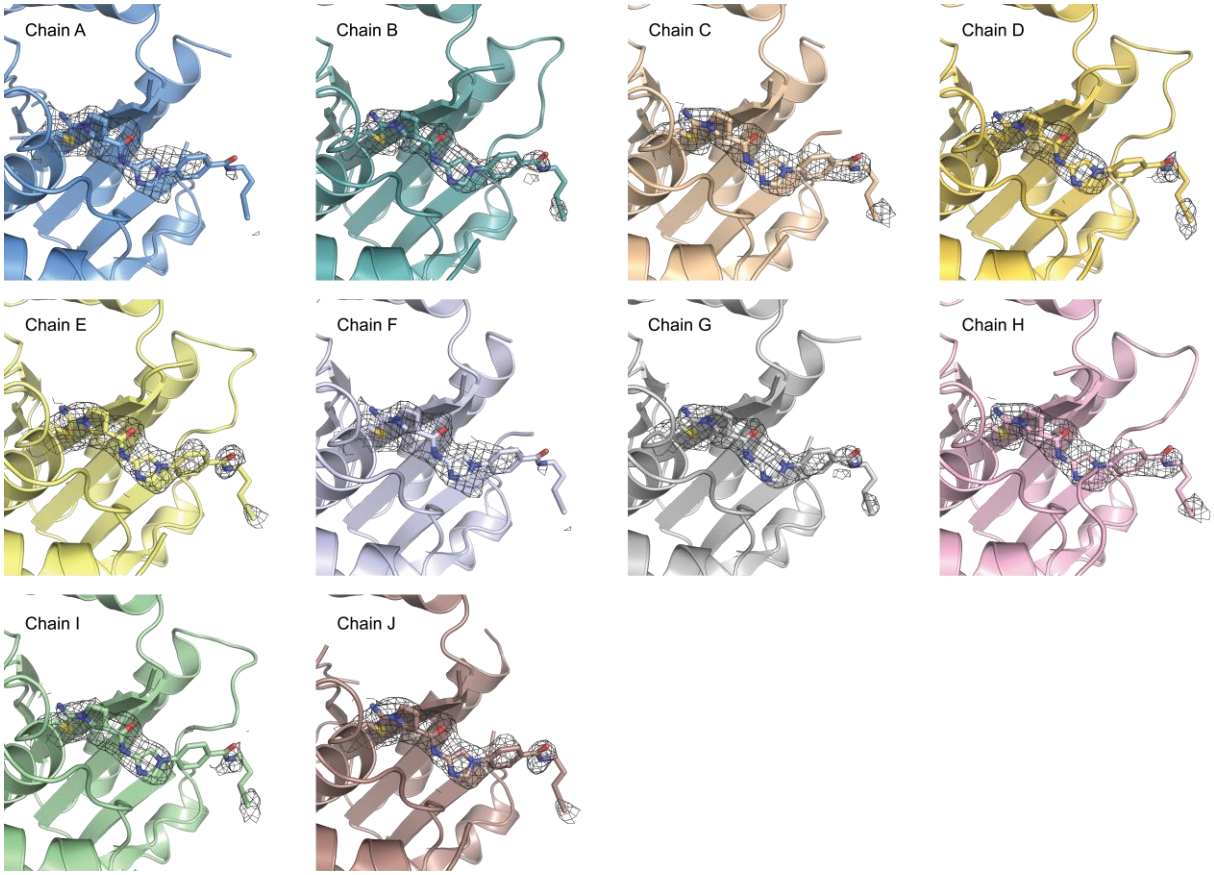

Figure 68. Individual cartoon representations of all 10 copies of the asymmetric unit of UCHL1~GK13S. UCHL1 is shown in cartoon representation. GK13S is shown as sticks with the electron density map overlaid in grey and contoured at 0.8 σ corresponding to the weighted |2F0 -FC| electron density.

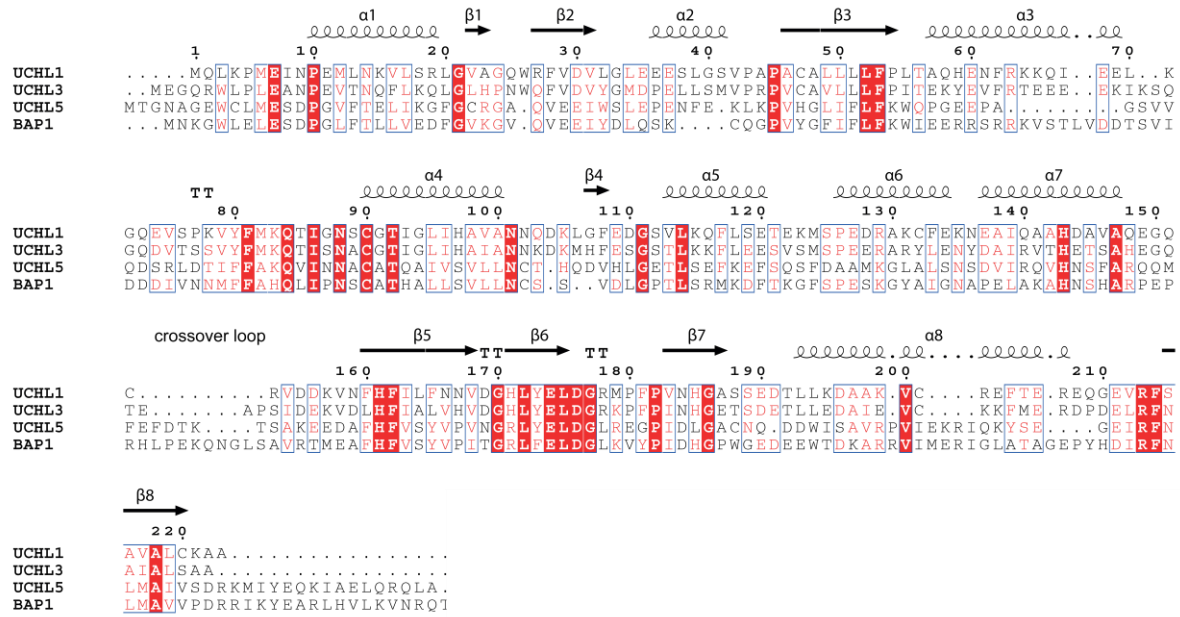

Figure 69. Full sequence alignment of human Ubiquitin C-terminal Hydrolase (UCH) family members. Secondary structure assignments are based on the UCHL1~GK13S structure.

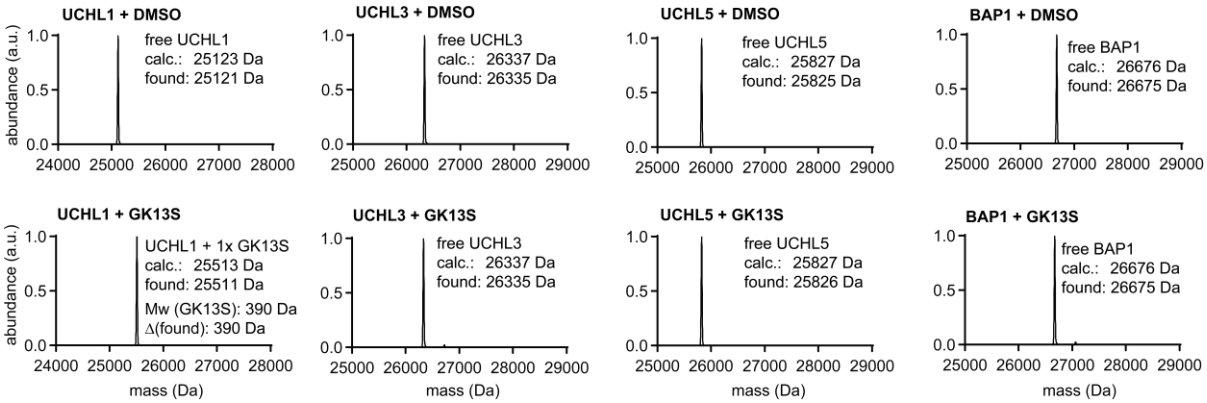

Figure 70. Intact protein mass spectrometry data of indicated UCH catalytic domains, treated with GK13S where indicated. Enzyme (3 µM) was treated with compound (10 µM) or DMSO for 1 h.

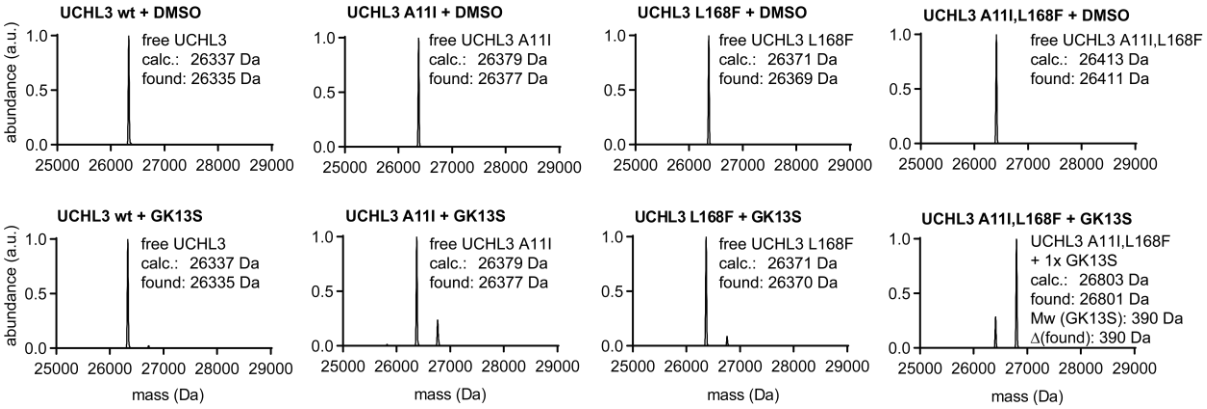

Figure 71. Intact protein mass spectrometry data of indicated UCHL3 catalytic domains, treated with GK13S where indicated. Enzyme (3 µM) was treated with compound (10 µM) or DMSO for 1 h.

Table 2. Data collection and refinement statistics for meUCHL1~GK13S.

	UCHL1^{methylated}~GK13S (PDB code: 7ZM0)
Data collection	
Beamline	SLS – PX2
Wavelength	1.000 Å
Space group	$P\ 2_12_12_1$
Cell dimensions	
a, *b*, *c* (Å)	101.93, 144.41, 158.25
α, β, γ (°)	90, 90, 90
Anisotropy correction	yes
Observed reflections	421721
Unique reflections	63622
Resolution (Å)	62.50 – 2.24 (2.54 – 2.24)
Ellipsoidal resolution limits (Å) [direction]	3.22 [a*] 2.70 [b*] 2.20 [c*]
R_{merge}	0.053 (0.457)
R_{meas}	0.057 (0.499)
$I/\sigma(I)$	18.0 (3.4)
$CC_{1/2}$	1.000 (0.917)
Spherical Completeness (%)	56.3 (10.7)
Ellipsoidal Completeness (%)	95.2 (83.0)
Redundancy	6.6 (6.3)
Wilson *B* (Å^2) [direction]	111 [a*] 71 [b*] 42 [c*]
Refinement	
Copies / a.s.u.	10
Resolution (Å)	2.24 Å
No. reflections	63574
R_{work} / R_{free} (%)	24.0 / 28.8
No. atoms	16195
Protein	15574
Ligand	290
Water	331
B factors (Å^2)	62.7
Protein (Å^2)	62.9
Ligand (Å^2)	69.7
Water (Å^2)	47.9
R.m.s.d.	
Bond lengths (Å)	0.003
Bond angles (°)	0.51
Ramachandran (favored / allowed / outlier) (%)	98.2 / 1.8 / 0
Clashscore	4.8
Rotamer outliers (%)	1.6

The dataset was collected from a single crystal. Values in parentheses are for highest-resolution shell. a.s.u., asymmetric unit. R.m.s.d., root mean square deviations.

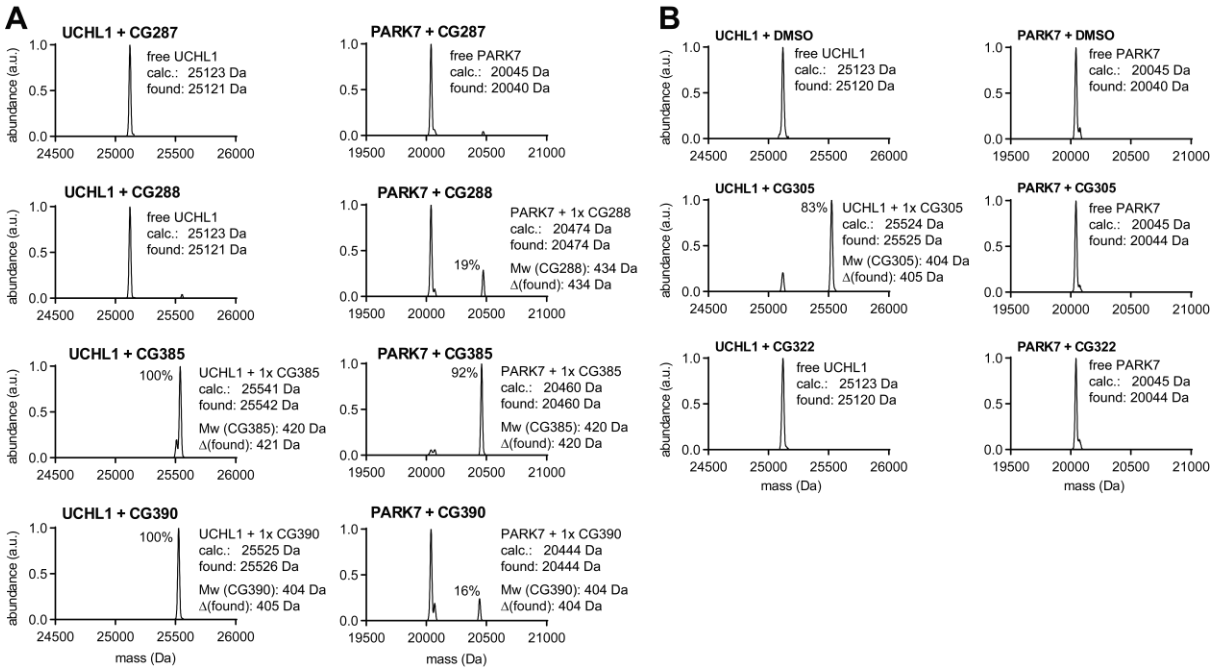

Figure 72. LC-MS binding characterisation of pyrrolidine (A)- and piperidine (B)-derivatives of GK13S to UCHL1 and PARK7. A, B. Intact protein mass spectrometry data of indicated compounds binding to recombinant UCHL1 or PARK7. UCHL1 (3 µM) or PARK7 (3 µM) were treated with compounds (10 µM) or DMSO for 1 h. Observed masses were assigned to given species with listed expected masses.

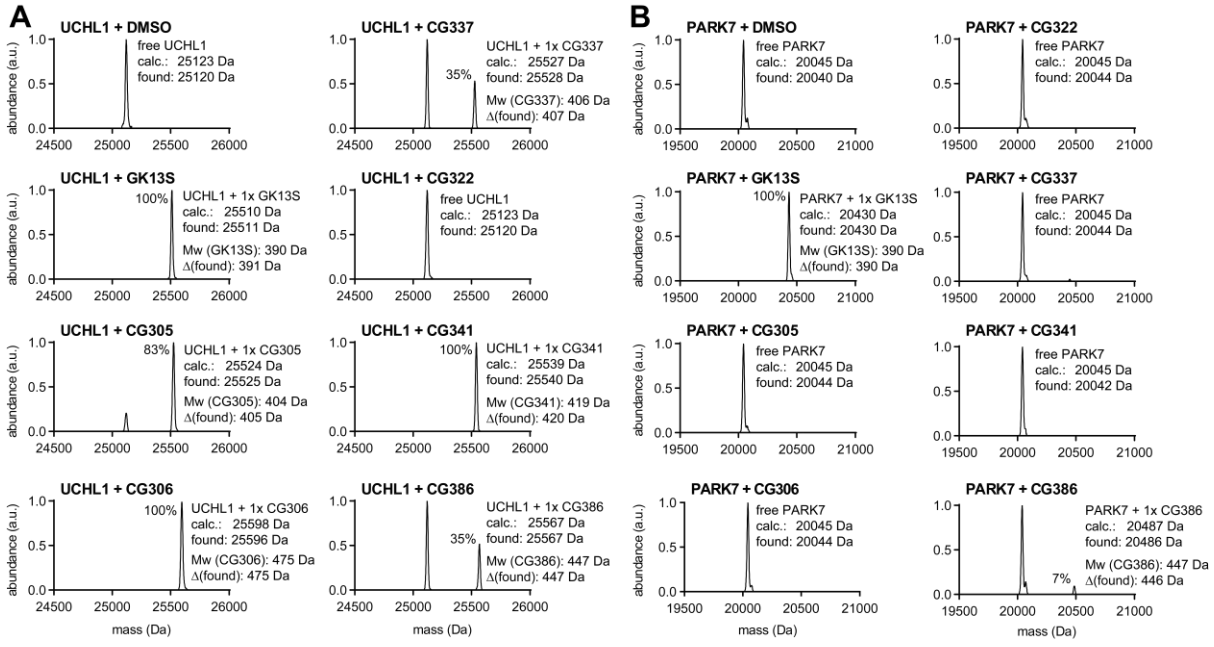

Figure 73. LC-MS binding characterisation of piperidine-, morpholine- and piperazine derivatives to UCHL1 (A) and PARK7 (B). A, B. Intact protein mass spectrometry data of indicated compounds binding to recombinant UCHL1 (**A**) or PARK7 (**B**). UCHL1 (3 µM) or PARK7 (3 µM) were treated with compounds (10 µM) or DMSO for 1 h. Observed masses were assigned to given species with listed expected masses.

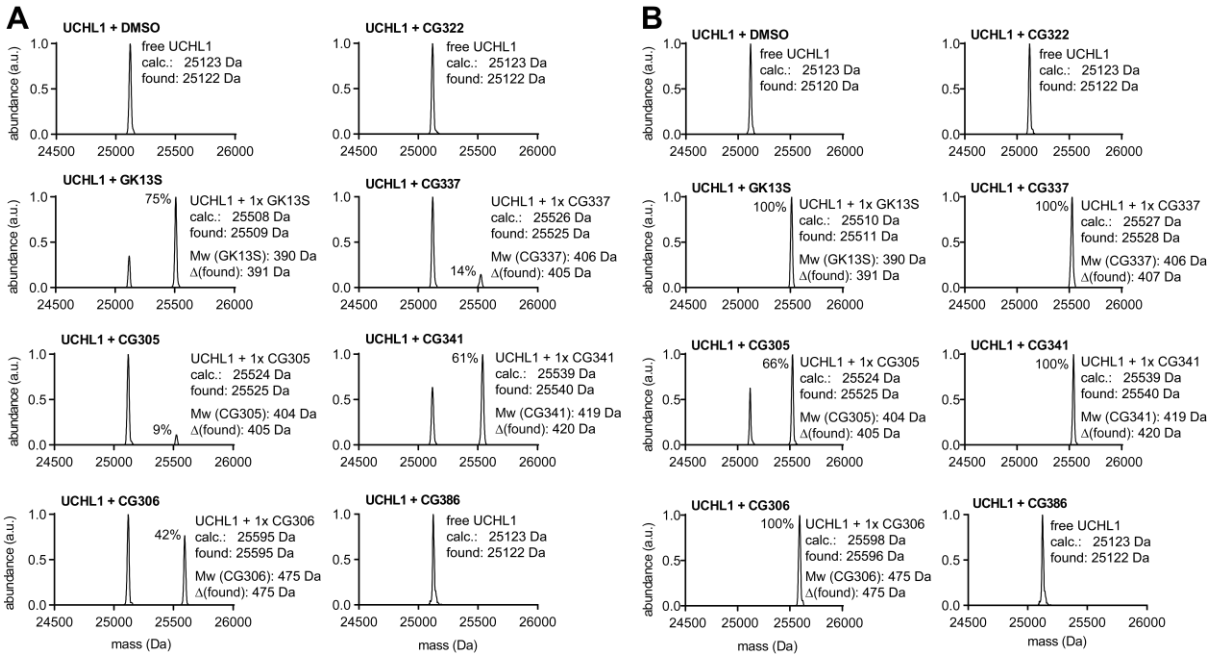

Figure 74. LC-MS binding characterisation of piperidine-, morpholine- and piperazine derivatives to UCHL1. A, B. Intact protein mass spectrometry data of indicated compounds binding to recombinant UCHL1. UCHL1 (0.8 µM) was treated with indicated compounds (1 µM) or DMSO for 1 h (**A**) or 14 h (**B**). Observed masses were assigned to given species with listed expected masses.

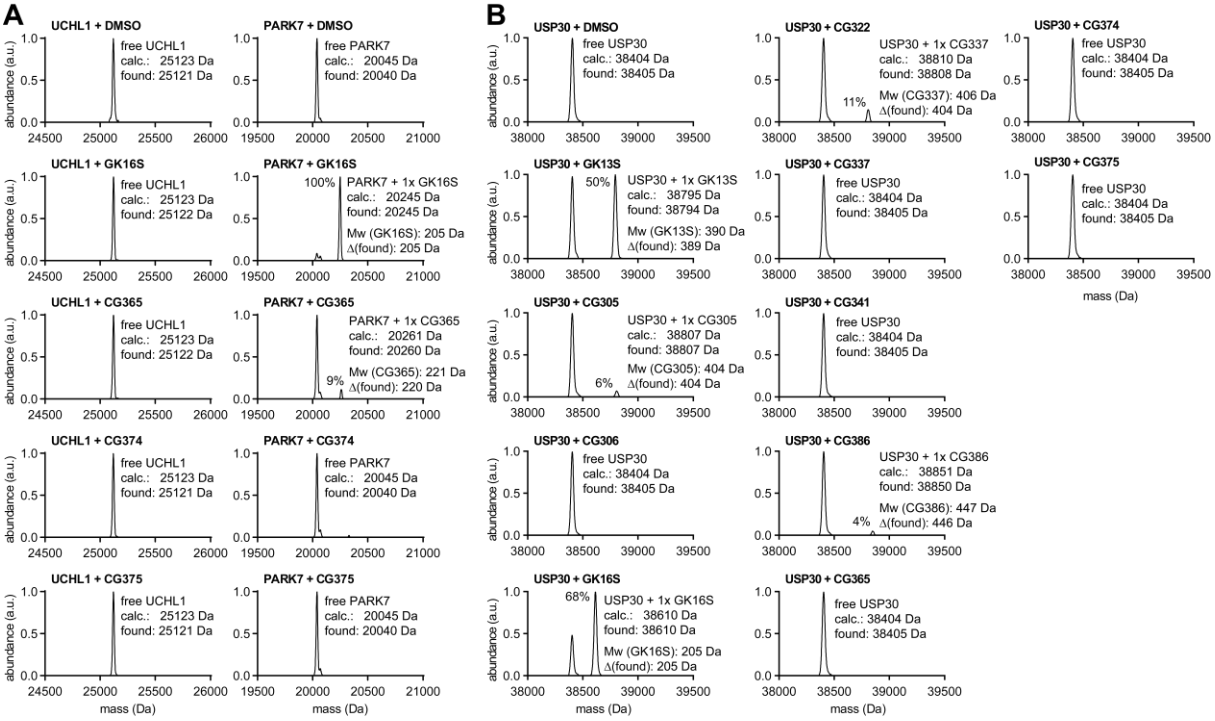

Figure 75. LC-MS binding characterisation of piperidine-, morpholine- and piperazine derivatives to UCHL1, PARK7 and USP30. A, B. Intact protein mass spectrometry data of indicated compounds binding to recombinant UCHL1 (**A**, left panel), PARK7 (**A**, right panel) or USP30 (**B**). Enzymes (3 µM) were treated with indicated compounds (10 µM) or DMSO for 1 h. Observed masses were assigned to given species with listed expected masses.

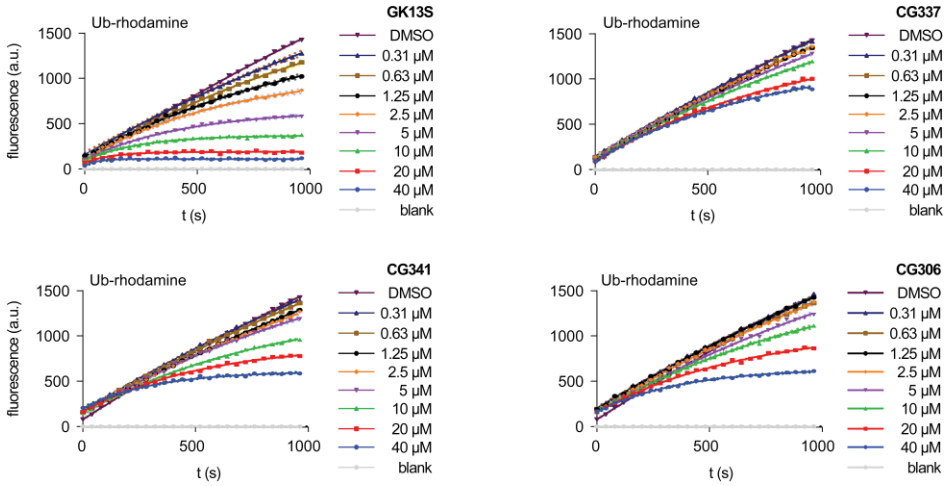

Figure 76. k_{obs}/[I] kinetic assay. Ubiquitin-Rhodamine cleavage assay of indicated probes and concentrations. Rate constants k_{obs} were determined from the linear slope of the plot and then plotted against inhibitor concentrations as shown in the main text.

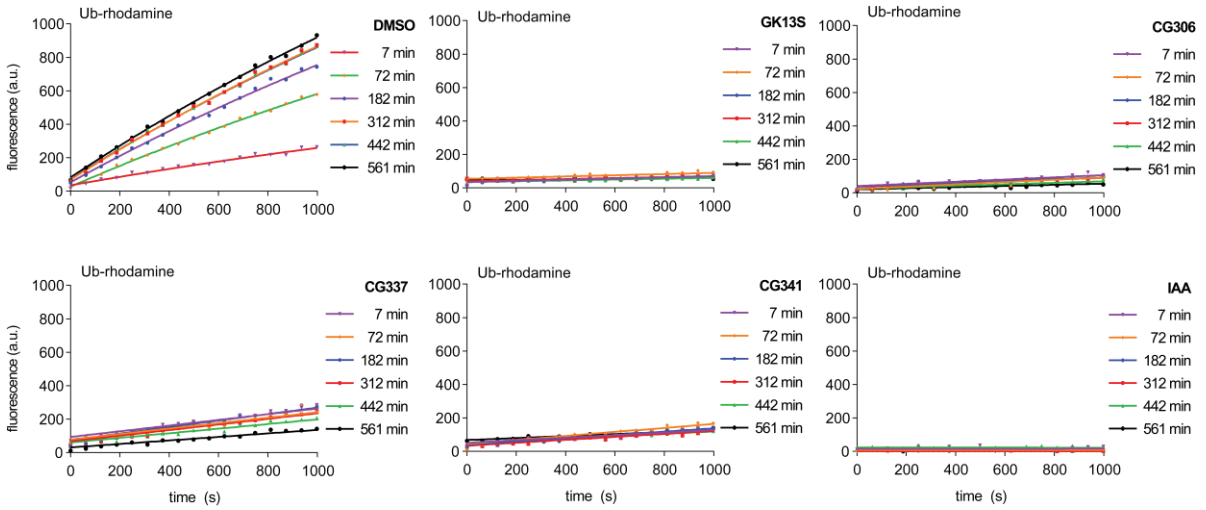

Figure 77. Jump-dilution assay. UCHL1 was treated with DMSO or an excess of indicated compound, thendiluted 100-fold, and its activity measured in Ub-Rhodamine cleavage assays after indicated timepoints.

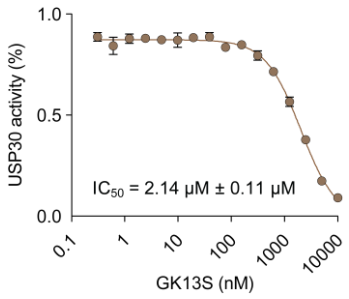

Figure 78. Inhibitory potency of GK13S binding to USP30 as determined from a Ubiquitin rhodamine cleavage assay. Compare **Figure 50B**. IC_{50} values were determined from 2 independent experiments and are given as mean ± standard deviation.

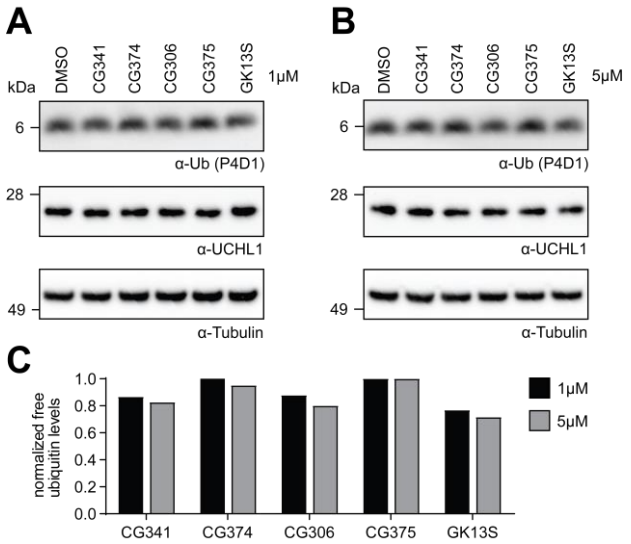

Figure 79. *N*-Cyanopiperazines CG341 and CG306 are able to phenocopy a UCHL1 mutant mouse. A-B. Western blots showing mono-Ubiquitin levels in U-87 MG cells treated with indicated compounds at 1µM (**A**) or 5µM (**B**) concentration. **C.** Quantification of mono-Ubiquitin intensities from **A** and **B**. Experiments were performed by MSc. M. Schmidt.

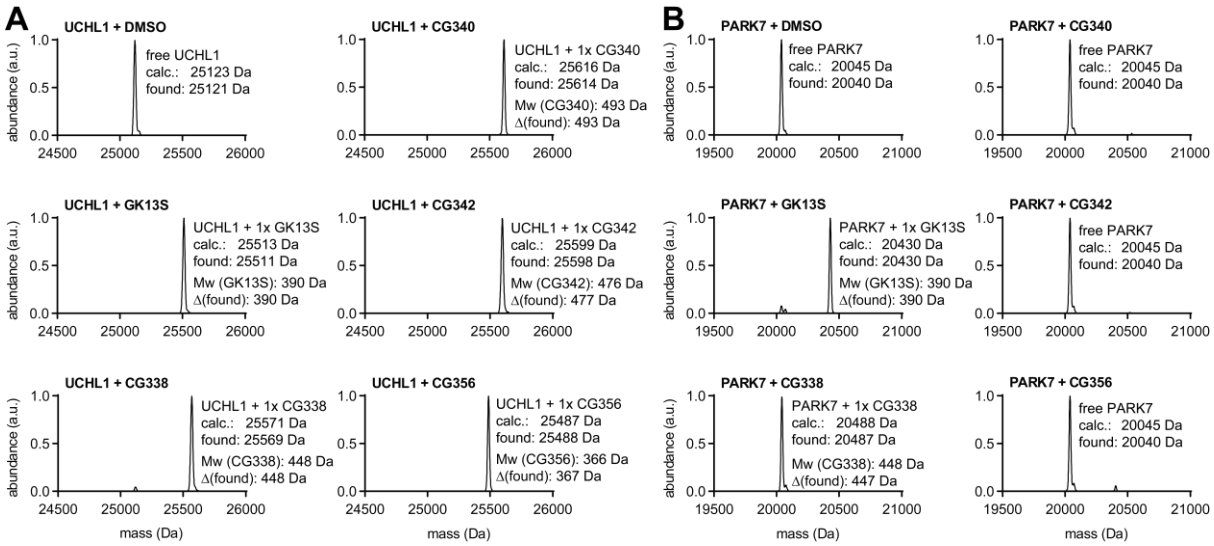

Figure 80. LC-MS binding characterisation of CG306 derivatives to UCHL1 (A) and PARK7 (B). A, B. Intact protein mass spectrometry data of indicated compounds binding to recombinant UCHL1 (**A**) or PARK7 (**B**). UCHL1 (3 µM) or PARK7 (3 µM) were treated with compounds (10 µM) or DMSO for 1 h. Observed masses were assigned to given species with listed expected masses.

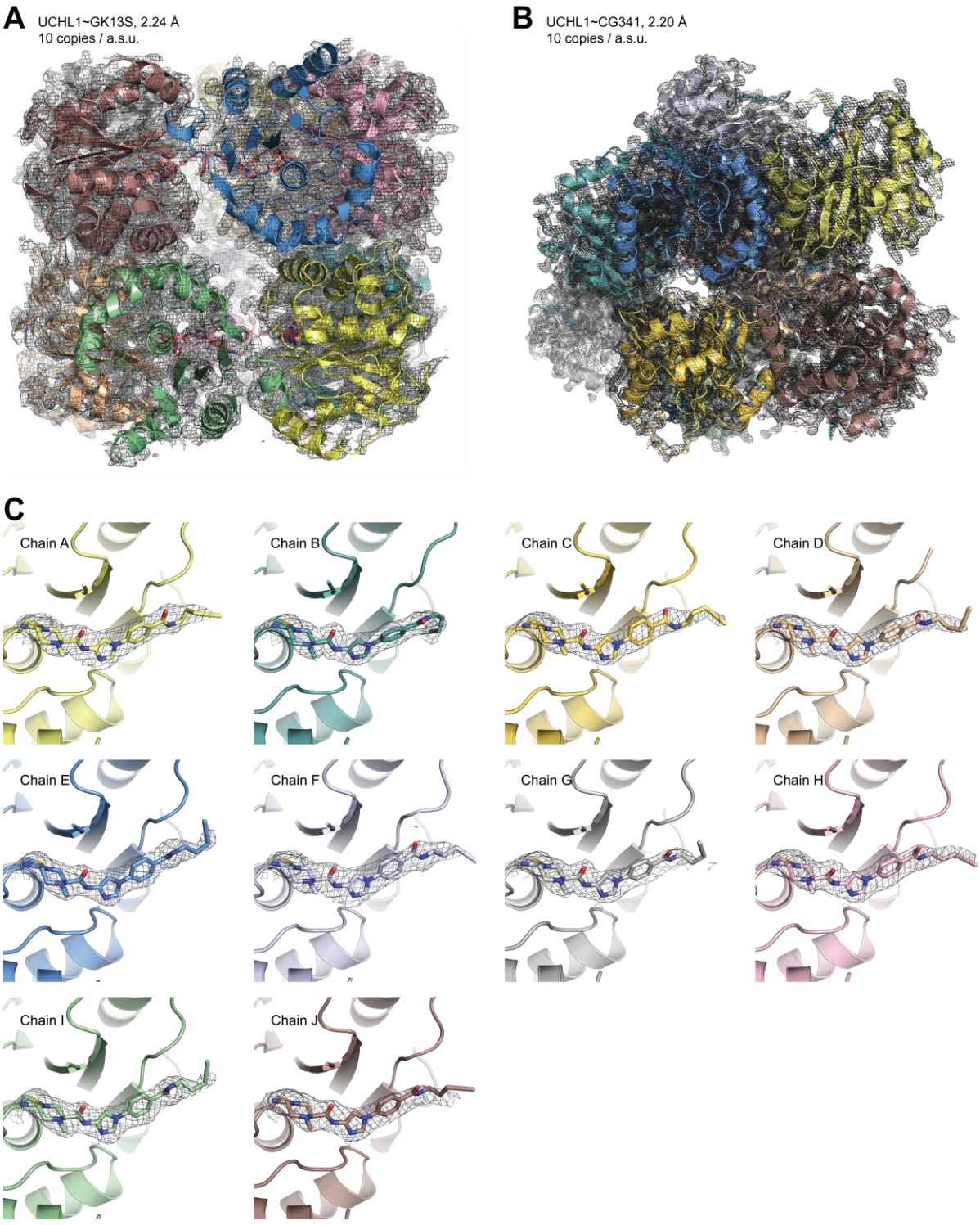

Figure 81. A, B. Asymmetric unit (a.s.u.) of the solved UCHL1~GK13S (A) and UCHL1~CG341 (B) structures including all 10 copies. The individual chains are shown in cartoon representation with the electron density map overlayed in grey and contoured at 0.8 σ corresponding to the weighted |2F0 -FC| electron density. **C.** Individual cartoon representations of all 10 copies of the asymmetric unit of UCHL1~GK13S. UCHL1 is shown in cartoon representation. GK13S is shown as sticks with the electron density map as in A and B. **C.** Individual cartoon representations of all 10 copies of the asymmetric unit of UCHL1~CG341. UCHL1 is shown in cartoon representation. GK13S is shown as sticks with the electron density map as in A and B.

Table 3. PARK7~GK16S. Data collection and refinement statistics.

	PARK7~GK16S (PDB code: 8PPW)
Beamline	SLS – PX2
Wavelength	1.000 Å
Resolution range	35.23 - 1.53 (1.585 - 1.53)
Space group	P 6_5 2 2
Unit cell	66.823 66.823 177.59 90 90 120
Total reflections	576332 (60186)
Unique reflections	36047 (3506)
Multiplicity	16.0 (17.2)
Completeness (%)	99.07 (98.34)
Mean I/sigma(I)	31.63 (2.31)
Wilson B-factor	27.30
R-merge	0.03934 (1.416)
R-meas	0.04067 (1.458)
R-pim	0.01015 (0.3453)
CC1/2	1 (0.768)
CC*	1 (0.932)
Reflections used in refinement	36039 (3505)
Reflections used for R-free	1812 (183)
R-work	0.1645 (0.3225)
R-free	0.1825 (0.3566)
CC(work)	0.967 (0.860)
CC(free)	0.956 (0.815)
Number of non-hydrogen atoms	1592
macromolecules	1360
ligands	15
solvent	217
Protein residues	186
RMS(bonds)	0.007
RMS(angles)	0.92
Ramachandran favored (%)	98.91
Ramachandran allowed (%)	0.54
Ramachandran outliers (%)	0.54
Rotamer outliers (%)	0.00
Clashscore	1.45
Average B-factor	35.94
macromolecules	33.97
ligands	49.33
solvent	47.38
Number of TLS groups	10

The dataset was collected from a single crystal. Values in parentheses are for highest-resolution shell.
a.s.u., asymmetric unit. R.m.s.d., root mean square deviations.

Table 4. meUCHL1~CG341. Data collection and refinement statistics.

	meUCHL1~CG341 (PDB code: 8PW1)
Beamline	SLS – PX2
Wavelength	1.000 Å
Resolution range	51.61 - 2.20 (2.279 - 2.20)
Space group	P 1
Unit cell	69.629 77.753 126.465 94.0933 104.06 113.798
Total reflections	409398 (38934)
Unique reflections	115147 (11238)
Multiplicity	3.6 (3.5)
Completeness (%)	98.08 (95.56)
Mean I/sigma(I)	11.19 (1.47)
Wilson B-factor	53.57
R-merge	0.04799 (0.8749)
R-meas	0.05681 (1.036)
R-pim	0.03 (0.5467)
CC1/2	0.995 (0.641)
CC*	0.999 (0.884)
Reflections used in refinement	115086 (11223)
Reflections used for R-free	5769 (595)
R-work	0.2285 (0.3734)
R-free	0.2703 (0.4107)
CC(work)	0.957 (0.767)
CC(free)	0.948 (0.673)
Number of non-hydrogen atoms	16561
macromolecules	16024
ligands	310
solvent	227
Protein residues	2196
RMS(bonds)	0.003
RMS(angles)	0.51
Ramachandran favored (%)	98.23
Ramachandran allowed (%)	1.77
Ramachandran outliers (%)	0.00
Rotamer outliers (%)	1.15
Clashscore	5.71
Average B-factor	80.79
macromolecules	81.29
ligands	66.23
solvent	65.63
Number of TLS groups	51

The dataset was collected from a single crystal. Values in parentheses are for highest-resolution shell.
a.s.u., asymmetric unit. R.m.s.d., root mean square deviations.

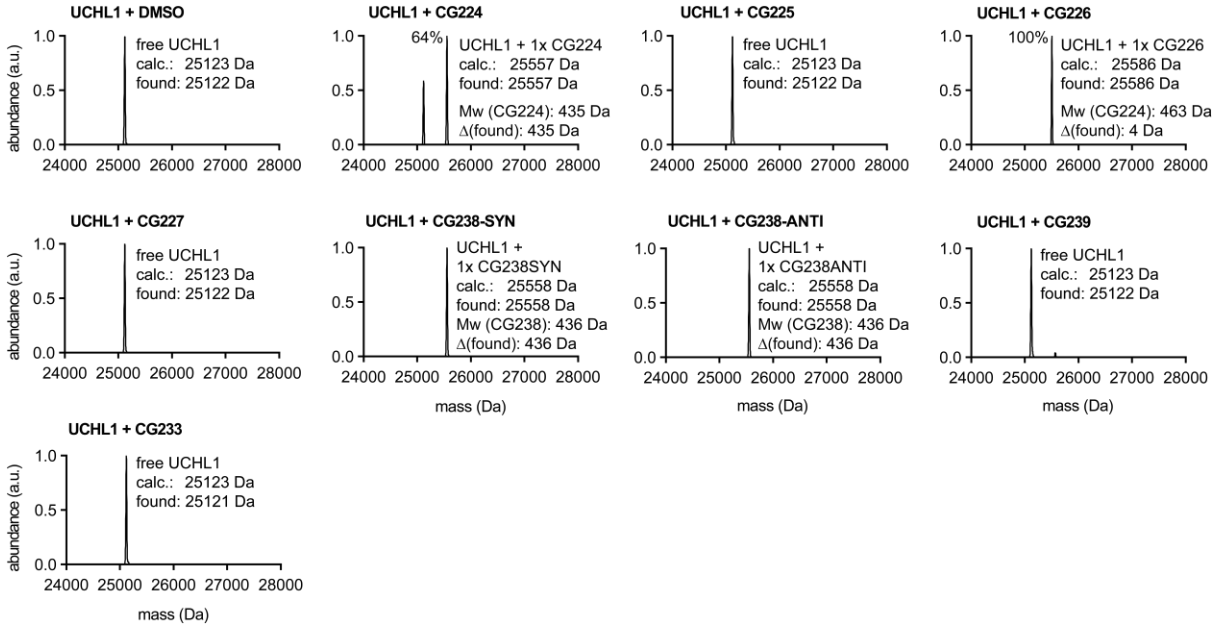

Figure 82. Intact protein mass spectrometry data of indicated dual-functional-warhead-based probes. UCHL1 (3 µM) was treated with compound (10 µM) or DMSO for 1 h. Observed masses were assigned to given species with listed expected masses.

9 Methods

9.1 Biological Methods

Methods for all biological experiments performed by other members of the lab, including Ubiquitin-probe assays, western blots, cellular target ID and target validation experiments, proteomic profiling, cell viability measurements and cellular characterisation experiments are not part of this thesis (for detailed contribution see chapter "Disclaimer"). Detailed information on these methods can be found either in Grethe and Schmidt et al.[1], in the PhD thesis of Mr M. Schmidt[4], or in the bachelor and master thesis of MSc. G. M. Kipka.[2,3]

Cloning and constructs

Human UCHL1 (UniProt: P09936, residues: 1-223), UCHL3 (UniProt: P15374, residues: 1-230), UCHL5 (UniProt: Q9Y5K5, residues: 1-228), BAP1 (UniProt: Q92560, residues: 1-235), and PARK7 (UniProt: Q99497, residues: 1-189) sequences were cloned from cDNA templates for bacterial expression into the pOPIN-B vector (for UCHL1 and PARK7, N-terminal His_6-3C-tag, an additional GS linker was used for UCHL1) or into the pOPIN-K vector (for UCHL3, UCHL5, and BAP1, N-terminal His_6-GST-3C tag) using the In-Fusion HD Cloning Kit (Takara Clonetech). Site-directed mutagenesis was carried out by splicing-by-overlap extension PCR using Phusion Polymerase (New England BioLabs).

Protein expression and purification

For bacterial expression of proteins, Rosetta2(DE3) pLacI cells were transformed with the respective vector. Overnight cultures were diluted 1:100 into 2xTY medium, which was supplemented with appropriate antibiotics, and cultures were grown shaking at 37 °C. When an A_{600} of 0.8 was reached, cultures were cooled to 18 °C, isopropyl-1-thio-β-d-galactopyranoside (IPTG) was added to a final concentration of 0.5 mM and cultures were grown overnight. Cells were harvested by centrifugation and stored at −80 °C. The pellets were thawed, resuspended in lysis buffer (50 mM H_2NaPO_4, 300 mM NaCl, 20 mM imidazole, pH 8.0, supplemented with lysozyme and DNAse, and with Complete protease inhibitors for UCHL5 and BAP1) and lysed by sonication on ice for 5 min. The lysates were cleared by centrifugation at 22,000×*g* for 30 min at 4 °C and sterile filtered. The clear lysate was then passed through a 5 mL HisTrap column (GE Healthcare), preequilibrated with buffer A (50 mM H_2NaPO_4, 300 mM NaCl, 20 mM imidazole, pH 8.0), using an ÄKTA Pure System (GE Healthcare). The protein was then eluted into buffer B (50 mM H_2NaPO_4, 300 mM NaCl, 500 mM imidazole, pH 8.0). Protein-containing fractions were pooled and concentrated. For UCHL1 and PARK7, GST-3C protease was added and the sample was dialysed into buffer C (20 mM Tris pH 8.0, 100 mM NaCl, 4 mM DTT) overnight. These proteins were further purified by size exclusion chromatography using a HiLoad 16/600 Superdex 75 pg column (GE Healthcare) with buffer C. PARK7 was dialysed subsequently into buffer D (20 mM KH_2PO_4 pH 7.0 and 5 mM DTT). For UCHL3, UCHL5, and BAP1, His_6-3C protease was added and the sample was dialysed into a lysis buffer. Dialysed samples were passed through a preequilibrated HisTrap column and the eluate was diluted into a low salt buffer (25 mM Tris pH 8.5, 50 mM NaCl, 4 mM DTT). These proteins were further purified by anion exchange chromatography on a ResQ column (GE Healthcare) by elution into a high salt buffer (25 mM Tris pH 8.5, 500 mM NaCl, 4 mM DTT) over 20 column volumes. Fractions containing pure protein were pooled, concentrated, and buffer exchanged into buffer C + 5% glycerol and protein concentrations were measured by UV absorbance on a Nanodrop 2000.

Lysine methylation of UCHL1

Methylation of primary amines in UCHL1 was achieved by adding 600 µL of freshly prepared dimethylamine-borane complex (1 M) and 1.2 mL formaldehyde solution (1 M) to 30 mL of UCHL1 (1 mg/mL) in buffer E (50 mM Hepes pH 7.5, 250 mM NaCl). After incubation for 2 h at 4 °C, 600 µL of

dimethylamine-borane complex (1 M) and 1.2 mL formaldehyde solution (1 M) were added and the incubation continued for an additional 2 h. Then 300 µL of dimethylamine-borane complex (1 M) was added and the reaction was incubated overnight at 4 °C. The next day precipitated protein was removed by centrifugation. After concentrating to a final volume of 1.5 mL, the protein was purified by size exclusion chromatography into buffer F (50 mM Tris pH 7.5, 200 mM NaCl). The protein was concentrated at 16 or 17 mg/mL and directly used for crystallisation experiments.

Co-crystallisation

Crystallisation was carried out in 96-well sitting-drop vapor diffusion plates in MRC format (Molecular Dimensions) at 18°C and set up using a mosquito HTS robot (TTP Labtech). Typical drop ratios of 200 nL + 200 nL, 100 nL + 200 nL, 200 +100 nL and 400 nL + 400 nL (protein solution + reservoir solution) were used for coarse screening and fine screening, respectively.

For co-crystallisation experiments PARK7 and methylated UCHL1 (meUCHL1) were preincubated with GK16S (1.2 eq) and GK13S (1.2 eq) and CG341 (1.2 eq), respectively. Covalent adduct formation was approved by LC-MS. PARK7~GK16S was concentrated to 15 mg/mL in 20 mM KH_2PO_4 pH 7.0 and 5 mM DTT and crystallised in 20 % PEG 3350 and 200 mM KNO_3 as long wedge-shaped crystals (606x109x109 μm^3). meUCHL1~GKX13 (c(meUCHL1) = 17 mg/mL) was crystallised in 2.3 M ammonium sulphate, 110 mM K_3PO_4 and 90 mM K_2HPO_4 as hexagonal prisms (120x45x45 μm^3). meUCHL1~CG341 (c(meUCHL1) = 16 mg/mL) was crystallised in 2.49 M ammonium sulphate and 86 mM trisodium citrate as hexagonal prisms.

Cryoprotection for PARK7~GK16S was achieved by placing the crystal for a few seconds in a cryo solution containing 20% PEG3350, 20 mM TRIS pH 8.0, 200 mM KNO_3 and 25% Glycerol followed by immediate vitrification in liquid nitrogen. Cryoprotection for meUCHL1~GK13S and meUCHL1~CG341 was achieved by placing the crystal for a few seconds into 3 M sodium malonate pH 7.0 with 1 mM GK13S and CG341, respectively, followed by immediate vitrification in liquid nitrogen.

Data collection, structure solution and refinement

Diffraction data were collected at 100 K at the Swiss Light Source (SLS, Villigen-PSI, Switzerland) on beamline PXII. The dataset leading to the structure of meUCHL1~GK13S was integrated using Dials[256] and anisotropically scaled using the STARANISO web server[257]. The structure was solved by molecular replacement using MR Phaser[258] and the apo protein as search model (pdb 2ETL). Model building using Coot[259] and refinement with Phenix.Refine[260] yielded the final structure. Data collection, anisotropy correction and refinement statistics are given in **Table 2**. Data have been deposited with the protein data bank under accession code 7ZM0. The same sequence of steps, except the anisotropic scaling, was implemented for the structures of PARK7~GK16S and meUCHL1~CG341 with apo protein (pdb: 4ZGG) and meUCHL1~GK13S (pdb: 7ZM0) as search model, respectively. Data collection and refinement statistics are given in **Table 3** and **Table 4**, respectively.

Ub-Rhodamine assay

Reactions were performed in black 384 well low volume non-binding surface plates (Greiner 784900) in a final volume of 20 µL. DUBs were diluted in reaction buffer H (20 mM Hepes pH 8.0, 50 mM NaCl, 0.05 mg/ml BSA) to a 4x stock (final concentrations: UCHL1: 0.06 nM; UCHL3: 0.25–0.5 pM; UCHL5: 0.01 nM; BAP1: 0.01 nM). DUBs were mixed in a 1:1 ratio with 4x compound dissolved in reaction buffer (final DMSO concentration: 0.1–1%). To each well was added 10 µL of DUB-compound solution in triplicates, followed by 1 h incubation time. Reactions were initiated by the addition of 10 µL Ub-Rhodamine 110 (Biomol, final concentration: 50 nM, diluted into reaction buffer supplemented with 5 mM DTT) and fluorescence (excitation = 492 nm, emission = 525) was read on a Tecan Spark plate reader with Tecan SparkControl software for 1 h in 1.5 min intervals at room temperature. Biochemical IC_{50} values were calculated using GraphPad Prism. The experiment with iodoacetamide (**Figure 36**) was carried out with a final concentration of 5 mM DTT in buffer H.

k_{obs}/[I] kinetic assay

Reactions were performed in 384 well plates as above. Compound (5 µL of a 4x stock in reaction buffer H supplemented with 2.5 mM TCEP; varying final concentrations ranging from 78 nM to 200 µM) and Ub-Rhodamine 110 (5 µL of a 4x stock in buffer H supplemented with 2.5 mM TCEP; final concentration: 50 nM) were mixed in a 1:1 ratio. To each well was added 10 µL of UCHL1 (2x stock in buffer H supplemented with 2.5 mM TCEP, final concentration: 0.06 nM) and fluorescence was recorded as described above. For compounds CG306, CG337, CG341 and GK13S as control, no TCEP was supplemented. The kinetic constant k_{obs} was obtained from fitting the curve with a one-phase association function to

$$Y(t)=Y0+(A-Y0)\cdot(1-e-kobs\cdot t)$$

wherein *Y(t)* denotes the fluorescence change over time *t*, starting at the initial fluorescence Y_0 and going up to a plateau *A*. The observed rate constant k_{obs} was plotted over the inhibitor concentration. Linear regression of the corresponding curve resulted in k_{obs}*/[I]*-values as slope, which enabled comparison of covalent inhibitor potencies.

Intact protein mass spectrometry

The recombinant protein was diluted to a final concentration of 3 or 0.8 µM in buffer I (20 mM Hepes pH 8.0, 50 mM NaCl) and treated with DMSO/compound to result in a final concentration of 10 or 1 µM, respectively. Followed by incubation of 1 h at room temperature, the samples were either run through a MassPrep Online Desalting 2.1 mm × 10 mm cartridge (Waters, flow rate 0.5 mL/min, runtime 7 min, column temperature 30 °C) or an AdvanceBio DesaltingRP 2.1 mm × 12.5 mm cartridge (Agilent, flow rate 0.4 mL/min, runtime 6 min, column temperature 32 °C) with solvents A = HPLC-grade H_2O + 0.1% TFA or formic acid and solvent B = HPLC-grade acetonitrile + 0.1% TFA or formic acid as mobile phases, respectively. A gradient from 20–90% solvent B (MassPrep Online Desalting cartridge) or 5–95% solvent B (AdvancedBio DesaltingRP) was programmed. The samples were either analysed on a Velos Pro Dual-Pressure Linear Ion Trap mass spectrometer (ThermoFisher, with Xcalibur software), equipped with an electrospray ion source in positive mode (capillary voltage 5 kV, desolvation gas flow 40 L/min, temperature 275 °C) or on an Agilent 1260 II Infinity system (Agilent, with Openlab software), equipped with an electrospray ion source in positive mode (capillary voltage 4 kV, desolvation gas flow 80 L/min, temperature 350 °C). Spectra were deconvoluted with ProMass (Enovatia).

Thermal shift assay

Reactions were performed in white 96-well PCR plates (Bio-Rad). UCHL1 was diluted in thermal shift buffer (1x PBS, 5 mM DTT) to a 4x concentration of 4 µM. The protein was then mixed with 4x compound dissolved in thermal shift buffer in a 1:1 ratio. To each well was added 20 µL of DUB-Inhibitor solution, followed by 1 h incubation time. To each well was then added 20 µL 4x SYPRO Orange in thermal shift buffer. After sealing the plates with a transparent film, thermal denaturation (gradient: 20–90 °C; Increment: 0.3 °C, hold for 5 s before read) was performed and monitored by a Bio-Rad Connect cycler.

Jump-dilution assay

Reactions were performed in similar 384 plates as above in a final volume of 20 µL. UCHL1 was diluted in reaction buffer H (20 mM Hepes pH 8.0, 50 mM NaCl, 0.1 mg/mL BSA) to a concentration of 12 nM (final concentration in well 0.06 nM). To this was added GK13S (1.25 µM), CG306 (5 µM), CG337 (10 µM), CG341 (5 µM), iodoacetamide (20 mM) or DMSO (20 mM) and the mixture was incubated for 2 h. Parts of this solution were diluted at 1:100 at different time points with buffer H. All samples were then diluted 1:2 with 100 nM Ub-Rho (buffer H, final concentration in well 50 nM) and fluorescence was recorded as described above. Half-life time was obtained by fitting the curve with a one-phase decay function to

$$Y(t)=A+(Y0-A)\cdot e-kobs\cdot t$$

wherein Y(t) denotes the fluorescence change over time *t*, starting at the initial fluorescence Y_0 and decreasing to a plateau *A*. The half-life time displays the time at which the curve reaches 50% of the plateau.

Dialysis dilution assay

UCHL1 (20 µM) was either incubated with DMSO or GK13S (40 µM) for 1 h to achieve near complete inhibition, and then diluted 1:5 with either PBS or 5 M of urea. A hole was cut into the lid of the 1.5 mL Eppendorf tubes and a SnakeSkin dialysis tubing membrane (3.5 K MWCO) was fit between the lid and the tube. The tubes were turned upside down, fastened in a floating rack and dialysed against 1 L of PBS overnight. Protein inhibition was quantified through LC/MS samples which were taken after indicated times of dialysis.

Statistics and reproducibility

Statistical significance of mono-Ubiquitin changes (project 1) was analysed using a one-sample, two-tailed *t*-test compared to a hypothetical mean of “1” as set for the DMSO or siScr samples using GraphPad Prism.

All observations reported in this thesis, if not mentioned otherwise, were made in at least two independent experiments, typically with technical triplicates, all with consistent results. Where possible, values were obtained as averages from multiple independent experiments as stated in the Figure legends.

9.2 Chemical Synthesis

Chemicals and solvents were used without further purification, and purchased from companies such as Acros, Activate Scientific, Alfa Aesar, Fluorchem, Merck, Novabiochem, Roth, Sigma-Aldrich, TCI and VWR. LDN-57444 was purchased from Sigma-Aldrich. Solvents used for all synthetic steps were named as follows. EA: ethyl acetate, DCM: dichloromethane, MeOH: methanol, PE: petroleum ether, CH: cyclohexane, DMF: dimethylformamide, THF: tetrahydrofuran, ACN: acetonitrile, H_2O: water, EtOH: ethanol. Thin-layer chromatography was carried out using silica gel aluminum plates (silica gel 60 F254, Merck). The detection was carried out using UV light (λ = 254/366 nm) and potassium permanganate or ninhydrin solution as staining reagents. For purification via column chromatography, silica gel 60 (60Å, 0.035-0.070 mm, Sigma Aldrich) was used. Automated column chromatographic purification was carried out on a Pure C-850 FlashPrep system or a Pure-C-810 Flash system (Büchi). For preparative HPLC, an 1260/1290 Infinity II series system (Agilent Technologies) with a VP125/21 Nucleodur C18 Gravity column (5 µm, Macherey Nagel) was used. Gradient A (40-60% ACN in H_2O + 0.1% TFA over 30 min) or gradient B (20-60% ACN in H_2O + 0.1% TFA over 60 min) was used to purify molecules before biological testing. For chiral HPLC, a Finnigan LTQ Orbitrap XL MS system (Thermo Scientific) with a Lux Cellulose-2 column (5 µm, Phenomenex), an Agilent 1200 Series G1312 binary pump, an Agilent G1315 DAD UV detector, and an Agilent 1200 Series G1367 Hip-ALS autosampler were used. Solvent A: Hexane + 0.1% TFA, solvent B: Isopropanol:MeOH (1:1) + 0.1% TFA; Flowrate: 0.5 ml/ min; Gradient:

Time (min)	Composition
0	A = 88%, B = 12%
16	A = 88%, B = 12%
49	A = 20%, B = 80%
58	A = 20%, B = 80%

For low resolution LC-MS analysis, a 1200 series HPLC system (Agilent Technologies) with a ZORBAX Eclipse XDB column (C18 80 Å; 4.6 x 150 mm; 5 µm) was used. High resolution mass spectrometry (HRMS) was carried out with an LTQ Orbitrap Fourier transform mass spectrometer (Thermo Electron). This spectrometer was coupled to an HPLC instrument from the same company (Hypersil Gold: Inner diameter 1 mm, length 50 mm, particle size 1.9 micron). The eluent gradients used were 0.1% v/v formic acid in H_2O and 0.1% v/v formic acid in ACN. The ionization mode was ESI (Electronspray ionization) with a source voltage source voltage of 3.8 kV. NMR spectra were recorded on the following devices (all from Bruker): AV 400 Avance III HD (400 MHz for ^{1}H and 101 MHz for ^{13}C NMR), AV 500 Avance III HD (500 MHz for ^{1}H and 125 MHz for ^{13}C NMR), AV 600 Avance III HD (600 MHz for ^{1}H and 151 MHz for ^{13}C NMR) and AV 700 Avance III HD (700 MHz for ^{1}H and 176 MHz for ^{13}C NMR). The chemical shifts of all spectra are specified in ppm. The coupling constants *J* are given in Hertz (Hz). Peaks are referenced to used deuterated solvent (DMSO-d_6: δ = 2.50 ppm / 39.52 ppm; $CDCl_3$: δ = 7.26 ppm / 77.16 ppm; MeOH-d_4: δ = 4.87 ppm / 49.15 ppm). The multiplicities of the signals in the ^{1}H spectra are abbreviated as follows. s (singlet), d (doublet), dd (doublet of doublets), t (triplet), td (triplet of doublets), q (quartet), m (multiplet) and br (broad). Certain NMR spectra showed the presence of two different rotamers, each displaying unique proton signals. The proton signals shared by both rotamers were collectively integrated and denoted by the label "d".

9.2.1 Structural basis for specific inhibition of UCHL1 (Project 1)

8.1.1.1 Synthesis of CG017

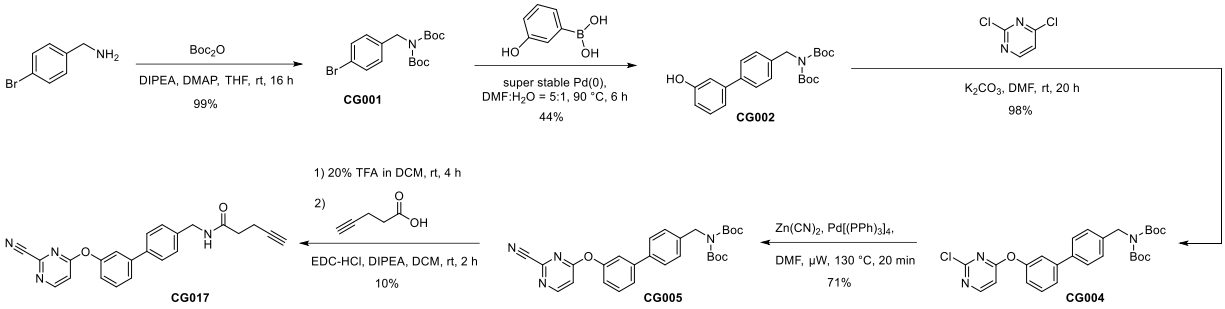

Scheme 18. Synthesis of compound CG017 based on [184].

tert-Butyl (4-bromobenzyl)(*tert*-butoxycarbonyl)carbamate (CG001)

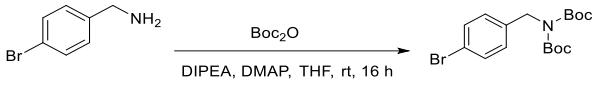

Diisopropylethylamine (DIPEA) (2.08 mL, 12.25 mmol, 1.2 eq) and dimethylaminopyridine (DMAP) (0.62 g, 5.1 mmol, 0.5 eq) were added to a suspension of 4-bromobenzylamine (2.0 g, 10.2 mmol, 1.0 eq) in THF (15 mL) at 0 °C under argon atmosphere. After stirring for 10 min, a solution of Boc-anhydride (Boc_2O) (5.6 g, 25.5 mmol, 2.5 eq) in THF (10 mL) was added dropwise via a cannula. The reaction mixture was stirred at room temperature for 16 h. The reaction mixture was poured into concentrated NH_4Cl (200 mL) and extracted with EA (200 mL). The organic layer was washed with sat. $NaHCO_3$ (100 mL) and brine (100 mL), dried over anhydrous Na_2SO_4 and filtered. The solvent was removed under reduced pressure and the crude product purified via a normal phase silica column. The product was eluting at 10-15% EA in PE and CG001 (3.9 g, 10.1 mmol, 99%) was obtained as a white solid. The analytical characterisation was in good agreement with previously reported data[261].

^{1}H NMR (400 MHz, $CDCl_3$) δ (ppm) = 7.43 (d, *J* = 8.3 Hz, 2H), 7.17 (dt, *J* = 8.1, 0.5 Hz, 2H), 4.72 (s, 2H), 1.46 (s, 18H).

^{13}C NMR (126 MHz, DMSO-d_6) δ (ppm) = 152.16, 137.85, 131.41, 129.24, 120.24, 82.38, 48.41, 27.64.

tert-Butyl (*tert*-butoxycarbonyl)((3'-hydroxy-[1,1'-biphenyl]-4-yl)methyl)-carbamate (CG002)

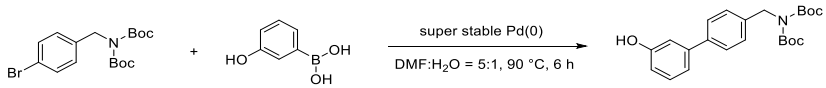

A suspension of CG001 (2.97 g, 7.7 mmol, 1.0 eq), 3-hydroxyphenylboronic acid (1.38 g, 10 mmol, 1.3 eq), tetrakis[tris[3,5-bis(trifluoromethyl)phenyl]phosphine]palladium(0) (super stable Pd(0)) (81.4 mg, 38.4 µmol, 0.005 eq) and K_2CO_3 (2.13 g, 15.4 mmol, 2.0 eq) in a mixture of DMF:H_2O = 5:1 (12 mL) was stirred for 6 h at 90 °C. The reaction mixture was filtered through Celite545 (Roth), poured into H_2O (100 mL) and extracted with EA (100 mL). The organic layer was washed with brine (100 mL), dried over anhydrous Na_2SO_4 and filtered. The organic layer was evaporated under reduced pressure and the crude product was purified on a normal phase silica column. The product was eluting at 15% EA in PE to obtain CG002 (1.3 g, 3.4 mmol, 44%) as a white solid.

^{1}H NMR (500 MHz, DMSO-d_6) δ (ppm) = 9.52 (s, 1H), 7.57 (d, *J* = 8.3 Hz, 2H), 7.32-7.27 (m, 2H), 7.24 (t, *J* = 7.9 Hz, 1H), 7.05 (dt, *J* = 7.8, 1.2 Hz, 1H), 7.01 (t, *J* = 2.1 Hz, 1H), 6.75 (ddd, *J* = 8.1, 2.4, 0.9 Hz, 1H), 4.71 (s, 2H), 1.41 (s, 18H).

^{13}C NMR (126 MHz, DMSO-d_6) δ (ppm) = 157.83, 152.23, 141.23, 139.14, 137.46, 129.95, 127.49, 126.58, 117.37, 114.42, 113.38, 82.13, 48.61, 27.59.

HRMS *m/z* for $C_{23}H_{30}NO_5^+$ ([M+H]$^+$) calculated: 400.2119, found: 400.2119.

***tert*-Butyl (*tert*-butoxycarbonyl)((3'-((2-Chloropyrimidin-4-yl)oxy)-[1,1'-biphenyl]-4-yl)methyl)-carbamate (CG004)**

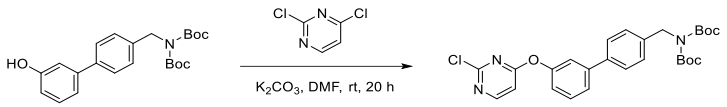

A mixture of CG002 (1.27 g, 3.2 mmol, 1.0 eq), 2,4-dichloropyrimidine (0.95 g, 6.4 mmol, 2.0 eq) and K_2CO_3 (0.88 g, 6.4 mmol, 2.0 eq) in DMF was stirred at room temperature for 20 h. This mixture was quenched with brine (100 mL) and extracted twice with EA (100 mL). The combined organic phases were dried over anhydrous Na_2SO_4, filtered and the solvent was evaporated. The resulting crude product was purified via a normal phase silica column. The product eluted at 20% EA in PE to afford pure CG004 (1.60 g, 3.13 mmol, 98%).

^{1}H NMR (500 MHz, DMSO-d_6) δ (ppm) = 8.63 (dd, *J* = 5.6, 0.9 Hz, 1H), 7.71 (d, *J* = 8.1 Hz, 2H), 7.66 (dt, *J* = 7.8, 1.4 Hz, 1H), 7.60 (s, 1H), 7.57 (t, *J* = 7.9 Hz, 1H), 7.32 (d, *J* = 8.1 Hz, 2H), 7.27 (ddd, *J* = 8.0, 2.3, 1.1 Hz, 1H), 7.20 (dd, *J* = 5.6, 1.0 Hz, 1H), 4.72 (s, 2H), 1.41 (s, 18H).

^{13}C NMR (126 MHz, DMSO-d_6) δ (ppm) = 170.17, 162.32, 161.53, 159.02, 152.20, 141.76, 138.15, 137.60, 130.61, 127.56, 126.79, 124.36, 120.47, 119.49, 107.70, 82.16, 48.58, 27.58.

HRMS *m/z* for $C_{27}H_{31}ClN_3O_5^+$ ([M+H]$^+$) calculated: 512.1947, found: 512.1949.

***tert*-Butyl (*tert*-butoxycarbonyl)((3'-((2-cyanopyrimidin-4-yl)oxy)-[1,1'-biphenyl]-4-yl)methyl)carbamate (CG005)**

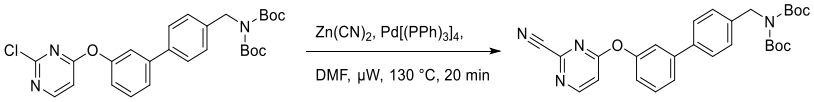

A mixture of CG004 (50 mg, 0.10 mmol, 1.0 eq), $Zn(CN)_2$ (11.5 mg, 0.10 mmol, 1.0 eq) and $Pd(PPh_3)_4$ (11.3 mg, 0.01 mmol, 0.1 eq) in DMF (1 mL) was irradiated in a microwave reactor at 130 °C for 20 min. The reaction was quenched with sat. $NaHCO_3$ (20 mL) and extracted with EA (30 mL). The organic layer was washed with brine (20 mL), dried over anhydrous Na_2SO_4 and the solvent was evaporated under reduced pressure. The product was purified using a silica column, eluting at 30% EA in PE to yield pure CG005 (149 mg, 0.30 mmol, 71%).

^{1}H NMR (600 MHz, DMSO-d_6) δ (ppm) = 8.86 (d, *J* = 5.9 Hz, 1H), 7.71 (d, *J* = 8.2 Hz, 2H), 7.67 (dt, *J* = 8.0, 1.2 Hz, 1H), 7.61 (d, *J* = 2.1 Hz, 1H), 7.59 (t, *J* = 7.9 Hz, 1H), 7.52 (d, *J* = 5.9 Hz, 1H), 7.32 (d, *J* = 8.0 Hz, 2H), 7.28 (dd, *J* = 8.0, 2.0 Hz, 1H), 4.72 (s, 2H), 1.41 (s, 18H).

^{13}C NMR (151 MHz, DMSO-d_6) δ (ppm) = 170.15, 161.50, 159.02, 152.26, 152.19, 141.76, 138.15, 137.60, 130.59, 127.55, 126.76, 124.33, 120.42, 119.44, 107.66, 82.16, 48.58, 27.60, 27.57.

HRMS *m/z* for $C_{28}H_{31}N_4O_5^+$ ([M+H]$^+$) calculated: 503.2289, found: 503.2289.

***N*-((3'-((2-Cyanopyrimidin-4-yl)oxy)-[1,1'-biphenyl]-4-yl)methyl)pent-4-ynamide (CG017)**

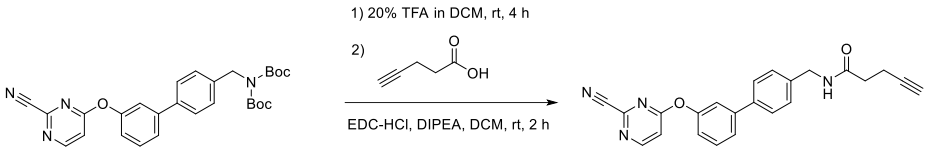

Step 1

CG005 (50 mg, 0.10 mmol, 1.0 eq) was dissolved in DCM (2 mL) and TFA (400 µL) was added dropwise to the solution. After completion of the deprotection, the reaction mixture was poured into sat. $NaHCO_3$ (50 mL) and extracted with EA (50 mL). The organic layer was washed with brine (50 mL), dried over anhydrous Na_2SO_4, filtered and the solvent evaporated under reduced pressure.

Step 2

4-Pentynoic acid (12.3 mg, 0.12 mmol, 1.2 eq), EDC-HCl (28.6 mg, 0.15 mmol, 1.5 eq) and DIPEA (25.4 µL, 0.15 mmol, 1.5 eq) were dissolved in DCM (1 mL) and stirred for 10 min at room temperature. To this reaction was added the crude product from step 1 in DCM (1 mL) dropwise. The reaction was stirred for 2 h until full conversion of the educt was observed by TLC. The reaction was quenched with sat. $NaHCO_3$ (30 mL) and extracted with EA (40 mL). The organic layer was washed with brine (30 mL), dried over anhydrous Na_2SO_4, filtered and the solvent evaporated under reduced pressure. The product was purified using a preparative HPLC to yield pure CG017 (4 mg, 0.01 mmol, 10%).

^{1}H NMR (600 MHz, $CDCl_3$) δ (ppm) = 8.79 (d, *J* = 4.8 Hz, 1H), 7.56 (d, *J* = 8.2 Hz, 2H), 7.52 (d, *J* = 5.1 Hz, 2H), 7.39 (s, 2H), 7.37 (d, *J* = 4.7 Hz, 2H), 7.19 – 7.15 (m, 1H), 5.99 (s, 1H), 4.52 (d, *J* = 5.7 Hz, 2H), 2.59 (td, *J* = 7.1, 2.7 Hz, 2H), 2.48 (t, *J* = 7.1 Hz, 2H), 2.01 (t, *J* = 2.6 Hz, 1H).

^{13}C NMR (151 MHz, $CDCl_3$) δ (ppm) = 171.32, 165.62, 162.15, 152.69, 143.42, 142.87, 139.54, 137.73, 130.31, 128.52, 127.64, 124.99, 120.42, 120.20, 119.29, 114.99, 82.97, 69.79, 43.59, 35.53, 15.12.

HRMS *m/z* for $C_{23}H_{19}N_4O_2^+$ ([M+H]$^+$) calculated: 383.1503, found: 383.1500.

8.1.1.2 Synthesis of CG041

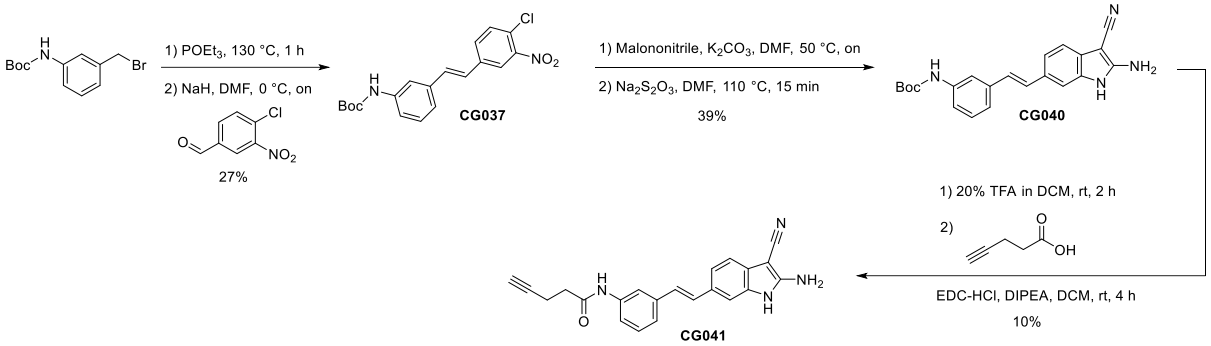

Scheme 19. Synthesis of compound CG041 based on [185].

***tert*-Butyl (*E*)-(3-(4-chloro-3-nitrostyryl)phenyl)carbamate (CG037)**

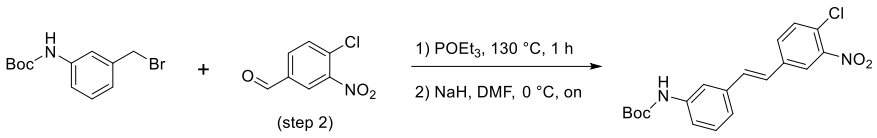

Step 1

tert-Butyl (3-(bromomethyl)phenyl)carbamate (463 mg, 1.6 mmol, 1.0 eq) and $POEt_3$ (448 µL, 1.6 mmol, 2.6 eq) were heated to 130 °C for 1 h until the formation of *tert*-butyl (3-((diethoxyphosphoryl)methyl)phenyl)carbamate was finished, as judged by LC-MS and TLC. Residual $POEt_3$ was removed under reduced pressure and the product was used for step 2 without further purification.

Step 2

The crude product from step 1 was diluted with DMF (3 mL) and cooled to 0 °C. NaH (129 mg, 3.2 mmol, 2.0 eq) was added portion wise to the solution at 0 °C. After stirring for 20 min, a solution of 4-chloro-3-nitrobenzaldehyde (300.0 mg, 1.6 mmol, 1.0 eq) in DMF (2 mL) was added dropwise at 0 °C. After 12 h the mixture was diluted with EA (50 mL) and the organic layer was washed with H_2O (30 mL) and brine (50 mL). After drying over anhydrous $MgSO_4$, the organic layer was filtered and concentrated under reduced pressure. The compound was purified via a silica column, eluting at 5% EA in PE, yielding CG037 (165 mg, 0.4 mmol, 27%) as a red solid.

^{1}H NMR (500 MHz, $CDCl_3$) δ (ppm) = 7.97 (d, *J* = 2.1 Hz, 1H), 7.74 (d, *J* = 4.7 Hz, 1H), 7.60 (dd, *J* = 8.4, 2.1 Hz, 1H), 7.51 (d, *J* = 8.4 Hz, 1H), 7.29 (t, *J* = 7.8 Hz, 1H), 7.20-7.15 (m, 2H), 7.13 (d, *J* = 16.4 Hz, 1H), 7.04 (d, *J* = 16.3 Hz, 1H), 6.55 (s, 1H), 1.54 (s, 9H).

^{13}C NMR (126 MHz, $CDCl_3$) δ (ppm) = 152.83, 148.31, 139.08, 137.66, 137.05, 132.19, 130.71, 129.54, 125.48, 125.39, 123.14, 121.88, 118.77, 116.56, 80.94, 28.48.

HRMS *m/z* for $C_{19}H_{20}ClN_2O_4^+$ ($[M+H]^+$) calculated: 375.1112, found: 375.1104.

***tert*-Butyl (*E*)-(3-(2-(2-amino-3-cyano-1*H*-indol-6-yl)vinyl)phenyl)carbamate (CG040)**

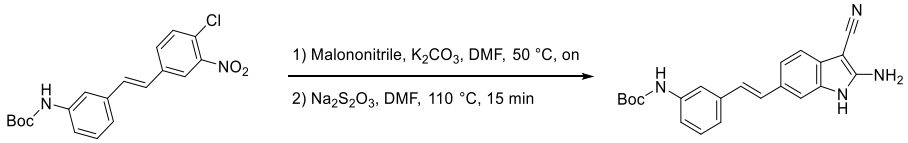

A stirred solution of CG037 (150 mg, 0.4 mmol, 1.0 eq) and malononitrile (66.1 mg, 1.0 mmol, 2.5 eq) in DMF (5 mL) was treated with K_2CO_3 (221 mg, 1.6 mmol, 4.0 eq). The mixture was stirred at 50 °C overnight. To this solution was added DMF (2 mL), H_2O (2 mL) and $Na_2S_2O_3$ (697 mg, 4.0 mmol, 10.0 eq) and the mixture heated to 110 °C for 15 min. The solution was poured into H_2O (50 mL) and extracted with EA (100 mL). The organic layer was washed with brine (100 mL), dried over anhydrous $MgSO_4$ and filtered. The solvent was evaporated, and the product purified on a reverse phase C18-column, eluting at 52% ACN in H_2O, yielding CG040 (58.8 mg, 0.16 mmol, 39%).

^{1}H NMR (500 MHz, DMSO-d_6) δ (ppm) = 10.75 (s, 1H), 9.34 (s, 1H), 7.66 (d, *J* = 2.0 Hz, 1H), 7.34 (d, *J* = 1.5 Hz, 1H), 7.26 (dd, *J* = 8.2, 1.6 Hz, 2H), 7.22 (t, *J* = 7.6 Hz, 1fH), 7.20-7.16 (m, 1H), 7.12 (d, *J* = 16.1 Hz, 1H), 7.10 (s, 1H), 6.99 (d, *J* = 16.4 Hz, 1H), 6.86 (br s, 2H), 1.49 (s, 9H).

^{13}C NMR (126 MHz, DMSO-d_6) δ (ppm) = 154.55, 152.85, 139.87, 138.00, 132.62, 129.66, 128.90, 128.46, 125.07, 119.96, 118.15, 117.71, 117.03, 115.76, 115.18, 114.72, 108.30, 79.05, 62.12, 28.18.

HRMS *m/z* for $C_{22}H_{23}N_4O_2^+$ ($[M+H]^+$) calculated: 375.1816, found: 375.1815.

(*E*)-*N*-(3-(2-(2-Amino-3-cyano-1*H*-indol-6-yl)vinyl)phenyl)pent-4-ynamide (CG041)

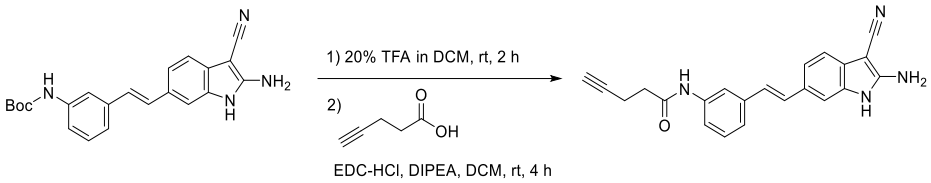

Step 1

CG040 (50 mg, 0.13 mmol, 1.0 eq) was dissolved in DCM (3 mL) and TFA (600 µL) was added dropwise. After the completion of the deprotection as judged by TLC, the reaction mixture was poured into sat. $NaHCO_3$ (50 mL) and extracted with EA (50 mL). The organic layer was washed with brine (50 mL), dried over anhydrous $MgSO_4$, filtered and the solvent evaporated under reduced pressure.

Step 2

The crude product from step 1, EDC-HCl (38.4 mg, 0.20 mmol, 1.5 eq), HOBt (20.4 mg, 0.13 mmol, 1.0 eq), 4-pentynoic acid (16.5 mg, 0.16 mmol, 1.2 eq) and DIPEA (34 µL, 0.20 mmol, 1.5 eq) were dissolved in DMF (2 mL) and stirred for 4 h at room temperature. The reaction was quenched with sat. $NaHCO_3$ (50 mL) and extracted with EA (100 mL). The organic layer was washed with brine (50 mL), dried over anhydrous $MgSO_4$, filtered and the solvent evaporated under reduced pressure. The product was purified using a preparative HPLC eluting at 55% ACN in H_2O, yielding CG041 (4.7 mg, 0.01 mmol, 10%).

^{1}H NMR (700 MHz, DMSO-d_6) δ (ppm) = 10.76 (s, 1H), 9.98 (s, 1H), 7.79 (t, *J* = 1.8 Hz, 1H), 7.43 (dt, *J* = 7.2, 2.1 Hz, 1H), 7.34 (d, *J* = 1.5 Hz, 1H), 7.29-7.24 (m, 3H), 7.15 (d, *J* = 16.3 Hz, 1H), 7.11 (d, *J* = 8.0 Hz, 1H), 7.02 (d, *J* = 16.3 Hz, 1H), 6.84 (s, 2H), 2.81 (t, *J* = 2.6 Hz, 1H), 2.54 (t, *J* = 7.0 Hz, 2H), 2.52-2.46 (m, 2H).

^{13}C NMR (176 MHz, DMSO-d_6) δ (ppm) = 169.38, 154.52, 139.44, 138.06, 132.58, 129.81, 128.97, 128.82, 128.48, 124.86, 121.07, 119.91, 117.85, 117.62, 116.56, 115.15, 108.29, 83.64, 71.49, 62.15, 35.22, 14.07.

HRMS *m/z* for $C_{22}H_{19}N_4O^+$ ([M+H]$^+$) calculated: 355.1553, found: 355.1551.

8.1.1.3 Synthesis of 3-carboxypyrrolidine-based probes and controls

Synthesis of GK12S/R and GK13S/R

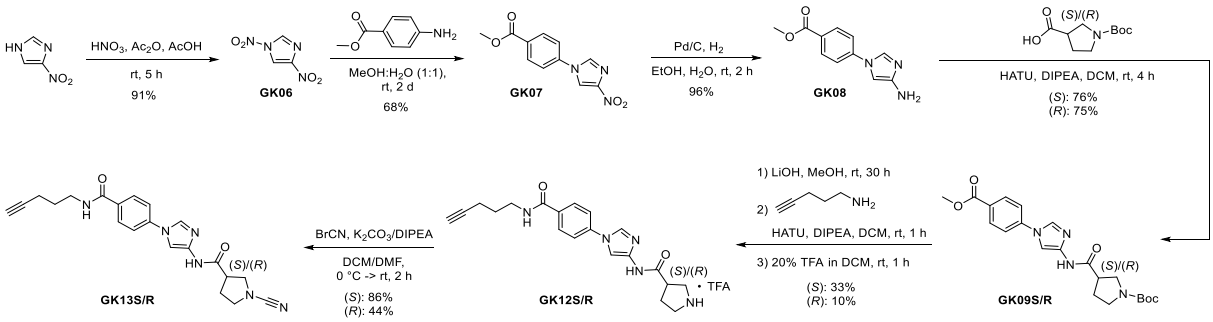

Scheme 20. Synthesis of compounds GK13S, GK13R, GK12S, and GK12R based on[181].

1,4-Dinitro-1*H*-imidazole (GK06)

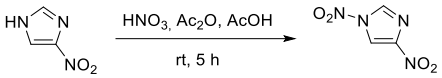

4-Nitroimidazole (2.00 g, 17.7 mmol, 1.0 eq) was dissolved in acetic acid (36 mL) and cooled to 0 °C. Concentrated nitric acid (9 mL) was added dropwise over 30 min. Then acetic anhydride (24 mL) was added dropwise over 30 min. The solution was stirred for 4 h at room temperature. The reaction was slowly poured into sat. K_2CO_3 solution (250 mL) and the aqueous phase was extracted twice with EA (50 mL). The combined organic layers were washed with sat. K_2CO_3 solution (100 mL), brine (100 mL) and dried with $MgSO_4$. The solvent was removed under reduced pressure. The obtained yellow crystals (2.56 g, 16.2 mmol, 91%) were used for the next reaction without further purification.

^{1}H NMR (700 MHz, DMSO-d_6) δ (ppm) = 9.42 (d, *J* = 1.6 Hz, 1H), 8.98 (d, *J* = 1.6 Hz, 1H).

^{13}C NMR (176 MHz, DMSO-d_6) δ (ppm) = 136.32, 133.14, 116.44.

Methyl 4-(4-nitro-1*H*-imidazol-1yl)benzoate (GK07)

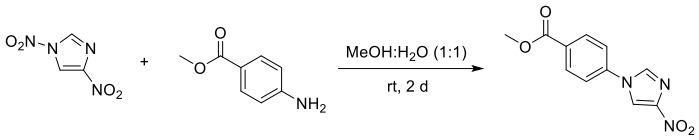

GK06 (2.56 g, 16.18 mmol, 1.0 eq) was dissolved in a 1:1 mixture of MeOH and H_2O (120 mL). Methyl 4-aminobenzoate (641 mg, 4.24 mmol, 1.0 eq) was added and the reaction mixture was stirred for two days at room temperature in darkness. The obtained red suspension was cooled down to 0 °C and the precipitate was filtered and washed with cold MeOH in H_2O (1:1). The red solid was recrystallised in a mixture of MeOH, H_2O and concentrated hydrochloric acid (2000:100:1) (100 mL) at 90 °C. The product was obtained as a yellow solid (2.74 g, 11.1 mmol, 68%). The analytical characterisation was in good agreement with previously reported data.[262]

^{1}H NMR (700 MHz, DMSO-d_6) δ (ppm) = 9.10 (d, *J* = 1.6 Hz, 1H), 8.60 (d, *J* = 1.5 Hz, 1H), 8.11 (d, *J* = 8.8 Hz, 2H), 7.99 (d, *J* = 8.8 Hz, 2H), 3.89 (s, 3H).

^{13}C NMR (176 MHz, DMSO-d_6) δ (ppm) = 165.26, 148.33, 138.95, 135.71, 130.84, 129.32, 121.23, 119.56, 52.44.

HRMS *m/z* for $C_{11}H_{10}N_3O_4^+$ ([M+H]$^+$) calculated: 248.0666, found: 248.0666.

Methyl 4-(4-amino-1*H*-imidazol-1yl)benzoate (GK08)

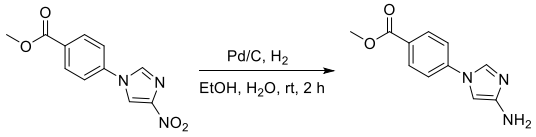

GK07 (500 mg, 2.02 mmol, 1.0 eq) was dissolved in EtOH (25 mL) and a few drops of H_2O were added. Palladium (10%) on activated charcoal (100 mg) was added under argon atmosphere. The reaction was flushed with H_2 and stirred for 2 h at room temperature. The reaction was filtered through celite545 which was then washed with EA. The solvent was dried over anhydrous $MgSO_4$ and removed under reduced pressure. The obtained yellow solid (423 mg, 1.94 mmol, 96%) was used for the next reaction without further purification. The analytical characterisation was in good agreement with previously reported data.[262]

^{1}H NMR (400 MHz, DMSO-d_6) δ (ppm) = 8.03 (d, *J* = 1.6 Hz, 1H), 8.00 (d, *J* = 8.9 Hz, 2H), 7.69 (d, *J* = 8.9 Hz, 2H), 6.73 (d, *J* = 1.7 Hz, 1H), 3.32 (s, 3H).

^{13}C NMR (126 MHz, DMSO-d_6) δ (ppm) = 165.59, 149.07, 140.75, 131.82, 130.96, 126.27, 118.43, 95.11, 52.21.

HRMS *m/z* for $C_{11}H_{12}N_3O_2^+$ ([M+H]$^+$) calculated: 218.0924, found: 218.0924.

tert-Butyl-(*S*)-3-((1-(4-(Methoxycarbonyl)phenyl)-1*H*-Imidazol-4-yl)carbamoyl)-pyrrolidine-1-carboxylate (GK09S)

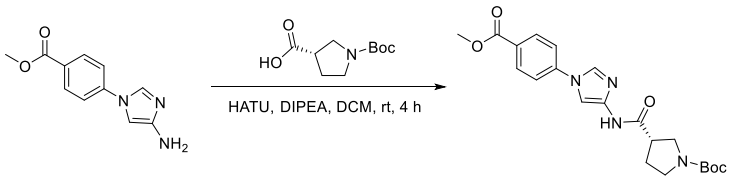

(*S*)-1-(*tert*-Butoxycarbonyl)pyrrolidine-3-carboxylic acid (198 mg, 0.92 mmol, 1.0 eq) was dissolved in DCM (5 mL), to which DIPEA (313 µL, 1.84 mmol, 2.0 eq) and HATU (525 mg, 1.38 mmol, 1.5 eq) were added. The solution was stirred for 30 min at room temperature. GK08 (200 mg, 0.60 mmol, 1.0 eq) dissolved in DCM (6 mL) was added dropwise to the reaction mixture. After additional 30 min the reaction mixture was quenched with sat. NH_4Cl-solution (20 ml) and extracted with DCM (40 mL). The organic phase was washed with brine (20 mL), dried over anhydrous $MgSO_4$ and the solvent was removed under reduced pressure. The compound was purified via a silica column eluting at 60% EA in PE, yielding GK09S (320 mg, 0.77 mmol, 76%) as a brown solid.

^{1}H NMR (500 MHz, $CDCl_3$) δ (ppm) = 9.89 (d, *J* = 110.6 Hz, 1H), 8.17 (d, *J* = 8.6 Hz, 2H), 7.93 (d, *J* = 12.8 Hz, 1H), 7.86 (s, 1H), 7.52 (d, *J* = 8.7 Hz, 2H), 3.95 (s, 3H), 3.85-3.65 (m, 1H), 3.65-3.53 (m, 2H), 3.43-3.32 (m, 1H), 3.21-3.09 (m, 1H), 2.33-2.15 (m, 2H), 1.45 (s, 9H).

^{13}C NMR (126 MHz, $CDCl_3$) δ (ppm) = 169.73, 165.50, 153.38, 140.36, 139.49, 132.30, 131.04, 127.37, 119.53, 103.90, 78.35, 54.96, 52.31, 48.48, 45.28, 43.14, 42.26, 28.20

HRMS *m/z* for $C_{21}H_{26}N_4O_5^+$ ([M+H]$^+$) calculated: 415.1976, found: 415.1976.

tert-Butyl-(*R*)-3-((1-(4-(Methoxycarbonyl)phenyl)-1*H*-Imidazol-4-yl)carbamoyl)-pyrrolidine-1-carboxylate (GK09R)

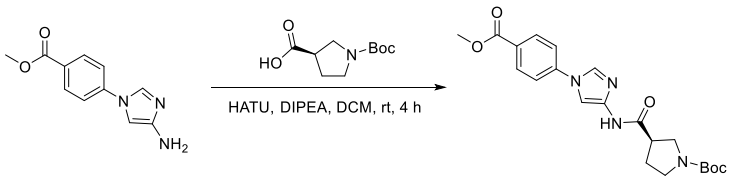

GK09R (313 mg, 0.76 mmol, 75%) was obtained as a brown solid from (*R*)-1-(*tert*-Butoxycarbonyl)pyrrolidine-3-carboxylic acid as described above for GK09S.

^{1}H NMR (500 MHz, $CDCl_3$) δ (ppm) = 9.97 (d, *J* = 103.4 Hz, 1H), 8.16 (d, *J* = 8.6 Hz, 2H), 7.89 (d, *J* = 12.9 Hz, 1H), 7.86 (s, 1H), 7.52 (d, *J* = 8.7 Hz, 2H), 3.94 (s, 3H), 3.86-3.67 (m, 1H), 3.63-3.54 (m, 2H), 3.44-3.33 (m, 1H), 3.23-3.09 (m, 1H), 2.35-2.15 (m, 2H), 1.45 (s, 9H).

^{13}C NMR (126 MHz, $CDCl_3$) δ (ppm) = 169.94, 166.00, 154.54, 140.19, 138.39, 131.76, 130.64, 129.56, 120.54, 106.14, 79.70, 52.58, 48.75, 45.65, 44.50, 28.62.

HRMS *m/z* for $C_{21}H_{26}N_4O_5^+$ ([M+H]$^+$) calculated: 415.1976, found: 415.1976.

(*S*)-*N*-(1-(4-(Pent-4-yn-1-ylcarbamoyl)phenyl)-1*H*-imidazol-4-yl)pyrrolidine-3-carboxamide TFA salt (GK12S)

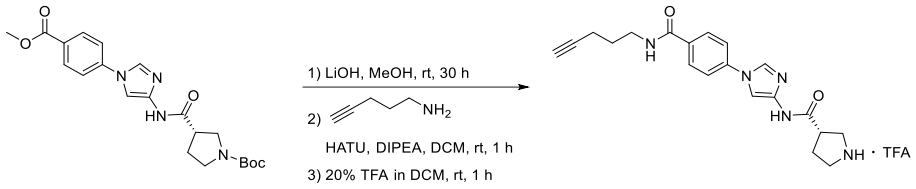

Step 1

GK09S (290 mg, 0.70 mmol, 1.0 eq) was dissolved in MeOH (7.5 mL). Aqueous 2M LiOH solution (875 µL) was added and the reaction mixture was stirred for 30 h at room temperature. To the reaction mixture was added 1 M hydrochloric acid (700 µL) to neutralise the excess of LiOH. The solvent was removed under reduced pressure and the obtained crude product was used for the next reaction without further purification.

Step 2

The crude product from step 1 was dissolved in DMF (4 mL) and DCM (3 mL). DIPEA (285 µL, 1.67 mmol, 2.0 eq) and HATU (636 mg, 1.67 mmol, 2.0 eq) were added and the reaction mixture was stirred for 30 min. 4-Pentyn-1-amine hydrochloride (100 mg, 0.84 mmol, 1.0 eq) was dissolved in DCM (2 mL) and added to the reaction dropwise. After 30 min the reaction mixture was quenched with sat. NH_4Cl solution (20 ml) and extracted with DCM (40 mL). The organic phase was washed with brine (20 mL), dried over $MgSO_4$ and the solvent was removed under reduced pressure. The obtained crude product was used for the next reaction without further purification.

Step 3

The crude product from step 2 was dissolved in DCM (4 mL) and TFA (1 mL) was added dropwise. The solution was stirred for 1 h at room temperature. The solvent was removed under reduced pressure. The product was purified by preparative HPLC eluting at 10-20% ACN in H_2O, yielding GK12S as a TFA salt (109 mg, 0.23 mmol, 33% yield).

^{1}H NMR (500 MHz, DMSO-d_6) δ (ppm) = 10.89 (s, 1H), 9.05 (s, 2H), 8.61 (t, *J* = 5.6 Hz, 1H), 8.28 (d, *J* = 1.7 Hz, 1H), 7.98 (d, *J* = 8.7 Hz, 2H), 7.79 (d, *J* = 1.7 Hz, 1H), 7.74 (d, *J* = 8.7 Hz, 2H), 3.48-3.39 (m, 1H), 3.34 (m, 4H), 3.29-3.17 (m, 2H), 2.80 (t, *J* = 2.6 Hz, 1H), 2.29-2.18 (m, 3H), 2.08-1.98 (m, 1H), 1.71 (p, *J* = 7.1 Hz, 2H).

^{13}C NMR (126 MHz, DMSO-d_6) δ (ppm) = 169.01, 165.30, 158.52 (q, *J* = 34.5 Hz), 139.01, 138.73, 132.56, 132.31, 129.09, 119.40, 116.25 (q, *J* = 293.8 Hz), 104.39, 84.21, 71.49, 47.04, 45.12, 42.03, 38.57, 29.02, 28.12, 15.61.

HRMS *m/z* for $C_{20}H_{24}N_5O_2^+$ ([M+H]$^+$) calculated: 366.1924, found: 366.1924.

(*R*)-*N*-(1-(4-(Pent-4-yn-1-ylcarbamoyl)phenyl)-1*H*-imidazol-4-yl)pyrrolidine-3-carboxamide (GK12R)

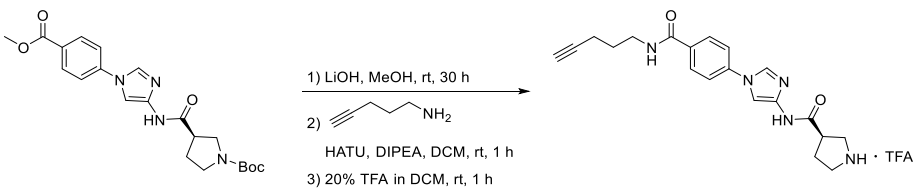

GK12R was obtained from GK09R as described above for GK12S. For step 3, the crude product was purified by column chromatography using a reverse phase silica column. The product was eluting at

15-25% ACN in H_2O. Parts of the product were further purified by preparative HPLC, eluting at 10-20% ACN, yielding GK12R as a TFA salt (39 mg, 0.08 mmol, 10%).

^{1}H NMR (500 MHz, DMSO-d_6) δ (ppm) = 10.88 (s, 1H), 9.03 (s, 2H), 8.60 (t, *J* = 5.6 Hz, 1H), 8.28 (d, *J* = 1.7 Hz, 1H), 8.00-7.96 (m, 2H), 7.79 (d, *J* = 1.6 Hz, 1H), 7.76-7.72 (m, 2H), 3.50-3.38 (m, 1H), 3.37-3.30 (m, 4H), 3.28-3.17 (m, 2H), 2.81 (t, *J* = 2.6 Hz, 1H), 2.23 (td, *J* = 7.1, 2.8 Hz, 3H), 2.03 (dq, *J* = 12.8, 7.3 Hz, 1H), 1.72 (p, *J* = 7.1 Hz, 2H).

^{13}C NMR (126 MHz, DMSO-d_6) δ (ppm) = 168.95, 165.24, 158.38 (q, *J* = 33.7 Hz), 139.08, 138.71, 132.51, 132.30, 129.05, 119.35, 116.50 (d, *J* = 295.3 Hz), 104.30, 84.18, 71.49, 47.02, 45.09, 42.00, 38.54, 28.99, 28.09, 15.58.

HRMS *m/z* for $C_{20}H_{24}N_5O_2^+$ ([M+H]$^+$) calculated: 366.1925, found: 366.1924.

(*S*)-1-Cyano-*N*-(1-(4-(pent-4-yn-1ylcarbamoyl)phenyl)-1*H*-imidazol-4-yl)pyrrolidine-3-carboxamide (GK13S).

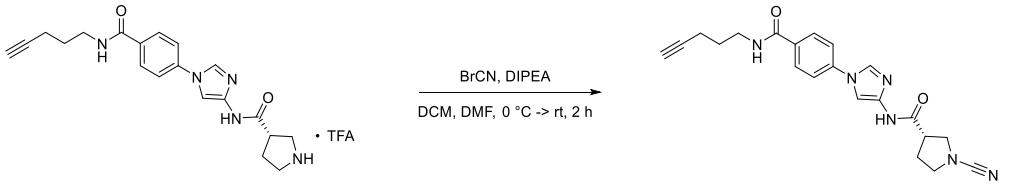

GK12S (70 mg, 0.15 mmol, 1.0 eq) was dissolved in DCM (3 mL) and DMF (1 mL), then DIPEA (127 µL, 0.73 mmol, 5.0 eq) was added. The mixture was cooled to 0 °C and stirred for 30 min. Then 3 M cyanogen bromide solution (58 µL, 0.18 mmol, 1.2 eq) was added and the mixture was stirred for 30 min at 0 °C. The reaction mixture was allowed to warm up to room temperature and stirred for another 2 h followed by the addition of H_2O (10 mL). The two phases were separated, and the aqueous phase was extracted two times with EA (20 mL). The combined organic layers were dried over anhydrous $MgSO_4$, filtered and the solvent was removed under reduced pressure. The corresponding product was purified via a silica column eluting at 4% MeOH in DCM, yielding GK13S (49 mg, 0.13 mmol, 86%) as light brown crystals.

^{1}H NMR (700 MHz, DMSO-d_6) δ (ppm) = 10.74 (s, 1H), 8.56 (t, *J* = 5.6 Hz, 1H), 8.25 (s, 1H), 7.97 (d, *J* = 8.2 Hz, 2H), 7.81 (s, 1H), 7.75 (d, *J* = 8.2 Hz, 2H), 3.60 (t, *J* = 8.6 Hz, 1H), 3.47 (td, *J* = 8.8, 8.3, 5.8 Hz, 2H), 3.40 (q, *J* = 7.7 Hz, 1H), 3.36 – 3.32 (m, 2H), 3.28 – 3.22 (m, 1H), 2.82 – 2.76 (m, 1H), 2.23 (dt, *J* = 7.2, 4.3 Hz, 3H), 2.09 (ddq, *J* = 81.0, 14.1, 7.1 Hz, 2H), 1.72 (p, *J* = 7.2 Hz, 2H).

^{13}C NMR (176 MHz, DMSO-d_6) δ (ppm) = 169.02, 165.19, 139.18, 138.71, 132.37, 132.09, 128.95, 119.20, 117.24, 104.17, 84.12, 71.39, 52.55, 50.03, 43.04, 38.48, 29.54, 28.04, 15.53.

HRMS *m/z* for $C_{21}H_{23}N_6O_2^+$ ([M+H]$^+$) calculated: 391.1877, found: 391.1881.

ee >99%, t_R (min) = 49.83.

(*R*)-1-Cyano-*N*-(1-(4-(pent-4-yn-1ylcarbamoyl)phenyl)-1*H*-imidazol-4-yl)pyrrolidine-3-carboxamide (GK13R)

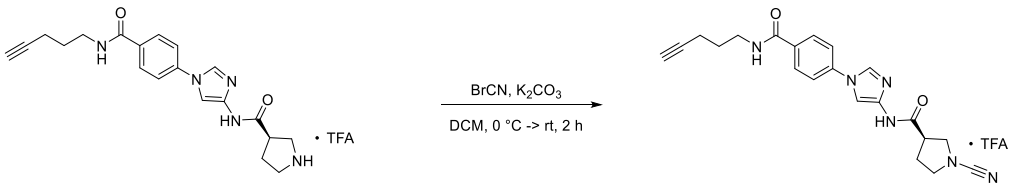

GK12R (53 mg, 0.11 mmol, 1.0 eq) was dissolved in DCM (3 mL) and K_2CO_3 (61 mg, 0.44 mmol, 4.0 eq) was added. The mixture was cooled to 0 °C and stirred for 30 min. Then 3 M cyanogen bromide

solution (44 µL, 0.13 mmol, 1.2 eq) was added and the mixture was stirred for 2 h at 0 °C. The reaction mixture was allowed to warm up to room temperature and stirred for another 2 h followed by the addition of H_2O (10 mL). The two phases were separated, and the aqueous phase was extracted two times with EA (20 mL). The combined organic layers were dried over anhydrous $MgSO_4$, filtered and the solvent was removed under reduced pressure. The corresponding product was purified via preparative HPLC eluting at 20-30% ACN in H_2O yielding GK13R as a TFA salt (21 mg, 0.05 mmol, 44%).

^{1}H NMR (500 MHz, DMSO-d_6) δ (ppm) = 10.77 (s, 1H), 8.58 (t, *J* = 5.6 Hz, 1H), 8.29 (s, 1H), 7.97 (d, *J* = 8.7 Hz, 2H), 7.82 (d, *J* = 1.7 Hz, 1H), 7.76 (d, *J* = 8.7 Hz, 2H), 3.60 (dd, *J* = 9.4, 7.7 Hz, 1H), 3.50 – 3.44 (m, 2H), 3.40 (dt, *J* = 9.0, 7.2 Hz, 1H), 3.33 (q, *J* = 6.4 Hz, 2H), 3.29 – 3.22 (m, 1H), 2.81 (t, *J* = 2.6 Hz, 1H), 2.23 (td, *J* = 7.1, 2.7 Hz, 2H), 2.18 – 1.99 (m, 2H), 1.71 (p, *J* = 7.1 Hz, 2H).

^{13}C NMR (126 MHz, DMSO-d_6) δ (ppm) = 169.12, 165.23, 158.26 (d, *J* = 36.9 Hz), 139.01, 138.70, 132.44, 132.14, 129.00, 119.29, 117.30, 104.30, 84.17, 71.48, 52.56, 50.05, 43.08, 38.52, 29.59, 28.08, 15.57.

HRMS *m/z* for $C_{21}H_{23}N_6O_2^+$ ($[M+H]^+$) calculated: 391.1877, found: 391.1880.

ee >99%, t_R (min) = 50.04.

Synthesis of the minimal probes

(*S*)-1-Cyano-*N*-(pent-4-yn-1-yl)pyrrolidine-3-carboxamide (GK16S)

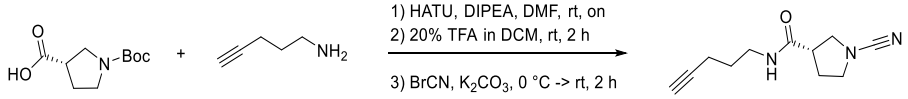

Step 1

(*S*)-*N*-Boc-pyrrolidine-3-carboxylic acid (50 mg, 0.23 mmol, 1.0 eq) was dissolved in 4 mL of DCM, then DIPEA (79 µL, 0.46 mmol, 2.0 eq) and HATU (525 mg, 1.38 mmol, 1.5 eq) were added to the solution. After stirring for 30 min at room temperature 4-pentyn-1-amine hydrochloride (33 mg, 1.38 mmol, 1.5 eq) was added and the solution was stirred overnight. The reaction mixture was poured into sat. NH_4Cl (50 mL) and extracted with EA (100 mL). The organic layer was washed with brine (100 mL), dried over anhydrous $MgSO_4$, filtered and the solvent was evaporated under reduced pressure. The obtained crude product was used for the next reaction without further purification.

Step 2

The crude product from step 1 was dissolved in 20% TFA in DCM (2 mL) and stirred for 2 h. To this solution toluene (1 mL) was added and the solvent was removed under reduced pressure yielding crude (*S*)-*N*-(pyrrolidin-3-yl)pent-4-ynamide.

Step 3

The crude product from step 2 was dissolved in DCM (4 mL), then K_2CO_3 (130 mg, 0.87 mmol, 4.0 eq) was added and the reaction mixture was stirred for 20 min at room temperature. The pH was adjusted to pH 7-8 by adding a few drops of 10 M NaOH. The solution was cooled to 0 °C and 3 M cyanogen bromide solution in DCM (106 µL, 0.25 mmol, 1.1 eq) was added dropwise. After 30 min the ice bath was removed, and the reaction mixture was stirred for 2 h at room temperature. The reaction was quenched by the addition of H_2O (50 mL) and extracted with DCM (100 mL). The aqueous phase was extracted with EA (100 mL) and the organic layers were combined and dried over anhydrous $MgSO_4$. After filtering, the solvent was removed under reduced pressure and the product purified via a silica column eluting at 0-1% MeOH in DCM. Pooling of pure fractions yielded GK16S (18.1 mg, 0.09 mmol, 39%) as a clear resin.

^{1}H NMR (700 MHz, DMSO-d_6) δ (ppm) = 8.04 (t, *J* = 5.6 Hz, 1H), 3.49 (dd, *J* = 9.3, 7.8 Hz, 1H), 3.41 (ddd, *J* = 9.1, 7.9, 5.2 Hz, 1H), 3.38-3.32 (m, 2H), 3.12 (tdd, *J* = 6.7, 5.5, 0.9 Hz, 2H), 2.94 (p, *J* = 7.4 Hz, 1H), 2.78 (t, *J* = 2.7 Hz, 1H), 2.16 (td, *J* = 7.2, 2.7 Hz, 2H), 2.03 (dtd, *J* = 12.6, 7.3, 5.2 Hz, 1H), 1.92 (dq, *J* = 12.5, 7.6 Hz, 1H), 1.57 (p, *J* = 7.1 Hz, 2H).

^{13}C NMR (176 MHz, DMSO-d_6) δ (ppm) =171.73, 117.76, 84.45, 71.88, 52.96, 50.52, 43.67, 38.25, 29.97, 28.42, 15.84.

HRMS *m/z* for $C_{11}H_{16}N_3O^+$ ([M+H]$^+$) calculated: 206.1288, found: 206.1288.

ee 98.7%, t_R (min) = 39.35.

(*R*)-1-Cyano-*N*-(pent-4-yn-1-yl)pyrrolidine-3-carboxamide (GK16R):

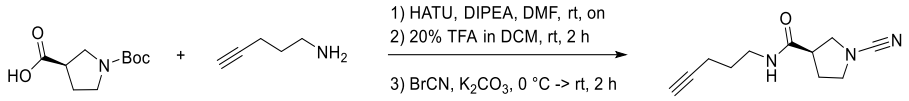

GK16R (24.3 mg, 0.12 mmol, 53%) as obtained as a clear resin from (*R*)-*N*-Boc-pyrrolidine-3-carboxylic acid as described above for GK16S.

^{1}H NMR (700 MHz, DMSO-d_6) δ (ppm) = 8.03 (t, *J* = 5.6 Hz, 1H), 3.49 (dd, *J* = 9.3, 7.8 Hz, 1H), 3.41 (ddd, *J* = 9.0, 7.8, 5.2 Hz, 1H), 3.38-3.32 (m, 2H), 3.12 (tdd, *J* = 6.7, 5.5, 0.9 Hz, 2H), 2.94 (p, *J* = 7.4 Hz, 1H), 2.77 (t, *J* = 2.7 Hz, 1H), 2.16 (td, *J* = 7.2, 2.7 Hz, 2H), 2.03 (dtd, *J* = 12.6, 7.3, 5.2 Hz, 1H), 1.92 (dq, *J* = 12.5, 7.6 Hz, 1H), 1.57 (p, *J* = 7.1 Hz, 2H).

^{13}C NMR (176 MHz, DMSO-d_6) δ (ppm) = 171.25, 117.27, 83.96, 71.38, 52.48, 50.04, 43.19, 37.76, 29.48, 27.94, 15.36.

HRMS *m/z* for $C_{11}H_{16}N_3O^+$ ([M+H]$^+$) calculated: 206.1288, found: 206.1288.

ee 94.9%, t_R (min) = 37.63.

8.1.1.4 Synthesis of parent inhibitor Cpd158

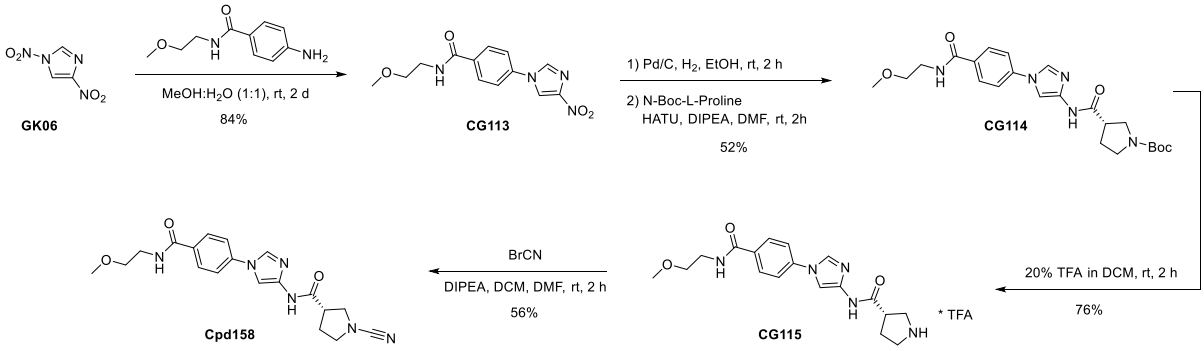

Scheme 21. Synthesis of compound Cpd158 (compound 158 in patent WO2016046530A1[181]).

***N*-(2-Methoxyethyl)-4-(4-nitro-1*H*-imidazol-1-yl)benzamide (CG113)**

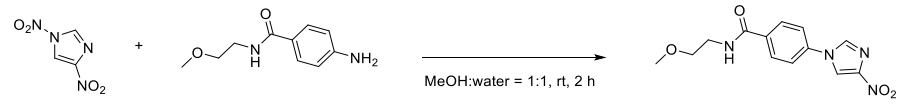

GK06 (300 mg, 1.54 mmol, 1.2 eq) was dissolved in a 1:1 mixture of MeOH and H_2O (10 mL). 4-Amino-*N*-(2-methoxyethyl)benzamide (292.98 mg, 1.85 mmol, 1.0 eq) was added and the reaction mixture was

stirred for 2 h at room temperature in darkness. The obtained suspension was cooled down to 0 °C and the precipitate was filtered and washed with cold MeOH in H_2O (1:1). The product was obtained as a yellow solid (377.4 mg, 1.30 mmol, 84%).

^{1}H NMR (600 MHz, DMSO-d_6) δ (ppm) = 9.10 (d, *J* = 1.6 Hz, 1H), 8.69 (t, *J* = 5.3 Hz, 1H), 8.58 (d, *J* = 1.6 Hz, 1H), 8.04 (d, *J* = 8.7 Hz, 2H), 7.94 (d, *J* = 8.7 Hz, 2H), 3.50-3.42 (m, 4H), 3.28 (s, 3H).

^{13}C NMR (151 MHz, DMSO-d_6) δ (ppm) = 164.96, 148.24, 137.39, 135.65, 134.00, 128.90, 120.78, 119.58, 70.40, 70.38, 57.95, 40.06.

HRMS *m/z* for $C_{13}H_{15}N_4O_4^+$ ([M+H]$^+$) calculated: 291.1088, found: 291.1091.

tert-Butyl (*S*)-3-((1-(4-((2-methoxyethyl)carbamoyl)phenyl)-1*H*-imidazol-4-yl)carbamoyl)pyrrolidine-1-carboxylate (CG114)

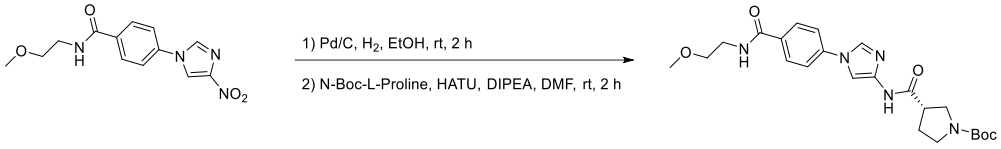

Step 1

CG113 (100 mg, 0.34 mmol, 1.0 eq) was dissolved in EtOH (5 mL) and a few drops of H_2O were added. Palladium (10%) on activated charcoal (20 mg) was added under argon atmosphere. Then the flask was flushed with hydrogen gas and the reaction mixture was stirred for 2 h at room temperature. The reaction was filtered through celite545 and was washed with EA. The solvent was dried over anhydrous $MgSO_4$ and removed under reduced pressure. The obtained yellow solid was used for the next reaction without further purification.

Step 2

(*S*)-1-(*tert*-Butoxycarbonyl)pyrrolidine-3-carboxylic acid (81.6 mg, 0.38 mmol, 1.1 eq) was dissolved in DMF (2 mL) and DIPEA (117 µL, 0.69 mmol, 2.0 eq) and HATU (157 mg, 0.41 mmol, 1.2 eq) were added. The solution was stirred for 30 min at room temperature. The crude product from step 1 was dissolved in DMF (1 mL) and added dropwise to the reaction mixture. After additional 2 h the reaction mixture was quenched with sat. NH_4Cl-solution (20 ml) and extracted with EA (40 mL). The organic phase was washed with brine (20 mL), dried over anhydrous $MgSO_4$ and the solvent was removed under reduced pressure. The compound was purified via a silica column eluting at 5% MeOH in DCM, yielding CG114 (82 mg, 0.18 mmol, 52%) as a light-brown solid.

^{1}H NMR (600 MHz, DMSO-d_6) δ (ppm) = 10.67 (d, *J* = 10.0 Hz, 1H), 8.61 (t, *J* = 5.4 Hz, 1H), 8.25 (d, *J* = 1.6 Hz, 1H), 8.03-7.96 (m, 2H), 7.81 (s, 1H), 7.76 (d, *J* = 8.7 Hz, 2H), 3.49 (dd, *J* = 11.1, 4.0 Hz, 1H), 3.48-3.41 (m, 4H), 3.41-3.34 (m, 2H), 3.28 (s, 3H), 3.26-3.14 (m, 2H), 2.09 (td, *J* = 11.7, 5.4 Hz, 1H), 2.06-1.95 (m, 1H), 1.41 (s, 9H).

^{13}C NMR (151 MHz, DMSO-d_6) δ (ppm) = 169.65, 165.20, 153.36, 139.29, 138.77, 132.04, 128.97, 119.17, 104.07, 78.31, 70.44, 57.93, 48.47, 45.41, 40.74, 33.49, 28.18, 24.10, 21.03.

HRMS *m/z* for $C_{23}H_{32}N_5O_5^+$ ([M+H]$^+$) calculated: 458.2398, found: 458.2393.

(*S*)-*N*-(1-(4-((2-Methoxyethyl)carbamoyl)phenyl)-1*H*-imidazol-4-yl)pyrrolidine-3-carboxamide TFA-salt (CG115)

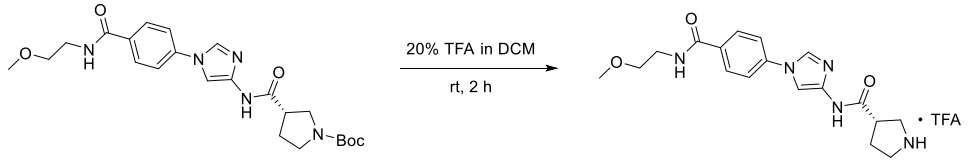

CG114 (75 mg, 0.16 mmol, 1.0 eq) was dissolved in a solution of 20% TFA in DCM (2 mL). The mixture was stirred for 2 h at room temperature. The solvent was removed under reduced pressure and the crude product purified by preparative HPLC eluting at 10-20% ACN in H_2O, yielding CG115 as a TFA salt (58.7 mg, 0.12 mmol, 76%).

^{1}H NMR (700 MHz, DMSO-d_6) δ (ppm) = 10.85 (s, 1H), 8.85 (d, *J* = 47.9 Hz, 2H), 8.61 (t, *J* = 5.4 Hz, 1H), 8.27 (d, *J* = 1.6 Hz, 1H), 7.99 (d, *J* = 8.6 Hz, 2H), 7.78 (d, *J* = 1.6 Hz, 1H), 7.74 (d, *J* = 8.6 Hz, 2H), 3.47 (dd, *J* = 6.3, 4.3 Hz, 2H), 3.44 (t, *J* = 5.2 Hz, 2H), 3.43-3.39 (m, 1H), 3.34 (tt, *J* = 11.6, 6.1 Hz, 2H), 3.27 (s, 3H), 3.24 (ddt, *J* = 25.6, 11.8, 3.0 Hz, 2H), 2.24 (dq, *J* = 14.0, 7.2 Hz, 1H), 2.03 (dq, *J* = 13.8, 7.2 Hz, 1H).

^{13}C NMR (176 MHz, DMSO-d_6) δ (ppm) = 168.87, 165.16, 158.01 (q, *J* = 33.9 Hz), 139.06, 138.69, 132.31, 132.25, 129.00, 119.29, 116.36 (q, *J* = 295.4 Hz), 104.22, 70.44, 57.92, 47.07, 45.10, 41.90, 40.02, 28.88.

HRMS *m/z* for $C_{18}H_{24}N_5O_3^+$ ($[M+H]^+$) calculated: 358.1874, found: 358.1875.

(*S*)-1-Cyano-*N*-(1-(4-((2-methoxyethyl)carbamoyl)phenyl)-1*H*-imidazol-4-yl)pyrrolidine-3-carboxamide (Cpd158)

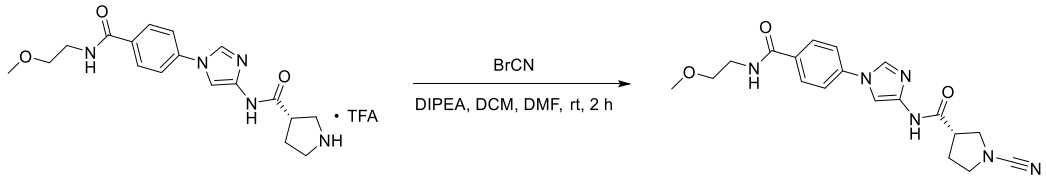

CG115 (40 mg, 0.08 mmol, 1.0 eq) was dissolved in DCM (2 mL) and K_2CO_3 (46.9 mg, 0.34 mmol, 4.0 eq) was added. A 3 M cyanogen bromide solution (34 µL, 0.10 mmol, 1.2 eq) was added and the mixture was stirred for 2 h. The reaction was quenched by the addition of H_2O (10 mL). The two phases were separated, and the aqueous phase were extracted two times with EA (20 mL). The combined organic layers were dried over anhydrous $MgSO_4$, filtered and the solvent was removed under reduced pressure. The corresponding product was purified via a silica column eluting at 6% MeOH in DCM, yielding Cpd158 (18.2 mg, 0.05 mmol, 56%) as a white solid.

^{1}H NMR (500 MHz, DMSO-d_6) δ (ppm) = 10.76 (s, 1H), 8.62 (t, *J* = 5.3 Hz, 1H), 8.26 (d, *J* = 1.7 Hz, 1H), 7.98 (d, *J* = 8.7 Hz, 2H), 7.81 (d, *J* = 1.6 Hz, 1H), 7.76 (d, *J* = 8.7 Hz, 2H), 3.60 (dd, *J* = 9.5, 7.7 Hz, 1zH), 3.52-3.37 (m, 7H), 3.27 (s, 3H), 2.14 (dtd, *J* = 12.8, 7.3, 5.6 Hz, 1H), 2.03 (dq, *J* = 12.6, 7.3 Hz, 1H), 1.25 (q, *J* = 6.9 Hz, 1H).

^{13}C NMR (126 MHz, DMSO-d_6) δ (ppm) = 169.50, 165.65, 139.66, 139.21, 132.63, 132.58, 129.45, 119.66, 117.73, 104.61, 70.91, 58.40, 53.00, 50.49, 43.50, 30.03.

HRMS *m/z* for $C_{19}H_{23}N_6O_3^+$ ($[M+H]^+$) calculated: 383.1826, found: 383.1829.

9.2.2 Structural basis for piperazine-specific inhibition of UCHL1 (Project 2)

8.1.1.5 Synthesis of CG287

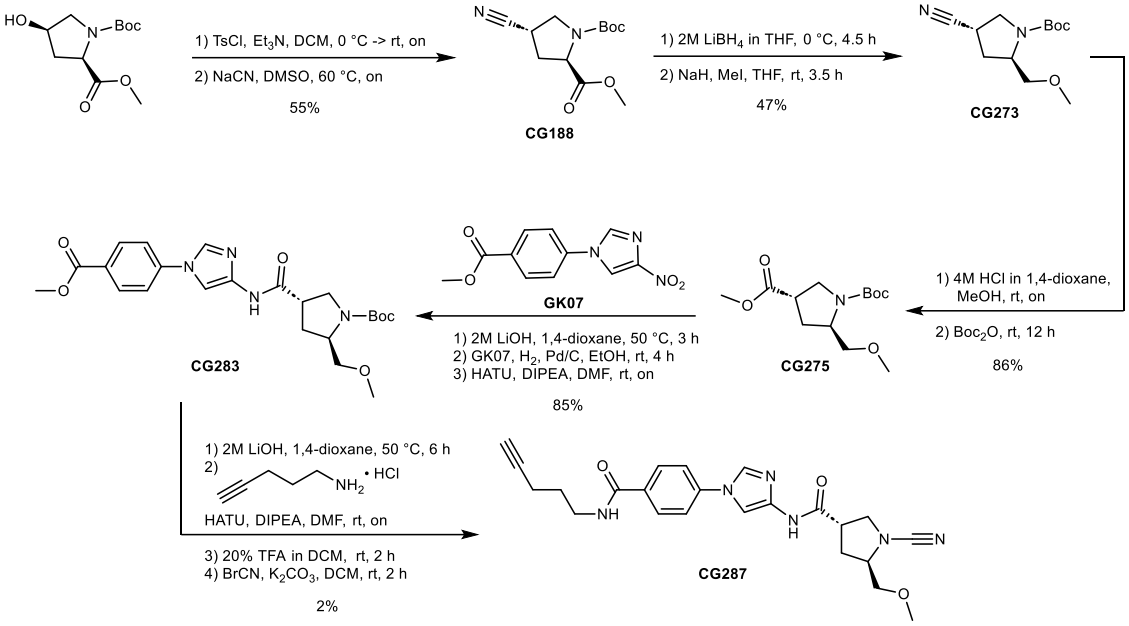

Scheme 22. Synthesis of CG287.

1-(*tert*-Butyl) 2-methyl (2*R*,4*S*)-4-cyanopyrrolidine-1,2-dicarboxylate (CG188)

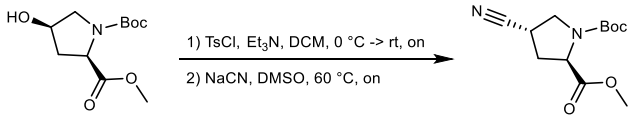

Step 1

Methyl *cis*-1-boc-4-hydroxy-*D*-prolinate (2.0 g, 8.15 mmol, 1.0 eq), triethylamine (Et_3N, 3.4 mL, 24.5 mmol, 3.0 eq) and DMAP (100 mg, 0.82 mmol, 0.1 eq) were dissolved in DCM (30 mL) and the solution cooled to 0 °C. 4-Toluenesulfonyl chloride (TsCl, 2.0 g, 10.6 mmol, 1.3 eq) was added portionwise to the solution at 0 °C. The reaction mixture was allowed to warm up to room temperature and stirred overnight. The reaction mixture was quenched with water (50 ml) and extracted with DCM (2x50 mL). The combined organic phases were washed with 10% citric acid (40 mL), sat. $NaHCO_3$ (40 mL) and brine (40 mL), dried over anhydrous $MgSO_4$ and the solvent was removed under reduced pressure. The product was used for step 2 without further purification.

^{1}H NMR (600 MHz, $CDCl_3$) δ (ppm) = 7.79 – 7.74 (m, 2H), 7.35 (t, *J* = 7.2 Hz, 2H), 5.11 – 4.99 (m, 1H), 4.38 (“d”dd, *J* = 66.0, 8.3, 4.0 Hz, 1H), 3.68 (“d”, *J* = 6.3 Hz, 3H), 3.67 – 3.63 (m, 1H), 3.63 – 3.54 (m, 1H), 2.45 (“d”, *J* = 2.4 Hz, 3H), 2.43 – 2.41 (m, 1H), 2.37 – 2.33 (m, 1H), 1.42 (“d”, *J* = 26.2 Hz, 9H).

^{13}C NMR (151 MHz, $CDCl_3$) δ (ppm) = 171.91 (“d”, *J* = 54.7 Hz), 153.68 (“d”, *J* = 66.3 Hz), 145.27 (“d”, *J* = 6.4 Hz), 133.76 (“d”, *J* = 22.6 Hz), 130.09 (“d”, *J* = 7.7 Hz), 127.88 (“d”, *J* = 4.1 Hz), 80.76 (“d”, *J* = 2.5 Hz), 78.35 (“d”, *J* = 172.3 Hz), 57.33 (“d”, *J* = 53.3 Hz), 52.46 (“d”, *J* = 23.0 Hz), 51.92 (“d”, *J* = 89.1 Hz), 36.63 (“d”, *J* = 149.2 Hz), 28.41 (“d”, *J* = 15.0 Hz), 21.83.

HRMS m/z for $C_{18}H_{26}NO_7S^+$ ($[M+H]^+$) calculated: 400.1425, found: 400.1425.

Step 2

The crude product from step 1 (1.0 g, 2.45 mmol, 1.0 eq) was dissolved in DMSO (25 mL) and sodium cyanide (180.3 mg, 3.68 mmol, 1.5 eq) was added. The reaction mixture was heated to 60 °C and stirred overnight. The reaction mixture was quenched by the addition of brine (50 ml) and extracted with EA (2x50 mL). The combined organic phases were dried over anhydrous $MgSO_4$ and the solvent was removed under reduced pressure. The product was purified via a silica column eluting at 10-20% EA in PE. CG188 (343.0 mg, 1.35 mmol, 55%) was obtained as a clear resin.

^{1}H NMR (700 MHz, $CDCl_3$) δ (ppm) = 4.44 (“d”dd, *J* = 67.1, 8.6, 3.4 Hz, 1H), 3.90 (“d”dd, *J* = 21.7, 10.6, 7.7 Hz, 1H), 3.75 (s, 3H), 3.65 (“d”dd, *J* = 42.5, 10.7, 7.4 Hz, 1H), 3.26 (“d”p, *J* = 22.7, 7.7 Hz, 1H), 2.50 (“d”dt, *J* = 43.3, 13.1, 8.9 Hz, 1H), 2.36 (“d”dd, *J* = 13.2, 6.8, 3.5 Hz, 1H), 1.44 (“d”, *J* = 38.6 Hz, 9H).

^{13}C NMR (176 MHz, $CDCl_3$) δ (ppm) = 172.41 (“d”, *J* = 15.7 Hz), 153.31 (“d”, *J* = 89.0 Hz), 119.12 (“d”, *J* = 14.6 Hz), 81.35 (“d”, *J* = 16.7 Hz), 57.91 (“d”, *J* = 36.4 Hz), 52.58, 49.25 (“d”, *J* = 18.6 Hz), 34.25 (“d”, *J* = 170.7 Hz), 28.38 (“d”, *J* = 20.6 Hz), 26.86 (“d”, *J* = 99.4 Hz).

HRMS m/z for $C_{12}H_{19}N_2O_4^+$ ($[M+H]^+$) calculated: 255.1339, found: 255.1340.

tert-Butyl (2*R*,4*S*)-4-cyano-2-(methoxymethyl)pyrrolidine-1-carboxylate (CG273)

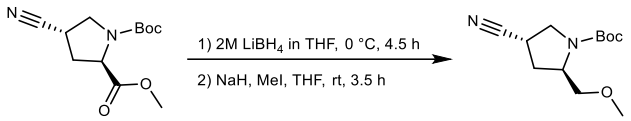

Step 1

To a solution of CG188 (500 mg, 1.97 mmol, 1.0 eq) in dry THF (9 mL) was added 2 M $LiBH_4$ in THF (1.08 mL, 2.16 mmol, 1.1 eq). The reaction mixture was stirred at 0 °C for 4.5 h. Drops of acetone were added slowly to quench the reaction. The resulting solution was poured into H_2O (40 mL) and extracted with EA (2x40 mL). The combined organic layers were washed with sat. $NaHCO_3$ (40 mL) and brine (40 mL), dried over anhydrous $MgSO_4$, filtered and the solvent was evaporated under reduced pressure. The resulting product was used for the next reaction without further purification.

HRMS *m/z* for $C_{11}H_{19}N_2O_3^+$ ($[M+H]^+$) calculated: 227.1391, found: 227.1390.

Step 2

The crude product from step 1 (282 mg, 1.25 mmol, 1.0 eq) was dissolved in dry THF (7 mL), then sodium hydride (60 wt.% in mineral oil, 59.8 mg, 1.50 mmol, 1.2 eq) was added portionwise and the mixture stirred at room temperature for 30 min. To the mixture was added methyl iodide (155.2 µL, 2.49 mmol, 2.0 eq) and stirring was continued at room temperature for 3 h. The reaction mixture was quenched by the addition of sat. NH_4Cl (30 ml) and extracted with EA (2x20 mL). The combined organic layers were washed with brine (40 mL), dried over anhydrous $MgSO_4$, filtered and the solvent was evaporated under reduced pressure. The product was purified via a silica column eluting at 10% EA in PE. CG273 (141.0 mg, 0.59 mmol, 47%) was obtained as a pale-yellow resin.

^{1}H NMR (700 MHz, $CDCl_3$) δ (ppm) = 4.05 (“d”, *J* = 67.3 Hz, 1H), 3.70 (“d”d, *J* = 10.7, 8.1 Hz, 1H), 3.58 (s, 1H), 3.48 (“d”d, *J* = 11.1, 7.3 Hz, 1H), 3.39 (“d”d, *J* = 9.8, 2.7 Hz, 1H), 3.32 (s, 3H), 3.01 (p, *J* = 7.6 Hz, 1H), 2.43 – 2.18 (m, 2H), 1.47 (“d”, *J* = 3.3 Hz, 9H).

^{13}C NMR (176 MHz, $CDCl_3$) δ (ppm) = 153.82, 120.24, 80.54, 76.98, 73.40, 59.42, 56.37, 49.82, 32.96, 28.56, 27.07.

HRMS *m/z* for $C_{12}H_{21}N_2O_3^+$ ($[M+H]^+$) calculated: 241.1547, found: 241.1546.

1-(*tert*-Butyl) 3-methyl (3*S*,5*R*)-5-(methoxymethyl)pyrrolidine-1,3-dicarboxylate (CG275)

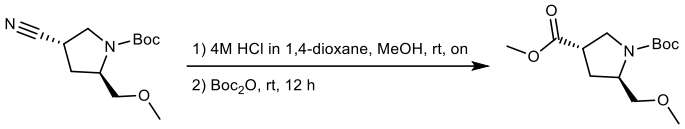

To a solution of CG273 (120.0 mg, 0.50 mmol, 1.0 eq) was added 4 M HCl in 1,4-dioxane (1.50 mL, 5.99 mmol, 12 eq) and the solution stirred overnight at room temperature. The reaction mixture was concentrated under reduced pressure and the crude intermediate dissolved in EA (4 mL) and basified with sat. aqueous $NaHCO_3$ (4 mL). Boc_2O (130.8 mg, 0.60 mmol, 1.2 eq) was added and the biphasic solution was stirred at rt for 12 h. The layers were then separated and the aqueous phase extracted with EA (30 mL). The organic phases were combined, washed with brine (50 mL), dried over anhydrous $MgSO_4$, filtered and the solvent was evaporated under reduced pressure. The product was purified via a silica column eluting at 1% EA in PE. CG275 (117.5 mg, 0.43 mmol, 86%) was obtained as a pale-yellow resin.

^{1}H NMR (600 MHz, DMSO-d_6) δ (ppm) = 3.88 (s, 1H), 3.62 (s, 3H), 3.44 – 3.38 (m, 2H), 3.36 (“d”d, *J* = 9.4, 3.4 Hz, 1H), 3.34 – 3.28 (m, 1H), 3.27 – 3.23 (m, 3H), 3.22 (s, 1H), 2.06 (“d”, *J* = 27.0 Hz, 2H), 1.40 (“d”, *J* = 1.3 Hz, 9H).

^{13}C NMR (151 MHz, DMSO-d_6) δ (ppm) = 173.11, 153.20, 78.75, 72.65 (“d”, *J* = 103.0 Hz), 58.50, 55.88, 51.79, 48.32 (“d”, *J* = 17.0 Hz), 40.92, 31.35 (“d”, *J* = 128.6 Hz), 28.08.

HRMS *m/z* for $C_{13}H_{24}NO_5^+$ ([M+H]$^+$) calculated: 274.1649, found: 274.1652.

***tert*-Butyl (2*R*,4*S*)-4-((1-(4-(methoxycarbonyl)phenyl)-1*H*-imidazol-4-yl)carbamoyl)-2-(methoxymethyl)pyrrolidine-1-carboxylate (CG283)**

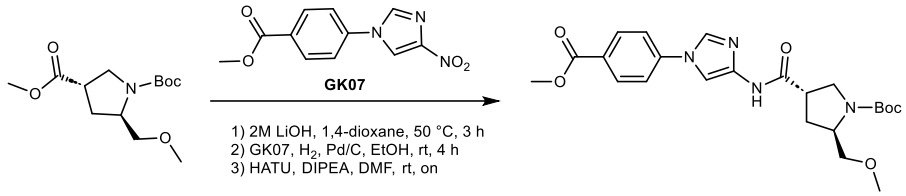

Step 1

CG275 (94.0 mg, 0.34 mmol, 1.0 eq) was dissolved in 1,4-dioxane (2 mL). Aqueous 2 M LiOH solution (344 µL, 0.69 mmol, 2.0 eq) was added and the reaction mixture was stirred for 3 h at 50 °C. The pH of the reaction mixture was adjusted to pH 7 by adding aqueous 1 M HCl dropwise. The solvent was removed under reduced pressure and the obtained product used for the next reaction without further purification.

Step 2

Methyl 4-(4-nitro-1*H*-imidazol-1-yl)benzoate (GK07[1]) (110.5 mg, 0.45 mmol, 1.3 eq) was dissolved in EtOH (10 mL) and a few drops of H_2O were added. Palladium (10%) on activated charcoal (11 mg) was added under an argon atmosphere. The reaction was flushed with H_2 and stirred for 4 h at room temperature. The reaction was filtered through Celite 545 which was then washed with EA. The solvent was removed under reduced pressure and the obtained product used for the next reaction without further purification.

Step 3

The crude product from step 1 was dissolved in DMF (2 mL), then DIPEA (175 µL, 1.03 mmol, 3.0 eq) and HATU (156.9 mg, 0.41 mmol, 1.2 eq) were added and the reaction mixture was stirred for 10 min at room temperature. The crude product from step 2 was dissolved in DMF (2 mL), added to the reaction

and the mixture stirred at room temperature overnight. The reaction mixture was quenched with sat. NH_4Cl solution (30 ml) and extracted with EA (2x30 mL). The combined organic layers were washed with brine (20 mL), dried over $MgSO_4$, filtered and the solvent was removed under reduced pressure. The product was purified via a silica column eluting at 65% EA in PE. CG283 (134.8 mg, 0.29 mmol, 85%) was obtained as a yellow solid.

^{1}H NMR (600 MHz, DMSO-d_6) δ (ppm) = 10.58 (“d”, *J* = 103.9 Hz, 1H), 8.32 – 8.26 (m, 1H), 8.09 – 8.03 (m, 2H), 7.81 (“d”q, *J* = 8.8, 2.4, 1.9 Hz, 3H), 3.94 – 3.88 (m, 1H), 3.87 (s, 3H), 3.53 – 3.38 (m, 2H), 3.38 – 3.33 (m, 1H), 3.31 (“d”, *J* = 3.4 Hz, 1H), 3.27 (“d”, *J* = 17.6 Hz, 3H), 3.24 (“d”, *J* = 11.9 Hz, 1H), 2.14 – 1.95 (m, 2H), 1.48 – 1.35 (m, 9H).

^{13}C NMR (151 MHz, DMSO-d_6) δ (ppm) = 171.12, 165.32, 157.52, 140.18, 139.16, 132.15, 131.02, 127.37, 119.55, 103.91, 78.67, 72.99, 58.52, 56.10, 52.09, 48.99, 42.62, 32.35, 28.11.

HRMS *m/z* for $C_{23}H_{31}N_4O_6^+$ ([M+H]$^+$) calculated: 459.2238, found: 459.2240.

(3*S*,5*R*)-1-Cyano-5-(methoxymethyl)-*N*-(1-(4-(pent-4-yn-1-ylcarbamoyl)phenyl)-1*H*-imidazol-4-yl)pyrrolidine-3-carboxamide (CG287)

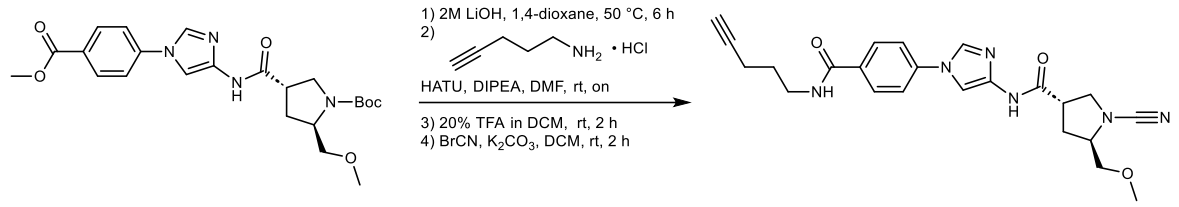

Step 1

CG283 (67.0 mg, 0.15 mmol, 1.0 eq) was dissolved in 1,4-dioxane (1 mL). Aqueous 2 M LiOH solution (102 µL, 0.20 mol, 1.4 eq) was added and the reaction mixture was stirred for 6 h at 50 °C. The pH of the reaction mixture was adjusted to pH 7 by adding aqueous 1 M HCl dropwise. The solvent was removed under reduced pressure and the obtained product used for the next reaction without further purification.

Step 2

The crude product from step 1 was dissolved in DMF (1 mL), then DIPEA (49.7 µL, 0.29 mmol, 2.0 eq) and HATU (72.2 mg, 0.19 mmol, 1.3 eq) were added and the reaction mixture was stirred for 10 min at room temperature. 4-Pentyn-1-amine (22.7 mg, 0.19 mmol, 1.3 eq) was dissolved in DMF (1 mL), added to the reaction and the mixture stirred at room temperature overnight. The reaction mixture was quenched with sat. NH_4Cl solution (30 ml) and extracted with EA (2x30 mL). The combined organic layers were washed with brine (20 mL), dried over $MgSO_4$, filtered and the solvent was removed under reduced pressure. The product was used for the next reaction without further purification.

Step 3

The crude product from step 2 was dissolved in DCM (2 mL) and TFA (0.4 mL) was added dropwise. The solution was stirred for 2 h at room temperature. The solvent was removed under reduced pressure and the product dried overnight in vacuo. Partial purification was achieved by preparative HPLC during which the desired product (3*S*,5*R*)-5-(methoxymethyl)-*N*-(1-(4-(pent-4-yn-1-ylcarbamoyl)phenyl)-1*H*-imidazol-4-yl)pyrrolidine-3-carboxamide TFA salt (9.6 mg, 0.02 mmol) co-eluted with uncharacterised impurities. Fractions containing the desired product as judged by LC-MS and TLC were combined, frozen, lyophilised and used for the next reaction without further purification.

Step 4

The crude product from step 3 was dissolved in DMF (1 mL) and DIPEA (12.5 µL, 0.07 mmol, 4.0 eq based on intermediate product of step 3) was added. The mixture was cooled to 0 °C and 3 M cyanogen bromide solution (7.3 µL, 0.02 mmol, 1.2 eq based on intermediate product of step 3) was added and the mixture was stirred for 30 min at 0 °C. The reaction mixture was allowed to warm up to room temperature and stirred for another 2 h followed by the addition of H_2O (20 mL). The mixture was extracted with EA (2x20 mL). The combined organic layers were washed with brine (20 mL), dried over anhydrous $MgSO_4$, filtered and the solvent was removed under reduced pressure. Partial purification was achieved by normal phase column chromatography using DCM and MeOH as eluents, during which the desired product (3*S*,5*R*)-5-(methoxymethyl)-*N*-(1-(4-(pent-4-yn-1-ylcarbamoyl)phenyl)-1*H*-imidazol-4-yl)pyrrolidine-3-carboxamide mainly co-eluted with an uncharacterised impurity (probably its (3*R*,5*R*)-diastereomer as judged by comparison of NMR spectra of similar compounds with *N*-cyanopyrrolidine warhead in (3*R*,5*R*)-configuration). Only selected fractions contained the desired, pure product, as judged by LC-MS and TLC. They were subsequently combined, frozen and lyophilised to obtain pure CG287 (1.5 mg, 3.45 µmol, 2% overall yield) as a white powder.

^{1}H NMR (700 MHz, DMSO-d_6) δ (ppm) = 10.71 (s, 1H), 8.56 (t, *J* = 5.6 Hz, 1H), 8.24 (d, *J* = 1.7 Hz, 1H), 8.00 – 7.93 (m, 2H), 7.80 (d, *J* = 1.7 Hz, 1H), 7.77 – 7.71 (m, 2H), 3.88 (dq, *J* = 7.8, 5.4 Hz, 1H), 3.65 (dd, *J* = 9.4, 7.3 Hz, 1H), 3.50 (dd, *J* = 9.4, 6.1 Hz, 1H), 3.43 – 3.36 (m, 2H), 3.36 – 3.33 (m, 2H), 3.31 (s, 3H), 3.30 – 3.24 (m, 1H), 2.80 (t, *J* = 2.7 Hz, 1H), 2.23 (td, *J* = 7.1, 2.7 Hz, 2H), 2.15 (ddd, *J* = 12.7, 7.9, 6.7 Hz, 1H), 1.94 (ddd, *J* = 12.9, 7.5, 5.5 Hz, 1H), 1.72 (p, *J* = 7.1 Hz, 2H).

^{13}C NMR (176 MHz, DMSO-d_6) δ (ppm) = 169.10, 165.18, 139.16, 138.70, 132.36, 132.09, 128.95, 119.19, 116.53, 104.17, 84.12, 73.19, 71.40, 60.51, 58.52, 53.13, 42.15, 38.48, 31.74, 28.04, 15.53.

HRMS *m/z* for $C_{23}H_{26}N_6O_3^+$ ([M+H]$^+$) calculated: 435.2139, found: 435.2139.

8.1.1.6 Synthesis of CG385

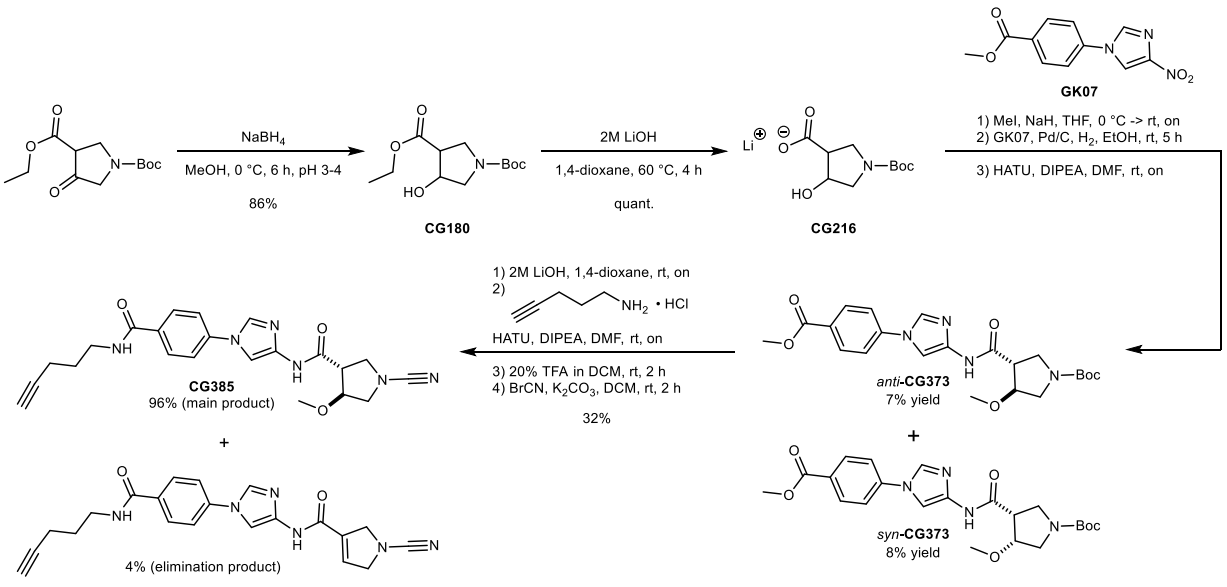

Scheme 23. Synthesis of CG385.

1-(*tert*-Butyl) 3-ethyl 4-hydroxypyrrolidine-1,3-dicarboxylate (CG180)

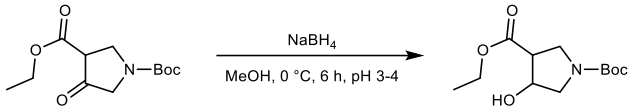

To a solution of 1-(*tert*-butyl) 3-ethyl 4-oxopyrrolidine-1,3-dicarboxylate (2.0 g, 7.77 mmol, 1.0 eq) in dry MeOH (40 mL) was added $NaBH_4$ (588.2 mg, 15.55 mmol, 2.0 eq). Aqueous 1 N HCl was added dropwise to adjust the pH to 3-4. The reaction mixture was stirred at 0 °C for 6 h. The reaction mixture was quenched by the addition of water (50 ml) and brine (50 mL) and then extracted with EA (6x40 mL). The organic layers were combined, dried over anhydrous $MgSO_4$, filtered and the solvent was evaporated under reduced pressure. The product was purified via a silica column eluting at 10-20% EA in PE. CG180 (1.735 g, 6.69 mmol, 86%) was obtained as a clear liquid.

^{1}H NMR (700 MHz, $CDCl_3$) δ (ppm) = 4.59 – 4.52 (m, 1H), 4.21 (“d”q, *J* = 21.5, 7.1 Hz, 2H), 3.78 – 3.74 (m, 1H), 3.74 – 3.68 (m, 1H), 3.63 – 3.53 (m, 1H), 3.53 – 3.24 (m, 1H), 3.08 – 2.93 (m, 1H), 1.46 (“d”, *J* = 2.0 Hz, 9H), 1.32 – 1.26 (m, 3H).

^{13}C NMR (176 MHz, $CDCl_3$) δ (ppm) = 171.91, 154.48 (“d”, *J* = 16.8 Hz), 79.91 (“d”, *J* = 10.3 Hz), 72.40, 61.46 (“d”, *J* = 16.4 Hz), 52.98 (“d”, *J* = 252.4 Hz), 50.85, 45.77 (“d”, *J* = 137.1 Hz), 28.61 (“d”, *J* = 3.7 Hz), 14.30 (“d”, *J* = 2.9 Hz).

HRMS *m/z* for $C_{12}H_{22}NO_5^+$ ([M+H]$^+$) calculated: 260.1493, found: 260.1491.

Lithium 1-(*tert*-butoxycarbonyl)-4-hydroxypyrrolidine-3-carboxylate (CG216)

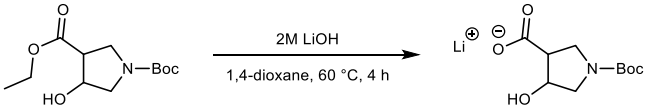

CG180 (500.0 mg, 1.93 mmol, 1.0 eq) was dissolved in 1,4-dioxane (2 mL). Aqueous 2 M LiOH solution (1.93 mL, 3.86 mmol, 2.0 eq) was added and the reaction mixture was stirred for 4 h at 60 °C. The pH of the reaction mixture was adjusted to pH 7 by adding aqueous 1 N HCl dropwise. The solvent was removed under reduced pressure yielding CG216 (389.0 mg, 1.64 mmol, 85%), which was used for following reactions without further purification.

***anti*-/*syn*-*tert*-Butyl-3-methoxy-4-((1-(4-(methoxycarbonyl)phenyl)-1*H*-imidazol-4-yl)carbamoyl)-pyrrolidine-1-carboxylate (CG373)**

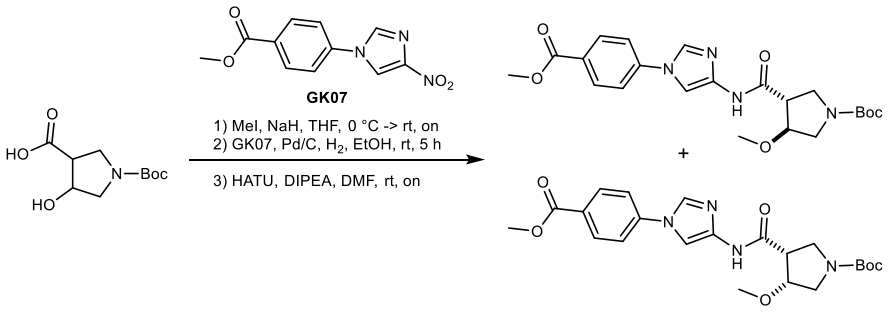

Step 1

CG216 (165.2 mg, 0.69 mmol, 1.0 eq) was dissolved in dry THF (8 mL), then sodium hydride (60 wt.% in mineral oil, 133.8 mg, 3.34 mmol, 4.8 eq) was added portionwise at 0 °C. The reaction was allowed to reach room temperature and stirred for another 30 min. To the mixture was added methyl iodide (104.1 µL, 1.67 mmol, 2.4 eq) and stirring was continued at room temperature overnight. The reaction

mixture was quenched by the addition of sat. NH_4Cl (30 ml) and extracted with EA (2x20 mL). The combined organic layers were washed with brine (40 mL), dried over anhydrous $MgSO_4$, filtered and the solvent was evaporated under reduced pressure. The product was used for the next reaction without further purification.

Step 2

GK07 (268.7 mg, 1.09 mmol, 1.6 eq) was dissolved in EtOH (20 mL) and a few drops of H_2O were added. Palladium (10%) on activated charcoal (27 mg) was added under an argon atmosphere. The reaction was flushed with H_2 and stirred for 5 h at room temperature. The reaction was filtered through Celite 545 which was then washed with EA. The solvent was removed under reduced pressure and the obtained product used for the next reaction without further purification.

Step 3

The crude product from step 1 was dissolved in DMF (2 mL), then DIPEA (568.8 µL, 3.34 mmol, 4.8 eq) and HATU (413.3 mg, 1.09 mmol, 1.6 eq) were added and the reaction mixture stirred for 10 min at room temperature. The crude product from step 2 was dissolved in DMF (2 mL), added to the reaction and the mixture stirred at room temperature overnight. The reaction mixture was quenched with sat. NH_4Cl solution (30 ml) and extracted with EA (2x30 mL). The combined organic layers were washed with brine (20 mL), dried over $MgSO_4$, filtered and the solvent was removed under reduced pressure. The product was purified via a silica column eluting at 40-60% EA in PE, yielding a mixture of both *syn*- and *anti*-CG373 as judged by LC-MS and NMR analysis. The product mixture was further purified by preparative HPLC eluting at 15-25% ACN in H_2O. Both isomers were able to be separated yielding *anti*-CG373 (20.6 mg, 0.05 mmol, 7%) and *syn*-CG373 (25.3 mg, 0.06 mmol, 8%), both as white solids.

anti-CG373

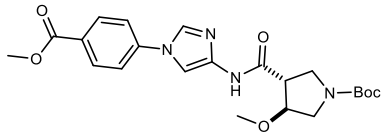

^{1}H NMR (700 MHz, DMSO-d_6) δ (ppm) = 10.65 (“d”, *J* = 8.5 Hz, 1H), 8.35 (“d”d, *J* = 2.7, 1.6 Hz, 1H), 8.06 (“d”d, *J* = 8.8, 2.1 Hz, 2H), 7.86 – 7.75 (m, 3H), 4.26 (td, *J* = 4.7, 2.7 Hz, 1H), 3.87 (s, 3H), 3.64 – 3.55 (m, 1H), 3.51 – 3.39 (m, 2H), 3.38 – 3.29 (m, 2H), 3.23 (“d”, *J* = 5.0 Hz, 3H), 1.41 (“d”, *J* = 1.5 Hz, 9H).

^{13}C NMR (176 MHz, DMSO-d_6) δ (ppm) = 166.47 (“d”, *J* = 27.5 Hz), 165.47, 158.33 (q, *J* = 37.6 Hz), 153.63 (“d”, *J* = 5.2 Hz), 140.27, 139.11 (“d”, *J* = 6.0 Hz), 132.12 (“d”, *J* = 5.8 Hz), 131.00 (“d”, *J* = 1.9 Hz), 127.48, 119.63 (“d”, *J* = 3.5 Hz), 115.30 (q, *J* = 289.7 Hz), 103.93 (“d”, *J* = 4.4 Hz), 79.92 (“d”, *J* = 134.3 Hz), 78.43, 56.82 (“d”, *J* = 20.0 Hz), 52.26, 49.75 (“d”, *J* = 40.4 Hz), 47.28 (“d”, *J* = 169.6 Hz), 45.47 (“d”, *J* = 19.7 Hz), 28.17.

HRMS *m/z* for $C_{22}H_{29}N_4O_6^+$ ($[M+H]^+$) calculated: 445.2082, found: 445.2087.

syn-CG373

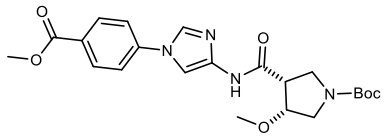

^{1}H NMR (700 MHz, DMSO-d_6) δ (ppm) = 10.85 (“d”, *J* = 10.1 Hz, 1H), 8.33 (d, *J* = 1.7 Hz, 1H), 8.09 – 8.00 (m, 2H), 7.84 (d, *J* = 1.7 Hz, 1H), 7.83 – 7.80 (m, 2H), 4.07 (q, *J* = 4.6, 4.2 Hz, 1H), 3.87 (s, 3H), 3.59 – 3.46 (m, 2H), 3.44 – 3.37 (m, 1H), 3.28 (s, 3H), 3.27 – 3.21 (m, 2H), 1.40 (s, 9H).

^{13}C NMR (176 MHz, DMSO-d_6) δ (ppm) = 168.67 (“d”, *J* = 10.9 Hz), 165.46, 158.31 (q, *J* = 37.2 Hz), 153.41 (“d”, *J* = 18.4 Hz), 140.27, 139.08, 132.29, 131.00, 127.48, 119.60, 115.41 (q, *J* = 290.3 Hz), 104.22, 81.33 (“d”, *J* = 151.1 Hz), 78.58, 56.50, 52.25, 50.31 (“d”, *J* = 54.3 Hz), 48.06 (“d”, *J* = 150.2 Hz), 47.21 (“d”, *J* = 33.0 Hz), 28.13.

HRMS *m/z* for $C_{22}H_{29}N_4O_6^+$ ([M+H]$^+$) calculated: 445.2082, found: 445.2085.

***anti*-1-Cyano-4-methoxy-*N*-(1-(4-(pent-4-yn-1-ylcarbamoyl)phenyl)-1*H*-imidazol-4-yl)pyrrolidine-3-carboxamide (CG385)**

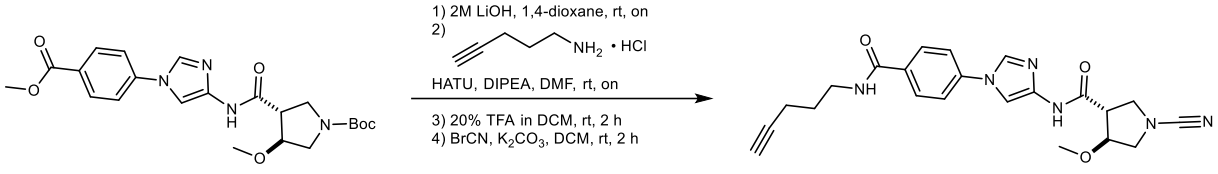

Step 1

anti-CG373 (5.9 mg, 0.13 mmol, 1.0 eq) was dissolved in 1,4-dioxane (0.5 mL). Aqueous 2 M LiOH solution (19.9 µL, 0.40 mol, 3 eq) was added and the reaction mixture was stirred at room temperature overnight. The pH of the reaction mixture was adjusted to pH 7 by adding a few drops of aqueous 1 M HCl. The solvent was removed under reduced pressure and the obtained product used for the next reaction without further purification.

Step 2

The crude product from step 1 was dissolved in DMF (1 mL), then DIPEA (9.3 µL, 0.53 mol, 4 eq) and HATU (6.6 mg, 0.17 mmol, 1.3 eq) were added and the reaction mixture was stirred for 10 min at room temperature. 4-Pentyn-1-amine HCl (2.1 mg, 0.17 mmol, 1.3 eq) was added to the reaction and the mixture stirred at room temperature overnight. The reaction mixture was quenched with sat. NH_4Cl solution (30 mL) and extracted with EA (2x30 mL). The combined organic layers were washed with brine (20 mL), dried over $MgSO_4$, filtered and the solvent was removed under reduced pressure. Partial purification was achieved by preparative HPLC during which the desired product *anti*-*tert*-butyl 3-methoxy-4-((1-(4-(pent-4-yn-1-ylcarbamoyl)phenyl)-1*H*-imidazol-4-yl)-carbamoyl)pyrrolidine-1-carboxylate TFA salt mainly co-eluted with an uncharacterised impurity. Selected fractions, containing only the desired and pure product as judged by LC-MS and TLC, were combined, frozen, lyophilised and used for the next reaction without further purification.

Step 3

The product from step 2 (4.1 mg, 0.07 mmol, 1.0 eq) was dissolved in DCM (2 mL) and TFA (0.4 mL) was added dropwise. The solution was stirred for 3 h at room temperature. EA (5 mL) was added to the mixture. Then the solvent and residual TFA were removed under reduced pressure and the product dried in vacuo.

Step 4

The crude product from step 3 was dissolved in DMF (1 mL) and DIPEA (9.2 µL, 0.05 mmol, 8.0 eq) was added. 3 M cyanogen bromide solution (4.5 µL, 0.01 mmol, 2.0 eq) was added and the mixture was stirred for 3 h at room temperature. The reaction was quenched by the addition of aqueous sat. $NaHCO_3$ (20 mL) and then extracted with EA (2x20 mL). The combined organic layers were washed with aqueous sat. NH_4Cl (20 mL) and brine (20 mL), dried over anhydrous $MgSO_4$, filtered and the solvent was removed under reduced pressure. The corresponding product was purified via a preparative HPLC (without TFA), eluting at 15-25% ACN (no TFA) in H_2O (no TFA), yielding *anti*-CG385 (1.8 mg, 4.28 µmol, 32% overall yield) as a white powder. Note that even after thorough selection of pure fractions after preparative HPLC, as judged by LC-MS, an impurity of 4% could be observed in the ^{1}H NMR spectrum, characterised as the elimination product 1-cyano-*N*-(1-(4-(pent-4-yn-1-

ylcarbamoyl)phenyl)-1*H*-imidazol-4-yl)-2,5-dihydro-1*H*-pyrrole-3-carboxamide as judged by 1D- and 2D-NMR analysis (e.g. characteristic chemical shift of alkene proton [δ = 6.91 ppm (s, 0.4 H ≙ 1 H)] as well as chemical equivalent pyrrolidine protons adjacent to the *N*-cyano-group [δ = 4.48 (s, 0.18 H ≙ 4 H).

^{1}H NMR (600 MHz, DMSO-d_6) δ (ppm) = 10.92 (s, 1H), 8.57 (t, *J* = 5.6 Hz, 1H), 8.26 (d, *J* = 1.6 Hz, 1H), 8.02 – 7.94 (m, 2H), 7.82 (d, *J* = 1.6 Hz, 1H), 7.78 – 7.73 (m, 2H), 4.10 (dt, *J* = 4.9, 2.6 Hz, 1H), 3.64 (dd, *J* = 9.9, 7.4 Hz, 1H), 3.57 – 3.48 (m, 2H), 3.43 (dd, *J* = 10.4, 2.3 Hz, 1H), 3.37 – 3.33 (m, 3H), 3.31 (s, 3H), 2.80 (t, *J* = 2.6 Hz, 1H), 2.23 (td, *J* = 7.1, 2.7 Hz, 2H), 1.72 (p, *J* = 7.1 Hz, 2H).

^{13}C NMR (151 MHz, DMSO-d_6) δ (ppm) = 167.88, 165.18, 139.01, 138.68, 132.39, 132.16, 128.96, 119.21, 117.12, 104.35, 84.12, 82.18, 71.41, 56.49, 54.52, 51.71, 48.53, 38.48, 28.04, 15.53.

HRMS *m/z* for $C_{22}H_{25}N_6O_3^+$ ([M+H]$^+$) calculated: 421.1983, found: 421.1987.

8.1.1.7 Synthesis of CG390

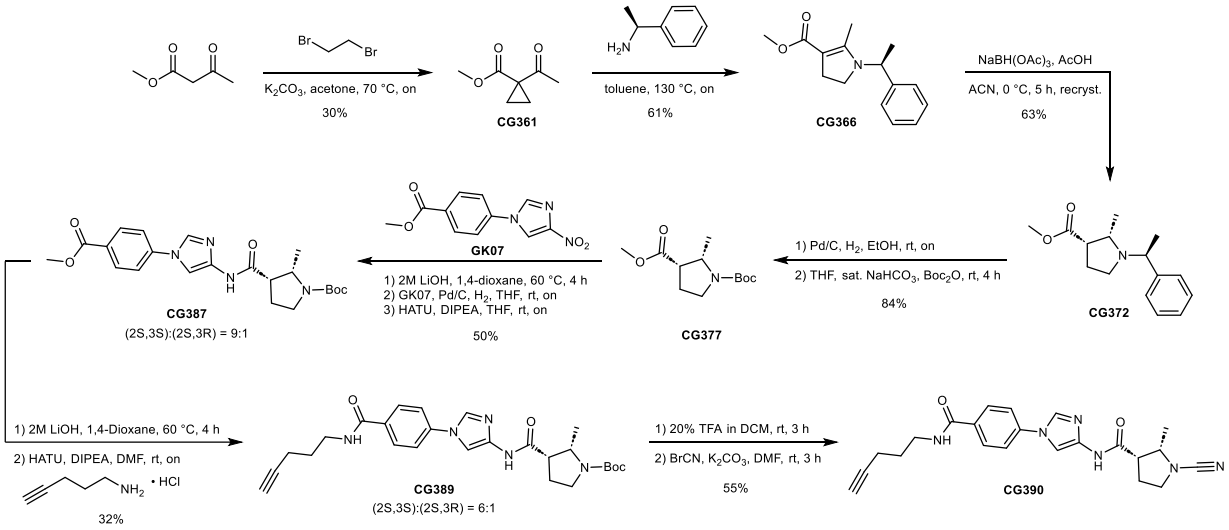

Scheme 24. Synthesis of compound CG390 based on the synthesis route described for Cpd74 [181].

Methyl 1-acetylcyclopropane-1-carboxylate (CG361)

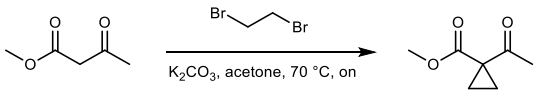

To a solution of methyl 3-oxobutanoate (1.0 mL, 9.27 mmol, 1.0 eq) and 1,2-dibromoethane (882 µL, 10.19 mmol, 1.1 eq) in acetone (20 mL) was added K_2CO_3 (1.92 g, 13.9 mmol, 1.5 eq) at room temperature. The reaction was heated to 70 °C and stirred for 24 h. The reaction mixture was allowed to cool down to room temperature and filtered through Celite 545 which was then washed with acetone. The filtrate was concentrated under reduced pressure and purified by normal phase column chromatography eluting at 2-5% EA in CH. CG361 (390.7 mg, 2.75 mmol, 30%) was obtained as a clear liquid.**^{1}H NMR** (600 MHz, $CDCl_3$) δ (ppm) = 3.74 (s, 3H), 2.47 (s, 3H), 1.48 (s, 4H).

^{13}C NMR (151 MHz, $CDCl_3$) δ (ppm) = 203.18, 171.67, 52.41, 35.07, 30.00, 19.44.

Methyl (*S*)-2-methyl-1-(1-phenylethyl)-4,5-dihydro-1*H*-pyrrole-3-carboxylate (CG366)

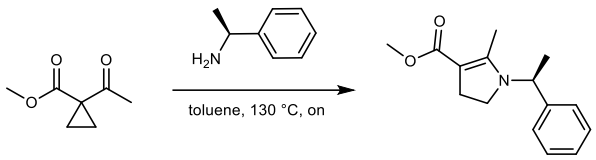

CG361 (380.0 mg, 2.67 mmol, 1.0 eq) was dissolved in toluene (4 mL) and (*S*)-1-phenylethan-1-amine (862 µL, 6.68 mmol, 2.5 eq) was added. The reaction was equipped with a Dean-Stark trap, heated to 130 °C and stirred overnight. The reaction mixture was allowed to cool down to room temperature and concentrated under reduced pressure. The corresponding product was purified via a normal phase column eluting at 6% EA in PE, yielding CG366 (397.7 mg, 1.62 mmol, 61%) as a red oil.

^{1}H NMR (700 MHz, DMSO-d_6) δ (ppm) = 7.42 – 7.33 (m, 2H), 7.31 – 7.18 (m, 3H), 4.94 (q, *J* = 7.0 Hz, 1H), 3.50 (s, 3H), 3.49 – 3.42 (m, 1H), 3.07 (ddd, *J* = 12.0, 10.3, 8.2 Hz, 1H), 2.60 – 2.51 (m, 2H), 2.25 (d, *J* = 1.4 Hz, 3H), 1.48 (d, *J* = 7.0 Hz, 3H).

^{13}C NMR (176 MHz, DMSO-d_6) δ (ppm) = 166.29, 160.70, 141.32, 128.50, 127.11, 126.61, 94.21, 52.16, 49.50, 44.63, 26.15, 17.44, 11.77.

HRMS *m/z* for $C_{15}H_{20}NO_2^+$ ([M+H]$^+$) calculated: 246.1489, found: 246.1483.

Methyl (2*S*,3*S*)-2-methyl-1-((S)-1-phenylethyl)pyrrolidine-3-carboxylate (CG372)

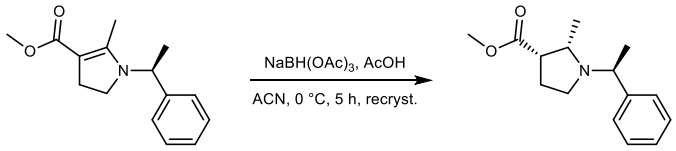

A solution of CG366 (390 mg, 1.59 mmol, 1.0 eq) and acetic acid (AcOH, 1.27 mL, 22.3 mmol, 14 eq) in ACN (4 mL) was cooled to 0°C, then sodium triacetoxyborohydride ($NaBH(OAc)_3$, 674 mg, 3.18 mmol, 2.0 eq) was added portionwise. After stirring the reaction for 5 h at 0 °C, the solvent was evaporated under reduced pressure and the resulting mixture poured into aqueous sat. $NaHCO_3$ solution (30 mL). The pH was adjusted to pH 9 followed by extraction with EA (3x30 mL). The combined organic layers were washed with brine (30 mL), dried over anhydrous $MgSO_4$, filtered and the solvent was removed under reduced pressure. The corresponding product was purified via normal phase column chromatography, eluting at 1-5% EA in CH. The product was further crystallised from hexane (30 mL) at -80 °C yielding CG372 (247.3 mg, 1.00 mmol, 63%) as white crystals.

^{1}H NMR (600 MHz, DMSO-d_6) δ (ppm) = 7.34 – 7.26 (m, 4H), 7.24 – 7.18 (m, 1H), 3.62 – 3.59 (m, 1H), 3.59 (s, 3H), 3.35 (dt, *J* = 7.8, 6.4 Hz, 1H), 3.06 (dt, *J* = 10.0, 8.1 Hz, 1H), 2.59 (td, *J* = 9.0, 3.7 Hz, 1H), 2.43 (dt, *J* = 9.2, 7.7 Hz, 1H), 1.98 (dddd, *J* = 12.6, 10.0, 8.7, 7.7 Hz, 1H), 1.85 – 1.76 (m, 1H), 1.26 (d, *J* = 6.5 Hz, 3H), 0.70 (d, *J* = 6.4 Hz, 3H).

^{13}C NMR (151 MHz, DMSO-d_6) δ (ppm) = 172.93, 145.40, 128.13, 127.19, 126.74, 59.60, 56.36, 51.29, 47.92, 46.68, 24.55, 20.19, 12.87.

HRMS *m/z* for $C_{15}H_{22}NO_2^+$ ([M+H]$^+$) calculated: 248.1645, found: 248.1642.

1-(*tert*-Butyl) 3-methyl (2*S*,3*S*)-2-methylpyrrolidine-1,3-dicarboxylate (CG377)

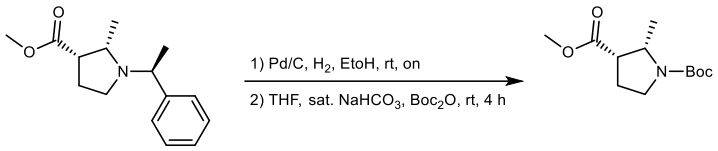

Step 1

To a solution of CG372 (500.0 mg, 2.02 mmol, 1.0 eq) in MeOH (10 mL) was added palladium (10%) on activated charcoal (50 mg) under an argon atmosphere. The reaction was flushed with H_2 and stirred overnight at room temperature. The reaction was filtered through Celite 545 which was then washed with EA. The solvent was removed under reduced pressure and the obtained product used for the next reaction without further purification.

Step 2

The crude product from step 1 was dissolved in a mixture of EA (2 mL) and aqueous sat. $NaHCO_3$ solution (1 mL). Boc2O (882 mg, 4.04 mmol, 2.0 eq) was added and the reaction vigorously stirred at room temperature for 4 h. The phases were separated and the aqueous phase extracted with EA (2x10 mL). The combined organic layers were washed with brine (30 mL), dried over anhydrous $MgSO_4$, filtered and the solvent was removed under reduced pressure. The corresponding product was purified via normal phase column chromatography, eluting at 12% EA in CH, yielding CG377 (415.8 mg, 1.71 mmol, 85%) as a white solid.

^{1}H NMR (600 MHz, DMSO-d_6) δ (ppm) = 4.01 (q, *J* = 7.1 Hz, 1H), 3.63 (s, 3H), 3.35 (t, *J* = 9.2 Hz, 1H), 3.20 (“d”q, *J* = 31.4, 9.8, 9.1 Hz, 2H), 2.24 – 2.03 (m, 1H), 1.99 – 1.89 (m, 1H), 1.39 (s, 9H), 0.95 (“d”, *J* = 6.4 Hz, 3H).

^{13}C NMR (151 MHz, DMSO-d_6) δ (ppm) = 171.42 (“d”, *J* = 16.5 Hz), 152.98, 78.42, 53.09, 51.59, 46.17 (“d”, *J* = 110.9 Hz), 44.45 (“d”, *J* = 47.9 Hz), 28.13, 24.19 (“d”, *J* = 159.0 Hz), 15.77 (“d”, *J* = 91.0 Hz).

HRMS *m/z* for $C_{12}H_{22}NO_4^+$ ([M+H]$^+$) calculated: 244.1543, found: 244.1537.

***tert*-Butyl (2S,3S)-3-((1-(4-(methoxycarbonyl)phenyl)-1H-imidazol-4-yl)carbamoyl)-2-methyl-pyrrolidine-1-carboxylate (CG387)**

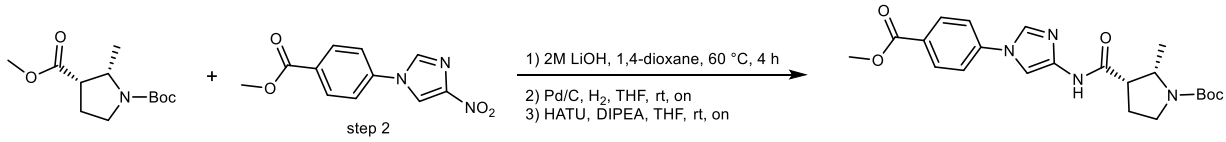

Step 1

CG377 (410.0 mg, 1.69 mmol, 1.0 eq) was dissolved in 1,4-dioxane (4 mL). Aqueous 2 M LiOH solution (1.52 mL, 3.03 mmol, 1.8 eq) was added and the reaction mixture was stirred for overnight at 50 °C. The pH of the reaction mixture was adjusted to pH 7 by adding aqueous 1 M HCl dropwise. The solvent was removed under reduced pressure and the obtained product used for the next reaction without further purification.

Step 2

GK07 (300.0 mg, 1.21 mmol, 1.0 eq) was dissolved in THF (5 mL) and palladium (10%) on activated charcoal (30 mg) was added under an argon atmosphere. The reaction was flushed with H_2 and stirred overnight at room temperature. The reaction was filtered through Celite 545 which was then washed with THF (20 mL) and the resulting solution was directly used for the next reaction.

Step 3

The crude product from step 1 was dissolved in THF (2 mL), then DIPEA (825 µL, 4.85 mmol, 4.0 eq) and HATU (553.7 mg, 1.46 mmol, 1.2 eq) were added and the reaction mixture was stirred for 10 min at room temperature. This reaction mixture was then transferred to the solution generated in step 2 and the reaction stirred at room temperature overnight. The reaction mixture was quenched with sat. NH_4Cl solution (30 mL) and extracted with EA (2x30 mL). The combined organic layers were washed with brine (30 mL), dried over $MgSO_4$, filtered and the solvent was removed under reduced pressure. The product was purified via a silica column eluting at 60-70% EA in CH. CG387 (258.3 mg, 0.60 mmol, 50%) was obtained as a 9:1 mixture of *(2S,3S):(2S,3R),* as judged by peak-ratios of corresponding H-atoms in the ^{1}H NMR Peak assignment was carried out by evaluation of 1D- and 2D-NMR spectra.

Spectral data are given for the main *(2S,3S)*-product.

^{1}H NMR (600 MHz, DMSO-d_6) δ (ppm) = 10.60 (“d”, *J* = 28.8 Hz, 1H), 8.29 (d, *J* = 1.6 Hz, 1H), 8.09 – 8.02 (m, 2H), 7.83 (q, *J* = 2.1, 1.6 Hz, 1H), 7.81 (q, *J* = 2.5, 2.0 Hz, 2H), 4.27 – 4.12 (m, 1H), 3.87 (s, 3H), 3.37 (td, *J* = 13.0, 12.5, 6.7 Hz, 1H), 3.19 (d, *J* = 9.2 Hz, 2H), 2.33 – 2.19 (m, 1H), 1.94 – 1.84 (m, 1H), 1.40 (“d”, *J* = 6.9 Hz, 9H), 0.93 (“d”d, *J* = 7.0, 3.0 Hz, 3H).

^{13}C NMR (151 MHz, DMSO-d_6) δ (ppm) = 167.36 (“d”, *J* = 17.5 Hz), 165.47, 153.06, 140.32, 139.47, 132.23, 131.00, 127.34, 119.50, 103.78, 78.30, 53.61, 52.26, 46.96 (“d”, *J* = 121.3 Hz), 44.46 (“d”, *J* = 45.9 Hz), 28.18, 24.11 (“d”, *J* = 155.7 Hz), 15.61 (“d”, *J* = 91.3 Hz).

HRMS *m/z* for $C_{22}H_{29}N_4O_5^+$ ([M+H]$^+$) calculated: 429.2133, found: 429.2135.

***tert*-Butyl (2*S*,3*S*)-2-methyl-3-((1-(4-(pent-4-yn-1-ylcarbamoyl)phenyl)-1*H*-imidazol-4-yl)carbamoyl)pyrrolidine-1-carboxylate (CG389)**

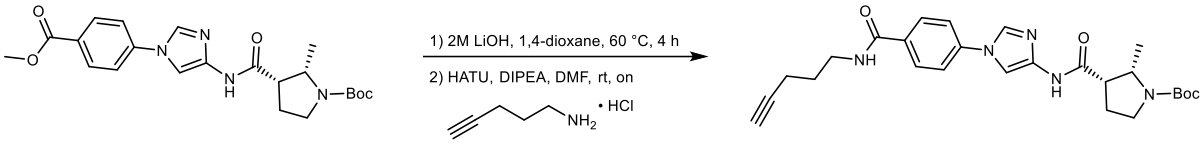

Step 1

CG387 (250.0 mg, 0.58 mmol, 1.0 eq) was dissolved in 1,4-dioxane (4 mL). Aqueous 2 M LiOH solution (379 µL, 0.76 mol, 1.3 eq) was added and the reaction mixture was stirred for 4 h at 60 °C. The pH of the reaction mixture was adjusted to pH 7 by adding aqueous 1 M HCl dropwise. The solvent was removed under reduced pressure and the obtained product used for the next reaction without further purification.

Step 2

The crude product from step 1 was dissolved in DMF (2 mL), then DIPEA (497.8 µL, 2.85 mmol, 5.0 eq) and HATU (281.8 mg, 0.74 mmol, 1.3 eq) were added and the reaction mixture was stirred for 10 min at room temperature. 4-Pentyn-1-amine HCl (75.0 mg, 0.63 mmol, 1.1 eq) was dissolved in DMF (2 mL), added to the reaction and the mixture stirred at room temperature overnight. The reaction mixture was quenched with sat. NH_4Cl solution (30 mL) and extracted with EA (2x30 mL). The combined organic layers were washed with brine (20 mL), dried over $MgSO_4$, filtered and the solvent was removed under reduced pressure. The product was purified via preparative HPLC eluting at 25-35% ACN (no TFA) in H_2O (no TFA), yielding CG389 (86.2 mg, 0.18 mmol, 31%) as a 6:1 mixture of *(2S,3S):(2S,3R),* as judged by peak-ratios of corresponding H-atoms in the ^{1}H NMR Peak assignment was carried out by evaluation of 1D- and 2D-NMR spectra. Spectral data are given for the main *(2S,3S)*-product

^{1}H NMR (700 MHz, DMSO-d_6) δ (ppm) = 10.57 (“d”, *J* = 33.3 Hz, 1H), 8.56 (t, *J* = 5.6 Hz, 1H), 8.25 (d, *J* = 1.6 Hz, 1H), 7.99 – 7.95 (m, 2H), 7.80 (d, *J* = 1.6 Hz, 1H), 7.76 – 7.73 (m, 2H), 4.22 – 4.13 (m, 1H),

3.43 – 3.36 (m, 1H), 3.36 – 3.32 (m, 2H), 3.18 (qd, *J* = 18.0, 14.6, 7.4 Hz, 2H), 2.80 (t, *J* = 2.6 Hz, 1H), 2.32 – 2.24 (m, 1H), 2.23 (td, *J* = 7.1, 2.7 Hz, 2H), 1.93 – 1.85 (m, 1H), 1.72 (p, *J* = 7.1 Hz, 2H), 1.40 ("d", *J* = 8.5 Hz, 9H), 0.94 ("d", *J* = 5.5 Hz, 3H). *(2S,3S):(2S,3R) = 5:1 mixture*

^{13}C NMR (176 MHz, DMSO-d_6) δ (ppm) = 167.31 ("d", *J* = 20.6 Hz), 165.19, 153.06, 139.18, 138.70, 132.34, 131.99, 128.94, 119.18, 104.02, 84.11, 78.29, 71.38, 53.61, 46.95 ("d", *J* = 141.2 Hz), 44.46 ("d", *J* = 53.6 Hz), 38.47, 28.18, 28.04, 24.12 ("d", *J* = 180.7 Hz), 15.91, 15.53.

HRMS *m/z* for $C_{26}H_{34}N_5O_4^+$ ([M+H]$^+$) calculated: 480.2605, found: 480.2607.

(2*S*,3*S*)-1-Cyano-2-methyl-*N*-(1-(4-(pent-4-yn-1-ylcarbamoyl)phenyl)-1*H*-imidazol-4-yl)pyrrolidine-3-carboxamide (CG390)

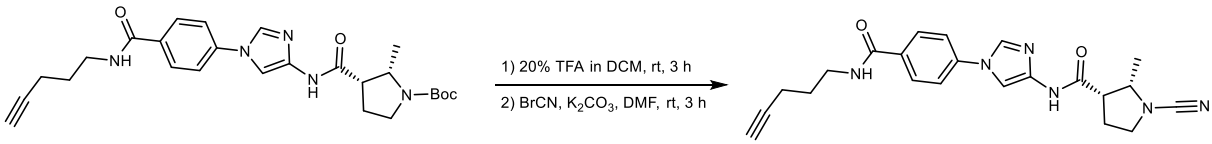

Step 1

CG389 (79 mg, 0.16 mmol, 1.0 eq) was dissolved in DCM (2 mL) and TFA (0.4 mL) was added dropwise. The solution was stirred for 3 h at room temperature. The solvent and residual TFA were removed under reduced pressure and the product dried in vacuo.

Step 2

The crude product from step 1 was dissolved in DMF (3 mL) and DIPEA (224.1 µL, 1.32 mmol, 8.0 eq) was added. 3 M cyanogen bromide solution (109.8 µL, 0.33 mmol, 2.0 eq) was added and the mixture was stirred for 3 h at room temperature. The reaction was quenched by the addition of aqueous sat. $NaHCO_3$ (50 mL). The mixture was extracted with EA (2x30 mL). The combined organic layers were washed with brine (30 mL), dried over anhydrous $MgSO_4$, filtered and the solvent was removed under reduced pressure. The corresponding product was purified via a preparative HPLC, eluting at 15-25% ACN (no TFA) in H_2O (no TFA), yielding CG390 (36.6 mg, 0.09 mmol, 55%) as a white powder.

^{1}H NMR (500 MHz, DMSO-d_6) δ (ppm) = 10.69 (s, 1H), 8.56 (q, *J* = 5.0, 4.5 Hz, 1H), 8.25 (d, *J* = 1.6 Hz, 1H), 7.99 – 7.94 (m, 2H), 7.82 (d, *J* = 1.6 Hz, 1H), 7.79 – 7.73 (m, 2H), 3.94 (p, *J* = 6.6 Hz, 1H), 3.63 (td, *J* = 8.3, 6.0 Hz, 1H), 3.40 (td, *J* = 8.4, 6.2 Hz, 1H), 3.37 – 3.32 (m, 2H), 3.21 (q, *J* = 6.8 Hz, 1H), 2.80 (t, *J* = 2.6 Hz, 1H), 2.23 (td, *J* = 7.1, 2.7 Hz, 2H), 2.15 (ddt, *J* = 12.5, 8.1, 6.1 Hz, 1H), 2.06 – 1.94 (m, 1H), 1.72 (p, *J* = 7.1 Hz, 2H), 1.11 (d, *J* = 6.6 Hz, 3H).

^{13}C NMR (126 MHz, DMSO-d_6) δ (ppm) = 167.81, 165.18, 139.05, 138.70, 132.33, 132.07, 128.94, 119.18, 116.31, 104.11, 84.12, 71.39, 58.11, 49.24, 46.52, 38.47, 28.04, 26.64, 15.53, 15.16.

HRMS m/z for $C_{22}H_{25}N_6O_2^+$ ([M+H]$^+$) calculated: 405.2034, found: 405.2034.

8.1.1.8 Synthesis of CG305

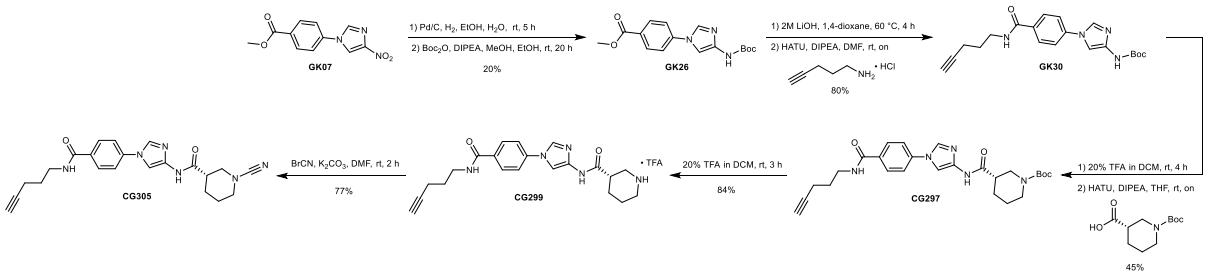

Scheme 25. Synthesis of CG305.

Methyl 4-(4-((*tert*-butoxycarbonyl)amino)-1*H*-imidazol-1-yl)benzoate (GK26)

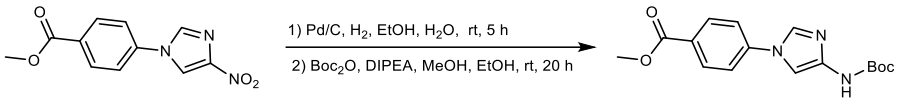

Step 1

GK07 (924 mg, 3.74 mmol, 1.0 eq) was dissolved in EtOH (30 mL) and a few drops of water were added. Palladium (10%) on activated charcoal (300 mg) was added under an argon atmosphere. Then the reaction mixture was stirred for five hours at room temperature under an atmosphere of hydrogen. The reaction mixture was filtrated through a pad of Celite 545 and washed with MeOH. The solution was directly used for the next reaction step without further purification.

Step 2

To the solution of crude product from step 1, Boc_2O (1.6 mL, 7.48 mmol, 2.0 eq) and DIPEA (1.3 mL, 7.48 mmol, 2.0 eq) were added and the reaction mixture was stirred for 20 h at room temperature. The mixture was concentrated under reduced pressure and EA (50 mL) was added to the residue. The mixture was washed with a sat. NH_4Cl-solution (50 mL) and brine (50 mL). The organic phase was dried and the solvent was removed under reduced pressure. The compound was purified via a silica column eluting at 5-40% EA in PE, yielding GK26 (242 mg, 0.76 mmol, 20%) as a yellow solid.

^{1}H NMR (700 MHz, DMSO-d_6) δ (ppm) = 9.64 (s, 1H), 8.22 (d, J = 1.6 Hz, 1H), 8.04 (d, J = 8.8 Hz, 2H), 7.81 (d, J = 8.5 Hz, 2H), 7.54 (s, 1H), 3.87 (s, 3H), 1.46 (s, 9H).

^{13}C NMR (176 MHz, DMSO-d_6) δ (ppm) = 165.47, 152.55, 140.39, 140.23, 132.13, 130.97, 127.15, 119.28, 102.27, 78.90, 52.22, 28.10.

***tert*-Butyl (1-(4-(pent-4-yn-1-ylcarbamoyl)phenyl)-1*H*-imidazol-4-yl)carbamate (GK30)**

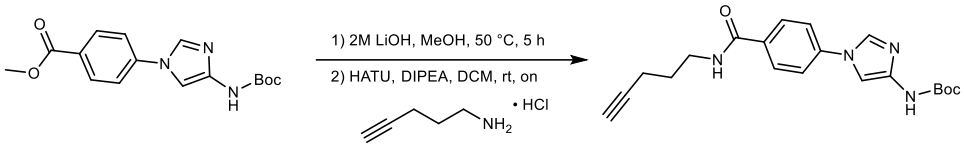

Step 1

GK26 (242 mg, 0.76 mmol, 1.0 eq) was dissolved in MeOH (5 mL), aqueous 2 M lithium hydroxide-solution (1.52 mL, 3.02 mmol, 4.0 eq) was added and the reaction mixture was stirred at 50 °C. After 5 hours the excess of lithium hydroxide was neutralised to a pH of 7 by addition of 1 M hydrochloric acid. The solvent was removed under reduced pressure and the crude product was obtained as a lithium salt and used for the next reaction without further purification.

Step 2

The crude product from step 1 was dissolved in DMF (6 mL) and DCM (10 mL). DIPEA (258 µL, 1.52 mmol, 2.0 eq) and HATU (422 mg, 1.14 mmol, 1.5 eq) were added and the reaction mixture stirred for 30 min. 4-Pentyn-1-amine hydrochloride (182 mg, 1.52 mmol, 2.0 eq) was added to the reaction mixture, followed by stirring for one day at room temperature. The reaction was quenched by the addition of sat. NH_4Cl-solution (30 mL), the phases were separated and the aqueous phase extracted with DCM (50 mL). The combined organic layers were washed with brine (50 mL), dried with $MgSO_4$ and the solvent was removed under reduced pressure. The product was purified via a silica column eluting at 0-20% EA in PE, yielding GK30 as a yellow solid (226 mg, 0.61 mmol, 80%).

^{1}H NMR (700 MHz, DMSO-d_6) δ (ppm) = 9.60 (s, 1H), 8.55 (t, *J* = 5.6 Hz, 1H), 8.16 (d, *J* = 1.7 Hz, 1H), 7.97 – 7.95 (m, 2H), 7.74 (d, *J* = 8.4 Hz, 2H), 7.56 – 7.47 (m, 1H), 3.34 (dd, *J* = 12.9, 6.8 Hz, 2H), 2.80 (t, *J* = 2.7 Hz, 1H), 2.23 (td, *J* = 7.1, 2.7 Hz, 2H), 1.72 (p, *J* = 7.1 Hz, 2H), 1.46 (s, 9H).

^{13}C NMR (176 MHz, DMSO-d_6) δ (ppm) =165.20, 152.57, 140.00, 138.79, 131.90, 128.91, 118.94, 102.50, 84.11, 80.46, 71.37, 56.02, 38.46, 28.10, 28.04, 15.53.

***tert*-Butyl (*S*)-3-((1-(4-(pent-4-yn-1-ylcarbamoyl)phenyl)-1*H*-imidazol-4-yl)carbamoyl)piperidine-1-carboxylate (CG297)**

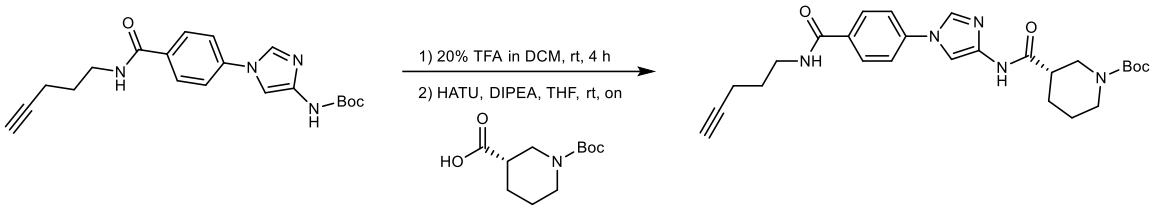

Step 1

GK30 (192.9 mg, 0.52 mmol, 1.2 eq) was dissolved in DCM (2 mL) and TFA (0.4 mL) was added dropwise. The solution was stirred for 4 h at room temperature. The solvent and residual TFA were removed under reduced pressure and the product dried in vacuo.

Step 2

(*S*)-1-(*tert*-Butoxycarbonyl)piperidine-3-carboxylic acid (100.0 mg, 0.44 mol, 1.0 eq) was dissolved in THF (2 mL), then DIPEA (151.9 µL, 0.87 mmol, 2.0 eq) and HATU (248.8 mg, 0.65 mmol, 1.5 eq) were added and the reaction mixture stirred for 30 min. The crude product from step 1 was dissolved in THF (2 mL) and added to the reaction dropwise. The resulting solution was stirred overnight at room temperature. The reaction was quenched by the addition of aqueous sat. $NaHCO_3$ (50 mL). The mixture was extracted with EA (2x30 mL). The combined organic layers were washed with brine (30 mL), dried over anhydrous $MgSO_4$, filtered and the solvent was removed under reduced pressure. The corresponding product was purified via a silica column eluting at 80-95% EA in PE, yielding CG297 (93.4 mg, 0.19 mmol, 45%) as a yellow solid.

^{1}H NMR (700 MHz, DMSO-d_6) δ (ppm) = 10.56 (s, 1H), 8.55 (t, *J* = 5.6 Hz, 1H), 8.23 (d, *J* = 1.6 Hz, 1H), 7.97 (d, *J* = 8.7 Hz, 2H), 7.77 (d, *J* = 1.6 Hz, 1H), 7.74 (d, *J* = 8.8 Hz, 2H), 3.85 (s, 1H), 3.34 (td, *J* = 7.1, 5.7 Hz, 2H), 2.80 (t, *J* = 2.7 Hz, 1H), 2.79 – 2.70 (m, 1H), 2.54 (dt, *J* = 11.1, 4.0 Hz, 1H), 2.23 (td, *J* = 7.1, 2.7 Hz, 2H), 2.03 – 1.95 (m, 1H), 1.92 – 1.86 (m, 1H), 1.72 (p, *J* = 7.1 Hz, 2H), 1.68 (s, 1H), 1.60 (q, *J* = 12.3 Hz, 1H), 1.40 (s, 9H), 1.36 – 1.24 (m, 2H).

^{13}C NMR (176 MHz, DMSO-d_6) δ (ppm) = 170.49, 165.19, 153.80, 139.22, 138.74, 132.33, 131.99, 128.94, 119.18, 104.04, 84.11, 78.71, 71.38, 41.71, 40.73, 40.15, 38.47, 28.70, 28.04, 27.51, 24.09, 15.52.

HRMS *m/z* for $C_{26}H_{34}N_5O_4^+$ ($[M+H]^+$) calculated: 480.2605, found: 480.2602.

(*S*)-*N*-(1-(4-(Pent-4-yn-1-ylcarbamoyl)phenyl)-1*H*-imidazol-4-yl)piperidine-3-carboxamide TFA salt (CG299)

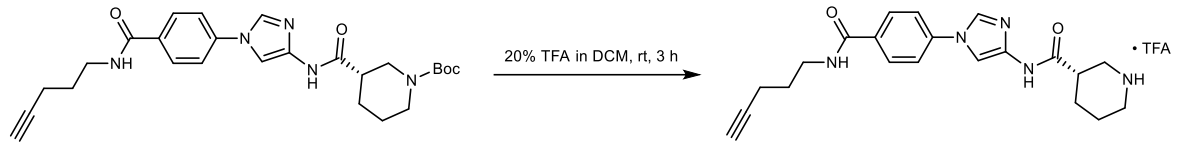

CG297 (90.0 mg, 0.19 mmol, 1.0 eq) was dissolved in DCM (2 mL) and TFA (0.4 mL) was added dropwise. The mixture was stirred for 3 h at room temperature. The solvent and residual TFA were removed under reduced pressure. The product was dried in vacuo and subsequently purified by preparative HPLC eluting at 10-20% ACN in H_2O, yielding CG299 as a TFA salt (77.4 mg, 0.16 mmol, 84%).

^{1}H NMR (700 MHz, DMSO-d_6) δ (ppm) = 10.79 (s, 1H), 8.57 (t, *J* = 5.6 Hz, 2H), 8.54 – 8.42 (m, 1H), 8.26 (d, *J* = 1.6 Hz, 1H), 8.03 – 7.92 (m, 2H), 7.76 (d, *J* = 1.6 Hz, 1H), 7.74 – 7.70 (m, 2H), 3.38 – 3.28 (m, 3H), 3.18 (d, *J* = 12.4 Hz, 1H), 3.11 – 3.01 (m, 1H), 2.97 – 2.85 (m, 2H), 2.81 (t, *J* = 2.7 Hz, 1H), 2.23 (td, *J* = 7.1, 2.7 Hz, 2H), 2.00 (dt, *J* = 11.9, 3.9 Hz, 1H), 1.82 (dq, *J* = 7.9, 3.9 Hz, 1H), 1.72 (p, *J* = 7.1 Hz, 2H), 1.69 – 1.56 (m, 2H).

^{13}C NMR (176 MHz, DMSO-d_6) δ (ppm) = 169.36, 165.16, 157.79 (q, *J* = 31.5 Hz), 138.99, 138.67, 132.45, 132.22, 128.99, 119.26, 117.08 (q, *J* = 299.3 Hz), 104.18, 84.11, 71.42, 44.22, 43.06, 38.57, 38.48, 28.05, 26.18, 21.15, 15.53.

HRMS *m/z* for $C_{18}H_{24}N_5O_3^+$ ([M+H]$^+$) calculated: 358.1874, found: 358.1875.

(*S*)-1-Cyano-*N*-(1-(4-(pent-4-yn-1-ylcarbamoyl)phenyl)-1*H*-imidazol-4-yl)piperidine-3-carboxamide (CG305)

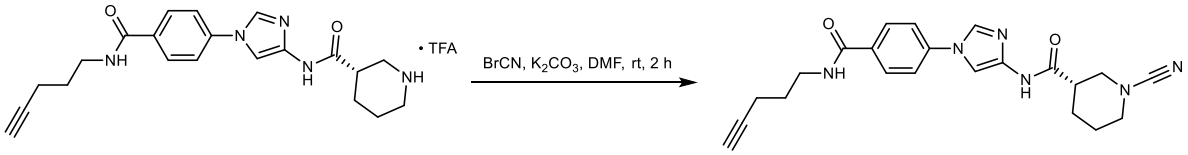

CG299 (70.0 mg, 0.14 mmol, 1.0 eq) was dissolved in DMF (2 mL) and K_2CO_3 (78.4 mg, 0.57 mmol, 4.0 eq) was added. After stirring for 30 min at room temperature, 3 M cyanogen bromide solution (56.7 µL, 0.17 mmol, 1.2 eq) was added to the mixture, and stirring was continued for 2 h. The reaction was quenched by the addition of aqueous sat. $NaHCO_3$ (50 mL). The mixture was extracted with EA (2x30 mL). The combined organic layers were washed with brine (30 mL), dried over anhydrous $MgSO_4$, filtered and the solvent was removed under reduced pressure. The corresponding product was purified via a silica column, eluting at 5% MeOH in DCM, yielding CG305 (44.1 mg, 0.11 mmol, 77%) as a white powder.

^{1}H NMR (700 MHz, DMSO-d_6) δ (ppm) = 10.62 (s, 1H), 8.55 (t, *J* = 5.5 Hz, 1H), 8.23 (d, *J* = 1.6 Hz, 1H), 7.99 – 7.94 (m, 2H), 7.76 (d, *J* = 1.6 Hz, 1H), 7.76 – 7.71 (m, 2H), 3.50 – 3.44 (m, 1H), 3.36 – 3.30 (m, 3H), 3.12 (dd, *J* = 12.5, 10.9 Hz, 1H), 3.02 (ddd, *J* = 12.8, 11.6, 3.2 Hz, 1H), 2.80 (t, *J* = 2.6 Hz, 1H), 2.79 – 2.73 (m, 1H), 2.23 (td, *J* = 7.1, 2.7 Hz, 2H), 1.96 – 1.89 (m, 1H), 1.72 (p, *J* = 7.1 Hz, 3H), 1.61 – 1.51 (m, 2H).

^{13}C NMR (176 MHz, DMSO-d_6) δ (ppm) = 169.45, 165.18, 139.14, 138.72, 132.35, 132.04, 128.94, 119.20, 117.93, 104.06, 84.11, 71.38, 50.64, 48.88, 40.75, 38.47, 28.03, 26.28, 23.18, 15.52.

HRMS *m/z* for $C_{22}H_{25}N_6O_2^+$ ([M+H]$^+$) calculated: 405.2034, found: 405.2035.

8.1.1.9 Synthesis of CG322

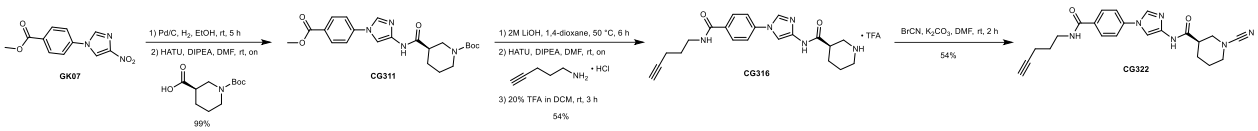

Scheme 26. Synthesis of CG322.

***tert*-Butyl (*R*)-3-((1-(4-(methoxycarbonyl)phenyl)-1*H*-imidazol-4-yl)carbamoyl)piperidine-1-carboxylate (CG311)**

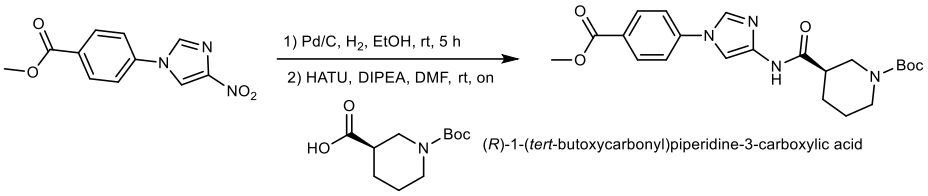

Step 1

GK07 (118.6 mg, 0.48 mmol, 1.1 eq) was dissolved in EtOH (20 mL) and palladium (10%) on activated charcoal (12 mg) was added under an argon atmosphere. The reaction was flushed with H_2 and stirred for 5 hours at room temperature. The reaction was filtered through Celite 545 which was then washed with EA. The solvent was removed under reduced pressure and the obtained product used for the next reaction without further purification.

Step 2

(*R*)-1-(*tert*-Butoxycarbonyl)piperidine-3-carboxylic acid (100.0 mg, 0.44 mol, 1.0 eq) was dissolved in DMF (2 mL), then DIPEA (222.5 µL, 1.31 mmol, 3.0 eq) and HATU (199.0 mg, 0.52 mmol, 1.2 eq) were added and the reaction mixture stirred for 20 min. The crude product from step 1 was dissolved in DMF (2 mL) and added to the reaction dropwise. The resulting solution was stirred overnight at room temperature. The reaction was quenched by the addition of aqueous sat. NH_4Cl (40 mL) and the mixture extracted with EA (2x30 mL). The combined organic layers were washed with brine (30 mL), dried over anhydrous $MgSO_4$, filtered and the solvent was removed under reduced pressure. The corresponding product was purified via a silica column eluting at 33% EA in PE, yielding CG311 (185.4 mg, 0.43 mmol, 99%) as a yellow solid.

^{1}H NMR (600 MHz, DMSO-d_6) δ (ppm) = 10.60 (s, 1H), 8.28 (d, *J* = 1.7 Hz, 1H), 8.08 – 8.03 (m, 2H), 7.82 – 7.80 (m, 2H), 7.79 (d, *J* = 1.7 Hz, 1H), 3.87 (s, 3H), 3.84 (s, 1H), 2.77 (d, *J* = 12.8 Hz, 1H), 2.54 (s, 2H), 1.89 (ddd, *J* = 13.8, 5.8, 3.3 Hz, 1H), 1.69 (d, *J* = 13.1 Hz, 1H), 1.64 – 1.55 (m, 1H), 1.47 – 1.41 (m, 1H), 1.39 (s, 9H), 1.37 – 1.25 (m, 1H).

^{13}C NMR (151 MHz, DMSO-d_6) δ (ppm) = 170.57, 165.47, 153.80, 140.35, 139.42, 132.23, 131.01, 127.35, 119.53, 103.84, 78.73, 52.26, 41.72, 40.74, 40.43, 28.04, 27.51, 24.10.

HRMS *m/z* for $C_{22}H_{29}N_4O_5^+$ ($[M+H]^+$) calculated: 429.2133, found: 429.2135.

(*R*)-*N*-(1-(4-(Pent-4-yn-1-ylcarbamoyl)phenyl)-1*H*-imidazol-4-yl)piperidine-3-carboxamide TFA salt (CG316)

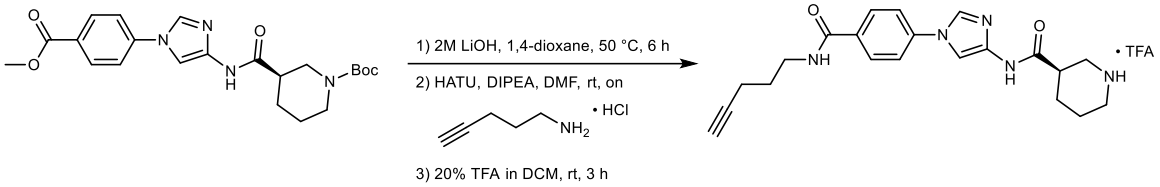

Step 1

CG311 (100.0 mg, 0.23 mmol, 1.0 eq) was dissolved in 1,4-dioxane (2 mL). Aqueous 2 M LiOH solution (163.4 µL, 0.33 mol, 1.4 eq) was added and the reaction mixture was stirred for 6 h at 50 °C. The pH of the reaction mixture was adjusted to pH 7 by adding aqueous 1 M HCl dropwise. The solvent was removed under reduced pressure and the obtained product used for the next reaction without further purification.

Step 2

The crude product from step 1 was dissolved in DMF (2 mL), then DIPEA (79.4 µL, 0.47 mmol, 2.0 eq) and HATU (115.4 mg, 0.30 mmol, 1.3 eq) were added and the reaction mixture was stirred for 10 min at room temperature. 4-Pentyn-1-amine HCl (33.5 mg, 0.28 mmol, 1.2 eq) was dissolved in DMF (2 mL), added to the reaction and the mixture stirred at room temperature overnight. The reaction mixture was quenched with sat. NH_4Cl solution (30 mL) and extracted with EA (2x30 mL). The combined organic layers were washed with brine (20 mL), dried over $MgSO_4$, filtered and the solvent was removed under reduced pressure. The crude product was directly used for the next step.

Step 3

The crude product from step 2 was dissolved in DCM (2 mL) and TFA (0.4 mL) was added dropwise. The solution was stirred for 3 h at room temperature. The solvent and residual TFA were removed under reduced pressure and the product dried in vacuo. The product was purified via preparative HPLC eluting at 20-30% ACN in H_2O, yielding CG316 (61.7 mg, 0.13 mmol, 54%) as a white TFA salt.

^{1}H NMR (600 MHz, DMSO-d_6) δ (ppm) = 10.79 (s, 1H), 8.57 (t, *J* = 5.6 Hz, 2H), 8.54 – 8.47 (m, 1H), 8.26 (d, *J* = 1.7 Hz, 1H), 8.01 – 7.96 (m, 2H), 7.76 (d, *J* = 2.0 Hz, 1H), 7.75 – 7.69 (m, 2H), 3.34 (q, *J* = 6.7 Hz, 2H), 3.31 (s, 1H), 3.19 (d, *J* = 12.4 Hz, 1H), 3.06 (q, *J* = 10.8 Hz, 1H), 2.92 (d, *J* = 11.1 Hz, 1H), 2.88 (dq, *J* = 9.3, 5.1, 4.0 Hz, 1H), 2.80 (q, *J* = 2.3 Hz, 1H), 2.23 (tt, *J* = 7.2, 1.9 Hz, 2H), 2.06 – 1.95 (m, 1H), 1.83 (dd, *J* = 10.6, 4.6 Hz, 1H), 1.72 (p, *J* = 7.1 Hz, 2H), 1.64 (q, *J* = 9.8, 9.1 Hz, 2H).

^{13}C NMR (151 MHz, DMSO-d_6) δ (ppm) = 169.85, 165.64, 158.54 (q, *J* = 34.5 Hz), 139.43, 139.14, 132.95, 132.69, 129.46, 119.75, 116.61 (d, *J* = 293.0 Hz), 104.69, 84.59, 71.88, 44.71, 43.54, 39.05, 38.96, 28.53, 26.65, 21.63, 16.01.

HRMS *m/z* for $C_{21}H_{26}N_5O_2^+$ ($[M+H]^+$) calculated: 380.2081, found: 380.2078.

(*R*)-1-Cyano-*N*-(1-(4-(pent-4-yn-1-ylcarbamoyl)phenyl)-1*H*-imidazol-4-yl)piperidine-3-carboxamide (CG322)

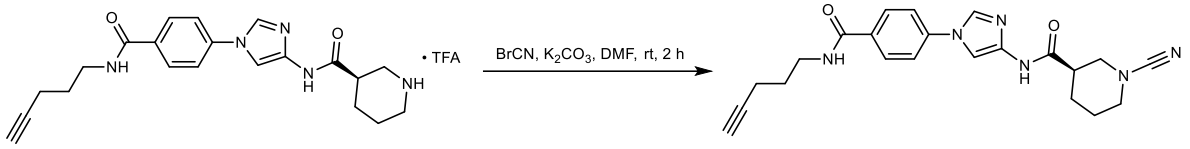

CG322 was obtained from CG316 (56.0 mg, 0.11 mmol, 1.0 eq) as described above for CG305. During column chromatography, the product was eluting at 75-100% EA in PE, yielding CG322 (24.6 mg, 0.06 mmol, 54%) as pale-yellow crystals.

^{1}H NMR (700 MHz, DMSO-d_6) δ (ppm) = 10.63 (s, 1H), 8.56 (t, *J* = 5.6 Hz, 1H), 8.23 (d, *J* = 1.6 Hz, 1H), 8.01 – 7.94 (m, 2H), 7.77 (d, *J* = 1.6 Hz, 1H), 7.76 – 7.70 (m, 2H), 3.48 (dd, *J* = 12.5, 4.1 Hz, 1H), 3.37 – 3.33 (m, 2H), 3.31 (s, 1H), 3.13 (dd, *J* = 12.6, 10.9 Hz, 1H), 3.03 (td, *J* = 12.3, 3.2 Hz, 1H), 2.80 (t, *J* = 2.6 Hz, 1H), 2.77 (tt, *J* = 10.8, 4.0 Hz, 1H), 2.24 (td, *J* = 7.2, 2.7 Hz, 2H), 1.97 – 1.89 (m, 1H), 1.73 (p, *J* = 7.1 Hz, 3H), 1.57 (qd, *J* = 13.5, 11.8, 8.3 Hz, 2H).

^{13}C NMR (176 MHz, DMSO-d_6) δ (ppm) = 169.46, 165.19, 139.14, 138.72, 132.36, 132.04, 128.94, 119.21, 117.93, 104.07, 84.11, 71.37, 50.65, 48.88, 40.76, 38.47, 28.04, 26.29, 23.18, 15.52.

HRMS *m/z* for $C_{22}H_{25}N_6O_2^+$ ([M+H]$^+$) calculated: 405.2034, found: 405.2034.

8.1.1.10 Synthesis of CG337

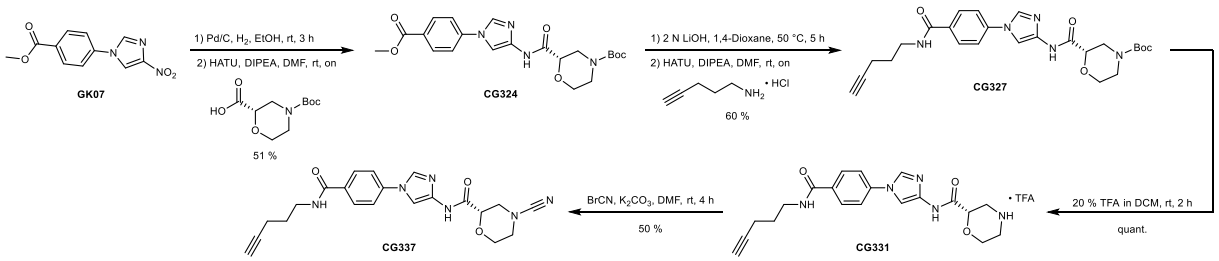

Scheme 27. Synthesis of CG337.

***tert*-Butyl (*S*)-2-((1-(4-(methoxycarbonyl)phenyl)-1*H*-imidazol-4-yl)carbamoyl)morpholine-4-carboxylate (CG324)**

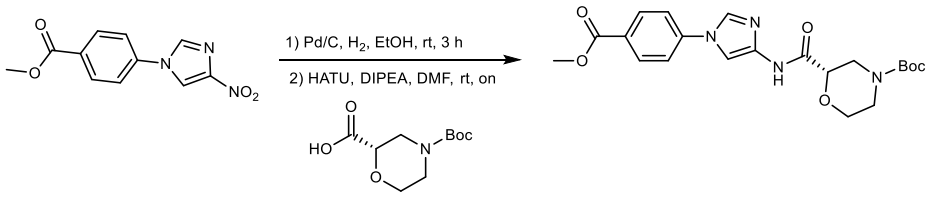

CG324 (56.9 mg, 0.13 mmol, 51%) was obtained as a yellow solid from (*S*)-4-(*tert*-butoxycarbonyl)morpholine-2-carboxylic acid (60.0 mg, 0.26 mmol, 1.0 eq) as described above for CG311.

^{1}H NMR (700 MHz, DMSO-d_6) δ (ppm) = 10.11 (s, 1H), 8.31 (d, *J* = 1.6 Hz, 1H), 8.10 – 8.02 (m, 2H), 7.83 (s, 1H), 7.83 (d, *J* = 6.7 Hz, 2H), 4.10 (dd, *J* = 10.2, 3.1 Hz, 1H), 4.00 – 3.92 (m, 2H), 3.88 (s, 3H), 3.74 – 3.67 (m, 1H), 3.51 (td, *J* = 11.4, 2.9 Hz, 1H), 2.69 (s, 2H), 1.42 (s, 9H).

^{13}C NMR (176 MHz, DMSO-d_6) δ (ppm) = 165.80, 165.45, 153.77, 140.24, 138.46, 132.49, 131.00, 127.49, 119.64, 104.42, 79.36, 74.34, 65.49, 52.26, 43.57, 38.23, 27.98.

HRMS *m/z* for $C_{21}H_{27}N_4O_6^+$ ([M+H]$^+$) calculated: 431.1925, found: 431.1926.

tert-Butyl (*S*)-2-((1-(4-(pent-4-yn-1-ylcarbamoyl)phenyl)-1*H*-imidazol-4-yl)carbamoyl)-morpholine-4-carboxylate (CG327)

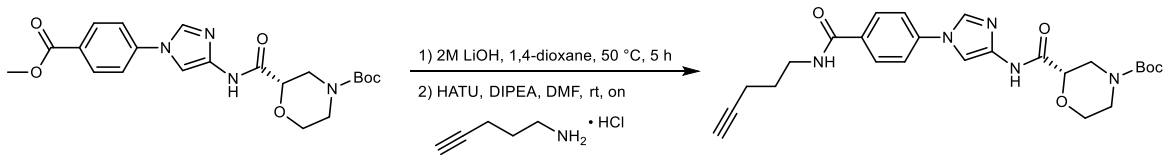

CG327 was obtained from CG324 (53.0 mg, 0.12 mmol, 1.0 eq) as described above for CG389. During column chromatography, the product was eluting at 3-4% MeOH in DCM, yielding CG327 (35.8 mg, 0.07 mmol, 60%) as a pale-yellow resin.

^{1}H NMR (700 MHz, DMSO-d_6) δ (ppm) = 10.08 (s, 1H), 8.57 (t, *J* = 5.6 Hz, 1H), 8.26 (d, *J* = 1.6 Hz, 1H), 7.97 (d, *J* = 8.7 Hz, 2H), 7.81 (d, *J* = 1.6 Hz, 1H), 7.80 – 7.73 (m, 2H), 4.10 (dd, *J* = 10.2, 3.1 Hz, 1H), 3.96 (s, 2H), 3.74 – 3.69 (m, 1H), 3.51 (td, *J* = 11.4, 3.0 Hz, 1H), 3.34 (td, *J* = 7.3, 5.9 Hz, 2H), 2.99 (s, 2H), 2.80 (t, *J* = 2.6 Hz, 1H), 2.23 (td, *J* = 7.1, 2.7 Hz, 2H), 1.72 (p, *J* = 7.1 Hz, 2H), 1.42 (s, 9H).

^{13}C NMR (176 MHz, DMSO-d_6) δ (ppm) = 165.75, 165.18, 153.78, 138.64, 138.26, 132.46, 132.29, 128.95, 119.29, 104.62, 84.12, 79.37, 74.33, 71.40, 65.50, 43.49, 40.16, 38.48, 28.04, 27.99, 15.53.

HRMS *m/z* for $C_{25}H_{32}N_5O_5^+$ ([M+H]$^+$) calculated: 482.2398, found: 482.2404.

(*S*)-*N*-(1-(4-(Pent-4-yn-1-ylcarbamoyl)phenyl)-1*H*-imidazol-4-yl)morpholine-2-carboxamide TFA salt (CG331)

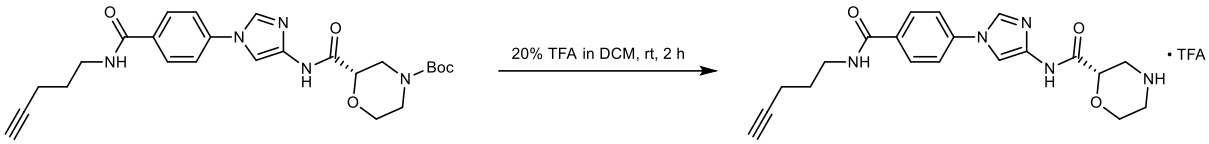

CG331 was obtained from CG327 (53.0 mg, 0.12 mmol, 1.0 eq) as described above for CG299. During preparative HPLC purification, the product was eluting at 15-25% ACN in H_2O, yielding CG331 (33.9 mg, 0.07 mmol, quant.) as a white TFA salt.

^{1}H NMR (700 MHz, DMSO-d_6) δ (ppm) = 10.50 (s, 1H), 9.06 (d, *J* = 23.2 Hz, 2H), 8.58 (t, *J* = 5.6 Hz, 1H), 8.29 (d, *J* = 1.6 Hz, 1H), 8.00 – 7.94 (m, 2H), 7.81 (d, *J* = 1.6 Hz, 1H), 7.77 – 7.71 (m, 2H), 4.44 (dd, *J* = 10.6, 2.8 Hz, 1H), 4.09 (ddd, *J* = 12.6, 3.9, 2.0 Hz, 1H), 3.80 (ddd, *J* = 12.6, 11.4, 2.5 Hz, 1H), 3.49 – 3.42 (m, 1H), 3.37 – 3.32 (m, 2H), 3.23 (d, *J* = 12.8 Hz, 1H), 3.16 (q, *J* = 10.6 Hz, 1H), 3.13 – 3.06 (m, 1H), 2.80 (t, *J* = 2.7 Hz, 1H), 2.23 (td, *J* = 7.1, 2.7 Hz, 2H), 1.72 (p, *J* = 7.1 Hz, 2H).

^{13}C NMR (176 MHz, DMSO-d_6) δ (ppm) = 165.15, 164.24, 158.11 (q, *J* = 34.5 Hz), 138.57, 138.17, 132.56, 132.46, 128.97, 119.36, 116.20 (q, *J* = 294.5 Hz), 104.80, 84.11, 72.18, 71.41, 63.22, 43.32, 42.10, 38.48, 28.05, 15.53.

HRMS *m/z* for $C_{20}H_{24}N_5O_3^+$ ([M+H]$^+$) calculated: 382.1874, found: 382.1878.

(*S*)-4-Cyano-*N*-(1-(4-(pent-4-yn-1-ylcarbamoyl)phenyl)-1*H*-imidazol-4-yl)morpholine-2-carboxamide (CG337)

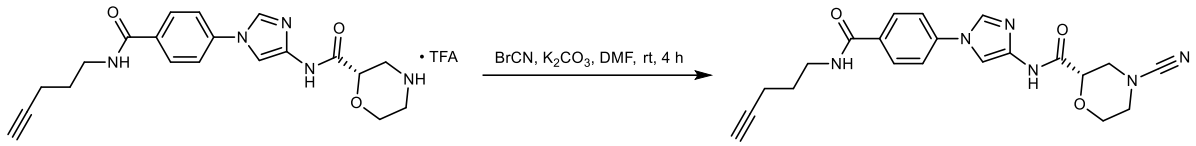

CG337 was obtained from CG331 (30.0 mg, 0.06 mmol, 1.0 eq) as described above for CG305. During column chromatography, the product was eluting at 8-10% MeOH in DCM, yielding CG327 (12.2 mg, 0.03 mmol, 50%) as pale-yellow crystals.

^{1}H NMR (700 MHz, DMSO-d_6) δ (ppm) = 10.30 (s, 1H), 8.57 (t, *J* = 5.5 Hz, 1H), 8.26 (d, *J* = 1.7 Hz, 1H), 8.01 – 7.94 (m, 2H), 7.80 (d, *J* = 1.6 Hz, 1H), 7.78 – 7.71 (m, 2H), 4.31 (dd, *J* = 9.9, 3.0 Hz, 1H), 3.95 (dt, *J* = 12.0, 2.7 Hz, 1H), 3.68 (td, *J* = 11.4, 3.0 Hz, 1H), 3.53 (dd, *J* = 12.7, 3.0 Hz, 1H), 3.36 – 3.33 (m, 2H), 3.30 (s, 1H), 3.28 – 3.25 (m, 1H), 3.25 – 3.21 (m, 1H), 2.80 (t, *J* = 2.6 Hz, 1H), 2.23 (td, *J* = 7.1, 2.7 Hz, 2H), 1.72 (p, *J* = 7.1 Hz, 2H).

^{13}C NMR (176 MHz, DMSO-d_6) δ (ppm) = 165.18, 164.81, 138.63, 138.30, 132.47, 132.33, 128.95, 119.32, 117.03, 104.64, 84.12, 73.52, 71.39, 64.80, 49.14, 47.44, 38.48, 28.04, 15.53.

HRMS *m/z* for $C_{21}H_{23}N_6O_3^+$ ([M+H]$^+$) calculated: 407.1826, found: 407.1829.

8.1.1.11 Synthesis of CG306

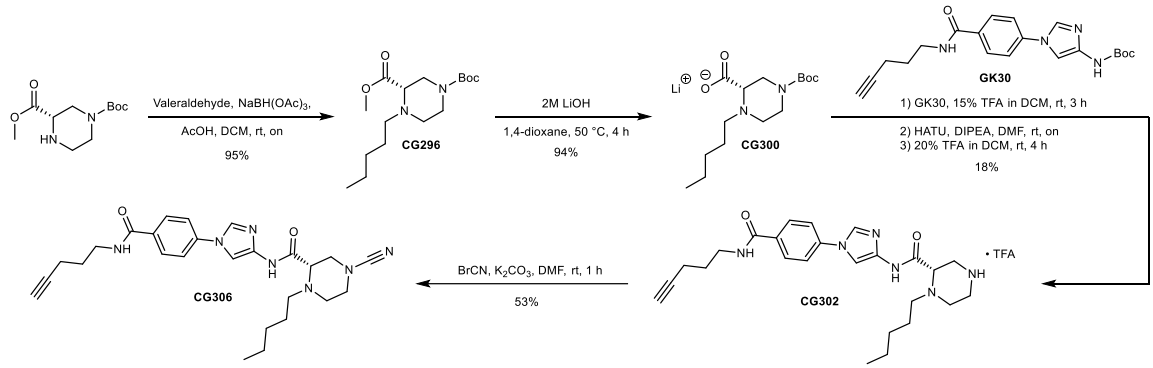

Scheme 28. Synthesis of CG306.

1-(*tert*-Butyl) 3-methyl (*S*)-4-pentylpiperazine-1,3-dicarboxylate (CG296)

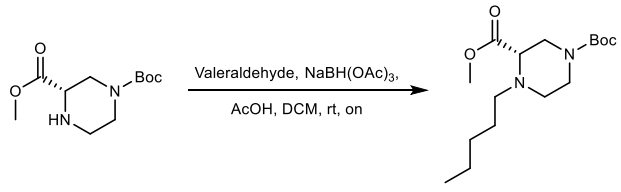

To a solution of 1-(*tert*-butyl) 3-methyl (*S*)-piperazine-1,3-dicarboxylate (100.0 mg, 0.41 mmol, 1.0 eq) in DCM (3 mL) was added valeraldehyde (86.0 µL, 0.82 mmol, 2.0 eq), followed by the addition of $NaBH(OAc)_3$ (433.8 mg, 2.05 mmol, 5.0 eq). The reaction was stirred for 10 min at room temperature. Acetic acid (468.2 µL, 8.19 mmol, 20.0 eq) was added dropwise and stirring continued overnight. The reaction was neutralised by adding 2 M NaOH, followed by addition of DCM (30 mL). After separating both layers, the aqueous phase was extracted with EA (2x30 mL). The combined organic layers were washed with brine (30 mL), dried over anhydrous $MgSO_4$, filtered and the solvent was removed under

reduced pressure. The obtained product CG296 (122.0 mg, 0.39 mmol, 95%) was used for the next reaction without further purification.

^{1}H NMR (700 MHz, DMSO-d_6) δ (ppm) = 3.92 – 3.66 (m, 1H), 3.61 (s, 3H), 3.68 – 3.43 (m, 2H), 3.30 – 3.29 (m, 1H), 3.28 – 3.27 (m, 1H), 2.95 (t, *J* = 9.7 Hz, 1H), 2.38 (s, 2H), 2.33 – 2.24 (m, 1H), 1.39 (ddd, *J* = 8.1, 4.2, 2.5 Hz, 2H), 1.37 (s, 9H), 1.30 – 1.24 (m, 2H), 1.24 – 1.16 (m, 2H), 0.85 (t, *J* = 7.2 Hz, 3H).

^{13}C NMR (176 MHz, DMSO-d_6) δ (ppm) = 171.32, 153.17, 78.84, 60.35, 54.54, 51.18, 46.43, 46.11, 42.58, 28.85, 27.94, 26.25, 21.94, 13.91.

HRMS *m/z* for $C_{16}H_{31}N_2O_4^+$ ([M+H]$^+$) calculated: 315.2278, found: 315.2279.

Lithium (*S*)-4-(*tert*-butoxycarbonyl)-1-pentylpiperazine-2-carboxylate (CG300)

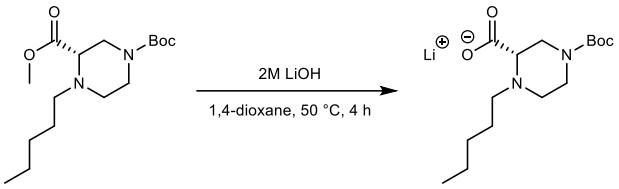

CG296 (118.0 mg, 0.38 mmol, 1.0 eq) was dissolved in 1,4-dioxane (2 mL). Aqueous 2 M LiOH solution (375.3 µL, 0.75 mmol, 2.0 eq) was added and the reaction mixture was stirred for 4 h at 50 °C. The pH of the reaction mixture was adjusted to pH 7 by adding aqueous 1 N HCl dropwise. The solvent was removed under reduced pressure yielding CG300 (108.0 mg, 0.35 mmol, 94%), which was used for following reactions without further purification.

(*S*)-*N*-(1-(4-(Pent-4-yn-1-ylcarbamoyl)phenyl)-1*H*-imidazol-4-yl)-1-pentylpiperazine-2-carboxamide TFA salt (CG302)

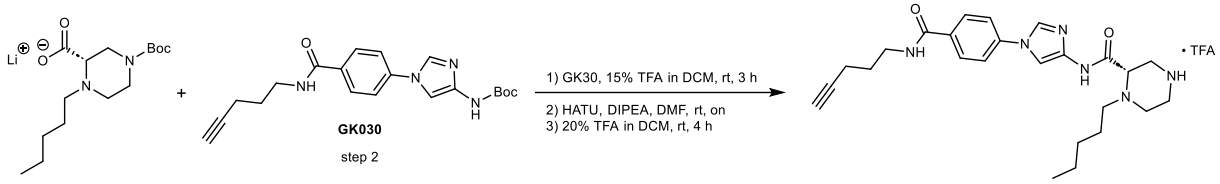

Step 1

GK30 (40.0 mg, 0.11 mmol, 1.0 eq) was dissolved in DCM (2 mL) and TFA (0.3 mL) was added dropwise. The solution was stirred for 3 h at room temperature. The solvent and residual TFA were removed under reduced pressure and the product dried in vacuo.

Step 2

CG300 (47.5 mg, 0.11 mol, 1.0 eq) was dissolved in DMF (2 mL), then DIPEA (56.7 µL, 0.33 mmol, 3.0 eq) and HATU (61.9 mg, 0.16 mmol, 1.5 eq) were added and the reaction mixture stirred for 30 min. The crude product from step 1 was dissolved in DMF (2 mL) and added to the reaction dropwise. The resulting solution was stirred overnight at room temperature. The reaction was quenched by the addition of aqueous sat. $NaHCO_3$ (50 mL). The mixture was extracted with EA (2x30 mL). The combined organic layers were washed with brine (30 mL), dried over anhydrous $MgSO_4$, filtered and the solvent was removed under reduced pressure. The corresponding product was used for the next reaction without further purification.

Step 3

The crude product from step 3 was dissolved in DCM (2 mL) and TFA (0.4 mL) was added dropwise. The solution was stirred for 4 h at room temperature. The solvent and residual TFA were removed under

reduced pressure and the product dried in vacuo. The product was purified via preparative HPLC eluting at 5-20% ACN in H_2O, yielding CG302 (11.3 mg, 0.02 mmol, 18%) as a white TFA salt.

^{1}H NMR (700 MHz, DMSO-d_6) δ (ppm) = 10.81 (s, 1H), 8.83 (s, 1H), 8.57 (t, *J* = 5.6 Hz, 1H), 8.49 (s, 1H), 8.29 (d, *J* = 1.6 Hz, 1H), 8.02 – 7.96 (m, 2H), 7.81 (d, *J* = 1.6 Hz, 1H), 7.78 – 7.70 (m, 2H), 3.51 (s, 1H), 3.34 (td, *J* = 7.2, 6.1 Hz, 2H), 3.28 (s, 2H), 3.19 – 3.08 (m, 3H), 2.80 (t, *J* = 2.6 Hz, 1H), 2.57 – 2.52 (m, 1H), 2.48 – 2.41 (m, 2H), 2.23 (td, *J* = 7.2, 2.7 Hz, 2H), 1.72 (p, *J* = 7.1 Hz, 2H), 1.45 (tt, *J* = 12.2, 7.2 Hz, 2H), 1.31 – 1.17 (m, 4H), 0.84 (t, *J* = 7.1 Hz, 3H).

^{13}C NMR (176 MHz, DMSO-d_6) δ (ppm) = 165.14, 157.72, 138.59, 138.40, 132.56, 132.43, 128.99, 119.35, 104.66, 84.10, 71.40, 60.02, 53.95, 45.26, 43.92, 42.42, 38.47, 28.75, 28.04, 25.56, 21.90, 15.52, 13.88.

HRMS *m/z* for $C_{25}H_{35}N_6O_2^+$ ([M+H]$^+$) calculated: 451.2816, found: 451.2816.

(*S*)-4-Cyano-*N*-(1-(4-(pent-4-yn-1-ylcarbamoyl)phenyl)-1*H*-imidazol-4-yl)-1-pentylpiperazine-2-carboxamide (CG306)

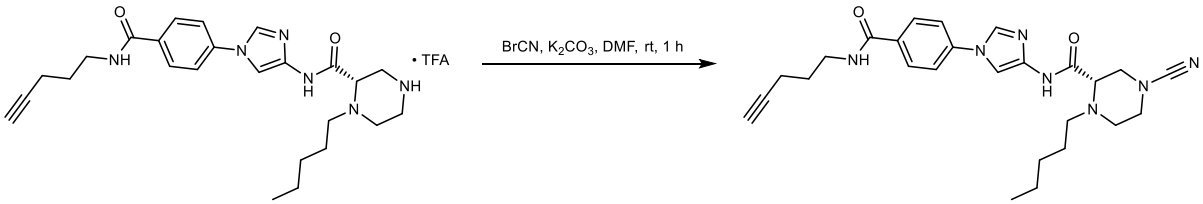

CG306 was obtained from CG302 (10.0 mg, 0.02 mmol, 1.0 eq) as described above for CG305. During column chromatography, the product was eluting at 8-10% MeOH in DCM, yielding CG306 (4.5 mg, 0.01 mmol, 53%) as a pale-yellow solid.

^{1}H NMR (700 MHz, DMSO-d_6) δ (ppm) = 10.49 (s, 1H), 8.56 (t, *J* = 5.6 Hz, 1H), 8.26 (d, *J* = 1.6 Hz, 1H), 8.00 – 7.93 (m, 2H), 7.82 (d, *J* = 1.6 Hz, 1H), 7.79 – 7.71 (m, 2H), 3.39 (d, *J* = 10.2 Hz, 1H), 3.37 – 3.30 (m, 4H), 3.31 – 3.27 (m, 1H), 3.21 (ddd, *J* = 12.3, 8.6, 3.2 Hz, 1H), 3.13 – 3.07 (m, 1H), 2.80 (t, *J* = 2.7 Hz, 1H), 2.55 – 2.51 (m, 1H), 2.37 – 2.30 (m, 2H), 2.23 (td, *J* = 7.1, 2.7 Hz, 2H), 1.72 (p, *J* = 7.1 Hz, 2H), 1.49 – 1.36 (m, 2H), 1.28 – 1.14 (m, 4H), 0.84 (t, *J* = 7.1 Hz, 3H).

^{13}C NMR (176 MHz, DMSO-d_6) δ (ppm) = 167.00, 165.18, 138.70, 138.67, 132.41, 132.18, 128.93, 119.27, 117.27, 104.31, 84.11, 71.38, 62.30, 54.26, 49.87, 47.90, 47.58, 38.47, 28.87, 28.04, 25.59, 21.96, 15.52, 13.89.

HRMS *m/z* for $C_{26}H_{34}N_7O_2^+$ ([M+H]$^+$) calculated: 476.2769, found: 476.2768.

8.1.1.12 Synthesis of CG341

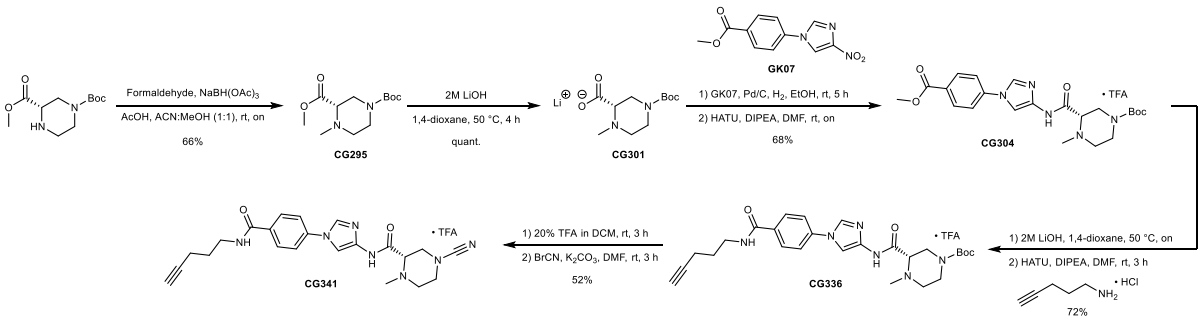

Scheme 29. Synthesis of CG341.

1-(*tert*-Butyl) 3-methyl (*S*)-4-methylpiperazine-1,3-dicarboxylate (CG295)

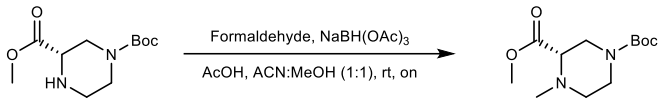

To a solution of 1-(*tert*-butyl) 3-methyl (*S*)-piperazine-1,3-dicarboxylate (300.0 mg, 1.23 mmol, 1.0 eq) in a 1:1 mixture of ACN:MeOH (24.6 mL) was added formaldehyde (37% aqueous, 3.3 mL, 44.46 mmol, 36.2 eq), followed by the addition of $NaBH(OAc)_3$ (1.041 g, 4.91 mmol, 4.0 eq). The reaction was stirred for 10 min at room temperature. Acetic acid (1.41 mL, 24.56 mmol, 20.0 eq) was added dropwise and stirring continued overnight. The solvent was removed under reduced pressure and the residue dissolved in DCM (60 mL) and neutralised by adding 2 M NaOH. Aqueous sat. $NaHCO_3$ (50 mL) was added and the layers were separated. The organic layer was washed with brine (40 mL), dried over anhydrous $MgSO_4$, filtered and the solvent was removed under reduced pressure. The obtained product CG295 (208.5 mg, 0.81 mmol, 66%) was used for the next reaction without further purification.

^{1}H NMR (700 MHz, DMSO-d_6) δ (ppm) = 3.63 (s, 3H), 3.59 – 3.42 (m, 2H), 3.41 – 3.34 (m, 1H), 3.29 – 3.19 (m, 1H), 3.15 – 2.97 (m, 1H), 2.89 (dt, *J* = 11.3, 5.1 Hz, 1H), 2.25 (s, 3H), 2.23 – 2.11 (m, 1H), 1.38 (s, 9H).

^{13}C NMR (176 MHz, DMSO-d_6) δ (ppm) = 170.91, 153.24, 79.00, 62.54, 51.38, 50.61, 49.72, 45.90, 42.81, 27.94.

HRMS *m/z* for $C_{12}H_{23}N_2O_4^+$ ([M+H]$^+$) calculated: 259.1652, found: 259.1654.

Lithium (*S*)-4-(*tert*-butoxycarbonyl)-1-methylpiperazine-2-carboxylate (CG301)

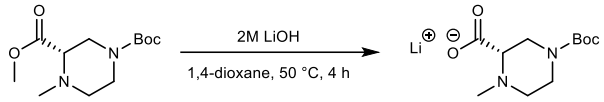

CG301 was obtained from CG295 (204.0 mg, 0.79 mmol, 1.0 eq) as described above for CG300. The obtained product CG301 (197.0 mg, 0.79 mmol, quant.) was used for following reactions without further purification.

***tert*-Butyl (*S*)-3-((1-(4-(methoxycarbonyl)phenyl)-1*H*-imidazol-4-yl)carbamoyl)-4-methyl-piperazine-1-carboxylate TFA salt (CG304)**

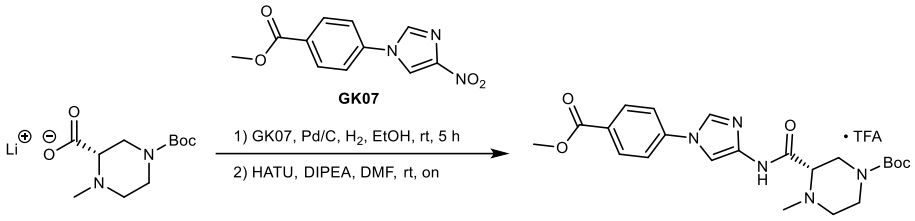

Step 1

GK07 (173.1 mg, 0.70 mmol, 1.3 eq) was dissolved in EtOH (20 mL) and palladium (10%) on activated charcoal (17 mg) was added under an argon atmosphere. The reaction was flushed with H_2 and stirred for 5 hours at room temperature. The reaction was filtered through Celite 545 which was then washed with EA. The solvent was removed under reduced pressure and the obtained product used for the next reaction without further purification.

Step 2

CG301 (135.0 mg, 0.54 mol, 1.0 eq) was dissolved in DMF (2 mL), then DIPEA (734.0 µL, 4.32 mmol, 8.0 eq) and HATU (246.2 mg, 0.65 mmol, 1.2 eq) were added and the reaction mixture stirred for 20 min

at room temperature. The crude product from step 1 was dissolved in DMF (2 mL) and added to the reaction dropwise. The resulting solution was stirred overnight at room temperature. The reaction was quenched by the addition of aqueous sat. NH_4Cl (40 mL) and the mixture extracted with EA (2x40 mL). The combined organic layers were washed with brine (30 mL), dried over anhydrous $MgSO_4$, filtered and the solvent was removed under reduced pressure. The corresponding product was purified via preparative HPLC, eluting at 5% ACN in H_2O, yielding CG304 (204.0 mg, 0.37 mmol, 68%) as a white TFA salt.

^{1}H NMR (600 MHz, DMSO-d_6) δ (ppm) = 11.67 (s, 1H), 8.38 (d, *J* = 1.7 Hz, 1H), 8.11 – 8.06 (m, 2H), 7.88 (d, *J* = 1.7 Hz, 1H), 7.84 (d, *J* = 8.7 Hz, 2H), 4.05 (s, 2H), 3.88 (s, 3H), 3.45 (s, 1H), 3.30 – 2.90 (m, 4H), 2.83 (s, 3H), 1.43 (s, 9H).

^{13}C NMR (151 MHz, DMSO-d_6) δ (ppm) = 168.69, 165.43, 157.97 (q, *J* = 33.1 Hz), 152.96, 140.11, 138.13, 132.93, 131.03, 127.78, 119.94, 116.56 (d, *J* = 296.8 Hz), 105.18, 80.27, 62.01, 58.22, 53.57, 52.32, 42.37, 41.21, 27.84.

HRMS *m/z* for $C_{22}H_{30}N_5O_5^+$ ($[M+H]^+$) calculated: 444.2242, found: 444.2247.

tert-Butyl (*S*)-4-methyl-3-((1-(4-(pent-4-yn-1-ylcarbamoyl)phenyl)-1*H*-imidazol-4-yl)carbamoyl)-piperazine-1-carboxylate TFA salt (CG336)

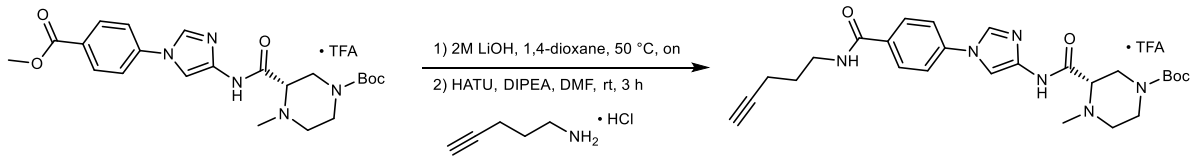

Step 1

CG304 (80.0 mg, 0.14 mmol, 1.0 eq) was dissolved in 1,4-dioxane (3 mL). Aqueous 2 M LiOH solution (151 µL, 0.30 mol, 2.1 eq) was added and the reaction mixture was stirred at 50 °C overnight. The pH of the reaction mixture was adjusted to pH 7 by adding aqueous 1 N HCl dropwise. The solvent was removed under reduced pressure and the obtained product used for the next reaction without further purification.

Step 2

The crude product from step 1 was dissolved in DMF (2 mL), then DIPEA (97.6 µL, 0.57 mmol, 4.0 eq) and HATU (70.9 mg, 0.19 mmol, 1.3 eq) were added and the reaction mixture was stirred for 10 min at room temperature. 4-Pentyn-1-amine HCl (51.5 mg, 0.43 mmol, 3.0 eq) was dissolved in DMF (2 mL), added to the reaction and the mixture stirred at room temperature for 3 h. The reaction mixture was quenched with sat. NH_4Cl solution (30 mL) and extracted with EA (2x30 mL). The combined organic layers were washed with brine (20 mL), dried over $MgSO_4$, filtered and the solvent was removed under reduced pressure. The product was purified via preparative HPLC eluting at 25-35% ACN in H_2O, yielding CG336 (62.5 mg, 0.10 mmol, 72%) as a white TFA salt.

^{1}H NMR (700 MHz, DMSO-d_6) δ (ppm) = 11.63 (s, 1H), 8.59 (t, *J* = 5.6 Hz, 1H), 8.33 (d, *J* = 1.7 Hz, 1H), 8.00 – 7.98 (m, 2H), 7.85 (d, *J* = 1.7 Hz, 1H), 7.80 – 7.73 (m, 2H), 4.03 (s, 2H), 3.44 (s, 1H), 3.39 – 3.32 (m, 2H), 3.31 – 3.12 (m, 3H), 2.90 (s, 1H), 2.82 (s, 3H), 2.81 (t, *J* = 2.6 Hz, 1H), 2.23 (td, *J* = 7.1, 2.6 Hz, 2H), 1.72 (p, *J* = 7.1 Hz, 3H), 1.50 – 1.32 (m, 9H).

^{13}C NMR (176 MHz, DMSO-d_6) δ (ppm) = 165.14, 160.95, 157.90 (q, *J* = 32.4 Hz), 152.97, 138.52, 137.93, 132.77, 132.73, 128.98, 119.58, 116.79 (d, *J* = 298.0 Hz), 105.32, 84.11, 80.25, 72.01, 71.41, 55.74, 52.12, 43.27, 41.24, 38.49, 28.05, 27.85, 15.53.

HRMS *m/z* for $C_{26}H_{35}N_6O_4^+$ ($[M+H]^+$) calculated: 495.2714, found: 495.2723.

(*S*)-4-Cyano-1-methyl-*N*-(1-(4-(pent-4-yn-1-ylcarbamoyl)phenyl)-1*H*-imidazol-4-yl)piperazine-2-carboxamide TFA salt (CG341)

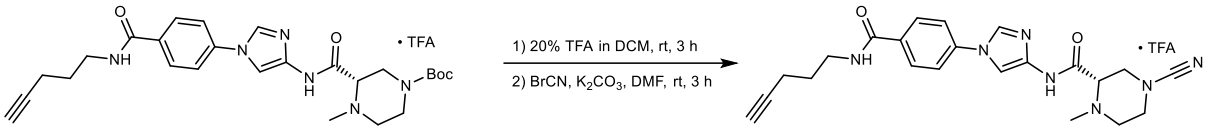

Step 1

CG336 (28.0 mg, 0.05 mmol, 1.0 eq) was dissolved in DCM (2 mL) and TFA (0.4 mL) was added dropwise. The solution was stirred for 3 h at room temperature. The solvent and residual TFA were removed under reduced pressure and the product dried in vacuo.

Step 2

The crude product from step 1 was dissolved in DMF (3 mL) and K_2CO_3 (25.4 mg, 0.18 mmol, 4.0 eq) was added. 3 M cyanogen bromide solution (23.0 µL, 0.07 mmol, 1.5 eq) was added and the mixture was stirred for 3 h at room temperature. The reaction was quenched by the addition of aqueous sat. $NaHCO_3$ (50 mL). The mixture was extracted with EA (2x30 mL). The combined organic layers were washed with brine (30 mL), dried over anhydrous $MgSO_4$, filtered and the solvent was removed under reduced pressure. The corresponding product was purified via preparative HPLC, eluting at 15-25% ACN in H_2O, yielding CG341 (12.7 mg, 0.02 mmol, 52%) as a white TFA salt.

^{1}H NMR (700 MHz, DMSO-d_6) δ (ppm) = 11.40 (s, 1H), 8.59 (t, *J* = 5.6 Hz, 1H), 8.32 (d, *J* = 1.6 Hz, 1H), 7.99 (d, *J* = 8.7 Hz, 2H), 7.84 (d, *J* = 1.6 Hz, 1H), 7.80 – 7.75 (m, 2H), 4.14 (s, 1H), 3.90 (d, *J* = 15.5 Hz, 1H), 3.66 (d, *J* = 14.2 Hz, 1H), 3.47 – 3.40 (m, 2H), 3.40 – 3.31 (m, 3H), 3.27 (s, 1H), 2.80 (t, *J* = 2.7 Hz, 1H), 2.78 (s, 3H), 2.23 (td, *J* = 7.1, 2.7 Hz, 2H), 1.72 (p, *J* = 7.1 Hz, 2H).

^{13}C NMR (176 MHz, DMSO-d_6) δ (ppm) = 165.16, 160.39, 158.04 (q, *J* = 33.9 Hz), 138.52, 137.91, 132.76, 132.72, 128.98, 119.60, 116.37 (q, *J* = 295.4 Hz), 115.78, 105.26, 84.12, 71.42, 63.46, 51.50, 48.88, 45.79, 41.60, 38.50, 28.06, 15.54.

HRMS *m/z* for $C_{22}H_{26}N_7O_2^+$ ([M+H]$^+$) calculated: 420.2143, found: 420.2146.

8.1.1.13 Synthesis of CG386

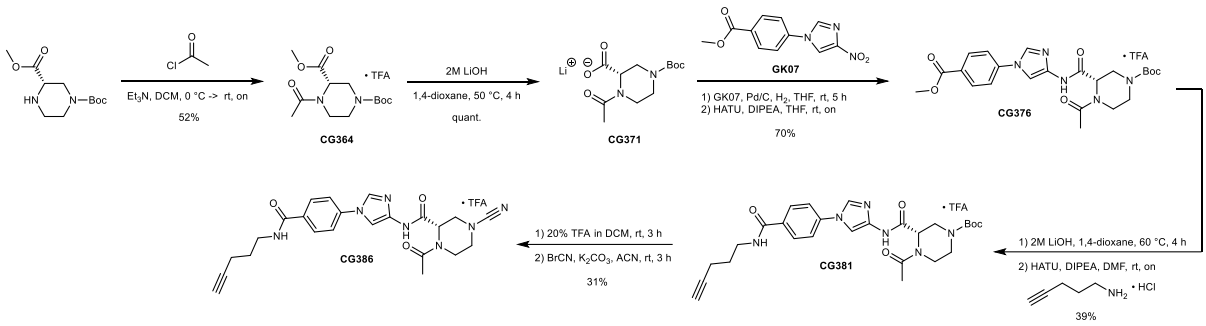

Scheme 30. Synthesis of CG386.

1-(*tert*-Butyl) 3-methyl (*S*)-4-acetylpiperazine-1,3-dicarboxylate TFA salt (CG364)

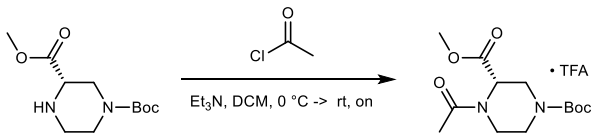

To a solution of 1-(*tert*-butyl) 3-methyl (*S*)-piperazine-1,3-dicarboxylate (200.0 mg, 0.82 mmol, 1.0 eq) in DCM (5 mL) was added acetyl chloride (76.0 µL, 1.06 mmol, 1.3 eq) at 0 °C. The reaction was

allowed to warm up to room temperature and stirred overnight. The reaction was quenched by the addition of aqueous sat. $NaHCO_3$ (40 mL) and the mixture extracted with DCM (2x30 mL). The combined organic layers were washed with brine (30 mL), dried over anhydrous $MgSO_4$, filtered and the solvent was removed under reduced pressure. The corresponding product was purified via preparative HPLC, eluting at 20-30% ACN in H_2O, yielding CG364 (12.1 mg, 0.03 mmol, 22%) as a white TFA salt.

^{1}H NMR (700 MHz, DMSO-d_6) δ (ppm) = 4.93 (s, 1H), 4.29 (d, *J* = 13.8 Hz, 1H), 4.14 (d, *J* = 13.0 Hz, 1H), 3.79 – 3.70 (m, 1H), 3.65 (s, 3H), 3.34 – 3.25 (m, 1H), 3.13 (s, 1H), 2.70 (s, 1H), 2.01 (d, *J* = 59.8 Hz, 3H), 1.38 (d, *J* = 6.8 Hz, 9H).

^{13}C NMR (176 MHz, DMSO-d_6) δ (ppm) = 170.42, 170.20, 158.16 (q, *J* = 36.6 Hz), 153.15, 115.57 (d, *J* = 291.2 Hz), 79.26, 52.14, 51.51, 44.41, 42.49, 38.07, 27.88, 21.31.

HRMS m/z for $C_{13}H_{23}N_2O_5^+$ ([M+H]$^+$) calculated: 287.1602, found: 287.1599.

Lithium (*S*)-1-acetyl-4-(*tert*-butoxycarbonyl)piperazine-2-carboxylate (CG371)

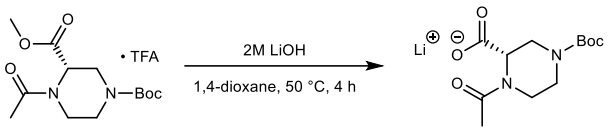

CG371 was obtained from CG364 (165.0 mg, 0.41 mmol, 1.0 eq) as described above for CG300. The obtained product CG371 (115.0 mg, 0.41 mmol, quant.) was used for following reactions without further purification.

***tert*-Butyl (*S*)-4-acetyl-3-((1-(4-(methoxycarbonyl)phenyl)-1*H*-imidazol-4-yl)carbamoyl)-piperazine-1-carboxylate TFA salt (CG376)**

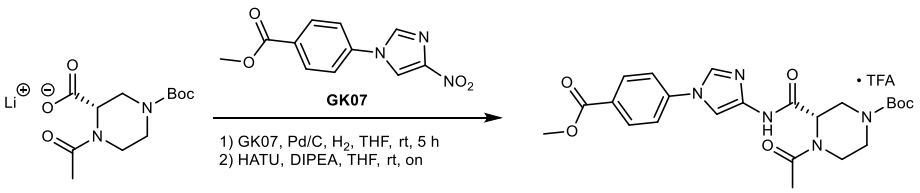

Step 1

GK07 (80.9 mg, 0.33 mmol, 1.3 eq) was dissolved in THF (3 mL) and palladium (10%) on activated charcoal (9 mg) was added under an argon atmosphere. The reaction was flushed with H_2 and stirred for 5 h at room temperature. The reaction was filtered through Celite 545 which was then washed with THF (20 mL) and the resulting solution was directly used for the next reaction.

Step 2

CG371 (70.0 mg, 0.25 mmol, 1.0 eq) was dissolved in THF (2 mL), then DIPEA (128 µL, 0.75 mmol, 3.0 eq) and HATU (124.4 mg, 0.33 mmol, 1.3 eq) were added and the reaction mixture was stirred for 15 min at room temperature. This reaction mixture was then transferred to the solution generated in step 1 and the reaction stirred at room temperature overnight. The reaction mixture was quenched with sat. NH_4Cl solution (40 mL) and extracted with EA (2x40 mL). The combined organic layers were washed with brine (30 mL), dried over $MgSO_4$, filtered and the solvent was removed under reduced pressure. The product was purified by preparative HPLC, eluting at 15-25% ACN in H_2O, yielding CG376 (83.0 mg, 0.18 mmol, 70%) as a white TFA salt.

^{1}H NMR (700 MHz, DMSO-d_6) δ (ppm) = 10.83 (d, *J* = 61.5 Hz, 1H), 8.34 (dd, *J* = 10.0, 1.7 Hz, 1H), 8.08 – 8.03 (m, 2H), 7.86 – 7.76 (m, 3H), 4.94 (dd, *J* = 4.8, 2.2 Hz, 1H), 4.40 (s, 1H), 3.98 – 3.87 (m,

1H), 3.87 (s, 3H), 3.75 – 3.60 (m, 2H), 3.22 (dd, *J* = 14.2, 4.8 Hz, 1H), 2.91 (s, 1H), 1.99 (d, *J* = 100.6 Hz, 3H), 1.27 (d, *J* = 105.9 Hz, 9H).

^{13}C NMR (176 MHz, DMSO-d_6) δ (ppm) = 170.58, 167.42, 165.44, 158.21 (q, *J* = 37.1 Hz), 153.30, 140.28, 139.37, 132.22, 131.03, 127.38, 119.41, 116.23 (q, *J* = 292.7 Hz), 103.62, 78.91, 52.25, 52.04, 45.66, 42.75, 42.24, 27.62, 21.55.

HRMS m/z for $C_{23}H_{30}N_5O_6^+$ ([M+H]$^+$) calculated: 472.2191, found: 472.2198.

tert-Butyl (*S*)-4-acetyl-3-((1-(4-(pent-4-yn-1-ylcarbamoyl)phenyl)-1*H*-imidazol-4-yl)carbamoyl)-piperazine-1-carboxylate TFA salt (CG381)

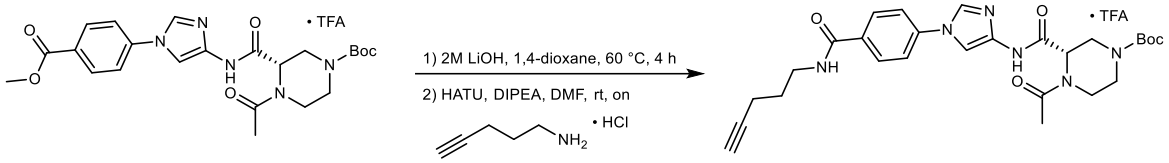

CG381 was obtained from CG376 (80.0 mg, 0.14 mmol, 1.0 eq) as described above for CG336. For step 1 the reaction was stirred at 60 °C for 4 h. For step 2 the reaction was stirred at room temperature overnight. The product was purified by preparative HPLC, eluting at 15-25% ACN in H_2O, yielding CG381 (34.2 mg, 0.05 mmol, 39%) as a white TFA salt.

^{1}H NMR (600 MHz, DMSO-d_6) δ (ppm) = 10.82 (d, *J* = 54.3 Hz, 1H), 8.56 (t, *J* = 5.6 Hz, 1H), 8.29 (dd, *J* = 8.8, 1.6 Hz, 1H), 7.98 – 7.94 (m, 2H), 7.76 (d, *J* = 4.9 Hz, 1H), 7.74 – 7.72 (m, 2H), 4.94 (dd, *J* = 4.8, 2.2 Hz, 1H), 4.40 (d, *J* = 13.9 Hz, 1H), 3.88 (s, 1H), 3.71 – 3.59 (m, 2H), 3.33 (q, *J* = 6.6 Hz, 2H), 3.22 (dd, *J* = 14.2, 4.8 Hz, 1H), 2.91 (s, 1H), 2.80 (t, *J* = 2.6 Hz, 1H), 2.23 (td, *J* = 7.1, 2.7 Hz, 2H), 1.99 (d, *J* = 85.9 Hz, 3H), 1.72 (p, *J* = 7.1 Hz, 2H), 1.27 (d, *J* = 89.2 Hz, 9H).

^{13}C NMR (151 MHz, DMSO-d_6) δ (ppm) = 170.70, 167.36, 165.18, 158.18 (q, *J* = 36.5 Hz), 153.29, 139.20, 138.68, 132.35, 132.00, 128.99, 119.04, 115.57 (q, *J* = 291.3 Hz), 103.76, 84.12, 78.94, 71.40, 51.99, 45.66, 42.77, 42.24, 38.47, 28.04, 27.63, 21.57, 15.53.

HRMS m/z for $C_{27}H_{35}N_6O_5^+$ ([M+H]$^+$) calculated: 523.2663, found: 523.2681.

(*S*)-1-Acetyl-4-cyano-*N*-(1-(4-(pent-4-yn-1-ylcarbamoyl)phenyl)-1*H*-imidazol-4-yl)piperazine-2-carboxamide (CG386)

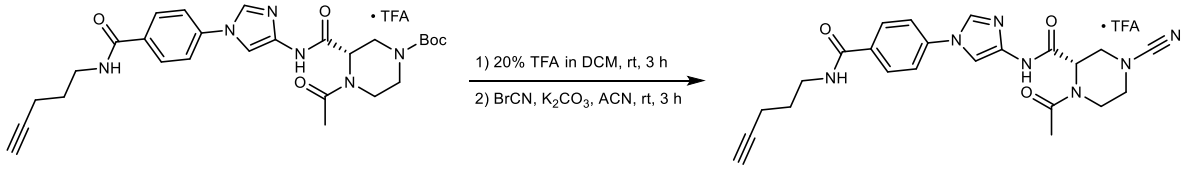

CG386 was obtained from CG381 (30.0 mg, 0.06 mmol, 1.0 eq) as described above for CG341. For step 2 the used based was DIPEA (78.1 µL, 0.46 mmol, 8.0 eq). The product was purified by preparative HPLC, eluting at 10% ACN in H_2O, yielding CG386 (20.2 mg, 0.05 mmol, 79%) as a white TFA salt.

^{1}H NMR (600 MHz, DMSO-d_6) δ (ppm) = 10.74 (s, 1H), 8.58 (t, *J* = 5.6 Hz, 1H), 8.36 – 8.31 (m, 1H), 8.00 – 7.94 (m, 2H), 7.90 – 7.83 (m, 1H), 7.81 – 7.73 (m, 2H), 5.13 (dd, *J* = 4.6, 1.9 Hz, 1H), 3.89 (dt, *J* = 13.3, 1.8 Hz, 1H), 3.80 (dt, *J* = 13.6, 3.0 Hz, 1H), 3.61 (ddd, *J* = 13.6, 12.0, 3.8 Hz, 1H), 3.44 – 3.40 (m, 1H), 3.38 (dd, *J* = 13.4, 4.7 Hz, 1H), 3.37 – 3.31 (m, 2H), 3.20 (td, *J* = 12.2, 3.6 Hz, 1H), 2.80 (t, *J* = 2.7 Hz, 1H), 2.23 (td, *J* = 7.1, 2.6 Hz, 2H), 2.10 (s, 3H), 1.72 (pd, *J* = 7.1, 2.1 Hz, 2H).

^{13}C NMR (151 MHz, DMSO-d_6) δ (ppm) = 170.61, 166.22, 165.20, 158.30 (q, *J* = 37.5 Hz), 138.63, 138.59, 132.52, 132.12, 128.97, 119.34, 117.01, 115.34 (q, *J* = 290.0 Hz), 104.77, 84.14, 71.41, 50.88, 49.26, 47.63, 42.42, 38.50, 28.05, 21.50, 15.55.

HRMS m/z for $C_{23}H_{26}N_7O_3^+$ ([M+H]$^+$) calculated: 448.2092, found: 448.2098.

8.1.1.14 Synthesis of minimal probes

Synthesis of (*S*)-4-cyano-*N*-(pent-4-yn-1-yl)morpholine-2-carboxamide (CG365)

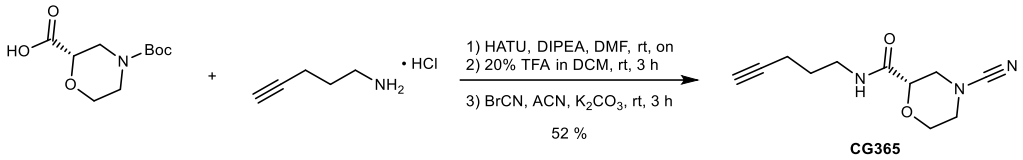

Scheme 31. Synthesis of CG365.

Step 1

(*S*)-4-(*tert*-Butoxycarbonyl)morpholine-2-carboxylic acid (100.0 mg, 0.43 mmol, 1.0 eq) was dissolved in 4 mL of DCM, then DIPEA (302.1 µL, 1.73 mmol, 4.0 eq) and HATU (230.2 mg, 0.61 mmol, 1.4 eq) were added to the solution. After stirring for 20 min at room temperature 4-pentyn-1-amine hydrochloride (62.1 mg, 0.52 mmol, 1.2 eq) was added and the solution was stirred overnight. The reaction mixture was poured into sat. NH_4Cl (50 mL) and extracted with EA (2x40 mL). The organic layer was washed with brine (30 mL), dried over anhydrous $MgSO_4$, filtered and the solvent was evaporated under reduced pressure. The obtained crude product was used for the next reaction without further purification.

Step 2

The crude product from step 1 was dissolved in DCM (2 mL) and TFA (0.4 mL) was added dropwise. The solution was stirred for 3 h at room temperature. The solvent and residual TFA were removed under reduced pressure and the product dried in vacuo. The crude product was used for the next reaction without further purification.

Step 3

The crude product from step 2 was dissolved in ACN (3 mL), then K_2CO_3 (239.1 mg, 1.73 mmol, 4.0 eq) was added to the reaction mixture. After stirring for 30 min at room temperature, 3 M cyanogen bromide solution (201.8 µL, 0.61 mmol, 1.4 eq) was added to the mixture, and stirring was continued for 3 h. The reaction was quenched by the addition of aqueous sat. $NaHCO_3$ (40 mL). The mixture was extracted with EA (2x30 mL). The combined organic layers were washed with brine (30 mL), dried over anhydrous $MgSO_4$, filtered and the solvent was removed under reduced pressure. The corresponding product was purified via preparative HPLC, eluting at 10-25% ACN in H_2O, yielding CG365 (50.0 mg, 0.23 mmol, 52%) as a clear resin.

^{1}H NMR (500 MHz, $CDCl_3$) δ (ppm) = 6.64 (s, 1H), 4.08 (dd, *J* = 10.8, 3.0 Hz, 1H), 3.98 (ddd, *J* = 11.9, 3.2, 1.6 Hz, 1H), 3.84 – 3.71 (m, 2H), 3.46 – 3.32 (m, 2H), 3.31 – 3.18 (m, 2H), 3.02 (dd, *J* = 12.9, 10.8 Hz, 1H), 2.25 (td, *J* = 7.0, 2.7 Hz, 2H), 1.99 (t, *J* = 2.7 Hz, 1H), 1.75 (p, *J* = 6.9 Hz, 2H).

^{13}C NMR (126 MHz, $CDCl_3$) δ (ppm) = 167.61, 116.61, 83.22, 74.20, 69.48, 65.66, 50.53, 48.27, 38.16, 28.11, 16.22.

HRMS *m/z* for $C_{11}H_{16}N_3O_2^+$ ([M+H]$^+$) calculated: 222.1237, found: 222.1232.

Synthesis of (*S*)-4-cyano-1-methyl-*N*-(pent-4-yn-1-yl)piperazine-2-carboxamide TFA salt (CG374)

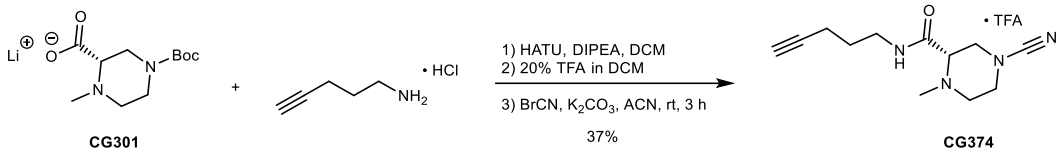

Scheme 32. Synthesis of CG374.

CG374 was obtained from CG301 (75.0 mg, 0.30 mmol, 1.0 eq) as described above for CG365. For step 1 ACN (2 mL) was used as solvent. For step 3 the product was purified by preparative HPLC, eluting at 15-25% ACN in H_2O, yielding CG374 (25.7 mg, 0.11 mmol, 37%) as a white TFA salt.

^{1}H NMR (700 MHz, DMSO-d_6) δ (ppm) = 8.82 (t, *J* = 5.7 Hz, 1H), 3.93 (d, *J* = 10.4 Hz, 1H), 3.80 (dt, *J* = 13.8, 2.8 Hz, 1H), 3.66 – 3.61 (m, 1H), 3.39 (td, *J* = 11.2, 9.7, 3.2 Hz, 2H), 3.30 – 3.23 (m, 2H), 3.21 (q, *J* = 6.7 Hz, 2H), 2.81 (t, *J* = 2.6 Hz, 1H), 2.73 (s, 3H), 2.20 (td, *J* = 7.2, 2.7 Hz, 2H), 1.62 (p, *J* = 7.0 Hz, 2H).

^{13}C NMR (176 MHz, DMSO-d_6) δ (ppm) = 164.34, 158.18 (q, *J* = 33.0 Hz), 116.68 (q, *J* = 296.9 Hz), 115.74, 83.73, 71.63, 63.49, 51.34, 48.79, 45.59, 41.35, 38.03, 27.48, 15.30.

HRMS *m/z* for $C_{12}H_{19}N_4O^+$ ([M+H]$^+$) calculated: 235.1553, found: 235.1549.

Synthesis of (*S*)-4-cyano-*N*-(pent-4-yn-1-yl)-1-pentylpiperazine-2-carboxamide TFA salt (CG375)

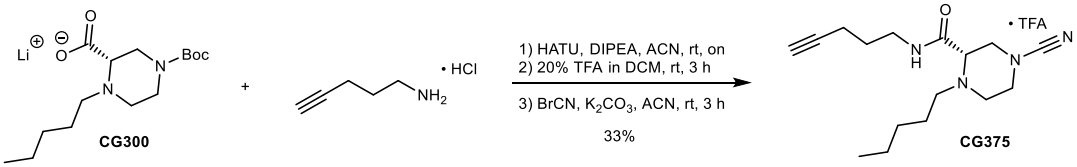

CG375 was obtained from CG300 (75.0 mg, 0.24 mmol, 1.0 eq) as described above for CG365. For step 1 ACN (2 mL) was used as solvent. For step 3 the product was purified by preparative HPLC, eluting at 15-25% ACN in H_2O, yielding CG375 (23.6 mg, 0.08 mmol, 33%) as a white TFA salt.

^{1}H NMR (700 MHz, DMSO-d_6) δ (ppm) = 8.77 (s, 1H), 3.90 (s, 1H), 3.77 (d, *J* = 13.9 Hz, 1H), 3.59 (d, *J* = 13.7 Hz, 1H), 3.54 – 3.46 (m, 1H), 3.41 (t, *J* = 12.3 Hz, 1H), 3.36 – 3.27 (m, 1H), 3.21 (ddd, *J* = 12.4, 6.9, 5.2 Hz, 2H), 3.17 – 3.10 (m, 1H), 2.91 (s, 2H), 2.81 (t, *J* = 2.7 Hz, 1H), 2.19 (td, *J* = 7.2, 2.6 Hz, 2H), 1.62 (pt, *J* = 7.1, 3.9 Hz, 3H), 1.56 (dq, *J* = 9.0, 5.2, 4.4 Hz, 1H), 1.34 – 1.14 (m, 4H), 0.86 (t, *J* = 7.1 Hz, 3H).

^{13}C NMR (176 MHz, DMSO-d_6) δ (ppm) = 158.09 (q, *J* = 32.6 Hz), 157.07, 116.77 (q, *J* = 297.6 Hz), 115.87, 83.68, 71.59, 62.77, 54.69, 48.82, 48.51, 45.75, 37.98, 28.08, 27.51, 23.04, 21.58, 15.28, 13.65.

HRMS *m/z* for $C_{16}H_{27}N_4O^+$ ([M+H]$^+$) calculated: 291.2179, found: 291.2177.

9.2.3 A Dual-Functional-Warhead Approach to Address novel DUBs (Project 3)

8.1.1.15 Warhead synthesis

Synthesis of 1-(*tert*-Butoxycarbonyl)-4-(prop-2-yn-1-yloxy)pyrrolidine-3-carboxylic acid (CG217)

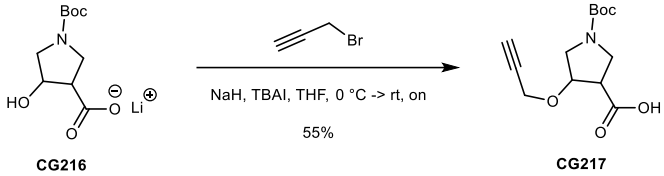

CG216 CG217

To a solution of CG216 (50.0 mg, 0.21 mmol, 1.0 eq) and tetrabutylammonium iodide (TBAI, 3.9 mg, 0.01 mmol, 0.05 eq) in dry THF (1 mL) was added sodium hydride (60 wt.% in mineral oil, 21.1 mg, 0.53 mmol, 2.5 eq) portion wise at 0 °C. The reaction was allowed to reach room temperature and stirred for another 30 min. To the mixture was added propargyl bromide (93.9 µL, 0.84 mmol, 4.0 eq) and stirring was continued at room temperature overnight. The reaction mixture was quenched by the addition of sat. NH_4Cl (30 ml) and extracted with EA (2x20 mL). The combined organic layers were washed with brine (40 mL), dried over anhydrous $MgSO_4$, filtered and the solvent was evaporated under reduced pressure. The product was purified via a silica column eluting at 20-35% EA (+ 0.1% AcOH) in PE. CG217 (31.1 mg, 0.12 mmol, 55%) was obtained as a clear resin.

^{1}H NMR (600 MHz, DMSO-d_6) δ (ppm) = 4.40 – 4.27 (m, 1H), 4.24 – 4.13 (m, 2H), 3.55 – 3.49 (m, 1H), 3.50 – 3.43 (m, 1H), 3.43 – 3.37 (m, 1H), 3.39 – 3.34 (m, 1H), 3.34 – 3.27 (m, 1H), 3.27 – 3.07 (m, 1H), 1.40 (“d”, *J* = 4.2 Hz, 9H).

^{13}C NMR (151 MHz, DMSO-d_6) δ (ppm) = 172.79, 153.47 (“d”, *J* = 23.5 Hz), 80.04 (“d”, *J* = 6.3 Hz), 78.68, 78.51 (“d”, *J* = 2.1 Hz), 77.37 (“d”, *J* = 18.5 Hz), 56.13 (“d”, *J* = 52.3 Hz), 50.32 (“d”, *J* = 41.0 Hz), 46.24 (“d”, *J* = 23.4 Hz), 45.10 (“d”, *J* = 32.1 Hz), 28.11 (“d”, *J* = 5.0 Hz).

HRMS m/z for $C_{13}H_{20}NO_5^+$ ([M+H]$^+$) calculated: 270.1336, found: 270.1337.

Synthesis of CG221

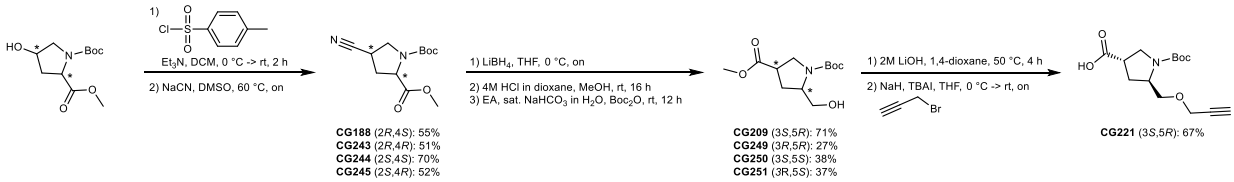

Scheme 33. Synthesis of CG221.

1-(*tert*-Butyl) 2-methyl (2*R*,4*R*)-4-cyanopyrrolidine-1,2-dicarboxylate (CG243)

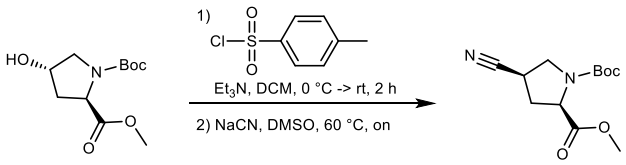

CG243 was obtained from 1-(*tert*-butyl) 2-methyl (2R,4S)-4-hydroxypyrrolidine-1,2-dicarboxylate (1.295 g, 5.28 mmol, 1.0 eq) as described above for CG188. For step 2, the product was eluting at 10-20% EA in PE. CG243 (681.5 mg, 2.68 mmol, 51%) was obtained as a clear resin.

^{1}H NMR (700 MHz, $CDCl_3$) δ (ppm) = 4.43 – 4.27 (m, 1H), 3.99 – 3.87 (m, 1H), 3.78 (s, 3H), 3.70 – 3.61 (m, 1H), 3.10 (dt, *J* = 19.3, 7.9 Hz, 1H), 2.75 – 2.62 (m, 1H), 2.34 – 2.24 (m, 1H), 1.47 – 1.38 (m, 9H).

^{13}C NMR (176 MHz, $CDCl_3$) δ (ppm) = 171.90 (“d”, *J* = 39.9 Hz), 153.30 (“d”, *J* = 86.9 Hz), 118.94, 81.36 (“d”, *J* = 8.5 Hz), 58.17 (“d”, *J* = 55.8 Hz), 52.66 (“d”, *J* = 31.0 Hz), 49.29 (“d”, *J* = 35.4 Hz), 34.06 (“d”, *J* = 175.3 Hz), 28.38 (“d”, *J* = 19.6 Hz), 27.02 (“d”, *J* = 129.2 Hz).

HRMS m/z for $C_{12}H_{19}N_2O_4^+$ ([M+H]$^+$) calculated: 255.1339, found: 255.1337.

1-(*tert*-Butyl) 2-methyl (2*S*,4*R*)-4-cyanopyrrolidine-1,2-dicarboxylate (CG245)

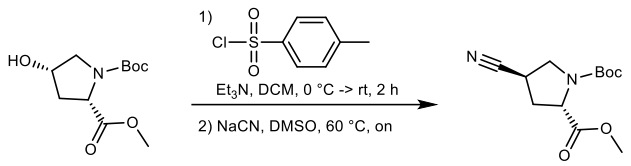

CG245 was obtained from 1-(*tert*-butyl) 2-methyl (2S,4S)-4-hydroxypyrrolidine-1,2-dicarboxylate (1.0 g, 4.08 mmol, 1.0 eq) as described above for CG188. For step 2, the product was eluting at 10-20% EA in PE. CG245 (541.7 mg, 2.13 mmol, 52%) was obtained as a clear resin.

^{1}H NMR (700 MHz, $CDCl_3$) δ (ppm) = 4.44 (“d”dd, *J* = 67.3, 8.7, 3.5 Hz, 1H), 3.91 (“d”dd, *J* = 21.9, 10.6, 7.8 Hz, 1H), 3.75 (s, 3H), 3.66 (“d”dd, *J* = 42.6, 10.7, 7.4 Hz, 1H), 3.26 (“d”p, *J* = 22.7, 7.7 Hz, 1H), 2.51 (“d”dt, *J* = 43.3, 13.0, 8.9 Hz, 1H), 2.36 (“d”dd, *J* = 13.1, 6.8, 3.5 Hz, 1H), 1.44 (“d”, *J* = 38.5 Hz, 9H).

^{13}C NMR (176 MHz, $CDCl_3$) δ (ppm) = 172.42 (“d”, *J* = 15.7 Hz), 153.33 (“d”, *J* = 95.2 Hz), 119.12 (“d”, *J* = 14.4 Hz), 81.35 (“d”, *J* = 16.6 Hz), 57.92 (“d”, *J* = 36.2 Hz), 52.67 (“d”, *J* = 31.5 Hz), 49.25 (“d”, *J* = 18.5 Hz), 34.25 (“d”, *J* = 170.7 Hz), 28.38 (“d”, *J* = 20.6 Hz), 26.86 (“d”, *J* = 99.2 Hz).

HRMS m/z for $C_{12}H_{19}N_2O_4^+$ ([M+H]$^+$) calculated: 255.1339, found: 255.1339.

1-(*tert*-Butyl) 3-methyl (3*S*,5*R*)-5-(hydroxymethyl)pyrrolidine-1,3-dicarboxylate (CG209)

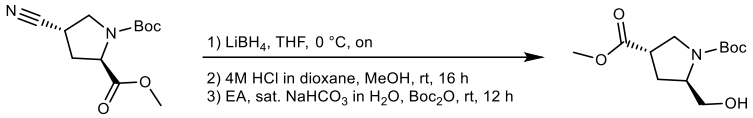

Step 1

To a solution of CG188 (100.0 mg, 0.39 mmol, 1.0 eq) in dry THF (2 mL) was added $LiBH_4$ (17.13 mg, 0.79 mmol, 2.0 eq). The reaction mixture was stirred at 0 °C overnight. Drops of acetone were added slowly to quench the reaction. The resulting solution was poured into H_2O (40 mL) and extracted with EA (2x40 mL). The combined organic layers were washed with sat. $NaHCO_3$ (40 mL) and brine (40 mL), dried over anhydrous $MgSO_4$, filtered and the solvent was evaporated under reduced pressure. The resulting product was used for the next reaction without further purification.

HRMS m/z for $C_{11}H_{19}N_2O_3^+$ ([M+H]$^+$) calculated: 227.1390, found: 227.1391.

Step 2

The crude product from step 1 was dissolved in MeOH (2.4 mL) and 4 M HCl in 1,4-dioxane (1.17 mL, 4.68 mmol, 12 e) was added dropwise. The solution was stirred at room temperature for 16 h.

Step3

The solvent was removed under reduced pressure and the crude intermediate dissolved in EA (2 mL) and basified with aqueous sat. $NaHCO_3$ (2 mL). Boc_2O (102.1 mg, 0.47 mmol, 1.2 eq) was added and the biphasic solution was vigorously stirred at room temperature for 12 h. The layers were then separated and the aqueous phase back extracted with EA (40 mL). The organic layers were combined, washed with brine (30 mL), dried over anhydrous $MgSO_4$, filtered and the solvent was evaporated under

reduced pressure. The product was purified via a silica column eluting at 12-30% EA in PE. CG209 (71.4 mg, 0.28 mmol, 71%) was obtained as a pale-yellow oil.

^{1}H NMR (500 MHz, $CDCl_3$) δ (ppm) = 4.09 (d, *J* = 8.2 Hz, 1H), 3.71 (s, 3H), 3.67 (dd, *J* = 11.1, 3.5 Hz, 1H), 3.64 (d, *J* = 7.7 Hz, 1H), 3.60 (d, *J* = 7.0 Hz, 1H), 3.60 – 3.52 (m, 1H), 3.17 – 3.04 (m, 1H), 2.28 (dt, *J* = 13.0, 8.3 Hz, 1H), 1.88 (p, *J* = 5.8 Hz, 1H), 1.47 (s, 9H).

^{13}C NMR (126 MHz, $CDCl_3$) δ (ppm) = 173.47, 156.77, 80.87, 67.20, 59.53, 52.33, 49.62, 41.76, 31.71, 28.54.

HRMS m/z for $C_{12}H_{22}NO_5^+$ ([M+H]$^+$) calculated: 260.1493, found: 260.1495.

1-(*tert*-Butyl) 3-methyl (3*R*,5*R*)-5-(hydroxymethyl)pyrrolidine-1,3-dicarboxylate (CG249)

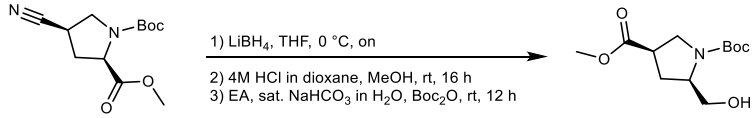

CG249 was obtained from CG243 (670.0 mg, 2.63 mmol, 1.0 eq) as described above for CG209. For step 2, $LiBH_4$ (2M in THF, 1.45 mL, 2.90 mmol, 1.1 eq) was used as reducing agent. For step 2, the product was eluting at 12-30% EA in PE. CG249 (181.0 mg, 0.70 mmol, 27%) was obtained as a pale-yellow oil.

Step 1

HRMS m/z for $C_{11}H_{19}N_2O_3^+$ ([M+H]$^+$) calculated: 227.1390, found: 227.1391.

Step 2

^{1}H NMR (700 MHz, DMSO-*d*$_6$) δ (ppm) = 4.70 (t, *J* = 5.5 Hz, 1H), 3.74 – 3.66 (m, 1H), 3.65 ("d"d, *J* = 10.8, 8.2 Hz, 1H), 3.62 (s, 3H), 3.48 ("d"dd, *J* = 10.4, 5.2, 3.3 Hz, 1H), 3.46 – 3.36 (m, 1H), 3.34 (q, *J* = 5.4, 4.8 Hz, 1H), 3.06 (s, 1H), 2.22 (s, 1H), 2.18 – 1.95 (m, 1H), 1.39 (s, 9H).

^{13}C NMR (176 MHz, DMSO-*d*$_6$) δ (ppm) = 173.15, 153.37 ("d", *J* = 34.5 Hz), 78.55, 61.69 ("d", *J* = 88.9 Hz), 58.27, 51.75 ("d", *J* = 2.4 Hz), 48.46 ("d", *J* = 18.9 Hz), 41.03 ("d", *J* = 51.6 Hz), 30.88 ("d", *J* = 140.0 Hz), 28.12.

HRMS m/z for $C_{12}H_{22}NO_5^+$ ([M+H]$^+$) calculated: 260.1493, found: 260.1495.

1-(*tert*-Butyl) 3-methyl (3*S*,5*S*)-5-(hydroxymethyl)pyrrolidine-1,3-dicarboxylate (CG250)

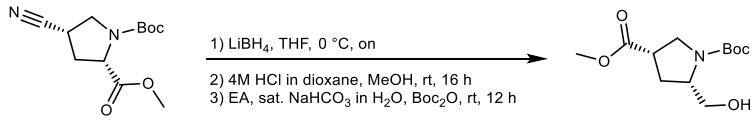

CG250 was obtained from CG244 (710.0 mg, 2.79 mmol, 1.0 eq) as described above for CG209. For step 2, $LiBH_4$ (2M in THF, 1.54 mL, 3.07 mmol, 1.1 eq) was used as reducing agent. For step 2, the product was eluting at 12-30% EA in PE. CG250 (277.2 mg, 1.07 mmol, 38%) was obtained as a pale-yellow oil.

Step 1

HRMS m/z for $C_{11}H_{19}N_2O_3^+$ ([M+H]$^+$) calculated: 227.1390, found: 227.1391.

Step 2

^{1}H NMR (700 MHz, DMSO-*d*$_6$) δ (ppm) = 4.70 (t, *J* = 5.5 Hz, 1H), 3.75 – 3.67 (m, 1H), 3.67 – 3.63 (m, 1H), 3.62 (s, 3H), 3.48 ("d"dt, *J* = 11.2, 5.9, 3.2 Hz, 1H), 3.46 – 3.38 (m, 1H), 3.34 (q, *J* = 5.4, 5.0 Hz, 1H), 3.07 (d, *J* = 15.2 Hz, 1H), 2.21 (d, *J* = 11.5 Hz, 1H), 2.14 – 2.01 (m, 1H), 1.39 ("d", *J* = 1.8 Hz, 9H).

^{13}C NMR (176 MHz, DMSO-d_6) δ (ppm) = 173.16, 153.38 (“d”, *J* = 35.4 Hz), 78.57, 61.70 (“d”, *J* = 87.0 Hz), 58.19 (“d”, *J* = 29.1 Hz), 51.74 (“d”, *J* = 2.4 Hz), 48.42 (“d”, *J* = 63.9 Hz), 40.90 (“d”, *J* = 95.8 Hz), 30.87 (“d”, *J* = 140.0 Hz), 28.12.

HRMS m/z for $C_{12}H_{22}NO_5^+$ ([M+H]$^+$) calculated: 260.1493, found: 260.1493.

1-(*tert*-Butyl) 3-methyl (3*R*,5*S*)-5-(hydroxymethyl)pyrrolidine-1,3-dicarboxylate (CG251)

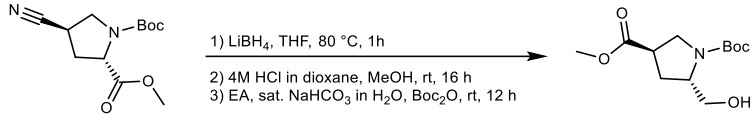

CG251 was obtained from CG245 (530.0 mg, 2.08 mmol, 1.0 eq) as described above for CG209. For step 2, $LiBH_4$ (2M in THF, 1.15 mL, 2.29 mmol, 1.1 eq) was used as reducing agent. For step 2, the product was eluting at 12-30% EA in PE. CG251 (201.2 mg, 0.78 mmol, 37%) was obtained as a pale-yellow oil.

Step 1

HRMS m/z for $C_{11}H_{19}N_2O_3^+$ ([M+H]$^+$) calculated: 227.1390, found: 227.1392.

Step 2

^{1}H NMR (700 MHz, DMSO-d_6) δ (ppm) = 4.76 (“d”d, *J* = 11.8, 5.5 Hz, 1H), 3.80 – 3.70 (m, 1H), 3.62 (s, 3H), 3.43 (“d”q, *J* = 7.5, 2.8, 2.3 Hz, 1H), 3.43 – 3.36 (m, 2H), 3.37 – 3.31 (m, 1H), 3.23 (tt, *J* = 16.1, 8.1 Hz, 1H), 2.12 (“d”t, *J* = 26.3, 9.8 Hz, 1H), 2.07 – 1.98 (m, 1H), 1.39 (s, 9H).

^{13}C NMR (176 MHz, DMSO-d_6) δ (ppm) = 173.32 (“d”, *J* = 31.9 Hz), 153.39 (“d”, *J* = 28.3 Hz), 78.53 (“d”, *J* = 8.2 Hz), 61.68 (“d”, *J* = 91.4 Hz), 58.27, 51.74 (“d”, *J* = 2.4 Hz), 48.46 (“d”, *J* = 18.6 Hz), 40.89, 30.87 (“d”, *J* = 138.6 Hz), 28.11.

HRMS m/z for $C_{12}H_{22}NO_5^+$ ([M+H]$^+$) calculated: 260.1493, found: 260.1494.

(3*S*,5*R*)-1-(*tert*-Butoxycarbonyl)-5-((prop-2-yn-1-yloxy)methyl)pyrrolidine-3-carboxylic acid (CG221)

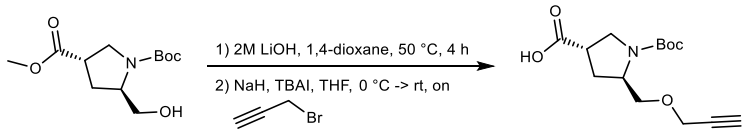

Step 1

CG209 (60.0 mg, 0.23 mmol, 1.0 eq) was dissolved in 1,4-dioxane (0.5 mL). Aqueous 2M LiOH solution (162.0 µL, 0.32 mmol, 1.4 eq) was added and the reaction mixture was stirred for 4 h at 50 °C. The pH of the reaction mixture was adjusted to pH 7 by adding aqueous 1 M HCl dropwise. The solvent was removed under reduced pressure and the obtained product used for the next reaction without further purification.

Step 2

To a solution of the crude product from step 1 and TBAI (4.2 mg, 0.01 mmol, 0.05 eq) in dry THF (2 mL) was added sodium hydride (60 wt.% in mineral oil, 23.0 mg, 0.57 mmol, 2.5 eq) portion wise at 0 °C. The reaction was allowed to reach room temperature and stirred for another 30 min. To the mixture was added propargyl bromide (102.5 µL, 0.92 mmol, 4.0 eq) and stirring was continued at room temperature overnight. The reaction mixture was quenched by the addition of sat. NH_4Cl (30 ml) and extracted with EA (2x20 mL). The combined organic layers were washed with brine (40 mL), dried over anhydrous $MgSO_4$, filtered and the solvent was evaporated under reduced pressure. The product was purified via

a silica column eluting at 20-35% EA (+ 0.1% AcOH) in PE. CG221 (43.8 mg, 0.15 mmol, 67%) was obtained as a pale-yellow oil.

^{1}H NMR (600 MHz, DMSO-d_6) δ (ppm) = 12.46 (s, 1H), 4.12 (d, *J* = 16.4 Hz, 2H), 3.88 (s, 1H), 3.51 (s, 1H), 3.47 – 3.43 (m, 1H), 3.42 – 3.37 (m, 3H), 3.18 – 3.05 (m, 1H), 2.05 (d, *J* = 38.1 Hz, 2H), 1.40 (s, 9H).

^{13}C NMR (151 MHz, DMSO-d_6) δ (ppm) = 174.21, 153.29 (“d”, *J* = 33.9 Hz), 80.24, 78.72, 77.24, 69.77 (“d”, *J* = 63.9 Hz), 57.77 (“d”, *J* = 11.6 Hz), 55.88 (“d”, *J* = 8.9 Hz), 48.44 (“d”, *J* = 21.2 Hz), 40.70 (“d”, *J* = 123.9 Hz), 31.39 (“d”, *J* = 130.0 Hz), 28.08.

HRMS m/z for $C_{14}H_{21}NO_5^+$ ([M+H]$^+$) calculated: 284.1492, found: 284.1490.

Synthesis of CG184

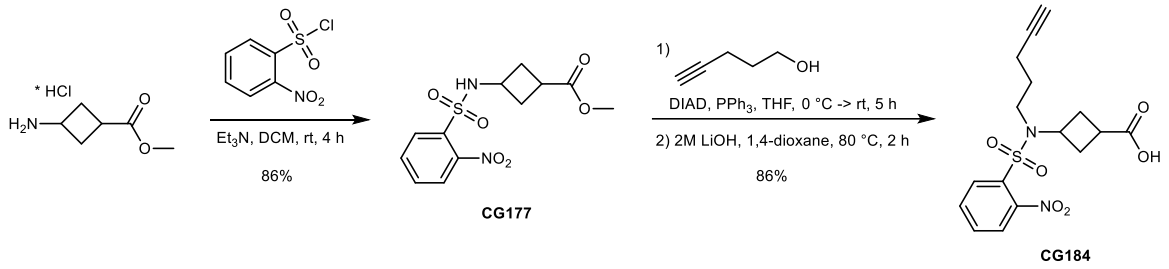

Scheme 34. Synthesis of CG184.

Methyl 3-((2-nitrophenyl)sulfonamido)cyclobutane-1-carboxylate (CG177)

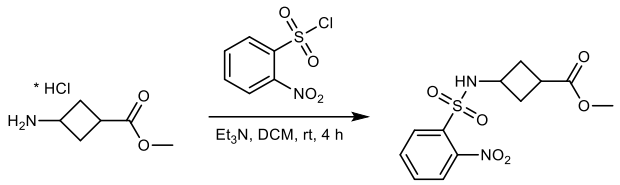

To a solution of methyl 3-aminocyclobutane-1-carboxylate HCl salt (300.0 g, 1.81 mmol, 1.0 eq) and Et_3N (504.9 µL, 3.62 mmol, 2.0 eq) in DCM (3 mL) was added 2-nitrobenzenesulfonyl chloride (602.2 mg, 2.72 mmol, 1.5 eq). The reaction mixture was stirred for 4 h at room temperature. The reaction mixture was quenched with water (30 ml) and extracted with DCM (2x40 mL). The combined organic layers were washed with sat. $NaHCO_3$ (30 mL) and brine (30 mL), dried over anhydrous $MgSO_4$ and the solvent was removed under reduced pressure. The product was purified via a silica column eluting at 12-30% EA in PE. CG177 (488.5 mg, 1.55 mmol, 86%) was obtained as a white solid.

^{1}H NMR (700 MHz, $CDCl_3$) δ (ppm) = 8.14 (ddd, *J* = 9.2, 6.0, 3.5 Hz, 1H), 7.86 (dt, *J* = 8.3, 3.1 Hz, 1H), 7.76 – 7.71 (m, 2H), 5.62 (d, *J* = 9.2 Hz, 1H), 3.96 (h, *J* = 8.5 Hz, 1H), 3.66 (s, 3H), 2.81 – 2.68 (m, 1H), 2.52 – 2.40 (m, 2H), 2.13 (qd, *J* = 9.3, 2.8 Hz, 2H).

^{13}C NMR (176 MHz, $CDCl_3$) δ (ppm) = 174.28, 148.15, 134.75, 133.88, 133.05, 130.85, 125.59, 52.19, 45.05, 34.60, 31.53.

HRMS m/z for $C_{12}H_{15}N_2O_6S^+$ ([M+H]$^+$) calculated: 315.0645, found: 315.0644.

3-((2-Nitro-*N*-(pent-4-yn-1-yl)phenyl)sulfonamido)cyclobutane-1-carboxylic acid (CG184)

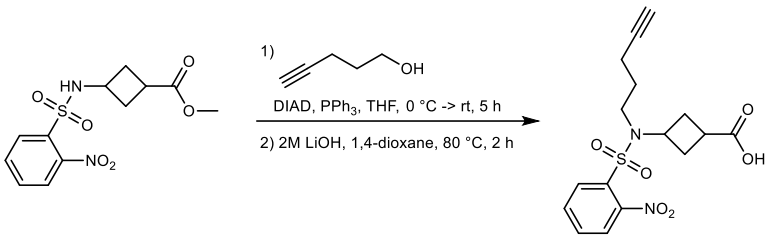

Step 1

A solution of pent-4-yn-1-ol (284.2 µL, 3.05 mmol, 2.0 eq), triphenylphosphine (PPh_3, 801.1 mg, 3.05 mmol, 2.0 eq) and diisopropyl azodicarboxylate (DIAD, 599.6 µL, 3.05 mmol, 2.0 eq) in dry THF (20 mL) was stirred at room temperature for 5 minutes. The solution was cooled to 0 °C followed by the addition of CG177 (480 mg, 1.53 mmol, 1.0 eq) and stirring was continued at 0 °C for 5 h. The reaction was filtered through celite545 which was then washed with EA. The solvent was removed under reduced pressure and the obtained product used for the next reaction without further purification.

Step 2

The crude product from step 1 was dissolved in 1,4-dioxane (3 mL). Aqueous 2M LiOH solution (1.07 mL, 2.14 mmol, 1.4 eq) was added and the reaction mixture was stirred for 2 h at 80 °C. To this reaction was added 1 M NaOH (50 mL), followed by extraction with DCM (2x30 mL). The aqueous phase was acidified with 1 M HCl to pH 1, followed by extraction with EA (2x30 mL). The organic EA layers were combined, dried over anhydrous $MgSO_4$ and the solvent was removed under reduced pressure. The product was recrystallised in EA at -20 °C, yielding CG184 (483.7 mg, 1.32 mmol, 86%) as white crystals.

^{1}H NMR (700 MHz, DMSO-d_6) δ (ppm) = 12.25 (s, 1H), 7.98 (dd, *J* = 7.9, 1.3 Hz, 1H), 7.94 (ddd, *J* = 25.2, 7.8, 1.5 Hz, 1H), 7.89 (td, *J* = 7.7, 1.4 Hz, 1H), 7.85 (td, *J* = 7.7, 1.4 Hz, 1H), 4.26 – 4.00 (m, 1H), 3.42 – 3.33 (m, 2H), 2.78 (t, *J* = 2.6 Hz, 1H), 2.68 (tt, *J* = 9.8, 7.7 Hz, 1H), 2.28 (dddd, *J* = 11.4, 7.6, 5.3, 2.5 Hz, 2H), 2.23 (ddd, *J* = 11.8, 8.4, 2.4 Hz, 2H), 2.19 (td, *J* = 7.1, 2.7 Hz, 2H), 1.69 (dq, *J* = 9.3, 7.2 Hz, 2H).

^{13}C NMR (176 MHz, DMSO-d_6) δ (ppm) = 174.74, 147.62, 134.64, 132.58, 131.82, 129.53, 124.36, 83.26, 71.72, 47.81, 43.81, 31.91, 30.51, 29.37, 15.09.

HRMS m/z for $C_{17}H_{21}N_2O_6S^+$ ([M+H]$^+$) calculated: 381.1115, found: 381.1117.

Synthesis of CG201

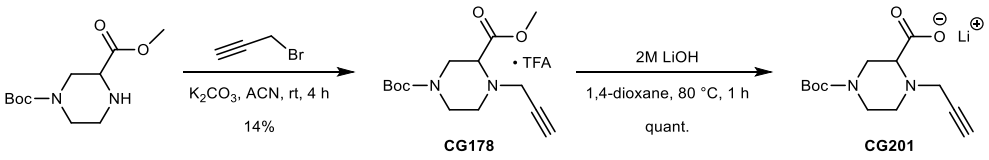

Scheme 35. Synthesis of CG201.

1-(*tert*-Butyl) 3-methyl 4-(prop-2-yn-1-yl)piperazine-1,3-dicarboxylate (CG178)

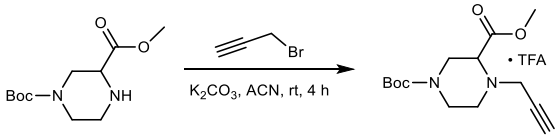

To a solution of 1-(*tert*-butyl) 3-methyl piperazine-1,3-dicarboxylate (100.0 mg, 0.41 mmol, 1.0 eq) and K_2CO_3 (113.2 mg, 0.82 mmol, 2.0 eq) in ACN (1 mL) was added propargyl bromide (46.5 µL,

0.61 mmol, 1.5 eq) and the reaction stirred at room temperature for 4 h. The reaction was filtered through celite545 which was then washed with EA. The solvent was removed under reduced pressure and the obtained product purified via a silica column, eluting at 10-20% EA in PE. Since the product still showed impurities, as judged by TLC and LC-MS, it was further purified by preparative HPLC, eluting at 20-30% ACN in H_2O, yielding CG178 (22.0 mg, 0.08 mmol, 14%) as a white TFA salt.

^{1}H NMR (600 MHz, $CDCl_3$) δ (ppm) = 4.04 – 3.78 (m, 1H), 3.74 (s, 3H), 3.69 (dt, *J* = 12.9, 4.2 Hz, 1H), 3.60 – 3.56 (m, 1H), 3.62 – 3.47 (m, 1H), 3.45 (dd, *J* = 17.2, 2.5 Hz, 1H), 3.43 – 3.40 (m, 1H), 3.33 (dt, *J* = 12.7, 4.4 Hz, 1H), 2.95 – 2.86 (m, 1H), 2.63 (t, *J* = 9.9 Hz, 1H), 2.27 (dt, *J* = 4.8, 2.4 Hz, 1H), 1.45 (s, 9H).

^{13}C NMR (151 MHz, $CDCl_3$) δ (ppm) = 171.19, 154.33, 80.35, 77.82, 74.25, 61.03, 52.22, 49.07, 46.60, 44.23, 42.79, 28.48.

HRMS m/z for $C_{14}H_{23}N_2O_4^+$ ($[M+H]^+$) calculated: 283.1652, found: 283.1655.

Lithium 4-(*tert*-butoxycarbonyl)-1-(prop-2-yn-1-yl)piperazine-2-carboxylate (CG201)

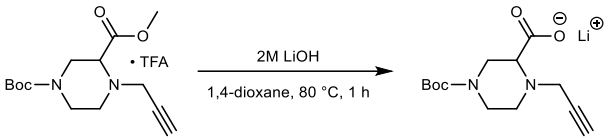

CG178 (20.0 mg, 0.05 mmol, 1.0 eq) was dissolved in 1,4-dioxane (0.5 mL). Aqueous 2M LiOH solution (100.9 µL, 0.20 mmol, 4.0 eq) was added and the reaction mixture was stirred for 1 h at 80 °C. The pH of the reaction mixture was adjusted to pH 7 by adding aqueous 1 N HCl dropwise. The solvent was removed under reduced pressure yielding CG201 (14.0 mg, 0.05 mmol, quant.), which was used for following reactions without further purification.

^{1}H NMR (700 MHz, D_2O) δ (ppm) = 3.99 (d, *J* = 11.7 Hz, 1H), 3.46 (d, *J* = 17.2 Hz, 1H), 3.40 (d, *J* = 17.2 Hz, 1H), 3.08 (ddd, *J* = 13.9, 11.1, 3.2 Hz, 2H), 3.04 – 3.00 (m, 2H), 2.88 (d, *J* = 13.3 Hz, 1H), 2.49 (td, *J* = 11.4, 3.4 Hz, 2H), 1.43 (s, 9H).

^{13}C NMR (176 MHz, D_2O) δ (ppm) = 177.15, 156.13, 82.10, 77.33, 66.54, 65.25, 56.49, 49.00, 43.23, 43.21, 27.58.

HRMS m/z for $C_{13}H_{21}N_2O_4^+$ ($[M+H]^+$) calculated: 269.1496, found: 269.1502.

Synthesis of 4-(*tert*-Butoxycarbonyl)-1-(pent-4-yn-1-yl)piperazine-2-carboxylic acid TFA salt (CG203)

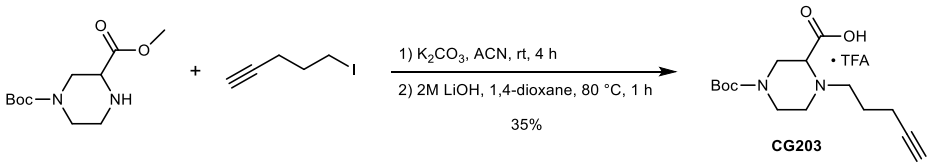

Step 1

To a solution of 1-(*tert*-butyl) 3-methyl piperazine-1,3-dicarboxylate (100.0 mg, 0.41 mmol, 1.0 eq) and K_2CO_3 (113.2 mg, 0.82 mmol, 2.0 eq) in ACN (1 mL) was added 5-iodopent-1-yne (70.1 µL, 0.61 mmol, 1.5 eq) and the reaction stirred at room temperature for 4 h. The reaction was filtered through celite545 which was then washed with EA. The solvent was removed under reduced pressure and the obtained product used for the next step without further purification.

Step 2

The crude product from step 1 was dissolved in 1,4-dioxane (1 mL). Aqueous 2M LiOH solution (811.9 µL, 1.62 mmol, 4.0 eq) was added and the reaction mixture was stirred for 1 h at 80 °C. The pH of the reaction mixture was adjusted to pH 7 by adding aqueous 1 N HCl dropwise. The solvent was removed under reduced pressure. The product was purified by preparative HPLC, eluting at 5-20% ACN in H_2O, yielding CG203 (42.6 mg, 0.14 mmol, 35%) as a white TFA salt.

^{1}H NMR (600 MHz, DMSO-d_6) δ (ppm) = 3.91 (s, 2H), 3.77 (s, 4H), 3.57 – 3.42 (m, 1H), 3.37 (s, 1H), 3.09 (s, 1H), 3.02 – 2.93 (m, 1H), 2.86 (s, 1H), 2.24 (td, *J* = 7.0, 2.7 Hz, 2H), 1.77 (s, 2H), 1.40 (s, 9H).

^{13}C NMR (151 MHz, DMSO-d_6) δ (ppm) = 168.06, 158.22, 158.00, 157.78, 157.56, 153.15, 119.65, 117.68, 115.71, 113.74, 83.22, 79.84, 72.01, 61.24, 53.57, 48.47, 48.04, 43.21, 27.88, 23.59, 15.22.

HRMS m/z for $C_{15}H_{25}N_2O_4^+$ ([M+H]$^+$) calculated: 297.1809, found: 297.1815.

Synthesis of CG202

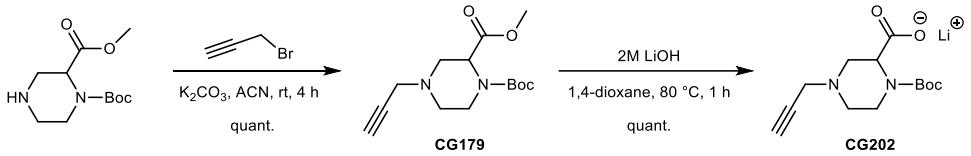

Scheme 36. Synthesis of CG202.

1-(*tert*-Butyl) 2-methyl 4-(prop-2-yn-1-yl)piperazine-1,2-dicarboxylate (CG179)

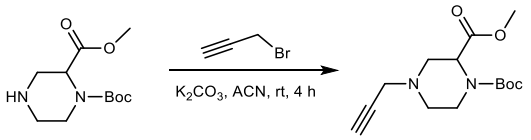

CG179 was obtained from 1-(*tert*-butyl) 2-methyl piperazine-1,2-dicarboxylate (100.0 mg, 0.41 mmol, 1.0 eq) as described above for CG178. The product was eluting at 0-10% EA in PE, yielding CG179 (115.0 mg, 0.41 mmol, quant.) as a clear oil.

^{1}H NMR (600 MHz, $CDCl_3$) δ (ppm) = 4.81 – 4.59 (m, 1H), 3.87 (dd, *J* = 57.9, 13.0 Hz, 1H), 3.75 (d, *J* = 7.2 Hz, 3H), 3.34 (dd, *J* = 2.4, 1.3 Hz, 2H), 3.33 – 3.27 (m, 1H), 3.27 – 3.11 (m, 1H), 2.69 (dd, *J* = 41.2, 11.2 Hz, 1H), 2.55 – 2.49 (m, 1H), 2.38 – 2.31 (m, 1H), 2.25 (t, *J* = 2.4 Hz, 1H), 1.45 (d, *J* = 25.2 Hz, 9H).

^{13}C NMR (151 MHz, $CDCl_3$) δ (ppm) = 171.41 (d, *J* = 48.4 Hz), 155.61 (d, *J* = 61.1 Hz), 80.57, 77.77, 73.97, 54.77 (d, *J* = 188.8 Hz), 52.46, 52.35, 50.87, 46.97, 41.41 (d, *J* = 142.0 Hz), 28.44 (d, *J* = 7.7 Hz).

HRMS m/z for $C_{14}H_{23}N_2O_4^+$ ([M+H]$^+$) calculated: 283.1652, found: 283.1654.

Lithium 1-(*tert*-Butoxycarbonyl)-4-(prop-2-yn-1-yl)piperazine-2-carboxylate (CG202)

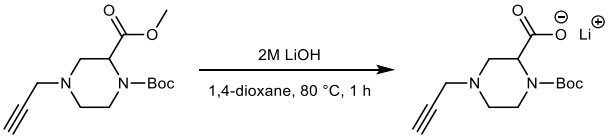

CG202 was obtained from CG179 (113.0 mg, 0.40 mmol, 1.0 eq) as described above for CG201. CG202 (110.0 mg, 0.40 mmol, quant.) was used for following reactions without further purification.

^{1}H NMR (700 MHz, D_2O) δ (ppm) = 4.47 (s, 1H), 3.89 (d, *J* = 108.9 Hz, 1H), 3.38 (d, *J* = 23.3 Hz, 1H), 3.29 (s, 2H), 3.23 – 3.15 (m, 2H), 2.85 (s, 1H), 2.47 (s, 1H), 2.28 (t, *J* = 11.8 Hz, 1H), 1.44 (s, 9H).

^{13}C NMR (176 MHz, D_2O) δ (ppm) = 181.49, 157.22, 81.84, 77.61, 66.55, 56.74, 52.69, 50.61, 45.90, 40.38, 27.59.

HRMS m/z for $C_{13}H_{21}N_2O_4^+$ ([M+H]$^+$) calculated: 269.1496, found: 269.1500.

Synthesis of 1-(*tert*-Butoxycarbonyl)-4-(pent-4-yn-1-yl)piperazine-2-carboxylic acid TFA salt (CG204)

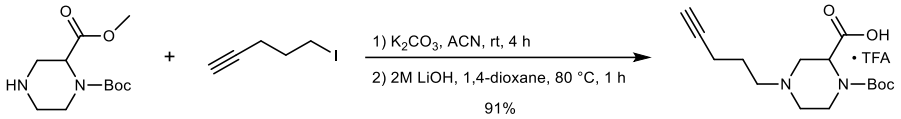

CG204 was obtained from 1-(*tert*-butyl) 2-methyl piperazine-1,2-dicarboxylate (100.0 mg, 0.41 mmol, 1.0 eq) as described above for CG203. The product was eluting at 5-20% ACN in H_2O, yielding CG204 (110.0 mg, 0.37 mmol, 91%) as a white TFA salt.

^{1}H NMR (600 MHz, DMSO-d_6) δ (ppm) = 4.17 (dd, *J* = 9.0, 3.5 Hz, 1H), 3.93 (s, 1H), 3.32 – 3.23 (m, 1H), 3.25 – 3.10 (m, 1H), 3.04 (tt, *J* = 9.6, 3.4 Hz, 2H), 2.90 (s, 1H), 2.80 (t, *J* = 2.6 Hz, 1H), 2.29 – 2.20 (m, 3H), 2.19 (td, *J* = 7.3, 2.7 Hz, 2H), 1.62 (p, *J* = 7.2 Hz, 2H), 1.40 (d, *J* = 22.9 Hz, 9H).

^{13}C NMR (151 MHz, DMSO-d_6) δ (ppm) = 168.54, 158.04 (q, *J* = 32.4 Hz), 154.11, 116.80 (q, *J* = 297.9 Hz), 84.01, 80.09, 71.51, 55.50, 54.58, 51.10, 48.63, 41.76, 27.80, 24.75, 15.36.

HRMS m/z for $C_{15}H_{25}N_2O_4^+$ ([M+H]$^+$) calculated: 297.1809, found: 297.1815.

8.1.1.16 Proof of concept (synthesis of GK13S analogues)

Synthesis of 4-Cyano-*N*-(1-(4-((2-methoxyethyl)carbamoyl)phenyl)-1*H*-imidazol-4-yl)-1-(prop-2-yn-1-yl)piperazine-2-carboxamide (CG224)

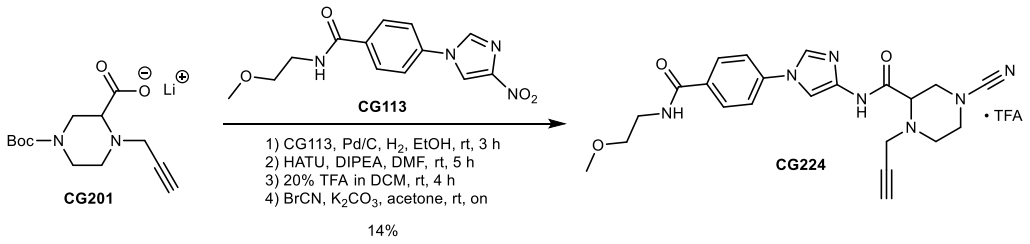

Step 1

CG113 (11.4 mg, 0.04 mmol, 1.2 eq) was dissolved in EtOH (5 mL) and a few drops of H_2O were added. Palladium (10%) on activated charcoal (2 mg) was added under argon atmosphere. The reaction was flushed with H_2 and stirred for 3 hours at room temperature. The reaction was filtered through celite545 which was then washed with EA. The solvent was removed under reduced pressure and the obtained product used for the next reaction without further purification.

Step 2

CG201 (9.0 mg, 0.03 mmol, 1.0 eq) was dissolved in DMF (1 mL), then DIPEA (11.2 µL, 0.07 mmol, 2.0 eq) and HATU (15.0 mg, 0.04 mmol, 1.2 eq) were added and the reaction mixture stirred for 20 minutes. The crude product from step 1 was dissolved in DMF (2 mL) and added to the reaction dropwise. The resulting solution was stirred for 5 h at room temperature. The reaction was quenched by the addition of aqueous sat. $NaHCO_3$ (30 mL). The mixture was extracted with EA (2x30 mL). The combined organic layers were washed with brine (30 mL), dried over anhydrous $MgSO_4$, filtered and

the solvent was removed under reduced pressure. The corresponding product was used for the next reaction without further purification.

Step 3

The crude product from step 2 was dissolved in DCM (2 mL) and TFA (0.4 mL) was added dropwise. The solution was stirred for 4 h at room temperature. The solvent and residual TFA were removed under reduced pressure and the product dried in vacuo.

Step 4

The crude product from step 3 was dissolved in acetone (2 mL) and K_2CO_3 (18.1 mg, 0.13 mmol, 4.0 eq) was added. 3 M cyanogen bromide solution (12.0 µL, 0.04 mmol, 1.1 eq) was added and the mixture was stirred overnight at room temperature. The reaction was quenched by the addition of aqueous sat. $NaHCO_3$ (30 mL). The mixture was extracted with EA (2x30 mL). The combined organic layers were washed with brine (30 mL), dried over anhydrous $MgSO_4$, filtered and the solvent was removed under reduced pressure. The corresponding product was purified via preparative HPLC, eluting at 10-20% ACN in H_2O, yielding CG224 (2.5 mg, 0.05 mmol, 14%) as a white TFA salt.

^{1}H NMR (700 MHz, DMSO-d_6) δ (ppm) = 10.75 (s, 1H), 8.61 (t, *J* = 5.4 Hz, 1H), 8.27 (d, *J* = 1.6 Hz, 1H), 7.98 (d, *J* = 8.7 Hz, 2H), 7.81 (d, *J* = 1.6 Hz, 1H), 7.76 (d, *J* = 8.7 Hz, 2H), 3.53 (dd, *J* = 9.4, 3.4 Hz, 1H), 3.50 – 3.33 (m, 8H), 3.29 (t, *J* = 2.4 Hz, 1H), 3.27 (s, 3H), 3.26 – 3.19 (m, 3H), 2.94 (dt, *J* = 12.1, 3.4 Hz, 1H), 2.64 (td, *J* = 11.3, 10.8, 3.3 Hz, 1H).

^{13}C NMR (176 MHz, DMSO-d_6) δ (ppm) = 170.83, 165.19, 138.69, 138.59, 132.30, 132.21, 128.96, 119.35, 116.97, 104.61, 77.97, 76.47, 70.43, 61.03, 57.92, 50.45, 48.03, 45.04, 42.93, 39.03.

HRMS m/z for $C_{22}H_{26}N_7O_3^+$ ($[M+H]^+$) calculated: 436.2092, found: 436.2090.

4-Cyano-*N*-(1-(4-((2-methoxyethyl)carbamoyl)phenyl)-1*H*-imidazol-4-yl)-1-(pent-4-yn-1-yl)piperazine-2-carboxamide (CG226)

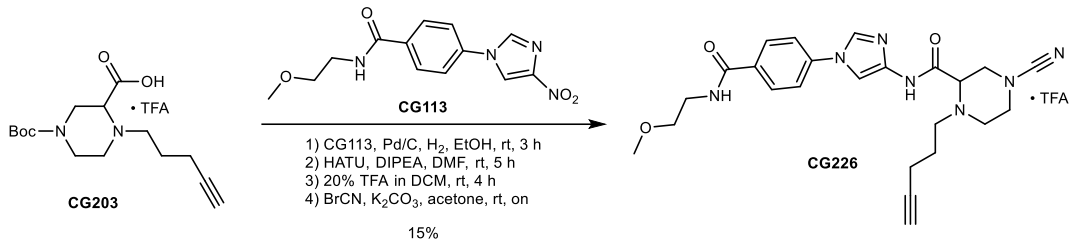

CG226 was obtained from CG203 (53.5 mg, 0.13 mmol, 1.0 eq) as described above for CG224. For step 4, the product was purified by preparative HPLC, eluting at 15-25% ACN in H_2O, yielding CG226 (11.0 mg, 0.02 mmol, 15%) as a white TFA salt.

^{1}H NMR (700 MHz, DMSO-d_6) δ (ppm) = 11.13 (s, 1H), 8.62 (t, *J* = 5.4 Hz, 1H), 8.30 (d, *J* = 1.7 Hz, 1H), 8.04 – 7.96 (m, 2H), 7.83 (d, *J* = 1.7 Hz, 1H), 7.80 – 7.74 (m, 2H), 3.97 (s, 1H), 3.75 (s, 2H), 3.54 (s, 2H), 3.47 (td, *J* = 5.4, 1.3 Hz, 2H), 3.46 – 3.42 (m, 2H), 3.39 (dd, *J* = 13.4, 9.4 Hz, 2H), 3.27 (s, 3H), 2.94 (s, 2H), 2.80 (t, *J* = 2.7 Hz, 1H), 2.25 (dtd, *J* = 16.9, 7.1, 2.7 Hz, 1H), 2.19 (dtd, *J* = 17.0, 7.1, 2.5 Hz, 1H), 1.81 (s, 1H), 1.77 – 1.69 (m, 1H).

^{13}C NMR (176 MHz, DMSO-d_6) δ (ppm) = 165.65, 158.53 (q, *J* = 34.7 Hz), 139.07, 138.61, 133.01, 132.94, 129.46, 119.98, 116.70, 116.64 (q, *J* = 294.6 Hz), 105.45, 83.77, 72.40, 70.92, 62.87, 58.41, 56.46, 54.39, 49.68, 48.87, 46.90, 39.53, 24.08, 15.76.

HRMS m/z for $C_{24}H_{30}N_7O_3^+$ ($[M+H]^+$) calculated: 464.2405, found: 464.2403.

Synthesis of 1-Cyano-*N*-(1-(4-((2-methoxyethyl)carbamoyl)phenyl)-1*H*-imidazol-4-yl)-4-(prop-2-yn-1-yl)piperazine-2-carboxamide (CG225)

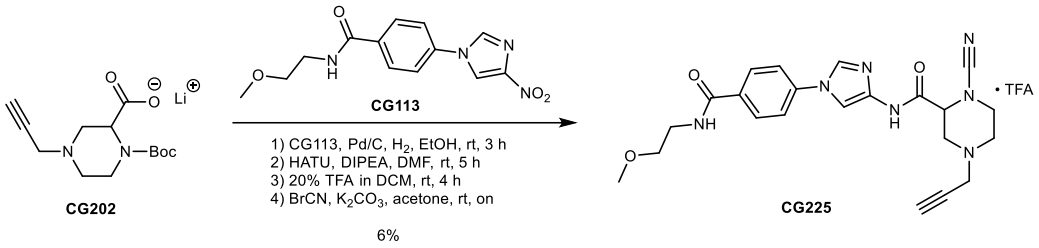

Step 1

CG113 (51.8 mg, 0.18 mmol, 1.1 eq) was dissolved in EtOH (5 mL) and a few drops of H_2O were added. Palladium (10%) on activated charcoal (6 mg) was added under argon atmosphere. The reaction was flushed with H_2 and stirred for 3 hours at room temperature. The reaction was filtered through celite545 which was then washed with EA. The solvent was removed under reduced pressure and the obtained product used for the next reaction without further purification.

Step 2

CG202 (44.5 mg, 0.16 mmol, 1.2 eq) was dissolved in DMF (2 mL), then DIPEA (55.2 µL, 0.32 mmol, 2.0 eq) and HATU (74.0 mg, 0.19 mmol, 1.2 eq) were added and the reaction mixture stirred for 20 minutes. The crude product from step 1 was dissolved in DMF (2 mL) and added to the reaction dropwise. The resulting solution was stirred for 5 h at room temperature. The reaction was quenched by the addition of aqueous sat. $NaHCO_3$ (30 mL). The mixture was extracted with EA (2x30 mL). The combined organic layers were washed with brine (30 mL), dried over anhydrous $MgSO_4$, filtered and the solvent was removed under reduced pressure. The corresponding product was used for the next reaction without further purification.

Step 3

The crude product from step 2 was dissolved in DCM (2 mL) and TFA (0.4 mL) was added dropwise. The solution was stirred for 4 h at room temperature. The solvent and residual TFA were removed under reduced pressure and the product dried in vacuo.

Step 4

The crude product from step 3 was dissolved in acetone (2 mL) and K_2CO_3 (89.7 mg, 0.65 mmol, 4.0 eq) was added. 3 M cyanogen bromide solution (59.5 µL, 0.18 mmol, 1.1 eq) was added and the mixture was stirred overnight at room temperature. The reaction was quenched by the addition of aqueous sat. $NaHCO_3$ (30 mL). The mixture was extracted with EA (2x30 mL). The combined organic layers were washed with brine (30 mL), dried over anhydrous $MgSO_4$, filtered and the solvent was removed under reduced pressure. The corresponding product was purified via preparative HPLC, eluting at 10-20% ACN in H_2O, yielding CG225 (5.3 mg, 0.01 mmol, 6%) as a white TFA salt.

^{1}H NMR (700 MHz, DMSO-d_6) δ (ppm) = 9.73 (s, 1H), 9.19 (s, 1H), 8.67 (t, *J* = 5.4 Hz, 1H), 8.61 (d, *J* = 1.6 Hz, 1H), 8.15 (d, *J* = 1.6 Hz, 1H), 8.07 – 8.02 (m, 2H), 7.87 – 7.81 (m, 2H), 4.68 (dd, *J* = 11.3, 4.7 Hz, 1H), 4.25 – 4.18 (m, 1H), 3.51 (dd, *J* = 4.4, 2.4 Hz, 2H), 3.48 (dd, *J* = 6.7, 3.6 Hz, 2H), 3.47 – 3.43 (m, 2H), 3.31 (t, *J* = 2.4 Hz, 1H), 3.28 (s, 3H), 3.25 (ddd, *J* = 10.9, 4.7, 1.4 Hz, 1H), 2.94 (dd, *J* = 11.8, 3.7 Hz, 1H), 2.55 (t, *J* = 11.1 Hz, 1H), 2.53 – 2.51 (m, 1H), 2.45 (td, *J* = 12.0, 3.7 Hz, 1H).

^{13}C NMR (176 MHz, DMSO-d_6) δ (ppm) = 168.73, 165.08, 157.81 (q, *J* = 32.3 Hz), 153.97, 138.04, 134.91, 133.34, 129.08, 120.05, 119.68, 114.86, 78.35, 76.75, 70.43, 57.94, 57.08, 50.15, 49.15, 45.47, 41.50, 39.10.

HRMS m/z for $C_{22}H_{26}N_7O_3^+$ ($[M+H]^+$) calculated: 436.2092, found: 436.2094.

Synthesis of 1-Cyano-*N*-(1-(4-((2-methoxyethyl)carbamoyl)phenyl)-1*H*-imidazol-4-yl)-4-(pent-4-yn-1-yl)piperazine-2-carboxamide (CG227)

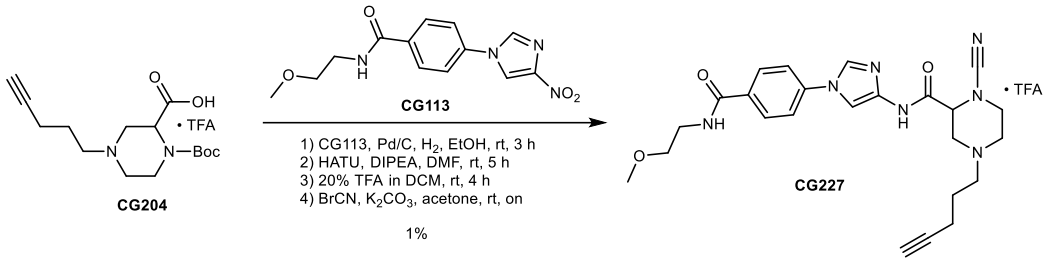

CG227 was obtained from CG204 (53.4 mg, 0.13 mmol, 1.0 eq) as described above for CG225. For step 4, the product was purified by preparative HPLC, eluting at 15-25% ACN in H_2O, yielding CG227 (0.9 mg, 1.56 µmol, 1%) as a white TFA salt.

HRMS m/z for $C_{24}H_{30}N_7O_3^+$ ($[M+H]^+$) calculated: 464.2405, found: 464.2401.

No NMR since too low yield!

Synthesis of CG233

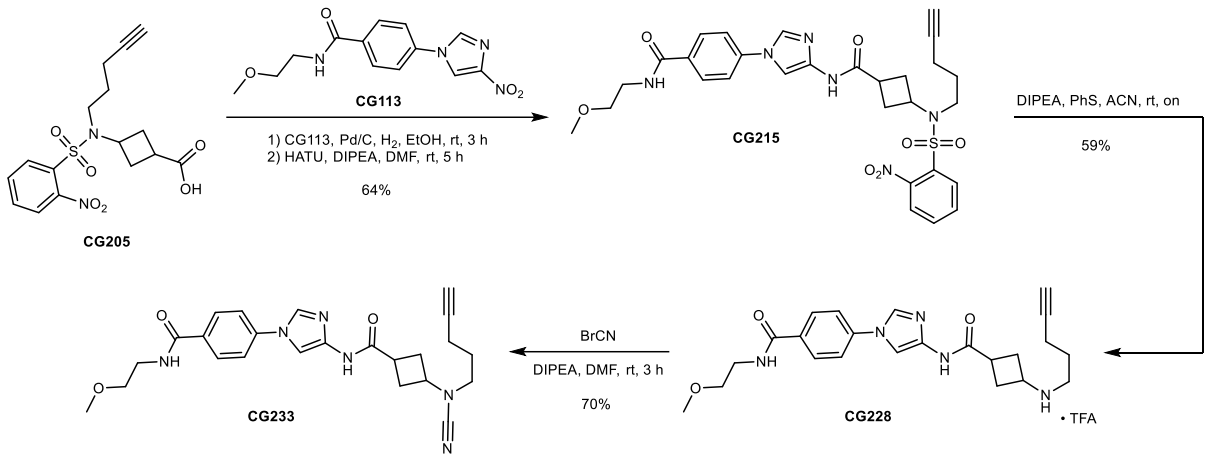

Scheme 37. Synthesis of CG233.

***N*-(2-Methoxyethyl)-4-(4-(3-((2-nitro-*N*-(pent-4-yn-1-yl)phenyl)sulfonamido)cyclobutane-1-carboxamido)-1*H*-imidazol-1-yl)benzamide (CG215)**

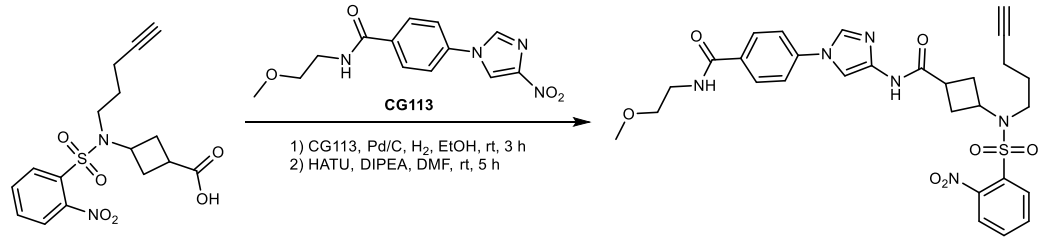

Step 1

CG113 (67.5 mg, 0.23 mmol, 1.2 eq) was dissolved in EtOH (10 mL) and palladium (10%) on activated charcoal (7 mg) was added under an argon atmosphere. The reaction was flushed with H_2 and stirred for 3 hours at room temperature. The reaction was filtered through celite545 which was then washed

with EA. The solvent was removed under reduced pressure and the obtained product used for the next reaction without further purification.

Step 2

CG184 (71.0 mg, 0.19 mol, 1.0 eq) was dissolved in DMF (2 mL), then DIPEA (98.9 µL, 0.58 mmol, 3.0 eq) and HATU (88.4 mg, 0.23 mmol, 1.2 eq) were added and the reaction mixture stirred for 20 minutes. The crude product from step 1 was dissolved in DMF (2 mL) and added to the reaction dropwise. The resulting solution was stirred for 5 h at room temperature. The reaction was quenched by the addition of aqueous sat. NH_4Cl (40 mL) and extracted with EA (2x30 mL). The combined organic layers were washed with brine (30 mL), dried over anhydrous $MgSO_4$, filtered and the solvent was removed under reduced pressure. The corresponding product was purified via a silica column eluting at 20-35% EA in PE, yielding CG215 (75.1 mg, 0.12 mmol, 64%) as a white solid and a mixture of *syn*- and *anti*-stereoisomers.

^{1}H NMR (600 MHz, DMSO-d_6) δ (ppm) = 10.52 (s, 1H), 8.61 (t, *J* = 5.4 Hz, 1H), 8.23 (dd, *J* = 3.7, 1.7 Hz, 1H), 8.03 – 7.96 (m, 4H), 7.90 (td, *J* = 7.7, 1.5 Hz, 1H), 7.88 – 7.84 (m, 1H), 7.80 (d, *J* = 1.7 Hz, 1H), 7.76 – 7.72 (m, 2H), 4.21 (tt, *J* = 9.7, 7.8 Hz, 1H), 3.47 (td, *J* = 5.4, 1.4 Hz, 2H), 3.44 (t, *J* = 5.4 Hz, 2H), 3.42 – 3.37 (m, 2H), 3.27 (s, 3H), 2.90 (tt, *J* = 9.3, 7.7 Hz, 1H), 2.83 (t, *J* = 2.6 Hz, 1H), 2.35 – 2.23 (m, 4H), 2.21 (td, *J* = 7.1, 2.6 Hz, 2H), 1.79 – 1.68 (m, 2H).

^{13}C NMR (151 MHz, DMSO-d_6) δ (ppm) = 169.90, 165.19, 147.63, 139.29, 138.77, 134.67, 132.59, 132.13, 132.02, 131.84, 129.66, 128.96, 124.35, 119.14, 104.03, 83.26, 71.87, 70.44, 57.93, 48.02, 43.83, 39.04, 31.81, 31.38, 29.49, 15.19.

HRMS m/z for $C_{29}H_{33}N_6O_7S^+$ ($[M+H]^+$) calculated: 609.2126, found: 609.2126.

N-(2-Methoxyethyl)-4-(4-(3-(pent-4-yn-1-ylamino)cyclobutane-1-carboxamido)-1*H*-imidazol-1-yl)benzamide TFA salt (CG228)

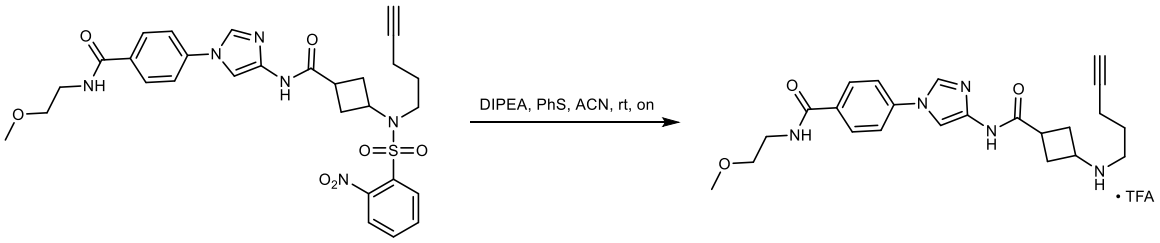

To a stirred solution of CG215 (72.0 mg, 0.12 mmol, 1.0 eq) in ACN (1 mL) was added DIPEA (80.5 µL, 0.47 mmol, 4.0 eq) and thiophenol (PhS, 362.0 µL, 3.55 mmol, 30.0 eq) and the mixture stirred at room temperature overnight. The reaction was quenched by the addition of H_2O (30 mL) and extracted with DCM (2x30 mL). To the aqueous phase was added 2M NaOH (30 mL), followed by extraction with EA (4x20 mL). The EA layers were combined, dried over anhydrous $MgSO_4$, filtered and the solvent was removed under reduced pressure. The corresponding product was purified via preparative HPLC, eluting at 5% ACN in H_2O. CG228 (37.5 mg, 0.07 mmol, 59%) was obtained as a white TFA salt and a mixture of *syn*- and *anti*-stereoisomers.

^{1}H NMR (700 MHz, DMSO-d_6) δ (ppm) = 10.58 (d, *J* = 6.7 Hz, 1H), 8.73 – 8.67 (m, 2H), 8.61 (t, *J* = 5.4 Hz, 1H), 8.25 (d, *J* = 1.6 Hz, 1H), 8.01 – 7.96 (m, 2H), 7.78 (d, *J* = 1.6 Hz, 1H), 7.76 – 7.70 (m, 2H), 3.72 (p, *J* = 6.7 Hz, 1H), 3.47 (td, *J* = 5.3, 1.3 Hz, 2H), 3.44 (qd, *J* = 5.4, 1.3 Hz, 2H), 3.27 (s, 3H), 3.07 (tt, *J* = 9.6, 7.9 Hz, 1H), 2.92 (t, *J* = 2.7 Hz, 1H), 2.91 – 2.84 (m, 2H), 2.47 – 2.41 (m, 2H), 2.33 (td, *J* = 9.3, 2.7 Hz, 2H), 2.28 (td, *J* = 7.1, 2.9 Hz, 2H), 1.74 (p, *J* = 7.1 Hz, 2H).

^{13}C NMR (176 MHz, DMSO-d_6) δ (ppm) = 169.49, 165.17, 157.96 (q, *J* = 34.0 Hz), 139.25, 138.73, 132.27, 132.19, 128.99, 119.29, 116.32 (d, *J* = 296.0 Hz), 104.01, 82.91, 72.29, 70.44, 57.93, 47.06, 43.35, 39.04, 31.50, 29.22, 24.57, 15.09.

HRMS m/z for $C_{23}H_{30}N_5O_3^+$ ($[M+H]^+$) calculated: 424.2343, found: 424.2344.

_N_-(2-Methoxyethyl)-4-(4-(3-(_N_-(pent-4-yn-1-yl)cyanamido)cyclobutane-1-carboxamido)-1_H_-imidazol-1-yl)benzamide (CG233)

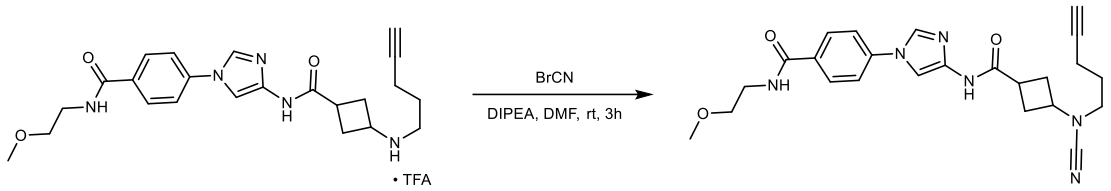

CG228 (25.0 mg, 0.05 mmol, 1.0 eq) was dissolved in DMF (1 mL) and DIPEA (31.6 mg, 0.19 mmol, 4.0 eq) was added. After stirring for 30 minutes at room temperature, 3 M cyanogen bromide solution (18.6 µL, 0.06 mmol, 1.2 eq) was added to the mixture, and stirring was continued for 3 h. The reaction was quenched by the addition of aqueous sat. $NaHCO_3$ (30 mL). The mixture was extracted with EA (2x30 mL). The combined organic layers were washed with brine (20 mL), dried over anhydrous $MgSO_4$, filtered and the solvent was removed under reduced pressure. The corresponding product was purified via a silica column, eluting at 4-8% MeOH in DCM, yielding CG233 (14.5 mg, 0.03 mmol, 70%) as a pale-yellow solid and a mixture of *syn*- and *anti*-stereoisomers.

^{1}H NMR (700 MHz, DMSO-d_6) δ (ppm) = 10.53 (s, 1H), 8.60 (t, *J* = 5.4 Hz, 1H), 8.23 (d, *J* = 1.6 Hz, 1H), 8.00 – 7.96 (m, 2H), 7.83 (d, *J* = 1.7 Hz, 1H), 7.77 – 7.73 (m, 2H), 3.60 (tt, *J* = 9.2, 7.3 Hz, 1H), 3.47 (td, *J* = 5.5, 1.3 Hz, 2H), 3.46 – 3.41 (m, 2H), 3.27 (s, 3H), 3.08 (dd, *J* = 7.7, 6.6 Hz, 2H), 2.92 (tt, *J* = 9.6, 7.6 Hz, 1H), 2.85 (t, *J* = 2.6 Hz, 1H), 2.40 (dtd, *J* = 8.5, 7.4, 2.7 Hz, 2H), 2.27 – 2.18 (m, 4H), 1.70 (p, *J* = 7.1 Hz, 2H).

^{13}C NMR (176 MHz, DMSO-d_6) δ (ppm) = 169.85, 165.20, 139.34, 138.78, 132.15, 131.99, 128.97, 119.14, 115.47, 104.05, 83.16, 71.94, 70.43, 57.92, 49.73, 48.62, 39.03, 31.52, 30.37, 26.53, 14.85.

HRMS m/z for $C_{24}H_{29}N_6O_3^+$ ([M+H]$^+$) calculated: 449.2296, found: 449.2300.

Synthesis of CG238SYN & CG238ANTI

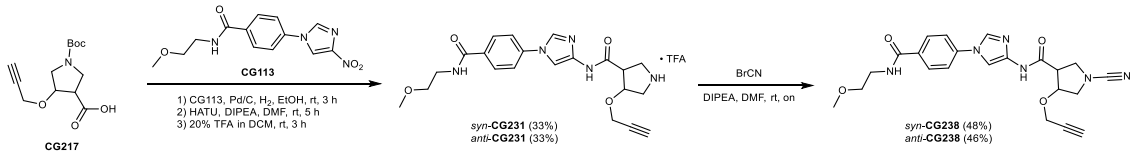

Scheme 38. Synthesis of CG238SYN & CG238ANTI.

***syn-lanti*-1-Cyano-*N*-(1-(4-((2-methoxyethyl)carbamoyl)phenyl)-1*H*-imidazol-4-yl)-4-(prop-2-yn-1-yloxy)pyrrolidine-3-carboxamide TFA salt (*syn-lanti*-CG231)**

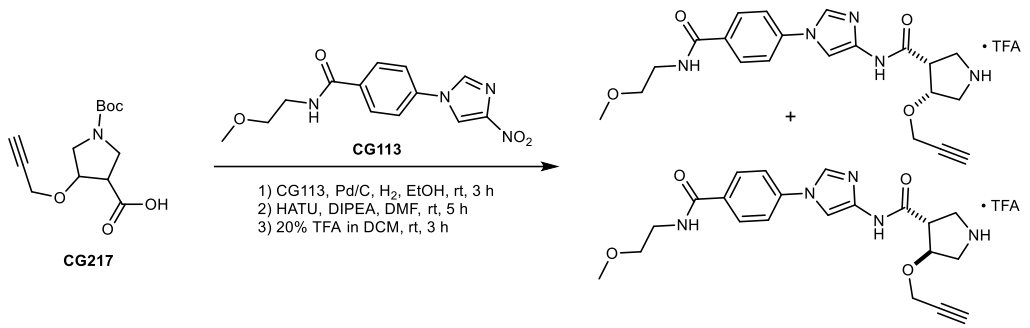

Step 1

CG113 (36.2 mg, 0.12 mmol, 1.2 eq) was dissolved in EtOH (10 mL) and palladium (10%) on activated charcoal (4 mg) was added under an argon atmosphere. The reaction was flushed with H_2 and stirred

for 3 hours at room temperature. The reaction was filtered through celite545 which was then washed with EA. The solvent was removed under reduced pressure and the obtained product used for the next reaction without further purification.

Step 2

CG217 (28.0 mg, 0.10 mol, 1.0 eq) was dissolved in DMF (2 mL), then DIPEA (35.4 µL, 0.21 mmol, 2.0 eq) and HATU (47.4 mg, 0.12 mmol, 1.2 eq) were added and the reaction mixture stirred for 20 minutes. The crude product from step 1 was dissolved in DMF (2 mL) and added to the reaction dropwise. The resulting solution was stirred for 5 h at room temperature. The reaction was quenched by the addition of aqueous sat. NH_4Cl (40 mL) and the mixture extracted with EA (2x30 mL). The combined organic layers were washed with brine (30 mL), dried over anhydrous $MgSO_4$, filtered and the solvent was removed under reduced pressure. The corresponding product was used for the next reaction without further purification.

Step 3

The crude product from step 2 was dissolved in DCM (2 mL) and TFA (0.4 mL) was added dropwise. The mixture was stirred for 3 h at room temperature. The solvent and residual TFA were removed under reduced pressure. The product was dried in vacuo and subsequently purified by preparative HPLC eluting at 15-18% ACN in H_2O. CG231 was eluting in 2 peaks, as judged by LC-MS, which could both be separated, yielding *syn*-CG231 (17.9 mg, 0.03 mmol, 33%) and *anti*-CG231 (18.2 mg, 0.03 mmol, 33%) as a TFA salt.

syn-CG231

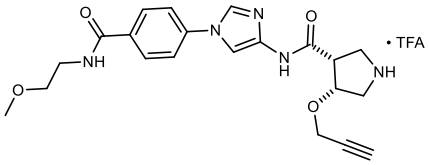

^{1}H NMR (700 MHz, DMSO-d_6) δ (ppm) = 10.82 (s, 1H), 9.07 (dd, *J* = 146.6, 36.2 Hz, 2H), 8.61 (t, *J* = 5.4 Hz, 1H), 8.26 (d, *J* = 1.6 Hz, 1H), 7.99 (d, *J* = 8.7 Hz, 2H), 7.76 (d, *J* = 1.7 Hz, 1H), 7.75 (d, *J* = 8.7 Hz, 2H), 4.70 (q, *J* = 2.3 Hz, 1H), 4.26 – 4.16 (m, 2H), 3.60 (dtd, *J* = 11.6, 7.7, 4.6 Hz, 1H), 3.50 (t, *J* = 2.4 Hz, 1H), 3.49 – 3.48 (m, 1H), 3.48 – 3.46 (m, 2H), 3.44 (t, *J* = 5.5 Hz, 2H), 3.46 – 3.42 (m, 1H), 3.41 – 3.40 (m, 1H), 3.30 (tt, *J* = 6.9, 4.7, 3.7 Hz, 1H), 3.27 (s, 3H).

^{13}C NMR (176 MHz, DMSO-d_6) δ (ppm) = 165.17, 164.49, 157.97 (q, *J* = 34.4 Hz), 139.10, 138.71, 132.26, 132.15, 128.98, 119.26, 116.17 (d, *J* = 294.9 Hz), 104.03, 79.56, 78.02, 77.23, 70.44, 57.92, 56.61, 49.06, 47.22, 44.45, 39.03.

HRMS m/z for $C_{21}H_{26}N_5O_4^+$ ($[M+H]^+$) calculated: 412.1979, found: 412.1980.

anti-CG231

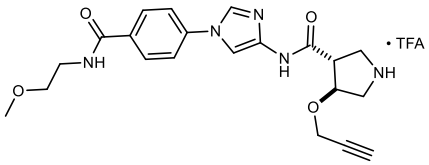

^{1}H NMR (700 MHz, DMSO-d_6) δ (ppm) = 11.10 (s, 1H), 9.32 – 9.20 (m, 2H), 8.61 (t, *J* = 5.4 Hz, 1H), 8.28 (d, *J* = 1.6 Hz, 1H), 7.99 (d, *J* = 8.7 Hz, 2H), 7.77 (d, *J* = 1.6 Hz, 1H), 7.74 (d, *J* = 8.7 Hz, 2H), 4.46 (dd, *J* = 4.2, 2.1 Hz, 1H), 4.34 (dd, *J* = 2.4, 1.1 Hz, 2H), 3.55 (t, *J* = 2.4 Hz, 1H), 3.53 – 3.48 (m, 1H), 3.48 – 3.45 (m, 2H), 3.48 – 3.41 (m, 2H), 3.44 (t, *J* = 5.4 Hz, 2H), 3.41 – 3.35 (m, 1H), 3.31 (ddd, *J* = 12.5, 7.4, 4.8 Hz, 1H), 3.27 (s, 3H).

^{13}C NMR (176 MHz, DMSO-d_6) δ (ppm) = 167.37, 165.14, 157.95 (q, *J* = 34.3 Hz), 138.83, 138.65, 132.38, 132.33, 129.01, 119.35, 116.24 (d, *J* = 295.0 Hz), 104.43, 79.70, 79.64, 77.94, 70.43, 57.92, 56.21, 49.56, 48.14, 46.12, 39.04.

HRMS m/z for $C_{21}H_{26}N_5O_4^+$ ([M+H]$^+$) calculated: 412.1979, found: 412.1985.

syn-1-Cyano-*N*-(1-(4-((2-methoxyethyl)carbamoyl)phenyl)-1*H*-imidazol-4-yl)-4-(prop-2-yn-1-yloxy)pyrrolidine-3-carboxamide (CG238-SYN)

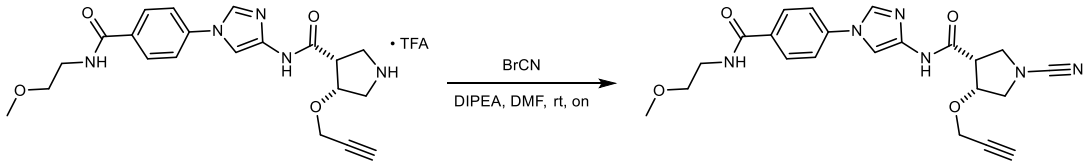

syn-CG231 (15.9 mg, 0.03 mmol, 1.0 eq) was dissolved in DMF (1 mL) and K_2CO_3 (16.7 mg, 0.12 mmol, 4.0 eq) was added. After stirring for 30 minutes at room temperature, 3 M cyanogen bromide solution (12.1 µL, 0.04 mmol, 1.2 eq) was added to the mixture, and stirring was continued overnight. The reaction was quenched by the addition of aqueous sat. $NaHCO_3$ (30 mL). The mixture was extracted with EA (2x30 mL). The combined organic layers were washed with brine (20 mL), dried over anhydrous $MgSO_4$, filtered and the solvent was removed under reduced pressure. The corresponding product was purified via a silica column, eluting at 6-8% MeOH in DCM, yielding CG238-SYN (6.3 mg, 0.01 mmol, 48%) as a pale-yellow solid.

^{1}H NMR (600 MHz, $CDCl_3$) δ (ppm) = 8.93 (s, 1H), 7.91 (d, *J* = 8.4 Hz, 2H), 7.78 (d, *J* = 1.7 Hz, 1H), 7.71 (d, *J* = 1.6 Hz, 1H), 7.48 (d, *J* = 8.5 Hz, 2H), 6.56 (t, *J* = 5.5 Hz, 1H), 4.61 (td, *J* = 4.7, 3.0 Hz, 1H), 4.35 (dd, *J* = 16.4, 2.4 Hz, 1H), 4.22 (dd, *J* = 16.3, 2.4 Hz, 1H), 3.96 (t, *J* = 9.1 Hz, 1H), 3.76 (dd, *J* = 9.4, 8.0 Hz, 1H), 3.72 – 3.62 (m, 4H), 3.59 (t, *J* = 5.0 Hz, 2H), 3.41 (s, 3H), 3.27 (td, *J* = 8.4, 5.0 Hz, 1H), 2.56 (t, *J* = 2.4 Hz, 1H).

^{13}C NMR (151 MHz, $CDCl_3$) δ (ppm) = 166.22, 164.79, 139.41, 138.50, 133.66, 131.19, 129.10, 120.71, 116.73, 106.10, 78.47, 76.90, 76.63, 71.20, 59.03, 57.59, 54.40, 50.70, 49.08, 39.98.

HRMS m/z for $C_{22}H_{25}N_6O_4^+$ ([M+H]$^+$) calculated: 437.1932, found: 437.1931.

anti-1-Cyano-*N*-(1-(4-((2-methoxyethyl)carbamoyl)phenyl)-1*H*-imidazol-4-yl)-4-(prop-2-yn-1-yloxy)pyrrolidine-3-carboxamide (CG238-ANTI)

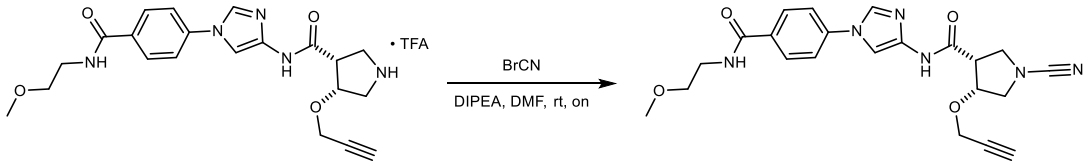

anti-CG238 was obtained from *anti*-CG231 (16.2 mg, 0.03 mmol, 1.0 eq) as described above for *syn*-CG231. The product was eluting at 6-8% MeOH in DCM, yielding CG238-ANTI (6.2 mg, 0.01 mmol, 46%) as a pale-yellow solid.

^{1}H NMR (700 MHz, $CDCl_3$) δ (ppm) = 9.48 (s, 1H), 7.92 (d, *J* = 8.5 Hz, 2H), 7.78 (d, *J* = 1.6 Hz, 1H), 7.76 (d, *J* = 1.7 Hz, 1H), 7.49 (d, *J* = 8.6 Hz, 2H), 6.56 (s, 1H), 4.51 (q, *J* = 5.0 Hz, 1H), 4.28 (dd, *J* = 16.1, 2.4 Hz, 1H), 4.22 (dd, *J* = 16.1, 2.4 Hz, 1H), 3.83 – 3.75 (m, 3H), 3.68 (q, *J* = 5.2 Hz, 2H), 3.59 (t, *J* = 5.1 Hz, 2H), 3.53 (dd, *J* = 10.4, 4.3 Hz, 1H), 3.41 (s, 3H), 3.24 (dt, *J* = 7.9, 6.2 Hz, 1H), 2.50 (t, *J* = 2.4 Hz, 1H).

^{13}C NMR (176 MHz, $CDCl_3$) δ (ppm) = 166.77, 166.18, 139.35, 138.60, 133.80, 131.40, 129.14, 120.78, 116.62, 106.21, 80.00, 78.63, 76.31, 71.20, 59.04, 57.80, 54.66, 51.00, 50.41, 39.99.

HRMS m/z for $C_{22}H_{25}N_6O_4^+$ ([M+H]$^+$) calculated: 437.1932, found: 437.1931.

Synthesis of CG239

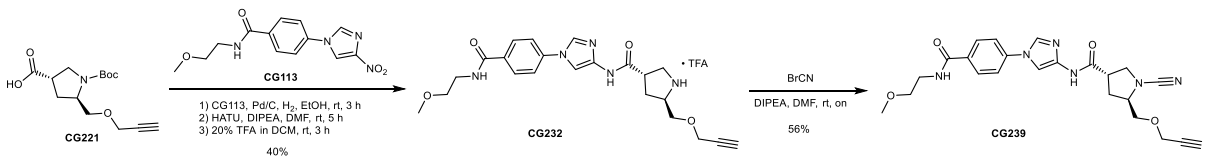

Scheme 39. Synthesis of CG239.

(3*S*,5*R*)-*N*-(1-(4-((2-Methoxyethyl)carbamoyl)phenyl)-1*H*-imidazol-4-yl)-5-((prop-2-yn-1-yloxy)methyl)pyrrolidine-3-carboxamide TFA salt (CG232)

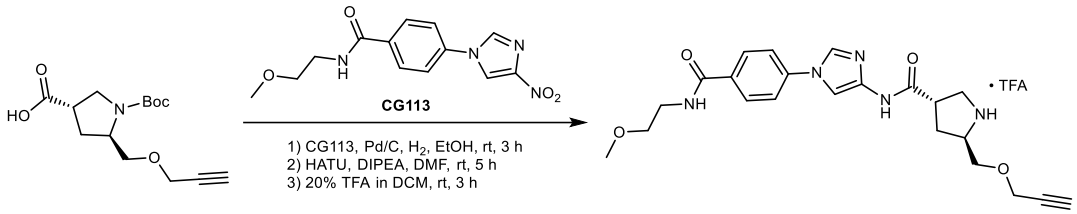

CG232 was obtained from CG221 (30.0 mg, 0.11 mmol, 1.0 eq) as described above for CG231. The product was eluting at 10-35% ACN in H_2O in DCM, yielding CG232 (22.6 mg, 0.04 mmol, 40%) as a white TFA salt.

^{1}H NMR (600 MHz, DMSO-d_6) δ (ppm) = 10.86 (s, 1H), 9.49 – 8.89 (m, 2H), 8.63 (t, *J* = 5.4 Hz, 1H), 8.28 (d, *J* = 1.6 Hz, 1H), 7.99 (d, *J* = 8.7 Hz, 2H), 7.78 (d, *J* = 1.6 Hz, 1H), 7.74 (d, *J* = 8.7 Hz, 2H), 4.25 (dd, *J* = 2.4, 1.6 Hz, 2H), 3.82 (q, *J* = 11.2, 10.3 Hz, 1H), 3.72 (dd, *J* = 10.5, 3.9 Hz, 1H), 3.60 (dd, *J* = 10.5, 7.9 Hz, 1H), 3.57 (t, *J* = 2.4 Hz, 1H), 3.48 (d, *J* = 1.8 Hz, 1H), 3.47 – 3.45 (m, 2H), 3.44 (t, *J* = 5.3 Hz, 2H), 3.43 – 3.38 (m, 1H), 3.35 (dq, *J* = 12.3, 6.2 Hz, 1H), 3.27 (s, 3H), 2.20 (ddd, *J* = 12.8, 7.8, 4.8 Hz, 1H), 2.07 – 1.93 (m, 1H).

^{13}C NMR (151 MHz, DMSO-d_6) δ (ppm) = 169.07, 165.16, 138.95, 138.67, 132.33, 132.26, 129.01, 119.31, 104.26, 79.68, 78.03, 70.44, 67.89, 58.19, 57.99, 57.93, 47.20, 41.30, 39.05, 31.00.

HRMS m/z for $C_{22}H_{28}N_5O_4^+$ ([M+H]$^+$) calculated: 426.2136, found: 426.2135.

(3*S*,5*R*)-1-Cyano-*N*-(1-(4-((2-methoxyethyl)carbamoyl)phenyl)-1*H*-imidazol-4-yl)-5-((prop-2-yn-1-yloxy)methyl)pyrrolidine-3-carboxamide (CG239)

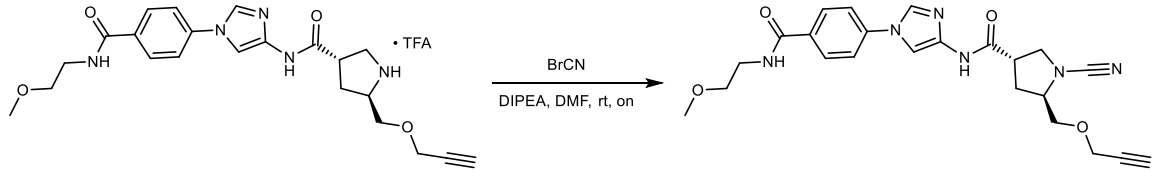

CG239 was obtained from CG232 (20.0 mg, 0.04 mmol, 1.0 eq) as described above for *syn*-CG231. The product was eluting at 4-6% MeOH in DCM, yielding CG239 (9.3 mg, 0.02 mmol, 56%) as a pale-yellow solid.

^{1}H NMR (700 MHz, $CDCl_3$) δ (ppm) = 10.26 (s, 1H), 7.93 (d, *J* = 8.0 Hz, 2H), 7.81 (s, 1H), 7.78 (s, 1H), 7.51 (d, *J* = 8.2 Hz, 2H), 6.61 (d, *J* = 5.3 Hz, 1H), 4.22 – 4.11 (m, 2H), 4.01 (dd, *J* = 8.5, 4.1 Hz, 1H), 3.78 (t, *J* = 8.5 Hz, 1H), 3.74 (td, *J* = 7.2, 6.6, 3.4 Hz, 2H), 3.67 (tt, *J* = 10.4, 4.1 Hz, 3H), 3.59 (t, *J* = 5.1

Hz, 2H), 3.41 (s, 3H), 3.36 (q, *J* = 8.2 Hz, 1H), 2.51 – 2.40 (m, 2H), 2.24 (ddd, *J* = 12.4, 7.6, 3.7 Hz, 1H).

^{13}C NMR (176 MHz, $CDCl_3$) δ (ppm) = 168.63, 166.20, 139.33, 139.00, 133.83, 131.13, 129.17, 120.86, 115.92, 106.33, 79.02, 75.59, 71.19, 70.38, 61.06, 59.02, 58.97, 53.79, 43.86, 39.98, 32.36.

HRMS m/z for $C_{22}H_{28}N_5O_4^+$ ([M+H]$^+$) calculated: 426.2136, found: 426.2135.

9.2.4 CG306 Binding Element Improvement

Synthesis of CG338

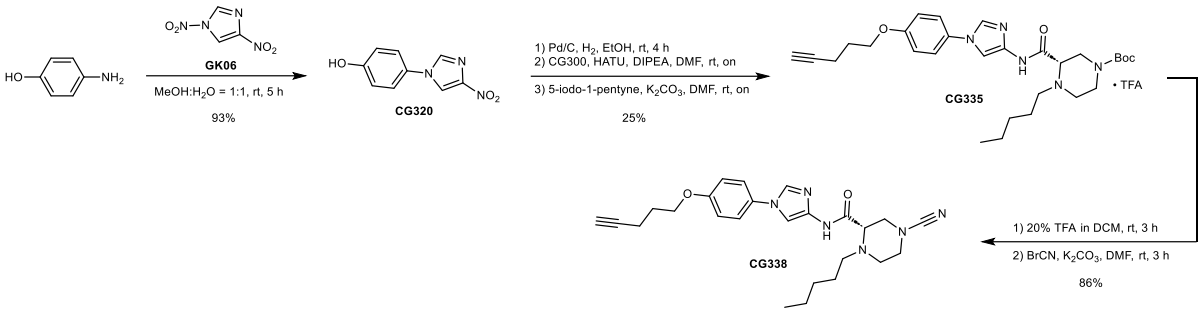

Scheme 40. Synthesis of CG338.

4-(4-Nitro-1*H*-imidazol-1-yl)phenol (CG320)

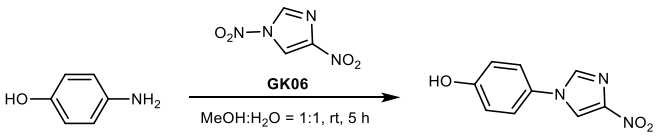

GK06 (500.0 mg, 3.16 mmol, 1.0 eq) was dissolved in a 1:1 mixture of MeOH and H_2O (30 mL). 4-Aminophenol (379.7 mg, 3.48 mmol, 1.1 eq) was added and the reaction mixture was stirred for 5 h at room temperature in darkness. The precipitated product was filtered, washed with H_2O (50 mL) and dried at 60 °C in a drying oven. CG320 (601.3 mg, 2.93 mmol, 93%) was obtained as a yellow solid.

^{1}H NMR (600 MHz, DMSO-d_6) δ (ppm) = 9.94 (d, *J* = 1.3 Hz, 1H), 8.83 (d, *J* = 1.5 Hz, 1H), 8.30 (d, *J* = 1.5 Hz, 1H), 7.56 (dd, *J* = 8.7, 1.4 Hz, 2H), 6.91 (dd, *J* = 8.7, 1.4 Hz, 2H).

^{13}C NMR (151 MHz, DMSO) δ (ppm) = 157.73, 147.75, 135.65, 127.33, 123.18, 119.95, 116.09.

HRMS *m/z* for $C_9H_8N_3O_3^+$ ([M+H]$^+$) calculated: 206.0560, found: 206.0564.

tert-Butyl (*S*)-3-((1-(4-(pent-4-yn-1-yloxy)phenyl)-1*H*-imidazol-4-yl)carbamoyl)-4-pentyl-piperazine-1-carboxylate TFA salt (CG335)

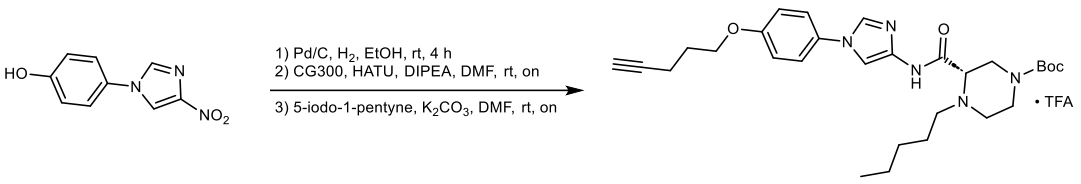

Step 1

CG320 (59.5 mg, 0.29 mmol, 1.2 eq) was dissolved in EtOH (20 mL) and palladium (10%) on activated charcoal (25 mg) was added under an argon atmosphere. The reaction was flushed with H_2 and stirred

for 4 h at room temperature. The reaction was filtered through Celite 545 which was then washed with EA (30 mL). The solvent was removed under reduced pressure and the obtained product used for the next reaction without further purification.

Step 2

CG300 (74.0 mg, 0.24 mol, 1.0 eq) was dissolved in DMF (2 mL), then DIPEA (123.2 µL, 0.72 mmol, 3.0 eq) and HATU (110.2 mg, 0.29 mmol, 1.2 eq) were added and the reaction mixture stirred for 10 min. The crude product from step 1 was dissolved in DMF (2 mL) and added to the reaction dropwise. The resulting solution was stirred overnight at room temperature. The reaction was quenched by the addition of aqueous sat. NH_4Cl (40 mL) and the mixture extracted with EA (2x30 mL). The combined organic layers were washed with brine (30 mL), dried over anhydrous $MgSO_4$, filtered and the solvent was removed under reduced pressure. Partial purification was achieved by preparative HPLC during which the desired product *tert*-butyl (*S*)-3-((1-(4-hydroxyphenyl)-1*H*-imidazol-4-yl)carbamoyl)-4-pentylpiperazine-1-carboxylate TFA salt (80.0 mg, 0.14 mmol) co-eluted with uncharacterised impurities. Fractions containing the desired product as judged by LC-MS and TLC were combined, frozen, lyophilised and used for the next reaction without further purification.

Step 3

The crude product from step 2 was dissolved in DMF (2 mL). 5-Iodo-1-pentyne (17.1 µL, 0.15 mmol, 1.2 eq) and K_2CO_3 (84.6 mg, 0.61 mmol, 5.0 eq) were added and the reaction stirred at room temperature overnight. The reaction was quenched by the addition of aqueous sat. $NaHCO_3$ (40 mL). The mixture was extracted with EA (2x30 mL). The combined organic layers were washed with brine (30 mL), dried over anhydrous $MgSO_4$, filtered and the solvent was removed under reduced pressure. The corresponding product was purified via preparative HPLC, eluting at 20-30% ACN in H_2O, yielding CG335 (38.0 mg, 0.06 mmol, 25%) as a white TFA salt.

^{1}H NMR (600 MHz, DMSO-d_6) δ (ppm) = 10.18 (s, 1H), 8.05 (s, 1H), 7.65 (s, 1H), 7.53 (d, *J* = 8.3 Hz, 2H), 7.13 – 7.04 (m, 2H), 4.08 (t, *J* = 6.2 Hz, 2H), 3.57 (s, 1H), 3.40 (br s, 5H), 3.25 (s, 1H), 3.10 (br s, 2H), 2.83 (t, *J* = 2.6 Hz, 1H), 2.35 (td, *J* = 7.1, 2.7 Hz, 2H), 1.94 – 1.85 (m, 2H), 1.62 (br s, 2H), 1.42 (s, 9H), 1.34 – 1.22 (m, 4H), 0.85 (t, *J* = 7.0 Hz, 3H).

^{13}C NMR (151 MHz, DMSO-d_6) δ (ppm) = 167.13, 158.02, 151.44, 138.85, 131.58, 130.12, 122.16, 115.50, 106.11, 83.59, 77.53, 71.69, 66.35, 63.71, 54.77, 46.45, 45.47, 44.52, 27.88, 27.84, 27.62, 25.40, 21.63, 14.44, 13.67.

HRMS *m/z* for $C_{29}H_{42}N_5O_4^+$ ([M+H]$^+$) calculated: 524.3231, found: 524.3243.

(*S*)-4-Cyano-*N*-(1-(4-(pent-4-yn-1-yloxy)phenyl)-1*H*-imidazol-4-yl)-1-pentylpiperazine-2-carboxamide (CG338)

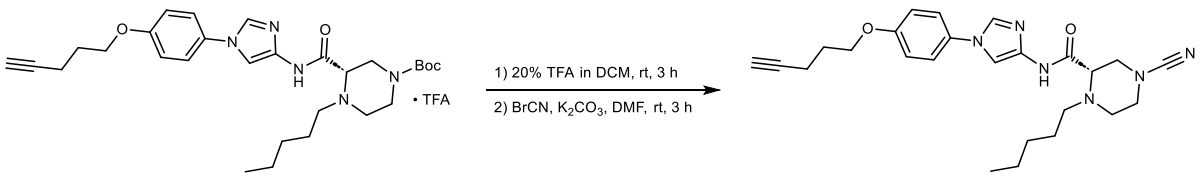

Step 1

CG335 (25.0 mg, 0.04 mmol, 1.0 eq) was dissolved in DCM (2 mL) and TFA (0.4 mL) was added dropwise. The solution was stirred for 3 h at room temperature. The solvent and residual TFA were removed under reduced pressure and the product dried in vacuo.

Step 2

The crude product from step 1 was dissolved in DMF (2 mL) and K_2CO_3 (21.7 mg, 0.16 mmol, 4.0 eq) was added. 3 M cyanogen bromide solution (19.6 µL, 0.06 mmol, 1.5 eq) was added and the mixture was stirred for 3 h at room temperature. The reaction was quenched by the addition of aqueous sat. $NaHCO_3$ (50 mL). The mixture was extracted with EA (2x30 mL). The combined organic layers were washed with brine (30 mL), dried over anhydrous $MgSO_4$, filtered and the solvent was removed under reduced pressure. The corresponding product was purified via a silica column, eluting at 100% DCM. The solvent was removed under reduced pressure. The oily residue was re-dissolved in ACN (1 mL), a few drops of water were added and the resulting solution frozen and lyophilised, yielding CG338 (15.1 mg, 0.03 mmol, 86%) as a white powder.

^{1}H NMR (600 MHz, DMSO-d_6) δ (ppm) = 10.42 (s, 1H), 7.99 (d, *J* = 1.6 Hz, 1H), 7.62 (d, *J* = 1.6 Hz, 1H), 7.57 – 7.46 (m, 2H), 7.13 – 6.99 (m, 2H), 4.08 (t, *J* = 6.2 Hz, 2H), 3.38 (q, *J* = 8.0 Hz, 1H), 3.32 – 3.26 (m, 3H), 3.20 (ddd, *J* = 12.5, 8.7, 3.1 Hz, 1H), 3.14 – 3.03 (m, 1H), 2.83 (t, *J* = 2.6 Hz, 1H), 2.54 – 2.47 (m, 1H), 2.34 (td, *J* = 7.1, 2.7 Hz, 2H), 2.34 – 2.24 (m, 2H), 1.94 – 1.87 (m, 2H), 1.51 – 1.37 (m, 2H), 1.33 – 1.12 (m, 4H), 0.83 (t, *J* = 7.1 Hz, 3H).

^{13}C NMR (151 MHz, DMSO-d_6) δ (ppm) = 166.80, 157.26, 138.20, 131.89, 130.27, 121.88, 117.28, 115.45, 105.17, 83.61, 71.69, 66.32, 62.42, 54.25, 49.88, 47.90, 47.65, 28.87, 27.65, 25.57, 21.97, 14.45, 13.90.

HRMS *m/z* for $C_{25}H_{33}N_6O_2^+$ ([M+H]$^+$) calculated: 449.2660, found: 449.2664.

Synthesis of CG340

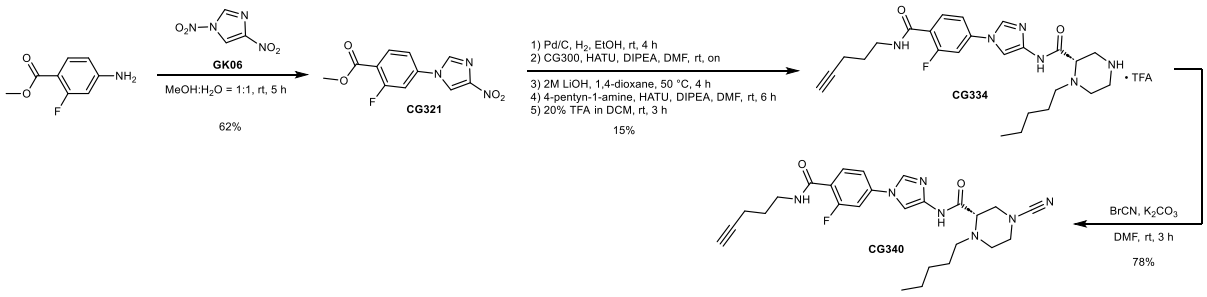

Scheme 41. Synthesis of CG340.

Methyl 2-fluoro-4-(4-nitro-1*H*-imidazol-1-yl)benzoate (CG321)

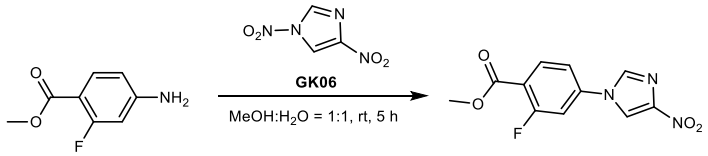

GK06 (400.0 mg, 2.53 mmol, 1.0 eq) was dissolved in a 1:1 mixture of MeOH and H_2O (40 mL). Methyl 4-amino-2-fluorobenzoate (470.8 mg, 2.78 mmol, 1.1 eq) was added and the reaction mixture was at 80 °C in darkness overnight. The reaction was allowed to cool down to room temperature and the precipitate was filtered and washed with H_2O. CG321 (416.5 mg, 1.57 mmol, 62%) was obtained as a red solid

^{1}H NMR (600 MHz, DMSO-d_6) δ (ppm) = 9.16 (d, *J* = 2.9 Hz, 1H), 8.65 (d, *J* = 2.9 Hz, 1H), 8.10 – 8.02 (m, 2H), 7.86 (dd, *J* = 8.5, 2.3 Hz, 1H), 3.90 – 3.84 (m, 3H).

^{13}C NMR (151 MHz, DMSO-d_6) δ (ppm) = 163.10, 161.37 (d, *J* = 258.6 Hz), 148.33, 140.02 (d, *J* = 10.9 Hz), 135.80, 133.35, 119.53, 117.53 (d, *J* = 10.4 Hz), 116.68 (d, *J* = 3.6 Hz), 109.99 (d, *J* = 27.6 Hz), 52.61.

HRMS *m/z* for $C_{11}H_9N_3O_4F^+$ ([M+H]$^+$) calculated: 266.0572, found: 266.0574.

(*S*)-*N*-(1-(3-Fluoro-4-(pent-4-yn-1-ylcarbamoyl)phenyl)-1H-imidazol-4-yl)-1-pentylpiperazine-2-carboxamide TFA salt (CG334)

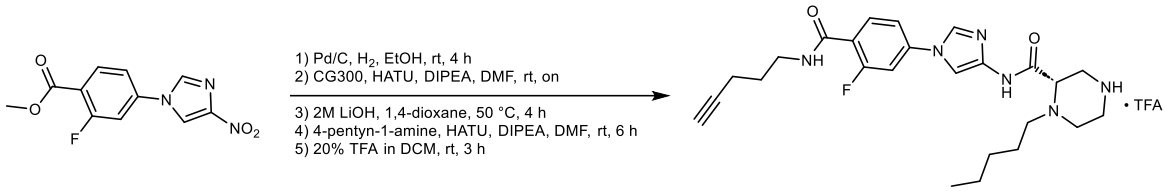

Step 1

CG321 (46.1 mg, 0.17 mmol, 1.2 eq) was dissolved in EtOH (20 mL) and palladium (10%) on activated charcoal (20 mg) was added under an argon atmosphere. The reaction was flushed with H_2 and stirred for 4 h at room temperature. The reaction was filtered through Celite 545 which was then washed with EA (30 mL). The solvent was removed under reduced pressure and the obtained product used for the next reaction without further purification.

Step 2

CG300 (44.4 mg, 0.14 mol, 1.0 eq) was dissolved in DMF (2 mL), then DIPEA (73.9 µL, 0.43 mmol, 3.0 eq) and HATU (66.1 mg, 0.17 mmol, 1.2 eq) were added and the reaction mixture stirred for 10 min at room temperature. The crude product from step 1 was dissolved in DMF (2 mL) and added to the reaction dropwise. The resulting solution was stirred overnight at room temperature. The reaction was quenched by the addition of aqueous sat. NH_4Cl (40 mL) and the mixture extracted with EA (2x30 mL). The combined organic layers were washed with brine (30 mL), dried over anhydrous $MgSO_4$, filtered and the solvent was removed under reduced pressure. Partial purification was achieved by preparative HPLC during which the desired product *tert*-butyl (*S*)-3-((1-(3-fluoro-4-(methoxycarbonyl)phenyl)-1*H*-imidazol-4-yl)carbamoyl)-4-pentylpiperazine-1-carboxylate TFA salt (28.4 mg, 0.04 mmol) co-eluted with uncharacterised impurities. Fractions containing the desired product as judged by LC-MS and TLC were combined, frozen, lyophilised and used for the next reaction without further purification.

Step 3

The crude product from step 2 was dissolved in 1,4-dioxane (2 mL). Aqueous 2M LiOH solution (41.6 µL, 0.08 mol, 2.1 eq) was added and the reaction mixture was stirred for 4 h at 50 °C. The pH of the reaction mixture was adjusted to pH 7 by adding aqueous 1 M HCl dropwise. The solvent was removed under reduced pressure and the obtained product used for the next reaction without further purification.

Step 4

The crude product from step 3 was dissolved in DMF (2 mL), then DIPEA (26.9 µL, 0.16 mmol, 4.0 eq) and HATU (19.6 mg, 0.05 mmol, 1.3 eq) were added and the reaction mixture was stirred for 10 min at room temperature. 4-Pentyn-1-amine HCl (14.2 mg, 0.12 mmol, 3.0 eq) was dissolved in DMF (2 mL), added to the reaction and the mixture stirred for 6 h at room temperature. The reaction mixture was quenched with sat. NH_4Cl solution (30 mL) and extracted with EA (2x30 mL). The combined organic layers were washed with brine (20 mL), dried over $MgSO_4$, filtered and the solvent was removed under reduced pressure. The crude product was directly used for the next step.

Step 5

The crude product from step 4 was dissolved in DCM (2 mL) and TFA (0.4 mL) was added dropwise. The solution was stirred for 3 h at room temperature. The solvent and residual TFA were removed under reduced pressure and the product dried in vacuo. The product was purified via preparative HPLC eluting at 18-24% ACN in H_2O, yielding CG334 (12.6 mg, 0.02 mmol, 15%) as a white TFA salt.

^{1}H NMR (600 MHz, DMSO-d_6) δ (ppm) = 10.84 (s, 1H), 8.85 (s, 1H), 8.55 (s, 1H), 8.40 (td, *J* = 5.8, 1.9 Hz, 1H), 8.33 (d, *J* = 1.7 Hz, 1H), 7.85 (d, *J* = 1.6 Hz, 1H), 7.76 (dd, *J* = 11.6, 2.2 Hz, 1H), 7.73 (t, *J* = 8.2 Hz, 1H), 7.58 (dd, *J* = 8.4, 2.2 Hz, 1H), 3.52 (t, *J* = 5.8 Hz, 1H), 3.32 (q, *J* = 6.6 Hz, 2H), 3.30 – 3.23 (m, 2H), 3.22 – 3.08 (m, 3H), 2.81 (t, *J* = 2.7 Hz, 1H), 2.56 (q, *J* = 9.1, 7.5 Hz, 1H), 2.48 – 2.41 (m, 2H), 2.23 (td, *J* = 7.2, 2.7 Hz, 2H), 1.70 (p, *J* = 7.1 Hz, 2H), 1.54 – 1.38 (m, 2H), 1.33 – 1.10 (m, 4H), 0.84 (t, *J* = 7.1 Hz, 3H).

^{13}C NMR (151 MHz, DMSO-d_6) δ (ppm) = 166.43, 160.88 (d, *J* = 606.5 Hz), 160.52, 157.94 (q, *J* = 33.1 Hz), 139.22 (d, *J* = 10.7 Hz), 138.47, 132.70, 131.63 (d, *J* = 4.3 Hz), 122.05 (d, *J* = 14.8 Hz), 115.29 (d, *J* = 3.2 Hz), 107.68 (d, *J* = 27.5 Hz), 104.69, 84.00, 71.46, 60.21, 53.99, 45.40, 43.90, 42.37, 38.40, 28.75, 27.92, 25.46, 21.91, 15.43, 13.89.

HRMS *m/z* for $C_{25}H_{34}N_6O_2^+$ ([M+H]$^+$) calculated: 469.2722, found: 469.2726.

(*S*)-4-Cyano-*N*-(1-(3-fluoro-4-(pent-4-yn-1-ylcarbamoyl)phenyl)-1*H*-imidazol-4-yl)-1-pentylpiperazine-2-carboxamide (CG340)

CG334 (10.0 mg, 0.02 mmol, 1.0 eq) was dissolved in DMF (2 mL) and K_2CO_3 (9.5 mg, 0.07 mmol, 4.0 eq) was added. 3 M cyanogen bromide solution (8.6 µL, 0.03 mmol, 1.5 eq) was added and the mixture was stirred for 3 h at room temperature. The reaction was quenched by the addition of aqueous sat. $NaHCO_3$ (30 mL). The mixture was extracted with EA (2x20 mL). The combined organic layers were washed with brine (20 mL), dried over anhydrous $MgSO_4$, filtered and the solvent was removed under reduced pressure. The corresponding product was purified via a silica column, eluting at 70-100% EA in PE. The solvent was removed under reduced pressure, yielding CG340 (6.6 mg, 0.01 mmol, 78%) as a yellow resin.

^{1}H NMR (700 MHz, DMSO-d_6) δ (ppm) = 10.52 (s, 1H), 8.39 (td, *J* = 5.6, 2.0 Hz, 1H), 8.31 (d, *J* = 1.7 Hz, 1H), 7.86 (d, *J* = 1.6 Hz, 1H), 7.77 (dd, *J* = 11.6, 2.2 Hz, 1H), 7.71 (t, *J* = 8.2 Hz, 1H), 7.61 (dd, *J* = 8.4, 2.2 Hz, 1H), 3.43 – 3.38 (m, 1H), 3.36 – 3.28 (m, 5H), 3.26 – 3.19 (m, 1H), 3.16 – 3.09 (m, 1H), 2.80 (t, *J* = 2.6 Hz, 1H), 2.54 – 2.50 (m, 1H), 2.37 – 2.29 (m, 2H), 2.23 (td, *J* = 7.2, 2.7 Hz, 2H), 1.70 (p, *J* = 7.2 Hz, 2H), 1.51 – 1.36 (m, 2H), 1.36 – 1.13 (m, 4H), 0.84 (t, *J* = 7.1 Hz, 3H).

^{13}C NMR (176 MHz, DMSO-d_6) δ (ppm) = 162.92, 160.95 (d, *J* = 690.5 Hz), 160.41, 139.25, 137.95, 132.50, 131.53 (d, *J* = 4.6 Hz), 121.91 (d, *J* = 13.5 Hz), 115.24, 114.88, 107.60 (d, *J* = 27.8 Hz), 104.42, 84.00, 71.43, 62.33, 54.33, 45.60, 43.65, 42.73, 38.40, 28.81, 27.91, 25.09, 21.93, 15.43, 13.88.

HRMS *m/z* for $C_{26}H_{33}N_7O_2F^+$ ([M+H]$^+$) calculated: 494.2674, found: 494.2681.

Synthesis of CG342

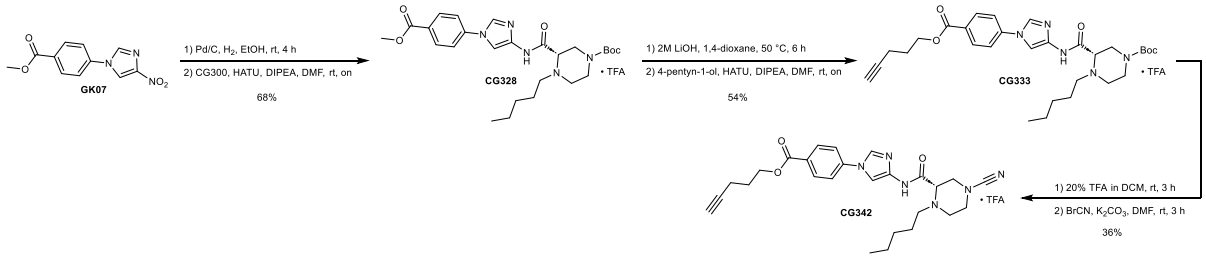

Scheme 42. Synthesis of CG342.

tert-Butyl (*S*)-3-((1-(4-(methoxycarbonyl)phenyl)-1*H*-imidazol-4-yl)carbamoyl)-4-pentyl-piperazine-1-carboxylate TFA salt (CG328)

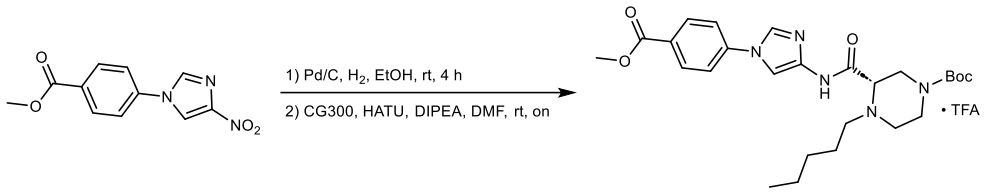

Step 1

GK07 (131.4 mg, 0.53 mmol, 1.1 eq) was dissolved in EtOH (20 mL) and palladium (10%) on activated charcoal (50 mg) was added under an argon atmosphere. The reaction was flushed with H_2 and stirred for 4 h at room temperature. The reaction was filtered through Celite 545 which was then washed with EA. The solvent was removed under reduced pressure and the obtained product used for the next reaction without further purification.

Step 2

CG300 (148.0 mg, 0.48 mol, 1.0 eq) was dissolved in DMF (2 mL), then DIPEA (246.5 µL, 1.45 mmol, 3.0 eq) and HATU (220.5 mg, 0.58 mmol, 1.2 eq) were added and the reaction mixture stirred for 10 min at room temperature. The crude product from step 1 was dissolved in DMF (2 mL) and added to the reaction dropwise. The resulting solution was stirred overnight at room temperature. The reaction was quenched by the addition of aqueous sat. NH_4Cl (40 mL) and the mixture extracted with EA (2x30 mL). The combined organic layers were washed with brine (30 mL), dried over anhydrous $MgSO_4$, filtered and the solvent was removed under reduced pressure. The product was purified via preparative HPLC eluting at 25-35% ACN in H_2O, yielding CG328 (201.0 mg, 0.33 mmol, 68%) as a white TFA salt.

^{1}H NMR (700 MHz, DMSO-d_6) δ (ppm) = 11.68 (s, 1H), 8.38 (d, *J* = 1.6 Hz, 1H), 8.12 – 8.04 (m, 2H), 7.87 (s, 1H), 7.84 (d, *J* = 8.2 Hz, 3H), 4.21 – 4.02 (m, 1H), 4.01 – 3.93 (m, 1H), 3.88 (s, 3H), 3.81 – 3.69 (m, 1H), 3.59 (br s, 1H), 3.37 – 3.24 (m, 2H), 3.16 (br s, 1H), 3.06 (br s, 2H), 1.67 (d, *J* = 35.0 Hz, 2H), 1.42 (s, 9H), 1.32 – 1.15 (m, 4H), 0.86 (t, *J* = 7.0 Hz, 3H).

^{13}C NMR (176 MHz, DMSO-d_6) δ (ppm) = 174.08, 165.91, 158.37 (q, *J* = 32.7 Hz), 153.42, 140.59, 138.57, 133.40, 131.51, 128.25, 120.42, 117.17 (q, *J* = 297.4 Hz), 105.67, 80.75, 56.22, 55.28, 52.80, 49.76, 48.01, 46.97, 28.48, 28.34, 23.47, 22.05, 14.11.

HRMS *m/z* for $C_{26}H_{38}N_5O_5^+$ ($[M+H]^+$) calculated: 500.2868, found: 500.2876.

tert-Butyl (_S_)-3-((1-(4-((pent-4-yn-1-yloxy)carbonyl)phenyl)-1_H_-imidazol-4-yl)carbamoyl)-4-pentyl-piperazine-1-carboxylate TFA salt (CG333)

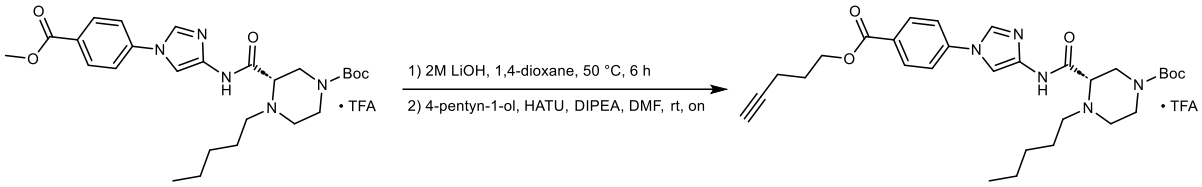

Step 1

CG328 (50.0 mg, 0.08 mmol, 1.0 eq) was dissolved in 1,4-dioxane (2 mL). Aqueous 2M LiOH solution (85.6 µL, 0.17 mol, 2.1 eq) was added and the reaction mixture was stirred at 50 °C overnight. The pH of the reaction mixture was adjusted to pH 7 by adding aqueous 1 N HCl dropwise. The solvent was removed under reduced pressure and the obtained product used for the next reaction without further purification.

Step 2

The crude product from step 1 was dissolved in DMF (2 mL), then DIPEA (55.4 µL, 0.33 mmol, 4.0 eq) and HATU (40.3 mg, 0.11 mmol, 1.3 eq) were added and the reaction mixture was stirred for 10 min at room temperature. 4-Pentyn-1-ol (22.7 µL, 0.24 mmol, 3.0 eq) was dissolved in DMF (2 mL), added to the reaction and the mixture stirred overnight at room temperature. The reaction mixture was quenched with sat. NH_4Cl solution (30 mL) and extracted with EA (2x30 mL). The combined organic layers were washed with brine (20 mL), dried over $MgSO_4$, filtered and the solvent was removed under reduced pressure. The product was purified via preparative HPLC eluting at 25-35% ACN in H_2O, yielding CG333 (29.3 mg, 0.04 mmol, 54%) as a white TFA salt.

^{1}H NMR (600 MHz, DMSO-d_6) δ (ppm) = 11.69 (s, 1H), 8.38 (d, J = 1.7 Hz, 1H), 8.12 – 8.07 (m, 2H), 7.87 (s, 1H), 7.83 (d, J = 8.4 Hz, 2H), 4.36 (t, J = 6.3 Hz, 2H), 4.34 (br s, 1H), 4.01 (d, J = 32.9 Hz, 2H), 3.58 (br s, 2H), 3.27 (br s, 1H), 3.05 (br s, 3H), 2.84 (t, J = 2.7 Hz, 1H), 2.36 (td, J = 7.1, 2.7 Hz, 2H), 1.92 (p, J = 6.7 Hz, 2H), 1.66 (d, J = 31.1 Hz, 2H), 1.42 (s, 9H), 1.33 – 1.12 (m, 4H), 0.85 (t, J = 7.0 Hz, 3H).

^{13}C NMR (151 MHz, DMSO-d_6) δ (ppm) = 174.39, 164.92, 157.79 (q, J = 31.8 Hz), 152.97, 140.14, 138.17, 132.89, 131.10, 127.84, 119.92, 116.99 (q, J = 299.1 Hz), 105.14, 83.49, 80.19, 71.76, 63.64, 61.94, 54.78, 49.39, 48.44, 47.67, 28.04, 27.87, 27.31, 27.13, 21.61, 14.65, 13.66.

HRMS *m/z* for $C_{30}H_{42}N_5O_5^+$ ($[M+H]^+$) calculated: 552.3181, found: 552.3192.

Pent-4-yn-1-yl (_S_)-4-(4-(4-cyano-1-pentylpiperazine-2-carboxamido)-1_H_-imidazol-1-yl)benzoate TFA salt (CG342)

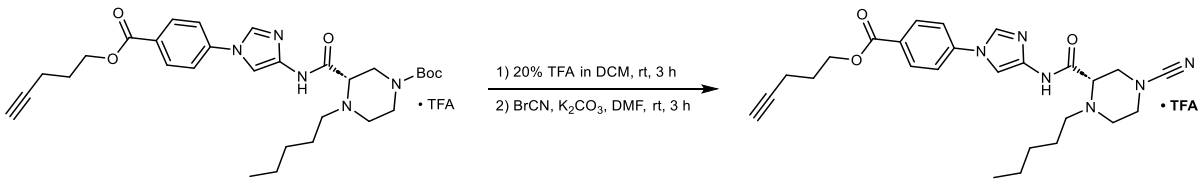

Step 1

CG333 (20.0 mg, 0.03 mmol, 1.0 eq) was dissolved in DCM (2 mL) and TFA (0.4 mL) was added dropwise. The solution was stirred for 3 h at room temperature. The solvent and residual TFA were removed under reduced pressure and the product dried in vacuo.

Step 2

The crude product from step 1 was dissolved in DMF (2 mL) and K_2CO_3 (16.6 mg, 0.12 mmol, 4.0 eq) was added. 3 M cyanogen bromide solution (15.0 µL, 0.05 mmol, 1.5 eq) was added and the mixture was stirred for 3 h at room temperature. The reaction was quenched by the addition of aqueous sat. $NaHCO_3$ (30 mL). The mixture was extracted with EA (2x30 mL). The combined organic layers were washed with brine (20 mL), dried over anhydrous $MgSO_4$, filtered and the solvent was removed under reduced pressure. The corresponding product was purified via preparative HPLC, eluting at 25-30% ACN in H_2O, yielding CG342 (6.3 mg, 0.01 mmol, 36%) as a white TFA salt.

^{1}H NMR (700 MHz, DMSO-d_6) δ (ppm) = 8.35 (d, *J* = 1.7 Hz, 1H), 8.13 – 8.05 (m, 2H), 7.86 (d, *J* = 1.6 Hz, 1H), 7.85 – 7.82 (m, 2H), 4.35 (t, *J* = 6.3 Hz, 2H), 3.47 (br s, 7H), 3.40 – 3.33 (m, 2H), 2.84 (t, *J* = 2.6 Hz, 1H), 2.36 (td, *J* = 7.1, 2.7 Hz, 2H), 1.92 (p, *J* = 6.7 Hz, 2H), 1.56 (d, *J* = 42.7 Hz, 2H), 1.37 – 1.15 (m, 4H), 0.85 (t, *J* = 7.1 Hz, 3H).

^{13}C NMR (176 MHz, DMSO-d_6) δ (ppm) = 174.53, 164.93, 157.82 (q, *J* = 32.1 Hz), 140.19, 138.41, 132.71, 131.07, 127.73, 119.81, 116.42, 116.91 (q, *J* = 297.9 Hz), 104.73, 83.49, 71.74, 63.63, 62.46, 54.70, 49.26, 48.21, 48.08, 28.38, 27.13, 25.09, 21.75, 14.65, 13.76.

HRMS *m/z* for $C_{26}H_{33}N_6O_3^+$ ([M+H]$^+$) calculated: 477.2609, found: 477.2616.

Synthesis of CG356

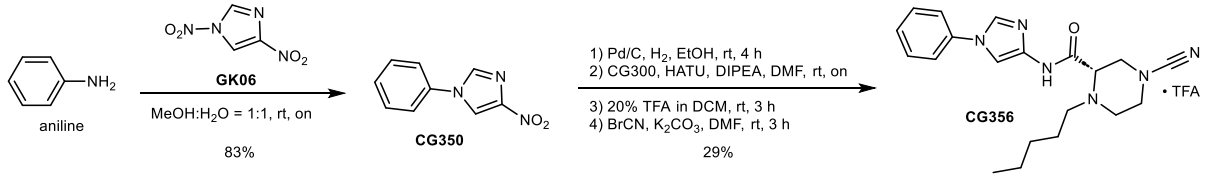

Scheme 43. Synthesis of CG356.

4-Nitro-1-phenyl-1*H*-imidazole (CG350)

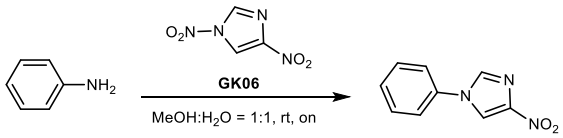

GK06 (300.0 mg, 1.90 mmol, 1.0 eq) was dissolved in a 1:1 mixture of MeOH and H_2O (20 mL). Aniline (259.9 µL, 2.85 mmol, 1.5 eq) was added and the reaction mixture was stirred overnight at room temperature and in darkness. The precipitated product was filtered, washed with H_2O (150 mL) and dried at 60 °C in a drying oven. CG352 (299.0 mg, 1.58 mmol, 83%) was obtained as a yellow solid.

^{1}H NMR (500 MHz, DMSO-d_6) δ (ppm) = 9.01 (d, *J* = 1.6 Hz, 1H), 8.49 (d, *J* = 1.6 Hz, 1H), 7.84 – 7.77 (m, 2H), 7.59 (t, *J* = 7.9 Hz, 2H), 7.52 – 7.45 (m, 1H).

^{13}C NMR (126 MHz, DMSO) δ (ppm) = 148.12, 135.70, 135.53, 130.01, 128.68, 121.38, 119.81.

HRMS *m/z* for $C_9H_8N_3O_2^+$ ([M+H]$^+$) calculated: 190.0611, found: 190.0611.

(*S*)-4-Cyano-1-pentyl-*N*-(1-phenyl-1*H*-imidazol-4-yl)piperazine-2-carboxamide TFA salt (CG356)

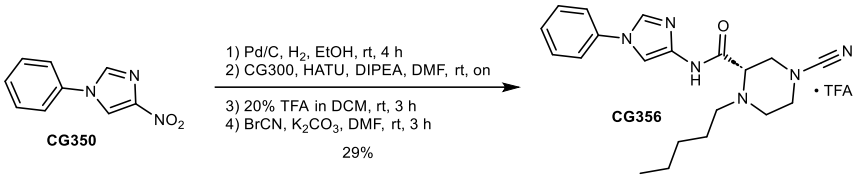

Step 1

CG350 (38.4 mg, 0.20 mmol, 1.2 eq) was dissolved in EtOH (10 mL) and palladium (10%) on activated charcoal (30 mg) was added under an argon atmosphere. The reaction was flushed with H_2 and stirred for 4 h at room temperature. The reaction was filtered through Celite 545 which was then washed with EA. The solvent was removed under reduced pressure and the obtained product used for the next reaction without further purification.

Step 2

CG300 (51.8 mg, 0.17 mol, 1.0 eq) was dissolved in DMF (2 mL), then DIPEA (86.3 µL, 0.51 mmol, 3.0 eq) and HATU (77.2 mg, 0.20 mmol, 1.2 eq) were added and the reaction mixture stirred for 10 min at room temperature. The crude product from step 1 was dissolved in DMF (2 mL) and added to the reaction dropwise. The resulting solution was stirred overnight at room temperature. The reaction was quenched by the addition of aqueous sat. NH_4Cl (30 mL) and the mixture extracted with EA (2x30 mL). The combined organic layers were washed with brine (30 mL), dried over anhydrous $MgSO_4$, filtered and the solvent was removed under reduced pressure. Partial purification was achieved by preparative HPLC during which the desired product *tert*-butyl (*S*)-4-pentyl-3-((1-phenyl-1*H*-imidazol-4-yl)carbamoyl)piperazine-1-carboxylate TFA salt (46.9 mg, 0.11 mmol) co-eluted with uncharacterised impurities. Fractions containing the desired product as judged by LC-MS and TLC were combined, frozen, lyophilised and used for the next reaction without further purification.

Step 3

The crude product from step 2 was dissolved in DCM (2 mL) and TFA (0.4 mL) was added dropwise. The solution was stirred for 3 h at room temperature. The solvent and residual TFA were removed under reduced pressure and the product dried in vacuo.

Step 4

The crude product from step 3 was dissolved in DMF (3 mL) and K_2CO_3 (56.3 mg, 0.41 mmol, 4.0 eq) was added. 3 M cyanogen bromide solution (44.2 µL, 0.13 mmol, 1.3 eq) was added and the mixture was stirred for 3 h at room temperature. The reaction was quenched by the addition of aqueous sat. $NaHCO_3$ (30 mL). The mixture was extracted with EA (2x30 mL). The combined organic layers were washed with brine (30 mL), dried over anhydrous $MgSO_4$, filtered and the solvent was removed under reduced pressure. The corresponding product was purified via preparative HPLC, eluting at 25-35% ACN in H_2O, yielding CG356 (28.3 mg, 0.06 mmol, 29%) as a white TFA salt.

^{1}H NMR (700 MHz, DMSO-d_6) δ (ppm) = 11.10 (s, 1H), 8.18 (d, *J* = 1.6 Hz, 1H), 7.75 (d, *J* = 1.6 Hz, 1H), 7.66 – 7.62 (m, 2H), 7.56 – 7.49 (m, 2H), 7.41 – 7.35 (m, 1H), 4.16 – 4.01 (m, 1H), 3.94 (br s, 1H), 3.75 (br s, 1H), 3.57 – 3.52 (m, 1H), 3.44 (br s, 1H), 3.42 – 3.38 (m, 2H), 2.85 (br s, 2H), 1.58 (d, *J* = 43.8 Hz, 2H), 1.35 – 1.13 (m, 4H), 0.84 (t, *J* = 7.1 Hz, 3H).

^{13}C NMR (176 MHz, DMSO-d_6) δ (ppm) = 157.98 (q, *J* = 32.2 Hz), 157.00, 137.91, 136.72, 132.36, 129.93, 127.07, 120.33, 116.23, 116.89 (q, *J* = 298.27 Hz), 105.33, 62.46, 54.74, 49.15, 48.29, 46.38, 28.30, 23.87, 21.71, 13.72.

HRMS *m/z* for $C_{20}H_{27}N_6O^+$ ([M+H]$^+$) calculated: 367.2241, found: 367.2244.

References

[1] C. Grethe, M. Schmidt, G. M. Kipka, R. O'Dea, K. Gallant, P. Janning, M. Gersch, *Nat Commun* **2022**, *13*, 5950.
[2] G. M. Kipka, TU Dortmund University **2019**.
[3] G. M. Kipka, TU Dortmund University **2022**.
[4] M. Schmidt, dissertation thesis, TU Dortmund University **unpublished**.
[5] W. Gui, P. Paudel, Z. Zhuang, in *Comprehensive Natural Products III*, **2020**, pp. 589-602.
[6] M. F. Schmidt, Z. Y. Gan, D. Komander, G. Dewson, *Cell Death Differ* **2021**, *28*, 570-590.
[7] Q. Yang, J. Zhao, D. Chen, Y. Wang, *Mol Biomed* **2021**, *2*, 23.
[8] T. E. T. Mevissen, D. Komander, *Annu Rev Biochem* **2017**, *86*, 159-192.
[9] J. Heideker, I. E. Wertz, *Biochem J* **2015**, *467*, 191.
[10] U. F. Cajee, R. Hull, M. Ntwasa, *Int J Mol Sci* **2012**, *13*, 11804-11831.
[11] C. J. Huang, D. Wu, F. A. Khan, L. J. Huo, *DNA Cell Biol* **2015**, *34*, 652-660.
[12] R. I. Enchev, B. A. Schulman, M. Peter, *Nat Rev Mol Cell Biol* **2015**, *16*, 30-44.
[13] A. G. van der Veen, H. L. Ploegh, *Annu Rev Biochem* **2012**, *81*, 323-357.
[14] A. M. Burroughs, L. M. Iyer, L. Aravind, *Front Biosci (Landmark Ed)* **2012**, *17*, 1433-1460.
[15] P. V. Hornbeck, B. Zhang, B. Murray, J. M. Kornhauser, V. Latham, E. Skrzypek, *Nucleic Acids Res* **2015**, *43*, D512-520.
[16] F. Ohtake, Y. Saeki, K. Sakamoto, K. Ohtake, H. Nishikawa, H. Tsuchiya, T. Ohta, K. Tanaka, J. Kanno, *EMBO Rep* **2015**, *16*, 192-201.
[17] Y. Leestemaker, H. Ovaa, *Drug Discov Today Technol* **2017**, *26*, 25-31.
[18] J. A. Harrigan, X. Jacq, N. M. Martin, S. P. Jackson, *Nat Rev Drug Discov* **2017**.
[19] G. Dittmar, K. F. Winklhofer, *Front Chem* **2019**, *7*, 915.
[20] I. Dikic, *Annu Rev Biochem* **2017**, *86*, 193-224.
[21] A. Hershko, A. Ciechanover, *Annu Rev Biochem* **1982**, *51*, 335-364.
[22] A. Ciechanover, Y. Hod, A. Hershko, *Biochem Biophys Res Commun* **1978**, *425*, 565-570.
[23] D. Komander, M. Rape, *Annu Rev Biochem* **2012**, *81*, 203-229.
[24] E. M. Cooper, C. Cutcliffe, T. Z. Kristiansen, A. Pandey, C. M. Pickart, R. E. Cohen, *EMBO J* **2009**, *28*, 621-631.
[25] R. Yau, M. Rape, *Nat Cell Biol* **2016**, *18*, 579-586.
[26] W. Kim, E. J. Bennett, E. L. Huttlin, A. Guo, J. Li, A. Possemato, M. E. Sowa, R. Rad, J. Rush, M. J. Comb, J. W. Harper, S. P. Gygi, *Mol Cell* **2011**, *44*, 325-340.
[27] J. R. Morris, E. Solomon, *Hum Mol Genet* **2004**, *13*, 807-817.
[28] K. E. Wickliffe, A. Williamson, H. J. Meyer, A. Kelly, M. Rape, *Trends Cell Biol* **2011**, *21*, 656-663.
[29] M. Tracz, W. Bialek, *Cell Mol Biol Lett* **2021**, *26*, 1.
[30] A. K. Al-Hakim, A. Zagorska, L. Chapman, M. Deak, M. Peggie, D. R. Alessi, *Biochem J* **2008**, *411*, 249-260.
[31] A. Rodriguez Carvajal, I. Grishkovskaya, C. Gomez Diaz, A. Vogel, A. Sonn-Segev, M. S. Kushwah, K. Schodl, L. Deszcz, Z. Orban-Nemeth, S. Sakamoto, K. Mechtler, P. Kukura, T. Clausen, D. Haselbach, F. Ikeda, *Elife* **2021**, *10*.
[32] F. Tokunaga, S. Sakata, Y. Saeki, Y. Satomi, T. Kirisako, K. Kamei, T. Nakagawa, M. Kato, S. Murata, S. Yamaoka, M. Yamamoto, S. Akira, T. Takao, K. Tanaka, K. Iwai, *Nat Cell Biol* **2009**, *11*, 123-132.
[33] E. Rivkin, S. M. Almeida, D. F. Ceccarelli, Y. C. Juang, T. A. MacLean, T. Srikumar, H. Huang, W. H. Dunham, R. Fukumura, G. Xie, Y. Gondo, B. Raught, A. C. Gingras, F. Sicheri, S. P. Cordes, *Nature* **2013**, *498*, 318-324.
[34] S. Ning, L. Luo, B. Yu, D. Mai, F. Wang, *J Leukoc Biol* **2022**, *112*, 799-811.
[35] H. J. Meyer, M. Rape, *Cell* **2014**, *157*, 910-921.
[36] R. G. Yau, K. Doerner, E. R. Castellanos, D. L. Haakonsen, A. Werner, N. Wang, X. W. Yang, N. Martinez-Martin, M. L. Matsumoto, V. M. Dixit, M. Rape, *Cell* **2017**, *171*, 918-933 e920.
[37] D. L. Haakonsen, M. Rape, *Trends Cell Biol* **2019**, *29*, 704-716.
[38] D. A. Perez Berrocal, K. F. Witting, H. Ovaa, M. P. C. Mulder, *Front Chem* **2019**, *7*, 931.
[39] C. M. Guzzo, C. E. Berndsen, J. Zhu, V. Gupta, A. Datta, R. A. Greenberg, C. Wolberger, M. J. Matunis, *Sci Signal* **2012**, *5*, ra88.
[40] S. L. Poulsen, R. K. Hansen, S. A. Wagner, L. van Cuijk, G. J. van Belle, W. Streicher, M. Wikstrom, C. Choudhary, A. B. Houtsmuller, J. A. Marteijn, S. Bekker-Jensen, N. Mailand, *J Cell Biol* **2013**, *201*, 797-807.

[41] E. Santonico, R. Nepravishta, W. Mandaliti, L. Castagnoli, G. Cesareni, M. Paci, *Int J Mol Sci* **2019**, *20*.
[42] N. V. Giannakopoulos, J. K. Luo, V. Papov, W. Zou, D. J. Lenschow, B. S. Jacobs, E. C. Borden, J. Li, H. W. Virgin, D. E. Zhang, *Biochem Biophys Res Commun* **2005**, *336*, 496-506.
[43] K. L. Rock, C. Gramm, L. Rothstein, K. Clark, R. Stein, L. Dick, D. Hwang, A. L. Goldberg, *Cell* **1994**, *78*, 761-771.
[44] P. Leznicki, Y. Kulathu, *Journal of Cell Science* **2017**.
[45] I. Dikic, S. Wakatsuki, K. J. Walters, *Nat Rev Mol Cell Biol* **2009**, *10*, 659-671.
[46] D. Komander, M. J. Clague, S. Urbe, *Nat Rev Mol Cell Biol* **2009**, *10*, 550-563.
[47] K. Patel, Z. S. Ahmed, X. Huang, Q. Yang, E. Ekinci, C. M. Neslund-Dudas, B. Mitra, F. A. Elnady, Y. H. Ahn, H. Yang, J. Liu, Q. P. Dou, *Future Med Chem* **2018**, *10*, 2087-2108.
[48] D. Komander, *Subcell Biochem* **2010**, *54*, 69-87.
[49] P. Hanpude, S. Bhattacharya, A. K. Dey, T. K. Maiti, *IUBMB Life* **2015**, *67*, 544-555.
[50] N. A. Snyder, G. M. Silva, *J Biol Chem* **2021**, *297*, 101077.
[51] D. Kwasna, S. A. Abdul Rehman, J. Natarajan, S. Matthews, R. Madden, V. De Cesare, S. Weidlich, S. Virdee, I. Ahel, I. Gibbs-Seymour, Y. Kulathu, *Mol Cell* **2018**, *70*, 150-164 e156.
[52] Y. Li, D. Reverter, *Int J Mol Sci* **2021**, *22*.
[53] D. Flierman, G. J. van der Heden van Noort, R. Ekkebus, P. P. Geurink, T. E. Mevissen, M. K. Hospenthal, D. Komander, H. Ovaa, *Cell Chem Biol* **2016**, *23*, 472-482.
[54] C. Gomez-Diaz, F. Ikeda, *Semin Cell Dev Biol* **2019**, *93*, 125-135.
[55] X. Huang, M. K. Summers, V. Pham, J. R. Lill, J. Liu, G. Lee, D. S. Kirkpatrick, P. K. Jackson, G. Fang, V. M. Dixit, *Mol Cell* **2011**, *42*, 511-523.
[56] L. Zhang, F. Zhou, Y. Drabsch, R. Gao, B. E. Snaar-Jagalska, C. Mickanin, H. Huang, K. A. Sheppard, J. A. Porter, C. X. Lu, P. ten Dijke, *Nat Cell Biol* **2012**, *14*, 717-726.
[57] M. J. Clague, I. Barsukov, J. M. Coulson, H. Liu, D. J. Rigden, S. Urbe, *Physiol Rev* **2013**, *93*, 1289-1315.
[58] Y. Ye, H. Scheel, K. Hofmann, D. Komander, *Mol Biosyst* **2009**, *5*, 1797-1808.
[59] T. Yao, L. Song, W. Xu, G. N. DeMartino, L. Florens, S. K. Swanson, M. P. Washburn, R. C. Conaway, J. W. Conaway, R. E. Cohen, *Nat Cell Biol* **2006**, *8*, 994-1002.
[60] E. J. Worden, C. Padovani, A. Martin, *Nat Struct Mol Biol* **2014**, *21*, 220-227.
[61] D. D. Sahtoe, W. J. van Dijk, F. El Oualid, R. Ekkebus, H. Ovaa, T. K. Sixma, *Mol Cell* **2015**, *57*, 887-900.
[62] Y. Kee, K. Yang, M. A. Cohn, W. Haas, S. P. Gygi, A. D. D'Andrea, *J Biol Chem* **2010**, *285*, 11252-11257.
[63] M. A. Cohn, Y. Kee, W. Haas, S. P. Gygi, A. D. D'Andrea, *J Biol Chem* **2009**, *284*, 5343-5351.
[64] A. C. Faesen, M. P. Luna-Vargas, P. P. Geurink, M. Clerici, R. Merkx, W. J. van Dijk, D. S. Hameed, F. El Oualid, H. Ovaa, T. K. Sixma, *Chem Biol* **2011**, *18*, 1550-1561.
[65] M. E. Sowa, E. J. Bennett, S. P. Gygi, J. W. Harper, *Cell* **2009**, *138*, 389-403.
[66] N. Nakamura, S. Hirose, *Mol Biol Cell* **2008**, *19*, 1903-1911.
[67] G. C. Hassink, B. Zhao, R. Sompallae, M. Altun, S. Gastaldello, N. V. Zinin, M. G. Masucci, K. Lindsten, *EMBO Rep* **2009**, *10*, 755-761.
[68] X. X. Sun, X. He, L. Yin, M. Komada, R. C. Sears, M. S. Dai, *Proc Natl Acad Sci U S A* **2015**, *112*, 3734-3739.
[69] M. J. Clague, S. Urbe, *Febs J* **2017**, *284*, 1753-1766.
[70] L. Herhaus, A. B. Perez-Oliva, G. Cozza, R. Gourlay, S. Weidlich, D. G. Campbell, L. A. Pinna, G. P. Sapkota, *Sci Signal* **2015**, *8*, ra35.
[71] M. A. Cohn, P. Kowal, K. Yang, W. Haas, T. T. Huang, S. P. Gygi, A. D. D'Andrea, *Mol Cell* **2007**, *28*, 786-797.
[72] D. Vucic, V. M. Dixit, I. E. Wertz, *Nat Rev Mol Cell Biol* **2011**, *12*, 439-452.
[73] J. M. Fraile, V. Quesada, D. Rodriguez, J. M. Freije, C. Lopez-Otin, *Oncogene* **2012**, *31*, 2373-2388.
[74] J. J. Sacco, T. Y. Yau, S. Darling, V. Patel, H. Liu, S. Urbe, M. J. Clague, J. M. Coulson, *Oncogene* **2014**, *33*, 4265-4272.
[75] M. S. Song, L. Salmena, A. Carracedo, A. Egia, F. Lo-Coco, J. Teruya-Feldstein, P. P. Pandolfi, *Nature* **2008**, *455*, 813-817.
[76] X. X. Sun, K. B. Challagundla, M. S. Dai, *EMBO J* **2012**, *31*, 576-592.
[77] M. Li, C. L. Brooks, N. Kon, W. Gu, *Mol Cell* **2004**, *13*, 879-886.
[78] F. Colland, E. Formstecher, X. Jacq, C. Reverdy, C. Planquette, S. Conrath, V. Trouplin, J. Bianchi, V. N. Aushev, J. Camonis, A. Calabrese, C. Borg-Capra, W. Sippl, V. Collura, G. Boissy, J. C. Rain, P. Guedat, R. Delansorne, L. Daviet, *Mol Cancer Ther* **2009**, *8*, 2286-2295.

[79] M. Schwickart, X. Huang, J. R. Lill, J. Liu, R. Ferrando, D. M. French, H. Maecker, K. O'Rourke, F. Bazan, J. Eastham-Anderson, P. Yue, D. Dornan, D. C. Huang, V. M. Dixit, *Nature* **2010**, *463*, 103-107.
[80] E. Graner, D. Tang, S. Rossi, A. Baron, T. Migita, L. J. Weinstein, M. Lechpammer, D. Huesken, J. Zimmermann, S. Signoretti, M. Loda, *Cancer Cell* **2004**, *5*, 253-261.
[81] T. Ozaki, A. Nakagawara, *Cancers (Basel)* **2011**, *3*, 994-1013.
[82] R. I. Oliveira, R. A. Guedes, J. A. R. Salvador, *Front Chem* **2022**, *10*, 1005727.
[83] Z. Wang, W. Kang, O. Li, F. Qi, J. Wang, Y. You, P. He, Z. Suo, Y. Zheng, H. M. Liu, *Acta Pharm Sin B* **2021**, *11*, 694-707.
[84] F. Morra, F. Merolla, V. Napolitano, G. Ilardi, C. Miro, S. Paladino, S. Staibano, A. Cerrato, A. Celetti, *Oncotarget* **2017**, *8*, 31815-31829.
[85] D. Su, S. Ma, L. Shan, Y. Wang, Y. Wang, C. Cao, B. Liu, C. Yang, L. Wang, S. Tian, X. Ding, X. Liu, N. Yu, N. Song, L. Liu, S. Yang, Q. Zhang, F. Yang, K. Zhang, L. Shi, *J Clin Invest* **2018**, *128*, 4280-4296.
[86] T. An, Y. Gong, X. Li, L. Kong, P. Ma, L. Gong, H. Zhu, C. Yu, J. Liu, H. Zhou, B. Mao, Y. Li, *Biochem Pharmacol* **2017**, *131*, 29-39.
[87] M. S. Ritorto, R. Ewan, A. B. Perez-Oliva, A. Knebel, S. J. Buhrlage, M. Wightman, S. M. Kelly, N. T. Wood, S. Virdee, N. S. Gray, N. A. Morrice, D. R. Alessi, M. Trost, *Nat Commun* **2014**, *5*, 4763.
[88] D. Chauhan, Z. Tian, B. Nicholson, K. G. Kumar, B. Zhou, R. Carrasco, J. L. McDermott, C. A. Leach, M. Fulcinniti, M. P. Kodrasov, J. Weinstock, W. D. Kingsbury, T. Hideshima, P. K. Shah, S. Minvielle, M. Altun, B. M. Kessler, R. Orlowski, P. Richardson, N. Munshi, K. C. Anderson, *Cancer Cell* **2012**, *22*, 345-358.
[89] M. Kemp, *Prog Med Chem* **2016**, *55*, 149-192.
[90] M. Y. W. Ng, T. Wai, A. Simonsen, *Dev Cell* **2021**, *56*, 881-905.
[91] B. Liu, J. Ruan, M. Chen, Z. Li, G. Manjengwa, D. Schluter, W. Song, X. Wang, *Mol Psychiatry* **2022**, *27*, 259-268.
[92] T. M. Durcan, E. A. Fon, *Front Neurol* **2013**, *4*, 46.
[93] J. Chakraborty, E. Ziviani, *Front Physiol* **2020**, *11*, 535.
[94] T. M. Durcan, M. Y. Tang, J. R. Perusse, E. A. Dashti, M. A. Aguileta, G. L. McLelland, P. Gros, T. A. Shaler, D. Faubert, B. Coulombe, E. A. Fon, *EMBO J* **2014**, *33*, 2473-2491.
[95] Z. Alexopoulou, J. Lang, R. M. Perrett, M. Elschami, M. E. Hurry, H. T. Kim, D. Mazaraki, A. Szabo, B. M. Kessler, A. L. Goldberg, O. Ansorge, T. A. Fulga, G. K. Tofaris, *Proc Natl Acad Sci U S A* **2016**, *113*, E4688-4697.
[96] M. Colombo, S. Vallese, I. Peretto, X. Jacq, J. C. Rain, F. Colland, P. Guedat, *ChemMedChem* **2010**, *5*, 552-558.
[97] S. von Stockum, A. Sanchez-Martinez, S. Corra, J. Chakraborty, E. Marchesan, L. Locatello, C. Da Re, P. Cusumano, F. Caicci, V. Ferrari, R. Costa, L. Bubacco, M. B. Rasotto, I. Szabo, A. J. Whitworth, L. Scorrano, E. Ziviani, *Life Sci Alliance* **2019**, *2*.
[98] B. Bingol, J. S. Tea, L. Phu, M. Reichelt, C. E. Bakalarski, Q. Song, O. Foreman, D. S. Kirkpatrick, M. Sheng, *Nature* **2014**, *510*, 370-375.
[99] B. Bingol, M. Sheng, *Free Radic Biol Med* **2016**, *100*, 210-222.
[100] F. Wang, Y. Gao, L. Zhou, J. Chen, Z. Xie, Z. Ye, Y. Wang, *Front Pharmacol* **2022**, *13*, 851654.
[101] E. V. Rusilowicz-Jones, F. G. Barone, F. M. Lopes, E. Stephen, H. Mortiboys, S. Urbe, M. J. Clague, *Life Sci Alliance* **2022**, *5*.
[102] A. F. Kluge, B. R. Lagu, P. Maiti, M. Jaleel, M. Webb, J. Malhotra, A. Mallat, P. A. Srinivas, J. E. Thompson, *Bioorg Med Chem Lett* **2018**, *28*, 2655-2659.
[103] E. Tsefou, A. S. Walker, E. H. Clark, A. R. Hicks, C. Luft, K. Takeda, T. Watanabe, B. Ramazio, J. M. Staddon, T. Briston, R. Ketteler, *Biochem J* **2021**, *478*, 4099-4118.
[104] A. Jones, M. Kemp, M. Stockley, K. Gibson, G. Whitlock, in *WO2016156816A1, Vol. WO2016156816A1* (Ed.: M. T. Ltd), **2016**.
[105] M. Therapeutics, *Mission Therapeutics authorised to initiate first clinical trial for lead DUB program, MTX652, in kidney disease* **2022**.
[106] R. Rott, R. Szargel, J. Haskin, R. Bandopadhyay, A. J. Lees, V. Shani, S. Engelender, *Proc Natl Acad Sci U S A* **2011**, *108*, 18666-18671.
[107] R. S. Magin, X. Liu, A. Felix, A. S. Bratt, W. C. Chan, S. J. Buhrlage, *Cell Chem Biol* **2021**, *28*, 1090-1100.
[108] K. D. Wilkinson, K. M. Lee, S. Deshpande, P. Duerksen-Hughes, J. M. Boss, J. Pohl, *Science* **1989**, *246*, 670-673.
[109] L. M. Lundberg, P. Alm, J. Wharton, J. M. Polak, *Histochemistry* **1988**, *90*, 9-17.

[110] P. Supraja, S. Tripathy, S. R. Krishna Vanjari, S. G. Singh, *Biosens Bioelectron* **2022**, *216*, 114631.
[111] P. Bishop, D. Rocca, J. M. Henley, *Biochem J* **2016**, *473*, 2453-2462.
[112] H. Osaka, Y. L. Wang, K. Takada, S. Takizawa, R. Setsuie, H. Li, Y. Sato, K. Nishikawa, Y. J. Sun, M. Sakurai, T. Harada, Y. Hara, I. Kimura, S. Chiba, K. Namikawa, H. Kiyama, M. Noda, S. Aoki, K. Wada, *Hum Mol Genet* **2003**, *12*, 1945-1958.
[113] C. Das, Q. Q. Hoang, C. A. Kreinbring, S. J. Luchansky, R. K. Meray, S. S. Ray, P. T. Lansbury, D. Ringe, G. A. Petsko, *Proc Natl Acad Sci U S A* **2006**, *103*, 4675-4680.
[114] J. I. Sulkowska, E. J. Rawdon, K. C. Millett, J. N. Onuchic, A. Stasiak, *Proc Natl Acad Sci U S A* **2012**, *109*, E1715-1723.
[115] P. Virnau, L. A. Mirny, M. Kardar, *PLoS Comput Biol* **2006**, *2*, e122.
[116] P. Virnau, A. Mallam, S. Jackson, *J Phys Condens Matter* **2011**, *23*, 033101.
[117] P. Bishop, P. Rubin, A. R. Thomson, D. Rocca, J. M. Henley, *J Biol Chem* **2014**, *289*, 36140-36149.
[118] H. J. Kim, H. J. Kim, J. E. Jeong, J. Y. Baek, J. Jeong, S. Kim, Y. M. Kim, Y. Kim, J. H. Nam, S. H. Huh, J. Seo, B. K. Jin, K. J. Lee, *PLoS One* **2014**, *9*, e99654.
[119] N. B. Last, A. D. Miranker, *Proc Natl Acad Sci U S A* **2013**, *110*, 6382-6387.
[120] E. Evangelisti, C. Cecchi, R. Cascella, C. Sgromo, M. Becatti, C. M. Dobson, F. Chiti, M. Stefani, *J Cell Sci* **2012**, *125*, 2416-2427.
[121] B. Bolognesi, J. R. Kumita, T. P. Barros, E. K. Esbjorner, L. M. Luheshi, D. C. Crowther, M. R. Wilson, C. M. Dobson, G. Favrin, J. J. Yerbury, *ACS Chem Biol* **2010**, *5*, 735-740.
[122] D. Komander, F. Reyes-Turcu, J. D. Licchesi, P. Odenwaelder, K. D. Wilkinson, D. Barford, *EMBO Rep* **2009**, *10*, 466-473.
[123] D. A. Boudreaux, T. K. Maiti, C. W. Davies, C. Das, *Proc Natl Acad Sci U S A* **2010**, *107*, 9117-9122.
[124] L. C. Dang, F. D. Melandri, R. L. Stein, *Biochemistry* **1998**, *37*, 1868-1879.
[125] C. N. Larsen, B. A. Krantz, K. D. Wilkinson, *Biochemistry* **1998**, *37*, 3358-3368.
[126] E. Kyratzi, M. Pavlaki, L. Stefanis, *Hum Mol Genet* **2008**, *17*, 2160-2171.
[127] K. Brinkmann, P. Zigrino, A. Witt, M. Schell, L. Ackermann, P. Broxtermann, S. Schull, M. Andree, O. Coutelle, B. Yazdanpanah, J. M. Seeger, D. Klubertz, U. Drebber, U. T. Hacker, M. Kronke, C. Mauch, T. Hoppe, H. Kashkar, *Cell Rep* **2013**, *3*, 881-891.
[128] H. J. Kim, V. Magesh, J. J. Lee, S. Kim, U. G. Knaus, K. J. Lee, *Oncotarget* **2015**, *6*, 16287-16303.
[129] J. S. Bett, M. S. Ritorto, R. Ewan, E. G. Jaffray, S. Virdee, J. W. Chin, A. Knebel, T. Kurz, M. Trost, M. H. Tatham, R. T. Hay, *Biochem J* **2015**, *466*, 489-498.
[130] T. Kabuta, A. Furuta, S. Aoki, K. Furuta, K. Wada, *J Biol Chem* **2008**, *283*, 23731-23738.
[131] A. Bheda, A. Gullapalli, M. Caplow, J. S. Pagano, J. Shackelford, *Cell Cycle* **2010**, *9*, 980-994.
[132] K. Saigoh, Y. L. Wang, J. G. Suh, T. Yamanishi, Y. Sakai, H. Kiyosawa, T. Harada, N. Ichihara, S. Wakana, T. Kikuchi, K. Wada, *Nat Genet* **1999**, *23*, 47-51.
[133] B. J. Walters, S. L. Campbell, P. C. Chen, A. P. Taylor, D. G. Schroeder, L. E. Dobrunz, K. Artavanis-Tsakonas, H. L. Ploegh, J. A. Wilson, G. A. Cox, S. M. Wilson, *Mol Cell Neurosci* **2008**, *39*, 539-548.
[134] F. Chen, Y. Sugiura, K. G. Myers, Y. Liu, W. Lin, *Proc Natl Acad Sci U S A* **2010**, *107*, 1636-1641.
[135] M. Mukoyama, K. Yamazaki, T. Kikuchi, T. Tomita, *Acta Neuropathol* **1989**, *79*, 294-299.
[136] J. H. Jara, B. Genc, G. A. Cox, M. C. Bohn, R. P. Roos, J. D. Macklis, E. Ulupinar, P. H. Ozdinler, *Cereb Cortex* **2015**, *25*, 4259-4272.
[137] K. Bilguvar, N. K. Tyagi, C. Ozkara, B. Tuysuz, M. Bakircioglu, M. Choi, S. Delil, A. O. Caglayan, J. F. Baranoski, O. Erturk, C. Yalcinkaya, M. Karacorlu, A. Dincer, M. H. Johnson, S. Mane, S. S. Chandra, A. Louvi, T. J. Boggon, R. P. Lifton, A. L. Horwich, M. Gunel, *Proc Natl Acad Sci U S A* **2013**, *110*, 3489-3494.
[138] E. Kesidou, R. Lagoudaki, O. Touloumi, K. N. Poulatsidou, C. Simeonidou, *Neural Regen Res* **2013**, *8*, 2275-2283.
[139] K. E. Larsen, D. Sulzer, *Histol Histopathol* **2002**, *17*, 897-908.
[140] L. M. Koharudin, H. Liu, R. Di Maio, R. B. Kodali, S. H. Graham, A. M. Gronenborn, *Proc Natl Acad Sci U S A* **2010**, *107*, 6835-6840.
[141] F. M. de Vrij, D. F. Fischer, F. W. van Leeuwen, E. M. Hol, *Prog Neurobiol* **2004**, *74*, 249-270.
[142] L. E. Donovan, L. Higginbotham, E. B. Dammer, M. Gearing, H. D. Rees, Q. Xia, D. M. Duong, N. T. Seyfried, J. J. Lah, A. I. Levey, *Proteomics Clin Appl* **2012**, *6*, 201-211.

[143] J. Choi, A. I. Levey, S. T. Weintraub, H. D. Rees, M. Gearing, L. S. Chin, L. Li, *J Biol Chem* **2004**, *279*, 13256-13264.
[144] M. G. Spillantini, M. Goedert, R. A. Crowther, J. R. Murrell, M. R. Farlow, B. Ghetti, *Proc Natl Acad Sci U S A* **1997**, *94*, 4113-4118.
[145] H. J. Kim, Y. M. Kim, S. Lim, Y. K. Nam, J. Jeong, H. J. Kim, K. J. Lee, *Oncogene* **2009**, *28*, 117-127.
[146] H. C. Lien, C. C. Wang, C. H. Lin, Y. S. Lu, C. S. Huang, L. P. Hsiao, Y. T. Yao, *Hum Pathol* **2013**, *44*, 1838-1848.
[147] S. Liu, R. Gonzalez-Prieto, M. Zhang, P. P. Geurink, R. Kooij, P. V. Iyengar, M. van Dinther, E. Bos, X. Zhang, S. E. Le Devedec, B. van de Water, R. I. Koning, H. J. Zhu, W. E. Mesker, A. C. O. Vertegaal, H. Ovaa, L. Zhang, J. W. M. Martens, P. Ten Dijke, *Clin Cancer Res* **2020**, *26*, 1460-1473.
[148] S. Hussain, T. Bedekovics, M. Chesi, P. L. Bergsagel, P. J. Galardy, *Oncotarget* **2015**, *6*, 40704-40718.
[149] T. Bedekovics, S. Hussain, A. L. Feldman, P. J. Galardy, *Blood* **2016**, *127*, 1564-1574.
[150] S. Hussain, O. Foreman, S. L. Perkins, T. E. Witzig, R. R. Miles, J. van Deursen, P. J. Galardy, *Leukemia* **2010**, *24*, 1641-1655.
[151] Y. Goto, L. Zeng, C. J. Yeom, Y. Zhu, A. Morinibu, K. Shinomiya, M. Kobayashi, K. Hirota, S. Itasaka, M. Yoshimura, K. Tanimoto, M. Torii, T. Sowa, T. Menju, M. Sonobe, H. Kakeya, M. Toi, H. Date, E. M. Hammond, M. Hiraoka, H. Harada, *Nat Commun* **2015**, *6*, 6153.
[152] A. D. Krabill, H. Chen, S. Hussain, C. Feng, A. Abdullah, C. Das, U. K. Aryal, C. B. Post, M. K. Wendt, P. J. Galardy, D. P. Flaherty, *Chembiochem* **2020**, *21*, 712-722.
[153] P. C. Sanchez-Diaz, J. C. Chang, E. S. Moses, T. Dao, Y. Chen, J. Y. Hung, *PLoS One* **2017**, *12*, e0176879.
[154] S. Hussain, T. Bedekovics, Q. Liu, W. Hu, H. Jeon, S. H. Johnson, G. Vasmatzis, D. G. May, K. J. Roux, P. J. Galardy, *Blood* **2018**, *132*, 2564-2574.
[155] M. Mondal, D. Conole, J. Nautiyal, E. W. Tate, *Br J Cancer* **2022**, *126*, 24-33.
[156] S. M. Lange, L. A. Armstrong, Y. Kulathu, *Mol Cell* **2022**, *82*, 15-29.
[157] Y. A. Ramirez, T. B. Adler, E. Altmann, T. Klemm, C. Tiesmeyer, F. Sauer, S. G. Kathman, A. V. Statsyuk, C. Sotriffer, C. Kisker, *ChemMedChem* **2018**, *13*, 2014-2023.
[158] D. S. Hewings, J. A. Flygare, M. Bogyo, I. E. Wertz, *Febs J* **2017**, *284*, 1555-1576.
[159] D. K. Nomura, M. M. Dix, B. F. Cravatt, *Nat Rev Cancer* **2010**, *10*, 630-638.
[160] R. E. Moellering, B. F. Cravatt, *Chem Biol* **2012**, *19*, 11-22.
[161] W. P. Heal, T. H. Dang, E. W. Tate, *Chem Soc Rev* **2011**, *40*, 246-257.
[162] D. Conole, M. Mondal, J. D. Majmudar, E. W. Tate, *Front Chem* **2019**, *7*, 876.
[163] J. F. McGouran, S. R. Gaertner, M. Altun, H. B. Kramer, B. M. Kessler, *Chem Biol* **2013**, *20*, 1447-1455.
[164] N. Haj-Yahya, H. P. Hemantha, R. Meledin, S. Bondalapati, M. Seenaiah, A. Brik, *Org Lett* **2014**, *16*, 540-543.
[165] M. P. Mulder, F. El Oualid, J. ter Beek, H. Ovaa, *Chembiochem* **2014**, *15*, 946-949.
[166] A. de Jong, K. Witting, R. Kooij, D. Flierman, H. Ovaa, *Angew Chem Int Ed Engl* **2017**, *56*, 12967-12970.
[167] W. Gui, C. A. Ott, K. Yang, J. S. Chung, S. Shen, Z. Zhuang, *J Am Chem Soc* **2018**, *140*, 12424-12433.
[168] J. H. L. Claessen, M. D. Witte, N. C. Yoder, A. Y. Zhu, E. Spooner, H. L. Ploegh, *Chembiochem* **2013**, *14*, 343-352.
[169] M. P. Mulder, K. Witting, I. Berlin, J. N. Pruneda, K. P. Wu, J. G. Chang, R. Merkx, J. Bialas, M. Groettrup, A. C. Vertegaal, B. A. Schulman, D. Komander, J. Neefjes, F. El Oualid, H. Ovaa, *Nat Chem Biol* **2016**, *12*, 523-530.
[170] M. Poreba, A. Szalek, P. Kasperkiewicz, W. Rut, G. S. Salvesen, M. Drag, *Chem Rev* **2015**, *115*, 12546-12629.
[171] X. Sui, Y. Wang, Y. X. Du, L. J. Liang, Q. Zheng, Y. M. Li, L. Liu, *Chem Sci* **2020**, *11*, 12633-12646.
[172] S. Serim, U. Haedke, S. H. Verhelst, *ChemMedChem* **2012**, *7*, 1146-1159.
[173] J. A. Ward, L. McLellan, M. Stockley, K. R. Gibson, G. A. Whitlock, C. Knights, J. A. Harrigan, X. Jacq, E. W. Tate, *ACS Chem Biol* **2016**, *11*, 3268-3272.
[174] V. AB, https://clinicaltrials.gov/ct2/show/study/NCT02372240, **2018**.
[175] J. A. Ward, A. Pinto-Fernandez, L. Cornelissen, S. Bonham, L. Diaz-Saez, O. Riant, K. V. M. Huber, B. M. Kessler, O. Feron, E. W. Tate, *J Med Chem* **2020**, *63*, 3756-3762.

[176] R. Kooij, S. Liu, A. Sapmaz, B. T. Xin, G. M. C. Janssen, P. A. van Veelen, H. Ovaa, P. T. Dijke, P. P. Geurink, *J Am Chem Soc* **2020**, *142*, 16825-16841.
[177] N. Panyain, A. Godinat, T. Lanyon-Hogg, S. Lachiondo-Ortega, E. J. Will, C. Soudy, M. Mondal, K. Mason, S. Elkhalifa, L. M. Smith, J. A. Harrigan, E. W. Tate, *J Am Chem Soc* **2020**, *142*, 12020-12026.
[178] N. Panyain, A. Godinat, A. R. Thawani, S. Lachiondo-Ortega, K. Mason, S. Elkhalifa, L. M. Smith, J. A. Harrigan, E. W. Tate, *RSC Med Chem* **2021**, *12*, 1935-1943.
[179] Y. Liu, H. A. Lashuel, S. Choi, X. Xing, A. Case, J. Ni, L. A. Yeh, G. D. Cuny, R. L. Stein, P. T. Lansbury, Jr., *Chem Biol* **2003**, *10*, 837-846.
[180] M. Stockley, M. Kemp, in *US20200172519A1, Vol. US20200172519A1* (Ed.: M. T. Ltd), **2020**.
[181] A. Jones, M. I. Kemp, M. L. Stockley, K. R. Gibson, G. A. Whitlock, A. Madin, in *WO2016046530A1, Vol. WO2016046530A1* (Ed.: M. T. Ltd), Google Patents, **2016**.
[182] M. Kemp, M. Stockley, A. Jones*, Vol. US20180194724A1* (Ed.: M. T. Ltd), **2018**.
[183] A. Tsherniak, F. Vazquez, P. G. Montgomery, B. A. Weir, G. Kryukov, G. S. Cowley, S. Gill, W. F. Harrington, S. Pantel, J. M. Krill-Burger, R. M. Meyers, L. Ali, A. Goodale, Y. Lee, G. Jiang, J. Hsiao, W. F. J. Gerath, S. Howell, E. Merkel, M. Ghandi, L. A. Garraway, D. E. Root, T. R. Golub, J. S. Boehm, W. C. Hahn, *Cell* **2017**, *170*, 564-576 e516.
[184] S. Flohr, P. Furet, P. Imbach, U. Hommel, H.-U. Litshcer, S. G. Parrado, U. Hassiepen, J. Zimmermann, in *US7700605B2, Vol. US7700605B2* (Ed.: N. AG), Google Patents, **2010**.
[185] J.-C. Arnould, T. G. Bird, F. T. Boyle, D. C. Blakey*, Vol. US7030123B2* (Ed.: AstraZeneca), **2006**.
[186] N. J. Donato, M. Talpaz, L. Peterson, M. Young, H. D. Showalter, C. Wobus, M. X. D. O'riordan, M. Ermann, in *WO2015054555A1, Vol. WO2015054555A1* (Ed.: T. R. O. T. U. O. Michigan), Google Patents, **2018**.
[187] P. Guedat, G. Boissy, C. Borg-Capra, F. Colland, L. Daviet, E. Formstecher, X. Jacq, J. C. Rain, R. Delansorne, I. Peretto, S. Vignando*, Vol. WO2007066200A2* (Ed.: Hybrigencis), **2007**.
[188] A. J. van der Zouwen, M. D. Witte, *Front Chem* **2021**, *9*, 644811.
[189] F. Huang, X. Han, X. Xiao, J. Zhou, *Molecules* **2022**, *27*.
[190] F. Bruening, L. E. Lovelle, *EurJOC* **2017**, 3222-3228.
[191] Q. Li, C. Ye, T. Tian, Q. Jiang, P. Zhao, X. Wang, F. Liu, J. Shan, J. Ruan, *Cell Death Dis* **2022**, *13*, 434.
[192] G. Iakobson, P. Beier, *Beilstein J Org Chem* **2012**, *8*, 1185-1190.
[193] Z. Wang, in *Comprehensive Organic Name Reactions and Reagents*, Wiley, **2010**, pp. 3031-3042.
[194] Y. M. Volovenko, T. A. Volovenko, *Chemistry of Heterocyclic Compounds* **2001**, *37*.
[195] J. R. Liang, A. Martinez, J. D. Lane, U. Mayor, M. J. Clague, S. Urbe, *EMBO Rep* **2015**, *16*, 618-627.
[196] T. Ishiyama, M. Murata, N. Miyaura, *The Journal of Organic Chemistry* **1995**, *60*, 7508-7510.
[197] L. Nie, C. Wang, X. Liu, H. Teng, S. Li, M. Huang, X. Feng, G. Pei, Q. Hang, Z. Zhao, B. Gan, L. Ma, J. Chen, *Genes Dev* **2022**, *36*, 1016-1030.
[198] C. M. Nickson, M. R. Fabbrizi, R. J. Carter, J. R. Hughes, A. Kacperek, M. A. Hill, J. L. Parsons, *Front Oncol* **2021**, *11*, 671431.
[199] A. Pinto-Fernandez, S. Davis, A. B. Schofield, H. C. Scott, P. Zhang, E. Salah, S. Mathea, P. D. Charles, A. Damianou, G. Bond, R. Fischer, B. M. Kessler, *Front Chem* **2019**, *7*, 592.
[200] J. J. Chen, C. A. Tsu, J. M. Gavin, M. A. Milhollen, F. J. Bruzzese, W. D. Mallender, M. D. Sintchak, N. J. Bump, X. Yang, J. Ma, H. K. Loke, Q. Xu, P. Li, N. F. Bence, J. E. Brownell, L. R. Dick, *J Biol Chem* **2011**, *286*, 40867-40877.
[201] W. Rut, K. Groborz, L. Zhang, X. Sun, M. Zmudzinski, B. Pawlik, X. Wang, D. Jochmans, J. Neyts, W. Mlynarski, R. Hilgenfeld, M. Drag, *Nat Chem Biol* **2021**, *17*, 222-228.
[202] A. T. Reinicke, K. Laban, M. Sachs, V. Kraus, M. Walden, M. Damme, W. Sachs, J. Reichelt, M. Schweizer, P. C. Janiesch, K. E. Duncan, P. Saftig, M. M. Rinschen, F. Morellini, C. Meyer-Schwesinger, *Proc Natl Acad Sci U S A* **2019**, *116*, 7963-7972.
[203] R. K. Meray, P. T. Lansbury, Jr., *J Biol Chem* **2007**, *282*, 10567-10575.
[204] I. Rayment, *Methods Enzymol* **1997**, *276*, 171-179.
[205] C. W. Davies, J. Chaney, G. Korbel, D. Ringe, G. A. Petsko, H. Ploegh, C. Das, *Bioorg Med Chem Lett* **2012**, *22*, 3900-3904.
[206] D. Choi, J. Kim, S. Ha, K. Kwon, E. H. Kim, H. Y. Lee, K. S. Ryu, C. Park, *Febs J* **2014**, *281*, 5447-5462.
[207] I. P. Heremans, F. Caligiore, I. Gerin, M. Bury, M. Lutz, J. Graff, V. Stroobant, D. Vertommen, A. A. Teleman, E. Van Schaftingen, G. T. Bommer, *P Natl Acad Sci USA* **2022**, *119*.

[208] F. Leisico, D. V. Vieira, T. A. Figueiredo, M. Silva, E. J. Cabrita, R. G. Sobral, A. M. Ludovice, J. Trincao, M. J. Romao, H. de Lencastre, T. Santos-Silva, *Sci Rep-Uk* **2018**, *8*.
[209] W. Lu, M. Kostic, T. Zhang, J. Che, M. P. Patricelli, L. H. Jones, E. T. Chouchani, N. S. Gray, *RSC Chem Biol* **2021**, *2*, 354-367.
[210] Y. Jia, R. Q. Kim, R. Kooij, H. Ovaa, A. Sapmaz, P. P. Geurink, *J Med Chem* **2022**, *65*, 13288-13304.
[211] S. Chamberland, Y. Ishida, V. J. Lee, R. Leger, K. Nakayama, T. Ohta, M. Ohtsuka, T. W. Renau, W. J. Watkins, Z. J. Zhang*, Vol. WO2000001714A1* (Ed.: M. Pharmaceuticals), **1999**.
[212] S. Planken, H. Cheng, M. R. Collins, J. E. SPANGLER, A. Brooun, A. Maderna, C. Palmer, M. A. Linton, A. Nagata, P. Chen*, Vol. US20190233440A1* (Ed.: P. Inc), **2019**.
[213] P. A. Barsanti, C. Hu, X. Jin, S. C. Ng, K. B. Pfister, M. Sendzik, J. Sutton*, Vol. WO2012101064A1* (Ed.: N. Ag), **2012**.
[214] S. Gellman, B. Huck*, Vol. US20020032334A1* (Ed.: W. A. R. Foundation), **2002**.
[215] H. Cheng, T. O. J. JR., J. C. Kath, K. K.-C. Liu, E. A. Lunney, A. Nagata, S. K. Nair, S. P. Planken, S. C. Sutton*, Vol. WO2013042006A1* (Ed.: P. Inc), **2013**.
[216] Z. I. Goldberg, J. C. Kath, S. P. Letrent, S. L. Weinrich*, Vol. WO2014140989A2* (Ed.: P. Inc), **2014**.
[217] T. Zhang, W. Shen, M. Liu, R. Zhang, M. Wang, L. Li, B. Wang, H. Guo, Y. Lu, *Eur J Med Chem* **2015**, *104*, 73-85.
[218] C. J. Oalmann, D. S. Yamashita, P. J. Stern*, Vol. WO2021242923A1* (Ed.: A. Therapeutics), **2021**.
[219] S. Sasmal, S. C. Gill, N. M. Lim, D. L. Mobley, *J Chem Theory Comput* **2020**, *16*, 1854-1865.
[220] S. Langdon, in *3.6. Strain and Conformation in Cyclic Molecules, Vol. 2023* (Ed.: S. Langdon), University of Saskatchewan.
[221] S. L. Degorce, M. S. Bodnarchuk, I. A. Cumming, J. S. Scott, *J Med Chem* **2018**, *61*, 8934-8943.
[222] S. L. Degorce, M. S. Bodnarchuk, J. S. Scott, *ACS Med Chem Lett* **2019**, *10*, 1198-1204.
[223] N. A. Meanwell, O. Loiseleur, *J Agric Food Chem* **2022**, *70*, 10942-10971.
[224] N. A. Meanwell, O. Loiseleur, *J Agric Food Chem* **2022**, *70*, 10972-11004.
[225] P. Patil, R. Madhavachary, K. Kurpiewska, J. Kalinowska-Tluscik, A. Domling, *Org Lett* **2017**, *19*, 642-645.
[226] M. Cronin, *Current Computer-Aided Drug Design* **2006**, *2*, 405-413.
[227] N. Wishart, M. A. Argiriadi, D. J. Calderwood, A. M. Ericsson, B. A. Fiamengo, K. E. Frank, M. Friedman, D. M. George, E. R. Goedken, N. S. Josephsohn, B. C. Li, M. J. Morytko, K. D. Stewart, J. W. Voss, G. A. Wallace, L. Wang, K. R. Woller*, Vol. WO2009152133A1* (Ed.: A. Laboratories), **2009**.
[228] D. Pizzirani, M. Biagetti, P. Ronchi, P. Bruno, S. Guariento, B. Bertani, D. Pala, A. Barilli*, Vol. WO2022013307A1* (Ed.: C. F. S.P.A.), **2022**.
[229] M. L. Stockley, M. I. Kemp, A. Madin*, Vol. WO2018065768A1* (Ed.: M. T. Ltd), **2018**.
[230] A. Jones, M. I. Kemp, M. L. Stockley, M. D. Woodrow*, Vol. WO2017163078A1* (Ed.: M. T. Ltd), **2017**.
[231] M. L. Stockley, M. I. Kemp, A. Madin, M. D. Woodrow, A. Jones*, Vol. WO2018060689A1* (Ed.: M. T. Ltd), **2018**.
[232] M. L. Stockley, M. I. Kemp*, Vol. WO2018060691A1* (Ed.: M. T. Ltd), **2018**.
[233] M. L. Stockley, M. I. Kemp, A. Madin*, Vol. WO2018060742A1* (Ed.: M. T. Ltd), **2018**.
[234] Y. Hosono, S. Uchida, M. Shinkai, C. E. Townsend, C. N. Kelly, M. R. Naylor, H. W. Lee, K. Kanamitsu, M. Ishii, R. Ueki, T. Ueda, K. Takeuchi, M. Sugita, Y. Akiyama, S. R. Lokey, J. Morimoto, S. Sando, *Nat Commun* **2023**, *14*, 1416.
[235] C. A. Lipinski, F. Lombardo, B. W. Dominy, P. J. Feeney, *Adv Drug Deliv Rev* **2001**, *46*, 3-26.
[236] D. S. Nielsen, N. E. Shepherd, W. Xu, A. J. Lucke, M. J. Stoermer, D. P. Fairlie, *Chem Rev* **2017**, *117*, 8094-8128.
[237] E. Biron, J. Chatterjee, O. Ovadia, D. Langenegger, J. Brueggen, D. Hoyer, H. A. Schmid, R. Jelinek, C. Gilon, A. Hoffman, H. Kessler, *Angew Chem Int Ed Engl* **2008**, *47*, 2595-2599.
[238] E. P. Gillis, K. J. Eastman, M. D. Hill, D. J. Donnelly, N. A. Meanwell, *J Med Chem* **2015**, *58*, 8315-8359.
[239] N. A. Meanwell, *Tactics in Contemporary Drug Design*, **2015**.
[240] A. P. Turnbull, S. Ioannidis, W. W. Krajewski, A. Pinto-Fernandez, C. Heride, A. C. L. Martin, L. M. Tonkin, E. C. Townsend, S. M. Buker, D. R. Lancia, J. A. Caravella, A. V. Toms, T. M. Charlton, J. Lahdenranta, E. Wilker, B. C. Follows, N. J. Evans, L. Stead, C. Alli, V. V. Zarayskiy, A. C. Talbot, A. J. Buckmelter, M. Wang, C. L. McKinnon, F. Saab, J. F. McGouran, H. Century,

M. Gersch, M. S. Pittman, C. G. Marshall, T. M. Raynham, M. Simcox, L. M. D. Stewart, S. B. McLoughlin, J. A. Escobedo, K. W. Bair, C. J. Dinsmore, T. R. Hammonds, S. Kim, S. Urbe, M. J. Clague, B. M. Kessler, D. Komander, *Nature* **2017**, *550*, 481-486.
[241] Y. Wang, Y. Jiang, S. Ding, J. Li, N. Song, Y. Ren, D. Hong, C. Wu, B. Li, F. Wang, W. He, J. Wang, Z. Mei, *Cell Res* **2018**, *28*, 1186-1194.
[242] G. Gavory, C. R. O'Dowd, M. D. Helm, J. Flasz, E. Arkoudis, A. Dossang, C. Hughes, E. Cassidy, K. McClelland, E. Odrzywol, N. Page, O. Barker, H. Miel, T. Harrison, *Nat Chem Biol* **2018**, *14*, 118-125.
[243] Y. M. Baez-Santos, S. J. Barraza, M. W. Wilson, M. P. Agius, A. M. Mielech, N. M. Davis, S. C. Baker, S. D. Larsen, A. D. Mesecar, *J Med Chem* **2014**, *57*, 2393-2412.
[244] M. W. Popp, K. Artavanis-Tsakonas, H. L. Ploegh, *J Biol Chem* **2009**, *284*, 3593-3602.
[245] X. Chen, H. Li, Q. Lin, S. Dai, S. Yue, L. Qu, M. Li, M. Guo, H. Wei, J. Li, L. Jiang, G. Xu, Y. Chen, *Commun Chem* **2022**, *5*, 36.
[246] E. Kobayashi, D. Hwang, A. Bheda-Malge, C. B. Whitehurst, A. V. Kabanov, S. Kondo, M. Aga, T. Yoshizaki, J. S. Pagano, M. Sokolsky, J. Shakelford, *Int J Mol Sci* **2019**, *20*.
[247] D. K. Kolmel, E. T. Kool, *Chem Rev* **2017**, *117*, 10358-10376.
[248] P. Workman, I. Collins, *Chem Biol* **2010**, *17*, 561-577.
[249] J. Blagg, P. Workman, *Cancer Cell* **2017**, *32*, 268-270.
[250] J. Loeffler-Ragg, S. Skvortsov, B. Sarg, I. Skvortsova, M. Witsch-Baumgartner, D. Mueller, H. Lindner, H. Zwierzina, *Eur J Cancer* **2005**, *41*, 2338-2346.
[251] Y. Jin, W. Zhang, J. Xu, H. Wang, Z. Zhang, C. Chu, X. Liu, Q. Zou, *Int J Clin Exp Pathol* **2015**, *8*, 12500-12508.
[252] A. Glogowska, J. Stetefeld, E. Weber, S. Ghavami, C. Hoang-Vu, T. Klonisch, *Neoplasia* **2012**, *14*, 396-409.
[253] R. Mao, X. Tan, Y. Xiao, X. Wang, Z. Wei, J. Wang, X. Wang, H. Zhou, L. Zhang, Y. Shi, *Cancer Sci* **2020**, *111*, 3174-3183.
[254] X. Han, Y. L. Zhang, T. T. Fu, P. B. Li, T. Cong, H. H. Li, *Hypertens Res* **2020**, *43*, 1089-1098.
[255] Y. Liu, R. Ding, Z. Xu, Y. Xue, D. Zhang, Y. Zhang, W. Li, X. Li, *Int J Mol Sci* **2021**, *23*.
[256] G. Winter, D. G. Waterman, J. M. Parkhurst, A. S. Brewster, R. J. Gildea, M. Gerstel, L. Fuentes-Montero, M. Vollmar, T. Michels-Clark, I. D. Young, N. K. Sauter, G. Evans, *Acta Crystallogr D Struct Biol* **2018**, *74*, 85-97.
[257] I. J. Tickle, C. Flensburg, P. Keller, W. Paciorek, A. Sharff, C. Vonrhein, G. Bricogne, *Cambridge, United Kingdom: Global Phasing Ltd.* **2018**.
[258] A. J. McCoy, R. W. Grosse-Kunstleve, P. D. Adams, M. D. Winn, L. C. Storoni, R. J. Read, *J Appl Crystallogr* **2007**, *40*, 658-674.
[259] P. Emsley, B. Lohkamp, W. G. Scott, K. Cowtan, *Acta Crystallogr D Biol Crystallogr* **2010**, *66*, 486-501.
[260] P. D. Adams, P. V. Afonine, G. Bunkoczi, V. B. Chen, N. Echols, J. J. Headd, L. W. Hung, S. Jain, G. J. Kapral, R. W. Grosse Kunstleve, A. J. McCoy, N. W. Moriarty, R. D. Oeffner, R. J. Read, D. C. Richardson, J. S. Richardson, T. C. Terwilliger, P. H. Zwart, *Methods* **2011**, *55*, 94-106.
[261] R. Eelkema, H. L. Anderson, *Macromolecules* **2008**, *41*, 9930-9933.
[262] M. A. Brodney, K. J. Coffman, *US Patent App. 11/971,272* **2008**.

Abbreviations

a.u.	arbitrary unit
ABP	Activity-Based Probe
ABPP	Activity-Based Protein Profiling
AD	Alzheimer's Disease
AMSH	Associated Molecule with the SH3-domain of STAM
APC/C	Anaphase Promoting Complex/ Cyclosome
ATXN3	Ataxin-3
AUC	Area Under the Curve
CKD	Chronic Kidney Disease
CPP	Cell-Penetrating Peptide
CYLD	CYLindDomatosis tumour-suppressor gene
DEUBAD	DEUBiquitinase ADaptor
DUB	deubiquitinase
ERα	estrogen receptor α
gad	gracile axonal dystrophy
HA	Hemagglutinin
HECT	Homologous to E6AP C-Terminus
HEK-293	Human embryonic kidney-293
HeLa	Henrietta Lacks
HOIL-1	RanBP-type and C3HC4-type zinc finger-containing protein 1
HOIP	HOIL-1-interacting protein
ISG15	Interferon-Stimulated Gene 15
ITC	Isothermal Titration Calorimetry
JAMMs	JAB1/MPN/Mov34 Metalloenzymes
KD	Knowck down
KMS11	Kawasaki Medical School-11
LB	Lysogeny Broth
LUBAC	Linear Ubiquitin chain Assembly Complex
MAP	Mitogen-Activated Protein
MAPK	MAP kinase
MCL1	Induced Myeloid Leukemia Cell differentiation protein 1
MDM2	Mouse Double Minute 2 homolog
MINDY	Motif Interacting with Ubiquitin-containing Novel DUB family
MJD	Machado-Joseph disease Domain
MS	Mass Spectrometry
mTOR	mammalian Target of Rapamycin
MYC	MYeloCytomatosis
NEDD8	Neural-precursor-cell-Expressed Developmentally Down-regulated 8
NFκB	nuclear factor k-light-chain-enhancer of activated B cells
OTU	Ovarian Tumour Protease
PAGE	PolyAcrylamide Gel Electrophoresis
PARK	Parkinsonism Associated Deglycase
PBS	Phosphate Buffered Saline
PD	Parkinson's Disease
PD-L1	Programmed cell Death-Ligand 1

PGP	P-GlykoProtein
PINK1	PTEN-Induced Kinase 1
PK	PharmacoKinetic
PKB	Protein Kinase B
PPI	Protein-Protein-Interaction
PTEN	Phosphatase and TENsin homolog
PTM	post translational modification
pVHL	Von Hippel-Lindau protein
RBR	RING-between-RING
RING	Really Interesting New Gene
RNAi	RNA interference
RP	Regulatory Particle
rpm	Rotations per minute
RPN11	Regulatory particle subunit number 11
RT-qPCR	Reverse Transcription qPCR
SD	Standard Deviation
SEM	Standard Error of Mean
SHARPIN	SHANK Associated RH Domain Interactor
siRNA	small interfering RNA
SUMO	Small Ubiquitin-Related Modifier
TB	Terrific Broth
TBI	Traumatic Brain Injury
TNF	tumour necrosis factor
TRAF6	TNF-Receptor Associated factor 6
TSA	Thermal Shift Assay
U2OS	U-2 OsteoSarcoma
U-87 MG	Uppsala 87 Malignant Glioma
UAF	USP1-associated factor
Ub	Ubiquitin
UBD	Ubiquitin binding domain
Ubl	Ubiquitin-like
Ubp	Ubiquitin-specific protease
UCH	Ubiquitin C-terminal Hydrolase
UPS	Ubiquitin proteasome system
USP	Ubiquitin Specific Protease
wt	wild type
ZUFSP	Zinc finger with UFM1 Specific Peptidase domain

Eidesstaatliche Versicherung (Affidavit)

Name, Vorname (Surname, first name) Matrikel-Nr. (Enrolment number)

Belehrung:

Wer vorsätzlich gegen eine die Täuschung über Prüfungsleistungen betreffende Regelung einer Hochschulprüfungsordnung verstößt, handelt ordnungswidrig. Die Ordnungswidrigkeit kann mit einer Geldbuße von bis zu 50.000,00 € geahndet werden. Zuständige Verwaltungs- behörde für die Verfolgung und Ahndung von Ordnungs- widrigkeiten ist der Kanzler/die Kanzlerin der Techni- schen Universität Dortmund. Im Falle eines mehrfachen oder sonstigen schwerwiegenden Täuschungsversu- ches kann der Prüfling zudem exmatrikuliert werden, § 63 Abs. 5 Hochschulgesetz NRW.

Die Abgabe einer falschen Versicherung an Eides statt ist strafbar.

Wer vorsätzlich eine falsche Versicherung an Eides statt abgibt, kann mit einer Freiheitsstrafe bis zu drei Jahren oder mit Geldstrafe bestraft werden, § 156 StGB. Die fahrlässige Abgabe einer falschen Versicherung an Eides statt kann mit einer Freiheitsstrafe bis zu einem Jahr oder Geldstrafe bestraft werden, § 161 StGB.

Die oben stehende Belehrung habe ich zur Kenntnis genommen:

Official notification:

Any person who intentionally breaches any regulation of university examination regulations relating to deception in examination performance is acting improperly. This offence can be punished with a fine of up to EUR 50,000.00. The competent administrative authority for the pursuit and prosecution of offences of this type is the chancellor of the TU Dortmund University. In the case of multiple or other serious attempts at deception, the candidate can also be unenrolled, Section 63, paragraph 5 of the Universities Act of North Rhine-Westphalia.

The submission of a false affidavit is punishable.

Any person who intentionally submits a false affidavit can be punished with a prison sentence of up to three years or a fine, Section 156 of the Criminal Code. The negligent submission of a false affidavit can be punished with a prison sentence of up to one year or a fine, Section 161 of the Criminal Code.

I have taken note of the above official notification.

Ort, Datum (Place, date) Unterschrift (Signature)

Titel der Dissertation:

(Title of the thesis):

Ich versichere hiermit an Eides statt, dass ich die vorliegende Dissertation mit dem Titel selbstständig und ohne unzulässige fremde Hilfe angefertigt habe. Ich habe keine anderen als die angegebenen Quellen und Hilfsmittel benutzt sowie wörtliche und sinngemäße Zitate kenntlich gemacht.

Die Arbeit hat in gegenwärtiger oder in einer anderen Fassung weder der TU Dortmund noch einer anderen Hochschule im Zusammenhang mit einer staatlichen oder akademischen Prüfung vorgelegen.

I hereby swear that I have completed the present dissertation independently and without inadmissible external support. I have not used any sources or tools other than those indicated and have identified literal and analogous quotations.

The thesis in its current version or another version has not been presented to the TU Dortmund University or another university in connection with a state or academic examination.*

*Please be aware that solely the German version of the affidavit ("Eidesstattliche Versicherung") for the PhD thesis is the official and legally binding version.

Ort, Datum (Place, date) Unterschrift (Signature)